INTERNATIONAL COUNCIL FOR RESEARCH AND INNOVATION
IN BUILDING AND CONSTRUCTION

WORKING COMMISSION W18 - TIMBER STRUCTURES

CIB - W18

MEETING THIRTY-SIX

COLORADO

USA

AUGUST 2003

CONTENTS

CIB-W18 Papers 36-2-1 up to 36-102-2

0 List of Participants

INTERNATIONAL COUNCIL FOR RESEARCH AND INNOVATION IN BUILDING AND CONSTRUCTION
WORKING COMMISSION W18 - TIMBER STRUCTURES

MEETING THIRTY-SIX
Colorado, USA 11-14 August 2003

LIST OF PARTICIPANTS

AUSTRALIA

B Leicester	CSIRO, Melbourne

CANADA

F Lam	University of British Columbia, Vancouver
I Smith	University of New Brunswick, Fredericton

DENMARK

P Ellegaard	Aalborg University
H J Larsen	Copenhagen

FINLAND

A Ranta-Maunus	VTT Technical Research Centre of Finland, Espoo

FRANCE

J P Biger	Bureau Veritas, Paris

GERMANY

H J Blaß	University of Karlsruhe
J Denzler	Technical University of Munich
R Görlacher	University of Karlsruhe
L Höfflin	Otto-Graf-Institute, Stuttgart
S Lehmann	Bauhaus University, Weimar
K U Schober	Bauhaus University, Weimar

ITALY

A Ceccotti	IVALSA-CNR, Florence
M Ballerini	University of Trento

JAPAN

J Jensen	Institute of Wood Technology, Akita Prefectural University
N Kawai	National Institute for Land and Infrastructure Management, Ibaraki
K Komatsu	Wood Research Institute, Kyoto University
S Nakajima	Building Research Institute, Tsukuba
M Yasumura	Shizuoka University

LATVIA

L Ozola   Latvia University of Agriculture, Jelgava

NEW ZEALAND

H Bier   Carter Holt Harvey fibre-gen, Rotorua

PORTUGAL

L F C Jorge   Polytechnic Institute of Castelo Branco

SLOVENIA

B Dujic   Faculty of Civil and Geodetic Engineering, Ljubljana

R Zarnic   Faculty of Civil and Geodetic Engineering, Ljubljana

SWEDEN

C Bengtsson   Swedish National Testing and Research Institute, Borås

M Hansson   Lund University

H Johnsson   Lulea University of Technology

R Kliger   Chalmers University of Technology

SWITZERLAND

J Köhler   ETH Zürich

THE NETHERLANDS

A Dias   TU Delft

A Jorissen   SHR Timber Research, Wageningen

A D Leijten   TU Delft

UK

B S Choo   Centre for Timber Engineering, Edinburgh

D Ridley-Ellis   Centre for Timber Engineering, Edinburgh

USA

D M Carradine   Washington State University

J D Dolan   Washington State University

R Gutkowski   Colorado State University

B Kasal   North Carolina State University

B Yeh   American Plywood Association, Tacoma

1. Chairman's Introduction

2. Timber Columns

3. Stress Grading

4. Stresses for Solid Timber

5. Timber Joints and Fasteners

6. Duration of Load

7. Environmental Condition

8. Laminated Members

9. Trussed Rafters

10. Structural Stability

11. Structural Design Codes

12. Any Other Business

13. Venue and Program for Next Meeting

14. Close

M I N U T E S
(B S Choo)

1 CHAIRMAN'S INTRODUCTION

Prof Hans Blaß opened the 36th CIB W18 meeting and Prof Richard Gutkowski of Colorado State University, the local host, welcomed participants to the meeting and to Colorado. Prof Gutkowski informed participants of the domestic arrangements and other technical activities and visits arranged.
Prof Blaß thanked Prof Gutkowski for the local arrangements and informed participants of the changes in the technical programme and visits.

2 TIMBER COLUMNS

36 - 2 - 1 The Reliability of Timber Columns Based on Stochastical Principles -
K Rautenstrauch, R Hartnack

Presented by: K U Schober

Kay Schober's presentation covered issues relating to actions in general and the material properties. Results based on virtual experiments the work enabled the influence of strength, modulus of elasticity, proportion of permanent actions and the slenderness ratio of the columns to be analysed. He concluded that the model enabled verification of experimental data and the adaptation of design concepts. It will also reduce the number of experiments and experimental duration and enabled the use of user defined climatic scenarios. He expects the work to lead to practical recommendations in a year or so.

3 STRESS GRADING

36 - 5 - 1 Settings for Strength Grading Machines – Evaluation of the Procedure
*according to prEN 14081, part 2 - **C Bengtsson, M Fonselius***

Presented by: Charlotte Bengtsson

In her presentation, Charlotte Bengtsson described the requirements of the new standards, prEN 14081, for strength grading and she also outlined the Nordic understanding of the procedures implied in the standard. She recommended that a clear procedure for use within the standard would both improve the standard and also facilitate the use of the standard and answered questions on the reluctance of saw millers to use different settings for combination grades outputs, the implications of the standard regarding use of factory tests for confirming the 5 percentile requirements. She confirmed that for high strength outputs, namely for grades C35 and above, some factory testing is required.

*36 - 5 -2   A Probabilistic Approach to Cost Optimal Timber Grading - **J Köhler, M Faber***

Presented by: Jochen Köhler

Jochen Köhler described the issues surrounding the probabilistic modelling of timber materials and the authors' assessment of the optimal grading procedure. He also described findings based on tests using 239 samples of Swedish and German spruce (58x120mm) in which tests were carried out on strength, elastic modulus and density using regression analysis. He concluded that the approach presented may be used for the optimisation of the output from sawmills and answered questions regarding his use of the terms quality control and grading.

4   STRESSES FOR SOLID TIMBER

36 - 6 - 1   Characteristic Shear Strength Values Based on Tests According to EN 1193 - **P Glos, J Denzler**

Presented by: Julia Denzler

In her presentation, Julia Denzler described the loading arrangement and testing requirements needed to comply with EN 1193. The work is based on tests carried out on 118 test specimens. She concluded that the test results did not agree with the values in EN338 and that fissures and knots cannot be accommodated and reported bonding problems between the test pieces and the steel plates. Regarding shear strength it was reported that there is no significant influence of density on characteristic strength. The presentation was followed by an interesting and detailed discussion regarding the various test methods available and the implications of using clear samples versus realistic samples. This included the use of torsion tests and practical issues and implications of the findings.

5   TIMBER JOINTS AND FASTENERS

*36 - 7 - 1   Shear Tests in Timber-LWAC with Screw-Type Connections - **L Jorge, H Cruz, S Lopes***

Presented by: Luis Jorge

Luis Jorge described experimental work, test results and analysis regarding the use of screws with washers to connect the timber to the concrete. He concluded that LWAC specimens without an interlayer could lead to strength reduction but with similar stiffness in comparison with NWC. His tests suggest that the use of LWAC could be a positive alternative to normal concrete. He answered question relating to failure modes, slip and slip modulus.

*36 - 7 - 2   Plug Shear Failure in Nailed Timber Connections: Experimental Studies - **H Johnsson***

Presented by: Helena Johnsson

Helena Johnsson stated that the purpose of her study was to evaluate existing predictive formulae for plug shear failures and based on the analysis of her test data, she recommended a formula provided the nail has not penetrated more than half the depth of the timber. She plans to use fracture mechanics and finite element approaches to further examine the issues involved and went on to answer questions relating to load duration and growth ring orientation.

36 - 7 - 3   Nail-Laminated Timber Elements in Natural Surface-Composite with Mineral Bound Layer - S Lehmann, K Rautenstrauch

Presented by: Steffen Lehmann

Steffen Lehmann described the experimental setup and also discussed his test data as well as the discrepancies between theoretical and measured tensile stresses. In summary, he concluded that shear stresses can be transferred across saw-rough lamella surfaces. There were questions and severe warnings relating to long term durability of the bond layers and the timber species used as the natural bond characteristics could be related to the species used. He also answered questions relating to the implications of the work to Eurocode 5.

36 - 7 - 4   Mechanical Properties of Timber-Concrete Joints Made With Steel Dowels - A Dias, J W G van de Kuilen, H Cruz

Presented by: Alfredo Dias

Alfredo Dias described the test programme which employed dowel type fasteners of 8 and 10 mm diameters. Timber specimens included spruce, maritime pine and chestnut. Comparisons were also made with reference to EC5. In general it was found that load capacity increased with concrete strength. And that in general, load capacity is conservative but that the slip modulus estimation is not conservative. He answered questions relating to the failure modes of the interlayer and the value of the embedding strength of the concrete and timber.

36 - 7 - 5   Comparison of Hysteresis Responses of Different Sheating to Framing Joints - B Dujič, R Zarnić

Presented by: Bruno Dujic

Bruno Dujic discussed the need for the research presented and the two-stage mathematical model of wood frame structures used. The experimental work involved 6 different joint configurations employing 3 specimens for each configuration. He concluded that the simulation of non-elastic behaviour of nailed connection is of crucial importance for the successful prediction of the behaviour of timber framed walls and timber structures subject to seismic excitation. Bruno's presentation was followed by an interesting discussion regarding to the use of the damping values obtained in relation to timber structures and their implications for design codes.

*36 - 7 - 6   Evaluation and Estimation of the Performance of the Nail Joints and Shear Walls under Dry/Humid Cyclic Climate - **S Nakajima***

Presented by: Shiro Nakajima

Shiro Nakajima indicated that the main objectives of the research he presented was to evaluate the effects of dry/humid cyclic climatic conditions of nailed joints in shear wall panels as the shear walls installed in timber houses experience these climatic cycles. He compared values obtained for plywood and OSB sheathed shear walls with those obtained numerically. In his conclusion he observed that the condition of the test specimen during the test affected the strength and stiffness of the joints. Questions were asked with regard to more than one cycle of dry/humid conditions. Shiro indicated that he plans to perform tests using multiple climatic cyclic conditions.

*36 - 7 - 7   Beams Transversally Loaded by Dowel-Type Joints: Influence on Splitting Strength of Beam Thickness and Dowel Size - **M Ballerini, A Giovanella***

Presented by: Marco Ballerini

Marco Ballerini introduced his presentation with a discussion of the issues relating to tensile strength perpendicular to the grain and the existing code (prEN 1995-1-1 and E DIN 1052) formulae for designing the situation. He indicated that the aims of the experimental studies are to obtain the actual influence of b on the splitting strength of the beams and to demonstrate the influence of the failure loads of the bearing capacity. He concluded that the thickness affects linearly the splitting strength of beams and that EC5 formula is able to correctly predict the experimental data "when calibrated on each test series". He then answered questions relating to practical design situations.

*36 - 7 - 8   Splitting Strength of Beams Loaded by Connections - **J L Jensen***

Presented by: Joergen Jensen

Joergen Jensen introduced his paper by discussing the need for this piece of research using fracture mechanics approach. Comparisons were made using the formulae provided by Jensen, Van der Put/Leijten and Gustafsson/Larsen using glulam and LVL beam examples. He concluded that the inclusion of normal forces in the Van der Put/Leijton formula is of limited practical importance. Jensen answered questions relating to the use of tensile strength values perpendicular to the grain, especially for glulam and LVL beams.

*36 - 7 - 9   A Tensile Fracture Model for Joints with Rods or Dowels loaded Perpendicular- to-Grain - **J L Jensen, P J Gustafsson, H J Larsen***

Presented by: J Larsen

J Larsen explained that the authors used the updated approach based on beam on elastic foundation approach using Timoshenko beam theory as published recently as a CIB-W18 paper. Comparisons were carried out using fracture mechanics and stress analysis

4

approaches. Analysis was also carried out using a double symmetrical "plate joint" model. Hans Larsen presented the experimental work used to verify the theoretical work described in the paper. This included tests carried out by Yasumura, and Quenneville and Mohammad, and Kasim and Quenneville. Comparisons of the test data with theoretical work raised questions about the use of fitting approaches.

These 2 presentations were followed by interesting discussions relating to the theoretical definition of stresses as well as the practical engineering design solution approaches to the perpendicular-to-the-grain tensile fracture situations.

*36 - 7 - 10   A Numerical Model to Simulate the Load-Displacement Time-History of Mutiple-Bolt Connections Subjected to Various Loadings - **C P Heine, J D Dolan***

Presented by: Dan Dolan

Dan Dolan introduced the paper by providing an overview of the problem of bolted joints. The research was limited to single shear load parallel to grain situations. The research looked at group action effects in both elastic and the inelastic range. Dan went on to answer questions relating to the way the program dealt with load reversal situations and also about the "black box" approach used versus the clarity of detailed engineering methodology needed to understand the methodology used.

*36 - 7 - 11   Reliability of Timber Structures, Theory and Dowel-Type Connection Failures - **A Ranta-Maunus, A Kevarinmäki***

Presented by: Alpo Ranta-Maunus

Alpo Ranta-Maunus explained that this research followed the collapse of 52m span glulam structure in Finland in February 2003. The structure was designed to EC5 requirements. He informed participants that the paper covered the effects of grading on the strength properties of timber structures and also about dowel joint design and manufacture. He indicated that the reported effects of grading on strength distribution is based on numerical simulation in accordance with PrEN 14081-2. He reported that the failure initiated at a joint where there were only 7 dowels instead of the required 33 dowels. Other reasons included poor manufacture quality and questionable stability supports. More importantly he concluded that EC5 provisions for multiple dowel joints are not adequate. A major conclusion from the research is that design rules for tension in dowel type joints must be revised for group effects and should also take into account block shear failure.

6   DURATION OF LOAD

*36 - 9 - 1   Load Duration Factors for Instantaneous Loads - **A J M Leijten, B Jansson***

Presented by: Ad Leijten

Ad Leijten began his presentation by giving an overview of the need to consider impact loading on guard rails and the choice of tropical hard wood. The research showed that the variation of dynamic strength as compared to static strength is dependent on species types.

He concluded that impact-bending strength depends on wood species and loading rate. Discussions which followed related to the question of whether the effect is on a reduction of strength or an increase in loading due to the impact loading and the parameters which need to be considered in the research.

7   ENVIRONMENTAL CONDITION

36 - 11 - 1 *Structural Durability of Timber in Ground Contact – R H Leicester, C H Wang, M N Nguyen, G C Foliente, C McKenzie*

Presented by: Bob Leicester

Bob Leicester's presentation began with engineering definitions of the terms such as decay and decay front. He went on to describe the on-site tests carried out from which decay attack patterns on treated and untreated heartwood, corewood and sapwood were observed as a function of the maintenance procedure used. He went on to describe the model developed to predict the service life and its applicability to other forms of decay such as termite attack. He went on to answer questions relating to the current trend of not using preservatives such as CCA and design life.

8   LAMINATED MEMBERS

36 - 12 - 1 *Problems with Shear and Bearing Strength of LVL in Highly Loaded Structures - H Bier*

Presented by: Hank Bier

Hank started his presentation by describing the background of the production of LVL in Australasia and the need for research due to the relatively large volume of production per capita. He went on to say that the aim of the research is to assess the reliability of the published shear and bearing capacity of the engineered products. From the test he concluded that only high grade specimens fail in shear, that shear characteristic based on bending is too conservative and that bearing failure needed to be examined. As a result follow on bearing tests were conducted from which he concluded that bearing deformation is important and that further work is necessary.

36 - 12 - 2 *Weibull Based Design of Round Holes in Glulam - L Höfflin, S Aicher*

Presented by: Lilian Höfflin

Lilian began her presentation with an overview of the mechanical problem and also commented on the requirements of DIN 1052 and EC5. She went on to conclude that the Weibull approach agreed well with experimental results which showed strong size effects and moment influence.

She then went on to answer questions relating to the practical design use of the methodology presented and its impact on EC5 requirements. The methodology was well received by the participants.

9   TRUSSED RAFTERS

*36 - 14 - 1   Effect of Chord Splice Joints on Force Distribution in Trusses with Punched Metal Plate Fasteners - **P Ellegaard***

Presented by: Peter Ellegaard

Peter Ellegaard began his presentation by outlining the reasons and methodology used for the research. He also discussed the new guidelines given in EC5 and in the Danish code for the design of chord splice joints. The numerical aspects of the work is carried out using TrussLab. The work also included tests on trusses without chord splice joints for comparison purposes. He concluded that the influence on shear and axial forces is insignificant. More importantly he concluded that the new guidelines are not necessary.

*36 - 14 - 2   Monte Carlo Simulation and Reliability Analysis of Roof Trusses with Punched Metal Plate Fasteners - **M Hansson, P Ellegaard***

Presented by: Martin Hansson

Martin Hansson began his presentation by describing the principles behind the use of load sharing system. He went on to describe the test data used in his research. He concluded that the strength of a roof truss taking experimental data as input parameters could be simulated. In the discussions which followed Martin clarified that by system he meant only a single roof truss rather than the whole roof.

*36 - 14 - 3   Truss Trouble – **R H Leicester, J Goldfinch, P Paevere, G C Foliente***

Presented by: Bob Leicester

Bob Leicester began his presentation by considering a recent structural truss rafter roof collapse and nail plate pull out. He also described lateral stability issues related to truss roofs and also discussed heel joint failure modes, buckling and local effects. His survey showed that nail plate pull out is not uncommon. In a particular case 12 out of 18 trusses had to be replaced due to nail plate pull out failures. From the study it is recommended that the strength of complex truss systems be verified via laboratory tests, that formal stability checks should be made for certain trusses and that special checks may need to be made for local grain slopes. Discussions centred on design code implications and the testing procedure for the heel joints.

10   STRUCTURAL STABILITY

*36 - 15 - 1   Monitoring Light-Frame Timber Buildings: Environmental Loads and Load Paths – **I Smith et al.***

Presented by: Ian Smith

Ian Smith made the presentation on behalf of 10 authors in 7 institutions in 3 countries. He began by stating that the design of timber structures is basically subjective although the

intention is to move towards a more performance/probabilistic approach. To be able to do so it is necessary to have synchronous data from full-scale timber structures which are complex. He went on to describe the various wooden buildings being monitored. The overall aim of the exercise is to achieve better design codes and rules leading to better building performance. He went on to inform participants of the expected project outcomes and technical challenges. The presentation was followed by an interesting discussion on the purpose, possible outcomes and implications for design of timber structures.

*36 - 15 - 2 Applicability of Design Methods to Prevent Premature Failure of Joints at Shear Wall Corners in Case of Post and Beam Construction - **N Kawai, H Isoda***

Presented by: Naohito Kawai

Naohito Kawai began his presentation by stating that the objective of the research is to confirm the adequacy of design calculation (empirical and rigid beam) methodologies relating to the prevention of premature failure of joints at shear wall corners. He went on to describe the test specimens used and compared the test data against the predictions from both design methods. In conclusion he stated that both design methods give larger tensile force values than that observed experimentally and although the methods are applicable there are differences which will need to be verified using finite element methods.

*36 - 15 - 3 Effects of Screw Spacing and Edge Boards on the Cyclic Performance of Timber Frame and Structural Insulated Panel Roof Systems - **D M Carradine, J D Dolan, F E Woeste***

Presented by: David Carradine

David Carradine began his presentation by describing contemporary timber frame design methodologies using SIP panels. He went on to describe the testing protocols and the SIP roof panel configurations used in his experimental work. David went on to discuss the design implications based on the findings of the research.

*36 - 15 - 4 Pseudo-Dynamic Tests on Conventional Timber Structures with Shear Walls - **M Yasumura***

Presented by: Motoi Yasumura

Motoi Yasumura described typical 3 storey timber framed buildings using shear walls and their ability to withstand seismic effects before going on to describe the test method, specimens used in the pseudo dynamic testing conducted and the data obtained. He concluded that pseudo-dynamic testing is a useful approach for assessing the ground level storey behaviour and that the hysteretic model accurately predicted the first storey behaviour but under-estimate the second storey behaviour.

36 - 15 - 5 Experimental Investigation of Laminated Timber Frames with Fiber-reinforced
*Connections under Earthquake Loads - **B Kasal, P Haller, S Pospisil,***
I Jirovsky, A Heiduschke, M Drdacky

Presented by: Bo Kasal

Bo Kasal indicated that his presentation is a follow on from the presentation by Peer Haller made in Kyoto last year. The problems with multi-storey heavy timber framed building in earthquakes relate to the relatively low mass and high strength/mass ratios of the structures. He went on to describe the full–scale and small (1:4) scale model tests conducted. He concluded by raising the various issues which should be resolved before composite reinforcements are used practically. Discussions on the paper included the need to relate W18 papers to at least work reported in previous W18 proceedings.

36 - 15 - 6 Effect of Test Configurations and Protocols on the Performance of Shear Walls
*- **F Lam, D Jossen, J Gu, N Yamaguchi, H G L Prion***

Presented by: Frank Lam

In his introduction Frank Lam discussed the possibility of an earthquake in Vancouver before going on to describe the test protocol, specimens and results obtained. The aim of the research is to investigate the influence of test configuration and protocols on the performance of shear walls. He observed that hold-down devices allow full racking capacity to be developed. He concluded that hold down devices have a strong influence on the behaviour of the structure. More importantly a large number of load cycles in testing may not truly reflect structural behaviour in an earthquake. Hence he recommended that cyclic testing protocols should consider the total energy dissipation characteristics of the structure under expected earthquake excitation.

36 - 15 - 7 Comparison of Monotonic and Cyclic Performance of Light-Frame Shear
*Walls - **J D Dolan, A J Toothman***

Presented by: Dan Dolan

Dan Dolan reported that the research, comparing the performance of shear walls constructed with 4 different sheeting materials was carried out at the Brooks Forest Products Research Centre at Virginia Tech. He then described the results obtained and also discussed the design code implications as the test results showed that the design code requirements gave values less than that obtained experimentally. In the discussion Dan confirmed that he used 9mm sheathing with 24 inches stud spacing – this was sufficient to prevent buckling problems.

11   STRUCTURAL DESIGN CODES

36 - 102 - 1 Predicted Reliability of Elements and Classification of Timber Structures -
L Ozola, T Keskküla

Presented by: Lilita Ozola

After acknowledging her co-author, Lilita Ozola discussed the approaches used to address the issue of uncertainties in design parameters. She went on to describe her database of timber framing systems, the sampling scheme used and the procedure used for determining the 5th percentile strength values. She proposed 3 classes of timber structures for design purposes, based on the required degree of reliability. Discussion centred on the relevance of the research to EC5.

36 - 102 - 2 Calibration of Reliability-Based Timber Design Codes: Choosing a Fatigue Model - I Smith

Presented by: Ian Smith

Ian Smith began his presentation by stating that although most engineers take "static" fatigue into account they frequently neglect the effects of "cyclic" fatigue. He showed that the choice of damage model is a major factor that controls reliability predictions and that common interpretation of static fatigue data does not match the expectations from theoretical mechanics. He then went on to discuss the features which need to be taken into account when choosing a damage model before suggesting a simple mathematical model. He concluded that damage models should be consistent with experimental data but this does not mean that they have to be complex. Discussion centred on the use of terms static and cyclic fatigue and the relationship of the work reported to other standard fatigue work on timber.

12   ANY OTHER BUSINESS

Hans Blaß informed participants who presented that a paper version of the paper needs to be sent to Rainer Goerlacher by end of September for publication purposes. Richard Gutkowski suggested that a mechanism for taking suggestions made during the meetings could be taken forward.

13   VENUE AND PROGRAMME FOR NEXT MEETING

Hans Blaß informed participants that the next W18 meeting will be held in Edinburgh, Scotland. The UK Centre for Timber Engineering (CTE) recently established at Napier University in Edinburgh will host the event. BS Choo gave a brief presentation on the CTE and informed participants of some of the many interesting activities and places of interest in Edinburgh.
Hans Blaß informed the participants that the venue of 2005 W18 meeting will be in Germany.
Ario Ceccotti offered Venice as a venue for 2006 and Roko Zarnic offered Bled, Slovenia as a venue thereafter.

14   CLOSE

Hans Blaß thanked Richard Gutkowski for organising the 36th CIB W18 meeting in Colorado and for the technical visits and social events before closing the meeting.

**15.   List of CIB-W18 Papers,
Colorado, USA 2003**

List of CIB-W18 Papers, Colorado, USA 2003

16.   Current List of CIB-W18(A) Papers

CURRENT LIST OF CIB-W18(A) PAPERS

Technical papers presented to CIB-W18(A) are identified by a code CIB-W18(A)/a-b-c, where:

a   denotes the meeting at which the paper was presented.
Meetings are classified in chronological order:

1   Princes Risborough, England; March 1973

2   Copenhagen, Denmark; October 1973

3   Delft, Netherlands; June 1974

4   Paris, France; February 1975

5   Karlsruhe, Federal Republic of Germany; October 1975

6   Aalborg, Denmark; June 1976

7   Stockholm, Sweden; February/March 1977

8   Brussels, Belgium; October 1977

9   Perth, Scotland; June 1978

10   Vancouver, Canada; August 1978

11   Vienna, Austria; March 1979

12   Bordeaux, France; October 1979

13   Otaniemi, Finland; June 1980

14   Warsaw, Poland; May 1981

15   Karlsruhe, Federal Republic of Germany; June 1982

16   Lillehammer, Norway; May/June 1983

17   Rapperswil, Switzerland; May 1984

18   Beit Oren, Israel; June 1985

19   Florence, Italy; September 1986

20   Dublin, Ireland; September 1987

21   Parksville, Canada; September 1988

22   Berlin, German Democratic Republic; September 1989

23   Lisbon, Portugal; September 1990

24   Oxford, United Kingdom; September 1991

25   Åhus, Sweden; August 1992

26   Athens, USA; August 1993

27   Sydney, Australia; July 1994

28   Copenhagen, Denmark; April 1995

29   Bordeaux, France; August 1996

30   Vancouver, Canada; August 1997

31   Savonlinna, Finland; August 1998

32   Graz, Austria, August 1999

33   Delft, The Netherlands; August 2000

34   Venice, Italy; August 2001

35   Kyoto, Japan; September 2002

36   Colorado, USA; August 2003

b   denotes the subject:

1   Limit State Design
2   Timber Columns
3   Symbols
4   Plywood
5   Stress Grading
6   Stresses for Solid Timber
7   Timber Joints and Fasteners
8   Load Sharing
9   Duration of Load
10   Timber Beams
11   Environmental Conditions
12   Laminated Members
13   Particle and Fibre Building Boards
14   Trussed Rafters
15   Structural Stability
16   Fire
17   Statistics and Data Analysis
18   Glued Joints
19   Fracture Mechanics
20   Serviceability
21   Test Methods
100   CIB Timber Code
101   Loading Codes
102   Structural Design Codes
103   International Standards Organisation
104   Joint Committee on Structural Safety
105   CIB Programme, Policy and Meetings
106   International Union of Forestry Research Organisations

c   is simply a number given to the papers in the order in which they appear:

Example: CIB-W18/4-102-5 refers to paper 5 on subject 102 presented at the fourth meeting of W18.

Listed below, by subjects, are all papers that have to date been presented to W18. When appropriate some papers are listed under more than one subject heading.

LIMIT STATE DESIGN

TIMBER COLUMNS

SYMBOLS

PLYWOOD

STRESS GRADING

STRESSES FOR SOLID TIMBER

TIMBER JOINTS AND FASTENERS

10

11

TIMBER BEAMS

ENVIRONMENTAL CONDITIONS

LAMINATED MEMBERS

PARTICLE AND FIBRE BUILDING BOARDS

TRUSSED RAFTERS

STRUCTURAL STABILITY

FIRE

STATISTICS AND DATA ANALYSIS

GLUED JOINTS

FRACTURE MECHANICS

| 30-19-1 | Failure Analysis of Single-Bolt Joints - L Daudeville, L Davenne and M Yasumura |

SERVICEABILITY

27-20-1	Codification of Serviceability Criteria - R H Leicester
27-20-2	On the Experimental Determination of Factor k_{def} and Slip Modulus k_{ser} from Short- and Long-Term Tests on a Timber-Concrete Composite (TCC) Beam - S Capretti and A Ceccotti
27-20-3	Serviceability Limit States: A Proposal for Updating Eurocode 5 with Respect to Eurocode 1 - P Racher and F Rouger
27-20-4	Creep Behavior of Timber under External Conditions - C Le Govic, F Rouger, T Toratti and P Morlier
30-20-1	Design Principles for Timber in Compression Perpendicular to Grain - S Thelandersson and A Mårtensson
30-20-2	Serviceability Performance of Timber Floors - Eurocode 5 and Full Scale Testing - R J Bainbridge and C J Mettem
32-20-1	Floor Vibrations - B Mohr

TEST METHODS

31-21-1	Development of an Optimised Test Configuration to Determine Shear Strength of Glued Laminated Timber - G Schickhofer and B Obermayr
31-21-2	An Impact Strength Test Method for Structural Timber. The Theory and a Preliminary Study - T D G Canisius
35-21-1	Full-Scale Edgewise Shear Tests for Laminated Veneer Lumber- B Yeh, T G Williamson

CIB TIMBER CODE

2-100-1	A Framework for the Production of an International Code of Practice for the Structural Use of Timber - W T Curry
5-100-1	Design of Solid Timber Columns (First Draft) - H J Larsen
5-100-2	A Draft Outline of a Code for Timber Structures - L G Booth
6-100-1	Comments on Document 5-100-1; Design of Solid Timber Columns - H J Larsen and E Theilgaard
6-100-2	CIB Timber Code: CIB Timber Standards - H J Larsen and E Theilgaard
7-100-1	CIB Timber Code Chapter 5.3 Mechanical Fasteners; CIB Timber Standard 06 and 07 - H J Larsen
8-100-1	CIB Timber Code - List of Contents (Second Draft) - H J Larsen
9-100-1	The CIB Timber Code (Second Draft)
11-100-1	CIB Structural Timber Design Code (Third Draft)
11-100-2	Comments Received on the CIB Code U Saarelainen; Y M Ivanov, R H Leicester, W Nozynski, W R A Meyer, P Beckmann; R Marsh
11-100-3	CIB Structural Timber Design Code; Chapter 3 - H J Larsen
12-100-1	Comment on the CIB Code - Sous-Commission Glulam
12-100-2	Comment on the CIB Code - R H Leicester
12-100-3	CIB Structural Timber Design Code (Fourth Draft)

INTERNATIONAL STANDARDS ORGANISATION

JOINT COMMITTEE ON STRUCTURAL SAFETY

CIB PROGRAMME, POLICY AND MEETINGS

INTERNATIONAL UNION OF FORESTRY RESEARCH ORGANISATIONS

**INTERNATIONAL COUNCIL FOR RESEARCH AND INNOVATION
IN BUILDING AND CONSTRUCTION**

WORKING COMMISSION W18 - TIMBER STRUCTURES

THE RELIABILITY OF TIMBER COLUMNS

BASED ON STOCHASTICAL PRINCIPLES

K Rautenstrauch

R Hartnack

K. U. Schober

Bauhaus-University Weimar

GERMANY

Presented by: K U Schober

Kay Schober's presentation covered issues relating to actions in general and the material properties. Results based on virtual experiments the work enabled the influence of strength, modulus of elasticity, proportion of permanent actions and the slenderness ratio of the columns to be analysed. He concluded that the model enabled verification of experimental data and the adaptation of design concepts. It will also reduce the number of experiments and experimental duration and enabled the use of user defined climatic scenarios. He expects the work to lead to practical recommendations in a year or so.

The reliabilty of timber columns

based on stochastical principles

Karl Rautenstrauch, Ralf Hartnack

Bauhaus-University Weimar, Chair of Timber and Masonry Engineering, Germany

1 Introduction

As already mentioned in publication 35-2-1 of CIB [8], the reliabilty of timber columns depends on a multitude of influencing variables and on the interaction of these variables. Firstly, the sector of hygrothermal long-time effects and basic principles of the calculating modell was specified in [8]. In addition to hygrothermal long-time effects described in [8] the spreading of influences and of material parameters which are to be described on the basic of probabilistic principles, have a decisive influence on the evaluation of the reliability of timber columns.

Due to the multitude of influencing variables a procedure solely based on experiments is hardly possible, so that the computer simulations of the structural behaviour presented in this work represent a reasonable and an efficient alternative. Thus the parameter of the influencing sector and also the parameter of the resistance's sector ([2], [7]) could be taken into account, based on probabilistic principles. Consequentially the load-bearing capacities, calculated by the software ISOBEAM are also distributed probabilistcally and they must be analysed accordingly.

The concepts of modern standards are also based on semiprobabilistic principles, so that the computer aided simulation models, presented in the following paper, could be made to verify or calibrate the semiprobabilisitic methods of design.

2 Modeling

Without describing the model in detail, the following work is done, referring to the publications in the context of CIB in the previous years ([1], [8]).

In this publication the stochastic relevant influence parameters are only described in a short and explicit way. First of all this has something to do with influences (load, climate, initial deformation) and with resistance (strength, stiffness).

2.1 Action

2.1.1 static loads

First of all static loads are divided into permanent and non-permanent loads. Because hygrothermal long-time effects depend on the duration of a load, permanent loads are seen as main causative for creep deformation and for the adherent reduction of the load-bearing capacity. But the spreading of permanent loads is marginal, therfore a deterministic investigation is choosen for this consideration.

Non-permanent loads are further divided by differentiating the causes. In this publication possible causes are live loads, snow loads and wind loads.

Live loads are usually caused by persons, furniture and the like. They could be hardly summed up using probabilistic principles. Short-term acting loads as loadings by persons do not produce a reduction of load-bearing capacity caused by creep. Mitchell et al. [10] observed in an investigation of a large number of office buildings that part of the non-permanent load could be considered as permanent acting. This loading is basically the result of furnishings which only change their place in huge intervals. More than ten years are characteristic for these intervals. The loading which is caused by furnishings is investigated by about 43 % of live load by German code. This part is added to the permanent loads as quasi-permant part of live loads. As a result the remaining part acts in a short term and therefore the relevance of this part is negligible small for the creep process. The quasi permanent load is assumed as deterministic.

Whereas the load acting duration of snow-loads has another character than that of live loads. If there appears snow-load according to the respective season and of the regional boundary conditions, it permanently acts for the duration of load influence. But no significant stochastic influence can be observed, if the equivalent water content of snow cover - which actually appears (choosen climate station of German weather service DWD) - is investigated. Investigations of Mårtensson [9] show that even if the snow load is present during more than 40 % of a year it does not have a decisive influence on creep oriented on the whole space of observation time. At the point of snow load action you can see a relatively great influence on deformation in dependence of load value. For shorter periods of time, own investigation (Fig. 1) show that the neglect of snow load is an acceptable simplification.
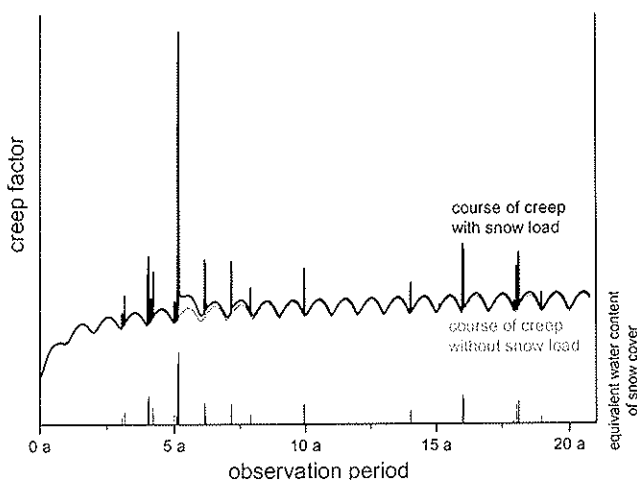
Figure 1: Influence of snow load on creep deformations

2

Normally wind loads have a very short duration of action. Therefore an influence on the long-term load bearing capacity can be excluded.

2.1.2 Imperfections

Beside the static load each installed structural member made of wood shows imperfections which brings the stressless prebend or the oblique position into account. In doing so prebend is the parabolic deflection of a beam. All kinds of columns are affected by prebend.

Ehlbeck et al. [6] investigated a multitude of installed columns to find out whether they had deflections. From their results you can derive the following formulas for prebend and oblique position:

prebend:
$$y_0 = \left(0,11501 \cdot 10^{-3} \pm 1,05381 \cdot 10^{-3}\right) \cdot L \qquad (1)$$

oblique position:
$$\psi = \frac{\left(0,22138 \cdot 10^{-3} \pm 4,82253 \cdot 10^{-3}\right)}{\sqrt{h}} \qquad (2)$$

2.1.3 Moisture Distribution

A further significant influence on the reliability of wooden columns is the surrounding climate and the moisture of the wood produced by it. The influence is described in more detail by Hartnack et al. [8]. Service class 2, which is defined in the mentioned publication, is used in the subsequent work.

2.2 Material parameters

2.2.1 probabilistic determination

The material properties of wood spread very strongly, because of the structural configuration of wood [5]. To determine values of resistance, especially the modulus of elasticity and strength, you have to analyse regression equations of Colling [2]. Becker [1] also used this procedure, but in a slightly modified way. Thereby specifying parameters of input are the bulk density of the material and the knot density, which are choosen at random on the principles of the so-called Monte-Carlo simulation.
For non finger-jointed areas Colling [2] states the following equation:

$$\ln\left(Y_i\right) = \ln\left(Y_{Reg,i}\right) + \Delta_B + X_i \qquad (3)$$

Y is the resistance value to be determined, Δ_B is the random distance of the treated structural member to straight regression line and X_i is the rest spreading. The index i shows the corresponding cell, for which the resistance value is determined. A cell comes into being by the regular dividing of the structural member along its longitudinal axis. The cell length is about 15 cm.
The equations (4) to (7) gives the allocation of each addend of equation (3) for the modulus of elasticity. It is acted on the assumption of a normal distribution with the form mean value $\pm$ standard deviation:

$$\ln\left(E_{Reg,i,tension}\right) = 8.20 + 3.13 \cdot 10^{-3} \cdot \rho_0 - 1.17 \cdot KAR \qquad (4)$$

3

$$\ln\left(E_{Reg,i,compression}\right) = 8.22 + 2.994 \cdot 10^{-3} \cdot \rho_0 - 0.76 \cdot KAR \tag{5}$$

$$\Delta_B = 0.00 \pm 0.16 \tag{6}$$

$$X_i = 0.00 \pm \left(0.079 \pm 0.027\right) \tag{7}$$

The equations (8) upto (10) allocate the addends for strength:

$$\ln\left(f_{Reg,i,tension}\right) = -4.22 + \ln\left(E_{i,tension}\right) \cdot \left(0,876 - 0,093 \cdot KAR\right) \tag{8}$$

$$\ln\left(f_{Reg,i,compression}\right) = 2.586 + 2.80 \cdot 10^{-3} \cdot \rho_0 - 0.825 \cdot KAR \tag{9}$$

$$\Delta_B = 0.00 \pm 0.13 \tag{10}$$

$$X_i = 0.00 \pm 0.13 \tag{11}$$

The so determined resistance values are allocated to each cell of the longitudinal discretisized structural member.

2.2.2 Test Diagram

Strength and modulus of elasticity, determined on stochastic principles, are assigned on the test diagram of Glos [7]. More detailed information could by taken from the paper 35-2-1 [8] or from [11].

3 Application flow of virtual experiments

First there are 1000 elements chosen as random samples from the basic population with the aid of the Monte-Carlo simulation. For this choice the stochastic basics as desbribed in section 2.2.1 are used. All elements of this random sample are loaded and the load is increased until the element fails. Hygrothermal long-term effects do not play any role so far i.e. the load is put on in a very short period of time. The element fails, if either the maximum of tension at the outer layer is reached or if no balance appears.

To investigate the reliability regarding hygrothermal long-time effects a further selection of random samples is made. With a possible load-bearing capacity after short-term loading ten columns from the region around the 5-%-fractiles and ten columns from the region around the mean value are choosen for further investigations. This procedure was verified as permissible in study with 1000 random samples which were investigated over a long-term period.

After choosing 22 elements these are investigated in connection with hygrothermal long-time effects. For that the characteristic load, which just meets the requirements of German Code, is put on. It is assumed that the modifying factor k_{mod} is 0,8. This is true, if at least one of the influences can be put into class "medium-term". This assumption is actually not true for the load degree 1,0, whereas it is right for each load degree, which is incrementally smaller than 1,0. Therefore this assumption is approximately permissible for the load degree 1,0, too. With it the load degree is the permanent load share of the whole load. This load is put on immediately after the beginning of the virtual experiment and it stays there for the whole period of time (about 20 years) without being changed. In this phase the additional deflections and stress redistributions arise as a result of creep. After this phase the load is increased until there is a failure as described by the first phase.

Beside the reduction of load-bearing capacity an increase of deflection can be observed. This fact, however, does not lead to failure.

4 Results

The virtual experiments are investigated for four cases of support following the classical Euler cases. But the analysis of the results shows that the reduction of the load-bearing capacity of different support cases does not significantly vary. Therefore just one representative case of support is chosen for the following results. Especially the influences of the degree of loading, of the slenderness ratio, of the strength and of the modulus of elasticity are investigated. Finally, the results are compared to characteristic load-bearing capacities by standard compared to safety values.

4.1 Influence of strength and modulus of elasticity

Before the running of the virtual long-term load-bearing capacities experiments are analysed first with the scope of correlation between the input parameters strength, modulus of elasticity and initial deflection. There was, however, no significant relation between the load-bearing capacity and the initial deflection.

If you compare the smallest strength of a test piece to the load-bearing capacity, you can observe a clear correlation as far as compact columns (figure 2) are concerned. On the other hand there is no correlation of strength as far as very slender columns are concerned.

Very slender columns show another picture. There a significant correlation between load-bearing capacity and modulus of elasticity can be observed (figure 3). Correspondingly, the load-bearing capacity of compact columns do not correlate with the modulus of elasticity.

These connections, which can also be derived from mechanical principles, are also shown in the presented simulation model and they can therefore be used for the verification of the model. Furthermore, the laod-bearing capacity of a column with the theoretical slender ratio zero only must depend on the weakest part which is represented by the smallest strength of a virtual test piece. On the other hand, the balance failure is decisive with increasing ratio of slenderness. This is directly proportiontal to the modulus of elasticity.
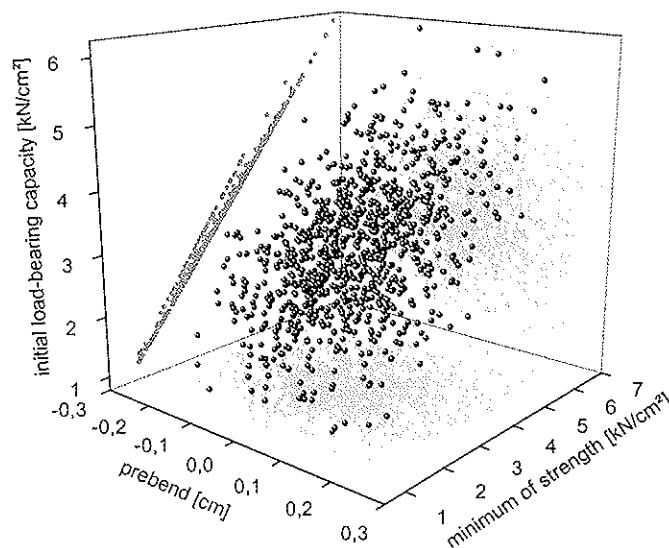
Figure 2: Correlation between minimum of strength and load-bearing capacity (slenderness ratio $\lambda = 20$)[11]
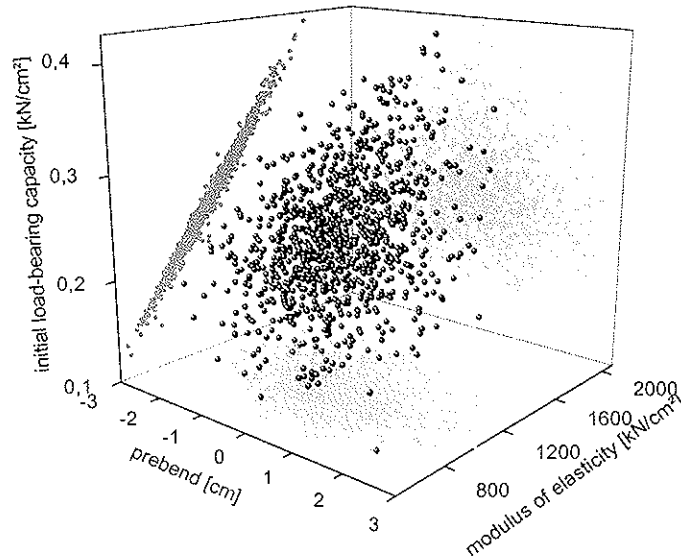
Figure 3: Correlation between middle modulus of elasticity and load-bearing capacity (slenderness ratio λ = 200)[11]

4.2 Influence of slenderness ratio

As already mentioned stress redistributions and increases of deflection arise as a result of hygrothermal long-time effects. If the reductions of load-bearing capacity are plotted against the slenderness ratio, first of all there will hardly have an influence on hygrothermal long-time effects on the load-bearing capacity for compact columns. As to very slender columns the influence can be actually classified as marginal. But in the region of middle slenderness ratios the influence is significant. Actually one exception has to be mentioned. The long-time effects also lead to significant reduction in the load-bearing capacity for high slenderness ratios, if the load degree is 1,0, that means permanent loads only act. Figure 4 shows the quotient of load-bearing capacities of the 5-%-fractiles of short-term load-bearing capacity. The quotient of the load-bearing capacity is defined as the quotient between the capacity after the virtual experiment and the capacity before the virtual experiment.
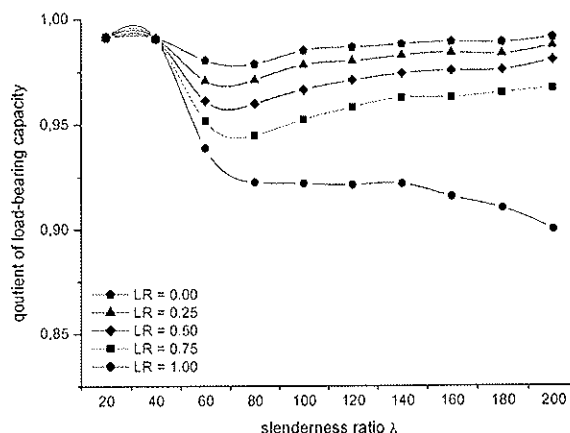
Figure 4: Quotient of load-bearing capacity Euler case 3 [11]

4.3 Influence of load degree and fractiles

Figure 4 already indicates that the load degree (portion of permanent load) also has significant influence on the reduction of the load-bearing capacity. In figure 5 the load –bearing

6

capacity of a column with the theoretical slenderness ratio zero is plotted in dependence of the load degree and the fractile. The significant influence of the laod-degree on the 5-% fractile could well be seen in figure 5. But it can also be observed that the influence on the mean value of the load-bearing capacities is much less. To show the effects clearly a slender column was used. Columns with middle slenderness ratios produce similar effects as well. As shown in figure 5, a significant and a designing relevant influence of hygrothermal effects can be constituted for load degress of 0,5 or higher.
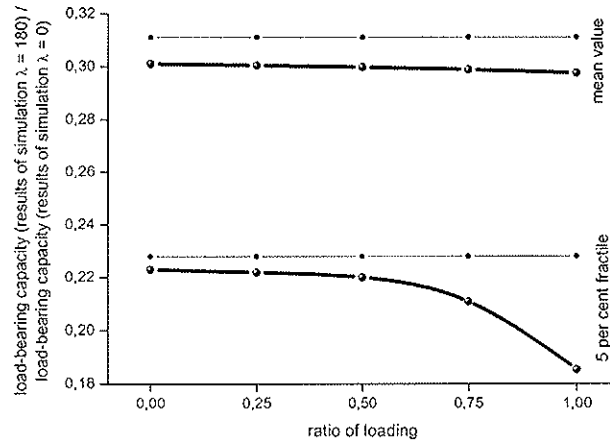
Figure 5: Reduction of load-bearing capacity (Euler case 2, λ=180)

4.4 Comparison to German Code DIN 1052

The results of the virtual experiments could now be compared and contrasted with the values of the standard. Results from the computer simulation (before and after the virtual experiment) and results from calculation for the model column method of German Code DIN 1052 (October 2002) and for the non-linear elastic method (by [3] and [4]) are plotted in figure 6. The differences of the non-linear elastic method between the two drafts result from the fact that 5-%-fratiles of modulus of elasticity which are divided by the partial safety factor γ_M, are used by [3]. [4] on the other hand uses mean values of modulus of elasticity which are divided by the partial safety factor γ_M. The influence of the two different assumptions could decisively be seen in figure 6. In the region of compact columns you can hardly observe any influence. Slenderness ratio 60 or higher shows a significant difference. This formation could be expected, because it is a change of modulus of elasticity. For this reason the modulus of elasticity is multiplied by factor $[1/(1+k_{def})]$ in a further calculation
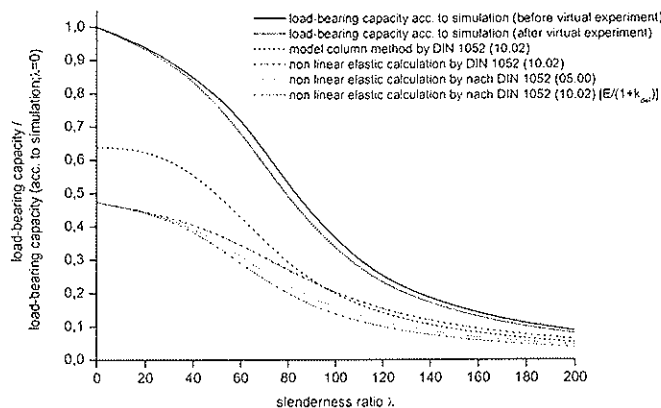
Figure 6: Comparison between the characteristic laod-bearing capacity by DIN 1052 and by computer simulations

7

For the further comparison between load-bearing capacities of the standard and of the computer simulation design values of standard are used. This facilitates to a better comparability between each of load degrees. On the principles of German Code DIN 1052 ([3] and [4]), you have to keep the safety margin γ_M/k_{mod} between the design value of action and the design resistance.
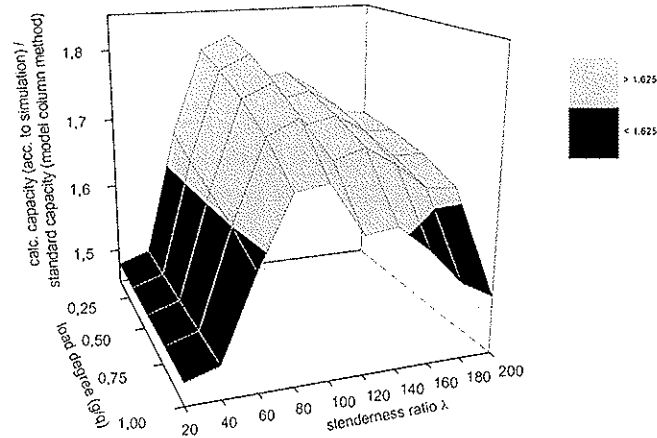
Figure 7: Comparison between the lnod-bearing capacity by computer simulatons and the model columns method by DIN 1052 for the example Euler case 3

Figure 7 shows the comparison between the load-bearing capacity of the computer simulation (after the virtual comparison) and the model column method according to German Code DIN 1052 [4] for the example Euler case three. It can be realised that design values of action are always conservative for modifying factors k_{mod} equal 1,1 resp. 0,9, but they are not conservative for modifying factors k_{mod} equal 0,7 resp. 0,6. The region changes in high dependency of the slenderness ratio and in slight dependency of load degree for modifying factors k_{mod} equal 0,8. The black regions of figure 7 show the non-conservative areas, but the grey ones show the conservative areas.

To investigate the non-linear elastic method, the characteristic values of the load-bearing capacity is faced to the computer simulation (after the virtual experiment). To get a better overview, the axis of load degree is eliminated and in each case one diagram for load degree zero (figure 8) and one diagram for the load degree one (figure 9) is plotted. In dependency of the modifying factor k_{mod} horizontal lines represent the ranges of the postulated safety by German Code DIN 1052 (10.02) [4]. The postulated safety can be calculated by the equation (12).

$$\gamma_{global} = \frac{\gamma_M \cdot \gamma_F}{k_{mod}}$$ (12)

According to this four safety ranges (is equal to four horizontal lines in figure 8) arise for load degree zero (modifying factors k_{mod} = 0,7 ... 1,1) and five safety ranges (is equal to five horizontal lines in figure 9) arise for load degree one.
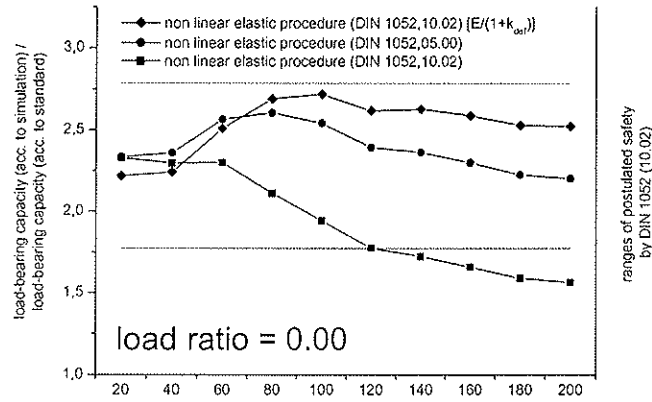
Figure 8: Ratio of load-bearing capacity of computer simulation to that by standard (load ratio 0,0)
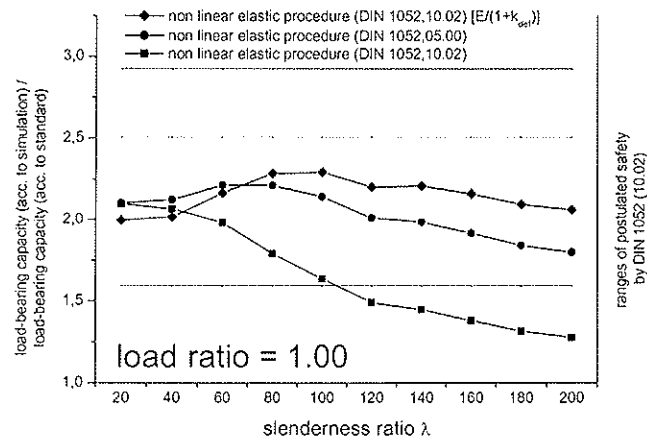
Figure 9: Ratio of load-bearing capacity of computer simulation to that by standard (load ratio 1,0)

If the accordant postulated levels of safety are taken as basis, the analysis of both diagrams show that design procedures are conservative or non-conservative in dependency of the modifying factor k_{mod}.

5 Summary

A tool has been created which is in a position to calculate the load-bearing capacity of wooden columns with the help of virtual experiments. The material parameters of wood are determined on pure probabilistic principles and they are respectively allocated to the structural member. Action is treated in the same way, but it is partly estimated as deterministic on the basis of reasonable simplifications. According to measured values of German climate stations the climatic boundary conditions are taken into account by approximated cyclic specifications.

The chosen approach by using computer simulations makes a confrontation and a comparison to the load-bearing capacity of standard possible, so that you are able to state facts as to the actual safety. Furthermore, the influence of creep on the reliability of timber columns is investigated in this study. Especially in the constructional convenient regions of slenderness ratio you can see a high influence. The influence of the load degree and the fractile are also investigated. The influence of hygrothermal long-time effects increases with an increasing load-degree and with a decreasing fractile value.

9

To evaluate the laod-bearing capacity of timber columns, the presented procedure on the basis of a probabilistic simulation model is excellently suitable for an economic supply of results, because such investigations are always based on a long-term observation period.

6 Acknowledgements

7 References

[1] Becker, P., Modellierung des zeit- und feuchteabhängigen Materialverhaltens zur Untersuchung des Langzeittragverhaltens von Druckstäben aus Holz, PhD-Thesis, Bauhaus-University Weimar, Weimar, 2002

[2] Colling, F., Tragfähigkeit von Biegeträgern aus Brettschichtholz in Abhängigkeit von den festigkeitsrelevanten Einflußgrößen, PhD-Thesis, University of Karlsruhe, Karlsruhe, 1990

[3] DIN 1052 (05.00), Entwurf, Berechnung und Bemessung von Holzbauwerken, 2000

[4] DIN 1052 (10.02), Entwurf, Berechnung und Bemessung von Holzbauwerken, 2002

[5] Dinwoodie, J.M., Timber: Its nature and behaviour, Second Edition, New York, 2000

[6] Ehlbeck, J., Blaß, H.J., "Imperfektionsannahmen für Holzdruckstäbe", Holz als Roh- und Werkstoff, Vol. 45, 1987, pp. 231-235

[7] Glos, P., Zur Bestimmung des Festigkeitsverhalten von Brettschichtholz bei Druck-beanspruchung aus Werkstoff- und Einwirkungsgrößen, PhD-Thesis, University of Munich, Munich, 1978

[8] Hartnack, R., Schober, K.-U., Rautenstrauch, K., Computer simulations on the reli-ability of timber columns regarding hygrothermal effects, CIB-W18 meeting 35, paper 35-2-1, Kyoto, 2002

[9] Mårtensson, A., Mechanical behaviour of wood exposed to humidity variations, Report TVBK-1006, Lund, 1992

[10] Mitchell, G.R., Woodgate, R.W., A survey of floor loadings in office buildings, Constuction Industry Research and Information Association Report 25, London, 1970

[11] Rautenstrauch, K., Hartnack, R., Zuverlässigkeit von Druckstäben aus Holz unter Berücksichtigung des zeit- und feuchteabhängigen Materialverhaltens. DFG-Abschlussbericht, Weimar, 2002

[12] Rautenstrauch, K., Hartnack, R., Becker, P., The reliability of timber columns – Computer simulations on the reliability regarding long-time effects, Second Interna-tional Conference of the European Society for Wood Mechanics, Stockholm 2003

**INTERNATIONAL COUNCIL FOR RESEARCH AND INNOVATION
IN BUILDING AND CONSTRUCTION**

WORKING COMMISSION W18 - TIMBER STRUCTURES

SETTINGS FOR STRENGTH GRADING MACHINES –

EVALUATION OF THE PROCEDURE ACCORDING TO PREN 14081, PART 2

C Bengtsson

SP Swedish National Testing and Research Institute, Borås

SWEDEN

M Fonselius

VTT

FINLAND

Presented by: Charlotte Bengtsson

In her presentation, Charlotte Bengtsson described the requirements of the new standards, prEN 14081, for strength grading and she also outlined the Nordic understanding of the procedures implied in the standard. She recommended that a clear procedure for use within the standard would both improve the standard and also facilitate the use of the standard and answered questions on the reluctance of saw millers to use different settings for combination grades outputs, the implications of the standard regarding use of factory tests for confirming the 5 percentile requirements. She confirmed that for high strength outputs, namely for grades C35 and above, some factory testing is required.

Settings for strength grading machines – evaluation of the procedure according to prEN 14081, part 2

Charlotte Bengtsson, SP Swedish National Testing and Research Institute, Wood Materials and Structures, Box 857, SE-501 15 Borås, Sweden

Mikael Fonselius, VTT Technical Research Centre of Finland, P.O. Box 1801, FIN-02044 VTT, Finland

1 Abstract

This paper presents experience gained during the application of the new standard prEN 14081-part 2. The standard contains a procedure for derivation of setting values for strength grading machines. The standard was applied for representative raw material from the Nordic countries (Sweden, Finland and Norway). Consequences when the raw material properties are better than those of the required grades and the importance of the choice of representative raw material data for derivation of settings are discussed. A "method for calculation" which would facilitate the use of the standard is suggested.

2 Background and introduction

A new standard "prEN 14081 Timber structures – Strength graded structural timber with rectangular cross section" is under development. This standard will harmonise the procedures for calculation of strength grading machine settings in Europe and results in the possibility to CE-mark structural timber. The standard consists of four different parts:

- Part 1: General requirements

- Part 2: Machine Grading – Additional requirements for initial type testing

- Part 3: Machine Grading – Additional requirements for factory production control

- Part 4: Machine Grading – Grading machine settings for machine controlled systems

In part two the procedure for calculating settings for strength grading machines are described. Settings determined according to part two are presented in part four separately for different machine types as well as for different growth areas of the timber to be graded. Settings approved by CEN/TC124/WG2/TG2 are included in part four of the standard.

The procedure for calculating the settings is denoted the "cost matrix method". The method was presented by Rouger (1997). The present version of the standard (dated February 2003) deviates from earlier versions concerning the sampling procedure and the procedure when the characteristic values of the material to be graded are higher than those required for the actual grade.

The standard requires that settings are calculated separately for raw material from different countries which means that raw material from one origin must be graded with the same settings independent of where it is graded. Restricting the use of settings to one country is a topic that has been discussed a lot. The Nordic countries (Sweden, Finland and Norway) have produced a document (Brundin et al. 2002) showing that raw material (spruce and pine) from these three countries has very similar relationships between modulus of elasticity and bending strength. As most grading machines measure stiffness it is appropriate to use this relationship as comparison. The variability within each country is as large as the variability between the countries. Hence, it was accepted by CEN/TC124/WG2/TG2 that Sweden, Finland and Norway can use the same settings.

2.1 Objectives of this paper

The objectives of this paper are to present experience gained during the application of the standard and to discuss some possible improvements.

This paper does not present a full evaluation of the standard but it focuses on some experiences found when applying it for a representative raw material from the Nordic countries (Sweden, Finland and Norway). The methodology used is based on a common understanding of the method for calculation of settings achieved within a Nordic project (Nordtest project number 1616-02).

3 Analysis

3.1 Methodology

The methodology for calculating settings (interpreted from the standard) can briefly be described as follows (references given in this section correspond to clauses in prEN 14081 part 2):

1. Establish a database containing the test data (ID number, bending strength (f_m), modulus of elasticity (E), density and indicating property (IP) measured by the machine). f_m shall be corrected to h=150 mm and E and density to 12% moisture content according to EN 384. Number of specimens and sub-samples shall be arranged according to 6.2.1. The sub-samples shall consist of at least 100 specimens and contain material from one growth area or source of production. A minimum number of four sub-samples must be included and at least 900 specimens are required.

2. Optimum grading according to 6.2.4.3. The "1,12 factor" according to EN 384 shall not be applied for grades above C30 and the 95% factor shall be used on E. The optimum grading shall be carried out by maximising the number of specimens in the highest grades for which settings are required.

3. Establish a model relating strength to IP measured by the machine. In the analysis presented here a model of the following form was used:

$$f_{mod,h=150} = k \cdot \left(\frac{t}{50}\right)^a \cdot \left(\frac{h}{150}\right)^b \cdot (IP)^c$$

4. Leave out one sub-sample and determine settings for actual grade combination so that the required characteristic strength (f_k), E and density are fulfilled. Repeat for all sub-samples.

5. Determine the "production settings" as the average of the settings obtained under point 4. Check that the difference between the average and the most conservative sub-sample setting is less than 15%. Otherwise correct according to 6.2.4.4.

6. Grade the whole raw material by using the production settings determined under 5. These grades are called "assigned grades".

7. Collect optimum grades and assigned grades in a "size matrix" according to 6.2.4.5. Example of a size matrix is shown in Table 1.

Table 1. Example of a size matrix for the grade combination C35-C24-C18-reject.

Optimum grade	Assigned grade			
	C35	C24	C18	Reject
C35	554	894	13	0
C24	34	414	60	0
C18	1	27	6	0
Reject	0	74	28	2

8. Determine the elementary cost matrix according to 6.2.4.6. An example is shown in Table 2.

Table 2. Example of an elementary cost matrix.

Optimum grade	Assigned grade			
	C35	C24	C18	Reject
C35	0	0,57	1,3	0
C24	1,53	0	0,69	0
C18	3,15	1,11	0	0
Reject	5,418	2,025	0,685	0

9. Determine the "global cost matrix" as described in 6.2.4.6. Each value in the global cost matrix is obtained by multiplying the number in each cell of the size matrix by corresponding value in the elementary cost matrix and then dividing by the total number of pieces in the assigned grade. For example see Table 3.

Table 3. Example of a global cost matrix.

Optimum grade	Assigned grade			
	C35	C24	C18	Reject
C35	0	0,362	0,158	0
C24	(34*1,53)/589=0,088	0	0,387	0
C18	0,005	0,021	0	0
Reject	0	0,106	0,179	0

10. Check that none of the cells in the global cost matrix which indicate pieces wrongly upgraded contains a figure greater than 0.2 (the cells with bold text in Table 3), 6.2.4.7. Otherwise, correct the IP (point 5) for actual grades and repeat until the requirement is fulfilled.

11. Check that the characteristic values are fulfilled (f_k, E and density) for the assigned grades, according to 6.2.4.8.

The above given interpretation of the standardised method was worked out by representatives for the Nordic countries. The standard would be considerably improved if such an interpretation was included in the standard.

3.2 Raw material used for the analysis

Test material from Norway Spruce (*Picea abies*) representing six different origins in Sweden, Finland and Norway, see Table 4, are used for the analysis presented in this paper. The material data are representative for spruce raw material from these countries. The whole material has a characteristic bending strength of 24,8 MPa, a mean modulus of elasticity of 12400 MPa and a characteristic density of 364 kg/m³.

Table 4. Spruce material used in this paper. The different sub-samples represent different locations in Sweden, Norway and Finland.

Sub-sample No.	Dimensions	No. specimens	Mean bending strength [MPa]	Mean modulus of elasticity [MPa]	Mean density [kg/m³]
1	34 x 95 34 x 145 45 x 145 45 x 195 70 x 220	395	43,0	11341	407
2	40 x 145	97	50,1	12789	466
3	40 x 145	683	45,3	12804	447
4	40 x 145	100	43,5	11330	437
5	40 x 145 45 x 120 35 x 55 35 x 60	522	46,5	12354	477
6	58 x 120 45 x 145	310	47,9	13138	419
Total		2107			

4 Results

To "speed up" the calculations according to the procedure described above a computer programme was developed. Our experience so far is that the procedure in prEN 14081, part two in general works well. However, during the forthcoming revision period the topics presented in this paper should seriously be analysed and discussed.

The examples given are valid for a bending type grading machine, in this case a Computermatic. This machine measures the deflection of a piece of timber when a constant bending stress is applied.

4

4.1 Influence of quality of the raw material

As shown above the "typical" raw material from the Nordic countries fulfils the requirements for C24 without grading. If settings for C24 or below are wanted the usual "cost matrix" procedure can not be used. The standard prescribes two ways of dealing with this case:

> 6.2.4.9 a) "The setting shall be derived from the model for a strength value of 0.5 times the required strength for the grade", or

> 6.2.4.9 b) "The setting shall be derived from the model for the worst indicating property value in the sample".

"If there is one or more test specimens in the sample with a strength value lower than 0.5 times the required value of the critical strength property for the grade, then case a) shall be used, otherwise case b) shall be used."

The consequences of these two cases are illustrated by examples below. For C18 the required strength is 16,1 MPa. Inserting 0,5 times this required strength (8,05 MPa, case a) in the model relating strength to indicating property results in unreasonable settings for the Computermatic grading machine. It is easily realised that this limit value is not realistic in the case of Computermatic when a bending stress of 13,8 MPa is applied when running the machine. The result is that settings 5-6 times less conservative than today will be accepted (this comparison is valid for C18 with a cross section of 50 x 150 mm). The allowed deflections to be measured by the Computermatic grading machine will be so high that they are not possible to measure.

Case b prescribes that the indicating property resulting in the lowest modelled strength within the sample should be used. For the data used in this paper the accepted deflection will be increased by 44 % compared to the deflection accepted today in Sweden (for C18, 50 x 150 in cross section). This value may be reasonable but it is not pleasing to base the setting on one single IP-value within the sample. Additionally, in case b the rule will give exactly the same setting for C16, C18 and C24.

To achieve more reasonable settings when the material quality is too good or the grades to be graded are too modest the following procedure is suggested:

If the lowest grade to be graded is so low that the characteristic values of the grade determining properties for the total sample (excluding those pieces in any higher grade) exceed those required for the grade, the production setting for the grade shall be derived following the method below:

1) Determine the setting for the lowest possible single grade by using the cost matrix method

2) For this grade establish the relationship: setting/required strength

3) Use that relationship for determining the setting for the actual grade

Example, deriving setting for grading C24 as a single grade (this example is not valid for exactly the same raw material as used otherwise in this paper):

1) The lowest single grade to be graded is C27. The "setting" for that grade, here denoted f_{mod} is 34,5.

2) Relationship setting/required strength: 34,5/(27/1,12)=1,43.

3) Setting for C24=(24/1,12)*1,43=30,6

The Figure below illustrates case a in the standard and the new proposal given here. The values above C24 are calculated according to the cost matrix method.
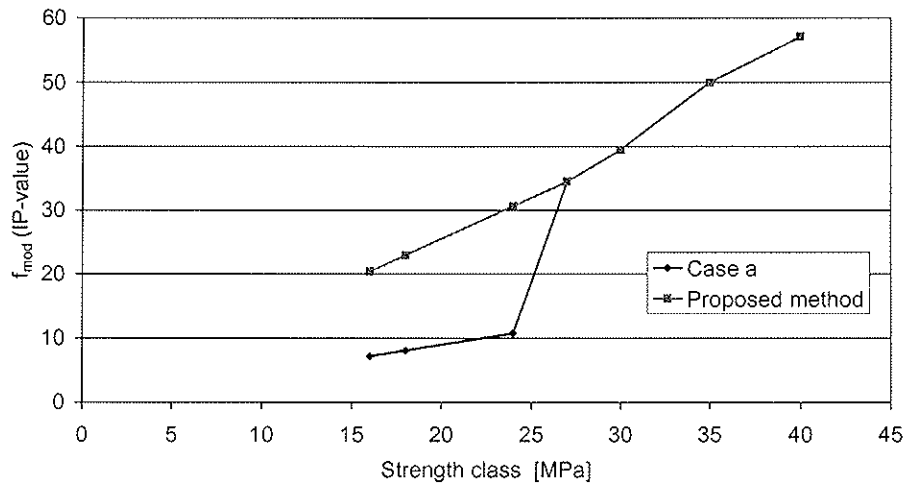
Figure 1. Illustration of two methods for calculating setting values when the characteristic values of the test material exceed those required for the actual grade.

It is obvious that the cost matrix method works well in the cases where the test material has properties corresponding to the properties of the required grade/grades. The main motivation for the proposal above is to use the mathematical model also for the lower strength classes and apply the same "level of safety" achieved by the cost matrix method also for lower grades. The mathematical model is based on several hundreds of test values and much more reliable than one single test value.

For the cases where the raw material is too good compared to the grades wanted a more conservative setting can be chosen. This is of course one option that is available, however it is not pleasing to have a standard permitting unreasonably liberal settings.

It may seem strange to grade good timber, as the Nordic one, to strength classes well below the strength of the timber itself. However, this is the need for many sawmills in the Nordic countries and is therefore an important topic to deal with.

4.2 "Upgrading" one case

The results when calculating settings for the combination C30-C24-C18-reject can be seen in Table 5. When the combination C30-C24-reject was chosen, the same settings were achieved, see Table 5. However, the requirement on the global cost matrix was not fulfilled, see Table 6. In the first case, both rejects and C18-pieces were wrongly upgraded to C24. In the second case only rejects are upgraded to C24, which is recognised more severe by the cost matrix method.

It is reasonable to think that the combination C30-C24-reject is derived directly from the combination C30-C24-C18-reject without a special calculation. The fact that the cost matrix is not fulfilled is then never discovered.

6

Table 5. Settings for two grade combinations.

Combination	Settings f_{mod}		
	C 30	C 24	C 18
C 30 – C 24	40,2	34,0	
C 30 – C 24 – C 18	40,2	34,0	23,0

Table 6. Global cost matrix for a) grade combination C30-C24-C18-reject, b) C30-C24-reject.

a)

Optimum grade	Assigned grade			
	C30	C24	C18	Reject
C30	0	0,22	0,576	0
C24	*0,009*	0	0,006	0
C18	*0,096*	*0,173*	0	0
Reject	*0,014*	*0,157*	*0,116*	0

b)

Optimum grade	Assigned grade		
	C30	C24	Reject
C30	0	0,22	0
C24	*0,009*	0	0
Reject	*0,104*	**0,248**	0

4.3 Influence of using different sub-samples

Using representative raw material is an absolutely crucial point for having correct and safe settings. In prEN 14081, part 2, it is prescribed that sub-samples shall be selected representing one growth area or source of production and that the minimum number of pieces in one sub-sample shall be 100. At least four sub-samples must be included and the total number of pieces must be at least 900. A test was made by using the raw material presented under point 3.2 in this paper. One sub-sample was left out and settings were calculated for the combination C30-reject. The results are presented in Table 7. It can be seen that the setting drops substantially when sub-sample 1 is left out. The difference between the least and most conservative setting for C30 is around 25%. Sub-sample 1 contains most of the dimensions and the material with the lowest density (for C30 the density is sometimes the governing parameter). The effects of location and the effects of timber size are not separated. In a coming version of the standard this must be cleared out.

Table 7. Settings for C30 when different sub-samples are included.

Sub-samples included	Setting (f_{mod}) for C30
2-6	**32,5**
1, 3-6	39,5
1-2, 4-6	**41,5**
1-3, 5-6	39,0
1-4, 6	40,0
1-5	36,8
All (1-6)	38,2

4.4 Different settings for the same strength class

According to EN 338 a timber population may be assigned to a strength class if the following three criteria are fulfilled:

- The characteristic value of bending strength, f_{mk}, is equal to or exceeds the corresponding value of that strength class.

- The mean value of modulus of elasticity, E, is equal to or exceeds 95 % of the corresponding value of that strength class.

- The characteristic value of density is equal to or exceeds the corresponding value of that strength class.

For strength grading machines the settings are determined in such a way that these three criteria are fulfilled. Additionally, the requirement not to wrongly upgrade too many timber pieces is checked.

Hence, the requirements are given for f_{mk}, E and density representing all the timber pieces in the same class. This means that the amount of timber pieces with a strength less than the required class strength can be increased by adding timber pieces with a strength above the class strength to the sample. (It may be wise in the forthcoming revision process to discuss an additional requirement to ensure that the weakest timber piece in each strength class is not too weak.)

Table 8 shows setting values for different grade combinations achieved by analysing the raw material presented in Table 4 (prEN 14081, part 2, version February 2003 was used). It can be seen that the settings for grading for example C24 on its own differs considerably from the setting for C24 when it is graded together with C30 and C18. Indeed the setting of 21,3 for C24 alone is considerably less restrictive than the setting of 34,0 for C24 but also less restrictive than the setting of 23,0 for C18!

Table 8. Settings for different grade combinations achieved when analysing the raw material presented in this paper.

Combination	Settings f_{mod}						
	C 40	C 35	C 30	C 27	C 24	C 18	C 16
C 24					21,3		
C 27				30,8			
C 30			38,2				
C 35		50,0					
C 27 – C 16				32,3			23,0
C 30 – C 18			38,2			21,3	
C 30 – C 24 – C 18			40,2		34,0	23,0	
C 35 – C 24 – C 18		50,0			34,0	23,0	
C 40 – C 27	57,6			32,3			

Although, it is in accordance with the European requirements it is confusing to have different settings for the same strength classes depending on the way the good material is handled. This may also be a problem for the quality control to be carried out, partly by the producer and partly by a third part body. If a producer uses the settings determined assuming saw falling material to be included in the class, it is of main importance for the quality control to ensure that nothing of that material has been creamed off before grading.

Although the three criteria presented above are also valid for visual grading it has in Europe been agreed to use some well defined national grading rules for assigning timber to the European strength classes. This means that the grading requirements are given for each individual timber piece instead of for a population of pieces. There are no possibilities to include low graded timber to a better class whatever high graded timber is included.

4.5 Use of the "1,12-factor"

According to EN 384 the characteristic value of the strength, f_k, is given by

$$f_k = f_{05} \cdot k_s \cdot k_v$$

where

f_{05} is the 5th percentile of the strength taking into account the different samples, clause 5.4 of EN 384.

k_s is a factor to adjust for the number of samples and their size.

k_v is stated to be a factor taking into account the lower variability of f_{05} values between samples for machine grades in comparison with visual grades. k_v is equal to 1,12 for machine grades with f_k equal to or less than 30 MPa. For all other machine grades and all visual grades k_v is equal to 1,00.

A discussion related to the k_v factor has been ongoing for several years and the factor included in the standard is a compromise that can not be defended statistically. At least not if the intention is to determine the characteristic value defined as the fifth percentile value for a certain confidence level on equal basis.

For timber machine graded to strength classes above C30 the variability of f_{05} values between samples is smaller than for machine grades to lower classes as well as smaller than for visual grades. Consequently, the k_v factor of 1,12 should be used also for these high grades but it is not the conclusion written down in the standard.

If the raw material used in present paper is graded to C30 and reject by using $k_v = 1,12$ as prescribed by the standard, then 1782 of the 2107 pieces are assigned to C30. The non-parametric 5th percentile value for these 1782 pieces is 28,9 MPa while the mean modulus of elasticity is 12900 MPa and the density is 380 kg/m^3 (the density was the governing factor). If the k_v factor 1,00 instead of 1,12 is used then only 1293 of the 2107 pieces will be assigned to the class C30. The non-parametric 5th percentile value for these 1293 pieces is 30,1 MPa while the mean modulus of elasticity is 13400 MPa and the density is 387 kg/m^3 (bending strength was the governing factor).

Lamellas to be used in the production of glued laminated timber can be either visually or machine graded. For machine graded lamellas the k_v factor shall be taken as 1,00 for all classes, according to EN 1194.

5 Conclusions and recommendations

During the work in CEN/TC124/WG2/TG2 by formulating and applying the suggested procedure for calculating settings different interpretations and understandings have come up. A clear procedure with examples, as presented under section 3.1 in this paper, would improve the standard considerably and facilitate the use of the standard.

The procedure for derivation of settings when the raw material is too good or the wanted grades are too modest need to be revised. A suggestion is given in this paper.

In the paper it is illustrated that the raw material used when deriving the settings must be representative for the material to be graded in production. It is shown that by deleting one of the sub-samples used in the present analysis the setting for C30 can vary by around 25%.

Further, consequences by deriving combinations of settings from already existing ones are pointed out. It is also pointed out that the methodology can result in considerably different settings for the same strength class.

6   Acknowledgement

7   References

Brundin, J., Bengtsson, C., Fonselius, M., Solli, K.: Nordic Spruce – A common growth area, paper accepted by CEN/TC124/WG2/TG2, March 2002.

Rouger, F.: A new statistical method for the establishment of machine settings, CIB W18, proceedings paper 30-17-1, Vancouver, Canada, 1997.

EN 384 Structural timber – Determination of characteristic values of mechanical properties

EN 338 Structural timber – Strength classes

EN 1194 Glued laminated timber – Strength classes and determination of characteristic values

prEN 14081 Timber structures – Strength graded structural timber with rectangular cross section, part 1-4

INTERNATIONAL COUNCIL FOR RESEARCH AND INNOVATION
IN BUILDING AND CONSTRUCTION

WORKING COMMISSION W18 - TIMBER STRUCTURES

A PROBABILISTIC APPROACH TO COST OPTIMAL TIMBER GRADING

J Köhler

M H Faber

Swiss Federal Institute of Technology

Zurich

SWITZERLAND

Presented by: Jochen Köhler

Jochen Köhler described the issues surrounding the probabilistic modelling of timber materials and the authors' assessment of the optimal grading procedure. He also described findings based on tests using 239 samples of Swedish and German spruce (58x120mm) in which tests were carried out on strength, elastic modulus and density using regression analysis. He concluded that the approach presented may be used for the optimisation of the output from sawmills and answered questions regarding his use of the terms quality control and grading.

A Probabilistic Approach to Cost Optimal Timber Grading

Jochen Köhler and Michael Havbro Faber

Swiss Federal Institute of Technology, Zurich, Switzerland

1   Introduction

Timber is by nature a very inhomogeneous building material. On a large scale the material properties are a product of e.g. the specific wood species and the geographical location where the wood has been grown. The material properties of timber may be ensured to fulfill given requirements only by quality control procedures – hereafter referred to as grading. For mechanical grading various schemes have been developed using different principles, however, the basic idea behind them all is that the relevant material properties such as, e.g. the bending strength, are assessed indirectly by means of other indicative properties (indicators) observed during a grading procedure such as e.g. the density or the modulus of elasticity, see also Madsen (1992) and Walker et al. (1993). The allocation into different grades is takes basis in acceptance criteria, which formulated in terms of the indicators. An acceptance criterion can be implemented by means of the settings of a grading machine, whereby a given grade is allocated to timber for which the indicators have values belonging to defined intervals. The timber graded in this way has to match given requirements implicitly defining the indicator value intervals. As an example, the European standard EN 338 defines grades in terms of the lower 5% fractile value of the graded timber bending strength, the mean value of the bending modulus of elasticity and the mean value of the density. These requirements can be implemented by adjusting the settings of the applied grading machine. The acceptance criterion, i.e. the grading machine settings, leading to normative grades are normally obtained and calibrated by performing many test of the graded timber.

Due to the special way timber material properties are ensured by means of grading in the production line, special considerations must be made when modeling their probabilistic characteristics. Previous work on this subject is reported in e.g. Glos (1981) and Rouger (1996). In Pöhlmann and Rackwitz (1981) a bi-variate Normal distribution model is suggested in order to describe the probabilistic characteristics of the graded timber. In Faber et al. (2003) a Bayesian approach is proposed allowing for a generalization of the bi-variate Normal distribution model such that the prior probability distribution function of the un-graded timber material properties may be chosen freely in accordance with statistical evidence.

The selection of a grading procedure, i.e. the type of grading machine and the acceptance criteria, could be made based on cost benefit considerations. Different procedures have different costs and different efficiency characteristics. In the present paper it is demonstrated how an optimal (in terms of monetary benefit) set of timber grades can be identified. Therefore, the approach suggested by Faber et al. (2003) is utilized to identify timber grades and quantify the probabilistic characteristics of their relevant material properties. This requires that the probabilistic characteristics of the relevant material properties of the ungraded timber are known together with their correlation to the indicator. An optimization problem can be defined for identifying the grading procedure, leading to the optimal set of timber grades.

2 Probabilistic Modeling of Timber Material Characteristics

In structural reliability applications it is necessary to be able to assess the probability distribution function of the relevant material properties. In the following the results of Faber et al. (2003) are summarized for easy reference. Assuming that a sufficiently large number of experiments have been performed regarding the relevant material property, it is in principle a straightforward task to select a probability density function and to estimate the parameters of this correspondingly. The resulting density function might be considered as a prior density function $f'_{\sigma_C}(s)$, i.e. the probability density function, which might be assumed if no grading procedures are invoked. However, when a grading procedure has been applied the prior density function is no longer representative for the graded timber specimens. In order to assess the representative probability density function use may be made of Bayes's rule yielding the posterior probability density function $f''_{\sigma_C}(s)$, i.e. the probability density function, which can be assumed for the material properties, categorized into a particular grade by application of the test acceptance criteria.

$$f''_{\sigma_C}(s) = P\big(\sigma_C = s\big|A_C\big) = \frac{1}{c} f'_{\sigma_C}(s) \cdot P(A_C|\sigma_C = s) \tag{1}$$

where $c = P\big(A_C\big)$.

It is seen from Equation (1) that it is necessary to estimate the likelihood of the implementation of the selection acceptance criteria, i.e. $P\big(A_C|\sigma_C = s\big)$ as a function of the specific value of the material property σ_C. This likelihood may, however, be assessed if test results are available from timber specimens tested both, in regard to the indirect characteristic, e.g. the flatwise bending stiffness, and the relevant material property, e.g. the edgewise bending strength. Assuming that such test results are available a regression analysis can be performed based on which the statistical characteristics of the indicator, e.g. the flatwise bending stiffness can be assessed for a given value of the relevant material property.

The regression analysis takes basis in n simultaneous observations of the relevant material property $\sigma_C = \big(\sigma_{C,1}, \sigma_{C,2}, \ldots, \sigma_{C,n}\big)^T$ and the indicator $I = \big(I_1, I_2, \ldots, I_n\big)^T$. Assuming that at least locally a linear relationship between σ_C and I exist the regression may be performed on the basis of

$$I = a_0 + a_1 \cdot \sigma_C + \varepsilon \tag{2}$$

where a_0 and a_1 are the regression coefficients and where ε is an error term. Assuming that the error term ε is normal distributed with zero mean and unknown standard deviation σ_ε the maximum likelihood method, see e.g. Lindley [7] may be used to estimate the mean values and covariance matrix for the parameters a_0, a_1, σ_ε.

The acceptance criteria applied for the categorization of timber into different grades may be formulated in terms of the values of the indicators. Typically the criteria have the following appearance

$$A_C = \{b_L \le I \le b_U\} \tag{3}$$

where b_L and b_U are lower and upper bounds for the indicators for a particular grade.

Having performed the regression analysis, it is possible to assess the acceptance probability i.e. $P(A_C | \sigma_C = s)$ by

$$P(A_C | \sigma_C = s) = P(b_L \le a_0 + a_1 \cdot \sigma_C + \varepsilon \le b_U | \sigma_C = s) = P(b_L \le a_0 + a_1 s + \varepsilon \le b_U) \tag{4}$$

which is straight forward to assess recognizing that the indicator I is normal distributed.

It is well known that especially the behavior of the probability distribution functions in the regions of the tails is of importance in reliability assessments. For load variables the upper tail is normally the most important whereas the lower tails are the important for resistance parameters.

One approach to estimate the probability distribution in the lower tail domain is by means of a censored Maximum Likelihood estimation where only observations in the lower tail domain i.e. below a given predefined threshold value are used explicitly. The other observations are only utilized implicitly to the extent that it is recognized that they exceed the threshold.

In this special case of a censored Maximum Likelihood estimation two different contributions to the likelihood are considered, i.e.

$$L1 = \prod_{i=1}^{j} f(x_i | \theta) \tag{5}$$

and

$$L2 = \left(1 - F(x_G | \theta)\right)^{n-j} \tag{6}$$

where $L1$ represents the relative likelihood of the j observations with values below or equal to the threshold value x_G. $L2$ represents the likelihood of the observations with values exceeding the threshold value x_G. $1 - F(x_G | \theta)$ is the probability that a value exceeds the threshold value x_G given the parameters of the probability distribution function θ. If n is the total number of observations $n - j$ is the number of observations exceeding the threshold value x_G.

The parameters are easily estimated by the solution of the optimization problem

$$\max_\theta (L1 \cdot L2) \tag{7}$$

3

The parameters are estimated as normal distributed random variables with means and covariances quantifying the statistical uncertainty due to the relative small number of observations below the threshold.

3 Assessment of the Optimal Grading Procedure

The selection of a grading procedure can be made based on cost benefit considerations. Based on the proposed statistical modeling of timber properties as a function of the type and efficiency of the grading procedures, a cost optimization scheme may be formulated for the identification of optimal grading. Therefore, the cost of the control and the benefit of fulfilling the requirements set for the material characteristics belonging to different grades have to be given.

The benefit of a set of timber grades identified by the grading procedure GP may be written as

$$B_T(f'_{\sigma_C}(s), A_C, GP) = \mathbf{V}^T \cdot \mathbf{C}_{grade} \tag{8}$$

where $\mathbf{V}$ is a vector of volumes of particular grades, which can be identified depending on the prior probability distribution of the relevant material property, the set of acceptance criteria and the grading procedure. $\mathbf{C}_{grade}$ is a vector of the (monetary) benefit of the timber grades per unit volume. If the prior probability distribution of the relevant material property, the grading procedure, the set of timber grades and their monetary benefits are known, the optimal set of acceptance criteria A_C may be found by solving the following optimization problem

$$\max_{A_c} B_T(f'_{\sigma_C}(s), A_C, GP) \tag{9}$$
$$\text{subject to: } \mathbf{N}_{req}, \mathbf{C}_{grade}$$

subject to normative requirements which have to be fulfilled by the grades, $\mathbf{N}_{req}$, and the cost vector $\mathbf{C}_{grade}$. Involving the investment, maintenance over lifetime costs, costs for personnel, etc. of a particular grading procedure by the function $C_G(GP)$ the optimal grading procedure may be identified by solving

$$\max_{GP} \left[\left(\max_{A_c} B_T(f'_{\sigma_C}(s), A_C, GP) \right) - C_G(GP) \right] \tag{10}$$
$$\text{subject to: } \mathbf{N}_{req}, \mathbf{C}_{grade}$$

3 Example

Consider as an example the case where the grading of the timber material is performed using the Computermatic grading machine. A data set from Johansson et al. (1992) is considered concerning the bending strength of 239 timber specimens of European spruce.

The Computermatic grading machine is a widely used grading machine, which considers the flatwise bending stiffness as an indicator of the bending strength. The stiffness characteristic is obtained through a measurement of the deflection under a fixed load applied at the centre of a span of 914 mm. The bending strength is obtained in four-point bending tests according to the European standard prEN 408 (1994). The entire population

of the 239 timber specimen is assumed to be un-graded. The probability distribution function of the bending strength, i.e. the prior probability distribution function, is assumed to be 2-parameter Weibull min distributed. The 2-parameter Weibull min distribution function is defined as

$$F_X(x) = 1 - \exp\left[-\left(\frac{x}{w}\right)^k\right]$$

(11)

where w is the location parameter and k is the scale parameter.

In the data from Johansson et al. (1992) not only the bending strength of the 239 specimens but also the Computermatic based indicator, the bending modulus of elasticity and the density for each specimen has been observed and recorded prior to or during the bending strength tests. By regression analysis of simultaneously measured bending strengths and the observed Computermatic based indicators the regression coefficients have been estimated according to Equations (2-4).

Using the Method of the Maximum Likelihood, both, the parameters of the prior probability distribution functions and the regression parameters are estimated as normal distributed random variables with mean values, standard deviations and correlations as given in Table 1. Neglecting the statistical uncertainty associated with the estimated parameters, which for the present case has been found to be insignificant, the acceptance probability may thus be assessed directly from Equation (4).

Table 1. Mean values, standard deviations and correlations of the parameters of the prior probability distribution function (w, k see also Equation (11)) together with the estimated parameters for the regression between bending strength and the Computermatic indicator.

	Prior Distribution Parameters (bending strength)			Regression Parameters (Computermatic)			
	Weibull parameters as normal distributed random variables		correlation	as normal distributed random variables			correlation
	w [MPa]	k [MPa]	ρ	a_0[Comp]	a_1[Comp/MPa]	σ_ε[Comp]	ρ
All data	$\mu = 48.0$ $\sigma = 0.76$	$\mu = 4.32$ $\sigma = 0.21$	$(w,k) = 0.33$	$\mu = 4673$ $\sigma = 291$	$\mu = 98.6$ $\sigma = 6.45$	$\mu = 1073$ $\sigma = 40.08$	$(a_0, a_1) = -0.02$ $(\sigma_\varepsilon, a_1) = 0$
Data lower 30%	$\mu = 43.9$ $\sigma = 0.02$	$\mu = 6.44$ $\sigma = 0.49$	$(w,k) = -0.06$				$(\sigma_\varepsilon, a_0) = 0$

In Figure 1 the acceptance probability for three different types of indicators is illustrated. The Computermatic based indicator is compared with the case when the timber density and edgewise bending modulus of elasticity are used as an indicator. The acceptance criterion for each probability curve is chosen such that the mean value of the expected bending strength is the same in all three cases. It is not surprising that the 'better' the linear regression is between the indicator and the relevant material property, the steeper is also the corresponding acceptance probability curve.

Assuming that the timber specimens are categorized in three grades of same volume according to the observed Computermatic indicators, i.e. 1) 4000 – 8100 MPa, 2) 8100 – 9650 MPa and 3) 9650 – 15000 MPa, the probability density function for the graded timber can be obtained directly from Equation (1).

In Figure 2 the prior probability density function of the bending strength for the un-graded timber (2-parameter Weibull min distributed with mean value 43.7 MPa and standard deviation 11.4 MPa) is shown together with the probability density functions for the three timber grades in accordance with the abovementioned acceptance criteria. Note that the

grading is performed using the prior probability density function with parameters estimated based on all data.
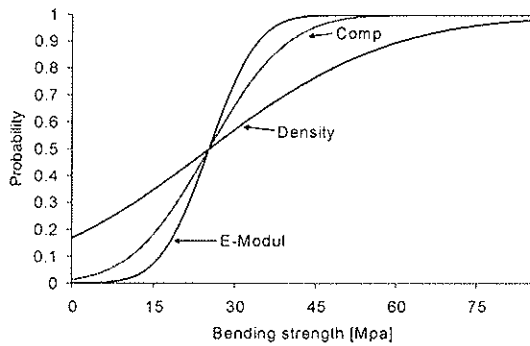
Figure 1. Acceptance probability of different indicators.
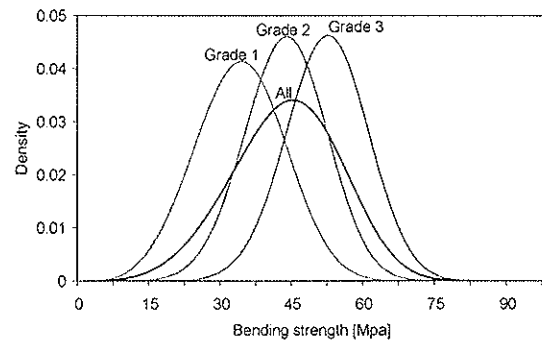
Figure 2. Illustration of the probability density functions for the bending strength for un-graded and graded timber specimens.

In Figure 3 the probability distribution function representing all data is compared to the probability distribution function estimated by using the censored maximum likelihood estimation according to Equation (5) and Equation (6) with a threshold value corresponding to the lower 30 % quantile. For purposes of comparison the sample probability distribution function using all observations is also illustrated. It is seen that a significant refinement of the representation of the strength data in the lower tail domain can be achieved, by using the distribution model fitted to the lower data set domain.
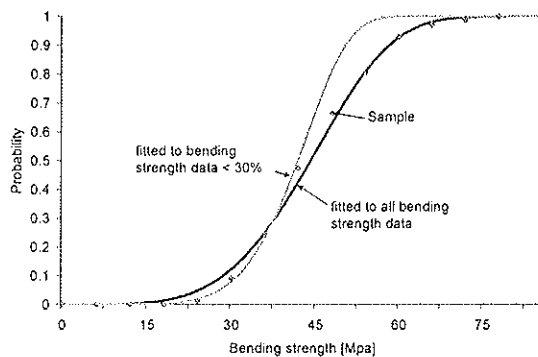
Figure 3. 2-parameter Weibull min probability distribution functions with parameters estimated using all data and data < 30%, compared with the sample probability distribution function (Sample PDF).
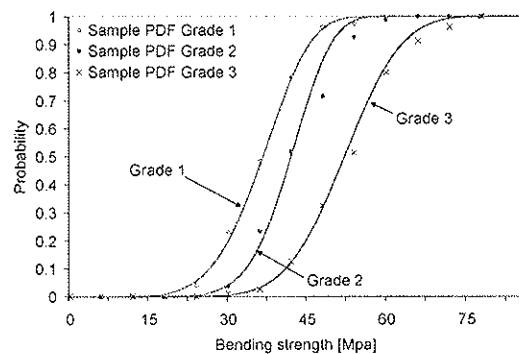
Figure 2. Probability distribution functions for the bending strength for three different grades togetherwith the corresponding sample probability distribution functions.

In Figure 4 the probability distribution functions for the different grades are shown in comparison with the sample probability distribution functions (sample PDF's) established from the experimental data fulfilling the respective acceptance criteria. The prior probability distribution function fitted to the lower 30% of the data was used to identify the posteriori distributions of grade 1 and 2. The data, which fulfills the grade 3 acceptance criteria, is mostly taken from the middle and upper part of the prior distribution. For that part the prior probability distribution function modeled under consideration of all data can be used.

From Figure 4 it is seen that a great benefit may be obtained by estimating the prior probability distribution with special consideration of the tail domain before the probability distributions of the graded specimens are evaluated.

Whether a prior fitted with special emphasis to the goodness of fit in the lower tail domain has to be preferred or not, depends on the domain for which the posterior is of special interest. It is thus difficult to provide any generally applicable rules for this selection. However, in most normal cases the selection would follow naturally from the available data on the simultaneous observations of an indicator and the bending strength together with previous experience to judge which approach is appropriate.

Considering the data and the inference from the foregoing, it can now be demonstrated how an optimal set of acceptance criteria for the considered grading procedure of the Computermatic grading machine can be found by applying Equation (9). The intention is to set up three different acceptance criteria to select three different timber grades. The grades have to fulfill the requirements for the grades according to EN 338 in terms of the 5% fractile value of the bending strength and the mean of bending modulus of elasticity and the density. The prior population is assumed to be checked according to visual defects of the timber as warp, insect damage etc. Five different grades according to EN 338 are selected to be possible grades and a reject domain is defined for timber, which not has to fulfill any requirements. They are shown together with example values for the monetary benefit and the material requirements in Table 2 therefore the vector $\mathbf{C}_{grade}$ (units : monetary unit per volume) becomes

$$\mathbf{C}_{grade} = (0.5, \quad 1.0, \quad 1.4, \quad 1.6, \quad 1.8, \quad 2.0)^T.$$

To identify three different Grades, three different acceptance criteria have to be defined,

$$A_{C_1} = \{a \leq I < b\}, \quad A_{C_2} = \{b \leq I < c\}, \quad A_{C_3} = \{c \leq I \leq d\}. \tag{12}$$

Table 2. Monetary benefit (example values) and requirements for grades according to EN338.

	'reject'	C16	C24	C30	C35	C40
Monetary Benefit	0.5	1.0	1.4	1.6	1.8	2.0
Bending strength, 5%-frac [MPa]	-	>16	>24	>30	>35	>40
Modulus of elasticity, mean value [MPa]	-	>8000	>11000	>12000	>13000	>14000
Density, mean value [kg/m³]	-	>310	>350	>380	>400	>420

In addition to the posteriori distributions of the ultimate bending strength for these three acceptance criteria $P(\sigma_C \leq s | A_{C_i})$, the posteriori distributions of the bending modulus of elasticity $P(E_B \leq s | A_{C_i})$ and of the density $P(\rho \leq s | A_{C_i})$ have to be assessed, according to the prior distribution parameters and the regression parameters given in Table 1, 3 and 4. These posteriori distributions are representing timber sub-populations with the property $I \in A_{C_i}$ and can be checked in regard to the requirements in Table 2.

The three acceptance criteria are defined through the values of a, b, c and d in Equation (12). The value d is fixed to an upper threshold value, namely $d = 16000 \, \text{MPa}$. The optimal values of a, b and c are then found by solving Equation (9) using the simplex algorithm, see e.g. Nelder and Mead (1965), for which differentiability of the objective function and constraints is not required. The applied algorithm does not allow for the definition of the constraints explicitly. Therefore the the constraints have been included directly into the formulation of the objective function $B_T(f'_{\sigma_C}(s), A_C, GP)$ in line with the requirements given in EN 338. Due to the discrete character of the objective function the

simplex algorithm is applied in conjunction with a random search to facilitate the identification of the optimal solution over the set of discrete optimization variables. In this search it has been found that 100 simulations provided stable results.

Table 3. Mean values, standard deviations and correlations of the parameters of the prior probability distribution function together with the estimated parameters for the regression between bending modulus of elasticity and the Computermatic indicator.

Prior Distribution Parameters (bending modulus of elasticity)			Regression Parameters (Computermatic)			
Log-normal parameters as normal distributed random variables		correlation	as normal distributed random variables			correlation
ξ [MPa]	δ [MPa]	ρ	a_0[Comp]	a_1[Comp/MPa]	σ_ϵ[Comp]	ρ
$\mu = 12749.1$ $\sigma = 160.7$	$\mu = 0.1949$ $\sigma = 0.0089$	$(\xi, \delta) = 0$	$\mu = 2892$ $\sigma = 332.1$	$\mu = 0.469$ $\sigma = 0.025$	$\mu = 961.7$ $\sigma = 35.91$	$(a_0, a_1) = -0.02$ $(\sigma_\epsilon, a_1) = 0$ $(\sigma_\epsilon, a_0) = 0$

Table 4. Mean values, standard deviations and correlations of the parameters of the prior probability distribution function together with the estimated parameters for the regression between density and the Computermatic indicator.

Prior Distribution Parameters (density)			Regression Parameters (Computermatic)			
Normal parameters as normal distributed random variables		Correlation	as normal distributed random variables			correlation
μ[kg/m^3]	δ [kg/m^3]	ρ	a_0[Comp]	a_1[Comp/ kg/m^3]	σ_ϵ[Comp]	ρ
$\mu = 406.3$ $\sigma = 2.295$	$\mu = 35.47$ $\sigma = 1.622$	$(\xi, \delta) = 0$	$\mu = 1063.6$ $\sigma = 997.24$	$\mu = 19.51$ $\sigma = 2.44$	$\mu = 1341.0$ $\sigma = 50.1$	$(a_0, a_1) = -0.02$ $(\sigma_\epsilon, a_1) = 0$ $(\sigma_\epsilon, a_0) = 0$

Table 5. Optimal set of timber grades, limiting properties are shaded and framed.

	I [MPa]	V_i	bending mod. of rupture 5%-fractile value [MPa]	Bend. mod. of elasticity mean value [MPa]	density 5%-fractile value [kg/m3]	Grade EN 338
A_{C_1}	[0,5255)	0.5%	reject			
A_{C_1}	[5255,8094)	29.5%	26.0	11000.4	339*	C24
A_{C_2}	[8094,10161)	49%	30.3	12952.34	351.6*	C30
A_{C_3}	[10161,16000]	21%	40.1	15738.9	366*	C40

*)density is not taken into account as a requirement

Subject to the given conditions summarized in Table 2, the optimal set of acceptance criteria is given in Table 5. From the assumed set of data the grades C24, C30 and C40 have been identified, where for the grade C24 the mean value of the bending modulus of elasticity is the limiting property. For the grades C30 and C40 the bending strength is limiting. The relationship between the computermatic indicator and the timber density is too weak to make any quantitative prediction about the density based on a computermatic indication. Therefore, in this example the density is not taken into account as a requirement for assigning grades.

As the Computermatic grading procedure apart from values of the flat wise bending stiffness (Indicator) also provides values of density, the parameters of Table 4 can be updated continuously. By doing spot test, e.g. for every 100th timber specimen, of the bending strength and the bending modulus of elasticity the parameters of Table 1 and 3 can also be updated continuously.

4   Discussion and Conclusions

It has been demonstrated how an optimal (in terms of monetary benefit) set of timber grades can be identified through the solution of an optimization problem. The objective function of the optimization problem is defined based on the findings reported previously by the authors where the statistical assessment of timber material properties has been considered with special emphasis on the modeling of the grading of timber. The identified timber grades can be described by means of the probabilistic characteristics of the relevant material properties as e.g. the bending strength, the bending modulus of elasticity and the density of the timber. The simplex algorithm for the optimization of non-differentiable object functions in conjunction with a simulation procedure has been applied for the identification of the optimal grading procedure. The constraints to the optimization problem, in terms of the requirements for timber grades according to EN 338 have been incorporated directly into the objective function.

An example has been presented illustrating the suggested approach to optimal timber grading. The assignment of monetary benefit to the different grades of timber has, however, been based on judgement rather than true values. In practice the benefit associated with timber of a particular grade would depend on a number of factors such as the size of the individual timber specimen, the total amount of available timber for a given grading, the production capacity of a given sawmill, the available grading machines and not least the market price for the different timber grades. The implementation of the proposed approach in practice would have to incorporate these and other factors more accurately into the formulation of the benefit function. Further studies in close collaboration with the timber industry should be undertaken and discussed to clarify these aspects and to set up a rational basis for their assessment. However, according to the preferences of a sawmill owner the proposed approach facilitates the identification and the calibration of a grading procedure and thus an increase in the overall production benefit.

Acknowledgments

References

COMPUTERMATIC "Manual" (2000). MPC Measuring and Process Control Ltd., Chelmsford, Essex, England.

EN 338, (1996) European Standard: Structural timber. Strength classes. European Committee of Standardization (CEN), 1996.

Faber, M.H., Kohler, J., Sorensen, J.D. (2003). "Probabilistic Modeling of Graded Timber Material Properties." Submitted to Structural Safety, April 2003.

Glos, P. (1981). "Zur Modellierung des Festigkeitsverhaltens von Bauholz bei druck-, Zug- und Biegebeanspruchung". Berichte zur Zuverlässigkeitstheorie der Bauwerke, SFB 96, Munich, Germany.

Johansson, C.-J.; Brundin, J.; Gruber, R. (1992). "Stress Grading of Swedish and German Timber. A comparison of machine stress grading". SP REPORT 1992:23

Joint Committee of Structural Safety (JCSS, 2001). "Probabilistic Model Code", Internet Publication: www.jcss.ethz.ch.

Lindley, D. V. (1965). "Introduction to Probability & Statistics" Cambridge University Press.

Madsen, B. (1992). "Structural Behavior of Timber". Timber Engineering Ltd., Vancouver, Canada.

Melchers, R.E. (1987). "Structural Reliability, Analysis and Prediction", John Wiley & Sons Limited.

Nelder, J.A., and Mead, R. (1965). "A simplex method for function minimization". Computer Journal 7, 308-313.

Pöhlmann, S. and Rackwitz, R. (1981). "Zur Verteilungsfunktion der Festigkeitseigenschaften bei kontinuierlich durchgeführter Sortierung". Materialprüfung 23, Hanser, Munich, Germany.

prEN 14081, (2000). European Standard: Timber structures – Strength graded structural timber with rectangular cross section. European Committee of Standardization (CEN), 2000.

prEN 408, (1994). European Standard: Timber structures - Structural Timber - Determination of some physical and mechanical properties. European Committee of Standardization (CEN), 1994.

Rouger, F. (1996). "Application of a modified statistical segmentation method to timber machine strength grading". Wood and Fiber Science, 28(4).

Walker, J.C.F. (1993). "Primary Wood Processing". Chapman &Hall.

INTERNATIONAL COUNCIL FOR RESEARCH AND INNOVATION
IN BUILDING AND CONSTRUCTION

WORKING COMMISSION W18 - TIMBER STRUCTURES

CHARACTERISTIC SHEAR STRENGTH VALUES BASED ON

TESTS ACCORDING TO EN 1193

P Glos

J Denzler

Wood Research Munich

GERMANY

Presented by: Julia Denzler

In her presentation, Julia Denzler described the loading arrangement and testing requirements needed to comply with EN 1193. The work is based on tests carried out on 118 test specimens. She concluded that the test results did not agree with the values in EN338 and that fissures and knots cannot be accommodated and reported bonding problems between the test pieces and the steel plates. Regarding shear strength it was reported that there is no significant influence of density on characteristic strength. The presentation was followed by an interesting and detailed discussion regarding the various test methods available and the implications of using clear samples versus realistic samples. This included the use of torsion tests and practical issues and implications of the findings.

Characteristic Shear Strength Values Based on Tests According to EN 1193

P. Glos, J. Denzler

Wood Research Munich, Germany

1 Introduction

Until today the effect of wood properties on shear strength of softwood is not completely understood. The European standard EN 384 (prEN 384:2002-10) assumes a direct relationship between shear and bending strength: $f_{v,k} = 0,2 \cdot (f_{m,k})^{0,8}$.

The strength properties proposed for the strength classes according to EN 338 (prEN 338:2002-10) are based on the same relationship. This means that the characteristic shear strength values are increasing with higher strength classes i.e. with increasing bending strength and density.

In contrast to this, the German standard E DIN 1052 defines a constant characteristic shear strength value for all strength classes. Up to strength class C 24 this value is higher than the corresponding values in EN 338 and for strength classes C 30 and above the value is lower than the values in EN 338. This is justified by the fact that so far a positive influence of density on shear strength has not yet been established and that the greater knot-ratio in the lower strength classes has a positive effect on shear strength.

Moreover, the different characteristic shear strength values may be explained by the fact that so far no satisfactory test method is available covering all strength influencing factors such as the cross sectional dimensions, the sawing pattern and fissures. Meanwhile a European standard for the determination of shear strength exists. Originally, this method was given in EN 1193. By now this method is transferred to EN 408 (prEN 408:2003-02) without being changed. However, in this paper we refer to EN 1193.

This test method was agreed upon after EN 338 and EN 384 had been drafted. Therefore it seems necessary to carry out tests according to EN 1193 in order to find out whether the test results are in accordance with the characteristic values as given in EN 338 and EN 384.

2 Material and methods

2.1 Material

Shear strength values are determined from 140 test pieces made of spruce (Picea abies) according to EN 1193. The pieces are cut out of glulam laminations parallel to the grain. One objective is to find out the effect of density, growth ring orientation and knots on shear strength values. 118 test pieces are defect free with varying density and growth ring orientation. The density varies from 330 to 590 kg/m^3. Following EN 338 the test pieces are subdivided into five groups (Table 1). Figure 1 classifies four groups of growth ring orientation into which the test pieces are divided.

radial	tangential	45 degrees	pith
$\not\lessgtr$ 60-90°	$\not\lessgtr$ 0-30°	$\not\lessgtr$ 30-60°	$\not\lessgtr$ 0-90°

| a | b | c | d |
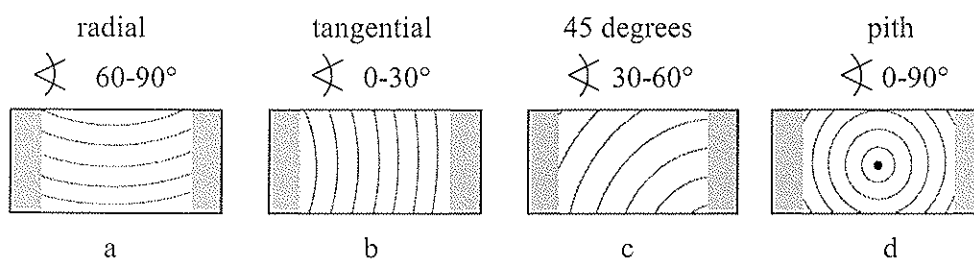
Figure 1: Definition of sub-groups with different ring width orientation.

In relation to the growth ring orientation test piece 1a will fail in radial direction with a fracture surface perpendicular to the growth rings. In contrast to this the test piece 1b will fail along a growth ring usually in the earlywood area. In this case the fracture surface is smooth and follows the curvature of the growth ring. Table 1 shows the distribution of the 118 defect free test pieces within the different sub-groups.

Table 1: Assignment of test pieces into sub-groups of density and growth ring orientation.

	$330 < \rho_{12} \leq 350$	$350 < \rho_{12} \leq 380$	$380 < \rho_{12} \leq 420$	$420 < \rho_{12} \leq 450$	$450 < \rho_{12} \leq 590$	Σ
radial	3	5	8	3	11	30
tangential	-	1	10	7	12	30
45 degrees	5	2	7	7	9	30
pith	-	7	5	7	9	28
Σ	8	15	30	24	41	118

In addition to the 118 pieces without defect, 22 pieces containing knots are tested to find out the influence of knots on the shear strength values. Each test piece with knots is matched with a test piece without knots in the way that both of them were cut out of the same lamination directly one after another. The small cross section of the timber test piece (Figure 2) does not allow to cover the full range of knot types and knot sizes. Therefore the presented results are not sufficient to explain the effect of knots totally but give some provisional orientation.

2

2.2 Loading arrangement

Figure 2 shows the loading arrangement according to EN 1193 and the small cross section of the timber test piece (32 x 55 m²).

timber test piece:

$w = 32$ mm $\pm$ 1mm

$h = 55$ mm $\pm$ 1mm

$\ell = 300$ mm $\pm$ 1mm

steel plates:

$w_s = 35$ mm $\pm$ 1mm

$h_s = 10$ mm $\pm$ 1mm

$\ell_s = 300$ mm $\pm$ 1mm

adhesive: **Terokal-221** solvent free two part epoxy adhesive
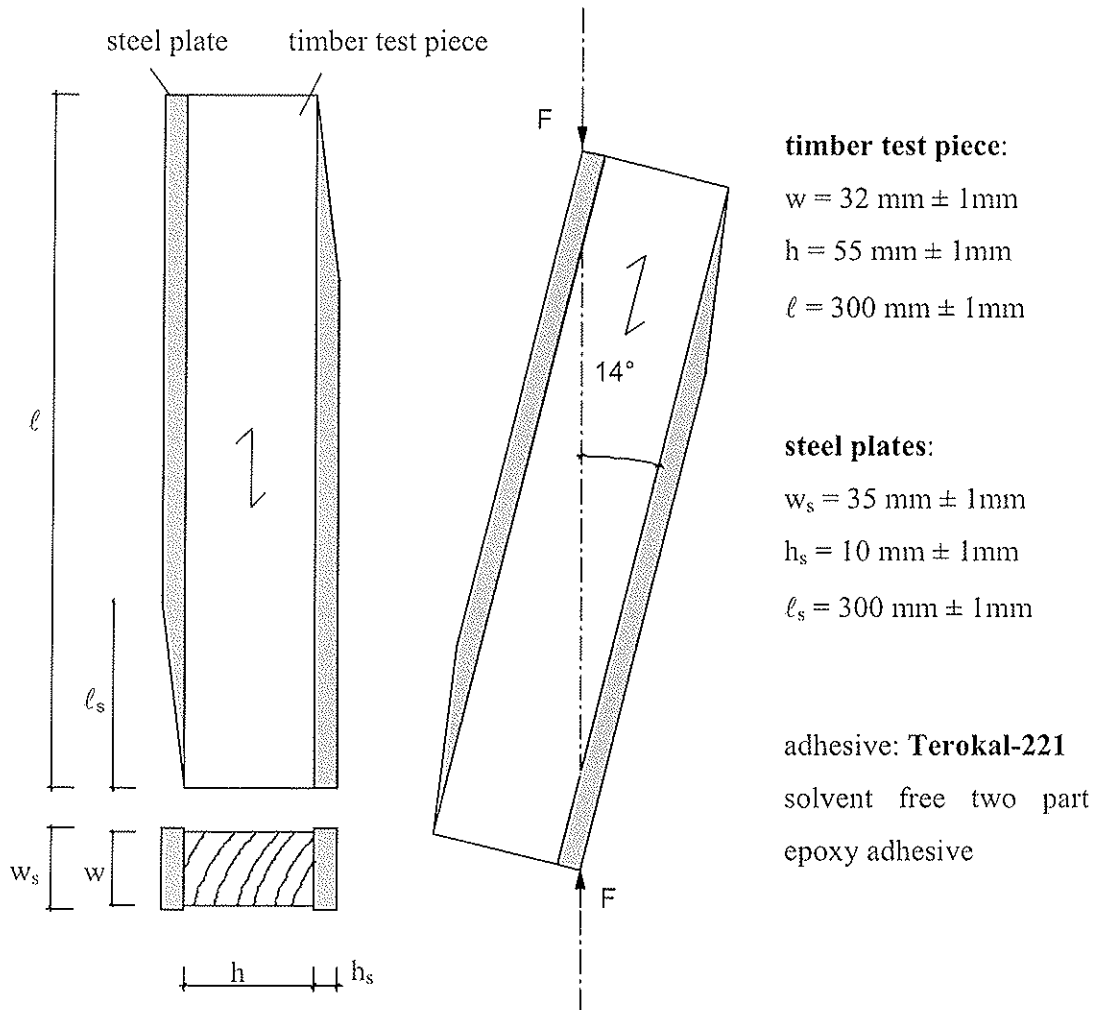
Figure 2: Timber test piece and loading arrangement according to EN 1193.

It is difficult to achieve a sufficient adhesion between the timber test pieces and the steel plates (BENHAM et. al., 1997). A failure in the glued area of the test piece/steel plate interface would result in invalid shear strength values. In preliminary tests at the Wood Research Munich good results were obtained when the two-part epoxy adhesive called Terokal 221 was used.

Moisture content, growth ring orientation and density are measured according to ISO 1030 and ISO 3131, resp., using a 2 cm thick test slice of full cross section cut from one end of the test piece after planing prior to cutting it to the required length.

The average moisture content of all 140 test pieces is 8.3%. According to SPENGLER (1982) there is no significant effect of moisture content on shear strength. Therefore, no correction factor is applied to the strength values.

3

The density values are adjusted to a reference moisture content of 12% using the adjustment factor given in EN 384 in order to make the values directly comparable with the values given in EN 338.

The steel plates were glued to the test pieces with a pressure of approximately 1,5 N/cm². To allow sufficient time for curing the adhesive the pieces were glued together at least four days before the shear test was carried out.

3 Results

3.1 General results

Table 2 shows the shear strength values of the 118 defect free test pieces separated into sub-groups of density and growth ring orientation.

Table 2: Shear strength results.

$f_{v,k}$ [N/mm²]		$330 < \rho_{12} \leq 350$	$350 < \rho_{12} \leq 380$	$380 < \rho_{12} \leq 420$	$420 < \rho_{12} \leq 450$	$450 < \rho_{12} \leq 590$	Σ
radial	number	3	5	8	3	11	30
	average	**4,9**	**5,0**	**6,4**	**6,4**	**7,6**	**6,5**
	stand. dev.	0,56	0,25	1,25	0,62	0,93	1,36
	minimum	4,4	4,8	4,4	5,9	6,1	4,4
	5th percentile						**4,4**
tangen-tial	number	-	1	10	7	12	30
	average		**4,9**	**5,4**	**5,5**	**5,5**	**5,4**
	stand. dev.		0,00	0,62	0,57	1,15	0,83
	minimum		4,9	4,5	4,8	3,8	3,8
	5th percentile						**4,0**
45 degree	number	5	2	7	7	9	30
	average	**4,3**	**5,6**	**5,2**	**5,5**	**6,0**	**5,4**
	stand. dev.	0,45	0,56	0,51	0,53	0,62	0,76
	minimum	3,6	5,2	4,3	4,6	4,8	3,6
	5th percentile						**4,0**
pith	number	-	7	5	7	9	28
	average		**5,3**	4,9	**6,0**	**5,8**	**5,6**
	stand. dev.		1,01	1,43	0,96	1,18	1,15
	minimum		3,6	3,3	4,9	3,6	3,3
	5th percentile						**3,4**
Σ	number	8	15	30	24	41	118
	average	**4,6**	**5,2**	**5,5**	**5,7**	**6,2**	**5,7**
	stand. dev.	0,54	0,72	1,07	0,74	1,30	1,13
	minimum	3,6	3,6	3,3	4,6	3,6	3,3
	5th percentile	**3,6**	**3,6**	**3,5**	**4,6**	**3,8**	**3,8**

3.2   Influence of growth ring orientation

Figure 3 shows the influence of growth ring orientation and density on the shear strength values. The horizontal lines indicate the average shear strength values of the ring-orientated sub-groups. Test pieces with radial growth ring orientation show the highest shear strength values, whereas for the remaining three sub-samples a similar lower strength level was obtained.
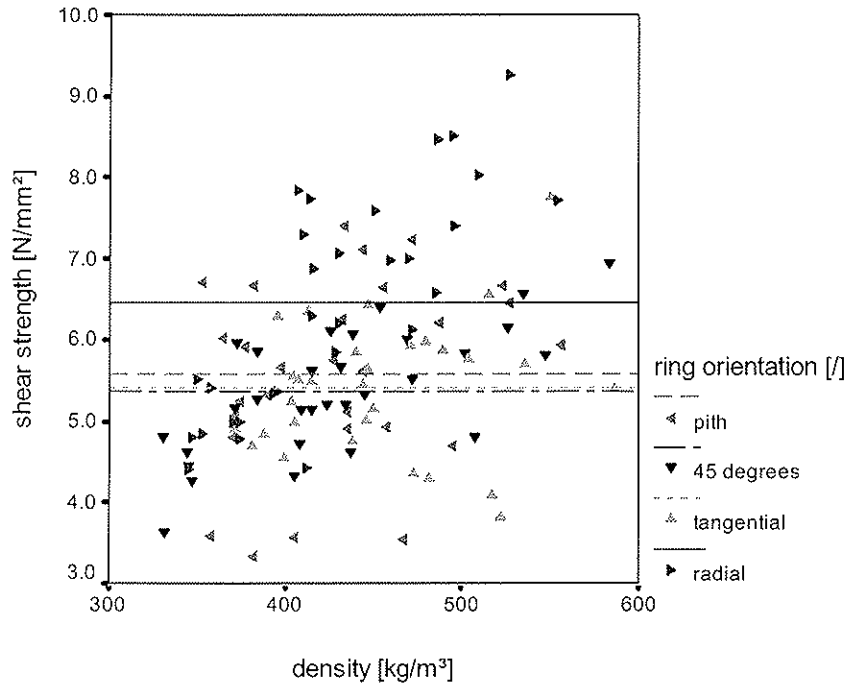
Figure 3: Shear strength as dependant on density divided into sub-groups of different growth ring orientation.

The higher average shear strength of the test pieces with radial growth ring orientation is correlated with the irregular fracture surface of these test pieces. The energy required to divide a piece of softwood perpendicular to the grain across latewood and earlywood areas is higher than the one for dividing a piece of softwood parallel to the grain. The fracture surface for radial failure is not plane whereas the one with tangential growth ring orientation or with 45 degrees is mostly smooth along an earlywood area. Two typical fracture surfaces are shown in Figure 4. On the 5th percentile level this influence is less pronounced.

The fact that radial growth ring orientation results in higher shear strength values than tangential orientated growth rings should be considered when fixing the characteristic shear strength values of glulam. Failures within glulam beams caused by shear loading usually have a tangential direction due to the typical growth ring orientation in laminations. Therefore the characteristic shear strength values for glulam beams should not be significantly higher than the ones for structural timber.

5
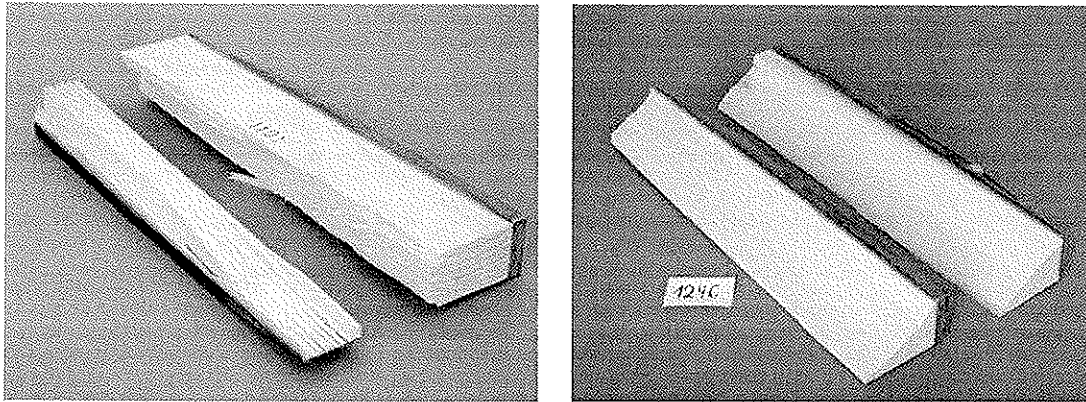
Figure 4: Fracture of a test piece with radial growth ring orientation (No. 1101) and a test piece with 45 degree ring width orientation (No. 1246).

3.3 Influence of density

The average shear strength increases with increasing density (Table 2, Figure 5). This influence is not obvious on the level of the characteristic strength values. The test pieces with radial growth ring orientation are the only sub-group with a significant increase of shear strength with increasing density as shown in Table 2. The other sub-groups do not show this tendency.
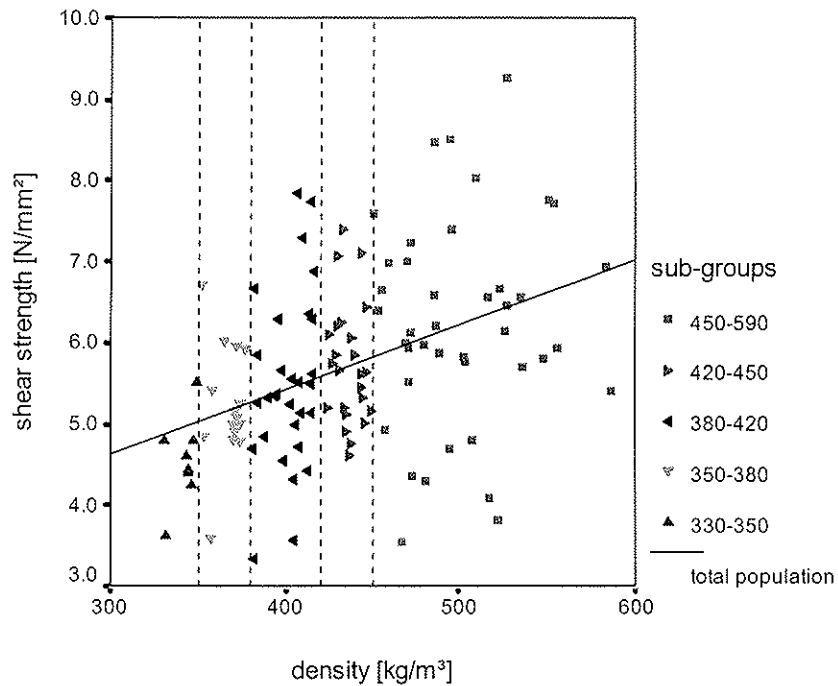
Figure 5: Shear strength as dependant on density separated for density sub-groups.

6

Table 3 shows the density values for the 118 defect free test pieces divided into the density sub-groups. The small standard deviation results from of the small range of each sub-group.

Table 3: Distribution of density in density sub-groups.

ρ_{12} [kg/m³]	$330 < \rho_{12} \leq 350$	$350 < \rho_{12} \leq 380$	$380 < \rho_{12} \leq 420$	$420 < \rho_{12} \leq 450$	$450 < \rho_{12} \leq 590$	Σ
number	8	15	30	24	41	118
average	342	367	401	437	502	435
stand. dev.	7,2	8,1	11,6	7,5	35,4	59,3
minimum	330	352	381	424	450	330
5th percentile	330	352	381	424	454	346

Table 4 compares the characteristic shear strength values of the shear tests with the values specified in EN 338 and E DIN 1052. Figure 5 shows this comparison graphically.

Table 4: Comparison of characteristic shear strength values according to EN 338, E DIN 1052 and strength test according to EN 1193.

poplar wood and softwood			C16	C18	C24	C30	C40	C50
EN 338	$f_{v,k}$	[N/mm²]	1,8	2,0	2,5	3,0	3,8	3,8
	ρ_k	[kg/m³]	310	320	350	380	420	460
	ρ_{mean}	[kg/m³]	370	380	420	460	500	550
E DIN 1052	$f_{v,k}$	[N/mm²]	2,7	-	2,7	2,7	2,7	-
	ρ_k	[kg/m³]	310	-	350	380	420	
test results	n	[/]	-	8	15	30	24	41
	$f_{v,k}$	[N/mm²]	-	3,6	3,6	3,5	4,6	3,8
	ρ_k	[kg/m³]	-	330	352	381	424	454
	ρ_{mean}	[kg/m³]	-	342	367	401	437	502
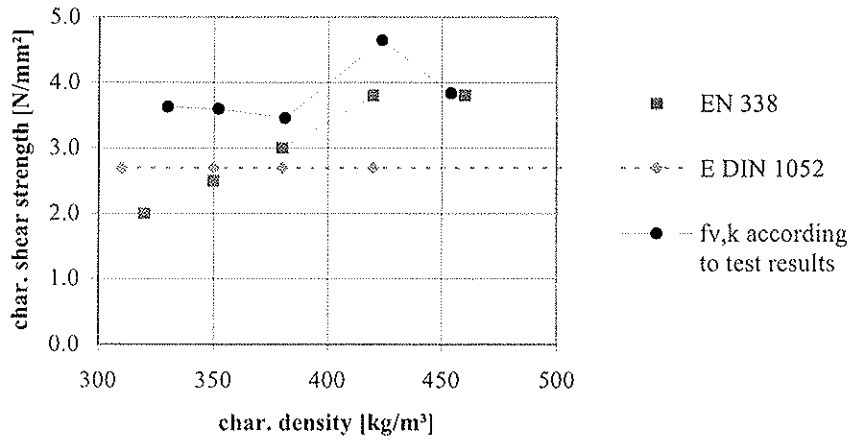
Figure 5: Characteristic shear strength values as dependant on characteristic density separated for test values and characteristic values according to EN 338 and E DIN 1052.

3.4 Influences of knots

Figure 6 shows the shear strength values of the matched test pieces with and without knots. The test results show neither a significant positive nor a significant negative effect of knots on shear strength values. Consistently higher shear strength values as expected for the test pieces with knots could not be confirmed by our tests.
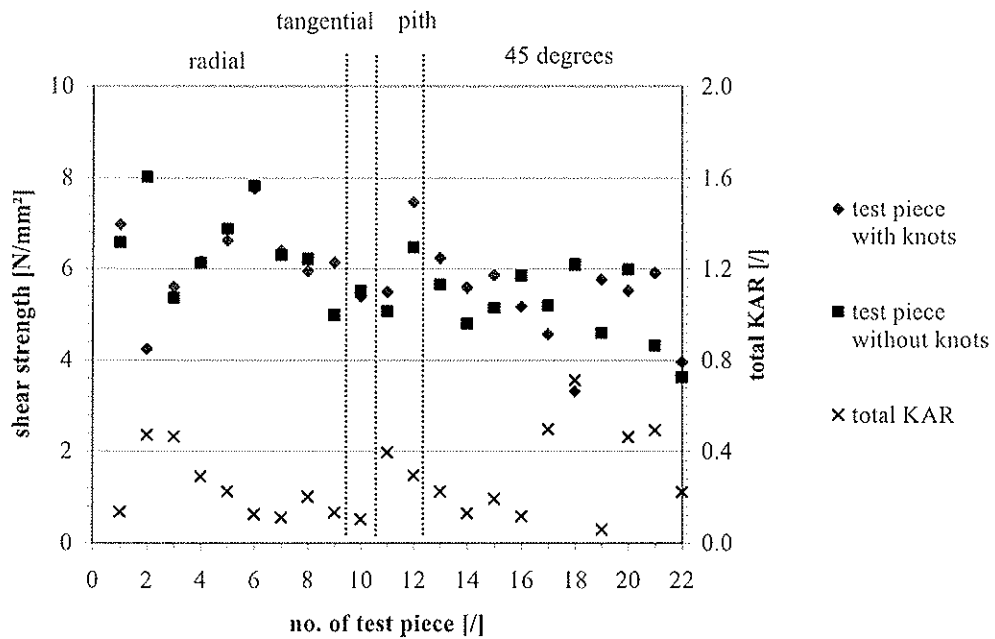
Figure 6: Shear strength and knot-ratio of matched test pieces with and without knots.

8

4 Conclusions

1. The influence of the density on the characteristic shear strength as given in EN 338 is not confirmed. A constant characteristic shear strength value independent of density as given in E DIN 1052 seems to be more appropriate.

2. The test results do not match with the shear strength values given in both standards. The test results are generally higher. Basically this difference seems justified because EN 1193 does not contain all negative influence factors on shear strength such as fissures. However, the values specified in a product standard must correspond with test results based on the test standard referenced in the product standard. To overcome this discrepancy, the product standards should consider these additional effects by applying an appropriate reduction factor.

3. According to the test results, the shear strength values of glulam beams should not be much higher than the shear strength values of structural timber because of the mainly tangential growth ring orientation of the laminations. At present the characteristic shear strength value for glulam beams in E DIN 1052 is 30% higher than the one for structural timber.

4. With regard to size effects on shear strength the test results according to EN 1193 were compared with results in the literature of test pieces with bigger cross sections (SPENGLER 1982). SPENGLER tested the shear strength of test pieces with cross sections from 22 x 80 mm² to 32 x 140 mm². His results ranging from 3 to 7 N/mm². Therefore based on the data presently available no size effect on shear strength values can be noticed.

5. The test method according to EN 1193 does not include all influences on shear strength. The small size of the test pieces does not allow to cover all kinds of fissures and knots. In order to avoid glueline failures in the test pieces/steel plates interface special attention has to be payed on the glueing process and to the appropriate selection of the adhesive. With the two-part epoxy Terokal 221 used in this study hardly no glueline failures were observed.

5   Literature

[1]   E DIN 1052:2002-10
Entwurf, Berechnung und Bemessung von Holzbauwerken – Allgemeine
Bemessungsregeln und Bemessungsregeln für den Hochbau

[2]   EN 1193:1997-10
Timber structures – Structural timber and glued laminated timber –
Determination of shear strength and mechanical properties perpendicular to the grain

[3]   ISO 1030:1975-12
Coniferous sawn timber; Defects; Measurement

[4]   ISO 3130:1975-11
Wood; Determination of moisture content for physical and mechanical tests

[5]   ISO 3131:1975-11
Wood; Determination of density for physical and mechanical tests

[6]   prEN 338:2002-10
Structural timber – strength classes

[7]   prEN 384:2002-10
Structural timber – Determination of characteristic values of mechanical properties
and density

[8]   prEN 408:2003-03
Timber structures - Structural timber and glued laminated timber - Determination of
some physical and mechanical properties

[9]   BENHAM et al. (1997)
BENHAM, C.A.; CANISIUS, T.D.G., MORRISON, P.A.G.
Compression, tension and shear strength properties for CEN strength classes based
on UK grown timber using new CEN methods. Centre for Timber Technology &
Construction, BRE CR 24/97. Watford, United Kingdom (1997).

[10]   SPENGLER, R. (1982)
Festigkeitsverhalten von Brettschichtholz unter zweiachsiger Beanspruchung –
Ermittlung des Festigkeitsverhaltens von Brettlamellen aus Fichte durch Versuche.
Sonderforschungsbereich 96, Heft 62. Laboratorium für den Konstruktiven
Ingenieurbau (LKI) Technische Universität München. München, Deutschland (1982)

INTERNATIONAL COUNCIL FOR RESEARCH AND INNOVATION
IN BUILDING AND CONSTRUCTION

WORKING COMMISSION W18 - TIMBER STRUCTURES

SHEAR TESTS IN TIMBER-LWAC JOINTS

WITH SCREW-TYPE CONNECTIONS

L Jorge

Castelo Branco Polytechnic Institute

H Cruz

LNEC

S Lopes

Coimbra University

PORTUGAL

Presented by: Luis Jorge

Luis Jorge described experimental work, test results and analysis regarding the use of screws with washers to connect the timber to the concrete. He concluded that LWAC specimens without an interlayer could lead to strength reduction but with similar stiffness in comparison with NWC. His tests suggest that the use of LWAC could be a positive alternative to normal concrete. He answered question relating to failure modes, slip and slip modulus.

Shear tests in timber-LWAC joints

with screw-type connections

Luís Jorge
Castelo Branco Polytechnic Institute, Portugal

Helena Cruz
LNEC, Portugal

Sérgio Lopes
Coimbra University, Portugal

1 Introduction

The use of timber-concrete slabs has been considered as a suitable alternative to traditional timber pavements, in terms of structural behaviour, acoustic and thermal insulation and fire resistance.

Typically these structures are made with normal-weight concrete (NWC), very seldom using light-weight aggregates concrete (LWAC).

The use of LWAC will most likely imply a different performance of the timber-concrete slab, due to the expected different short term and long term behaviour of the joints. Although the accepted failure modes for the joints with NWC would involve fasteners and timber only, it should be checked whether the same is valid when LWAC is used. The interest and relevance of developing further research work on the use of light-weight concrete in composite timber-concrete slabs has been pointed out by several authors [3, 6].

The lower modulus of elasticity of this concrete, directly related to its lower density, will imply a higher global deformation of the composite structure, which has to be counterbalanced by its lower self weight.

The self-weight reduction has other advantages, like less needs for prop, a better fire performance and a higher acoustic insulation to impact sounds as compared to NWC composite slabs.

With the purpose to study the suitability of using LWAC in timber-concrete slabs, composite shear tests on composite specimens were carried out. Special screws were used to connect timber to concrete as described below.

2 Test specimens

This paper presents the test results of eight different test specimen configurations, corresponding to combinations of concrete properties, screw type and also the presence or absence of an interlayer simulating the presence of floorboards in a real application.

The chosen fastener, a special screw - *SFS VB 48x7.5x100*, has been used before in several studies and a number of practical applications (site jobs), allowing an effective comparison with normal concrete composite test results referred in [6] and [5]. Two versions of this screw were used in the present study: the standard one and a modified version resulting from fixing a washer underneath the screw head thus increasing its contact area (Figure 1).
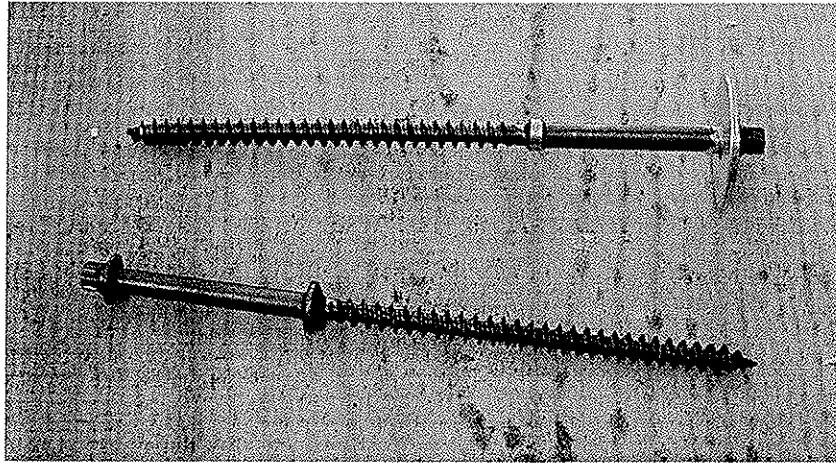
Figure 1 – Used screw in both versions: with and without the washer

This option resulted from perceiving that the pull-through resistance of the original screw embedded in LWAC might be quite different from that of NWC. The motivation was therefore to produce a wider bearing area to average the different resistance to pull-through from mortar and light-weight aggregates. This situation has also been exploited by Selle [4].

Table 1 – Characteristics of light-weight aggregates, LECA® used in this work [7].

assignment	particle size [mm]	apparent oven-dry density [kg/m³]	compression strength [MPa]	water absorption over 30min. [%]
Leca 2/4®	1.6 – 3	415	1.4	23
Leca 3/8F®	5 – 11.2	322	0.9	32

Two different admixtures were adopted for the concrete used in the experimental programme, made with the aggregates identified in Table 1, leading to the concretes shown in Figure 2. Thus, the concrete assigned for LWAC I was produced with resource the aggregate Leca 2/4® while concrete LWAC II included the two types of aggregate: Leca 2/4® e Leca 3/8F®.

These have quite distinct characteristics, namely strength and density, being identified as LWAC I (f_{clm}>30MPa, ρ>1500kg/m³) and LWAC II (f_{clm}<25MPa, ρ<1500kg/m³).

2
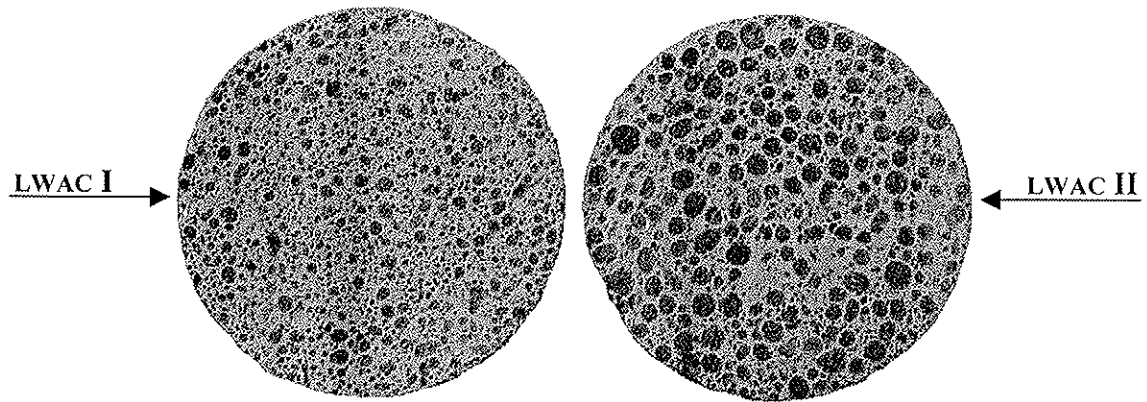
Figure 2 – Appearance of light-weight concretes used in the study.

Table 2 summarises the characteristics of the eight composite test specimen types produced for shear tests. Each specimen had two pairs of screws (one pair per shear plane) driven at an angle of ±45° to the shear plane.

Table 2 – Summary of shear test specimens.

batch	concrete	screw	25mm interlayer
A	LWAC I	with a washer	with
B	LWAC I	with a washer	without
C	LWAC II	with a washer	with
D	LWAC II	with a washer	without
E	LWAC I	without a washer	with
F	LWAC I	without a washer	without
G	LWAC II	without a washer	with
H	LWAC II	without a washer	without

Timber blocks of (glued laminated) spruce were used. The interlayer consisted of a 25mm thick maritime pine timber (*Pinus pinaster*, Ait.) board.

Around 20 replicates were tested for each specimen configuration (batch).

3   Preparation of test specimens and test procedure

Every piece of timber used was measured and weighted for density evaluation. Sampling evaluation of timber moisture content was also done (in 4 specimens per batch).

When producing the composite sheer tests, timber blocks were wrapped in thin polyethylene foil prior to concrete casting in order to prevent moisture take up in the timber and to reduce friction between timber and concrete.
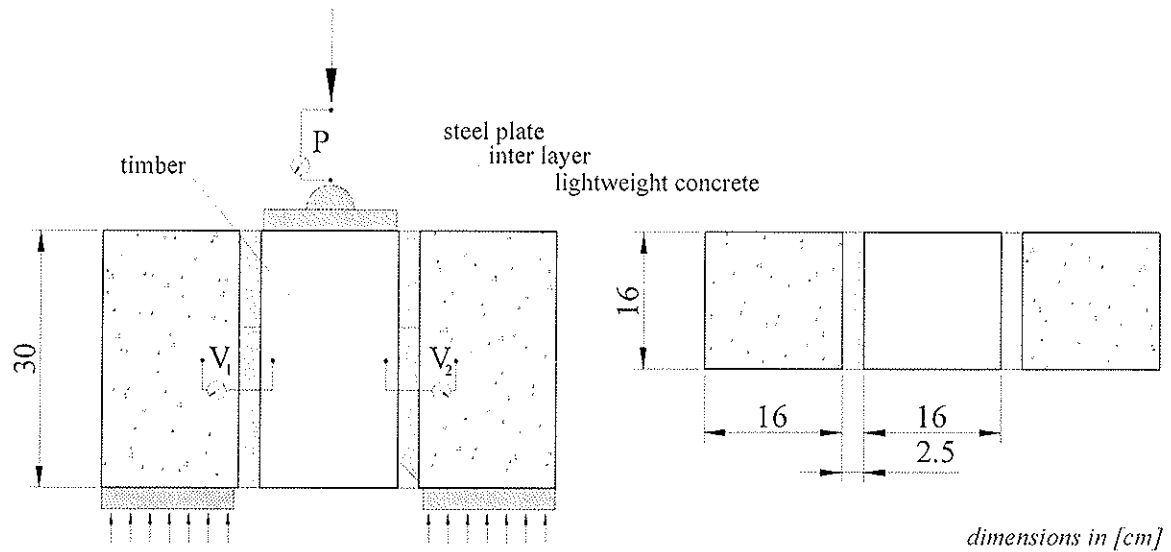
Figure 3 – Shear test set up.

Figure 3 illustrates the test specimen and set up used. The test specimen consists of a 160x160x300mm timber piece and two blocks of LWAC connected with one pair of screws per shear plane. The compression load is applied to the specimen through a steel device that provides load distribution over the timber piece and is free to rotate during the test. Four LVDT's are used (two on each side), to account for any specimen twist. These were placed in such a way that they measured only the slip between timber and concrete, disregarding any compression deformation. Measured slips and applied load were recorded continuously (every second readings).

An universal testing machine was used (Figure 4), programmed to apply a load history as described in EN 26891 (ISO 6891) [1].
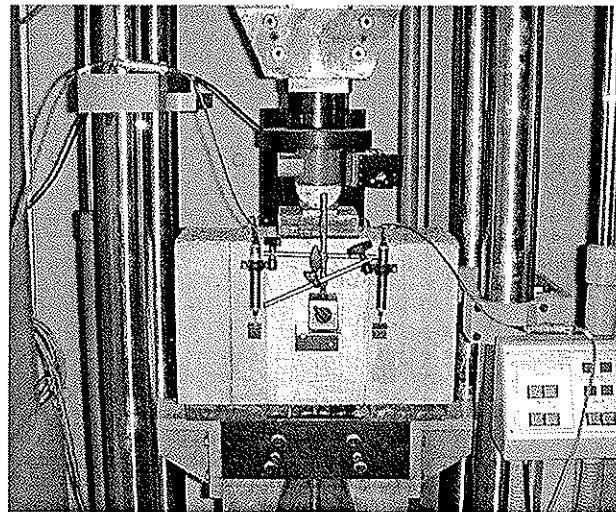
Figure 4 – Shear test.

4

4 Results

Table 3 presents, for each test batch, mean load capacity (F_{max}) and mean slip modulus (k_s), as well as the corresponding coefficients of variation.

Table 3 – Test results.

BATCH	no. specimens	JOINT strength, F_{max} mean value [kN]	JOINT strength, F_{max} coef. of variation [%]	JOINT slip modulus, k_s mean value [kN/mm]	JOINT slip modulus, k_s coef. of variation [%]	CONCRETE compression strength [MPa]	CONCRETE oven-dry density [kg/m³]	TIMBER moisture content [%]	TIMBER density at that moisture content [kg/m³]
A	20	**14.9**	10.4	**17.4**	13.2	27.9	1539	13.8	426
B	19	**16.9**	7.2	**26.0**	9.7	30.8	1595	13.9	428
C	18	**14.6**	9.0	**14.8**	19.7	25.5	1480	14.2	434
D	20	**17.6**	9.5	**26.1**	11.4	22.5	1485	13.8	436
E	24	**15.9**	6.6	**19.5**	9.0	31.3	1561	13.0	431
F	20	**16.8**	8.1	**28.7**	11.7	29.6	1533	14.8	430
G	24	**15.6**	8.2	**18.4**	11.7	22.6	1477	12.6	428
H	20	**14.6**	12.1	**31.1**	14.2	24.6	1461	12.6	433

Concrete mechanical properties (compressive strength and density) were determined simultaneously to the corresponding shear tests, between 28 and 35 days after casting of both specimens.

5 Analysis of results

5.1. Influence of concrete quality

5.1.1 Light-weight concrete type

Figures 5 and 6 present some typical load-slip diagrams obtained for composite shear joints tests on specimens with standard screws, for both LWAC concrete types, in the case of specimens without and with interlayer, respectively.

5
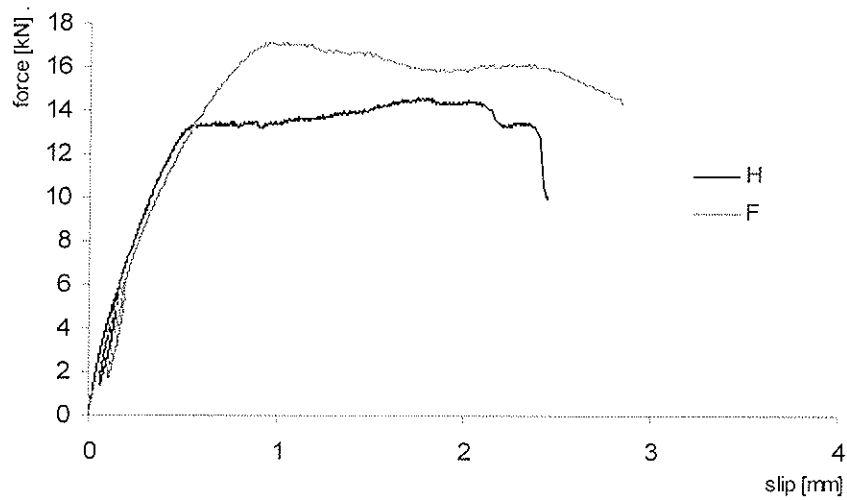
Figure 5 – Load-slip diagrams of typical specimens from batches F (LWAC I) and H (LWAC II)
(no washer, no interlayer).
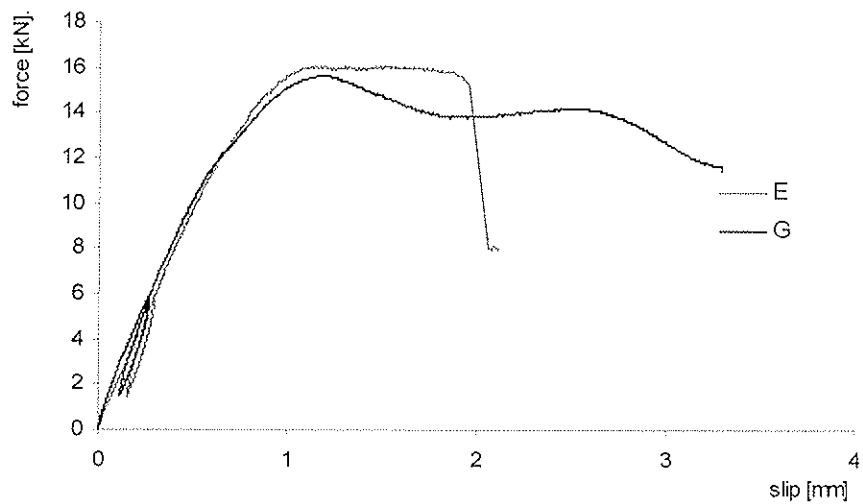
Figure 6 – Load-slip diagrams of typical specimens from batches E (LWAC I) and G (LWAC II)
(no washer, with interlayer).

When comparing the two LWAC used (Table 4), the biggest difference is found for the specimens without interlayer (F e H) – the higher strength and density concrete producing 15% stronger but 8% less rigid shear joints.

For batches E and G made with the standard screw and with interlayer, the influence of concrete quality is not so obvious. This may be due to the fact that the shorter penetration length of the screws in the timber is controlling the joint performance in these specimens.

Table 4 – Strength and slip-modulus ratios (specimens made with LWACII / made with LWAC I).

batches in comparison		batches differential [%]	
		strength	slip modulus
LWAC I	LWAC II	F_{max}	k_s
A	C	2	15
B	D	-4	0
E	G	2	6
F	H	15	-8

5.1.2. Comparison with NWC composite joints performance

In order to assess the influence of using LWAC, as compared to NWC, in the performance of timber-concrete joints, the results from the present study were compared with test data (batches LI - no interlayer; LII – interlayer 19mm thickness; LIII – interlayer 28mm thickness) reported by Mario van der Linden [6], who used similar standard fasteners in his work (Table 5). Similar test results to the above had been obtained with normal concrete with the same type of screw by Timmermam and Meierhofer [5], as referred by van der Linden.

Table 5 – Test results obtained by Mario van der Linden [6].

BATCH	n.° specimens	JOINT				CONCRETE		TIMBER	
		strength, F_{max}		*slip modulus, k_s*					density at that moisture content
		mean value	*coef. of variation*	*mean value*	*coef. of variation*	compression strength	oven-dry density	moisture content	moisture content
		[kN]	[%]	[kN/mm]	[%]	[MPa]	[kg/m³]	[%]	[kg/m³]
LI	5	**22.0**	5.0	**29.2**	20.5			-	-
LII	10	**15.3**	20.3	**12.9**	14.1	33.5	2320	14.4	393
LIII	16	**15.0**	11.7	**15.6**	8.1			15.5	438

As compared to the use of NWC, LWAC leads to a strength reduction of the shear joint between around 30% and 50%, for joints without interlayer. In the presence of interlayer, this difference is not so evident.

On the contrary, the use of LWAC does not clearly alter the joint stiffness for joints without interlayer, but it increases the slip modulus by about 15% to 35% in the presence on interlayer.

Table 6 – Strength and slip-modulus differences (specimens made with LWAC – made with NWC)

| batches in comparison | | batches differential [%] | |
L. Jorge	van der Linden	strength F_{max}	slip modulus k_s
F	LI	-31	-2
H	LI	-51	6
E	LII , LIII	4 , 6	34 , 20
G	LII , LIII	2 , 4	30 , 15

5.2. Influence of interlayer

Figures 7 and 8 present some typical load-slip diagrams obtained for specimens made with standard screws, with and without interlayer, for both LWAC concrete types, respectively.
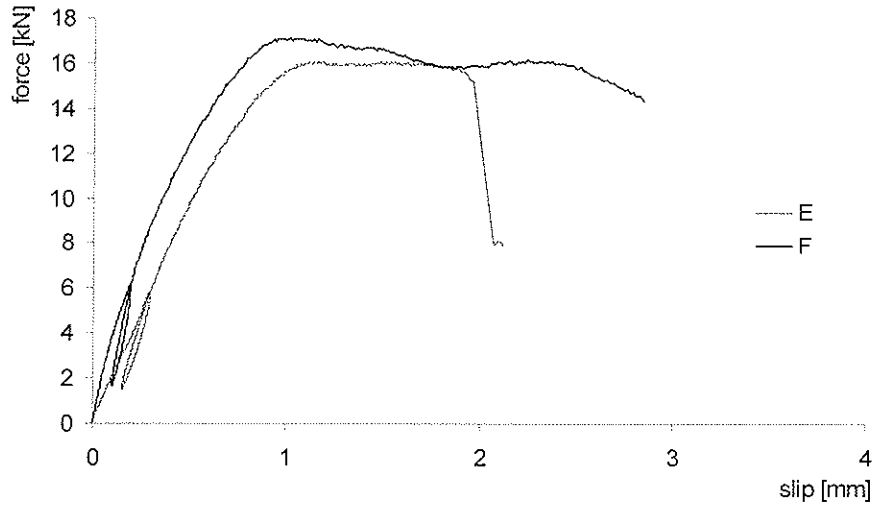
Figure 7 – Load-slip diagrams of typical specimens from batches E (with interlayer) and F (without interlayer) - (no washer, LWAC I).
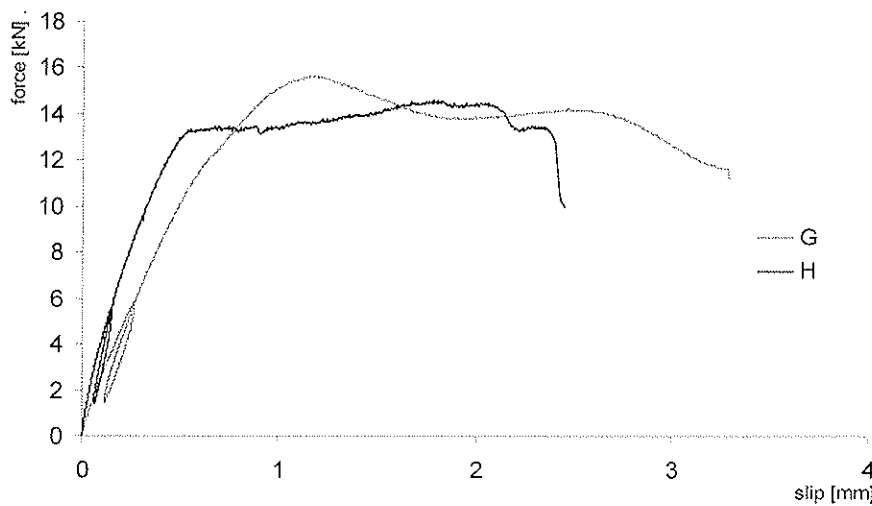
Figure 8 – Load-slip diagrams of typical specimens from batches G (with interlayer) and H (without interlayer) - (no washer, LWAC II).

When analysing the effect of the presence of interlayer only (Table 7), it can be seen that it lowers significantly the slip–modulus (between 50 and 75%).

As concerning the load capacity, only in the joints with the modified screw (with washer) the presence of interlayer makes some difference, by reducing strength by 15 to 20%. This situation is quite different from the one reported for shear tests with NWC [6], where the presence of the interlayer introduces much higher strength decreases, despite different interlayer thickness.

Table 7 – Strength and slip-modulus ratios (specimens made with interlayer / without interlayer).

| batches in comparison | | batches differential [%] | |
with interlayer	without interlayer	strength F_{max}	slip modulus k_s
A	B	-13	-49
C	D	-21	-76
E	F	-6	-47
G	H	6	-69

8

5.3. Influence of washer

The washer fixed underneath the screw head does not seem to increase the joint strength, except for batches D and H (with the less strong, less dense concrete). This may indicate an increasing effect of the washer for decreasing mechanical properties of concrete.

However, concerning to slip modulus, standard screws (without the washer) exhibit a (10% to 25%) better performance.
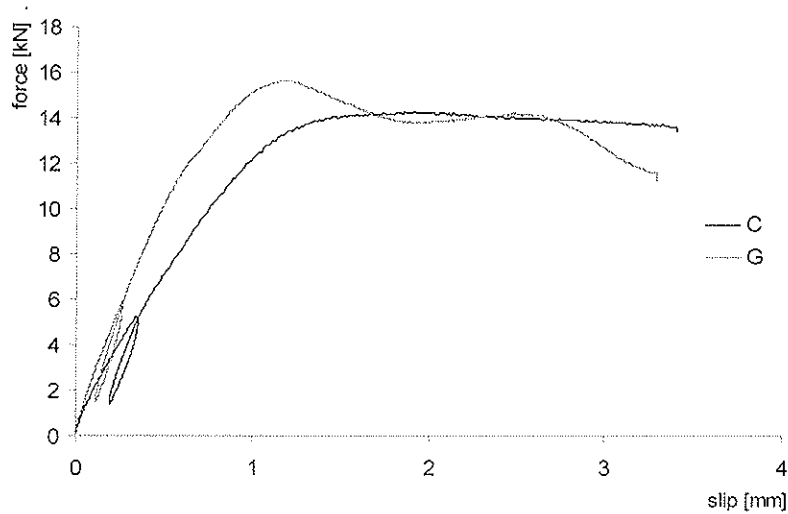
Figure 9 - Load-slip diagrams of typical specimens from batches C (washer) and G (no washer) (LWAC II, with interlayer).
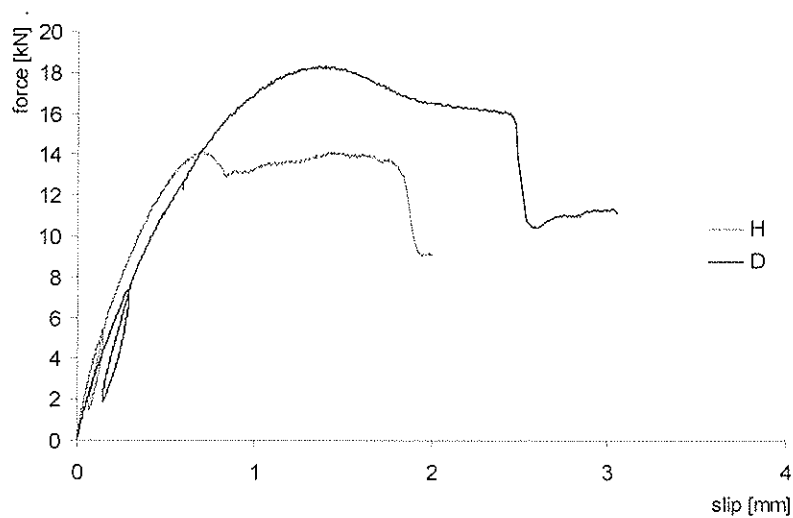
Figure 10 - Load-slip diagrams of typical specimens from batches D (washer) and H (no washer) (LWAC II, without interlayer).

Table 8 – Strength and slip-modulus ratios (specimens made with washer / without washer).

batches in comparison		batches differential [%]	
with washer	without washer	strength F_{max}	slip modulus k_s
A	E	-7	-12
B	F	1	-10
C	G	-7	-24
D	H	17	-19

9

6 Concluding remarks

The tests carried out indicate that the use of LWAC, in timber-concrete joints without interlayer lead to a strength reduction of the joint capacity but to a similar stiffness than the use of NWC.

On the contrary, in the presence of the interlayer, the use of LWAC conducts to higher slip modulus and to similar strength than the use of NWC. This is particularly promising for repair works since the studied interlayer simulates the floor boards existing in most old buildings that would generally benefit from reduced dead loads.

The modification of the screw (by introducing the washer) did not work as expected. However, the results suggest that this may be of some help in the case of using concrete admixtures even less dense and less resistant than the ones considered in the present study.

For standard screws (no washer), the presence of interlayer did not affect joint strength. Although resumed to one type of fastener only, test data suggest that the use of light-weight aggregates concrete may be suitable for timber-concrete composite slabs and a perfectly competitive alternative to the use of normal-weight concrete. Nevertheless, further research on the behaviour of timber-concrete slabs with LWAC should be carried out, namely by extending the focus to concretes of lighter density (class D1,4 [2]) and to the use of other fastener types.

7 Acknowledgement

8 References

1. EN 26891 – *Timber Structures – Joints made with mechanical fasteners – General principles for the determination of strength and deformation characteristics.* CEN. 1991.

2. prEN 206-1 – *Concrete Part 1: Specification, performance, production and conformity.* CEN. January 2000.

3. Rilem TC 111 CST – *Behaviour of timber-concrete composite load-bearing structures.* Proceedings of ACMAR-Ravenna International Symposium, Department of Civil Engineering, University of Florence, Italy. 1992.

4. Selle, R., Faust, T. – *Properties of composite joints of timber-LWAC composite structures.* LACER n°4. Leipzig University.1999.

5. Timmermam, K., Meierhofer, U. A. – *Holz/Beton-Verbundkonstuktionen. Untersuchungen und Entwicklungen zum mechanischen Verbund von Holz und Beton.* Forschungsbericht 115/30, Eidgenossische Material- und Prufanstald. Swiss. 1993.

6. van der LINDEN, M. L.R. – *Timber-concrete composite floor systems.* Doctoral Thesis. Technical University of Delft, Netherland. 1999.

7. Lourenço, J. – *Estudos de Composição para a Produção de Betões de Agregados Leves de Argila Expandida.* Betão, n°4. APEB. 2000.

**INTERNATIONAL COUNCIL FOR RESEARCH AND INNOVATION
IN BUILDING AND CONSTRUCTION**

WORKING COMMISSION W18 - TIMBER STRUCTURES

PLUG SHEAR FAILURE IN NAILED TIMBER CONNECTIONS:

EXPERIMENTAL STUDIES

H Johnsson

Div. of Timber Structures

Luleå University of Technology

SWEDEN

Presented by: Helena Johnsson

Helena Johnsson stated that the purpose of her study was to evaluate existing predictive formulae for plug shear failures and based on the analysis of her test data, she recommended a formula provided the nail has not penetrated more than half the depth of the timber. She plans to use fracture mechanics and finite element approaches to further examine the issues involved and went on to answer questions relating to load duration and growth ring orientation.

Plug Shear Failure in Nailed Timber Connections: Experimental Studies

Lic. Tech. Helena Johnsson

Div. of Timber Structures, Luleå University of Technology, SE-971 87 LULEÅ, e-mail: Helena.Johnsson@ce.luth.se

Abstract

Brittle failures in mechanical timber joints should be avoided, because this often results in low resistance and brittle failure of the structure. Nailed joints experience three ultimate failure modes: embedding, splitting or plug shear failure. Plug shear failure is limiting for large nailed connections loaded in tension parallel to the grain. To avoid plug shear failure, short and wide joints are preferred, minimising the number of fasteners in line with the load and grain direction. The aim of the study is to evaluate existing prediction formulas. Furthermore, knowledge of the parameters governing the plug shear failure is sought. Plug shear failure was examined in short-term experiments on nailed steel-to-timber joints in glulam loaded in tension parallel to the grain with varying joint geometries. Test results from four different test series are presented. Using hypothesis testing, a suitable prediction formula is derived based on more than 70 experiments. It is concluded that for engineering purposes the existing modelling approach is sufficient and plug shear resistance for the shear failure mode is modelled by the shear resistance of the bottom area of the joint.

Keywords: shear-plug failure, plug shear failure, block shear failure, timber connections, timber joints, nailed joints

1   Introduction

When timber is stressed by a group of fasteners loaded in tension parallel to the grain it results in both tension and shear stresses parallel to the grain, Fig. 1, where the bottom and side areas are in shear. The resistance of the joint is the lowest value of the nail embedding and the plug shear resistance, which involves tensile, R_t, and shear, R_v, capacities. In Kangas and Vesa (1998) a model is proposed for predicting the plug shear resistance, Eqn. 1. In Eqn. 1 t_{ef} is the distance

Figure 1: Schematic plug shear failure

between the two plastic hinges and is calculated according to Eurocode 5 (2003) assuming failure mode III, $t_{ef} = 2(M_y/(f_h d))^{1/2}$, Kangas and Vesa (1998). M_y denotes the yield moment of the nail, f_h the embedding strength of wood and d the diameter of the nail. The effective width b_{ef} is the width b reduced by the edge distances d_y and the nail diameters in one column, n_c. All other parameters are defined in Fig. 2.

1

$$R_{plug} = b_{ef}\left(t_{ef}f_t + lf_v\right) \qquad (1)$$

$$R_{plug} = \min\begin{cases} \dfrac{f_t t\left(b - 2d_y\right)}{K_t\beta_t\alpha_t\gamma_h} \\[2mm] \dfrac{2f_v tl}{K_s\beta_s\gamma_h} \end{cases} \qquad (2)$$

$$R_{plug} = \max\begin{cases} 1.5b_{ef}t_{ef}f_t \\[2mm] 0.7\left(b_{ef}l + 2t_{ef}l\right)f_v \end{cases} \qquad (3)$$

Figure 2: Definition of parameters (after Foschi and Longworth (1975)).

Timber is described through its tensile strength parallel to grain, f_t, and its shear strength, f_v, which also appear in Eqn. 2 proposed by Foschi and Longworth (1975). The numerically derived factors K, β, α and γ account for the number of nail rows and columns, nail spacing, timber thickness and penetration depth, h, respectively. Finally, Eqn. 3 is a proposal for Eurocode 5 (2003), Annex A. In Eqn. 1 the tensile and shear capacities are assumed to be additive, while Eqn. 2 and 3 separates them and it is natural to speak about a shear failure mode and a tensile failure mode. In Eqn. 1 the shear area along the bottom of the joint is assumed to carry the shear load, while in Eqn. 2 it is the side areas of the joint. Eqn. 3 assumes both shear areas to be effective. The phenomenological difference between the models in describing the plug shear failure is apparent. The aim with this paper is to compare the models in Eqn. 1, 2 and 3 using a statistical approach and propose a suitable prediction model.

2　Materials and Methods

Full size joints in glulam (Picea Abies) were tested in tension parallel to grain. The timber member cross sections were $90 \times 225\text{-}360$ mm^2 from glulam of strength class GL32, Eurocode 5 (2003). The timber member length varied between 650 and 1100 mm. In the RECTX series the thickness of the specimen was varied between 66, 78, 90 and 140 mm. In the ASP series one joint consisted of two 5 mm thick nail plates with annular ringed shank nails pressed into them welded back-to-back to form a Multiple Nail Connector, Fig. 3b. In the other series, one joint consisted of one steel plate 5 or 10 mm thick with a yield strength, $f_y = 355$ MPa, and annular ringed shank nails with diameter, $d = 4.0$ mm, and nail penetration depth, $t = 35$ or 40 mm respectively. Nail holes were pre-drilled in series RECT-, GRP-, SPREAD and NORM. The investigation comprised 14 series with a grand total of 74 specimens. The nail patterns varied between the different series, Table 1. The GRP- series had nails placed in groups with a distance e between them. The basic nail pattern is designed with distances between nails parallel to grain of 10d and perpendicular to grain of 5d (10d/5d). A reduction of the distances with a factor 0.7 was also tested (7d/3.5d). The P2, L6, T3 and T5 series in Table 1 were conducted by Bark and Martinsson (1991) and the ASP series by Burstrand and Salmonsson (1996). The specimens were conditioned to a temperature of 20°C and a relative humidity of 65 % according to ISO 6891 (1983). The tests were conducted with a time to failure between 8 and 15 minutes using a servo hydraulic testing machine with a maximum load of 600 kN and a maximum error of 1 % over the entire measuring range.

2
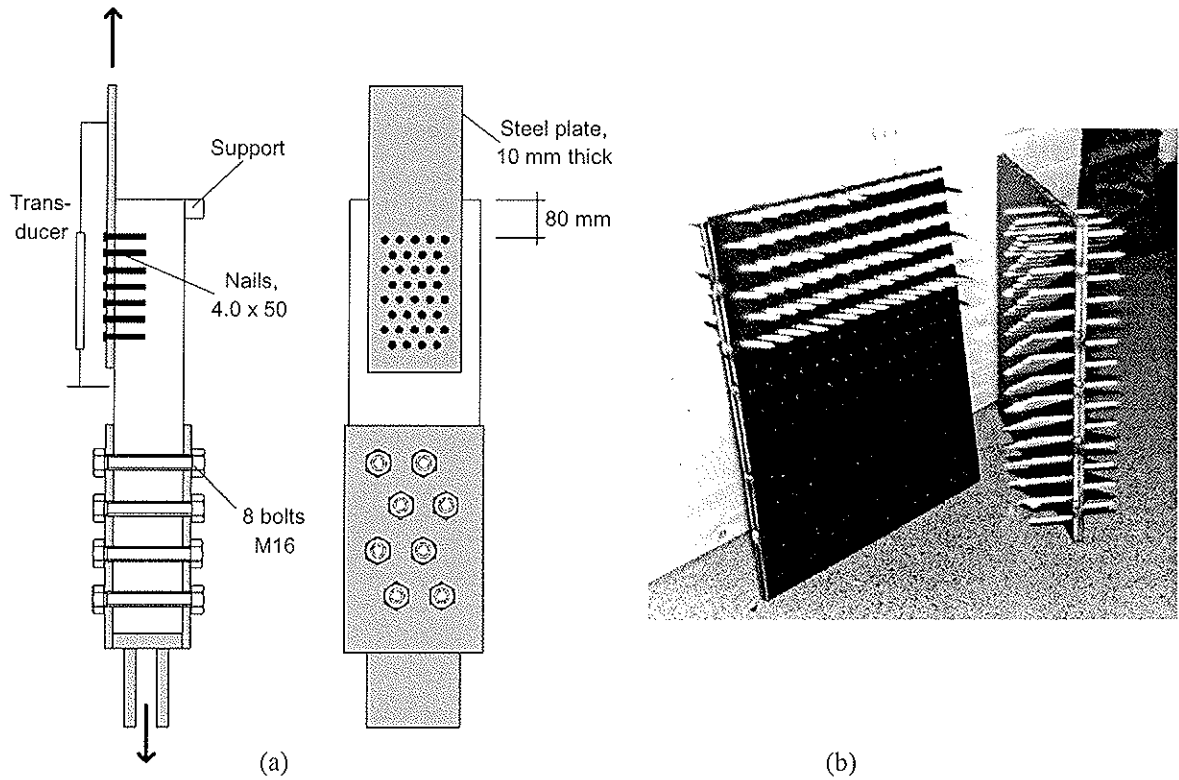
Figure 3: a) Experimental set-up and b) Multiple Nail Connectors.

Table 1: Specimen characteristics (b_{cf} includes/excludes the nail diameters, l includes the edge distance)

Series	No. of specimen	n_c	n_r	No. of nails	b_{cf} [mm]	l [mm]	t [mm]	t_{cf} [mm]	Nail pattern
P2	2	3	7	12	60/48	80	55	20	5d/2.5d
L6	6	10	14	70	130/102	240	55	20	10d/5d
T3	1	10	5	25	40/32	240	55	20	10d/5d
T5	5	10	7	35	60/48	240	55	20	10d/5d
ASP80	3	24	7	84/side	60/48	540	35	19	10d/5d
ASP120	4	15	11	82/side	100/80	360	35	19	10d/5d
RECTS	5	14	9	59	56/40	248	40	16-17	7d/3.5d
RECTL	5	15	19	143	126/90	276	40	15-17	7d/3.5d
RECTX	20	29	19	276	126/90	452	40	16-18	7d/3.5d
GRPS	5	15	19	143	126/90	337	40	16	7d/3.5d
GRPL	5	15	19	143	126/90	412	40	16-17	7d/3.5d
GRPX	5	15	19	143	126/90	482	40	16-18	7d/3.5d
SPREA	5	15	19	143	126/90	336	40	15-16	10d/3.5d
NORM	3	21	15	157	136/108	460	40	16-17	10d/5d

During the tests, displacements were measured by displacement transducers (LVDT, 0 - 50 mm, Vishay) placed centrally in the joint region. Data was sampled with a frequency of 2 Hz. The density and moisture content of the wood were determined according to ISO 3131 (1975) and ISO 3130 (1975) respectively. Measurements were made on two samples taken in the inner lamellas of the joints. The size of the samples was $40 \times 40 \times 40$ mm^3.

3 Results

The ultimate load from all 14 test series are presented in Table 2 together with results from the determination of density and moisture content.

Table 2: Test results (values are placed in corresponding order within cells)

Series	Ultimate load, R [kN]	Ult. displacement [mm]	Density, ρ [kg/m^3]	Moisture content, w [%]	Note
P2	33.1, 34.5	8.2, 12	480	13.6	
L6	170, 181, 191, 195, 197, 200	9, 9.5, 12.4, 12, 11.8, 17	480	13.6	Samples taken
T3	60.5	8.0	480	13.6	randomly
T5	75.5, 78.6, 88.6, 90.0, 94.6	9.2, 11.5, 9.2, 7.5, 12.7	480	13.6	
ASP80	158, 163, 166	3.2, 7.0, 5.0	458, -, -	8.6, -, -	
ASP120	154, 155, 167, 172	4.5, 4.0, 2.0, 4.0	533, -, -, 437	9.3, -, -, 8.9	
RECTS	76.2, 84.5, 92.1, 94.1, 94.9	1.7, 1.4, 1.5, 1.8, 1.5	473, 392, 425, -, 413	11.2, 11.0, 10.3, -, 10.6	
RECTL	150, 158, 162, 167, 171	1.2, 1.2, 1.8, 1.7, 1.3	467, 450, 415, 488, 431	11.1, 10.7, 10.5, 10.7, 11.3	
RECTX0	224, 233, 252, 262, 281	2.9, 2.2, 1.8, 2.3, 2.4	441, 431, 456, 420, 455	10.0, 9.30, 10.0, 9.44, 10.1	
RECTX1	169, 184, 203, 222, 224	2.2, 2.6, 2.0, 3.0, 2.1	418, 382, 448, 454, 366	10.3, 10.2, 10.8, 10.7, 10.1	c = 66 mm
RECTX2	214, 231, 248, 285, 306	1.9, 1.5, 1.8, 2.2, 1.9	436, 476, 457, 471, 432	10.2, 10.5, 10.4, 10.6, 10.3	c = 78 mm
RECTX4	238, 244, 247, 252, 295	2.9, 1.3, 2.0, 1.8, 2.0	412, 396, 436, 426, 415	9.61, 11.8, 11.0, 9.82, 9.75	c = 140 mm
GRPS	160, 178, 186, 187, 195	1.9, 2.2, 2.7, 1.6, 1.0	475, 472, 434, 458, 455	11.3, 11.2, 10.8, 11.1, 11.4	e = 75 mm
GRPL	202, 209, 221, 225, 230	2.0, 2.5, 2.6, 2.9, 2.1	422, 485, 446, 480, 465	10.7, 11.9, 11.7, 11.6, 11.4	e = 150 mm
GRPX	205, 218, 229, 243, 250	4.5, 2.3, 4.0, 2.7, 4.0	409, -, 365, 426, 443	9.19, -, 8.6, 9.33, 9.98	e = 300 mm
SPREAD	245, 246, 250, 261, 264	2.7, 3.0, 2.2, 2.6, 2.2	490, 455, 489, 446, 473	10.2, 9.86, 11.1, 9.69, 9.33	
NORM	276, 297, 305	2.8, 3.5, 3.9	414, 444, 487	9.10, 9.53, 10.56	

All tests experienced the shear failure mode, apart from the RECTX1 series where tensile failure was governing. From experimental observations (RECT-, SPREAD- and GRP-series) the general behaviour can be described:

1. A crack develops internally along one of the sides of the joint, Fig. 1. Probably the failure starts at the nail farthest from the free end. This occurs in most cases before ultimate load is reached.

2. The crack reaches the free end and is visible on the end face. The same development goes for the other side of the joint.

3. The final failure starts when a shear crack along the bottom face joins the two side cracks.

4. When the bottom side of the joint fails in shear, the tensile area of the joint cannot resist the load any longer and the joint fails.

Points 3 and 4 in the list of events occur almost simultaneously. It is possible that the tensile area fails before the bottom shear area. This is difficult to observe during the experiment. In the case of a thin member, such as series RECTX1 where c = 63 mm, the bottom

4

face crack never develops. Instead the side cracks protrude through the member to the back face and final failure is reached when the tensile area fails. Bark and Martinsson (1991) measured the plastic moment of nails $M_y = 9.16$ Nm for annular ringed shank nails used in all test series in Table 3. The value is used to obtain t_{ef} in Table 1.

4 Analysis

4.1 Strength values for wood

Test results should be compared to predictions made on the average strength level, not on the characteristic level. Gathering of appropriate strength data for glulam of Nordic origin (Picea Abies) is therefore necessary.

4.1.1 Shear strength

In Johansson and Stehn (2002) the shear strength of glulam was tested with an average value of $f_v = 9.6$ MPa. The area loaded in shear during the test was 45×45 mm^2. The shear strength of wood is affected by a volume effect and in Kuipers and Vermeyden (1964) an empirical relation between shear area and shear strength is presented based on an experimental study of ring-shear connectors, which also fail in plug shear failure, Eqn. 4.

$$f_v = K \cdot A_s^{-0.25} \quad \Rightarrow \quad K = \frac{f_v}{A_s^{-0.25}} = \frac{9.62}{2025^{-0.25}} = 64.5 \text{ N/mm}^{1.5} \qquad (4)$$

The parameter K is suggested as $K = 20$ on the characteristic level. Using the test result $f_v = 9.6$ MPa and $A_s = 45 \times 45 = 2025$ mm^2, $K = 64.5$ is calculated. Eqn. 4 is used with $K = 64.5$ in the evaluation of the shear strength for the hypothesis testing.

4.1.2 Tensile strength

Johansson et al. (1998) tested the tensile strength of glulam laminations of Nordic origin (Picea Abies). The results showed $f_t = 37.7$ MPa in the outer laminations and $f_t = 28.4$ MPa in the inner. All joints reported in Table 2 are mounted in the inner laminations. When the laminations are assembled to a glulam beam, the apparent tensile strength increases, Colling and Falk (1993). In their study, Colling and Falk (1993) separates the different constituents of the lamination effect, λ, into; i) the effect of test procedure, ii) the reinforcements of defects and iii) the dispersion of low-strength lumber, Eqn. 5.

$$\lambda = \frac{f_{m,beam}}{f_{t,lam}} = k_{test} \cdot k_{reinf} \cdot k_{disp} \quad \Rightarrow \quad f_t = f_{t,lam} \cdot k_{test} \cdot k_{reinf} = 28.4 \cdot 1.2 \cdot 1.2 = 40.9 \text{ MPa} \qquad (5)$$

Tensile failure in the outmost lamination is most often governing in bending failures and therefore $\lambda = f_{t,lam} / f_t$ is tentatively valid. Most of the joints tested in this study have only 3-4 laminations loaded in tension, why the dispersion effect does not apply. Guidelines for selecting the factors k_{test} and k_{reinf} are presented in Colling and Falk (1993) and leads to the determination of $f_t = 40.9$ MPa, Eqn. 5, which is used in the hypothesis testing procedure.

4.2 Influence from variation in density and moisture content

To make the different test series in Table 2 comparable regarding moisture content and density variations, a procedure for estimating the impact of these parameters is applied. The specific gravity is obtained as $G = \rho_{dry\ wood}/\rho_{water}$, and the elastic modulus is calculated for softwoods as $E = 25.156 \cdot G^{0.9454}$, Dinwoodie (1981). The tensile strength f_t of wood is

related to the elastic modulus through $f_t = 0.0038 \cdot E - 13.09$, Johansson et al. (1998). The relations are used to linearly promote or punish stronger or weaker wooden material in relation to series P2, which is chosen as a reference since the compressive strength measured by Bark and Martinsson (1991) corresponded closely to the strength values in Eurocode 5 (2003). The variation in f_v with density is ignored since Glos (1995) reports $f_v = 0.2 f_m^{0.8}$, which for the present range produces a variation of 6 %, whereas the variation in f_t is 25 %.

4.3 Analysis of variance

The aim of the analysis of variance, ANOVA, is to determine a prediction model for plug shear failure through hypothesis testing using the experimental data in Table 2. The hypotheses are based on different assumptions regarding active load-carrying areas, Table 3.

Table 3: Hypotheses used in the analysis of variance.

Hypothesis [kN]	Normalised unit of analysis	Comment
H_1: $2 \cdot t_{ef} \cdot l \cdot f_v$	$D_1 = (H_1-R)/100$	Only side shear areas, Eqn. 1
H_2: $b_{ef} \cdot t_{ef} \cdot f_t$	$D_2 = (H_2-R)/100$	Only tensile area, Eqn. 1 and 3
H_3: $b \cdot l \cdot f_v$	$D_3 = (H_3-R)/100$	Only bottom shear area
H_4: $2 \cdot t_{ef} \cdot l \cdot f_v + b \cdot l \cdot f_v$	$D_4 = (H_4-R)/100$	Both side and bottom shear areas, Eqn. 3
H_5: $2 \cdot t_{ef} \cdot l \cdot f_v + b_{ef} \cdot t_{ef} \cdot f_t$	$D_5 = (H_5-R)/100$	Side shear areas + tensile area
H_6: $b_{ef} \cdot t_{ef} \cdot f_t + b \cdot l \cdot f_v$	$D_6 = (H_6-R)/100$	Bottom shear area + tensile area, Eqn. 2
H_7: $b_{ef} \cdot t_{ef} \cdot f_t + b \cdot l \cdot f_v + 2 \cdot t_{ef} \cdot l \cdot f_v$	$D_7 = (H_7-R)/100$	All enclosing areas

The data set presented in Table 2 consists of many different test series with varying geometrical parameters entering hypothesis $H_1 - H_7$. The unit of analysis is changed from the direct hypothesis to a normalised difference as in Table 3. The hypothesis testing could be performed on the separate test series, but the variation between samples would be ignored and valuable information lost. The ANOVA, is based on the assumptions of equal within samples variance, which is correct on the 95 % confidence level. A good prediction model shows up in the ANOVA as a model with small between samples variance equally distributed around zero. The between samples variation is however large and strictly statistically speaking one cannot state that all test series belong to the same distribution. It is probable that the large natural variation of wood strength is the cause for the large scatter. In the analysis, series RECTX1 and RECTX2 were ignored since these series did not experience the exact same course of failure as the others. Some general conclusions from the ANOVA analysis are presented together with reflections from the experimental behaviour:

- Hypothesis H_1 underestimates the capacity. This is in line with the observed course of the plug shear failure where the side shear areas fail before ultimate load is reached.
- Hypothesis H_2 underestimates the capacity. That the tensile area fails before final failure is not confirmed through experimental observation, but could be true anyway.
- Hypothesis H_3 predicts the capacity well. The bottom shear area always remains active in the load uptake until maximum load is reached.
- Hypothesis H_4 predicts the capacity well. The sum of the shear areas is probably not useful as a prediction model since the side shear areas are observed to fail before maximum load is reached.
- Hypothesis H_5 underestimates the capacity. Combining H_1 and H_2 still leads to an underestimation.
- Hypothesis H_6 and H_7 overestimates the capacity heavily.

To examine the validity of the strength data, f_v and f_t were changed to characteristic values, which lead to the conclusion that H_6 or H_7 are the best prediction models. This is not in accordance with experimental observations. After the ANOVA two hypotheses remain and a plot of predicted resistances versus experimental values is constructed, leading to clarification on separating H_3: $R = b l f_v$ and H_4: $R = 2 t_{ef} l f_v + b l f_v$. H_4 is the approach in Eurocode 5 (2003), Annex A. In Fig. 4 one can see that both H_3 and H_4 seem to be good predictors, but

6

the prediction by H₄ falls mainly on the unsafe side. Therefore, H₃: R = blf$_v$ is suggested as a suitable prediction model based on experimental observations. In Eurocode 0 (1990), Annex D, a method is presented where the characteristic value of a prediction model can be determined. This leads to Eqn. 6 for the shear failure mode in plug shear failure:

$$R_{vk} = 0.81blf_{vk} \qquad (6)$$

The difference between Eqn. 6 and Eqn. 3 (H₄) is that only the bottom shear area is incorporated and the effective width and length are not used since nail holes are small and can be neglected (6 % of the bottom area). However, the use of effective width and length is an assumption on the safe side.

Figure 4: Test results versus predicted resistances.

5   Discussion

It is of course interesting to compare the suggested model for the shear failure mode with results from other researchers. Both Kangas and Vesa (1998) and Foschi and Longworth (1975) report failure modes in shear not in tension. The shear strength was not measured by Kangas and Vesa (1998)

Table 5. Material properties

	ρ [kg/m³]	f$_v$ [MPa]	A$_s$ [mm²]
Douglas Fir	525	17.4	645
Kerto-S-LVL	520	6.9	9894
Kerto-Q-LVL	520	6.9	9894
Spruce	380	9.6	2025

so average strength values were obtained from Finnforest (2003). Foschi and Longworth (1975) report strength values for shear and an approach for incorporating the volume effect. The material properties are gathered in Table 5 and used for producing Fig. 5. The experimental data from Foschi and Longworth (1975) and Kangas and Vesa (1998) are presented in Fig. 5 plotted against the prediction by R = blf$_v$. The scatter is larger than in Fig. 4, which is understandable

Figure 5: Test results versus predicted resistance including other sources (grand total is 108 experiments).

since the material properties are assumed average values, not measured quantities. A regression line fit for the data in Fig. 5 reveals that Test = 1.12*Predicted. The hypothesis that Test = Predicted (the 45° line in Fig. 5) is rejected on the 95 % confidence level since the major part of the values fall on the safe side in Fig. 5.

7

To increase the understanding and the knowledge on plug shear failure an approach for a prediction model based on fracture mechanics would be beneficial. Linear elastic fracture mechanics combined with 2D FE analysis is a natural first approach.

6   Conclusions

64 experiments on plug shear failure in nailed steel-to-wood connections were conducted. Based on experimental observations and the assumptions presented regarding material parameters, the model for predicting the characteristic plug shear resistance in the shear failure mode is suggested as Eqn. 7.

$$R_{vk} = 0.81 b l f_{vk} \qquad (7)$$

This model differs from the one suggested in Eurocode 5 (2003), Annex A, and leads to a safer design.

7   References

Bark T and Martinsson S (1991) Shear Force Capacity of Glulam Rivet Connections – Influence of Geometrical Design. Master thesis 1991:096E, Div. of Steel Structures, Luleå University of Technology, ISSN 0349-6023.

Burstrand H and Salmonsson J (1996) Design of Nailed Connections for Large Glulam Trusses. Master thesis 1996:197E, Div. of Steel Structures, Luleå University of Technology, ISSN 0349-6023.

Colling F and Falk RH (1993) Investigation of Laminating Effects in Glued Laminated Timber. In proceedings of CIB-W18, paper 26-12-3, August 1993, Athens, Georgia, USA.

Dinwoodie JM (1981) Timber – Its Nature and Behaviour. Van Nostrand Reninhold Co. Ltd, Berkshire, England. ISBN 0-442-30446-3.

Eurocode 0 (1990) Annex D (informative) Design assisted by testing, prEN 1990:2001.

Eurocode 5 (2003) Eurocode 5 - Design of timber structures. ENV 1995-1-1:1993. Final draft 2003-05-06.

Finnforest (2003) Personal communication.

Foschi RO, Longworth J (1975) Analysis and Design of Griplam Nailed Connections. Journal of the Structural Division, 101(12): 2537-2555.

Glos P (1995) Solid timber- Strength classes. In Timber Engineering STEP 1, Centrum Hout, the Netherlands.

ISO 3130 (1975) Wood – Determination of moisture content for physical and mechanical tests.

ISO 3131 (1975) Wood – Determination of density for physical and mechanical tests.

ISO 6891 (1983) Timber Structures – Joints made with mechanical fasteners – General principles and determination of strength and deformation characteristics.

Johansson C-J et al. (1998) Laminations for glued laminated timber: establishment of strength classes for visual strength grades and machine settings for glulam laminations of Nordic origin. SP Report 1998:38, ISSN 0284-5172, SP, Borås, Sweden.

Johansson H and Stehn L (2002) Causes for the Initiation of Shear-plug Failure in Nailed Connections. In proceedings from the 7th World Conference on Timber Engineering, WCTE 2002, Shah Alam, Malaysia, 12-15th August 2002.

Kangas J, Vesa J (1998) Design on Timber Capacity in Nailed Steel-to-Timber Joints. In proceedings from CIB-W18 – Timber Structures, CIB-W18, paper 31-7-4, meeting 31, Savonlinna, Finland.

Kuipers and Vermeyden (1964) Research on Timber Joints in the Netherlands. Rapport 4-64-15, Onderzoek v-7, Stevin-Laboratorium, Technische Hogeschool Delft, Netherlands.

**INTERNATIONAL COUNCIL FOR RESEARCH AND INNOVATION
IN BUILDING AND CONSTRUCTION**

WORKING COMMISSION W18 - TIMBER STRUCTURES

NAIL LAMINATED TIMBER ELEMENTS IN NATURAL SURFACE COMPOSITE

WITH MINERAL BOUND LAYER

S Lehmann

K Rautenstrauch

Bauhaus-University Weimar

GERMANY

Presented by: Steffen Lehmann

Steffen Lehmann described the experimental setup and also discussed his test data as well as the discrepancies between theoretical and measured tensile stresses. In summary, he concluded that shear stresses can be transferred across saw-rough lamella surfaces. There were questions and severe warnings relating to long term durability of the bond layers and the timber species used as the natural bond characteristics could be related to the species used. He also answered questions relating to the implications of the work to Eurocode 5.

Nail-laminated timber floor elements

in natural surface bond with mineral surface layer

S. Lehmann, K. Rautenstrauch

Institute of Structural Engineering, Bauhaus- University Weimar, Germany

1   Introduction

Recently the idea was focused on combining favourable characteristics of mineral surface layer and timber in composite elements. Thereby tension-stressed timber and compression-stressed mineral surface layer, for instance concrete, offer good load behaviour. The connection between timber and concrete is of fundamental importance for stiffness and carrying performance. Since these systems have usually been realised as timber-concrete composite beams mainly taken for bridges or revitalisation of timber beam floors, dowel type connectors were usually studied and taken for transfer of shear forces.

A research program was initiated at the Bauhaus-University Weimar, to test natural adhesion and modified timber surface structure for the transfer of shear forces in timber-mineral surface layer -composite slabs. It is a matter of saw-rough and additionally profiled lamellas of nail-laminated timber elements in combination with usual mineral surface layer. An overview of shear tests („slip-block-tests") and tension tests, performed to examine the load-slip is also given. Test data and figures are presented. Based on these test results the behaviour of the connection method is described.

2   Construction of surface bond

Transmission of shear stress in the contact area of timber-mineral surface layer was usually realised by steel connecting device [1][2][3][4][5]. The separating layer prevented thereby a direct, overall bond.

The accomplished tests were completely done without dowel type connectors and separating layer. Only the natural adhesive bond between timber and fresh mineral surface layer should be sufficient to transfer the shear- and tension forces in the compound joint. For all test series saw-rough lamellas with a width of 4,0 cm. were taken
As a basic version for surface structure (type R) the saw-rough lamellas of same height were jointed. The simplest mechanical modification of timber finishing are the 2,0 cm differently high jointed lamellas of type V. In the upward supernatant lamellas lateral profiling is in-milled in equal distances (type P). The filling out with the fresh mineral

topping of the lamellas of different height as well as the profiled lamellas is thus warranted. The shear forces between laminated timber-elements and mineral surface layer are transferred by the concrete-filled in-milled slots during the time bending stress of.

Additionally can be assumed that the surface layer becomes wedged with sufficient transverse stiffness between the set up lamellas. Among the modification of the timber finishing, different mineral surface layers were tested, like concrete, cement screed, anhydrite screed and the new concrete of geopolymer for load-bearing capacity of compound. The different investigated types are summarised in the following figure 1:
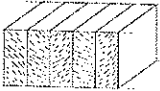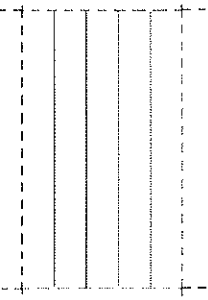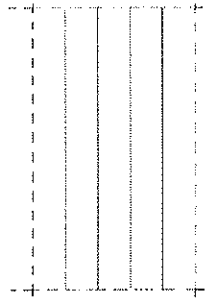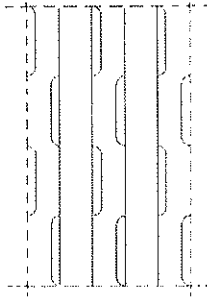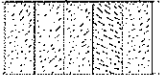
	type R	type V	type P
surface condition of nail-laminated timber elements (C24, picea abies)			
mineral surface layer			
concrete (C20/25)	BR	BV	BP
cement screed (ZE20)	ZR	ZV	ZP
anhydrite screed (AE 20)	AR	AV	AP
concrete of geoplolymer	GR	GV	GP

Figure 1: Variants of specimens

3 Shear tests as slip-block-tests

The behaviour of the shear connector in the composite joint between timber and mineral surface layer is extremely important for the carrying and deformation performance of composite structures with rigid bond. To enable a structural model the load-slip-characteristics, failure load and failure mechanism of each bond type was determined by experimental tests. Because of the sudden failure of the rigid bond in the test phases, a shear test with single lap shear joint is preferred to a pushout test. For such a test arrangement to determine the rigid bond the term "slip-block-test" was proposed [6]. The vertical force to work against the rotation force caused by the test specimen has to be located exactly. From the knowledge of the force position its value can be determined. Thus the coefficient of friction μ and friction portion could be defined.

Experimental procedure and applied load history were taken according to DIN ENV 26891. Test setup with dial indicators and load cells are illustrated in figures 2 and 3.
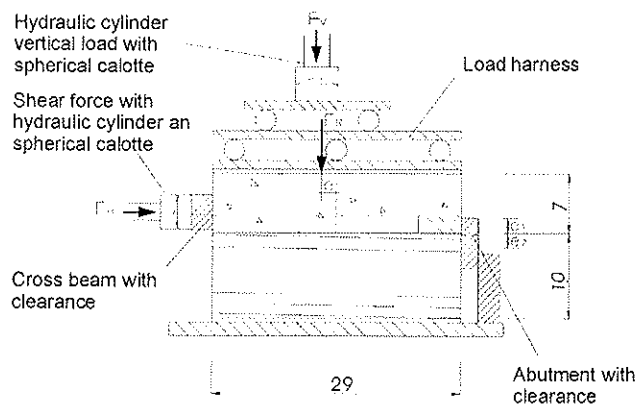
Figure 2: Principle test setup
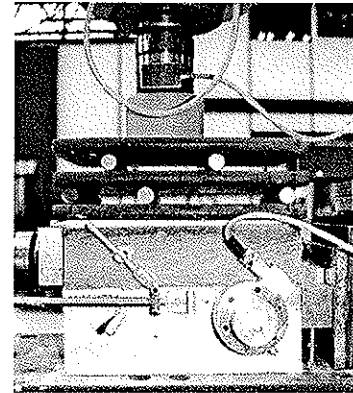
Figure 3: Measuring points

4 Tension test

The investigations of the friction, accomplished first in the slip-block-tests, should not serve alone for the determination of the coefficient of friction. To specify material parameter of the bond joint slip-block-tests should be completed by tension tests.

By variation of the load in the shear tests the internal friction φ between the partners of bond could be determined. The value of friction is the angle of friction between the respective shear test and the axis of normal stress σ_N. The Coulomb failure criterion gives only a reliable statement within the range of pressure perpendicularly to the shear joint.

The extension of the failure straight line from the shear test supplies the theoretically possible tensile strength $f_{jt}*$ perpendicular to the joint. At the same time the theory of [7], which explains the discrepancy of the theoretical and the experimentally observed tensile strength, requires a more exact view of this problem (figure 4). It remains to clarify, how theoretical and real tensile strength correspond.
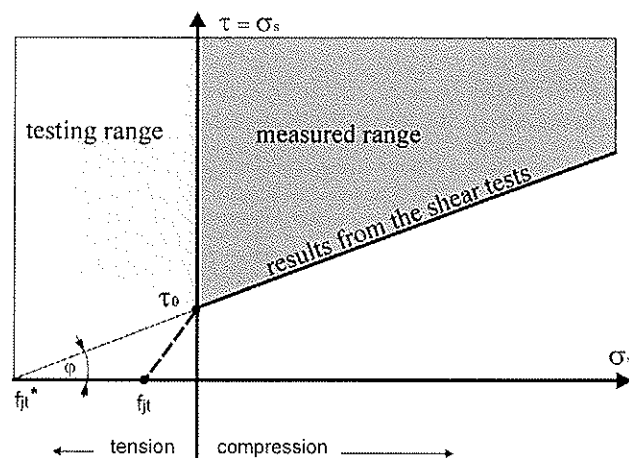
Figure 4: Coulomb-failure criterion in Mohr-diagram

For the formulation of a closed solution of the failure criterion the investigation of the tensile load perpendicular to the bond joint is of great importance. This has even now been uninvestigated.

For the better evaluation of this range in the figure the real axial tensile strength in the bond joint f_{jt} between nail-laminated timber element and mineral surface layer had to be determined experimentally.

Experimental procedure and applied load history were taken according to DIN EN 582. Principle test setup with dial indicators and load cells are illustrated in figures 5 and 6.
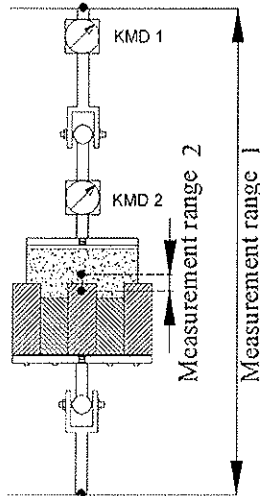
Figure 5: Principle test setup   Figure 6: Measuring points
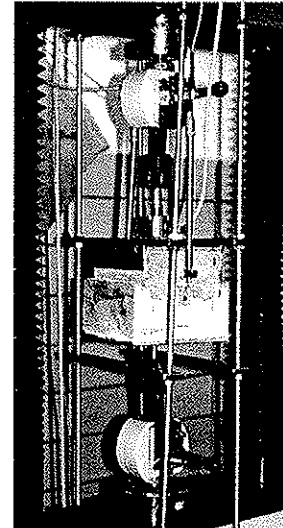
In agreement with applying the away-steered and supplied adhesive strength and the specific failure energy for this bond.

5   Results and conclusion

5.1   Results of the shear tests

In order to receive meaningful test results, to each type of the shear transferring a sufficient number of short time shear tests was conduced. With a specified experimental procedure and applied load history the following results for the maximally applied forces $F_{H,mean}$ and the adhesive shear strength $f_{v,mean}$ were measured and calculated (Table 1).

Table 1: Average value of adherence bonding strength $f_{v,mean}$ without friction

Type	$F_{H,mean}$ [kN]	μ [--]	$F_{V,eff}$ [kN]	$F_R = \mu * F_V$ [kN]	$F_{HV} = F_{H,mean} - F_R$ [kN]	$f_{v,mean}$ [N/mm²]
HVS/HV/AP	49,24	1,85	20,59	38,10	11,14	0,31
HVS/HV/AR	30,20	0,90	30,52	27,53	2,67	0,07
HVS/HV/BP	45,60	1,46	20,68	30,29	15,32	0,42

HVS/HV/BR	42,92	0,89	31,07	27,65	15,27	0,38
HVS/HV/BV	33,47	0,92	20,61	19,01	14,47	0,32
HVS/HV/GP	49,79	1,21	20,61	24,89	24,90	0,68
HVS/HV/GR	49,25	0,96	30,54	29,23	20,02	0,50
HVS/HV/GV	36,69	1,00	20,64	20,66	16,03	0,35
HVS/HV/ZP	50,27	1,76	20,59	36,23	14,04	0,39
HVS/HV/ZR	40,69	0,92	30,60	28,24	12,45	0,31

Consequently it is possible to transfer high shear forces between the layers by favourable combinations of materials for the mineral surface layer and surface design of the lamellas. The best bond of shear was determined between timber and concrete of geopolymer.

The concrete of geopolymer has only a small strength of material. But the high alkalinity of the mixture affected the bond positively. The smallest adhesive bond was observed with anhydrite screed.

Normal concrete and cement screed, both with the bonding agent cement, stand with their shearing strengths between the "specialised concrete". The comparison between the timber surface modifications vary evidently. The bond could be improved by the profiled surface versus the simple rigid surfaces by at least 20 %.

It was surprising that the values of the samples with transfers in altitude lamellas were smaller than with even rigid surface. An explanation for this can be the influence of swelling and shrinking of the timber and shrinking of the surface topping. The structural mechanism of the composite components is still to be still followed.

The total shear stiffness of such combination elements depends first on the adhesive bond, the friction and the wedge within the flutings. The adhesive bond is characterised by the fact that it also works without additional external forces.
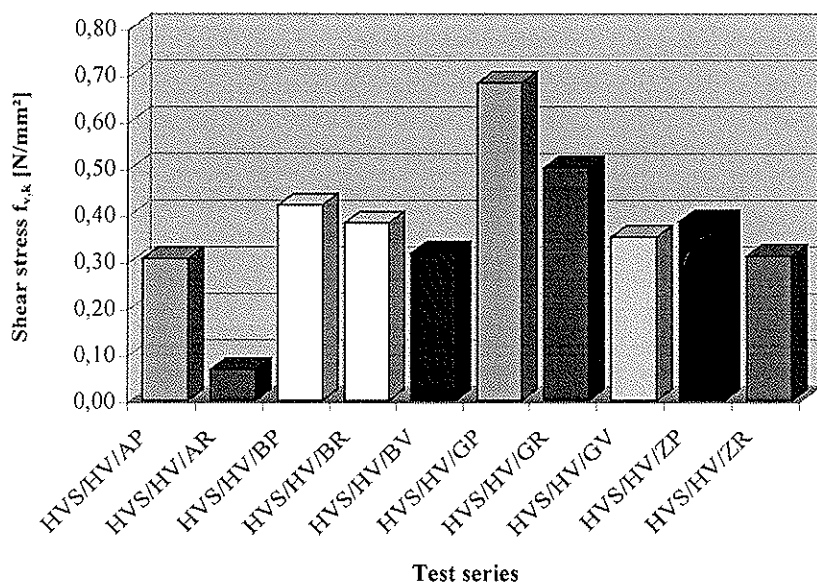
Figure 7: Transmittable shear stress without friction

After overstepping this value sudden failure occurs. The elongation up to the failure were all clearly under a half per cent. Therefore the adhesive bond works no more and cannot reset itself.

During the time of adhesive bond and after its failure the friction force works between the layers. It is dependent on the load.

Figure 8 shows the typical load-displacement-curve of the variants of bond type R, V and P with concrete as mineral surface layer.
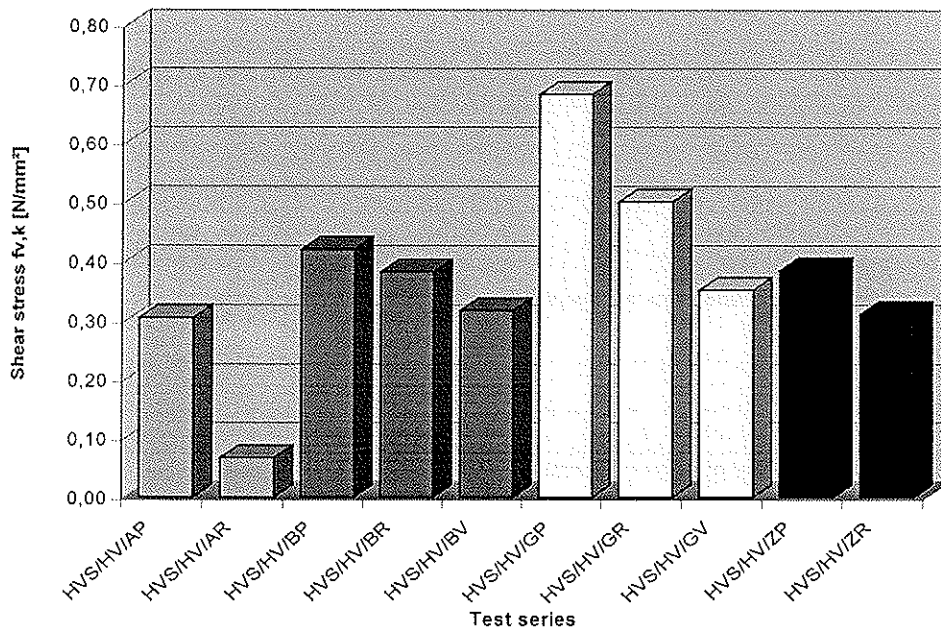
Figure 8: Load-displacement-curves of slip-block-tests type R, V and P with concrete as mineral surface layer

In the test a vertical load was applied on the test specimens. This led to friction between concrete surface layer and timber finishing. However the determination of the value is only possible if the load is known.

In literature a coefficient of friction called μ_f = 0.8... 1.0 between timber and concrete is itspecified. This coefficient could be confirmed in the test series "rigid surface (BR)".

During exact consideration it could be noticed that after the test arrears of concrete within the fine grain range presented loosely on the timber surface. The abrasion worked as a kind of glide layer. Burkhardt [8] observed in his tests of new concrete on old concrete slabs similar effects. A clear increase was obtained with the profiled test specimens.

The broken out remainder of mineral surface layer staying in the lateral profiles increased the resistance. Furthermore the statements about the internal angle of friction formed the basis for the theoretical quantification of the joint tensile strength (Figure 9).

6
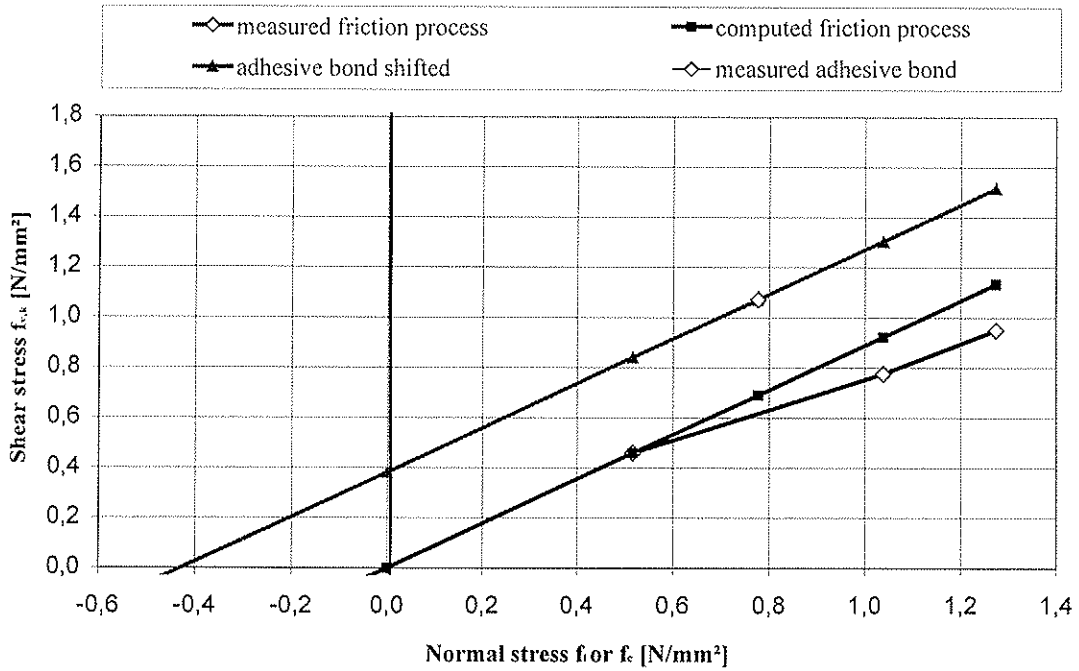
Figure 9: Determination of theoretical adhesive tensile strength by the
internal friction type BR

The straight line in figure 9 was shifted parallel into the measured value of adhesive bond
and extended into the negative range. The tangent with the angle φ defines the internal
friction. On the abscissa the theoretical detention adhesive tensile strength can be
determined.

5.2 Results of the adhesive tensile tests

In order to receive meaningful test results, to each type of the shear transfer a sufficient
number of short time tensile tests was realised.

With a specified experimental procedure and applied load history the following results for
the average adhesive tensile strength f_{jt} and the average failure energy were measured and
calculated (Table 2). The results of adhesive tensile strength perpendicular to the composite
joint represent a completion of the results of the shearing and friction tests.

Table 2: Average adhesive tensile strength and average friction energy

Type	Number	Average adhesive tensile strength [N/mm²]	Average friction energy [N/mm]
HZ/HV/BR	4	0,102	0,0249
HZ/HV/ZR	4	0,049	0,0113
HZ/HV/AR	4	0,018	0,0142
HZ/HV/GR	4	0,024	0,0047
HZ/HV/BV	4	0,123	0,7874
HZ/HV/ZV	4	0,093	0,8097

7

HZ/HV/AV	4	0,056	0,3886
HZ/HV/GV	4	0,016	0,0205
HZ/HV/BP	4	0,178	1,1157
HZ/HV/ZP	4	0,113	0,8787
HZ/HV/AP	4	0,103	0,8667
HZ/HV/GP	4	0,015	0,0156

For a better comparison of reached adhesive tensile strengths f_{jt} of the different variants of specimens were the average values of adhesive strengths f_{jt} confronted in figure 10.
The tensile strengths perpendicular to the joint result from the destabilisation phases and structural behaviour phases.

	Type P	Type V	Type R
Concrete	0,178	0,123	0,102
Cement screed	0,113	0,093	0,049
Anhydrite screed	0,103	0,056	0,018
Concrete of geopolymer	0,015	0,016	0,024
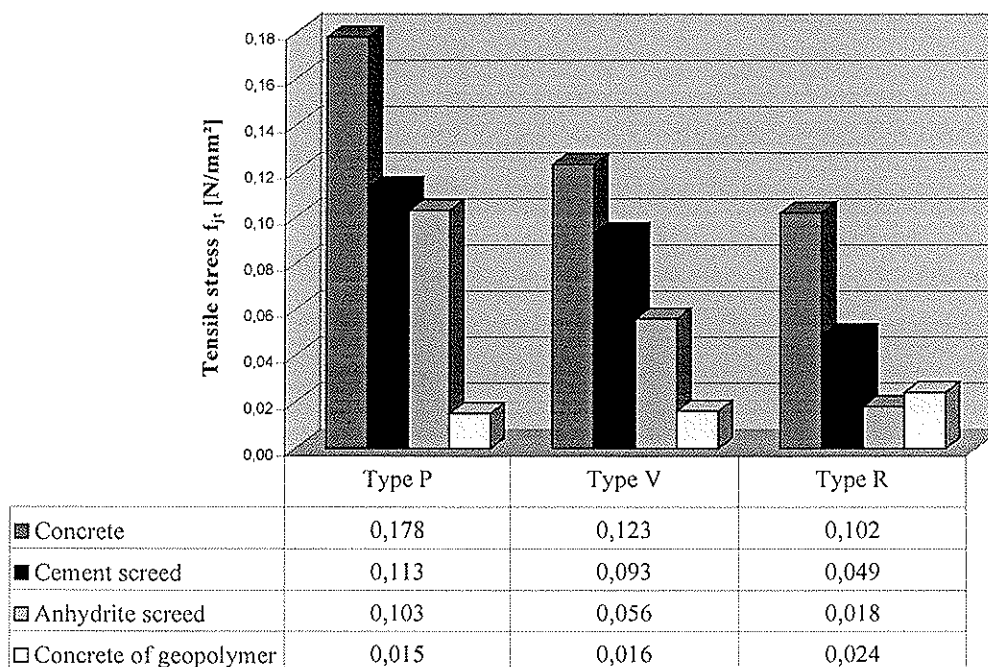
Figure10: Comparison of average tensile strength

In the following figure 11 the characteristics of the curve in principle of the test specimen variants BP, BV and BR are shown.
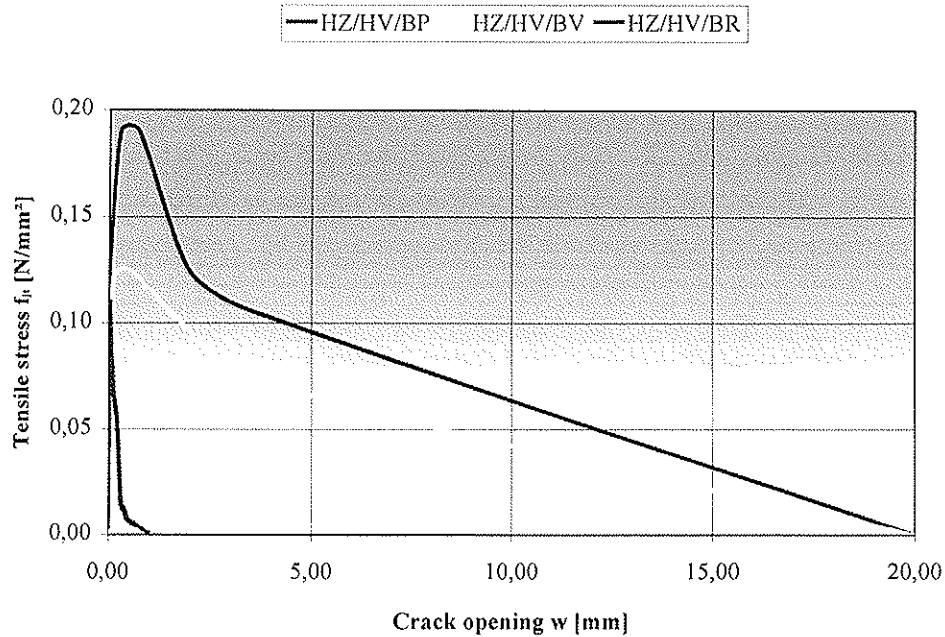
Figure 11: Stress-crack opening-curve of type BR, BV and BP with concrete surface layer

In a detailed comparison of the characteristics of the curve, depending upon type of specimen, different destabilisation phases are noticeable. For each component a certain portion of the entire destabilisation can be assigned:

- Phase I :   Failure of the adhesive bond between timber and mineral topping
- Phase II: Failure of the lateral profiles
- Phase III: friction of flank

Depending upon execution of the specimen occur the destabilisation phases mentioned above individually or in overlaid form. Finally the measured tensile strengths f_{jt} is to be compared with the theoretical tensile strengths $f_{jt}{}^*$ received by extension of the failure straight line to the shear tests $f_{jt}{}^*$. The figure 12 shows the result of the special specimens type BR, BV and BP.

	Type P	Type V	Type R
▨ fjt (measured)	0,178	0,123	0,102
■ fjt* (theoretical)	0,243	0,367	0,429
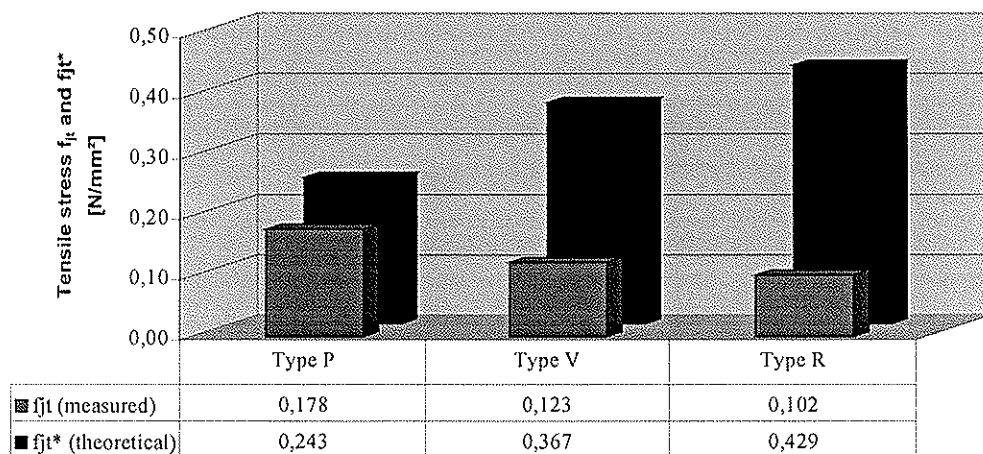
Figure 12: Comparison of the theoretical adhesive tensile strength with the measured adhesive tensile strength in example with concrete topping

9

6 Summary

Aim of the work was to examine by means of experiment the bond behaviour of nail-laminated timber elements and mineral surface layer without additional connecting devices. With the simplest formation of the composite joint, already a typical normal concrete on rigid wood surface, shear stresses can be transferred by $f_v = 0.38$ N/mm². The coefficient of friction between wood and concrete with the value $\mu = 0,9$ of normal concrete on even nail-laminated timber element well-known in the literature could be observed.

With normal concrete and profiled lamellas the shear stress amounted to $f_v = 0.42$ N/mm². The adhesive tensile tests confirmed the realisations of Griffith [7] that the actual tensile strength is smaller than the theoretical tensile strength received by the shear tests. Particularly high tensile strength f_{it} supplied the nail-laminated timber elements variant of the type P with a concrete surface layer (HZ/BP). The average tensile strength for this variant amounted about 0.18 N/mm². Compared with other bonds of material the reached tensile strength approximately corresponds to those of bond by stone on mortar.

The evaluation of the stiffness-crack opening curves showed different destabilisation phases dependent on nail-lamellas geometry. This differentiation represents a demarcation of the destabilisation procedures and thus a destabilisation model of the tested variants.

As a total result a formulation of the relationships between nail-laminated timber elements and mineral topping without separating layer is possible.

7 References

[1]   Allgemeine bauaufsichtliche Zulassung Z-9.1-473: Brettstapel-Beton-Verbunddecken mit Flachstahlschlössern; DIBT; Berlin 10/2002.

[2]   Blaß, H. J.; Ehlbeck, J., Schlager, M.: Trag- und Verformungsverhalten von Holz-Beton- Verbundkonstruktionen; Bauen mit Holz; Teil 1 (05/96) S.392-398; Teil 2 (06/96) S. 472-477.

[3]   Kreuzinger, H.: Holz- Beton- Verbundbauweise; Tagungsband Informationsdienst Holz

[4]   Lehmann, S.; Grosse, M.; Rautenstrauch, K.: New connector types of laminated timber concrete composite element joints; Proceedings of the International RILEM Symposium: Joints of timber structures; University of Stuttgart, 12 - 14 September 2001.

[5]   Meierhofer, U.A.: Anwendung von Holz- Beton- Verbund im Hochbau; Schweizer Ingenieur und Architekt Nr. 37 (09/94)

[6]   Minas, F.: Beitrag zur versuchsgestützten Bemessung von Profilblechverbunddecken mit nachgiebiger Verdübelung; Dissertation, Universität Kaiserslautern 1999.

[7]   Griffith, A. A.: The Phenomena of Ruptureand Flow in Solids; Philosophical Transaction, Royal Society of London, Series A, Vol. 221, 1920, pp. 163-198

[8]   Burkhardt, M.: Zum Tragverhalten von Stahlbeton-Verbundträgern mit nachgiebiger Verbundfuge unter Berücksichtigung nichtlinearen Tragverhaltens. Dissertation Hochschule für Architektur und Bauwesen Weimar 1991.

INTERNATIONAL COUNCIL FOR RESEARCH AND INNOVATION
IN BUILDING AND CONSTRUCTION

WORKING COMMISSION W18 - TIMBER STRUCTURES

MECHANICAL PROPERTIES OF TIMBER-CONCRETE JOINTS

MADE WITH STEEL DOWELS

A Dias

Coimbra University

Delft University of Technology

J W G van de Kuilen

Delft University of Technology

THE NETHERLANDS

H Cruz

LNEC

PORTUGAL

Presented by: Alfredo Dias

Alfredo Dias described the test programme which employed dowel type fasteners of 8 and 10 mm diameters. Timber specimens included spruce, maritime pine and chestnut. Comparisons were also made with reference to EC5. In general it was found that load capacity increased with concrete strength. And that in general, load capacity is conservative but that the slip modulus estimation is not conservative. He answered questions relating to the failure modes of the interlayer and the value of the embedding strength of the concrete and timber.

Mechanical Properties of Timber-Concrete Joints Made with Steel Dowels

A. Dias,

Coimbra University, Portugal

Delft University of Technology, The Netherlands

J.W.G. van de Kuilen.

Delft University of Technology, The Netherlands

H. Cruz.

LNEC, Portugal

1 Introduction

The effectiveness of a timber-concrete composite structure is highly dependent on the stiffness of the joints that connect the timber and the concrete. Many different types of joints have been developed and are already used in practice. One of the most used, for its simplicity and availability, are the dowel type fasteners. A research project was started in Coimbra University and Delft University of Technology (DUT) to improve the knowledge on the mechanical behaviour of these joints. Part of that research project consists of timber-concrete shear tests with dowel type fasteners with different conditions and materials. The results and analysis of those tests are presented. The results are also compared with the values computed using the equations given in EC5 part 1 and part 2.

2 Shear tests

2.1 Characteristics

Eight different configurations have been tested, six in Coimbra University and the other two at DUT (10mm-B and 10mm-INT). In Table 1 the most important characteristics for all test series are given. A wide range of situations is considered with the use of different timbers (maritime pine, "MP", chestnut "CH", Spruce) concretes (High strength concrete "HSC", Lightweight aggregates concrete "LWC"), dowel diameters ("8mm", "10mm") and interlayer ("10mm-INT").

Table 1.Configuration of the 8 tested series

Test	nr tests	joint	Timber	Steel	Concrete
CH	21	10mm-dowel[1]	Chestnut	480 [3]	48 [4]
MP	21	10mm-dowel[1]	Maritime pine	480 [3]	44 [4]
HSC	21	10mm-dowel[1]	Spruce	480 [3]	84 [4]
10mm-A	21	10mm-dowel[1]	Spruce	480 [3]	46 [4]
LWC	21	10mm-dowel[1]	Spruce	480 [3]	27 [4]
8mm	21	8mm-dowel[1]	Spruce	480 [3]	40 [4]
10mm-B	10	10mm-dowel[2]	Spruce	S500	50 [4]
10mm-INT[5]	10	10mm-dowel[2]	Spruce	S500	47 [4]

[1] – Reinforcement smooth bar ,[2] – Reinforcement bar with ribs, [3] – Mean value of ultimate tensile strength of the bars used in MPa,[4] – Mean value of compression strength of concrete used in each series, [5] – Interlayer made of spruce planks with 20mm thickness nailed with 2 nails/plank to the timber blocks

A middle concrete member and two side timber members constituted the test specimens as presented in Figure 1.

The fastener holes were pre-drilled with the same nominal diameter as the dowel. In all the joints, either a thin plastic film or paint, was applied between the timber and concrete, in order to prevent friction and movement of water.

**Delft
University**

**Coimbra
University**
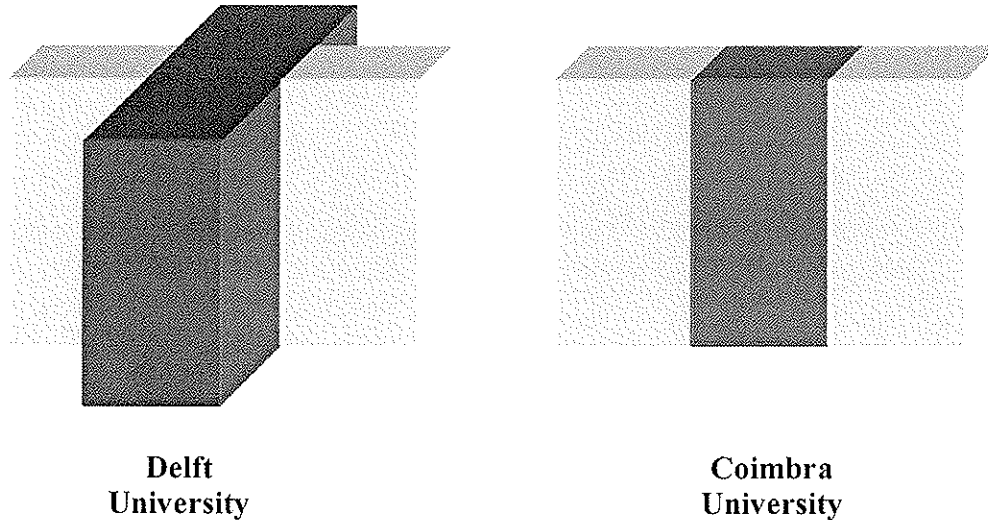
Figure 1. Test specimens configuration

The dimensions and characteristics of the tests performed in Delft and Coimbra were slightly different. The most significant difference is the use of only one fastener for each shear plane in Coimbra and two in Delft.

All the tests were performed according to EN26891 (1991); the estimated loads were evaluated based on preliminary tests. The displacement was measured on four sides of the specimen, as shown in figure 2
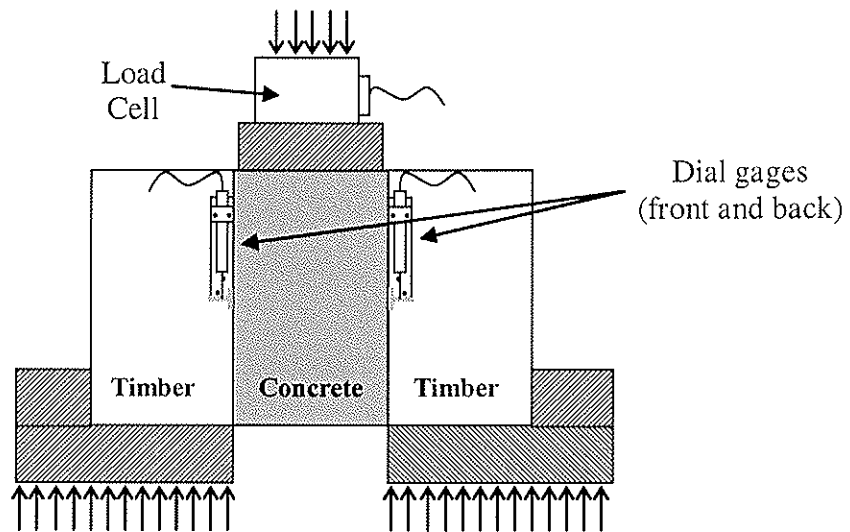
Figure 2. Test specimens set up

On the tests specimens with interlayer, the slip of the planks against the concrete member was also measured, at the same four points.

2.2 Characterization of the materials used

The purpose of this research was to study the mechanical behaviour of timber-concrete joints with different materials and conditions. For that reason, a good evaluation of the

mechanical properties of the materials involved in the shear tests was required. The followed procedure was the experimental evaluation of those properties, which was done for timber, concrete and steel. Particular attention was given to the timber because of the relatively high scatter in mechanical properties but also because the timber has the largest influence on the behaviour of the joint.

For concrete cubes (15cm side) were tested in series of three, on at least 4 ages in order to assess density and compression strength.

In order to evaluate the steel properties, tension tests were performed, one for each bar that was used and from them both the yield strength, tensile strength and modulus of elasticity were determined. The dowels used at DUT were produced from reinforcement bars of steel S500, for that reason the mechanical values from the standard were considered as accurate enough and no tests were performed.

For timber, two different situations occurred. At DUT only spruce was used. Since it is a timber with very well known mechanical properties, only some samples were collected to determine the mean value of the density and the moisture content. At Coimbra University all the timber specimens were conditioned at 20 °C and 65% air humidity. For those specimens the density was determined and embedding tests performed. That was done for each one of the timber pieces used on the shear tests. In order to assess embedment properties as close as possible from the shear test, the samples were collected from the part of the timber block immediately next to the area affected by the shear test, as can be seen from Figure 3.
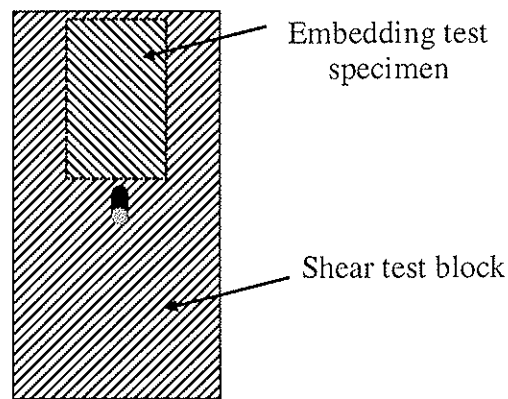
Figure 3. Collected timber for the embedding test

2.3 Presentation of the results

Almost every test specimens reached the displacement of at least 15mm, as stated in EN 26891. In two tests, one from the series 10mm-B and another from the series 10mm-INT, cracks developed in the concrete block causing early failure of the test specimen. That occurred for displacements of 8.8 mm and 14.6mm respectively.

On the CH series the steel dowels have reacted with the chestnut timber during the curing period forming a cover of rust around the dowel. That corrosion has increased the friction between the timber and the steel. After the test, when the dowels were separated from the timber a mean value of around 8 kN was obtained for the pulling-out.

The parameters from EN26891 (1991) were computed and on Table 2 are presented the mean values, the standard deviation and the characteristic values from the load capacity and slip modulus for all the tests series. The characteristic values were computed

considering the 0.05 fractile and a confidence level of 0.75 according with ISO 2394 (1998).

Table 2. F_{max} and k_{ser} values from the tests

Strength – F_{max} (kN)				
Test	**Nr tests**	**Mean value**	**Standard deviation**	**Characteristic value**
CH	21	26.2	1.8	22.7
MP	21	25.5	2.1	21.4
HSC	21	23.6	1.8	20.2
10mm-A	21	22.6	2.2	18.3
LWC	21	18.5	0.67	17.2
8mm	21	13.6	0.74	12.2
10mm-B[1]	10	34.3	3.0	27.9
10mm-INT[1]	10	31.7	1.48	28.6

Stiffness – k_{ser} (kN/mm)				
Test	**Nr tests**	**Mean value**	**Standard deviation**	**Characteristic value**
CH	21	30.4	6.7	17.5
MP	21	24.4	6.7	11.4
HSC	21	13.8	3.7	6.7
10mm-A	21	15.2	4.1	7.2
LWC	21	14.5	3.7	7.3
8mm	21	11.5	1.9	7.9
10mm-B[1]	10	17.1	3.2	10.5
10mm-INT[1]	10	11.1	1.4	8.3

[1] – The results presented are referred only to two joints of the four tested in each test

3 Analysis of the Results

3.1 Comparison between series

A general analysis of the results shows that the scatter for the strength properties is much lower than for stiffness properties. Although it was intended to vary only one property from series to series, there is always some variation in the concrete, in steel and particularly in timber properties. However, these variations are relatively small and the following conclusions are thus allowed.

Influence of concrete quality

Three different types of concrete were considered: lightweight aggregates, normal and high strength concrete whose compression strength mean values were found to be 27, 46 and 84 MPa respectively. Since these concrete types cover a wide range of compression strengths any relevant influence in the behaviour of the joints should become clear on this research.

The values of the load carrying capacity of the joints show some difference for different concrete types, 23.6, 22.6 and 18.5 for high strength, normal and lightweight aggregates concrete respectively. These results indicate that the load capacity increases with the

4

compression strength of the concrete. The higher difference between lightweight aggregates and normal may indicate that the influence is higher for concretes with low strength. The explanation for this may be that for higher strength concretes, the damage of the concrete is relatively small compared to the damage in the timber, in other words, the concrete act as a perfect constraint and then the damage on timber has increased its importance.

No evidence of a relation between the slip modulus and concrete strength can be found from these results. Indeed, the results of the series with normal concrete show the highest slip modulus; it is followed by lightweight aggregates concrete and, the lowest one, correspond to the high strength concrete. Since the slip modulus is calculated with slip values from the beginning of the test, no damage in concrete has occurred yet and the strength properties do not influence it. However, the compression strength of concrete is somehow connected with its elasticity modulus and then some relation could be expected. According with EC2 the elasticity modulus of the used concretes should be around 29, 34 and 42 GPa for lightweight aggregates, normal and high strength concrete respectively. One explanation could be that the deformations on concrete are small compared to those in timber at these low load levels. The differences in the slip modulus would then be also small and could easily be hidden by other effects such as hole clearance or friction between timber and concrete.

Timber

Two softwood species, spruce and maritime pine and one hardwood, chestnut, were used. The mean density values were found to be respectively, 454, 584 and 566 kg/m^3.

Looking at the results it becomes clear that the load carrying capacity of the maritime pine (MP) series is only slightly lower than the chestnut (CH) (3%) while the spruce (10mm) difference is almost 14%. The same calculations for slip modulus show a difference of around 20% from chestnut (CH) to maritime pine (MP) and 50% from spruce to chestnut. The influence of the density in the mechanical properties seems to be much higher for slip modulus than for the load carrying capacity.

The higher values of the mechanical properties values from the chestnut compared to maritime pine are probably due to the higher friction between timber and dowel in the chestnut series.

Influence of interlayer

The presence of interlayer decreases the mechanical performance of the joints. The value of the shear strength decreases around 8% and the slip modulus decreases around 35% as compared to similar joints without interlayer. The measurements of the slip indicate that for small deformations, the connection planks-timber is weak, however, for larger displacements that connection becomes more effective and is already able to take some load, which came in line with the shear tests results.

3.2 Models from EC5 and others

Rules to design timber-concrete joints with dowel type fasteners are given in EC5 part 2 (1997). The design rules presented there are based on the models for timber-timber joints presented on EC5 part 1 (2003), equations 1 to 3. The equations for timber-concrete are the same, but the results may be increased up to 20% for the load capacity and 100% for the slip modulus.

The load capacity of timber-timber joints, when β is considered as equal to 1, is given by:

$$F = \left[1.15\sqrt{2M_{y,Rk}f_{h,1,k}d} + \frac{F_{ax,Rk}}{4} \right]$$ (1)

Where:

$f_{h,1,k} = f_{h,2,k}$ - is the embedding strength of the timber members,

$\dfrac{F_{ax,Rk}}{4}$ - is the withdrawal capacity which shall be considered 0 for dowels,

$M_{y,Rk}$ - is the yielding moment of the dowel and can be calculated from:

$$M_{y,Rk} = \frac{f_u}{600}180d^{2.6}$$ (2)

where f_u is the tensile strength of the dowel.

The slip modulus of timber-timber joints is given by:

$$K_{ser} = \left[\frac{\rho_m^{1.5}d}{23} \right]$$ (3)

Where

d - is the diameter of the dowel,

ρ - is the mean value of the density of the timber in kg/m^3.

For joints with interlayer, the EC5 (1997) does not give calculation models and advises that the design values should be based either on suitable numeric models or on experimental work. In the literature, a model was presented by Blass and Laskewitz (2003), that considers the interlayer in the calculations of the load capacity of this type of joints. This model is given in equation 4, considering once again the value 1 for β:

$$F = f_{h,1}d\frac{1}{2}\left(-t_{zw} + \sqrt{t_{zw}^2 + 8\frac{M_y}{f_{h,1}d} + \delta t_{zw}^2} \right)$$ (4)

where:

$$\delta = \frac{f_{h,zw}}{f_{h,1}}$$

$f_{h,zw}$ - is the embedding strength of the interlayer member,

t_{zw} - is the interlayer thickness.

The values of material properties of the shear test specimens were used in the equations. Since each of these shear tests was composed of two joints, each one of them was computed independently, using equations 1 to 3, adding both results and then multiplied it by the factors given on EC5 part 2 (1997) for timber-concrete joints as presented on Equation 5.

$$f_{SST} = C \times \left[f_1(\text{joint 1}) + f_2(\text{joint 2}) \right]$$ (5)

where :

6

f_{SST} - is the expected value for the shear test,

f_1 and f_2 - are the values expected for each single joint

C – 1.2 for load capacity and 2 for slip modulus in accordance with EC5 part 2, for joints with interlayer no values are given so it was considered 1.

3.3 Analysis of results

Calculations of the load carrying capacity and slip modulus were done for all geometries. The correlation coefficients between the calculated data (according with EC5) and the data from the tests are presented in Table 3 for each test series. On the same table are also presented the mean values of the relation between the theoretical model and the experimental results for each series.

Table 3. Correlation coefficient and relation between experimental and models data

Test Series	F_{max} EC5/Experimental		k_{ser} EC5/Experimental	
	Ratio (mean value)	Correlation coefficient	Ratio (mean value)	Correlation coefficient
CH	0.80	0.37	0.79	no correlation
MP	0.85	0.86	1.1	0.70
HSC	0.81	0.83	1.3	0.66
10mm-A	0.88	0.87	1.2	0.33
LWC	0.98	0.61	1.2	0.46
8mm	0.90	0.64	1.2	0.44
10mm-B	0.51/0.58 [1]	*	0.93	*
10mm-INT[2]	0.28	*	*	*

[1] – considering f_h given by the equations from EC5 / considering f_h determined from tests

[2] – on the calculations δ was considered $=2/3$ (Equation 4)
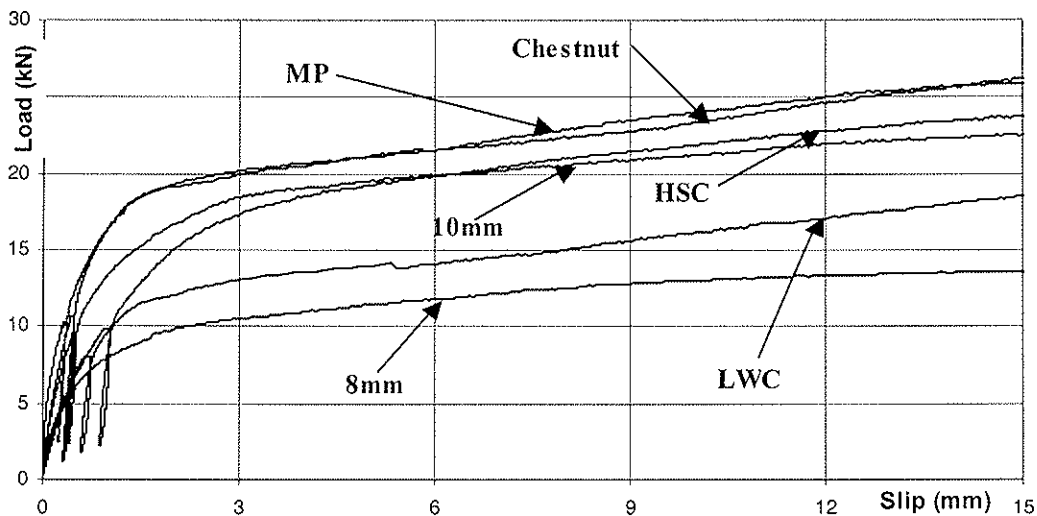
Figure 4. Mean load-slip diagrams for each series

The numerical modelling results and test data were also plotted in diagrams from Figure 5 and Figure 6. On those diagrams only the categories HSC, LWC, 10mm-A and MP are

7

plotted, because for a number of reasons the results from the other series are not comparable.
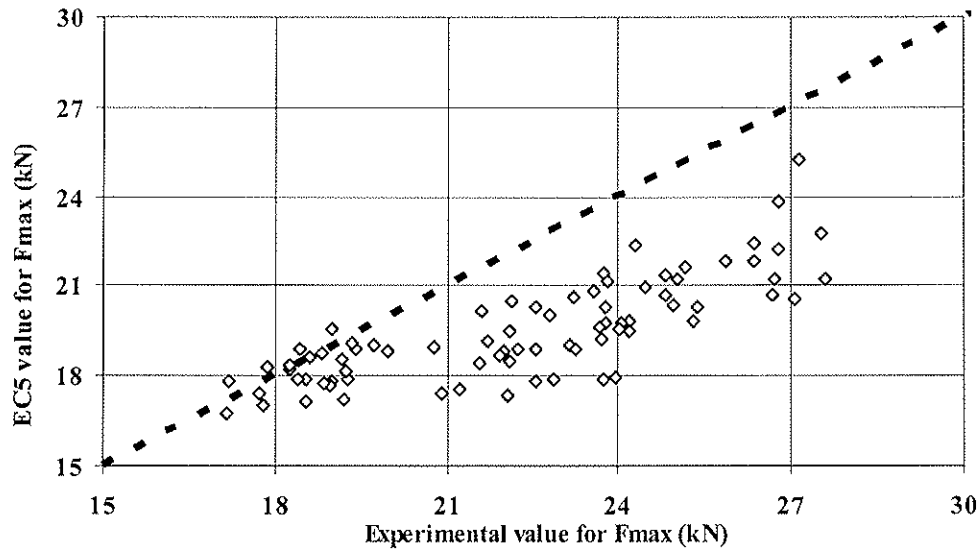
Figure 5. Experimental versus theoretical results for the load capacity
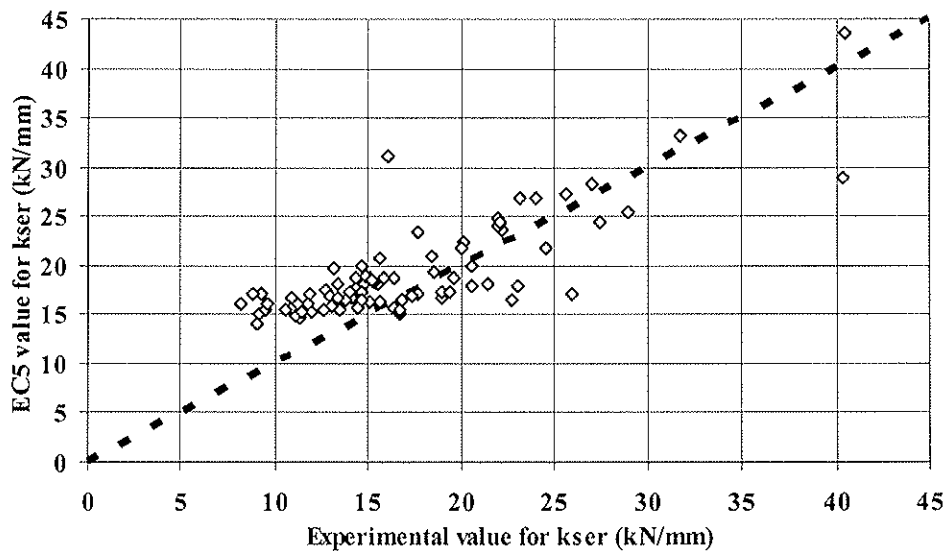
Figure 6. Experimental versus theoretical results for the slip modulus

Referring to Table 3, a different behaviour of the series with chestnut in comparison to the others can be detected. Not only the relations between model and experimental data show a different tendency but also the correlation coefficients between those values are much weaker for the chestnut series. The discrepancy may be due to the corrosion on the fasteners surface at the time of the tests.

Load carrying capacity

The results presented on Table 3 show that the estimation made with the models given in EC5 tend to underestimate the experimental value of the load capacity of the joints with differences from 2% to almost 50%.

A more detailed analysis of the results reveals that the ratio EC5 model-experimental results decreases with the increase of the compression strength of the concrete. The value

8

for lightweight aggregates concrete is 0.98 and for high strength concrete is 0.81, while the values for normal concrete are between those two. This argument strengthens the idea that the concrete compression strength influences the load capacity. Higher compression strength leads to a higher load carrying capacity of timber-concrete joints.

The values given by EC5 for CH series are only 80% of the values from the tests. However, that situation would change if a pulling out strength $F_{ax,Rk}$ would have been considered in the models due to the high friction as a result of rust of the dowels. Considering a pull-out strength of 8 kN (reasonable enough when considering the values measured for pulling-out) the relation would increase from 0.80 to 0.87, which is in line with what was found in other categories with normal concrete.

Slip modulus

The models given in EC5 to determine the slip modulus of dowel type fasteners joints overestimate the experimental value. In average, they are 20% higher than the values found in the tests. Only in the chestnut series the opposite occurred, the EC5 values are 20% lower than the theoretical value. On that series the test results indicate a decrease in slip modulus with an increase of the timber density. But here friction seems to have masked the results.

The correlation coefficients between experimental and theoretical results are always smaller than for the load carrying capacity on the same series. The main reason for that should be the problems and difficulties in the evaluation of the stiffness properties as described before.

4 Conclusions

The results presented here show that the load carrying capacity of timber-concrete joints is, among others, affected by the compression strength of concrete, a parameter that until now has been disregarded. On the other hand, no indications were found of any influence of the concrete strength on the slip modulus of the joints.

Both slip modulus and load carrying capacity are affected by the timber density and embedding strength. However, the effect on slip modulus seems to be much higher.

The effect of an interlayer is again higher for the slip modulus than for the load carrying capacity. In both cases the mechanical properties decrease if the interlayer is present.

This research found some indications that the effect of friction of smooth dowels may not be always negligible on these kind of joints, however further research is needed to confirm it.

The models given in the EC5 for the load capacity of these joints seem to be able to evaluate their actual load carrying capacities. The values from the models are always conservative when compared with the experimental data. Nevertheless these results also show that the properties of the concrete could be considered in the models, giving values with increased accuracy. Considering these results, the load carrying capacity of joints with concretes of higher classes, for instance of strengths of 60 MPa and more, could benefit from an increase of up to 20 %.

The ability of the model presented in EC5 to evaluate the slip modulus also seems to be good. However the values given by those models are always around 20% higher than the ones obtained from tests. That may indicate that the factor 2 given in EC5 part 2 (discarding the deformations of the concrete) is too high on this situation.

Acknowledgements

References:

EC5 (2003), Design of timber structures. Part 1-1- General rules and rules for buildings, CEN 2003.

EC5 (1997) , Design of timber structures. Part 2- Bridges, CEN 1997

EC2 (1997), Design of concrete structures. Part 1-1- General rules and rules for buildings, CEN 1997.

EN 26891 (1991), Joints made with mechanical fasteners – General principles for the determination of strength and deformation characteristics, CEN 1991.

ISO 2394 (1998), General principles on reliability for structures, 1998

Blass, H.J. ; Laskewitz, B., (2003) Tragfahigkeit von Verbindungen mit stiftformigen Verbindungsmitteln und Zwischenschichten, Bauen mit holz, 1/2003, pp. 26-35.

**INTERNATIONAL COUNCIL FOR RESEARCH AND INNOVATION
IN BUILDING AND CONSTRUCTION**

WORKING COMMISSION W18 - TIMBER STRUCTURES

COMPARISON OF HYSTERESIS RESPONSES OF DIFFERENT SHEATHING TO FRAMING JOINTS

B Dujic
R Zarnic

University of Ljubljana, Faculty of Civil and Geodetic Engineering

SLOVENIA

Presented by: Bruno Dujic

Bruno Dujic discussed the need for the research presented and the two-stage mathematical model of wood frame structures used. The experimental work involved 6 different joint configurations employing 3 specimens for each configuration. He concluded that the simulation of non-elastic behaviour of nailed connection is of crucial importance for the successful prediction of the behaviour of timber framed walls and timber structures subject to seismic excitation. Bruno's presentation was followed by an interesting discussion regarding to the use of the damping values obtained in relation to timber structures and their implications for design codes.

Comparison of Hysteresis Responses of Different Sheathing to Framing Joints

B. Dujic and R. Zarnic

University of Ljubljana, Faculty of Civil and Geodetic Engineering, Ljubljana, Slovenia

Abstract

Paper discusses the behaviour of six different configurations of single shear joint under cyclic load. The joints represent connection between timber frame elements and different sheathing plates with nails and steel staples. The kinds of joint specimens are based on typical construction types of European light timber-frame buildings. Four typical sheathing plates are generally used in European timber frame construction industry: oriented strand board, cement-splinter board, gypsum-fiber board and particleboard. Six series of different joints were loaded parallel to the wood fibers of framing member with increasing amplitudes of cyclic load. The analysis is focused on comparison of hysteretic behaviour of different sheathing to framing connections with stiffness deterioration and strength degradation between the first and the last repeated cycle at the same slip in joint, dissipation of energy by hysteresis loops, the equivalent viscous damping ratio and the failure mode.

1 Introduction

Earthquake resistance of timber frame buildings is in the great extend governed by connectors that tie together structural elements and entire structure to foundations. Fasteners and anchors play also an important role of energy dissipaters and controllers of dynamic properties of structural system. They might be designed and constructed as engineered devices but also the ordinary ones give their valuable contribution to behaviour of structure while exposed to dynamic load. The behaviour of connectors together with connected parts of structure may be considered as cyclic while entire structure is under dynamic excitation. This assumption enables relatively simple procedure of testing [1], [2] and [3] where only the choice of loading protocol is an issue to be carefully taken into account. Data on cyclic response of joints are valuable source of information needed for development, calibration and verification of inelastic computational models of timber frame buildings. There is a constant need for databases of behaviour of different structural connections and joints are one of them [4]. The variety of joint design, mechanical properties of local materials, types of fasteners and sheathings demand an extensive worldwide testing campaign that enables comparison of behaviour of different joint configurations and looking for possibilities of potential generalisation of behavioural mechanisms.

There are four major types of sheathing to framing joints that can be found in timber frame buildings produced in Slovenia that are also exported to European market. Due to lack of data on their behaviour, they were recently tested by cyclic loading in laboratory at Faculty of Civil and Geodetic Engineering, University of Ljubljana, Slovenia. The main purpose of testing was obtaining data needed for modelling of inelastic response of lateral resistance of timber-frame walls [5] and seismic response of timber-frame buildings [6].

2   Cyclic tests of joints

Altogether 6 different joint configurations were prepared for testing, three samples of each (Table 1, Fig. 1a). All specimens were made of the same type of wood and different sheathing plates fastened with different types of fasteners (Fig. 2). All materials used for preparation of specimens are available on Slovenian market and are regularly used by Slovenian wooden house producers. The only exception is annularly threaded nail that is common on Canadian market. The specimens with Canadian type of fastener were tested to be compared with other tested ones. Only the upper half of sheathing plate was fixed to wood frame element with tested fasteners. Nails were hammered in wood parallel to grain direction and staples with angle of 45° between the direction of staple crown and grain direction. The lower part of board was glued to wood element have higher shear resistance than upper part. Wooden elements were gripped with toothed metal plates that provided uniform distribution of acting force. Gripped specimens were fixed in Amsler HA 100 servo hydraulic testing machine and tested according to [7] and [8] with cyclic loading following the refined protocol. Load protocol is shown in Fig. 3.
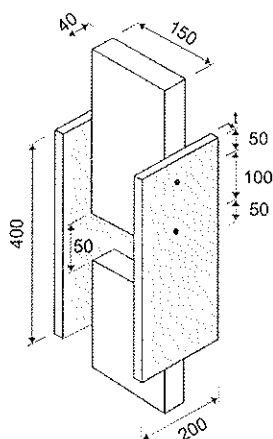
Figure 1: Sketch of specimen   *Figure 2: Fasteners in order as listed in Table 1*
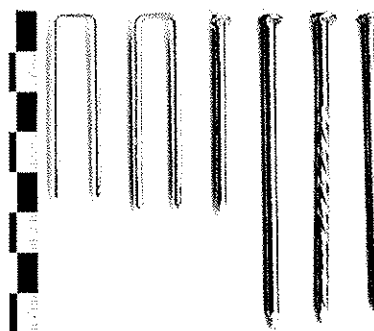
Table 1: Configuration and properties of tested specimens

Name	Frame	Sheathing	Fastener
GFB	SPF (spruce-pine-fir) 40/150 mm	gypsum-fiber board, t = 15 mm	steel staple NIKO 1.34 x 1.62/47 mm
CSB		cement-splinter board, t = 16 mm	steel staple Haubold 1.83 x 2.06/50 mm
PB_smN		particle board, t = 10 mm	smooth nail, 2.5/50 mm
OSB_smN		oriented strand board t = 11 mm	smooth nail, 3.1/80 mm
OSB_spN			spiral nail, 3.1/80 mm
OSB_anN			annular nail, 2.8/75 mm

The load protocol consisted of two parts that divided tests in two phases. Within the first phase the loading rate was 0.1 mm/s and in the second one 0.5 mm/s. Each displacement level was repeated three times as shown in Fig. 4. The protocol was designed following the idea of

applying significant number of cycles under the yield limit of joint and post yield cycling with following linear ascending ramp of amplitude. After reaching the load-carrying limit of joint, test continued monotonically until joint failure.
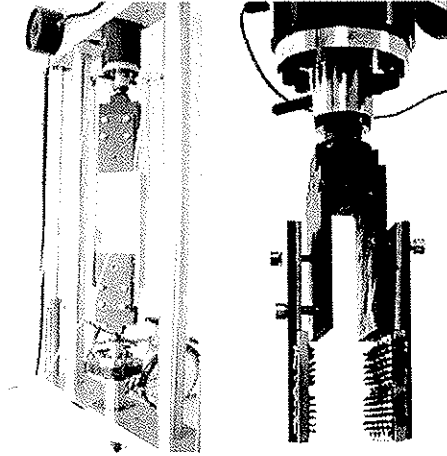
Figure 3: Specimen fixed in servo hydraulic testing machine Amsler HA 100 and detail of toothed metal plate
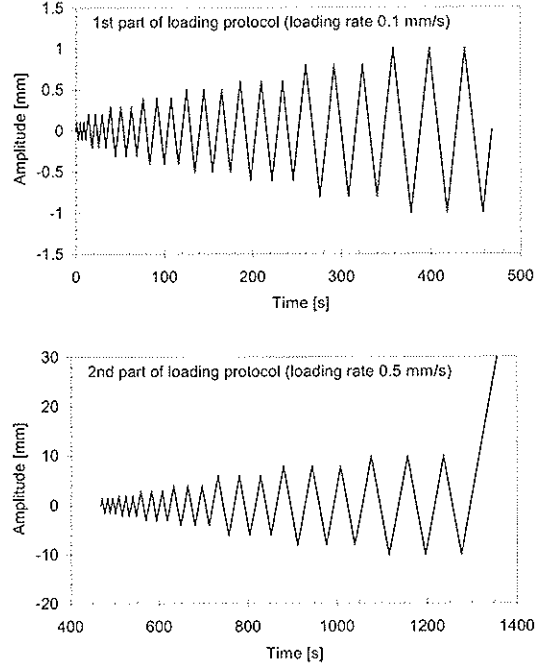
Figure 4: The quasi-static cyclic loading protocols.

3 Cyclic behaviour of joints

The main sources of information regarding response of joints on cyclic load are hysteresis loops obtained during testing and post failure visual inspection of tested joints. In following figures 5, 6 and 7 are presented typical load vs. joint slip relationships and other relations derived from hysteresis loops. Each type of tested joints is presented with typical hysteresis, comparison of envelopes of all three specimens of kind with calculated average envelope, stiffness vs. joint slip relationship and equivalent viscous damping vs. joint slip relationship. Presented envelopes were calculated as average envelopes of positive and negative branch of envelope obtained by testing. The stiffness of single hysteresis loop was defined as straight-line approximation between the positive and negative peak of a hysteresis loop according to [9]:

$$K^i = \frac{F^i_{max} - F^i_{min}}{\delta^i_{max} - \delta^i_{min}} \tag{1}$$

where F_{max} and F_{min} are peak values of attained load in observed positive and negative cycle and δ_{max} and δ_{min} are the corresponding joint slips. The equivalent viscous damping was calculated from hystersis using the equation suggested in [10]:

$$V_{eq} = \frac{E_d}{2\pi \cdot E_p} \tag{2}$$

where E_d is dissipated energy per cycle and E_p is available potential energy.

GFB

CSB
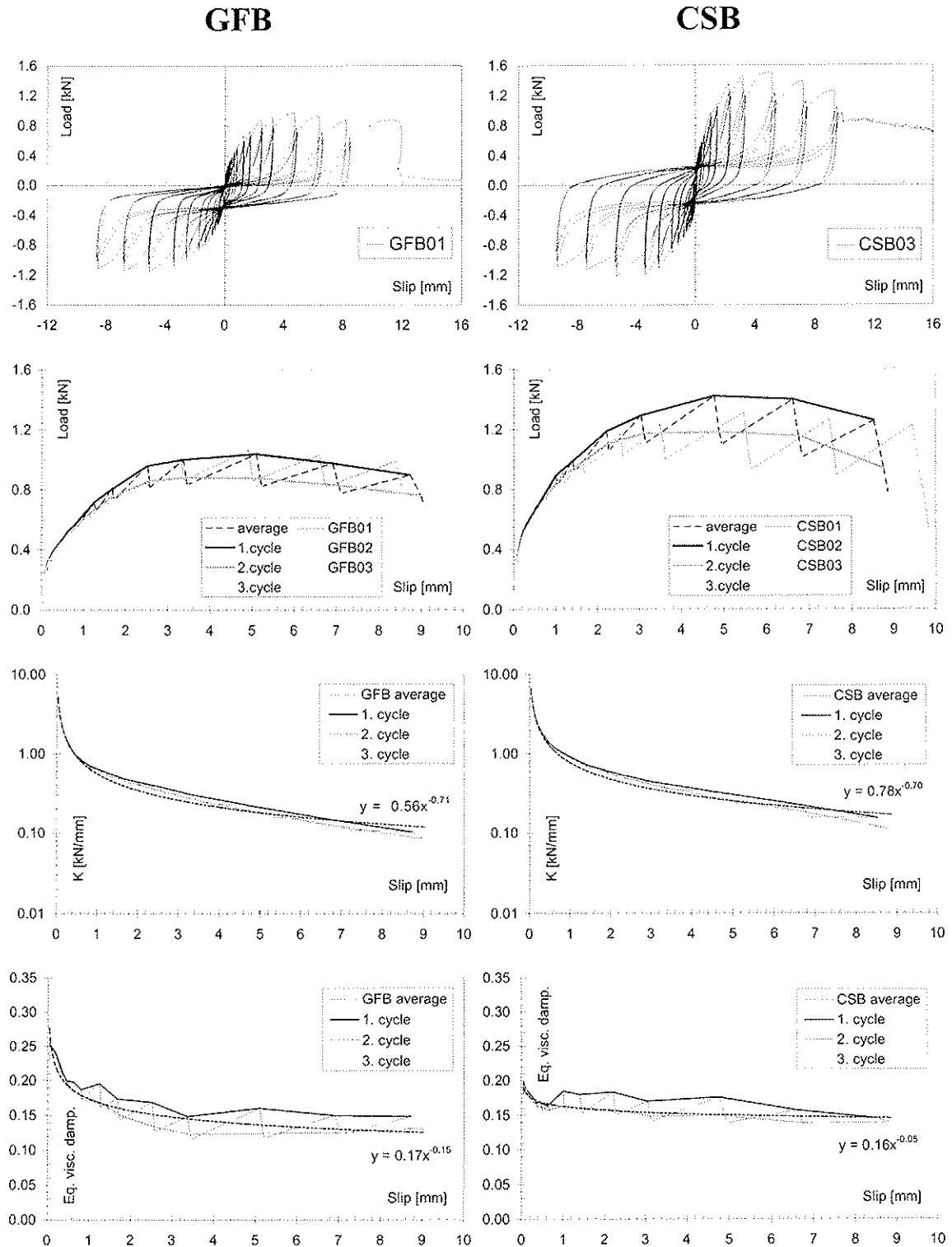
Figure 5: Response diagrams of gypsum fiber board fastened with steel staples to SPF wood

Figure 6: Response diagrams of cement splinter board fastened with steel staples to SPF wood

PB_smN
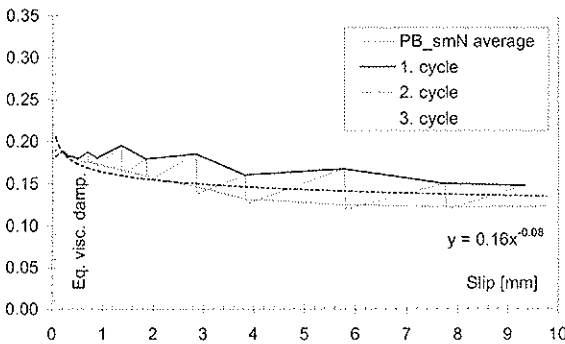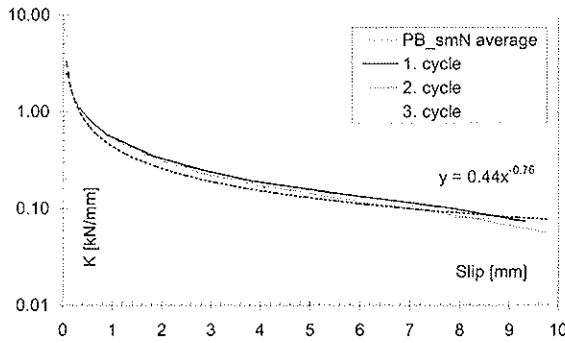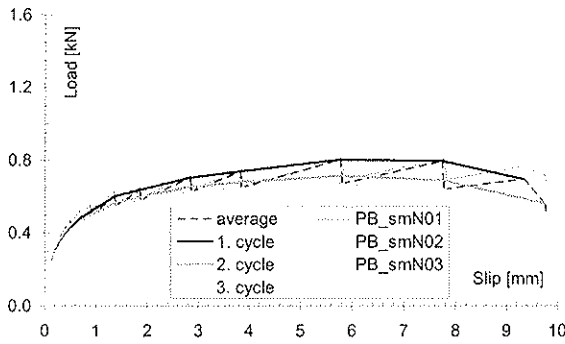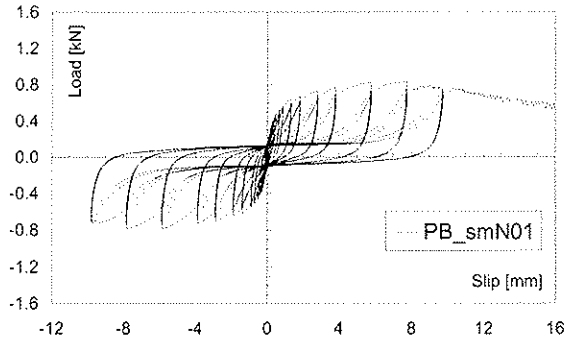
OSB_smN
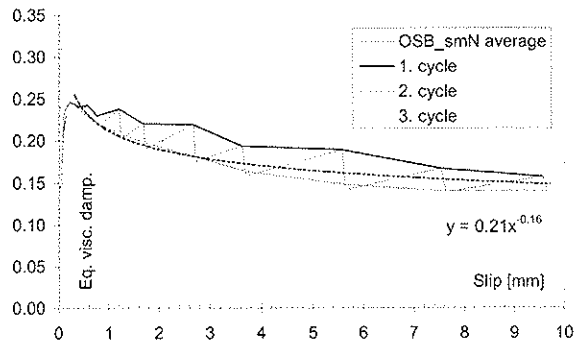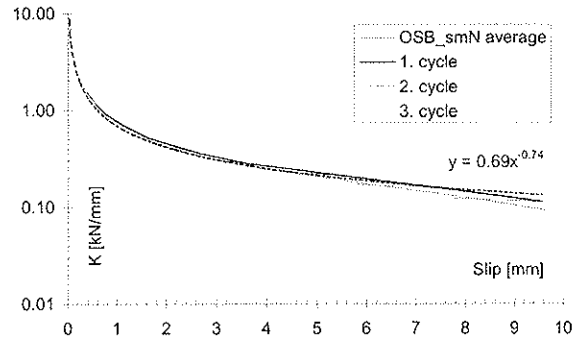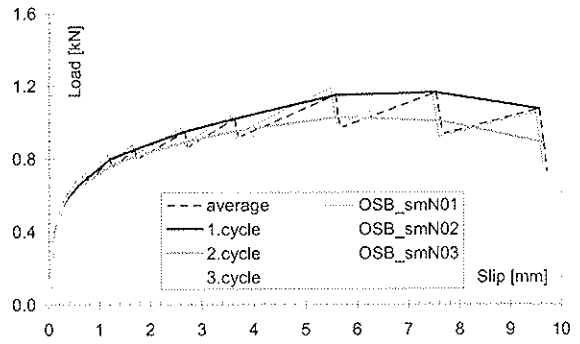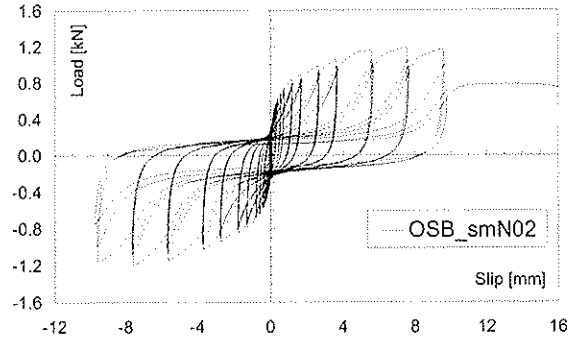
Figure 7: Response diagrams of particle board fastened with smooth nails to SPF wood

Figure 8: Response diagrams of oriented strand board fastened with smooth nails to SPF wood

OSB_spN

OSB_anN
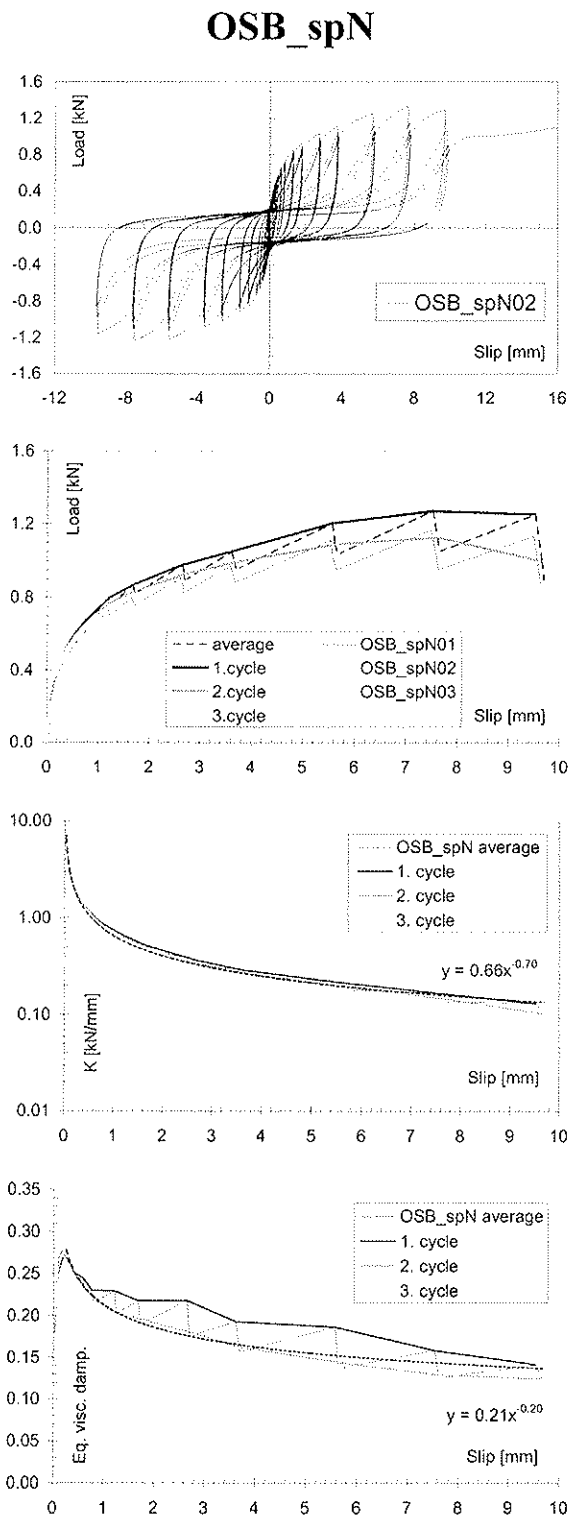
Figure 9: Response diagrams of oriented strand board fastened with spiral nails to SPF wood
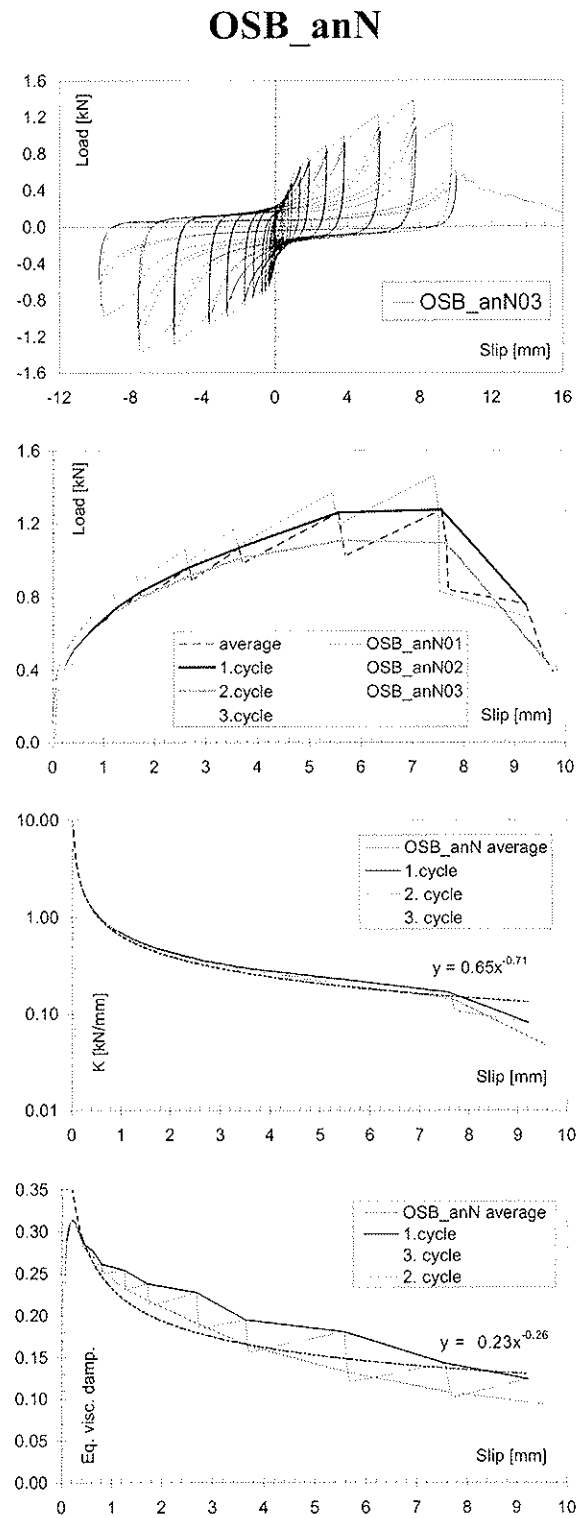
Figure 10: Response diagrams of oriented strand board fastened with annular nails to SPF wood

From above diagrams, some general observation may be highlighted. In the cases of nailed joints, the ultimate load was attained at higher magnitudes of joint slips. Two different failure modes were observed in cases of nailed joints and only one in the cases of stapled joints (Figure 11). Nails having smaller diameter failed due to fatigue after forming plastic hinge inside wooden element in depth approximately equal to thickness of sheathing plate. Joints having thicker nails failed with pull-through of nail head while nails exhibit plastic deformations. In both cases of stapled joints staples gradually pulled out of wood element and plastic hinge formation moved along the staple legs. Stapled joints show significant post ultimate load ductility due to described failure mechanism. Generally, all failures occurred after the last cycle defined in load protocol.

(a)　　　　(b)　　　　(c)　　　　(d)　　　　(e)
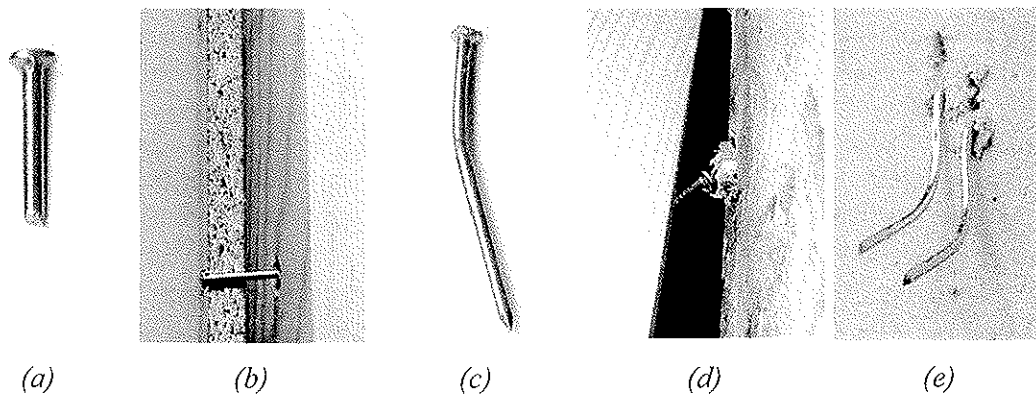
Figure 11: Different failure modes of joints: plastic hinge failure of nail (a), (b) as observed in cases of PB_smN and OSB_anN, plastic hinge deformation ending with pull-through of nail head (c), (d) as observed in cases of OSB_smN and OSB_spN and plastic hinging along the staple legs (e) as observed in cases of GFB and CSB

4 Discussion of test results

Three sets of parameters obtained from test results are chosen for discussion of joint behaviour. The first one deals with major events observed from envelope curves. The second set of parameters describes load degradation and stiffness deterioration. The third one is related to the equivalent viscous damping calculated from hysteresis loops.
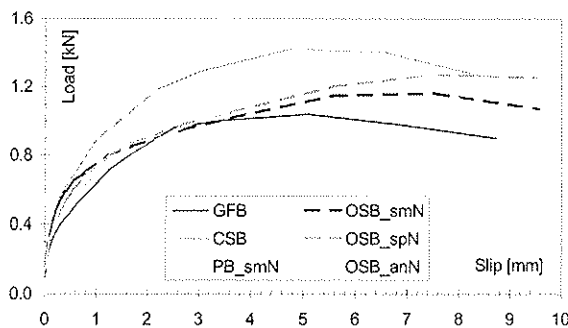
Figure 12: Comparison of average envelopes of the first cycles
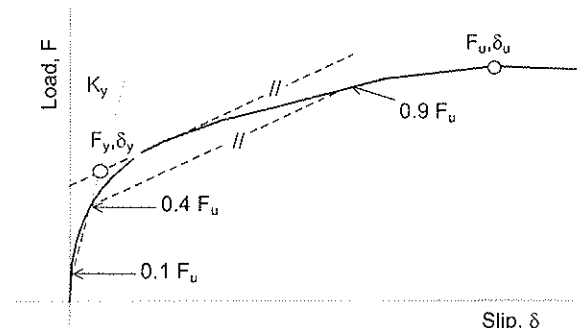
Figure 13: Definition of Yield Limit State (YLS)

In Figure 12 the average envelops of the first cycles of each tested joint configuration are presented. The purpose of herein reported tests was not the comparison of joints based on their load capacity but based on the mechanisms of their behaviour. It is clear that the type of fastener due to its geometrical and mechanical characteristics governs the load carrying capacity of joint. In our case wood element were made of the same sort of wood. However, basic information about the parameters of average hysteresis envelopes are summarized in Table 2. From the hystersis envelopes Yield Limit State (YLS) and Ultimate Limit State (ULS) can be identified. There are various approaches to YLS and ULS definitions. Both can be observed as events that signify the demarcation between two behaviour states. YLS is defined as the transition of the specimen behaviour from elastic to inelastic response. Often YLS is defined as the point of intersection of secants or/and tangents on the skeleton curve of hysteretic response of joints. In our case, YLS was defined as the point of intersection between two lines. The lines are the secant of the skeleton curve defined by points at 0.1 F_u (10 % of maximal horizontal load capacity) and 0.4 F_u and tangent on the upper part of the envelope, which is parallel to the secant through the skeleton curve at 0.4 F_u and 0.9 F_u (Fig. 13).

Ductility is defined as ratio between ULS and YLS slip and post ULS ductility as ratio between slip corresponding to 10% lower of post ULS and YLS slip. The interesting finding of test comparisons is that the ratio between ultimate and yield load is in range between 0.5 and 0.6. All tested joints exhibit ductility regarding ULS over value of 10.

Table 2: The parameters of average hysteresis envelop (F – force, δ - joint slip)

Name of specimen	YLS			ULS		F_y/F_u	Ductility $d_u=\delta_u/\delta_y$	Post ULS ductility $d_f=\delta_f/\delta_y$
	K_y [kN/mm]	F_y [kN]	δ_y [mm]	F_u [kN]	δ_u [mm]			
GFB	1.15	0.51	0.45	1.04	5.10	0.49	11.4	17.5
CSB	1.69	0.74	0.44	1.42	4.77	0.52	10.9	18.7
PB_smN	1.19	0.48	0.40	0.80	5.78	0.60	14.3	22.2
OSB_smN	2.18	0.66	0.30	1.16	7.54	0.57	24.8	27.5
OSB_spN	1.33	0.70	0.53	1.27	7.53	0.55	14.3	26.5
OSB_anN	1.13	0.65	0.57	1.27	7.56	0.51	13.1	14.1
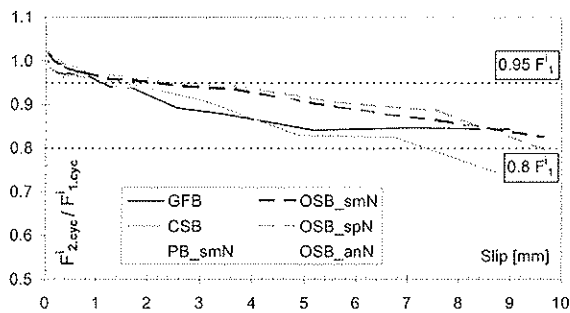
Figure 14: Load degradation from the first to the second cycle
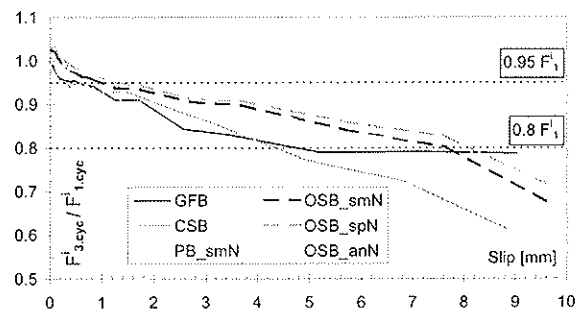
Figure 15: Load degradation from the first to the third cycle

Diagrams presented in Figures 14 and 15 have roughly linear, descending shape in all cases of tested specimens and in both comparisons of test cycles. The degradation process if faster in the cases of stapled joints than in the cases of nailed joints. This information is valuable for development of mathematical models of joints. Levels of 0.95 and 0.8 of the first cycle load gives information needed for definition of YLS and ULS according to known concepts. The method for YLS determination used in this paper shows that YLS is in all tested cases above 0.95 limits. Presented diagrams can serve as aid for definition of three linear envelope curve that is valuable simplification for modelling of inelastic behaviour of joints [6].
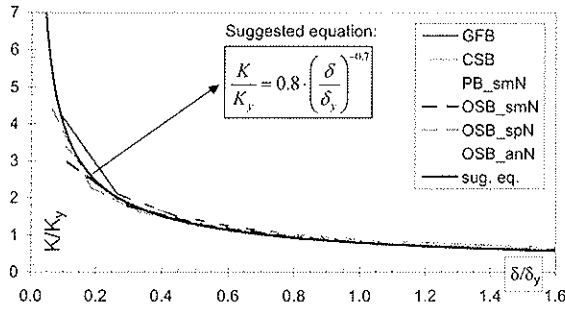
Figure 16: Normalized stiffness deterioration as derived from experimental results
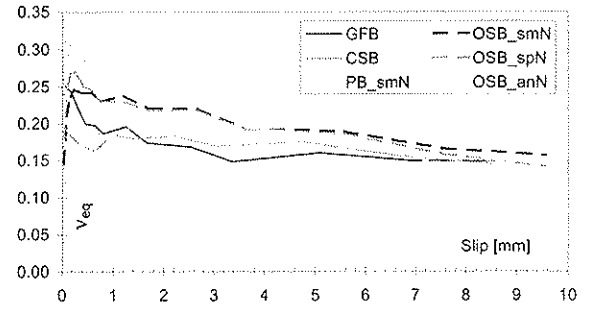
Figure 17: Comparison of equivalent viscous damping calculated from the first cycles

Stiffness deteoration curves shown in Figures 5 to 10 are very similar and have shapes of power functions. The initial elastic stiffness of joint is relatively high, but after several cycles in the range of low slip amplitudes stiffness drop to one that defines YLS. The observed drop is in range of magnitude of 3 to 7. All stiffness degradation curves were normalized by stiffness and joint slip at YLS and then unified through regression power curve obtained by simple curve fitting (Figure 16). Relatively simple equation was derived from curve fitting:

$$\frac{K}{K_y} = 0.8 \left(\frac{\delta}{\delta_y} \right)^{-0.7} \tag{3}$$

where K_y and δ_y are stiffness and joint slip at YLS, respectively.

Because tested types of joints have characteristic non-linear behaviour from the very beginning, the proposed equation (3) may be useful for construction of "synthetic" load - slip curve. However, the basis of such approach can be a sufficiently large data basis on joint behaviour.

Equivalent viscous damping diagrams of different joint assemblages (Fig. 17) show two different mechanisms of behaviour. One is characteristic for stapled joints and another for nailed joints. In the case of stapled joints, the yield points moved along the staple legs due to their gradual pulling of the wood element. It results in relatively constant damping from the YLS to ULS having approximate value of 0.17 in tested cases. In the case of nailed joints the damping at YLS is higher than 0.25 and roughly linearly descend to value of 0.17 at ULS.

5 Conclusions

Although the main purpose of tests was obtaining data needed for mathematical modelling of joints, some general conclusions about behaviour of tested joint configurations can be derived. Stapled joints (GFB and CSB) and nailed joints with shorter nails (PB_smN) reach ULS at about 30% lower magnitude of joint slip than joints nailed with about 37 % longer nails (OSB_smN, OSB_spN and OSB_anN). Load degradation of stapled joints is faster than load degradation of nailed joints. In the case of stapled joints, degradation at ULS has double value in comparison of nailed joints degradation at same slip. Nevertheless, the stiffness degradation of all tested types can be expressed with the almost equal power curve. The interesting characteristic of stapled joints is almost constant equivalent viscous damping from YLS to ULS and beyond. The initial equivalent viscous damping of nailed joints is significantly higher than those of stapled joints and meets their magnitude near to ULS.

6 References

[1]   RILEM TC 109-TSA, 1994. "Timber Structures in Seismic Regions: RILEM State-of-the-Art Report", Materials and Structures, Vol. 27: 157-184.

[2]   Dolan, J. D., Madsen, B., 1992. "Monotonic and cyclic nail connection tests", Canadian Journal of Civil Engineering, Vol. 19: 97-104.

[3]   Yasumura, M., 1998. "Mechanical properties of dowel type joints under reversed cyclic lateral loading", Proceedings of CIB-W18/31-7-1, Savonlinna, Finland.

[4]   Smith, I., Foliente, G., 2002. "Load and resistance factor design of timber joints: International practice and future direction", Journal of Structural Engineering, Vol. 128, 1: 48-59.

[5]   Dujic, B., Zarnic R., 2002. "Influence of Vertical Load on Lateral Resistance of Timber-Framed Walls", Proceedings of CIB-W18/35-15-4, Kyoto, Japan.

[6]   Dujic, B., Zarnic, R., 2003. "Blind Prediction of Seismic Response of Timber-Frame House", International Conference SE-40EEE, Skopje & Ohrid, FYR of Macedonia.

[7]   EN 1381:1999, Timber structures - Test methods – Load bearing stapled joints, CEN/TC 124.

[8]   prEN 1380:1994, Timber structures - Test methods – Load bearing nailed joints, CEN/TC 124.

[9]   Shenton, H.W., III, Dinehart, D.W., and Elliot, T.E. , 1998, "Stiffness and energy degradation of wood frame shear walls", Can. J. Civ. Eng., 25, 412-423.

[10]   prEN 12512:1996, Timber structures - Test methods – Cyclic testing of joints made with mechanical fasteners, CEN/TC 124.

INTERNATIONAL COUNCIL FOR RESEARCH AND INNOVATION
IN BUILDING AND CONSTRUCTION

WORKING COMMISSION W18 - TIMBER STRUCTURES

EVALUATION AND ESTIMATION OF THE PERFORMANCE OF THE NAIL JOINTS AND SHEAR WALLS UNDER DRY/HUMID CYCLIC CLIMATE

S NAKAJIMA

Building Research Institute

JAPAN

Presented by: Shiro Nakajima

Shiro Nakajima indicated that the main objectives of the research he presented was to evaluate the effects of dry/humid cyclic climatic conditions of nailed joints in shear wall panels as the shear walls installed in timber houses experience these climatic cycles. He compared values obtained for plywood and OSB sheathed shear walls with those obtained numerically. In his conclusion he observed that the condition of the test specimen during the test affected the strength and stiffness of the joints.
Questions were asked with regard to more than one cycle of dry/humid conditions. Shiro indicated that he plans to perform tests using multiple climatic cyclic conditions.

Evaluation and estimation of the performance of the nail joints and shear walls under dry/humid cyclic climate

Shiro NAKAJIMA

Building Research Institute, JAPAN

1   Abstract

As shear walls installed in timber houses usually experience dry and humid cyclic climate during their service life the effect of the humid and dry climate on the performance of the nail joints was evaluated.   Lateral nail resistance tests were conducted after conditioning the test specimens in the dry/humid/dry cyclic climate.   The tests were conducted for all possible combination of the surface grain direction of the studs and the sheathing materials and the loading direction.   The strength reduction of the shear walls due to the dry and humid cyclic climate was estimated by the simplified model.

Not only the conditioning schedule but also the final condition, i.e. the condition of the test specimens during the test, affected on the strength and stiffness of the nail joints.   The condition of the test specimens, i.e. wet or dry, was supposed to be one issue that should be discussed in the process of evaluating the stiffness and strength of the joints and the shear walls that will be exposed to a certain humid climate.

2   Introduction

The moisture contents of wooden materials and components affect on the strength and stiffness properties of the joints and the shear walls of wooden structures.   In most cases the strength and stiffness properties of the joints and the shear walls are evaluated from the test results of the test pieces that are conditioned in the standard condition, temperature 20°C and relative humidity 65%.   Wooden structures are actually used in various conditions and the performance of the joints and the shear walls of these structures should be properly evaluated according to the conditions in which they are used.   As it is quite difficult to conduct full size shear wall tests in various conditions it is quite necessary to develop an appropriate method to estimate the performance of the shear walls from the performance data of the materials and the joints.

In Japan the allowable shear strengths of the shear walls constructed by the 2X4-construction system were decided by analyzing the test data of the series of shear wall tests conducted in 1972 (Building Research Institute 1975).   In the process of calculating

the allowable shear strengths of the shear walls a modification factor that represented the durability of the sheathing panels was also multiplied to the shear strength. As most of these values were derived from the test results of the lateral nail resistance test of the nailed joints it is quite necessary to verify the adequacy of the values of modification factor by the full size shear wall tests.

On the other hand the three-service classes system was proposed in the Enforcement Order No.1446 in June 2001. The three service classes represented the climates "constantly wet", "intermittently wet" and "dry".

The effect of the constantly humid climate on the performance of the nail joints and the shear walls was reported in the last two papers (Nakajima2001, 2002) and the yield strength reduction of the shear walls caused by the humid climate was predicted by the simplified model. As shear walls installed in timber houses usually experience dry and humid cyclic climate during their service life the strength and stiffness of the nail joints under the humid and dry climate was measured and the strength and stiffness of the shear walls in this climate was estimated using the test results of the nail joints.

3   Previous test results

Shear walls sheathed with plywood or OSB were constructed by the 2X4-construction system and tested in two climates, temperature 20°C & relative humidity 65% and temperature 20°C & relative humidity 90% to clarify the effect of the moisture contents on the racking strength and stiffness of the shear walls. The panel shear test and the lateral nail resistance tests were also conducted after conditioning the test specimens in these two climates. The test results derived are as follows:

(1) In the humid climate the yield strength, the ultimate strength and the initial stiffness of the plywood sheathed shear walls were reduced to 85%, 87% and 79% respectively.

(2) In the humid climate the yield and the ultimate strength of the OSB sheathed shear walls were reduced to 90% and 91% respectively. And the initial stiffness of the OSB sheathed shear walls increase 5% after conditioned at the climate of 20°C and 90% R.H.

(3) The reduction of the panel shear modulus of rigidity due to the wet condition was 24% for plywood and 43% for OSB and the reduction of the panel shear strength was 24% for plywood and 23% for OSB. Both sheathing materials particularly OSB becomes more ductile when it is in a wet condition.

(4) Having an except for the nail joints with the surface grain directions of the framing members and the sheathing materials perpendicular to each other and the loading direction parallel to the surface grain direction of the sheathing materials, the yield strength of the "plywood - lumber" nail joints was reduced to almost 85% after being conditioned at the climate of temperature 20°C and relative humidity 90%.

(5) Having an except for the nail joints with the surface grain directions of the framing members and the sheathing materials perpendicular to each other and the loading direction parallel to the surface grain direction of the sheathing materials, the yield strength of the "OSB - lumber" nail joints was not reduced even after conditioned at the climate of temperature 20°C and relative humidity 90%.

4 Reverse-cyclic test of nail joints

4.1 Test specimens

Eight different types of nail joints were tested to evaluate the performance of the nail joints. Plywood and OSB panels were connected to the studs (204 lumbers) by the common nails 50mm in length (CN50). Considering the surface grain direction of the lumbers and the sheathing materials and also the loading direction four different types of test specimens were prepared. The detail of the size and shape of the test specimens are described in the previous paper (Nakajima2002). And the detail specification of the test specimens are as follows:

Joint A: Joint A represents the nail joints located at the vertical frames. The surface grain directions of the framing members and the sheathing materials are parallel to each other and the loading direction is parallel to both the surface grain direction of the framing members and the sheathing materials.

Joint B: Joint B represents the nail joints located at the top and bottom plates. The surface grain directions of the framing members and the sheathing materials are perpendicular to each other and the loading direction is parallel to the surface grain direction of the framing members.

Joint C: Joint C represents the nail joints located at the top and bottom plates. The surface grain directions of the framing members and the sheathing materials are perpendicular to each other and the loading direction is parallel to the surface grain direction of the sheathing materials.

Joint D: Joint D represents the nail joints located at the vertical frames. The surface grain directions of the framing members and the sheathing materials are parallel to each other and the loading direction is perpendicular to both the surface grain direction of the framing members and the sheathing materials.

Six test specimens were prepared for all types of nail joints. The test specimens were conditioned in a chamber after being assembled. The test specimens were conditioned at the climate of temperature 20°C and relative humidity 65% for 1week and then conditioned at the climate of temperature 20°C and relative humidity 90% for 3 weeks. And after this humid conditioning the test specimens were conditioned at the climate of temperature 20°C and relative humidity 65% for another 3 weeks.

4.2 Testing methods

Both ends of the studs (204 lumbers) were connected to the testing equipment and the reverse-cyclic load was applied to the test specimens. The loading schedule followed the ISO/DIS 16670 protocol. The slip between the sheathing materials and the studs were measured.

5 Test results

5.1 Thickness swelling of the sheathing materials

The thickness swelling and the increase of the weight of the sheathed materials caused during the conditioning process are summarized in table 1. After experiencing the humid

climate, temperature 20°C and relative humidity 90%, for 3 weeks the thickness of the plywood increased for almost 5%. And the thickness swelling was reduced to almost 2% after being conditioned in the standard condition, temperature 20°C and relative humidity 65% for 3 weeks. The thickness swelling of the OSB was three times higher than that of the plywood. After experiencing the humid climate, temperature 20°C and relative humidity 90%, for 3 weeks the thickness of the OSB increased for almost 15%. And the thickness swelling was reduced to almost 10% after being conditioned in the standard condition, temperature 20°C and relative humidity 65% for 3 weeks.

The increase of the weight of both the plywood and the OSB was almost same. The increase ratio of the weight of the panels after being conditioned at the humid climate was around 5% to 7% and the increase of the weight was reduced to almost 1% after experiencing the standard condition for 3 weeks.

Table 1   Thickness swelling and weight increase of the sheathing materials.

Material	Joint type	Thickness Swelling		Weight	
		After conditioned at 20°C 90% for 3weeks	After conditioned at 20°C 65% for 3weeks	After conditioned at 20°C 90% for 3weeks	After conditioned at 20°C 65% for 3weeks
Plywood	Joint A	6%	2%	7%	1%
	Joint B	5%	2%	7%	1%
	Joint C	5%	3%	5%	1%
	Joint D	5%	2%	5%	1%
OSB	Joint A	15%	9%	7%	2%
	Joint B	17%	10%	7%	3%
	Joint C	16%	10%	6%	1%
	Joint D	13%	9%	6%	1%

5.2   Shear strength of the plywood nailed joints

All the test results of the "plywood - lumber" nail joints are summarized in table 2. The yield strength (P_y), the yield deformation (D_y), the ultimate strength (P_u), the ultimate deformation (D_u), the initial stiffness (K) and the typical failure mode are tabulated.

The yield strength of the nail joints was not reduced by the humid and dry conditioning process and was almost same or approximately 15% higher than that of the nail joints conditioned at the standard climate. The reduction ratios of the initial stiffness of the "plywood - lumber" nail joints due to the humid and dry conditioning process ranged from 53% to 60%.

The failure modes of the "plywood - lumber" nail joints are summarized in figure 1. The failure modes of nail joints conditioned at the humid and dry cyclic climate were similar to those of the nail joints conditioned at the standard climate where the failure mode of the nail joints conditioned at the constantly humid climate differed from the nail joints conditioned at the standard climate.

4

Table 2　Summary of test results of the reverse-cyclic test of plywood nail joints.

Type of the test specimen	Conditioning [1]	Py (kN)	Dy (mm)	K (kN/mm)	Pu (kN)	Du (mm)	Dominant failure mode [2]
Joint A	65% R.H. const.	0.51	0.68	0.82	0.79	14.09	P6, W12, N22
	90% R.H. const.	0.43	0.61	0.85	0.69	10.97	P40, W0, N0
	Reduction ratio	*0.84*	*0.90*	*1.04*	*0.88*	*0.78*	-
	Humid/Dry	0.59	1.36	0.45	0.91	16.44	P4, W14, N6
	Reduction ratio	*1.17*	*2.00*	*0.56*	*1.15*	*1.17*	-
Joint B	65% R.H. const.	0.54	0.64	0.94	0.86	12.68	P24, W10, N2
	90% R.H. const.	0.46	0.96	0.53	0.75	12.68	P40, W0, N0
	Reduction ratio	*0.85*	*1.50*	*0.56*	*0.88*	*1.00*	-
	Humid/Dry	0.55	1.20	0.50	0.88	17.25	P14, W7, N3
	Reduction ratio	*1.02*	*1.87*	*0.53*	*1.03*	*1.36*	-
Joint C	65% R.H. const.	0.51	0.73	0.73	0.78	12.24	P13, W27, N0
	90% R.H. const.	0.51	1.07	0.52	0.78	14.35	P7, W12, N21
	Reduction ratio	*1.01*	*1.45*	*0.72*	*1.00*	*1.17*	-
	Humid/Dry	0.57	1.41	0.44	0.82	22.84	P0, W13, N11
	Reduction ratio	*1.12*	*1.92*	*0.60*	*1.05*	*1.87*	-
Joint D	65% R.H. const.	0.53	0.80	0.72	0.80	12.27	P0, W23, N17
	90% R.H. const.	0.45	0.95	0.56	0.70	12.33	P39, W0, N1
	Reduction ratio	*0.84*	*1.18*	*0.78*	*0.87*	*0.93*	-
	Humid/Dry	0.54	1.32	0.42	0.81	20.74	P0, W14, N10
	Reduction ratio	*1.01*	*1.64*	*0.58*	*1.01*	*1.56*	-

Note 1:　The temperature of the conditioning room is 20°C.
Note 2:　Failure mode "P", "W" and "N" represent "punching out", "nail withdrawal" and "nail failure" respectively and the figures beside the alphabet represent the amount of the nails.
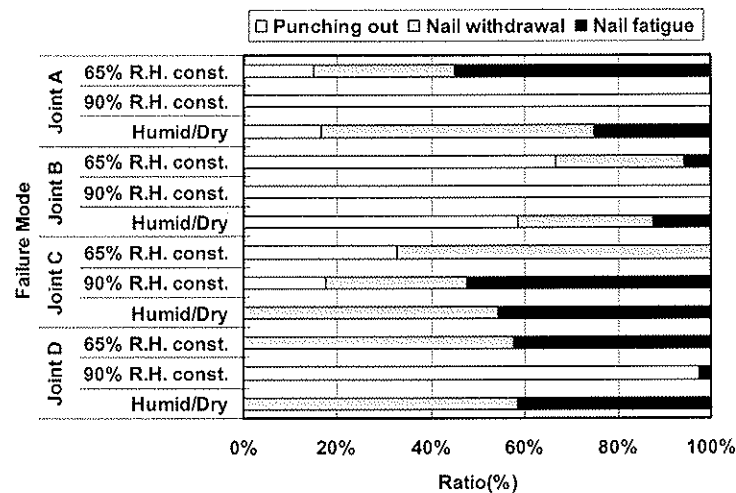
Figure 1　Failure mode of the "plywood- lumber" nail joints..

5.3   Shear strength of the OSB nailed joints

All the test results of the "OSB - lumber" nail joints are summarized in table 3.   The yield shear strength of the joint type B, C and D was reduced to 92%, 94% and 87% respectively by the humid and dry conditioning process.   The yield strength of the joint type A (both the surface grain of the 204 lumber pieces and the surface grain of the OSB panels parallel to the loading direction) was not reduced by the humid and dry process.   The reduction ratios of the initial stiffness of the "OSB - lumber" nail joints due to the humid and dry conditioning process ranged from 48% to 65%.

The failure modes of the "OSB - lumber" nail joints are summarized in figure 2.   The failure modes of nail joints being conditioned at the humid and dry cyclic climate were similar to those of the nail joints conditioned at the standard climate.   And the failure mode of the nail joints conditioned at the humid climate differed from that of the nail joints conditioned at the standard climate.   The dominant failure mode of the nail joints at the standard climate or the wet and dry cyclic climate was nail withdrawal where the dominant failure mode of the nail joints at the constantly humid climate was punching out.

Table 3   Summary of test results of the reverse-cyclic test of OSB nail joints.

Type of the test specimen	Conditioning [1]	P_y (kN)	D_y (mm)	K (kN/mm)	P_u (kN)	D_u (mm)	Dominant failure mode [2]
	65% R.H. const.	0.57	0.47	1.29	0.86	13.74	P12, W27, N1
	90% R.H. const.	0.59	0.57	1.15	0.90	13.63	P39, W1, N0
Joint A	*Reduction ratio*	*1.05*	*1.23*	*0.89*	*1.04*	*0.99*	-
	Humid/Dry	0.58	0.89	0.70	0.88	17.58	P2, W16, N6
	Reduction ratio	*1.08*	*1.66*	*0.65*	*1.07*	*1.22*	-
	65% R.H. const.	0.54	0.54	1.07	0.83	14.40	P4, W31, N5
	90% R.H. const.	0.62	0.59	1.17	0.95	13.88	P37, W3, N0
Joint B	*Reduction ratio*	*1.15*	*1.10*	*1.09*	*1.15*	*0.96*	-
	Humid/Dry	0.52	0.89	0.64	0.79	16.29	P6, W15, N3
	Reduction ratio	*0.92*	*1.90*	*0.50*	*0.92*	*1.19*	-
	65% R.H. const.	0.59	0.73	0.99	0.88	12.15	P1, W39, N0
	90% R.H. const.	0.57	0.69	1.04	0.86	13.30	P10, W11, N19
Joint C	*Reduction ratio*	*0.67*	*0.96*	*1.05*	*0.98*	*1.09*	-
	Humid/Dry	0.53	1.16	0.50	0.81	14.20	P0, W24, N0
	Reduction ratio	*0.94*	*1.72*	*0.55*	*0.96*	*1.17*	-
	65% R.H. const.	0.57	0.67	0.90	0.84	12.15	P2, W33, N5
	90% R.H. const.	0.60	0.62	1.07	0.91	12.61	P23, W7, N10
Joint D	*Reduction ratio*	*1.05*	*0.91*	*1.18*	*1.08*	*1.04*	-
	Humid/Dry	0.51	1.10	0.48	0.76	15.40	P1, W23, N0
	Reduction ratio	*0.87*	*1.51*	*0.48*	*0.87*	*1.27*	-

Note 1:   The temperature of the conditioning room is 20°C.

Note 2:   Failure mode "P", "W" and "N" represent "punching out", "nail withdrawal" and "nail failure" respectively and the figures beside the alphabet represent the amount of the nails.
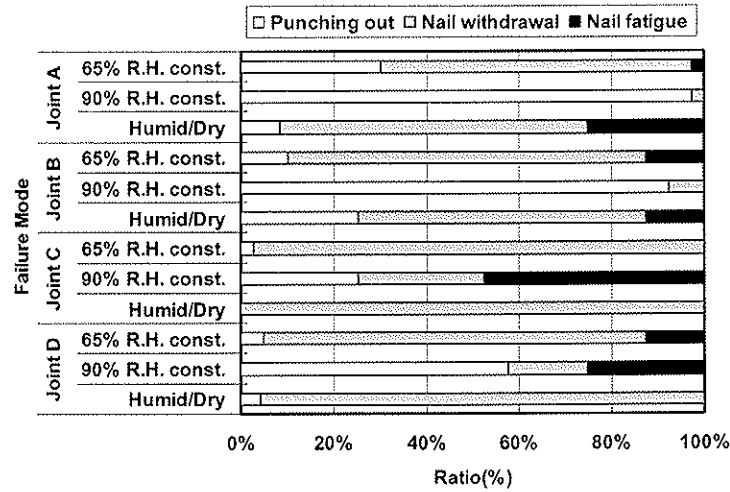
Figure 2   Failure mode of the "OSB- lumber" nail joints.

6   Prediction of the yield strength of the shear walls

6.1   Simple numerical model

To predict the reduction of the yield shear strength of the shear walls under the humid or the humid and dry cyclic climate the simple structural model proposed by Hirai (Hirai et.al. 1999) was referred.   The shear walls were modeled as shown in figure 3.

The model is a simplified model and the true shear deformation of the shear walls are assumed to be the summation of the shear deformation caused by the slip of the nail joints and the shear deformation of the sheathing panels.   When a horizontal load P is applied at the top of the shear wall the true shear deformation of the shear wall γ can be calculated by summing the shear deformation of the sheathing panels γ_s and the shear deformation caused by the slip of the nailed joints γ_n.

$$\gamma = \gamma_s + \gamma_n$$
---(1)

where ,

γ_s represents the shear deformation of the sheathing panels, and

γ_n represents the shear deformation caused by the slip of the nailed joints.

Figure 3   Modeling of the nailed shear walls.

When the load and deformation are in linear the shear deformation of the shear wall γ and the load P can be easily calculated by a simple numerical calculation.   Equation 2 shows the relationship between the load applied at the top of the shear wall and the shear deformation of the shear wall caused by the slip of the nail joints.

$$P = \frac{h_e}{2} \left(\sum_{i=1}^{n} k_{si} \cdot R_i^2 + \sum_{j=1}^{m} k_{si} \cdot R_j^2 \right) \cdot \gamma_n \qquad --- (2)$$

where,

k_{si} is the slip modulus of the nail joints at the horizontal framing members,

k_{sj} is the slip modulus of the nail joints at the vertical framing members,

and,

$$R_i = \frac{1}{1+\lambda^2}\left\{1 + \lambda^2\left(1 - \frac{2(i-1)}{n-1}\right)^2\right\}^{\frac{1}{2}} \qquad \text{---(3)}$$

$$R_j = \frac{1}{1+\lambda^2}\left\{\lambda^2 + \left(1 - \frac{2(j-1)}{m-1}\right)^2\right\}^{\frac{1}{2}} \qquad \text{---(4)}$$

$$\lambda = \frac{h_e}{l_e} \qquad \text{---(5)}$$

The slip of the nails nailed to the horizontal framing members s_i and the slip of the nails nailed to the vertical framing members s_j are given as shown in equation 6. The slip modulus of the nail joints located at the horizontal framing members k_{si} and the slip modulus of the nail joints located at the vertical framing members k_{sj} can be derived from the test results of lateral nail tests of the nail joints. Thus equation 2 gives the load P that can deform the shear wall to a certain shear deformation γ_n, the shear deformation caused by the slip of the nail joints.

$$s_i = \frac{h_e \gamma_n}{2} \cdot R_i, \qquad s_j = \frac{h_e \gamma_n}{2} \cdot R_j \qquad \text{---(6)}$$

Equation 7 gives the shear deformation of the sheathing panels γ_s caused by the load P applied at the top of the shear wall.

$$\gamma_s = \frac{P}{Gl_e t} \qquad \text{---(7)}$$

where,

G is the panel shear modulus of rigidity, and

t is the thickness of the panel.

Equation 1, 2 and 7 gives the total shear deformation of the shear wall and the load P carried by the shear wall.

6.2   Results and discussion

The length of the shear wall l_e was 948mm and the height h_e was 2450mm. And the number of the nail joints located at the vertical framing member m was 25 and the number of the nail joints located at the horizontal framing member n was 11. The slip modulus of the nail joints located at the horizontal framing members k_{si}, the slip modulus of the nail joints located at the vertical framing members k_{sj} at a certain displacement level can be derived from the load-slip curve of the nail joints.

To simplify the calculation the actual load-slip curves were express by the following functions:

$$Load = a\ln(1 + b \times disp.) \qquad \text{---(8)}$$

where,

a and b are constants obtained from the test results.

The panel-shear modulus of rigidity of the sheathing panels is summarized in table 4.   As

the panel shear tests were not conducted for the panels conditioned at the humid and dry cyclic climate the panel shear modulus of rigidity of the sheathing panels conditioned at the climate of 20°C, 90% R.H. were refered to calculate the load-deformation curve of the shear walls.

Table 4 The panel shear modulus of rigidity of the sheathing panels.

Climate:	(1) 20°C, 65%		(2) 20°C, 90%	
Sheathing material:	Plywood	OSB	Plywood	OSB
Panel shear modulus of rigidity (Mpa)	460	1650	350	940

The results of the calculation are summarized in figure 4 and figure 5. The results of the calculation indicate that the initial stiffness of plywood sheathed shear walls are reduced both by the humid climate and the humid/dry cyclic climate. And the initial stiffness of shear walls conditioned at the humid/dry cyclic climate was more reduced than the initial stiffness of the shear walls conditioned at the constantly humid climate. Though the initial stiffness of the OSB sheathed shear walls was also reduced by the constantly humid climate or the humid/dry cyclic climate the initial stiffness of the OSB sheathed shear walls conditioned at the constantly humid climate was not so much reduced and was almost same as that of the OSB sheathed shear walls conditioned at the 20°C, 65% R.H. climate.

As the measured yield deformation (Dy) of the shear walls was around 10mm the load carrying capacities of the shear walls at this deformation level were calculated to evaluate the effect of the humid climate on the load carrying capacities of the shear walls. The load carried by the plywood sheathed shear walls was reduced for almost 20% when the shear walls were conditioned at the constantly humid climate or at the humid/dry cyclic climate. And the load carried by the OSB sheathed shear walls were reduced for 25% when the shear walls were conditioned at the humid/dry cyclic climate. The load carrying capacities of the OSB sheathed shear walls were not reduced by the constantly humid climate.

The results above mentioned are based on the characteristics of the nail joints and the sheathing panels. The results indicated that not only the conditioning schedule but also the final condition, i.e. the condition of the test specimens during the test, affects on the strength and stiffness of the nail joints and the shear walls. And how they affect on the characteristic values of the nail joints and the shear walls depends on the type of the
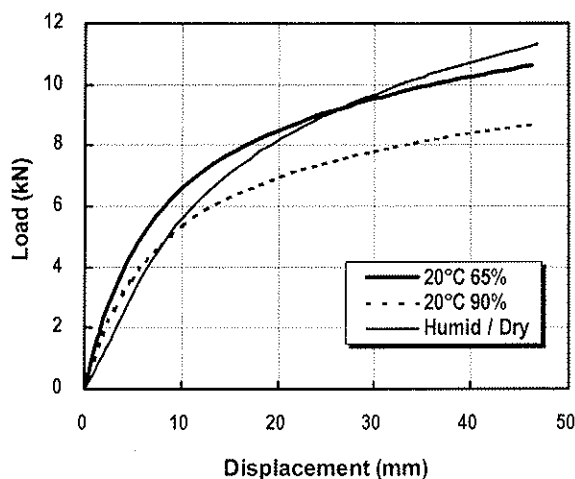
Figure 4   Estimated load-deformation curve of the plywood sheathed shear walls.
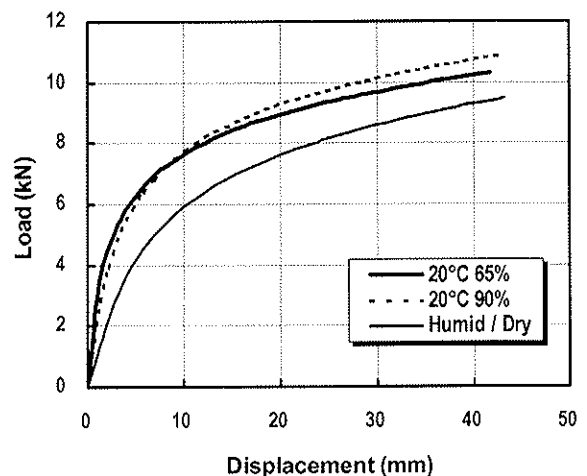
Figure 5   Estimated load-deformation curve of the OSB sheathed shear walls.

9

sheathing materials. The condition of the test specimens, i.e. wet or dry, is supposed to be one issue that should be discussed when evaluating the stiffness and strength of the joints and shear walls that are expected to be exposed to a certain humid climate.

7 Conclusion

The yield strength of the "plywood - lumber" nail joints was not reduced by the humid and dry conditioning process and was almost same or approximately 15% higher than that of the nail joints conditioned at the standard climate. The reduction ratios of the initial stiffness of the "plywood - lumber" nail joints due to the humid and dry conditioning process ranged from 53% to 60%.

Basically the yield shear strength of the "OSB - lumber" joint was reduced to approximately 10% by the humid and dry conditioning. The reduction ratios of the initial stiffness of the "OSB - lumber" nail joints due to the humid and dry conditioning process ranged from 48% to 65%.

Not only the conditioning schedule but also the final condition, i.e. the condition of the test specimens during the test, affected on the strength and stiffness of the nail joints. The condition of the test specimens, i.e. wet or dry, is supposed to be one issue that should be discussed when evaluating the stiffness and strength of the joints and the shear walls that will be exposed to a certain humid climate.

Reference

Building Research Institute MOC 1975. 'Annual Report of the General Technology Development Project – Development of the Construction Methods for the Small Scale Wooden houses'. Building Research Institute MOC.

Nakajima S, 2001. The effect of the moisture content on the performance of the shear walls. Proceedings of CIB-W18/34-15-2.

Nakajima S, 2002. Evaluation and estimation of the performance of the shear walls in humid climate. Proceedings of CIB-W18/35-15-3.

Takurou Hirai, Pei-Wen Zhang, Yasutaka Irie and Yoshiaki Wakashima, 1999. Lateral resistance of nailed timber joints with structural wooden panels. Journal of Japan Wood Science Society, 45(2), 120-129.

INTERNATIONAL COUNCIL FOR RESEARCH AND INNOVATION
IN BUILDING AND CONSTRUCTION

WORKING COMMISSION W18 - TIMBER STRUCTURES

BEAMS TRANSVERSALLY LOADED BY DOWEL-TYPE JOINTS:

INFLUENCE ON SPLITTING STRENGTH OF BEAM THICKNESS

AND DOWEL SIZE

M Ballerini

A Giovanella

University of Trento

Department of Mechanics & Structural Engineering

ITALY

Presented by: Marco Ballerini

Marco Ballerini introduced his presentation with a discussion of the issues relating to tensile strength perpendicular to the grain and the existing code (prEN 1995-1-1 and E DIN 1052) formulae for designing the situation. He indicated that the aims of the experimental studies are to obtain the actual influence of b on the splitting strength of the beams and to demonstrate the influence of the failure loads of the bearing capacity. He concluded that the thickness affects linearly the splitting strength of beams and that EC5 formula is able to correctly predict the experimental data "when calibrated on each test series". He then answered questions relating to practical design situations.

Beams transversally loaded by dowel-type joints: influence on splitting strength of beam thickness and dowel size

M. Ballerini, A. Giovanella

University of Trento, Department of Mechanics & Structural Engineering, Italy

Abstract: The paper reports the results of a new set of experimental tests on beams loaded perpendicular-to-grain by dowel-type connections. The experimental programme consists of two different test series. The first one, which concerns large specimens with multiple dowel connections, has been performed essentially to investigate the actual influence of the beam thickness on the splitting strength. The second one, which involves smaller specimens with single dowel joints, has been carried out to confirm the soundness of the results of a previous research and to demonstrate the limited effect of the connection strength on the splitting resistance of beams.

The experimental results of both test series are illustrated and discussed with reference also to the results of previous researches. Finally, the failure loads are compared with the bearing capacity predicted by the final drafts of the new European and German design codes for timber structures.

1   Introduction

The evaluation of the splitting strength of beams loaded perpendicular-to-grain by dowel-type connections is a difficult task due to the large number of involved parameters. Nevertheless, the need of a valid prediction formula is widely recognised as shown by the number of experimental, numerical and theoretical recent works on this item.

The most recent drafts for the new European (EC5, 2002 [1]) and German (E DIN 1052, 2002 [2]) design codes for timber structures suggest two different design formulae which take into account the several parameters in a very different way.

The design formula embodied in the latest draft of new EC5 is based on the work originally developed by Van der Put ([3, 4]), on the basis of an energetic approach in the framework of the Linear Elastic Fracture Mechanics, and recently put forward again by Van der Put and Leijten in [5]. Essentially, this formula assumes a linear relationship with the beam thickness and an influence of the square root of the distance of the furthest row of fasteners from the loaded edge of the beam (h_e). On the contrary, it doesn't take into account any effect of the joint geometry.

The design formula embodied in the latest draft of new E DIN 1052 is an evolution of the prediction formula derived by Ehlbeck, Görlacher and Werner [6, 7], which was based on both empirical and theoretical considerations. Besides the influence of the loaded edge distance (by means of the not-dimensional parameter $\alpha = h_e/h$), it explicitly considers the influence of the joint configuration and assumes a non-linear relationship of both the beam thickness and height as a result of the Weibull failure theory.

To obtain a better knowledge on the actual influence of some fundamental parameters, not deeply investigated up to now, a new experimental research has been carried out at the University of Trento.

1

The research consists of two different test series. In the first one, deep beams with multiple dowel connections have been tested. The intent of these tests is essentially to investigate the actual influence of the beam thickness on the splitting strength and the influence of the joint configuration.

The second one concerns smaller beams loaded by single dowel joints. These tests have been carried out to confirm the reliability of the results of a previous research on single dowel connections (Ballerini, [8]) and to demonstrate the negligible effect of dowel size on the beams splitting strength.

In the following, the experimental programme and the test set-up will be described in detail. The results, in terms of failure loads and types of failure, will be illustrated and discussed with reference to the investigated parameters.

Finally, the failure loads will be compared with the bearing capacity predicted by the latest drafts of the new European and German design codes for timber structures.

2 The experimental programme and the testing procedure

The experimental programme consists of two series of bending tests on simply supported glulam beams (European whitewood – Picea abies) loaded at mid-span by means of perpendicular-to-grain dowel connections. A detailed description of the research is reported in Giovanella [9].

In the first series, 24 tests have been performed on glulam beams characterized by a depth of 800 mm, a thickness ranging from 80 to 200 mm, and a test span of 2800 mm.

Steel-to-timber joints according to the three joint configurations shown in Figure 1 have been adopted for these specimens. The connections consist of 8 or 12 dowels with a diameter of 20 mm; the maximum slenderness of dowels occours for the 200 mm thick beam and is equal to 10.

Two distances of the furthest row of fasteners from the beams' loaded edge (h_e), 260 and 540 mm (corresponding respectively to α of 0.325 and 0.675), have been investigated.

Figure 1 – Investigated joint configuration

In the second series, beams loaded by single-dowel connections were tested. In detail, 24 tests have been performed on glulam beams with a cross section of 40 by 200 mm, and 24 tests have been carried out on beams with a cross section of 40 by 400 mm. The test spans were respectively 1200 and 1400 mm. In this series, the ratio α (h_e/h) ranges from 0.25 to 0.7 for beams 200 mm high and from 0.15 to 0.7 for beams 400 mm high. The dowel diameter has been selected according to the value of the loaded edge distance h_e; in detail diameters of 24 and 30 mm were selected for the 200 mm beams and diameters of 24, 30 and 35 mm for the 400 mm ones.

The tests have been carried out upside-down with the test set-up shown in Figure 2. The load was applied by means of a servo-hydraulic actuator with a capacity of 250 kN. As a basis, three tests in displacement control have been performed on each configuration. The displacement rate of the head of the actuator has been fixed equal to 1 mm/min for all beam sizes. Mostly, the testing time ranged between 7 to 12 minutes.

The average mid-span deflections of the unloaded and of the loaded edges of the beams, as well as the average connection displacement, and the average elongations across the splitting line (5 cm away from the left and right connection sides) have been automatically collected during the tests.

2

Figure 2 – Test set-up and arrangement of displacement transducers

3 Tests results

The results of the experimental programme are summarised in Table 1 for specimens 800 mm high and in Table 2 for specimens 200 and 400 mm high. In tables only the relevant parameters have been reported; for deeper beams, the first letter of *specimens id* identifies the joint configuration.

The average density of the wood of glulam beams was about 450 kg/m³ and the moisture content of laminations was in the range of 10-12%.

Table 1 – Experimental results of 800 mm high beams.

Specimen id	b (mm)	h_e (mm)	$\alpha = \dfrac{h_e}{h}$	F_u (kN)			Type of failure
specimens with h = 800 mm, joints with 4 by 3 or 4 by 2 d = 20 mm dowels, L/h = 3.5							
A08-8032	80	260	0.325	58.2	67.4	58.2	LS – TS – LS
A12-8032	120	260	0.325	105.1	86.8	101.7	TS
A16-8032	160	260	0.325	118.2	108.3	109.1	TS – TS – LS
A20-8032	200	260	0.325	169.4	130.5	148.8	LS – TS – TS
B08-8032	80	260	0.325	55.5	59.7	61.2	TS – TS – LS
C08-8032	80	260	0.325	47.4	64.1	64.8	TS
A08-8067	80	540	0.675	135.7	145.6	131.6	TS – LS – TS
C08-8067	80	540	0.675	109.2	128.1	128.1	TS

LS: limited splitting; TS: total splitting

Table 2 – Experimental results of 200 and 400 mm high beams.

Specimen id	d (mm)	h_e (mm)	$\alpha = \dfrac{h_e}{h}$	F_u (kN)				Type of failure
specimens with b = 40 mm, h = 200 mm, 1 dowel joint, L/h = 6								
D04-2025	24	50	0.25	10.1	8.2	7.0		LS
D04-2035	24	70	0.35	11.9	10.1	11.7		LS
D04-2045	24	90	0.45	11.6	10.3	13.0		LS – TS – TS
D04-2050	24	100	0.50	10.9	13.6	13.8		TS
D04-2055	24	110	0.55	11.5	11.8	12.1		TS
D04-2060	30	120	0.60	15.5	14.2	14.2		TS
D04-2065	30	130	0.65	14.6	14.1	17.4		LS – TS – TS
D04-2070	30	140	0.70	15.6	15.4	16.2		TS – LS – LS
specimens with b = 40 mm, h = 400 mm, 1 dowel joint, L/h = 3.5								
D04-4015	24	60	0.15	9.7	11.3			LS
D04-4025	24	100	0.25	11.3	8.8			LS
D04-4035	24	140	0.35	12.2	11.5	11.2		LS
D04-4040	30	160	0.40	15.7	16.0			LS
D04-4045	30	180	0.45	17.6	12.4			LS
D04-4050	30	200	0.50	17.7	15.5	15.8		LS
D04-4055	35	220	0.55	25.4	22.9	17.9	16.6	LS
D04-4060	35	240	0.60	20.9	16.6			LS
D04-2065	35	260	0.65	21.4	18.1			LS
D04-2070	35	280	0.70	22.4	22.9			LS

LS: limited splitting; TS: total splitting

All specimens have experienced splitting failure after stable crack propagation till the maximum load. Two different splitting failures have been noticed as shown in Figure 3: total splitting (TS) and limited splitting (LS).

The 800 mm high beams have experienced both types of splitting failures; the failure types are quite randomly distributed with no evidence of a direct influence of the α ratio.

The 400 mm high beams experienced only the limited splitting failure, while the 200 mm high beams have shown both splitting failures. In these latter beams, the failure types seem linked to the α ratio; in detail, limited splitting was predominantly in beams characterized by low α values, while total splitting was predominantly in beams with higher α values. The behaviour of the 200 mm high beams (which have the greater slenderness) can be ascribed to the amount of internal work accumulated before failure that increases as the α ratio (and consequently of the failure load) increases.

Differently from the results presented by Ballerini in [8], in these test series no separation of beams in two elements has been recorded; this is due to the large difference in specimens slenderness of the two experimental programmes.

The dowels used in this experimental research were very stocky in the 200 and 400 mm high beams and quite stocky (the maximum slenderness ratio was 10) in the 800 mm high specimens. As a consequence, the dowels remained straight in all tests and then they transferred the load quite uniformly to the wood.
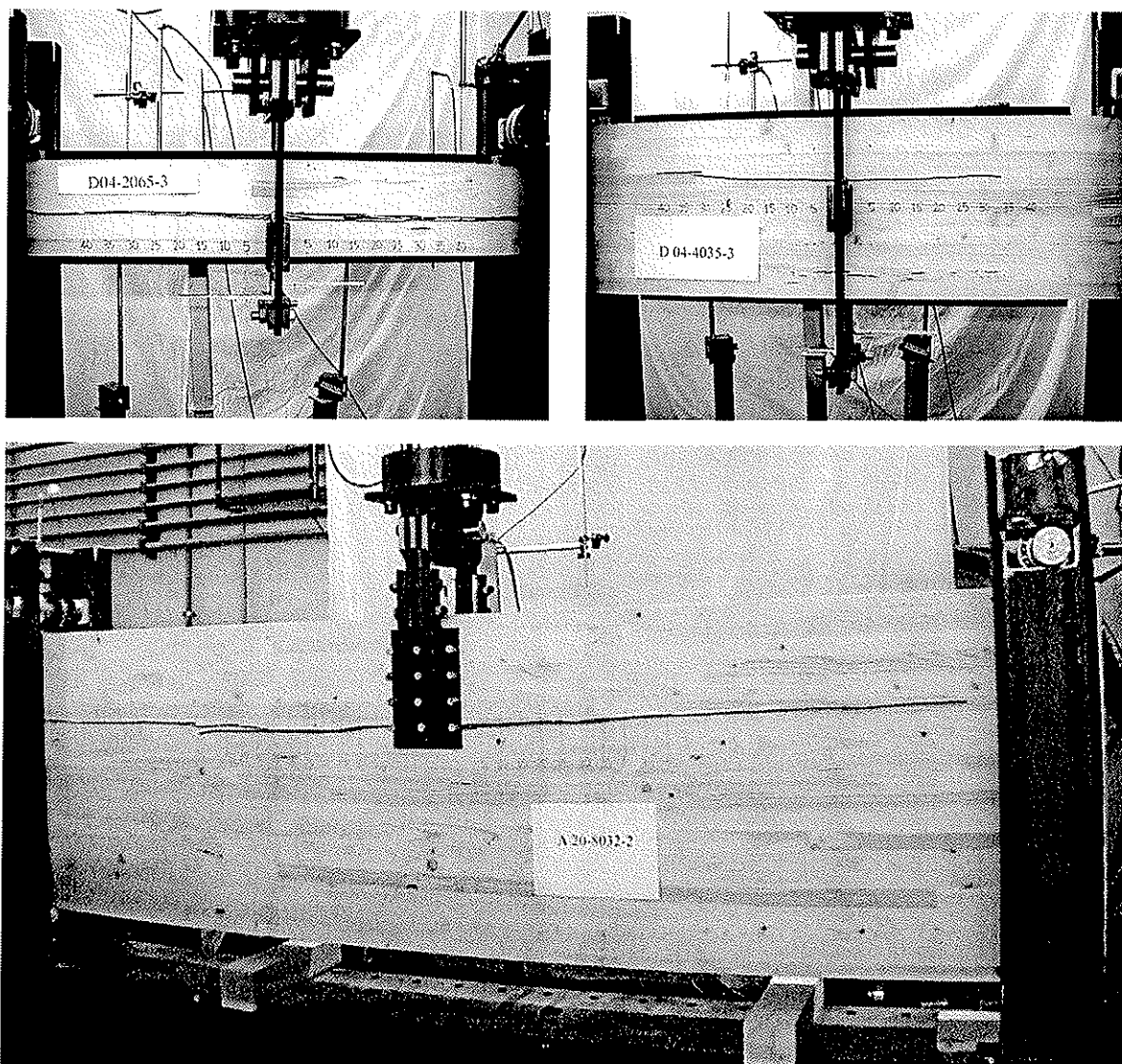
Figure 3 – Examples of recorded splitting failure types.

In spite of the small values of the bearing stresses beneath the dowels (as will be illustrated later) due to the above mentioned quite uniform load transfer and dowel sizes, few specimens of the second series have shown quite large plastic deformations. These deformations don't exhibit an evident correlation with joint parameter h_e but seem more linked to the quality of the wood just beneath the dowel.

4 Analysis of test results

The test results have been analysed and compared, with the ones of previous researches, separately for the specimens of the two series.

4.1 First test series – 800 mm high specimens

The analysis will be performed on the basis of Figures 4, 5, 6, and 7.

Figure 4 concerns the influence of the beam thickness on the splitting strength. In the graph are reported the results of this experimental research together with the ones of previous researches: Ehlbeck and Görlacher [EG, 10], Reske [11], Reske, Mohammad and Quenneville [RMQ, 12]. Moreover, for each series of data, two regression curves, the linear passing through zero and the power ones, are illustrated.

5
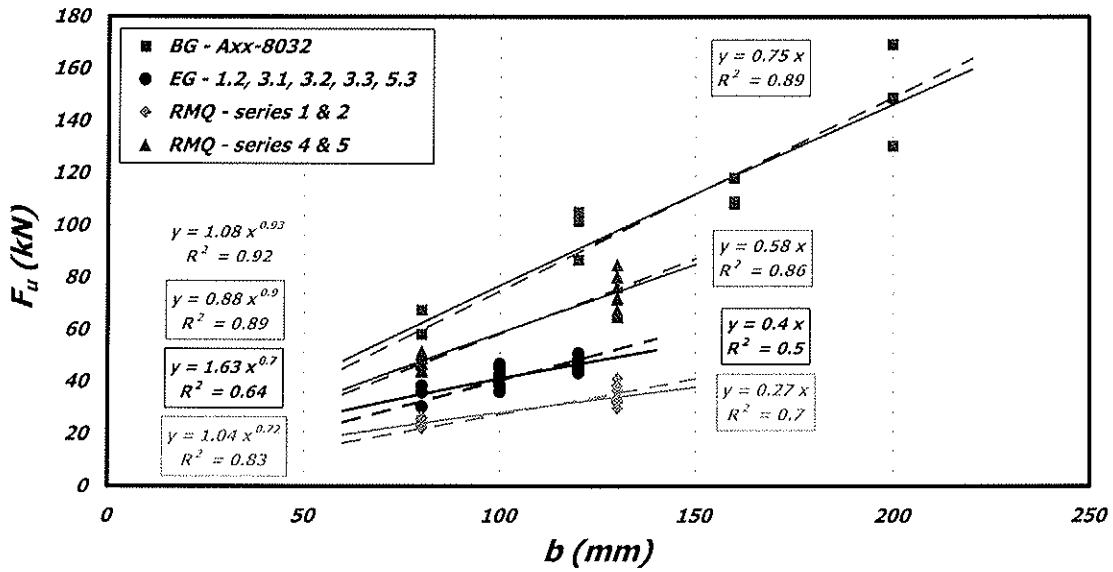
Figure 4 – Failure loads versus thickness
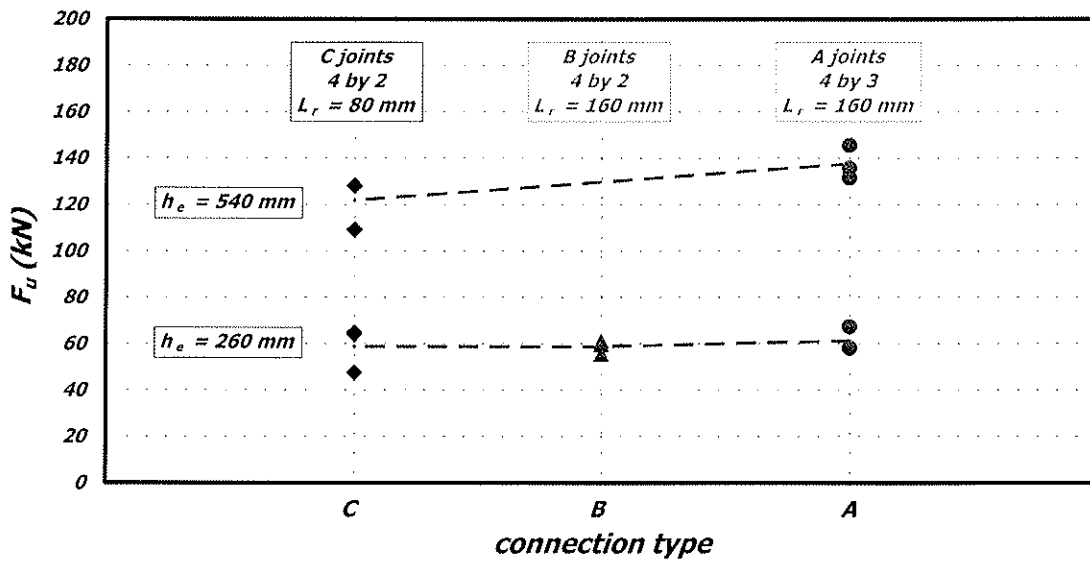
Figure 5 – Failure loads versus joints configuration
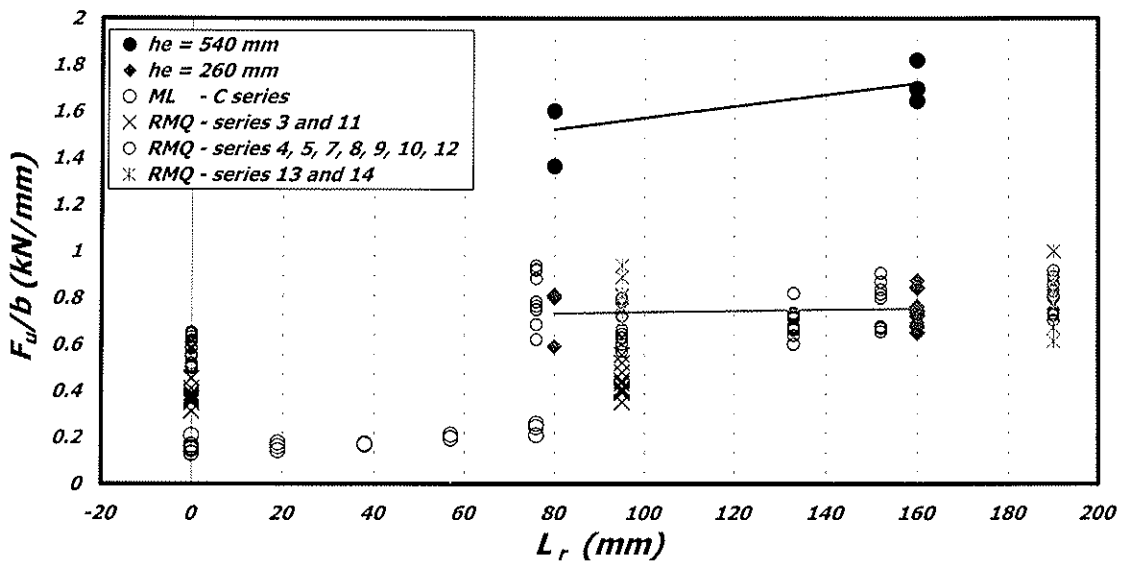
Figure 6 – Unit width failure loads versus joints width L_r

6
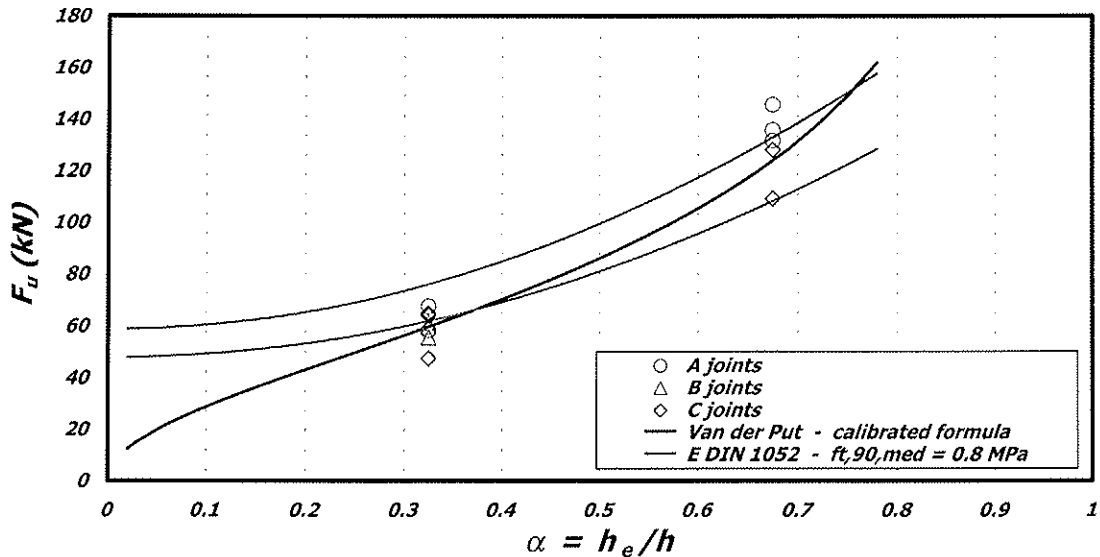
Figure 7 – Failure loads versus α

Although it is evident that power regression curves fit better the experimental data, the graph shows clearly that also the linear ones provide a good fitting. The differences between the two types of regression curves are very limited in the range of the investigated values and lower than the variability of test results. In the present research, this fact is emphasized due to the wider thickness range investigated.

The effect of the number of fasteners columns and of joint width L_r, are reported in Figures 5 and 6. From Figure 5 an influence of the joint width is appreciable only for the specimens with higher h_e. On the contrary, the specimens with lower h_e don't show any influence of both number of fasteners columns and joint width L_r. These results are confirmed in Figure 6 where also the results of other researches are reported (Möhler and Lautenschläger [ML, 13]). From the picture indeed, only a limited influence of L_r can be recognised for very low values of this parameter.

Finally, Figure 7 concerns with the effect of the α ratio. In addition to the tests results, the curves based on the Van der Put prediction formula (opportunely calibrated) and on the last E DIN 1052 design formula (based on a calibrated value of the average tensile resistance perpendicular to grain) are reported. As it is possible to notice, the above prediction curves are in good agreement with tests results.

4.2 Second test series – 200 and 400 mm high specimens

The influence of the distance from the loaded edge of the furthest row of fasteners h_e is analysed on the basis of the graphs reported in Figure 8, 9 and 10. Figure 8 concerns directly with the influence of h_e. From the picture, it is easy to notice a non-linear relationship between the failure loads and h_e; in detail, as the power regression curves show, failure loads are in good correlation with the square root of h_e for both beam sizes. From the same figure, it is also possible to notice the negligible influence of the dowel diameter on the splitting strength.

Figures 9 and 10 report the data of both beam sizes as a function of the α ratio. The bearing capacity predicted by both the Van der Put and E DIN 1052 prediction formulae, calibrated on this set of data, are also reported.

With regard to the Van der Put formula, it shows a good trend with the experimental data of both beam sizes even if it tends to overestimate the strength of specimens characterised by high α ratios and to underestimate the strength of the ones with low α ratios.

7
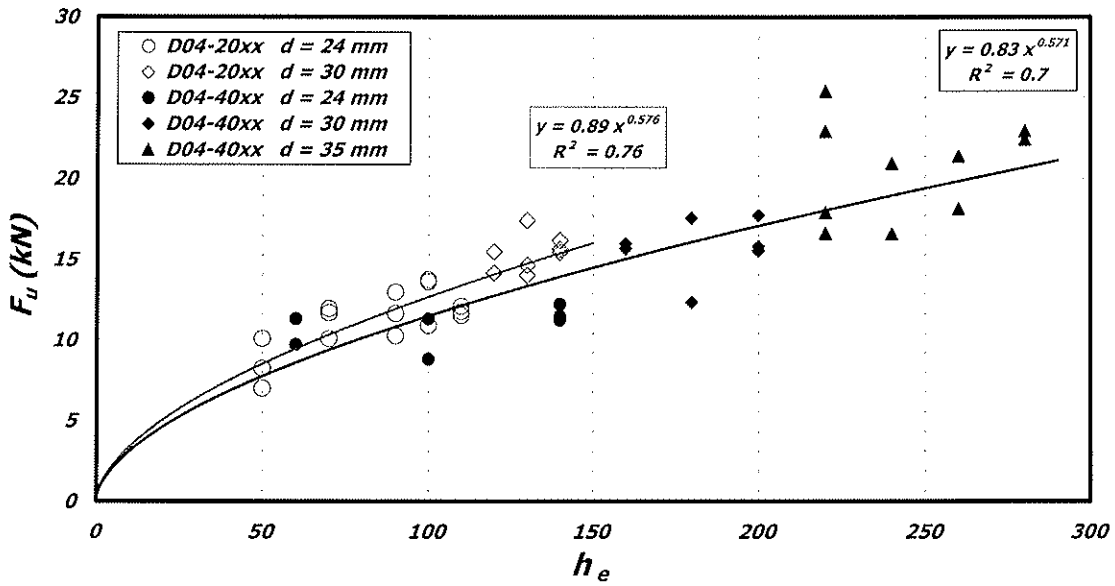
Figure 8 – Failure loads versus h_e of specimens with 200 and 400 mm
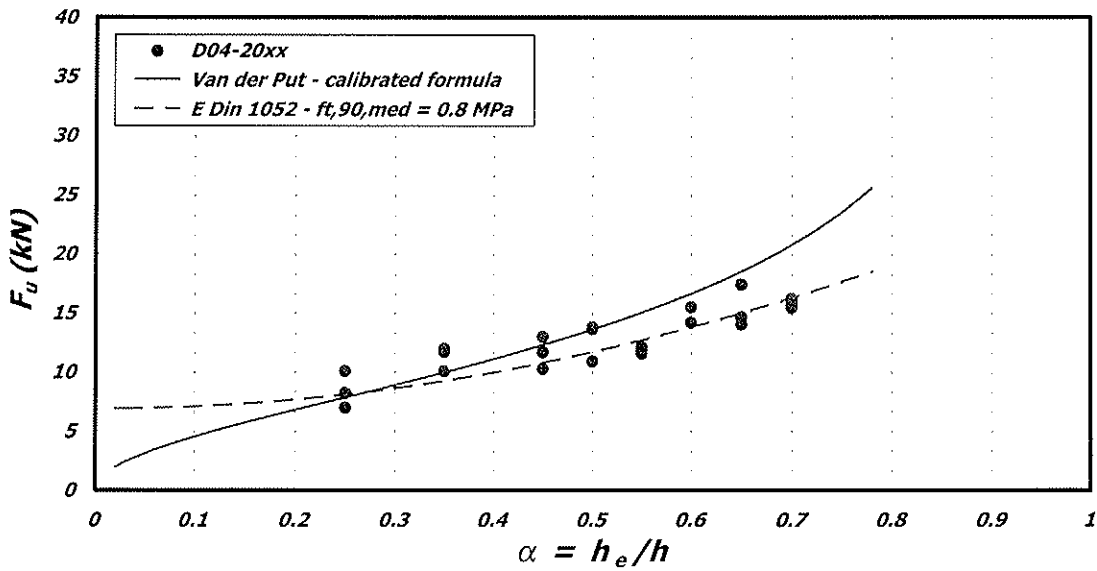
Figure 9 – Failure loads versus of specimens 200 mm high vesus α
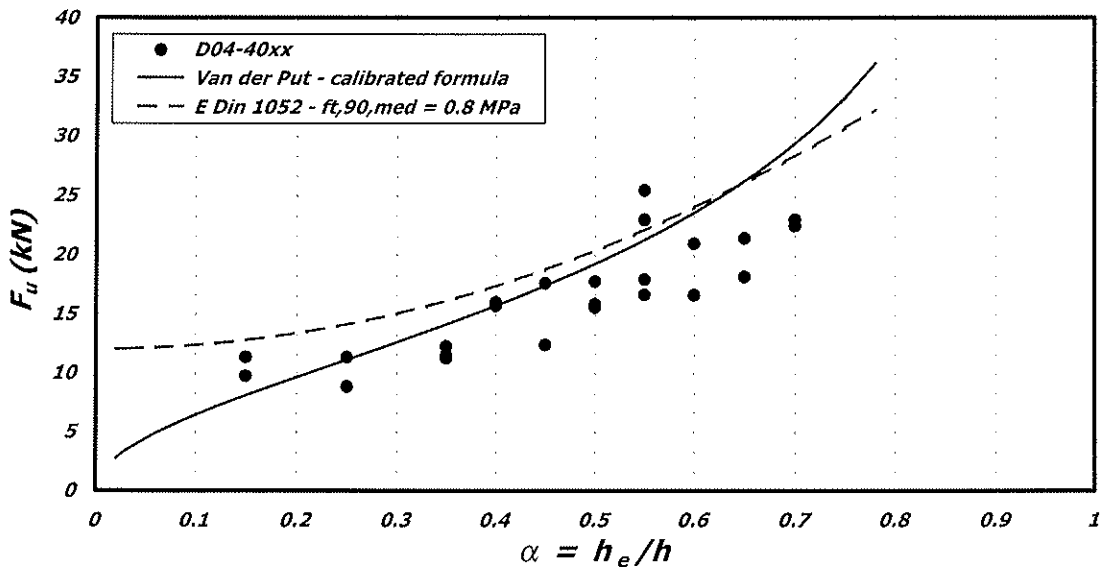
Figure 10 – Failure loads versus of specimens 400 mm high vesus α
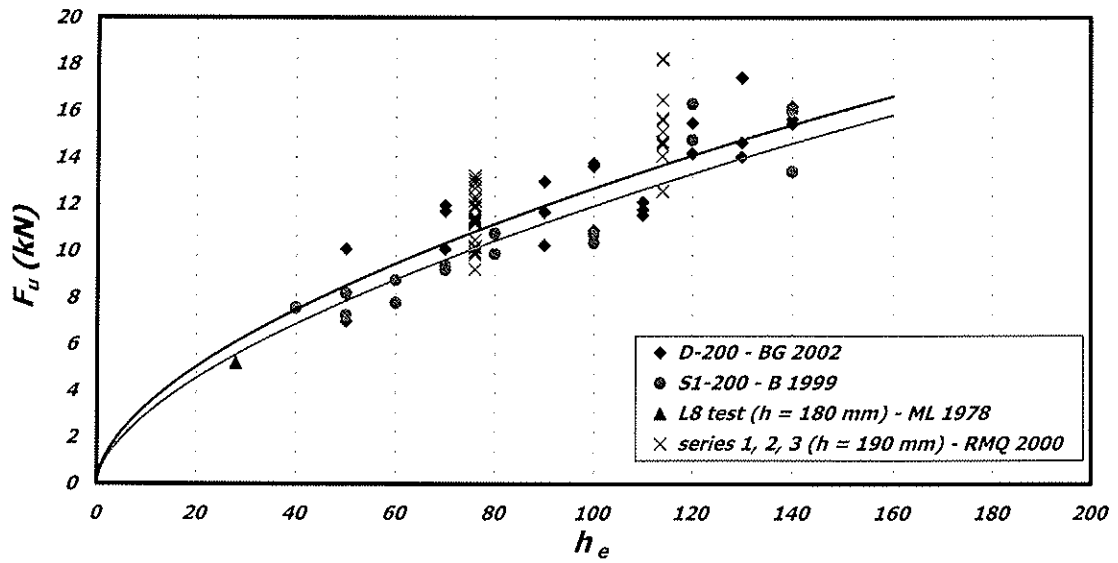
Figure 11 – Comparison of failure loads for 200 mm specimens
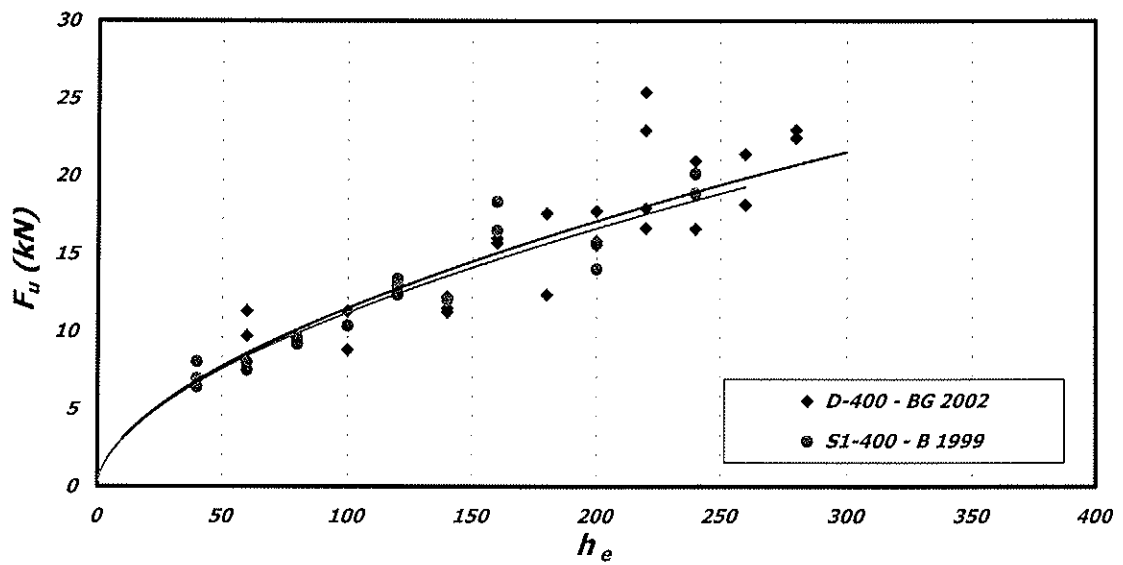
Figure 12 – Comparison of failure loads for 400 mm specimens
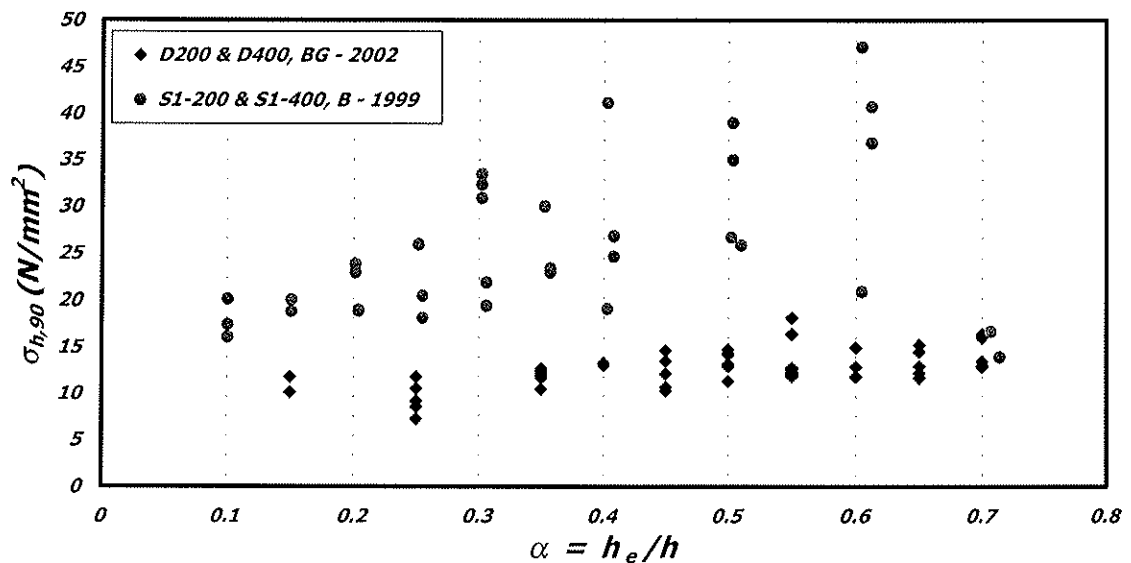
Figure 13 – Comparison of bearing stress values

9

The prediction of the E DIN 1052 design formula agrees quite perfectly with the data of 200 mm high beams, while overestimate the strength of the 400 mm high specimens. Nevertheless, it contrasts with physical evidence since it predicts a strength different form zero also for α values that tend to zero.

Figures 11 and 12 compare the results of 200 and 400 mm high beams with the ones of previous researches. In detail, in Figure 11 the comparison is established with the data of the researches reported in [8], [11, 12] and [13], while in Figure 12 the comparison is limited to the data available in [8]. In Figure 11 the size of the dowels in the different specimens, is respectively equal to 8, 10, 19, 24 and 30 mm. Instead, in Figure 12, it is equal to 10, 24, 30 and 35 mm.

In spite of the great variability of the dowels diameter, and consequently in the nominal strength of the connections, no evidence of the influence of the dowels size can be detected from the graphs on the splitting load bearing capacity.

The Figure 13, which reports the bearing stresses at failure of the specimens of this research and of the ones available in [8], confirms indirectly this result.

5 Comparison with design code formulae

The splitting failure loads of this experimental programme have been compared with the design formulae reported in the latest drafts of new Eurocode 5 and E DIN 1052.

In detail, accordingly with the characteristic lower bound of C_1 factor adopted by Van der Put and Leijten in [5], the comparison with the formula of the new Eurocode 5 has been done assuming an average strength equal to 1.5 the characteristic one. For the comparison with the formula reported in the new E DIN 1052, an average value of the tensile strength perpendicular to grain equal to 0.8 MPa has been assumed.

The results of the comparisons are shown in Figure 14, in terms of the experimental failure loads versus bearing capacity predictions, and in Figures 15 and 16 in terms of the ratios between the experimental values and the predicted ones versus the α ratio.

From figure 14, it is evident that the new E DIN 1052 formula globally gives a better prediction. In detail, for the beams of the second series, it seems less accurate with respect to the prediction of the Eurocode 5 formula; on the contrary it gives a better appraisal of failure loads for the beams of the first series.
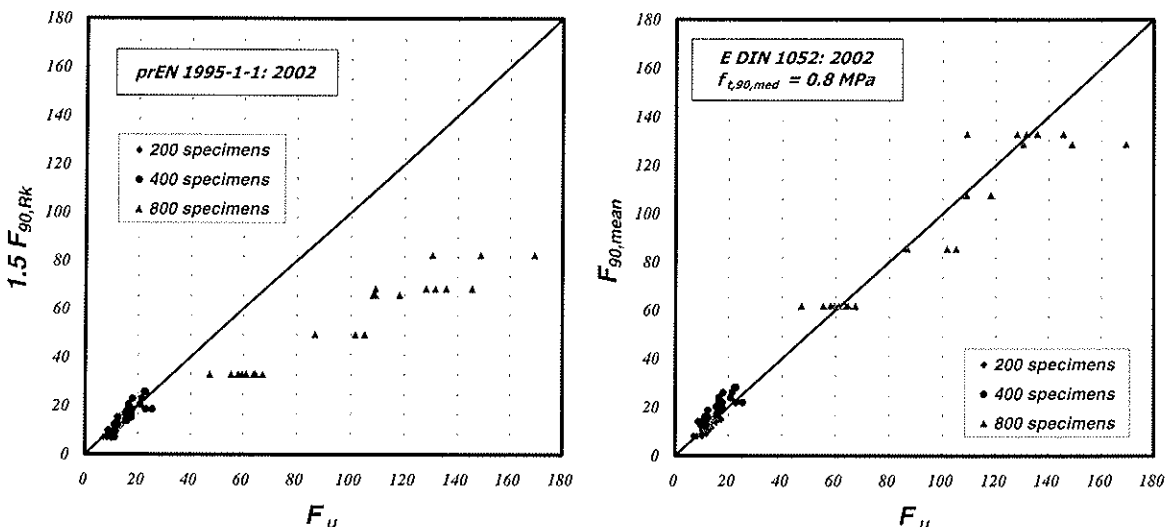
Figure 14 – Experimental failure loads versus the new Eurocode 5 (left) and E DIN 1052 (right) bearing capacity predictions
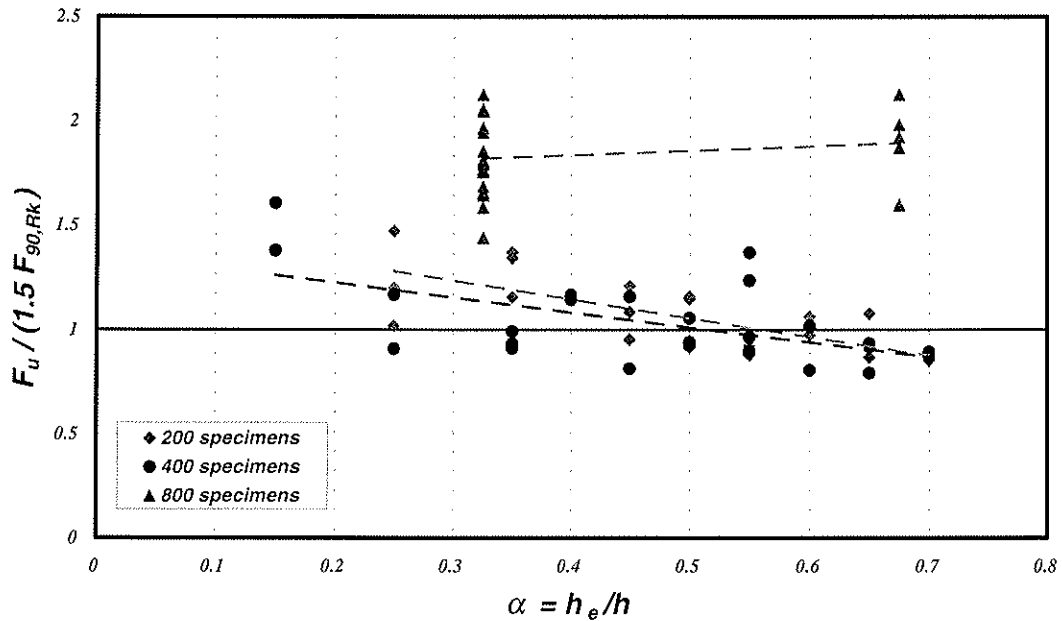
Figure 15 – Ratios $F_{u,exp}/F_{90,\,mean}$ according to new Eurocode 5 versus α
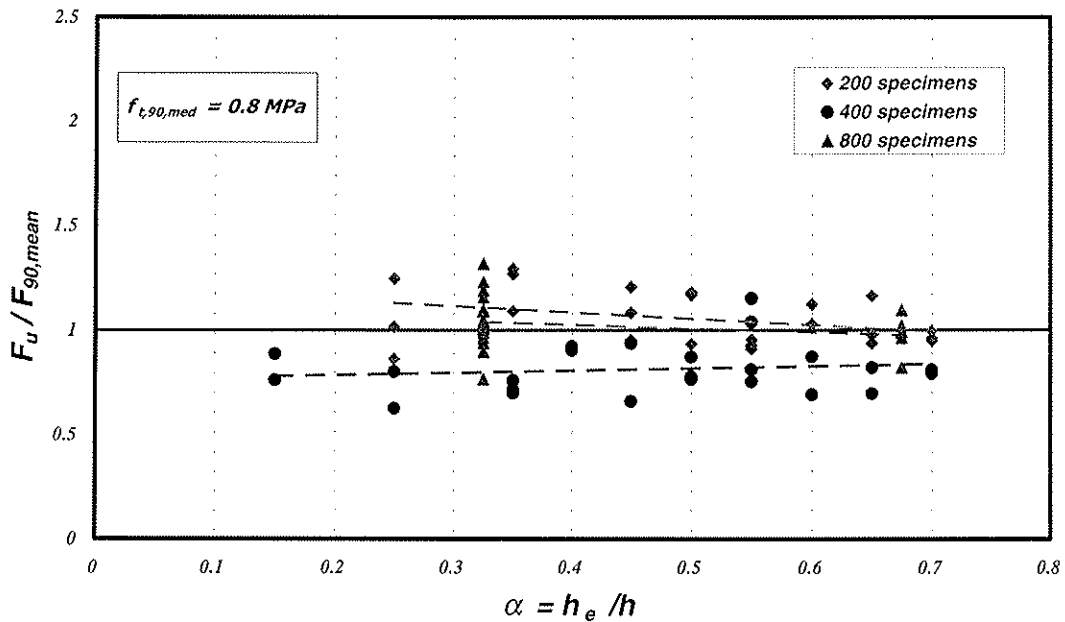
Figure 16 – Ratios $F_{u,exp}/F_{90,\,mean}$ according to new E DIN 1052 versus α

From Figures 15 and 16 the prediction ability of the design formulae can be appreciated in better detail. From Figure 15, it is easy to notice the good prediction ability of the formula for the beams of the second series and the severe underestimation of the experimental data for the beams of the first series. The better prediction ability of the E DIN 1052 formula appears clearly in Figure 16; nevertheless, the overestimation of the strength of 400 mm high beams is evident.

6   Conclusions

The results of a new experimental programme on the splitting strength of beams loaded perpendicular to the grain by dowel type connections, performed to investigate the actual

influence of the thickness of the beams and of the fasteners size, have been illustrated and discussed in detail.

The main features of this experimental research are the dimensions of the beams of the first series (800 mm high beams with a width ranging form 80 to 200 mm), and the size of fasteners' diameter.

The analysis of the results allows deriving the following drawings:

- the tests data show that beam thickness affects linearly the splitting strength;
- the tested joint configurations show to have no, or a very limited influence on the strength;
- the results on beams with single dowel connections show that the dowel diameter (and consequently the embedding strength of the joint) doesn't affect the splitting strength of beams;
- consequently, the tests results of the present research confirm the soundness of the results reported in [8].

Finally, the comparison of tests results with the design formulae included in the latest drafts of the new Eurocode 5 and E DIN 1052 shows the following:

- the design rule proposed by new Eurocode 5 describes quite well the strength of specimens with single dowel connections but it appears not able to estimate the strength of specimens with a more complex joint configuration;
- the design rule suggested by new E DIN 1052 is able to predict quite well the strength of specimens of both test series in spite of the fact that it estimates a strength greater than zero when α tends to zero.

References

[1] **prEN 1995-1-1**, 2002: *Eurocode 5 - Design of timber structures. Part 1-1: General rules and rules for buildings.* CEN/TC250/SC5, N195, Final Draft, October 2002.

[2] **E DIN 1052**, 07/2002: *Entwurf, Berechnung und Bemessung von Holzbauwerken.* Schlussentwurf Bemessungsnorm Holzbau BEKS, 2002.

[3] **Van der Put T.A.C.M.**, 1990: *Tension perpendicular to the grain at notches and joints.* CIB-W18, paper 23-10-1, Lisbon, Portugal.

[4] **Van der Put T.A.C.M.**, 1992: *Energy approach for fracture of joints loaded perpendicular to the grain.* COST 508, Workshop on fracture mechanics in wooden structures, Bordeaux, France.

[5] **Van der Put T.A.C.M., Leijten A.J.M.**, 2000: *Fracture of beams loaded by joints perpendicular to the grain.* CIB-W18, paper 33-7-7, Deltf, The Netherlands.

[6] **Ehlbeck J., Görlacher R., Werner H.**, 1989: *Determination of perpendicular-to-grain tensile stresses in joints with dowel-type fasteners: a draft proposal for design rules.* CIB-W18, paper 22-7-2, Berlin, German Democratic Republic.

[7] **Ehlbeck J., Görlacher R.**, 1995: *Tension perpendicular to the grain in joints.* Lecture C2:, STEP 1 - Timber Engineering, Centrum Hout, The Netherlands.

[8] **Ballerini M.**, 1999: *A new set of experimental tests on beam loaded perpendicular-to-grain by dowel-type joints.* CIB-W18, paper 32-7-2, Graz, Austria.

[9] **Giovanella A.**, 2002: *Experimental investigation on the splitting strength of beams loaded perpendicular to grain by dowel-type connections* (in Italian). Degree Thesis, University of Trento, Faculty of Engineering, march 27th, 2002.

[10] **Ehlbeck J., Görlacher R.,** 1983: *Tragverhalten von Queranschlüssen mittels Stahlblechformteilen, insbesondere Balkenschuhe, im Holzbau.* Forschungsbericht der Versuchsanstalt für Stahl, Holz und Steine, Abt. Ingenieurholzbau, Universität Karlsruhe.

[11] **Reske R.G.,** 1999: *Bolted timber connections loaded perpendicular-to-grain: influence of joint configuration parameters on strength.* M. Sc. Thesis. Dept. of Civil Engineering, Royal Military College of Canada, Kingston, ON.

[12] **Reske R.G., Mohammad M., Quenneville J.H.P.,** 2000: *Influence of joint configuration parameters on strength of perpendicular-to-grain bolted timber connections.* Proceedings of 6th World Timber Engineering Conference, WCTE 2000, Whistler, B.C., Canada.

[13] **Möhler K., Lautenschläger R.,** 1978: *Großflächige Queranschlüsse bei Brettschichtholz.* Forschungsbericht des Lehrstuhls für Ingenieurholzbau und Baukonstruktionen, Universität Karlsruhe.

INTERNATIONAL COUNCIL FOR RESEARCH AND INNOVATION
IN BUILDING AND CONSTRUCTION

WORKING COMMISSION W18 - TIMBER STRUCTURES

SPLITTING STRENGTH OF BEAMS LOADED BY CONNECTIONS

J L Jensen

Institute of Wood Technology
Akita Prefectural University

JAPAN

Presented by: Joergen Jensen

Joergen Jensen introduced his paper by discussing the need for this piece of research using fracture mechanics approach. Comparisons were made using the formulae provided by Jensen, Van der Put/Leijten and Gustafsson/Larsen using glulam and LVL beam examples. He concluded that the inclusion of normal forces in the Van der Put/Leijton formula is of limited practical importance. Jensen answered questions relating to the use of tensile strength values perpendicular to the grain, especially for glulam and LVL beams.

Splitting strength of beams loaded by connections

J. L. JENSEN

Institute of Wood Technology, Akita Prefectural University, Japan

1 Abstract

A fracture mechanics model for calculation of the splitting strength of dowel-type fastener joints loaded perpendicular to grain has previously been presented by Van der Put & Leijten [1], Leijten & Jorissen [2], Leijten [3], and Leijten [4], and now forms the basis for design in Eurocode 5. The Van der Put/Leijten model is based on an assumed distribution of sectional forces in the cracked part of the beam. Especially the disregard of normal forces has been subject to some discussions at previous CIB-meetings. In the present paper, a model is presented using a distribution of sectional forces, which includes normal forces and satisfies the static equilibrium equations. The solution obtained is essentially the same as the Van der Put/Leijten solution, but is derived without any simplifying assumptions. The Van der Put/Leijten expression appears as a special case of the present model, namely by assuming zero crack length or by only including the contributions from shear deformations.

The abovementioned models consider a single joint loaded perpendicular to grain. However, tests have indicated that the failure load of two single joints spaced along the grain is less than twice the failure load of a single joint. An attempt was made to use models based on the same approach as applied to the single joints to analyze beams with two joints. However, the two-joint models based on the present approach seem not to successfully explain the interaction phenomenon observed in tests.

2 Introduction

Dowel-type fastener joints subjected to loading perpendicular to grain may fail in either a ductile manner, characterized by bending of the fastener and/or embedment of the fastener into the wood, or in a brittle manner characterized by splitting of the wood.

The ductile failure modes are well understood and can fairly accurately be predicted by the European Yield Model (or extended theories), originally proposed by Johansen [5], which now forms the basis of design of dowel-type fastener joints in major design codes.

For brittle failure modes, no simple theory suitable for implementation in design codes has yet gained widely acceptance. Recently, however, two simple theoretical models based on fracture mechanics have been proposed by Van der Put & Leijten [1] and by Larsen & Gustafsson [6]. A large number of test data compiled from the literature was analyzed by Leijten [3], and the two models seem to be able to predict the splitting failure fairly well (at least if introducing appropriate empirically determined effectiveness factors). The Van der Put/Leijten model now forms the basis of design in Eurocode 5, but discussions about its theoretical foundation still occur. Main objections concentrate on the assumed distribution of sectional forces, especially the disregard of normal forces

in the cracked parts of the beam. In the present paper, a model based on the same approach as the Van der Put/Leijten model, but using a distribution of sectional forces, which includes the normal forces and fulfill the static equilibrium equations, is presented.

Tests (see for instance Larsen & Gustafsson [6] and Kasim & Quenneville [9]) have indicated that the failure load of two joints spaced along the grain of a beam is less than twice the failure load of a single joint. In particular for small spacing, tests indicate that the failure load of two joints does not increase (decrease is even reported) as compared with a single joint. An attempt was therefore made to derive models based on the same approach as applied to the single-joint model to analyze beams with two joints.

"Single joints" and "two joints" here means that the total load on a beam is assumed to be applied in one or two points, respectively. The purpose of two-joint models (in general multiple-joint models) is to account for the decrease in failure load per joint due to interacting stress fields in the beam stemming from the individual joints. A single joint may here thus be perceived as a single row of fasteners (aligned perpendicular to grain) within a joint containing two or more rows of fasteners, or as a joint (with one or more rows of fasteners) in a beam with one or more single joints, see Fig. 1.
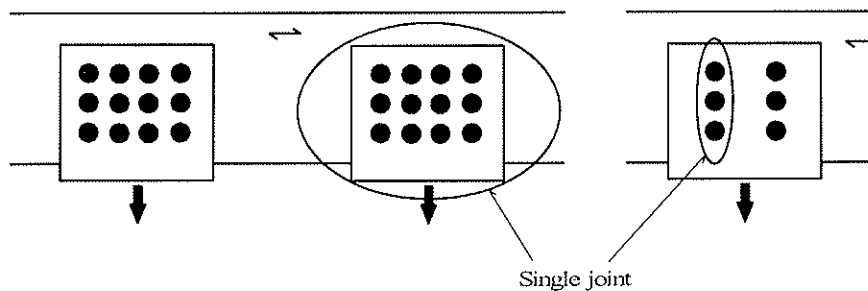
Fig. 1 *Definition of single joint*

3   Strength analysis

3.1   Linear elastic fracture mechanics

For a linear elastic body loaded by a single load, P, the crack propagation energy release rate, G, is given by (see for instance Hellan [7])

$$G = \frac{P^2}{2b} \frac{dC}{da} \tag{1}$$

where b is the width of the body, a is crack length, and C is the compliance given by

$$C = \frac{\delta}{P} \tag{2}$$

δ being the deflection of the loading point.

A crack starts propagating when the energy release rate reaches the critical value, G_c. Assuming

static or quasi-static conditions and no energy dissipation outside the fracture region, $\mathcal{G}_c$ is equal to the fracture energy, $\mathcal{G}_f$, of the material.

The failure load, P_c, of the body is thus given by

$$P_c = \sqrt{\frac{2b\mathcal{G}_f}{\dfrac{\mathrm{d}C}{\mathrm{d}a}}} \tag{3}$$

3.2 Single joint

A simply supported beam loaded perpendicular to grain by a single joint is shown in Fig. 2. Splitting failure, which occurs at the fastener located furthest from the loaded edge, is considered. It is here assumed that the fasteners are sufficiently stiff to ensure that the crack propagates along the grain simultaneously through the entire width of the beam, i.e. the problem is considered two-dimensional.

The cracked beam is modeled using ordinary beam theory (though beam theory is formally not valid for small crack lengths). The static model used is shown in Fig. 3 for a symmetrical crack of length a = $2\beta h$, h being the beam depth. The span of the beam is $2L$, and the load applied at mid-span is denoted P.
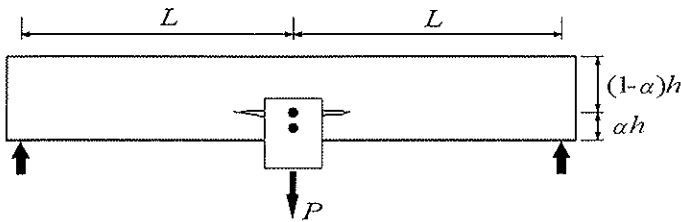
Fig. 2 *Splitting failure in beam loaded perpendicular to grain by a single joint*
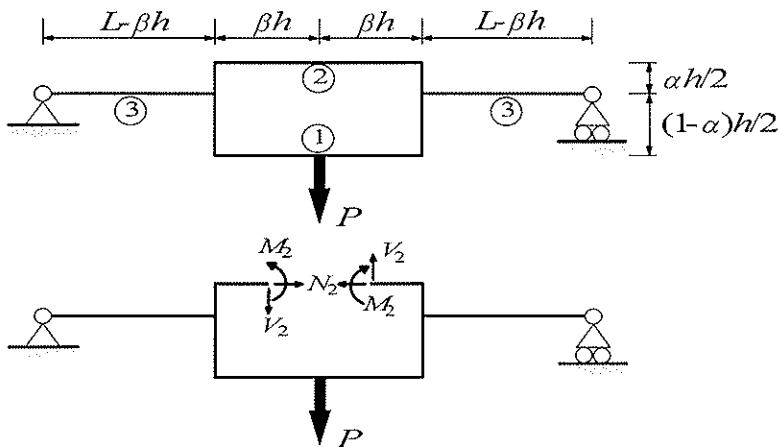
Fig. 3 *Static model for cracked beam with a single joint*

The beam structure shown in Fig. 2 is three times statically indeterminate. The unknown variables N_2, V_2, and M_2 are chosen as the sectional forces at the center of beam 2, and are found to be

$$N_2 = -\frac{3}{2}PL\frac{1}{h}\left(2 - \frac{\beta h}{L}\right)\alpha(1-\alpha) \quad , \quad M_2 = -\frac{h}{6}\frac{(1-\alpha)^2}{\alpha}N_2 \quad , \quad V_2 = 0 \tag{4}$$

The deflection at the loading point, δ, is given by

$$\delta = \frac{3}{5}\frac{P}{GA}\left(L + \beta h\frac{1-\alpha}{\alpha}\right) + \frac{P}{6EI}\left((L-\beta h)^3 + \frac{\beta h}{\alpha^3}\left(3L(L-\beta h) + (\beta h)^2 - \tfrac{3}{4}(2L-\beta h)^2(1-\alpha^3)\right)\right) \tag{5}$$

where E is modulus of elasticity, G is shear modulus, A is cross-sectional area and I is moment of inertia of the un-cracked beam cross section (width: b, depth: h).

By means of Eqs. (3) and (5), the failure load, P_c, is found to be

$$P_c = 2b\sqrt{\frac{\alpha h G \mathcal{G}_f}{\tfrac{1}{5}(1-\alpha) + \frac{3}{2}\frac{G}{E}\left(\frac{\beta}{\alpha}\right)^2(1-\alpha^3)}} \tag{6}$$

Zero crack length ($\beta \to 0$) or only considering the contribution to the deflection from the shear force ($E \to \infty$ or simply disregarding the second term in Eq. (5)) leads to the solution previously presented by Van der Put & Leijten [1], namely

$$P_c = 2b\sqrt{\tfrac{1}{3}G\mathcal{G}_f h\frac{\alpha}{1-\alpha}} \tag{7}$$

An alternative way of arriving at the same solution as given by Eq. (6) is to use the solution for a beam with a crack as given by Petersson [8]. The left side of the crack (see also Figs. 2 and 3) is shown in Fig. 4.
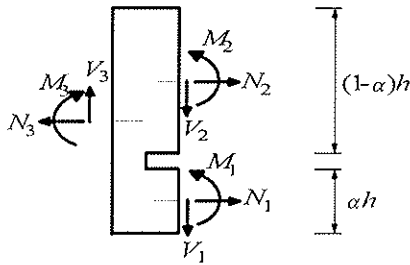
Fig. 4 *Sectional forces at crack-tip*

The sectional forces are given by Eq. (4) and by

$$N_1 = -N_2 \quad , \quad N_3 = 0$$
$$V_1 = \tfrac{1}{2}P \quad , \quad V_3 = \tfrac{1}{2}P \tag{8}$$
$$M_1 = \tfrac{1}{2}P(L-\beta h) + \tfrac{1}{2}hN_2 - M_2 \quad , \quad M_3 = \tfrac{1}{2}P(L-\beta h)$$

4

The critical load multiplication factor, λ_c, is given by

$$\lambda_c = \sqrt{\frac{2bG_f}{\dfrac{V_1^2}{\frac{5}{6}GA_1} + \dfrac{V_2^2}{\frac{5}{6}GA_2} - \dfrac{V_3^2}{\frac{5}{6}GA} + \dfrac{M_1^2}{EI_1} + \dfrac{M_2^2}{EI_2} - \dfrac{M_3^2}{EI} + \dfrac{N_1^2}{EA_1} + \dfrac{N_2^2}{EA_2} - \dfrac{N_3^2}{EA}}} \qquad (9)$$

where $A = bh$, $A_1 = \alpha A$, $A_2 = (1-\alpha)A$, $I = bh^3/12$, $I_1 = \alpha^3 I$, $I_2 = (1-\alpha)^3 I$.

Inserting the sectional forces as given by Eqs. (4) and (8) in Eq. (9), the failure load, $P_c = \lambda_c P$, is found to be given by Eq. (6).

3.3 Two joints

A beam with two joints as shown in Fig. 5 is considered. The joint spacing is $2s$. Cracks are assumed to develop symmetrically at both joints, and a state is considered where the cracks between the two joints have not yet merged. The distribution of sectional forces in the cracked beam is again calculated using a beam model as shown in Fig. 5.
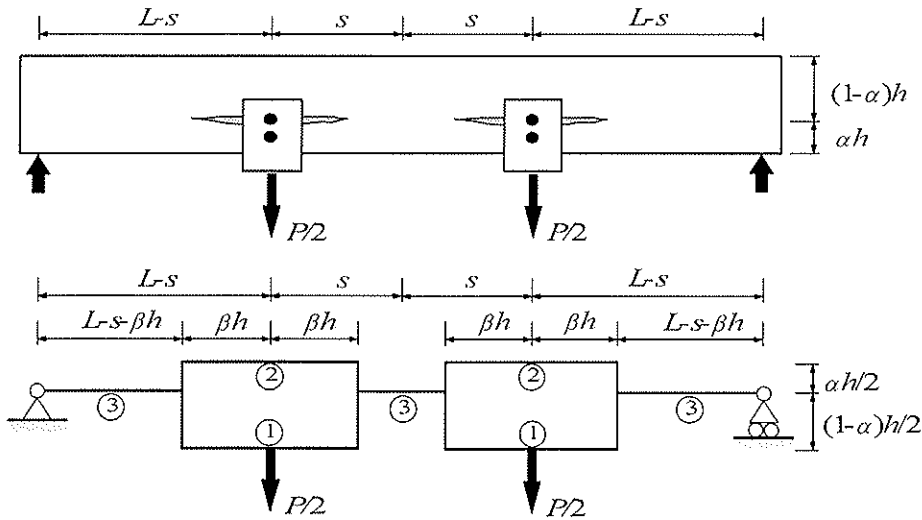
Fig. 5 *Splitting failure in beam loaded perpendicular to grain by two joints and corresponding static model. Case where cracks between the joints have not yet merged.*

The failure load, P_c, is found to be

$$P_c = 4b\sqrt{\frac{\frac{1}{2}\alpha h G G_f}{\frac{3}{5}(1-\alpha-\xi-\eta)+\frac{3}{2}\frac{G}{E}\left(\frac{\beta}{\alpha}\right)^2\left(\frac{5}{2}(1-\alpha^3)-4\xi-\frac{4}{3}\eta\right)}} \qquad (10)$$

where ξ and η are given by

$$\xi = \frac{1}{2}\,\frac{\dfrac{3}{10}\dfrac{E}{G}+\left(\dfrac{\beta}{\alpha}\right)^{2}}{\dfrac{3}{10}\dfrac{E}{G}\dfrac{1}{1-\alpha}+\left(\dfrac{\beta}{\alpha}\right)^{2}\left(1+\left(\dfrac{\alpha}{1-\alpha}\right)^{3}\right)} \qquad \eta = \frac{\dfrac{3}{10}\dfrac{E}{G}\left(\dfrac{\beta}{\alpha}\right)^{2}\dfrac{\alpha(1-2\alpha)}{(1-\alpha)^{3}}}{\left(\dfrac{3}{10}\dfrac{E}{G}\dfrac{1}{1-\alpha}+\left(\dfrac{\beta}{\alpha}\right)^{2}\left(1+\left(\dfrac{\alpha}{1-\alpha}\right)^{3}\right)\right)^{2}} \tag{11}$$

Maximum failure load is obtained for $\beta \rightarrow 0$, i.e. zero crack length, resulting in

$$P_c = 4b\sqrt{\frac{2}{3}GG_f h\frac{\alpha}{1-\alpha}} \tag{12}$$

The failure load as given by Eq. (12) is exactly twice the failure load as given by Eq. (7).

Notice that the joint spacing, $2s$, as well as the beam length, $2L$, does not appear in Eqs. (10) and (12). The present model for two joints seems therefore not useful for explaining test results, e.g. Larsen & Gustafsson [6] and Kasim & Quenneville [9], which indicate that two joints do not give twice the strength of a single joint; in particular two joints seem for small spacing to give the same (or even lower) failure load as a single joint.

In Fig. 6 is shown a situation where the part of the beam between the two joints is supposed to be cracked.
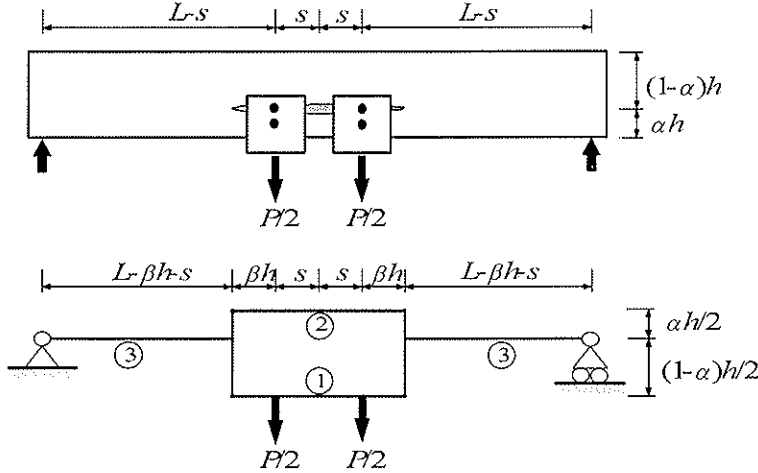
Fig. 6 *Splitting failure in beam loaded perpendicular to grain by two joints and corresponding static model. Case where the cracks between the joints have merged.*

The failure load, P_c, is in this case found to be given by Eq. (13), which for $s \rightarrow 0$ results in the same failure load as given by Eq. (6) for a single joint. For $\beta \rightarrow 0$ the solution previously presented by Van der Put & Leijten [1], and given by Eq. (7), is obtained.

$$P_c = 2b\sqrt{\frac{\alpha h G G_f}{\dfrac{2}{3}(1-\alpha)+\dfrac{3}{2}\dfrac{G}{E}\left(\dfrac{\beta}{\alpha}\right)^{2}(1-\alpha^{3})\dfrac{(\beta h)^{2}+4s(\beta h+s)}{(\beta h+s)^{2}}}} \tag{13}$$

4 Conclusions

A linear elastic fracture mechanics model for calculation of the splitting failure load for dowel-type fastener joints loaded perpendicular to grain was presented. The model is based on an approach similar to a previous model presented by Van der Put & Leijten [1], but includes normal forces in the cracked parts of the beam. The Van der Put/Leijten solution appears as a special case, namely for zero crack length or by only considering contributions from shear deformations.
Models for two joints spaced along the grain were developed based on the same approach as used in the abovementioned model. Those models predict either the same failure load as the single-joint model (cracks merged between the joints) or twice the failure load of the single-joint model (cracks not yet merged between the joints). This, however, seems not valuable for explaining existing test data.

5 References

1. Van der Put TACM & Leijten AJM (2000) Evaluation of perpendicular to grain failure of beams caused by concentrated loads of joints. CIB-W18/33-7-7
2. Leijten AJM & Jorissen AJM (2001) Splitting strength of beam loaded by connections perpendicular to grain, model validation. CIB-W18/34-7-1
3. Leijten AJM (2002) Splitting strength of beams loaded by connections, model comparison. CIB-W18/35-7-7
4. Leijten AJM (2002) Perpendicular to grain failure of beams caused by concentrated loads of joints. Proceedings of the 7th World Conference on Timber Engineering, Shah Alam, Malaysia.
5. Johansen KW (1941) Forsøg med træforbindelser. Bygningsstatiske Meddelelser, årgang XII.
6. Larsen HJ & Gustafsson PJ (2001) Dowel joints loaded perpendicular to grain. CIB-W18/34-7-3
7. Hellan K (1984) Introduction to fracture mechanics. McGraw-Hill Book Company.
8. Petersson, H (2002) Energy release rate analysis. In "Fracture mechanics models for strength analysis of timber beams with a hole or a notch- A Report of RILEM TC-133", edited by P-J Gustafsson, Report TVSM-7134, Lund University, Sweden.
9. Kasim M & Quenneville P (2002) Effect of row spacing on the capacity of bolted timber connections loaded perpendicular-to-grain. CIB-W18/35-7-6

INTERNATIONAL COUNCIL FOR RESEARCH AND INNOVATION
IN BUILDING AND CONSTRUCTION

WORKING COMMISSION W18 - TIMBER STRUCTURES

A TENSILE FRACTURE MODEL FOR JOINTS WITH RODS OR DOWELS

LOADED PERPENDICULAR- TO-GRAIN

J L Jensen

Inst. of Wood Technology, Akita Prefectural University

JAPAN

P J Gustafsson

H J Larsen

Div. of Structural Mechanics, Lund University

SWEDEN

Presented by: J Larsen

J Larsen explained that the authors used the updated approach based on beam on elastic foundation approach using Timoshenko beam theory as published recently as a CIB-W18 paper. Comparisons were carried out using fracture mechanics and stress analysis approaches. Analysis was also carried out using a double symmetrical "plate joint" model.

Hans Larsen presented the experimental work used to verify the theoretical work described in the paper. This included tests carried out by Yasumura, and Quenneville and Mohammad, and Kasim and Quenneville. Comparisons of the test data with theoretical work raised questions about the use of fitting approaches.

These 2 presentations were followed by interesting discussions relating to the theoretical definition of stresses as well as the practical engineering design solution approaches to the perpendicular-to-the-grain tensile fracture situations.

A tensile fracture model for joints with rods or dowels loaded perpendicular-to-grain

J. L. JENSEN

Inst. of Wood Technology, Akita Prefectural University, Japan

P. J. GUSTAFSSON   and   H. J. LARSEN
Div. of Structural Mechanics, Lund University, Sweden

1 Abstract

Tensile splitting failure from glued-in rods or dowels loaded perpendicular to grain is studied. A new quasi-nonlinear fracture mechanics model based on beam-on-elastic-foundation (BEF) theory is presented. The model is applied to plates with edge dowels, to beams with dowels, and to beam splice joints made up of rods glued in along grain. The BEF theory is verified by FEM calculations and test results for the same three kinds of joints. The test results for dowel joints in plates agree very well with the theory. The same applies for dowel joints in beams with small edge distances. For larger edge distances both the BEF and the FEM calculations overestimate the load-carrying capacity. In this case it may partly be explained by a change of failure mode from pure splitting to a combination of compression failure perpendicular to grain and splitting. Also the test results for beam splice joints with glued-in rods agree well with the theory.

2 Introduction

Several theoretical and experimental studies of tensile failures perpendicular to grain in dowel joints have been presented in recent years. Among others may be mentioned those by Gustafsson & Larsen [1], Jensen [3], Jensen & Gustafsson [4], Larsen & Gustafsson [5], [Leijten [6], Leijten [7], Leijten & Jorissen [8] and Van der Put & Leijten [10]. These studies represent rational models based on fracture mechanics, being simple enough to allow derivation of explicit strength equations that don't require any numerical analysis.

In models based on linear fracture mechanics, LEFM, it is assumed that fracture takes place as crack development by propagation of a fracture process region, which is small compared to relevant dimensions of the structural element. The material properties that govern joint strength are in this case E, G and G_f, being the modulus of elasticity, the shear modulus and the fracture energy, respectively.

In quasi-non-linear fracture mechanics, introduced in Gustafsson [2], the fracture region, its non-zero size. its limited stress capacity and its deformation capacity are taken into account by a deformation layer located along the potential fracture propagation path. The layer is assumed to be linear elastic with properties chosen in such a way that the fracture energy and the tensile strength of the wood are correctly reproduced. The material properties that govern joint strength are in this case the fracture toughness, $(E G_f)^{1/2}$ or $(G G_f)^{1/2}$, and the perpendicular to grain tensile strength, f_t.

The joint strength is in general affected by both parameters. However, in the extreme case of completely uniform stress distribution the strength is proportional to f_t and independent of $(EG_f)^{1/2}$, and vice versa in the extreme case of concentrated local stress at the tip of a deep crack in a large structural element.

3 Theory

3.1 Dowel joints in plates

3.1.1 Multiple dowels

A double symmetrical plate joint with two dowels in a row parallel to grain as shown in Fig. 1 is considered.
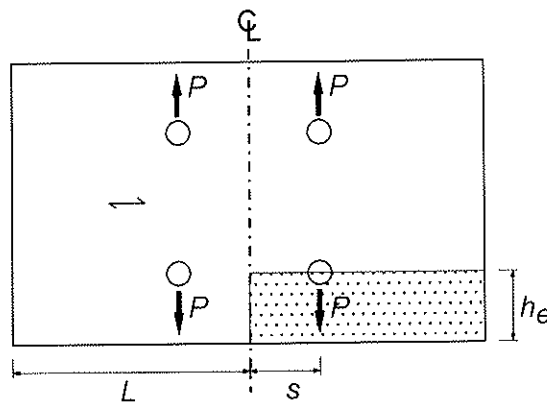
Fig. 1 *Double symmetrical plate with two dowels in a row parallel to grain.*
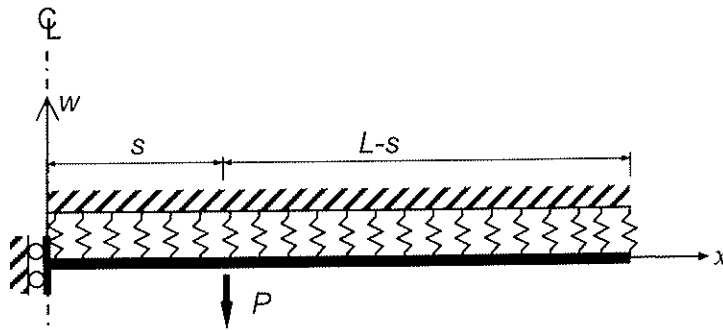
Fig. 2 *Beam-on-elastic-foundation model. Load, geometry, and boundary conditions.*

The shaded area is as shown in Fig. 2 treated as an elastic Timoshenko beam of finite length supported by a stiff foundation through linear elastic springs. The perpendicular-to-grain stress acting on the beam, σ, is given by

$$\sigma(x) = -Kw(x) \tag{1}$$

where K (unit: N/m^3) is the foundation modulus and $w(x)$ is the deflection of the beam axis, which may also be written

$$w(x) = -P\Phi(x) \tag{2}$$

Taking into account deformations of the beam due to bending and shear, the function $\Phi(x)$ (see Pilkey [9]) becomes

$$\Phi(x) = -\frac{e_1(x)}{EI\nabla}\{e_4(L)e_2(L-s) + \tfrac{1}{2}[e_1(L) - \eta e_3(L)]e_1(L-s)\} + \frac{e_3(x)}{EI\nabla}\{e_2(L)e_2(L-s) - e_3(L)e_1(L-s)\} + \frac{e_1\langle x-s \rangle}{EI} - \frac{e_2\langle x-s \rangle}{GA_s} \tag{3}$$

$$\nabla = -\lambda e_3(L)e_4(L) - e_2(L)[e_1(L) - \eta e_3(L)]$$

$$e_i\langle x-s \rangle = \begin{cases} 0 & \text{if } x < s \\ e_i(x-s) & \text{if } x \geq s \end{cases}$$

Case 1: $(\lambda \geq \tfrac{1}{4}\eta^2)$

$$e_1(z) = \frac{1}{2uv}\left[2uv \cosh vz \cos uz + \frac{\eta}{2}\sinh vz \sin uz\right]$$

$$e_2(z) = \frac{1}{2uv}[v \cosh vz \sin uz + u \sinh vz \cos uz]$$

$$e_3(z) = \frac{1}{2uv}\sinh vz \sin uz$$

$$e_4(z) = \frac{1}{2uv}\frac{1}{\sqrt{\lambda}}[v \cosh vz \sin uz - u \sinh vz \cos uz]$$

$$u^2 = \tfrac{1}{2}\sqrt{\lambda} - \tfrac{1}{4}\eta \quad , \quad v^2 = \tfrac{1}{2}\sqrt{\lambda} + \tfrac{1}{4}\eta$$

Case 2: $(\lambda < \tfrac{1}{4}\eta^2)$

$$e_1(z) = \frac{1}{v^2 - u^2}[v^2 \cosh vz - u^2 \cosh uz]$$

$$e_2(z) = \frac{1}{v^2 - u^2}[v \sinh vz - u \sinh uz]$$

$$e_3(z) = \frac{1}{v^2 - u^2}[\cosh vz - \cosh uz]$$

$$e_4(z) = \frac{1}{v^2 - u^2}[\tfrac{1}{v}\sinh vz - \tfrac{1}{u}\sinh uz]$$

$$u^2 = \tfrac{1}{2}\eta - \sqrt{\tfrac{1}{4}\eta^2 - \lambda} \quad , \quad v^2 = \tfrac{1}{2}\eta + \sqrt{\tfrac{1}{4}\eta^2 - \lambda}$$

where

$$\lambda = \frac{Kb}{EI} \quad , \quad \eta = \frac{Kb}{GA_s} \tag{4}$$

b being the width of the beam, E the modulus of elasticity, G the shear modulus, I the moment of inertia, and A_s the equivalent shear area of the beam cross section ($A_s = 5bh_c/6$ for a rectangular cross section with beam depth h_c).

The springs are intended to model the strength and fracture performance of the wood perpendicular to grain. The damage and fracture performance of wood is non-linear, but is in the present analysis represented by a linear response that is equivalent in terms of peak stress, f_t, and fracture energy dissipation, G_f. Since the energy dissipation in the case of linear performance is

$$G_f = \tfrac{1}{2}f_t\left(\frac{f_t}{K}\right) \quad \text{it follows that} \quad K = \frac{f_t^2}{2G_f} \tag{5}$$

The foundation stress in a joint with one ($s = 0$) or two dowels is thus given by Eqs. (1) - (5). Failure is assumed to occur when the maximum stress, $\sigma(x)$, equals the tensile strength perpendicular to grain, f_t, of the wood. For joints with three or more of dowels in a row parallel to grain, the stress distribution may be calculated by superposition. The superposition is straight forward if the load sharing between the dowels is known. The load sharing can be calculated by deformation conditions if not known or assumed in advance.

3

The present strength analysis of mode I failure is an analogy to the fracture mechanics application of the Volkersen-model to strength analysis of mode II failure in lap joints, see Gustafsson [2]. In Jensen & Gustafsson [4] it was shown that the stress criterion $\sigma = f_t$ gives exactly the same failure load predictions as the energy release rate criterion $G = G_f$ if using the present theory with a deformation layer with stiffness according to Eq. (5).

The limit between the two cases considered in Eq. (3) may be characterized by a requirement to the depth, h_e.

$$\text{Case 1:} \quad h_e \leq \frac{200}{3} \frac{G^2}{E} \frac{G_f}{f_t^2} \qquad\qquad \text{Case 2:} \quad h_e \geq \frac{200}{3} \frac{G^2}{E} \frac{G_f}{f_t^2} \qquad\qquad (6)$$

3.1.2 Two dowels

In case of two dowels in a row parallel to grain, the maximum stress usually occurs at the location of the dowels ($x = s$). In this case it is possible to give a closed-form solution as outlined below. In some special cases, e.g. for very small end distances, where the maximum stress does not occur at the location of the dowels, the solutions below are slightly non-conservative.

Eqs. (1), (2), and (6) give the plate failure load, P_p

$$P_p = \frac{2G_f}{f_t \Phi(s)} \qquad\qquad (7)$$

where $\Phi(s)$ may be written

Case 1: ($\lambda \geq \tfrac{1}{4}\eta^2$)

$$\Phi(s) = \frac{1}{EI} \frac{1}{\lambda} \frac{1}{4uv} \frac{4v^4 C_1 - v^3 u C_2 + 4v^2 u^2 C_3 + vu^3 C_4 - 4u^4 C_5}{v \sin 2uL + u \sinh 2vL} \qquad\qquad (8a)$$

$C_1 = \left[\sin u(L-s)\cosh^2 vs + \cos uL \sin us \right] \sin u(L-s)$, $C_2 = 3\sinh 2vs \sin 2u(L-s) + \sin 2us \sinh 2v(L-s)$

$C_3 = \cosh^2 vs - \sin^2 us$
$\qquad + 3\left\{ \left[\cosh^2 vL - \sin^2 uL\right]\left[\cosh^2 vs \cos^2 us - \sinh^2 vs \sin^2 us\right] + \tfrac{1}{4}\left[\cosh 2vs \sin 2uL \sin 2us - \cos 2us \sinh 2vL \sinh 2vs\right]\right\}$

$C_4 = 3\sin 2us \sinh 2v(L-s) + \sinh 2vs \sin 2u(L-s)$, $C_5 = \left[\sinh v(L-s)\cos^2 us + \cosh vL \sinh vs\right]\sinh v(L-s)$

Case 2: ($\lambda < \tfrac{1}{4}\eta^2$)

$$\Phi(s) = \frac{1}{EI} \frac{1}{\lambda} \frac{1}{(v^2 - u^2)^2} \frac{v^6 C_1 - v^5 u C_2 + v^4 u^2 C_3 + v^3 u^3 C_4 - v^2 u^4 C_5 + vu^5 C_6 - u^6 C_7}{v \cosh uL \sinh vL - u \cosh vL \sinh uL} \qquad\qquad (8b)$$

$C_1 = \cosh uL \cosh vs \cosh v(L-s)$, $C_2 = \sinh uL \cosh vs \sinh v(L-s)$
$C_3 = -2\cosh vs \cosh us - \cosh uL \cosh vs \cosh v(L-s)$, $C_4 = \cosh vs \sinh uL \sinh v(L-s) - \cosh us \sinh vL \sinh u(L-s)$
$C_5 = -2\cosh us \cosh vs - \cosh vL \cosh us \cosh u(L-s)$, $C_6 = \sinh vL \cosh us \sinh u(L-s)$
$C_7 = \cosh vL \cosh us \cosh u(L-s)$

λ, η, u, and v are defined in Eqs. (3) and (4).

For an infinitely long plate ($L \rightarrow \infty$) the failure load is reduced to the following comparatively simple expression

Case 1 ($\lambda \geq \eta^2/4$): $\quad P_P = 4bf_t \dfrac{e^{2vs}}{\frac{1}{u}\left(\sqrt{\lambda} - \eta\right)\sin 2us + \frac{1}{v}\left(\sqrt{\lambda} + \eta\right)\left(e^{2vs} + \cos 2us\right)}$ (9a)

Case 2 ($\lambda < \eta^2/4$): $\quad P_P = 2bf_t \dfrac{(v-u)\left(v^2 - u^2\right)^2}{v^4\left(v^2 - vu - u^2\right)\left(1 + e^{-2vs}\right) + v^3u^3\left(e^{-2vs} - e^{-2us}\right) - u^4\left(u^2 - uv - v^2\right)\left(1 + e^{-2us}\right)}$ (9b)

3.1.3 Single dowel

The failure load, P_P, of a joint with a single dowel is obtained from Eq. (8) by setting $s = 0$ (and multiplying by 2)

Case 1 ($\lambda \geq \eta^2/4$): $\quad P_P = 2bf_t \dfrac{\frac{1}{u}\sin 2uL + \frac{1}{v}\sinh 2vL}{4 - \left[3 - \left(\dfrac{v}{u}\right)^2\right]\sin^2 uL + \left[3 - \left(\dfrac{u}{v}\right)^2\right]\sinh^2 vL}$ (10a)

Case 2 ($\lambda < \eta^2/4$): $\quad P_P = 2bf_t \dfrac{\left(v^2 - u^2\right)^2\left(v\tanh vL - u\tanh uL\right)}{v^6 - u^6 - vu\left(v^4 - u^4\right)\tanh vL \tanh uL - v^2u^2\left(v^2 - u^2\right)\left(1 + \dfrac{2}{\cosh vL \cosh uL}\right)}$ (10b)

For an infinitely long plate ($L \rightarrow \infty$) the solutions for case 1 and case 2 merge and may be given as

$$P_P = \mu P_{P,\text{LEFM}}$$ (11)

where the linear elastic fracture mechanics solution, $P_{P,\text{LEFM}}$, is given by

$$P_{P,\text{LEFM}} = b\sqrt{\tfrac{20}{3}GG_f h_e} \approx 2.58b\sqrt{GG_f h_e}$$ (12)

and μ is given by

$$\mu = \frac{\sqrt{2\zeta + 1}}{\zeta + 1} \quad, \quad \zeta = \frac{5}{\sqrt{3}}\frac{G}{E}\sqrt{\frac{2EG_f}{h_e f_t^2}}$$ (13)

As seen from Eq. (13), the linear elastic fracture mechanics solution is obtained for $EG_f/(h_e f_t^2)$ or $GG_f/(h_e f_t^2)$ approaching zero, i.e. for brittle performance of the material or for large absolute size of the structural element.

Gustafsson & Larsen [1] previously derived the solution

5

$$P_p = 2\xi b\sqrt{2GG_f h_e} \approx 2.83\xi b\sqrt{GG_f h_e} \tag{14}$$

where ξ was introduced as an empirical efficiency factor. By means of the present theory ξ can be given as $\xi = \mu\sqrt{5/6}$, where μ is given by Eq. (13). The theoretically estimated values of ξ are in very good agreement with the experimentally determined values given in Larsen & Gustafsson [5].

The influence of dowel spacing is illustrated in Fig. 3. The ratio P_2/P_1 is given as a function of the normalized dowel spacing, $2s/h_e$, where P_2 is the failure load per dowel in a joint with two dowels as given by Eq. (9). P_1 is the failure load of a single dowel joint as given by Eqs. (11) – (13). The figure is based on $h_e = 56$ mm, $E = 12700$ MPa, $G = 870$ MPa and $G_f = 0.25$ N/mm. For case 1: $f_t = 0.89$ MPa. For case 2: $f_t = 5.0$ MPa.
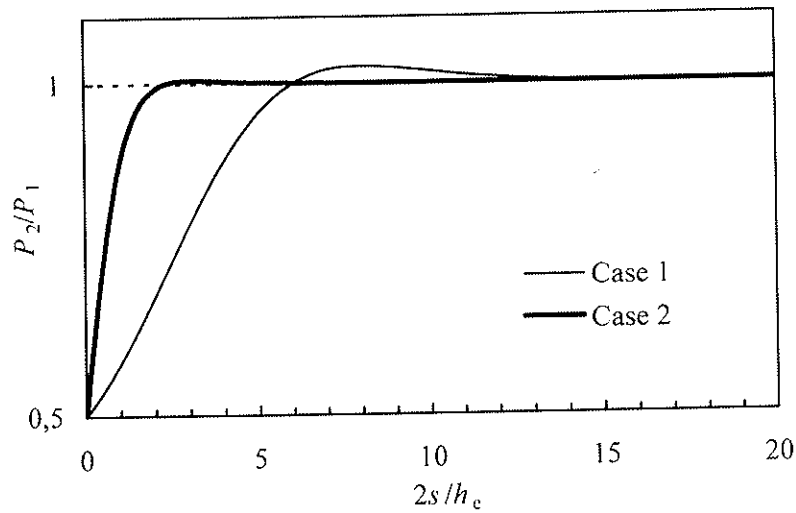
Fig. 3 *Influence of dowel spacing*

3.2 Dowel joints in beams

3.2.1 Beam on elastic foundation solution

In Fig. 4 is shown a joint with two dowels with edge distance h_e in a beam with total depth h. The shaded part of the beam distributes the dowel load to the rest of the beam partly as tensile stress perpendicular to grain, σ, partly as shear stress, τ.

For dowel joints in plates, the assumption that the springs rest on a fixed foundation is fulfilled due to the symmetry. For dowels in a beam, this is only the case if $h_e \ll h$, and the stress distribution can moreover be expected to be somewhat different from the stress distribution in the double symmetrical plate joints. As a simplifying approximation, however, the tensile stress distribution, σ, and the load per dowel P_P carried by the tensile stress is assumed to be the same as the distribution in the corresponding double-symmetrical plate joint.

The load per dowel carried by the shear stress is denoted P_S, and the total load per dowel is denoted P_B.
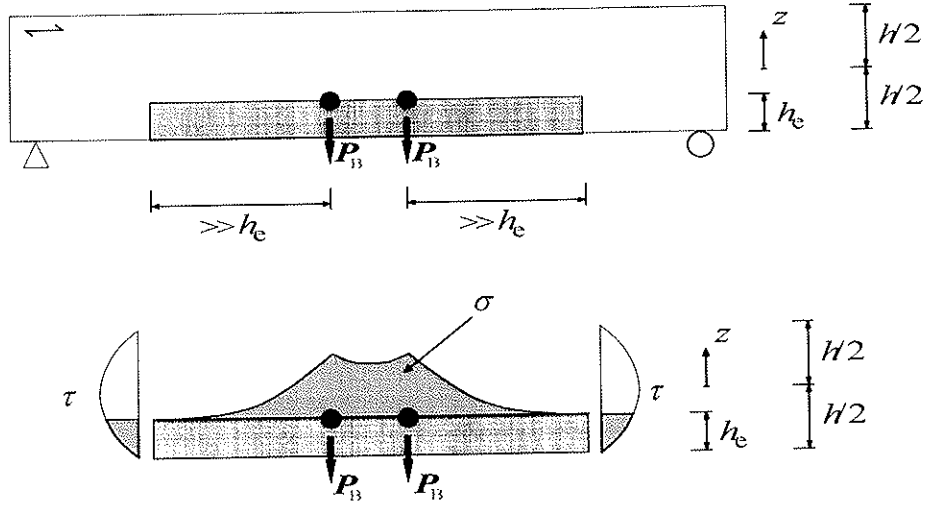
Fig. 4 *Dowel joint in beam*

The free body diagram gives the equilibrium equation

$$P_B = P_S + P_P \qquad \Rightarrow \qquad P_B = P_P /(1 - P_S / P_B) \tag{15}$$

The ratio P_S/P_B is calculated from the parabolic distribution of the shear stress, valid in beams at distances $\gg h_e$ from the dowels and other local stress disturbances:

$$\frac{P_S}{P_B} = \frac{\int_{-h/2}^{-h/2+h_e} b\,\tau dz}{\int_{-h/2}^{h/2} b\,\tau dz} = 3\left(\frac{h_e}{h}\right)^2 - 2\left(\frac{h_e}{h}\right)^3 \tag{16}$$

and the total load per dowel in a beam joint, P_B, may thus be given as

$$P_B = \kappa P_P \quad , \qquad \kappa = \frac{1}{1 - 3\left(\dfrac{h_e}{h}\right)^2 + 2\left(\dfrac{h_e}{h}\right)^3} \tag{17}$$

3.2.2 Finite element solution

7
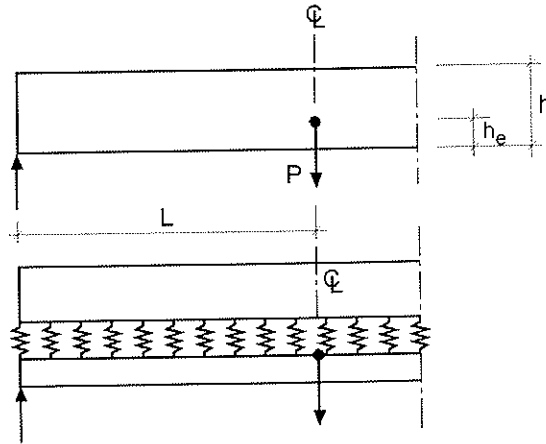
Fig. 5 *Finite element model of a beam with one dowel.*

A finite element model has been used to evaluate the accuracy of Eq. (17), which in general is on the unsafe side, and to verify the BEF Eqs. (9) and (10). A symmetrical beam with one or more dowels, see Fig. 5, is modeled as two Timoshenko beams, one on top of the other, with an intermediate layer composed of elastic springs with the normal stiffness $K_n = f_t^2/(2\,\mathcal{G}_f)$ and a shear stiffness K_v. The exact value of K_v appears not to be of very great importance for the present applications and was throughout the present calculations set equal to $3K_n$. One may expect the results of the FE-calculations to coincide exactly with the results of BEF calculations if in FE-calculations K_v is set equal to zero and the stiffness of the upper beam is made infinitely large. The initial length of the springs representing the elastic layer is zero and they are located between the upper edge of lower beam and the lower edge of the upper beam, and accordingly not between the centerlines of the two beams.

Theoretical results for the increase factor P_B/P_p, indicating the ratio between load capacity of a dowel in a beam and at the edge of a plate are given in Table 1. The FEM results were obtained for $L = 1000$ mm, $h = 250$ mm, $G = 870$ MPa, $E = 12700$ MPa, $f_t = 1.0$ MPa, $\mathcal{G}_f = 0.30$ N/mm and $K_v/K_n = 3$.

Table 1 *Ratio P_B/P_p from FEM calculations and from an approximate beam theory estimation.*

h/h_e	0.1	0.2	0.3	0.4	0.5	0.6	0.7	0.8	0.9
FEM	1.01	1.03	1.08	1.21	1.55	2.27	3.65	6.16	12.0
κ, Eq. (17)	1.03	1.12	1.28	1.54	2.00	2.84	4.63	9.6	35.7

3.3 Glued-in rod beam splice joints

In Fig. 6 is shown a symmetrical beam splice joint with rods glued in parallel to grain. Shear failure may occur as splitting failure in the beam as indicated in the figure. For this case a fracture mechanics solution based on beam-on-elastic-foundation theory as described above for dowel-type fastener joints was used in Jensen & Gustafsson [4].

8
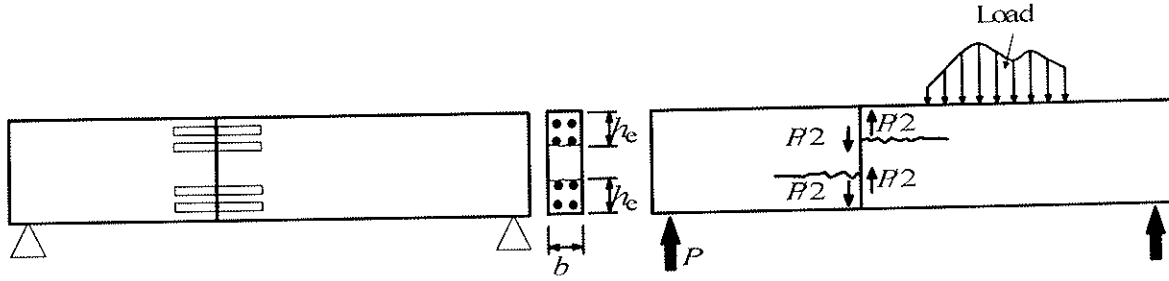
Fig. 6. *Splitting failure in symmetrical beam splice joint with glued-in rods.*

In the analysis of dowel joints, the beam-end was assumed to be fixed against rotations (see Fig. 2). In case of a splice joint, however, the beam-end is in reality only partially restrained. Two solutions were therefore developed; an upper-bound solution assuming no rotation at the beam-end, and a lower-bound solution assuming a free beam-end. The real failure load should in general be expected to fall between the upper-bound and lower-bound estimates.

Assuming infinite length of the beam on elastic foundation will for all practical joints cause only insignificant errors.

The upper-bound solution, $P_{c,U}$, is given by Eqs. (11) – (13), i.e.

$$P_{c,U} = \mu b \sqrt{\tfrac{20}{3} G \mathcal{G}_f h_e}$$
(18)

and the lower-bound solution may be written

$$P_{c,L} = \gamma P_{c,U}$$
(19)

where

$$\mu = \frac{\sqrt{2\zeta + 1}}{\zeta + 1} \quad , \quad \gamma = \frac{\zeta + 1}{2\zeta + 1} \quad , \quad \zeta = \frac{5}{\sqrt{3}} \frac{G}{E} \sqrt{\frac{2E\mathcal{G}_f}{h_e f_t^2}}$$
(20)

The beam efficiency factor κ as derived in section 3.2 may also be applied here.

4 Tests

4.1 Dowel joints

4.1.1 LVL plates and beams

Tests were made with plate and beam specimens as shown in Fig. 7a and Fig. 7b respectively. The geometries are shown in Table 2 and 3, where also the test values and the theoretical values are given and compared. The test values indicated are the average values for each test series and the theoretical values are for the plates those obtained by BEF calculations (Eq. (9,10)) and for beams

those obtained by FEM calculations. All specimens were 40 mm thick and made of Laminated Veneer Lumber (LVL) with a density of 475 kg/m^3 at 12 % moisture content. The dowel diameter was 14 mm. The test series 1.1-280a, 1.2, 1.3 and 2-56a (shaded) are reported in details in Gustafsson & Larsen [1], where also tests with tension and DCB specimens are described. The tensile strength perpendicular to grain was estimated to $f_t = 0.89$ MPa and the fracture energy to $G_f = 0.25$ N/mm. The number of specimens in a series was 10 for tension and DCB tests and more than 50 for the dowel tests. The following parameters were estimated from the density: $E = 12700$ MPa and $G = 870$ MPa.
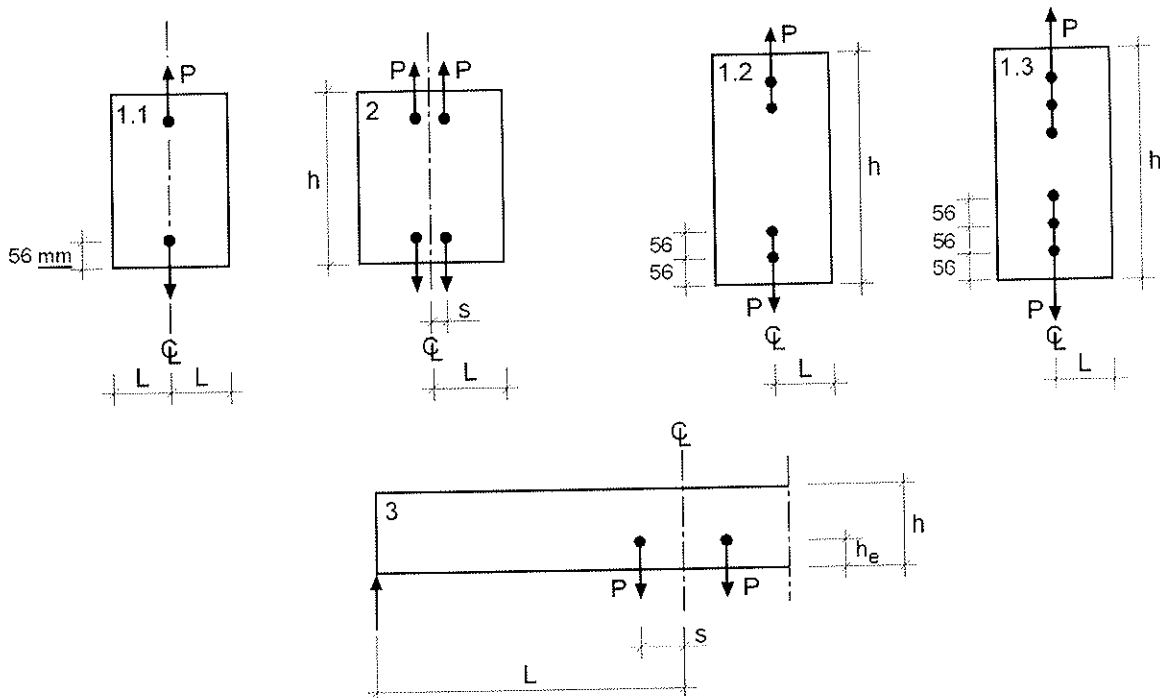
Fig. 7 *Test specimens. All plates are double symmetrical and all beams are symmetrical.*

The other test series were made from a very limited amount of LVL left over from the shaded tests marked in bold, and the number of specimens was only 6 (for plate tests) and 4 (for beam tests).

Table 2 *Geometry of plate specimens and failure loads (Theory and test) in kN. All measurements in mm.*

	1.1-56	1.1-112	1.1-168	1.1-224	1.1-280a	1.1-280b	1.2	1.3	2-28a	2-28b	2-56	2-84	2-112
$2L$	56	112	168	224	280	280	400	500	168	140	140	140	140
s									28	28	56	84	112
$L - s$										112	84	56	28
h	200	200	200	200	280	200	200	200	280	200	200	200	200
h_c	56	56	56	56	56	56	112	168	56	56	56	56	56
L/h_c	0.5	1.0	1.5	2.0	2.5	2.5	1.8	1.5					
s/h_c									0.5	0.5	1.0	1.5	2.0
Theory	1.97	3.82	5.39	6.56	7.27	7.27	10.82	13.61	4.10	4.10	4.54	4.62	4.08
Test	1.54	3.49	5.57	6.53	7.55	7.50	11.05	14.53	3.75	3.77	4.19	3.98	2.88
Test/Theory	0.78	0.91	1.03	1.00	1.04	1.03	1.02	1.07	0.91	0.92	0.92	0.86	0.71

The main conclusion is that the theory predicts the failure loads satisfactorily. This applies both to the absolute values and to the trends predicted in Fig. 3.

Table 3 *Geometry of beam specimens and failure loads (Theory and test) in kN. All measurements in mm.*

	3-0	3-56	3-84	3-112	3-140
s	0	56	84	112	140
h	200	200	200	200	200
h_e	56	56	56	56	56
s/h_e	0	1.0	1.5	2.0	2.5
L	750	750	750	750	750
Theory	5.01	6.80	7.88	8.85	9.57
Test	5.15	5.87	7.42	8.85	9.74
Test/Theory	0.97	0.86	0.94	1.00	1.02

4.1.2 Glulam

The theory has also been used to evaluate the tests with beams reported in Yasumura [11], Quenneville & Mohammad [12] and Kasim & Quenneville [13]. Calculations were carried out by the BEF solution, Eqs. (9) and (10), as well as by FEM. For loading and boundary conditions corresponding to a plate are the same results obtained by BEF calculations as by FEM calculations with $K_v = 0$. The FEM results indicated in the below tables were all obtained with $K_v = 3K_n$.

All these tests were made with glulam beams with rather short spans $3h$–$6h$.The main geometry of the test specimens are given in Fig. 8 and Table 4 – 6, where also the calculated failure loads and the test values for the relevant test series are given. σ_h is the embedding stress at failure.
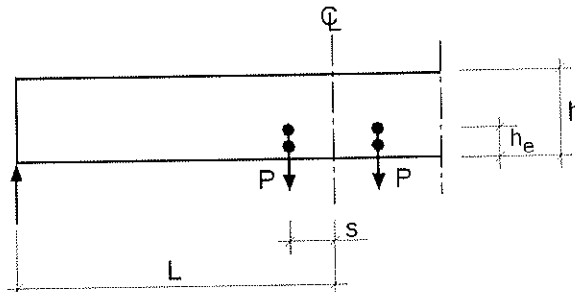
Fig. 8 *Test specimens.*

There is little information about the materials and the theoretical calculations have been made with the following material properties: $E = 12700$ MPa and $G = 870$ MPa. f_t and G_f have been estimated from the tests. Generally the best fit to the test results is obtained for $f_t = 1.0$ MPa and $G_f = 0.3$ N/mm. For Yasumura's tests, however, the best fit is found for $f_t = 5.0$ MPa and $G_f = 0.4$ N/mm, values much higher than expected, but consistent with the very high embeddings stresses at failure.

The plate load-carrying capacities according to the BEF theory and the FEM model agree well, the difference is due to the introduction of the shear stiffness (K_v) in the FEM-model. The load capacity of the beams tested by Quenneville & Mohammad [12] and Kasim & Quenneville [13]

11

are for large edge distances significantly over-estimated by the theoretical calculations. This may partly be explained by a change of failure mode from pure splitting to a combination of compression failure perpendicular to grain and splitting. This is supported by the high stresses perpendicular to grain at failure.

Table 4 *Summary of Yasumura's tests [11]*

b mm	h_c mm	h mm	h_c/h	No. of columns	s mm	P_{test} kN (B)	σ_h MPa	P_{theory} (kN) plate BEF Eq. (9,10)	FEM	P_{theory} (kN) beam FEM (A)	P_{theory}/P_{test} beam (A)/(B)
30	64	224	0.29	1	0	15.87	16.5	10.9	11.1	12.6	0.79
30	112	224	0.5	1	0	24.03	25.0	14.7	14.8	26.1	1.09
30	160	224	0.71	1	0	33.23	34.6	17.7	17.8	36.8	1.11
30	96	336	0.29	1	0	15.03	15.7	13.6	13.7	15.8	1.05
30	168	336	0.5	1	0	30.30	31.5	18.2	18.3	25.9	0.97
30	128	448	0.29	1	0	24.17	25.2	15.8	15.9	18.4	0.76
30	224	448	0.5	1	0	27.47	28.6	21.1	21.3	30.0	1.09

Dowel diameter: 16 mm

Table 5 *Summary of Quenneville & Mohammad's tests [12]*

Test No.	b mm	h_c mm	h mm	h_c/h	No. of columns	s mm	P_{test} kN (B)	σ_h MPa	P_{theory} (kN) plate BEF Eq.(9,10)	FEM	P_{theory} (kN) beam FEM (A)	P_{theory}/P_{test} beam (A)/(B)
1	130	76	190	0.4	1	0	41	8.3	33.8	35.0	40.8	1.00
2	80	76	190	0.4	1	0	26	8.6	20.8	21.6	25.1	0.97
3	130	114	190	0.6	1	0	59	11.9	43.6	44.6	80.5	1.36
4	130	133	190	0.7	1	0	85	17.2	47.5	48.2	120	1.41
5	80	133	190	0.7	1	0	52	17.1	29.2	29.7	73.7	1.42
6	130	171	228	0.75	1	0	100	20.2	55.8	57.9	165	1.65
7	130	133	190	0.7	2	47.5	104	10.5	54.3	57.0	167	1.61
8	80	133	190	0.7	2	37	75	12.3	32.8	33.4	96.6	1.29
9	130	133	190	0.7	2	66.5	107	10.8	56.1	60.4	187	1.75
11	130	114	190	0.6	2	47.5	73	7.4	49.6	53.3	103	1.41
13	130	171	228	0.75	2	47.5	122	12.4	62.7	65.5	233	1.91

Dowel diameter: 19 mm.

Table 6 *Summary of Kasim & Quenneville's tests [13]*

b mm	h mm	H_e mm	h_e/h	No. of columns	s mm	P_{test} kN (B)	σ_h MPa	P_{theory} (kN) plate		P_{theory} (kN) beam FEM (A)	P_{theory}/P_{test} Beam (A)/(B)
								BEF Eq. (9,10)	FEM		
80	304	134	0.44	1	0	41.1	13.5	29.9	30.9	37.8	0.92
80	304	134	0.44	2	77	32.6	3.4	35.3	39.9	50.1	1.54
80	304	134	0.44	2	155	41.5	6.8	40.2	48.7	62.1	1.28
80	304	134	0.44	2	225	58.7	9.7	44.8	56.9	75.1	1.28
80	304	134	0.44	2	320	63.2	10.4	50.8	61.4	87.1	1.38
80	304	204	0.70	1	0	68.2	22.4	39.7	40.6	93.6	1.37
80	304	204	0.70	2	77	66.6	11.0	45.6	49.8	137	2.1
80	304	204	0.70	2	225	83.8	13.8	55.1	67.6	183	2.2
80	304	204	0.70	2	320	83.2	13.7	61.2	74.2	196	2.4
80	304	204	0.70	2	418	100.4	16.5	67.6	76.1	218	2.2

Dowel diameter: 19 mm.

4.2 Glued-in rod beam splice joints

4.2.1 Test set-up and specimens

Tests were conducted in a test set-up as shown in Fig. 9, which gives pure shear at the location of the joint. The geometry of the eight types of joints tested is shown in Fig. 10.
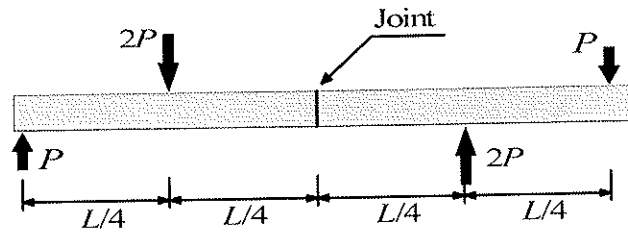
Fig. 9 *Test set-up for joints subjected to pure shear*
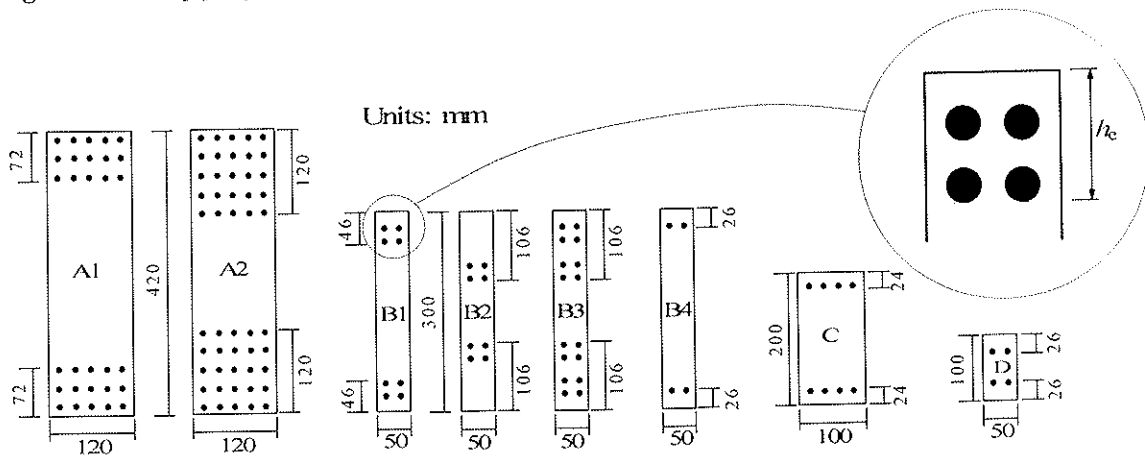
Fig. 10 *Geometry of joints with glued-in hardwood dowels tested in pure shear*

13

The glulam beams (30 mm laminae) used in the testing program were made of Japanese cedar (*Cryptomeria japonica*) with a dynamic E as given in Table 7. The moisture content was between 12% and 13%, and the corresponding density about 420 kg/m^3. The dowels, with a diameter of 12 mm, were made of hard maple (*Acer saccharum*) with $E \sim 15$ GPa. The moisture content was about 11%, and the corresponding density about 740 kg/m^3. The adhesive used was a one-component polyurethane C3060 from Nihon Polyurethane or #930 from Sunstar Engineering. The glulam beams and the dowels, as well as the specimens after gluing, were stored in the laboratory without controlling temperature and humidity.

The fracture energy was determined using DCB-specimens, and the tensile strength perpendicular to grain was determined using necked-down specimens with 10x10 mm^2 cross section. The material for tensile strength specimens and DCB-specimens was cut from beams already used for shear test and was taken without special selection to avoid defects such as knots.

4.2.2 Test results

The mean tensile strength was $f_t = 4.1$ MPa with a standard deviation of 1.3 MPa. The mean fracture energy was $G_f = 0.28$ with a standard deviation of 0.14 N/mm. The large variations are due to the presence of knots, which have a reinforcing effect and increased the fracture energy.

The results are given in Table 7 and compared with the calculated failure loads according to the lower-bound and upper-bound solutions as given by Eqs. (19) and (18), respectively. Generally the test results fall within the predicted interval.

Table 7 *Failure shear load of joints subjected to pure shear*

Specimen	No. of replicates	MOE (MPa)	b [mm]	h [mm]	h_e [mm]	κ	κP_c [kN] Test	Eq. (19	Eq. (18)
A1	3	8670	120	420	72	1.08	31.5 ± 4.2	25.7	32.0
A2	6	9310	120	420	120	1.25	51.3 ± 8.2	41.4	50.0
B1	3	8340	50	300	46	1.07	7.3 ± 0.9	8.0	10.3
B2	3	8340	50	300	106	1.40	12.9 ± 2.2	17.2	20.7
B3	6	9950	50	300	106	1.40	19.8 ± 2.9	18.5	22.5
B4	3	9950	50	300	26	1.02	7.0 ± 0.6	5.7	7.8
C	7	8300	100	200	24	1.04	11.0 ± 1.2	10.4	14.0
D	3	9950	50	100	26	1.20	6.9 ± 0.8	6.7	9.1

Note: Calculations based on $G = E/18$, $f_t = 4.1$ MPa and $G_f = 0.28$ N/mm. Test results given as mean ± standard deviation

5 References

1. Gustafsson P. J. & Larsen H. J. (2001): Dowel joints loaded perpendicular to grain. In: Aicher S. and Reinhardt H.W. (ed.): Joints in Timber Structures, Proceedings of the International RILEM Symposium, Stuttgart, Germany.

2. Gustafsson P. J. (1987): Analysis of generalized Volkersen-joints in terms of non-linear fracture mechanics. In: Verchery G. & Cardon A. H. (ed): Mechanical behaviour of adhesive joints. Pluralis.

3. Jensen J. L. (2003): Splitting strength of beams loaded by connections. Proceedings of CIB-W18, Colorado, paper CIB-W18/36-7-8.

4. Jensen J. L. & Gustafsson P. J. (2004?): Shear strength of beam splice joints with glued-in rods. Journal of Wood Science. In press.

5. Larsen H. J. & Gustafsson P. J. (2001): Dowel joints loaded perpendicular to grain. Proceedings of CIB-W18, Venice, paper CIB-W18/34-7-3

6. Leijten A. J. M. (2002): Perpendicular to grain failure of beams caused by concentrated loads of joints. Proceedings of the 7th World Conference on Timber Engineering, Shah Alam, Malaysia.

7. Leijten A. J. M. (2002): Splitting strength of beams loaded by connections, model comparison. Proceedings of CIB-W18, Kyoto, paper CIB-W18/35-7-7.

8. Leijten A. J. M. & Jorissen A. J. M. (2001): Splitting strength of beam loaded by connections perpendicular to grain, model validation. Proceedings of CIB-W18, Venice, paper CIB-W18/34-7-1.

9. Pilkey W. D. (1994): Formulas for stress, strain, and structural matrices. John Wiley & Sons, Inc.

10. Van der Put T. A. C. M. & Leijten A. J. M. (2000): Evaluation of perpendicular to grain failure of beams caused by concentrated loads of joints. Proceedings of CIB-W18, Delft, paper CIB-W18/33-7-7.

11. Yasumura, M. (2001): Criteria for damage and failure of dowel-type joints subjected to force perpendicular to the grain. Proceedings of CIB-W18, Venice, paper CIB-W18/34-7-9.

12. Quenneville, J. H. P. & Mohammad, M.(2001): A proposed Canadian design approach for bolted connections loaded perpendicular-to-grain. In: Aicher S. and Reinhardt H.W. (ed.): Joints in Timber Structures, Proceedings of the International RILEM Symposium, Stuttgart, Germany.

13. Kasim, M. & Quenneville, J. H. P. & (2002): Effect of row spacing on the capacity of perpendicular to grain loaded timber joints with multiple timber connections loaded perpendicular-to-grain. Proceedings of CIB-W18, Kyoto, paper CIB-W18/35-7-6

**INTERNATIONAL COUNCIL FOR RESEARCH AND INNOVATION
IN BUILDING AND CONSTRUCTION**

WORKING COMMISSION W18 - TIMBER STRUCTURES

A NUMERICAL MODEL TO SIMULATE THE
LOAD- DISPLACEMENT TIME-HISTORY OF MULTIPLE-BOLT CONNECTIONS
SUBJECTED TO VARIOUS LOADINGS

C P Heine

Botch Inc.

GERMANY

J D Dolan

Washington State University

USA

Presented by: Dan Dolan

Dan Dolan introduced the paper by providing an overview of the problem of bolted joints. The research was limited to single shear load parallel to grain situations. The research looked at group action effects in both elastic and the inelastic range. Dan went on to answer questions relating to the way the program dealt with load reversal situations and also about the "black box" approach used versus the clarity of detailed engineering methodology needed to understand the methodology used.

A Numerical Model to Simulate the Load-Displacement Time-History of Multiple-Bolt Connections Subjected to Various Loadings

C. P. Heine, Botch Inc., Germany

and

J. D. Dolan Washington State Univeristy, USA

ABSTRACT

A novel, general, numerical model is described that is capable of predicting the dynamic load-displacement relationship up to capacity of multiple-bolt joints in timber. The model consists of five parts. A new mathematical hysteresis model describes the stiffness of the individual bolt at each time step increment and accounts for non-linear and slack behavior; a mechanically-based structural stiffness model explains the interaction of one bolt with another bolt within a joint; an analytically-based failure model computes the stresses at each time step and initiates failure if crack length equals fastener spacing; a stochastic routine accounts for material property variation; and a heuristic optimization routine estimates the parameters needed.

The core model is a modified array of differential equations whose solution describes accurate hysteresis shapes for slack systems. Hysteresis parameter identification is carried out by a genetic algorithm routine that searches for the best-fit parameters following evolutionary principles (survival of the fittest). The structural model is a linear spring model. Failure is predicted based on a newly developed 'Displaced-Volume-Method' in conjunction with beam on elastic foundation theory, elastic theory, and a modified Tsai-Wu Failure criterion.

The devised computer model enhances the understanding of the mechanics of multiple-bolt joints in timber, and yields valid predictions of joint response of two-member multiple-bolt joints. This research represents a significant step towards the simulation of structural wood components.

INTRODUCTION

One of the most important elements of a timber structure is the connector. In fact, it is well established that the overall response of a wooden structure is a function of the performance of its connectors.

Constituting the simplest loading condition and joint configuration, single-bolt joints tested under unidirectional loading have attracted much research. Therefore, most of the information on bolts available today is based on single-bolt connections subjected to unidirectional displacing functions. Past research, however, demonstrated that the behavior of single-bolt joints cannot be extrapolated to predict the response of multiple-bolt configurations. This is especially true for stiffer bolts, which cause stress concentrations that may reach material strength and prematurely fail a joint.

Studies advanced by Moss and Carr (1988), Stewart et al. (1988), Dolan and Foschi (1989), Dolan and Madsen (1992), and Dolan et al. (1996a and b) have established the importance of cyclic and dynamic testing and analysis. Joints exhibit different and much more complex deformation mechanisms under cyclic or dynamic loading than when exposed to unidirectional forces. One characteristic that provides much difficulty for prediction models is the response dependency on loading history of joints in wood, also referred to as the "memory effect". Load history dependency describes the case where hole oversize or parts of the hole may grow because the elastic limit in the wood was

exceeded in a previous cycle and the surrounding wood fibers were crushed locally. Another problem is that, when loaded cyclically, a multiple-bolt joint whose holes are drilled oversize turns into a slack system.

OBJECTIVE

In view of improving the understanding of single- and multiple-bolt joints in timber, a theoretical model that furnishes scientists and designers alike with accurate information of the load-displacement relation of single and multiple-bolt connections, independent of the displacing function, would be beneficial. Thus, the primary objective of this paper was to describe a general model that is capable of predicting the load-displacement relationship, load distribution, capacity, and energy absorption characteristics of multiple-bolt timber joints of various configurations when subjected to reversed cyclic displacing functions. Using the model along with complementary testing, it should be possible to make inferences about the group action effect as a result of varying numbers of bolts in a row. The group action factor describes the effect of the number of bolts in a row on normalized joint capacity.

EXISTING MODELS

The first models attempting to predict the behavior of multiple-fastener joints in timber were based on linear elastic analysis and unidirectional loading conditions (Cramer 1968, Lantos 1969). Wilkinson (1986) expanded upon Lantos' solution to include fabrication tolerance and a piecewise linear approximation of the load-slip relation of each bolt. A nonlinear, comprehensive computer model predicting unidirectional strength of multiple-bolt joints was advanced by Jorissen (1998). The model is a hybrid of the elastic formulations developed by Lantos (1969) and stress analysis to include behavior in the inelastic range. Jorissen determined shear stresses and stresses perpendicular to the grain to predict failure due to splitting and to establish an analytical formulation that considers load redistribution due to accumulated stresses around single bolts beyond the elastic range. The model's prediction of the load-slip relation was relatively poor, but good agreement with experimental data was achieved for prediction of capacity.

The study of the unidirectional behavior of joints is a specialization of the general case however, which is joints subjected to random input including reversed cyclic loading or displacement. Mathematical models that have been devised to predict monotonic behavior of dowel-type joints all exclude important information such as effects due to displacement or loading history and energy dissipation. Despite the appealing nature of monotonic loading or displacement input, it is rare in real structures. Attributed to its rheological and non-linear elastic plastic characteristics, wood exhibits "memory". It is clear then that general analytical models accounting for random input are of increased complexity when compared to their more specialized monotonic counterparts. While some monotonic derivations such as failure models may be applicable for cyclic loading, analytical models for the general case are entirely different in structure. Under reversed cyclic loading up to joint capacity (beyond the elastic range), joint stiffness is related to load history. Hence, it is not possible to simply apply existing methods used to model static behavior of joints for connections subjected to cyclic excitations. In addition, conventional models used to approximate the elastic-plastic behavior of steel and concrete are not applicable for timber structures, as they do not allow for incorporation of slackness or pinching (Deam 1994). The core of a model to describe the cyclic response of timber structures is the formulation or method that describes the hysteresis, and several hysteresis models were developed previously.

In an effort to model numerically the cyclic behavior of shear walls, Stewart (1987) advanced a hysteretic approximation consisting of a series of straight-line segments. Dolan (1989) developed two hysteresis formulations as part of a finite element program that

numerically analyses the cyclic response of timber framed shear walls with plywood or waferboard sheathing. Other hysteresis models have been devised most of which are also part of comprehensive finite element analyses (Ceccotti and Vignoli 1990, Foschi 1993, Lee 1987, Komatsu et al. 1988; White and Dolan 1995, Tarabia and Itani 1994).

Apart from hysteresis models designed to be solved in a numerical, stepwise manner, mathematical solutions are rare. Most of the above models are not general in the sense that the solution depends on a set of programmed cases that are executed using 'IF – THEN – ELSE' statements, which makes modeling computationally inefficient and increasingly inaccurate if random input functions such as earthquake records are used.

One of the first truly mathematically closed-form hysteresis models for structures was put forth by Bouc (1967) and further modified and improved by Wen (1980), Baber and Wen (1981), and Baber and Noori (1985, 1986) (BWBN model). Foliente (1993) slightly altered the pinching function of the model and tested its applicability to wood structures. He presented an excellent and very detailed discussion of the BWBN model (Foliente 1993). The BWBN model relies on a "black-box approach", in that the complex mechanics involved in any structure that is stressed beyond the elastic limit, and that exhibits hysteretic behavior, are by and large disregarded. Instead, the modeled object is simplified and represented by an equivalent system consisting of a mass connected parallel to a linear spring, a linear viscous damper and a hysteretic element. The properties of the elements of the simplified structure are empirically adjusted to fit the problem at hand. In spite of this, the BWBN model is not to be mistaken as purely empirical. Empirical models have the disadvantage that extrapolation to cases outside the studied bounds is usually not valid. Using physical entities such as damper, spring and mass, the BWBN model, on the other hand, is valid for a wide range of input functions. Because of its versatility, the BWBN model constitutes the basis for the hysteresis model developed in this work.

MODEL DEVELOPMENT

The main focus of this study was the development of MULTBOLT, a generic model that predicts the load-displacement behavior of multiple-bolt joints under reversed cyclic and other displacement functions within the elastic *and* inelastic response range up to maximum load. MULTBOLT is an array of five models that are quite different in approach and nature. The individual models are briefly described below. A detailed description of the derivation of each model can be found in Heine (2001), and the experimental investigation used to validate the model is found in Anderson (2001).

Hysteresis Model

The hysteresis model is the core of MULTBOLT and is based on the BWBN model. But to incorporate slack, reduce the dependency on energy dissipation, make it applicable to multiple fastener joints, and reduce the number of parameters that need to be identified, the BWBN model was significantly modified.

A slack system, such as a single-bolt joint with oversized hole, typically exhibits zero or close-to-zero stiffness at small displacements. In case of stiff fasteners, this is true even if slack is very small or approaches zero, which is evident from embedment test data published by Wilkinson (1991), Brinkman (1996), Stamato and Calil (1999), and from load-displacement data of bolted joints reported by Stelmokas (1995). Because of settlement effects, as the fastener presses into the wood, stiffness increases from zero or close to zero in almost all cases. The equation of motion of a nonlinear, slack system may be written as (normalized by the mass per fastener) which describes the response of the

$$\ddot{u}(t) + 2 \cdot \xi \cdot \omega \cdot \dot{u}(t) + \omega^2 \cdot u(t) \cdot H(z,\Delta,t) + \omega^2 \cdot T(z,\Delta,t) = f(t) \qquad (1)$$

3

equivalent mass-hysteretic spring-dashpot system The parameters ξ and ω denote the linear elastic damping ratio and the pseudo-natural frequency of the nonlinear system, respectively. The right-hand side of Equation (1) is the mass-normalized input forcing function. Nonlinear and linear components are separated. Functions H and T describe the nonlinear part. Total displacement of the mass is described by u, whereas the force of the nonlinear element is a function of the fictitious displacement z, which is related to u in a rate-type manner. That is, z varies with u at different rates depending on direction of movement (positive or negative velocity) and displacement level. For example, an elliptic hysteresis is obtained if z increases more rapidly at small negative u and positive velocity and decreases more rapidly at large positive u and negative velocity. The parameter $H(z,\Delta,t)$, links slack growth to displacement level. $T(z,\Delta,t)$ describes the maximum displacement amplitudes (positive or negative) reached before or at time t.

Parameter Estimation

The hysteresis model describes the load displacement relation of the individual fastener. Therefore, it must be calibrated to cyclic test results of single-bolt joints where the two principal geometries, bolt diameter and member thickness, are the same as for the multiple-bolt joint whose performance is to be predicted, provided that minimum edge and end distances are not violated. While this may seem like a limitation, it only exists until there is sufficient test data available to allow stochastic predictions of hysteresis parameters based on bolt diameter, member thickness and specific gravity. Because the hysteresis model is derived from a physical system, it is, if properly calibrated, applicable to random input functions. This is important since each fastener in a multiple bolt joint experiences a unique displacing or loading function due to material deformations.

To fit the model to experimental data, a systematic parameter search routine was written using the Genetic Algorithm (GA) method. A GA recently published by Lybanon and Messa (1999) was specifically developed and optimized for model fitting to solve a satellite altimetry problem.

Structural Model

The purpose of the structural model is to account for the interaction of the individual fasteners in a multiple-bolt joint. Traditionally, material deformations were thought to be the main cause of the group action factor (unequal load sharing among bolts) and premature failure. Since all non-linearities, including slack, are explained by the hysteresis model, the structural model in MULTBOLT is an elastic spring model, where the individual fasteners and the member parts between the fasteners, or between the fastener and force application location, are modeled as springs with assigned stiffness. Key to developing the structural model is the assumption that bolt stiffness is constant within a single time step (secant stiffness). The structural model then becomes a solvable, dynamic system of linear equations with which the force or displacement distribution among the fasteners can be determined for each time step.

Failure Model

Brittle failure can be accurately predicted without the use of fracture mechanics. A newly developed method named the Displaced Volume Method in combination with the European Yield Theory, a modified Tsai-Wu failure criterion, and considerably modified stress computations based on the approach advanced by Jorissen (1998) provides an effective means of simulating brittle failure of multiple-bolt joints in timber. The model applies to both rigid and slender fasteners. Failure model output controls forces computed by the modified hysteresis/structural model. If failure is detected, forces are effectively reduced.

4

Stochastic Model

Not any one material can claim truly constant properties both spatially and specimen specific. MULTBOLT includes stochastic modeling to reflect the variable performance of timber joints and to allow statistical inferences about average model predictions and average test results. While the random effect of many parameters and their interaction may influence joint performance, it was desired to keep the number of input parameters small and rely on correlations reported in the literature. Hence, material properties are related to the parallel-to-grain modulus of elasticity (MOE). MULTBOLT offers the option to vary the parallel-to-grain MOE in two ways. The user can specify a *between-member* standard deviation, which describes the variation of the average MOE of each joint member when measured for many members. In addition, MULTBOLT allows MOE to vary *within* a member using lengthwise correlation based on the average value generated from the between-member variation. Parallel-to-grain MOE does not vary randomly along the length of a piece of lumber. Rather, it has been established that MOE measured in one segment is correlated with the MOE measured in adjacent segments. Hence, spatial variation of MOE was modeled using the second-order Markov model as published by Kline et al. (1985). With the exception of standard deviation, coefficients were used as estimated by Kline et al.

MODEL RESULTS

To validate MULTBOLT, 72 displacement-controlled experiments were conducted using both cyclic and unidirectional displacing functions. Yield Modes II and IV were investigated. Basic input parameters are listed in Table 1 (Yield moment was computed from published yield strength.)

Table 1: Basic input parameters used to validate MULTBOLT.

Input	Value	Unit	Reference
E_{para}	10.313	kN/mm^2	Bodig & Jayne (1982)
COV_{Epara}	32	%	Loferski (2000)
friction b/w bolt & wood	30	degrees	Jorissen (1998)
bolt yield moment[1]	105.923	kN mm	NDS (AF&PA 1997)
bolt ∅	12.7	mm	
number of bolts	1 or 3 or 5		
member thickness	38.1 or 88.9	mm	
member width	139.7	mm	
fastener spacing	50.8	mm	
spacing COV	0.5	%	(estimated)
hole oversize	1.59	mm	
yield mode	II or III or IV		
end distance	88.9	mm	

It must be emphasized that observed yield modes varied within given multiple-bolt joint configurations. In joints designed to yield in Mode IV, some bolts were observed to develop a single plastic hinge (Mode III), others did not develop any plastic hinge before catastrophic failure due to splitting occurred. This behavior may have several causes. It is hypothesized here that the higher yield modes "evolved" from lower modes at increasing displacement amplitude (Heine 2001). That is, because of oversized holes, the joint starts to deform like a Mode II yield, then various bolts change to Mode III and then possibly to Mode IV. The latter actually rarely formed in the multiple-bolt joints tested, while single bolt connections always produced Mode IV yield when predicted.

MULTBOLT accurately predicted the load-deflection relation of 10 multiple-bolt joints yielding in Mode II, both for reversed cyclic and unidirectional displacement input,

although the hysteresis model was fit to single bolt cyclic data only (Figures 2a-c). Based on limited data, MULTBOLT predicted well average monotonic performance of a 5-bolt joint configuration yielding in Mode II (Figure 2a). Furthermore, MULTBOLT correctly predicted higher capacity for joints stressed monotonically. The reason for this is the lower energy demand of monotonic tests resulting in reduced system degradation.

a) Comparison of average load-slip

b) Comparison of average cyclic load-displacement plot

c) Comparison of average absorbed energy up to capacity
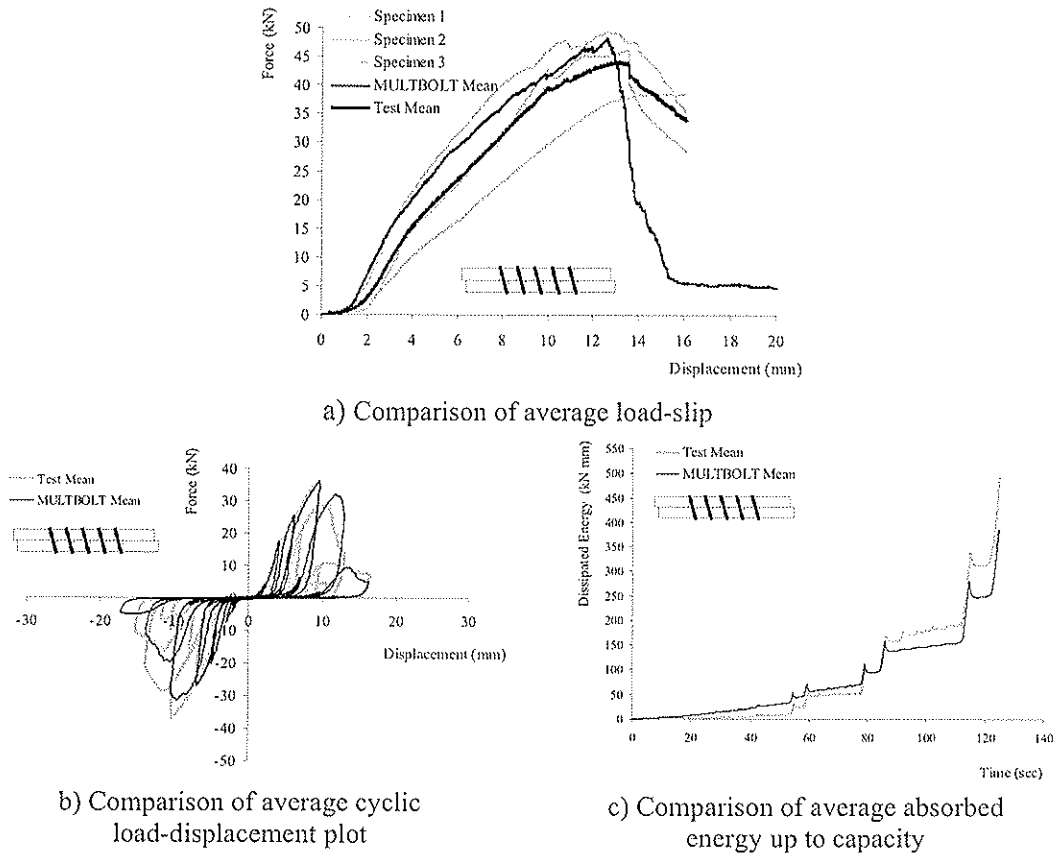
Figure 2. Comparison of predicted and experimental results for MODE II.

Probably as a result of defects contained in the larger members (drying checks, juvenile wood, and associated lower specific gravity) and most likely because yield modes varied within joints, MULTBOLT had more difficulties predicting the absorbed energy of higher yield modes (Figure 3b). However, load-displacement predictions are adequate (Figure 3a). Despite the fact that the current failure model does not account for varying yield modes within a given joint, good predictions were achieved by inputting the highest mode that was actually observed. Statistical tests revealed high correlation between experiments and predictions (Pearson's coefficient r > 0.90).

PARAMETRIC STUDY ON GROUP ACTION

The purpose of the parametric study was to investigate the group action effect. Comparisons of MULTBOLT predictions with group action characteristics outlined in the NDS (AF&PA 1997) are made. It is important to note, however, that this study is concerned with group action at limit state (i.e. maximum load) and not, as is the case with NDS equations, at proportional limit. The NDS equations were derived by Zahn (1991) from linear elastic analysis advanced by Lantos (1969). Nevertheless, comparisons with NDS predictions are made in this paper to highlight a principal issue. As shown below,

6
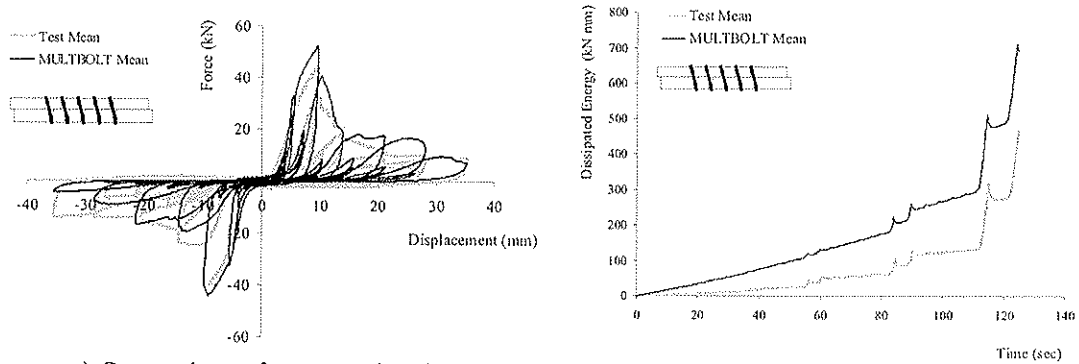
a) Comparison of average absorbed energy up to capacity

b) Comparison of average load-slip plot

Figure 3. Comparison of predicted and experimental results for connection designed for MODE IV but observed as MODE III.

group action at limit state differs in mechanism from group action at proportional limit. Group action effects are a safety limit state and therefore design values should be determined using capacity values. Current NDS values are working stress values at which the effects of group action are minimal. It seems unreasonable to base group action on linear elastic analysis, if, as is demonstrated here, the group action effects that cause failure are quite different.

MULTBOLT was run with stochastic variation turned off. In other words, material properties were not allowed to vary either per member or spatially, and spacing was constant between fasteners. The slight variation in the group action factors, as can be observed in the figures, is caused by numerical error.

Fastener spacing has substantial influence on group action (Figure 4). With an end distance of 89 mm (7D as recommended by the NDS), simulated joints exhibit the largest relative load drop when the number of fasteners is increased from 1 to 2. In contrast, the effect of member strain on group action as first described by Cramer (1968) and Lantos (1969) is actually very small at limit state (Heine 2001). This is partly because of inelastic material deformations and subsequent load redistribution, and partly because of high material stiffness parallel to the grain compared to fastener stiffness. Hence, MULTBOLT predicts that group action changes little with increasing number of bolts and is only influenced by the diminishing interaction effects of perpendicular-to-grain stresses and parallel-to-grain stresses, which impact the Tsai-Wu failure model. The trends shown here are substantiated by experimental results obtained from double-shear joints as reported by Jorissen (1998) and results obtained from joints tested for this study (Anderson 2001).

The trend predicted by MULTBOLT opposes the trend predicted by equations published in the 1997 NDS. Based on proportional limit, the NDS does not predict any group action factor for the joint containing 2 bolts in a row, but group action progressively increases with increasing number of bolts. Considering failure limit state, however, given the findings of this work, both experimental and theoretical, it is difficult to envision that two bolts with diameter of 12.7 mm, spaced 4 bolt diameters apart in a joint with common members (38 x 140 mm^2) do not interact, and hence do not negatively affect joint capacity.

Derived from the understanding that has been gained during the development of MULTBOLT, it seems unreasonable to treat fastener spacing different from end distance in terms of the effect on joint capacity, as is currently the case in the NDS. The area of influence of two adjacent bolts is mainly concentrated between the bolts. Although perpendicular-to-the grain stresses induced by a particular bolt are transferred along the members, they are concentrated at the fastener and decrease rapidly away from the fastener. Additionally, shear stresses are not transferred and the hole of the next fastener

7

$$C_g = \frac{F_{max,\ joint}}{N \cdot F_{max,\ single}}$$

Bolt spacing:
- o — 7D
- • — 6D
- □ — 5D
- ■ — 4D
- △ — 2D
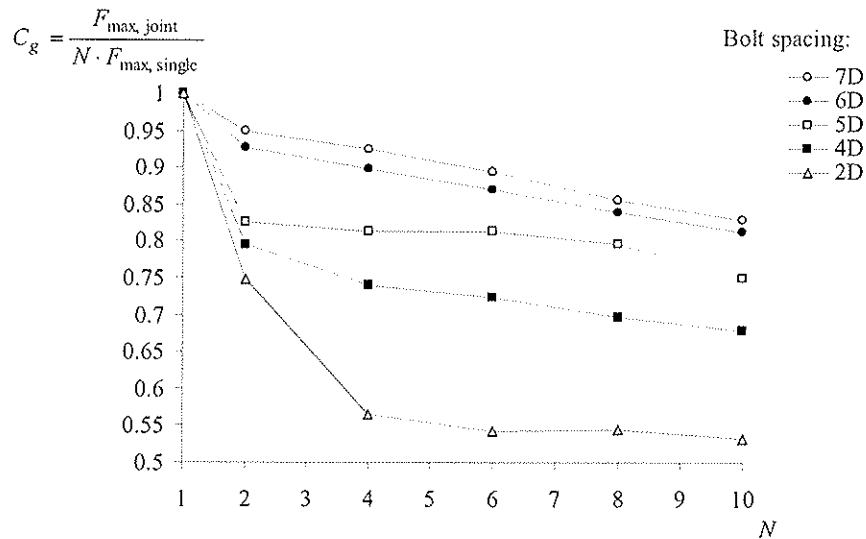
Figure 4: Group action effect of joints displaced cyclically. N denotes the number of bolts in a row. The y-axis represents the predicted group action factor C_g (relative capacity per bolt in a multiple-bolt joint compared with the capacity of a single-bolt joint). Results of joints containing 1, 2, 4, 6, 8, 10 bolts spaced 2D, 4D, 5D, 6D, 7D are shown (bolt diameter D = 12.7 mm, southern pine members 38 x 140 mm².

acts similar to a free end. The interaction of shear stress and tension perpendicular-to-the grain stress in combination with a higher normal stress parallel to the grain than at member ends, makes the distance to an adjacent hole an equally effective parameter as end distance. Thus, for bolted joints, minimum spacing requirements for full capacity should equal minimum end distance.

CONCLUSIONS

MULTBOLT produces valid predictions for single-shear, multiple-bolt joints based on various displacement functions. Joints were tested to minimize effects caused by connection eccentricity, which allowed out-of-shear-plane forces to be neglected. Predictions are not limited to tight-fit bolts. Instead, MULTBOLT can simulate joints with holes drilled oversize. The model handles random displacement input as well as static cyclic and unidirectional displacing functions. Joint load per displacement point and brittle joint failure are accurately predicted.

A new, fully mathematically tractable, hysteresis model was devised that is capable of accurately tracing the force-displacement interaction of slack systems with hysteretic behavior. The hysteresis model was successfully interfaced with a relatively simple structural model to account for the interaction of multiple bolts in a row. A linear-stiffness-based abstraction of the joint is sufficiently accurate to describe bolt interaction, since non-linear behavior is accounted for by the hysteresis model. A relatively novel approach, the Genetic Algorithm method (heuristic optimizer with global potential), was effectively utilized to estimate parameters for the hysteresis model.

Current group action equations recommended for design of bolted joints in the U.S.A should be revised to reflect the findings of this work. Reversed cyclic and unidirectional group action at limit state differs substantially from group action at proportional limit (basis of NDS) and is most affected by fastener spacing. Relative drop in maximum load per fastener was determined to be greatest when the number of bolts was increased from one to two. On the other hand, an increase from 3 to 10 bolts per row produced diminishing group action effects. This is because the effect of member strain on

8

group action is negligible for most joint configurations due to the high stiffness of wood parallel to the grain and inelastic load redistribution. Group action determination for multiple-bolt joints currently applied in the U.S. is based on the member strain effect.

Bolt spacing and end distance should not be treated differently for full capacity design. Thus, minimum allowable fastener spacing for full design capacity of multiple-bolt joints should be raised to seven times fastener diameter, which is equal to the required minimum end distance.

ACKNOWLEDGEMENTS

LITERATURE CITED

[1] American Forest and Paper Association (AF&PA). 1997. ANSI/NfoPA NDS 1997. National Design Specification for Wood Construction. AFPA, Washington, DC.

[2] Anderson, G.T. 2001. Experimental Investigation of Group Action Factor for Bolted Wood Connections. MS Thesis, Virginia Polytechnic Institute and State University, Blacksburg, VA.

[3] Baber, T. and M.N. Noori. 1985. Random vibration of degrading pinching systems. Journal of Engineering Mechanics, ASCE, Vol. 111 (8): 1010 – 1026.

[4] Baber, T. and M.N. Noori. 1986. Modeling general hysteresis behavior and random vibration application. Journal of Engineering Mechanics, ASCE, Vol. 107 (EM6): 1069 – 1089.

[5] Baber, T. and Y.K. Wen. 1981. Random vibration of hysteretic degrading systems. Acoustics, Stress and Reliability in Design. Vol. 108: 411 – 420.

[6] Bouc, R. 1967. Forced vibration of mechanical systems with hysteresis. Abstract in Proceedings of the 4th Conference on Nonlinear Oscillation.

[7] Brinkman, T. 1996. Unpublished research results. Virginia Polytechnic Institute and State University, Blacksburg, VA

[8] Ceccotti, A. and A. Vignoli. 1990. Engineered timber structures: an evaluation of their seismic behavior. Proceedings of 1990 International Timber Engineering Conference, Tokyo, Japan. 946 – 953 pp.

[9] Cramer, C.O. 1968. Load distribution in multiple bolt tension joints. Journal of the Structural Division. Vol. 94 (5): 1101 – 1117.

[10] Deam, B. and A. King. 1994. The seismic behavior of timber structures. Proceedings of the Pacific Timber Engineering Conference, Gold Coast Australia, July 11 – July 15.

[11] Dolan, J.D. 1989. The dynamic response of timber shear walls. Ph.D. Dissertation, University of British Columbia, Vancouver, British Columbia.

[12] Dolan, J.D. and B. Madsen. 1992. Monotonic and cyclic nail connection tests. Canadian Journal of Civil Engineering. Ottawa, Canada. 19 (1): 97-104.

[13] Dolan, J.D. and R.O. Foschi. 1989. Structural analysis models for timber shear walls. Structural Design, Analysis and Testing. A.H-S. August edition, ASCE, New York, N.Y., pp143-152.

[14] Dolan, J.D., Gutshall S.T., and McLain T.E. 1996a. Monotonic and cyclic tests to determine short-term load duration performance of nail and bolt connections. Research Report No. TE-1994-001. Virginia Polytechnic Institute and State University, Blacksburg, VA.

[15] Dolan, J.D., Gutshall S.T., and McLain T.E. 1996b. Determination of short-term duration-of-load performance of nailed and bolted connections using sequential

phased displacement tests. Research Report No. TE-1994-003. Virginia Polytechnic Institute and State University, Blacksburg, VA.

[16] Foliente, G.C. 1993. Stochastic Dynamic Response of Wood Structural Systems. Ph.D. Dissertation, Virginia Polytechnic Institute and State University, Blacksburg, Virginia.

[17] Foschi, R.O. 1993. P.S.A. – General Plane Structures Analysis Program with P-Delta Effects. Department of Civil Engineering, University of British Columbia, Conada.

[18] Heine, C.P. 2001. Simulated Response of Degrading Hysteretic Joints with Slack Behavior. PhD Dissertation, Virginia Polytechnic Institute and State University, Blacksburg, VA (available online at: http://.etd.vt.edu).

[19] Jorissen, A.J.M. 1998. Double Shear Timber Connections with Dowel Type Fasteners. PhD Thesis, Delft University Press, Deft, Netherlands. 264 pp.

[20] Kline, D.E., Woeste, F.E. and B.A. Bendtsen. 1985. Stochastic model for modulus of elasticity of lumber. Wood and Fiber Science. Vol. 18 (2): 228 – 238.

[21] Komatsu K., Kamiya F., and Y. Hirashima. 1988. Full size test and analysis on glulam two-storied portal frames. Proceedings of the 1988 International Timber Engineering Conference, Tokyo, Japan, vol. 2: 626 – 632 pp.

[22] Lantos, G. 1969. Load distribution in a row of fasteners subjected to lateral load. Wood Science. Vol. 1 (3): 129 – 136.

[23] Lee, C.S. 1987. A Composite-beam Finite Element for Seismic Analysis of Wood-framed Buildings. Ph.D. Dissertation, Oregon State University, Corvallis, Oregon.

[24] Lybanon, M. and K.C. Messa. 1999. Genetic algorithm model fitting. In: Practical Handbook of Genetic Algorithms. Complex Coding Systems. Volume III. Edited by L. D. Chambers. CRC Press, New York.

[25] Moss, P.J. and A.J. Carr, 1988. Earthquake response of low-rise timber buildings. Proceedings of the International Conference on Timber Engineering, Vol.1, pp. 848-858.

[26] Stamato, G.C. and C.Calil. 1999. Plywood embedment strength. Proceedings of Pacific Timber Engineering Conference, Rotorua, New Zealand. pp. 362-369.

[27] Stelmokas, J.W. 1995. Two Novel Techniques to Study Multiple-Bolted Wood Connection Behavior. Master of Science Thesis. Virginia Polytechnic Institute and State University, Blacksburg, VA.

[28] Stewart, W.G. 1987. The Seismic Design of Plywood-Sheathed Shearwalls. Ph.D. Dissertation, University of Canterbury, Christchurch, New Zealand.

[29] Stewart, W.G., Dean, J.A., and A.J. Carr, 1988. The earthquake behavior of plywood sheathed shearwalls. Proceedings of the International Conference on Timber Engineering, Vol. 2, pp. 248-261.

[30] Tarabia, A.M. and R.Y. Itani. 1994. Seismic analysis of light frame wood structures. Proceedings of the 2nd International Workshop on Full-scale Behavior of Low-rise Buildings, Townsville, Australia, 15pp.

[31] Wen, Y.K. 1980. Equivalent linearization for hysteretic stystems under random excitation. Journal of Applied Mechanics. Vol. 47: 150 – 154.

[32] Wilkinson, T.L. 1991. Dowel Bearing Strength. Res. Pap. FPL-RP-505. Madison, WI: U.S. Department of Agriculture, Forest Service, Forest Products Laboratory. 9p.

[33] Wilkinson, T.L. 1986. Load distribution among bolts parallel to load. Journal of Structural Engineering, Vol. 112 (4): 835 - 852.

[34] White, M.W., and Dolan, J.D. 1995. Nonlinear shear-wall analysis. Journal of Structural Engineering, Vol. 121, No. 11, pp. 1629-1635.

[35] Zahn, J.J. 1991. Design equations for multiple-fastener wood connections. U.S. Department of Agriculture, Forest Service, Forest Products Laboratory, Madison, WI.

**INTERNATIONAL COUNCIL FOR RESEARCH AND INNOVATION
IN BUILDING AND CONSTRUCTION**

WORKING COMMISSION W18 - TIMBER STRUCTURES

RELIABILITIY OF TIMBER STRUCTURES

THEORY AND DOWEL-TYPE CONNECTION FAILURES

A Ranta-Maunus

A Kevarinmäki

VTT

FINLAND

Presented by: Alpo Ranta-Maunus

Alpo Ranta-Maunus explained that this research followed the collapse of 52m span glulam structure in Finland in February 2003. The structure was designed to EC5 requirements. He informed participants that the paper covered the effects of grading on the strength properties of timber structures and also about dowel joint design and manufacture. He indicated that the reported effects of grading on strength distribution is based on numerical simulation in accordance with PrEN 14081-2. He reported that the failure initiated at a joint where there were only 7 dowels instead of the required 33 dowels. Other reasons included poor manufacture quality and questionable stability supports. More importantly he concluded that EC5 provisions for multiple dowel joints are not adequate. A major conclusion from the research is that design rules for tension in dowel type joints must be revised for group effects and should also take into account block shear failure.

Reliability of timber structures,

theory and dowel-type connection failures

Alpo Ranta-Maunus, Ari Kevarinmäki

VTT, Finland

1   Introduction

This paper has two separate parts both dealing with the reliability of timber structures. The first part is a theoretical one related to strength distribution of timber materials and to the theoretical effect of lower tail strength on safety factors in code calibration. Some results on the strength distributions of machine strength graded timber are discussed.

In the second part a recent failure case is reported. This is considered urgent because the failure was caused partly by inadequacy of the pre-standard version of Eurocode 5, which can now be used in many European countries. Because of the accident, supplementary national guidelines will be given in Finland concerning the design of dowel-type joints, including block shear failure. The draft guidelines are given in appendix.

2   Tail properties of timber strength

In structural reliability analysis the lower tail distribution of strength is one of the major contributors to the result. Therefore the effect of strength grading on the lower tail form is discussed in the following.

2.1   Strength distribution of unsorted sawn timber

In recent studies (Ranta-Maunus et al 2001) it was concluded that the bending strength distribution of unsorted spruce timber grown in Finland follows quite nicely normal distribution with mean 43.1 MPa and coefficient of variation COV = 27%. This is based on a sample size of 1508 including different timber sizes. If lognormal distribution is fitted to the data, we obtain parameter values $\mu = 3.721$ and $\sigma = 0.309$, the latter being the parameter corresponding closely to COV calculated from a lognormally distributed sample. This lognormal curve does not fit well to the lowest strength values. When lognormal distribution is fitted to the lowest 10% of the values, we obtain a much higher COV parameter $\sigma = 0.544$.

A sub-sample (N = 589) of the same spruce timber cited above, with constant 150 mm depth, is more homogeneous and has a mean of 44.2 MPa and coefficient of variation COV

= 25%. If lognormal distribution is fitted to the data, we obtain parameter values $\mu = 3.775$ and $\sigma = 0.292$. When lognormal distribution is fitted to the lowest 10% of the values, we obtain the COV parameter $\sigma = 0.517$.

2.2 Effect of grading on strength

The strength distribution of graded timber was studied experimentally by grading the same spruce population of 1508 samples both visually and by bending-type machine. Both gradings were made for one strength class only: visual for C24 and machine grading for C30. The machine graded population had a mean of 47.8 MPa and coefficient of variation COV = 21%. The sample size was now 986. If lognormal distribution is fitted to the data, we obtain parameter values $\mu = 3.844$ and $\sigma = 0.220$. When lognormal distribution is fitted to the lowest 10% of the values, we obtain a higher COV parameter $\sigma = 0.305$ indicating, however, improvement over the unsorted sample. When a machine graded sample with depth 150 mm is analysed, we obtain a COV parameter $\sigma = 0.284$ when fitted to the lower tail of the results.

Information on the lowest tail values is restricted due to the limited sample size used. This is why we wanted to study the effect of grading by numerical simulation. Starting from a normally distributed population of bending strength, modulus of elasticity, and density, which are the grade-determining properties, and with known correlations between these and assumed relations to the grading parameter (such as MOE in flatwise bending), we simulated larger samples of values, performed grading according to the CEN procedure, and finally ended up with strength distributions of various grades (Ranta-Maunus 2002, Turk et al 2003).

Here the results of simulations are briefly summarised, as strength distributions are of concern. In simulations, the statistical characteristics of unsorted material were based on data related to spruce with depth of 150 mm cited above.

Grading was done simultaneously into three European strength classes C40, C30 and C18. 0.5 and 5 percentile values of strength were determined. Lognormal distributions were fitted through these two points and the curves are shown in Figure 1.
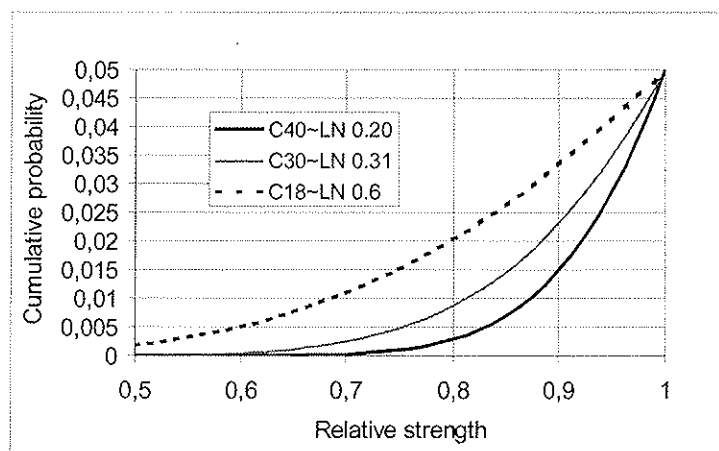
Figure 1. *Lower tail distributions of strength based on simulation of simultaneous grading into three grades.*

2

Lower tail strength distribution is quite different for each grade. The simulated result for C30 is similar to the result we obtained by destructive testing of the same material, as cited above. For other grades we have no experimental material for comparison.

If the lognormal distributions obtained in simulation are used in structural reliability analysis for the purpose of code calibration, we obtain partial safety factors for material having ratios 1.2 : 1.35 : 1.8 for C40, C30 and C18, respectively.

3   Learning from failures: Jyväskylä case

3.1   Description of failure

A considerable part of the roof (2000 m^2) of an exhibition hall in Jyväskylä collapsed on 1.2.2003. More than 10 people were in the building that morning, fortunately managing to escape before collapse.

The collapsed part of building was new and had only been in use for 2 weeks. The load bearing structure was a glulam truss with 52 m span, connected by steel-to-timber dowel joints with four shear planes, 12 mm dowels, and 8 mm thick steel plates. The strength class of glulam was GL32 (L40). Two trusses were placed side by side. The snow load on the roof was estimated to be 52 kg/m^2, which is 25% of the design value for snow load. The total load at the time of failure was 50% of the characteristic load estimated by the designer. The design calculation was made following the pre-standard (ENV) version of Eurocode 5.

Figure 2. *Photograph of the failed roof in Jyväskylä. The arrow shows the joint where dowels were lacking.*

3.2   Experiments

3.2.1   Loading of truss to failure on site

After the roof failure, one of the remaining trusses was loaded to failure on site. The failure load was 51% of the expected characteristic capacity of the truss (Hassinen et al 2003), and a tension connection in the middle of bottom chord failed, as seen in Figure 3. The cross-

section of the bottom chord was H x W = 630 x 215 mm. Two trusses were connected to each other. The failed joint was composed of two steel plates each having a thickness of 8 mm, and of 2 x 48 steel dowels (diameter 12 mm, strength class 8.8) on the both sides of the connection of the bottom chord of the double truss system. The dowels were placed in eight rows in the longitudinal direction of the chord, each row including six dowels in the direction of the tensile force of the chord (Figure 3 b, c). The connection failed under a tensile force of 2539 kN. The estimated characteristic short-term tensile resistance of the connection corresponding to the duration of the testing is 4964 kN. The estimation is based on ENV 1995-1-1 and the Finnish NAD (RIL 205-1997).

a)   b)

c)   d)
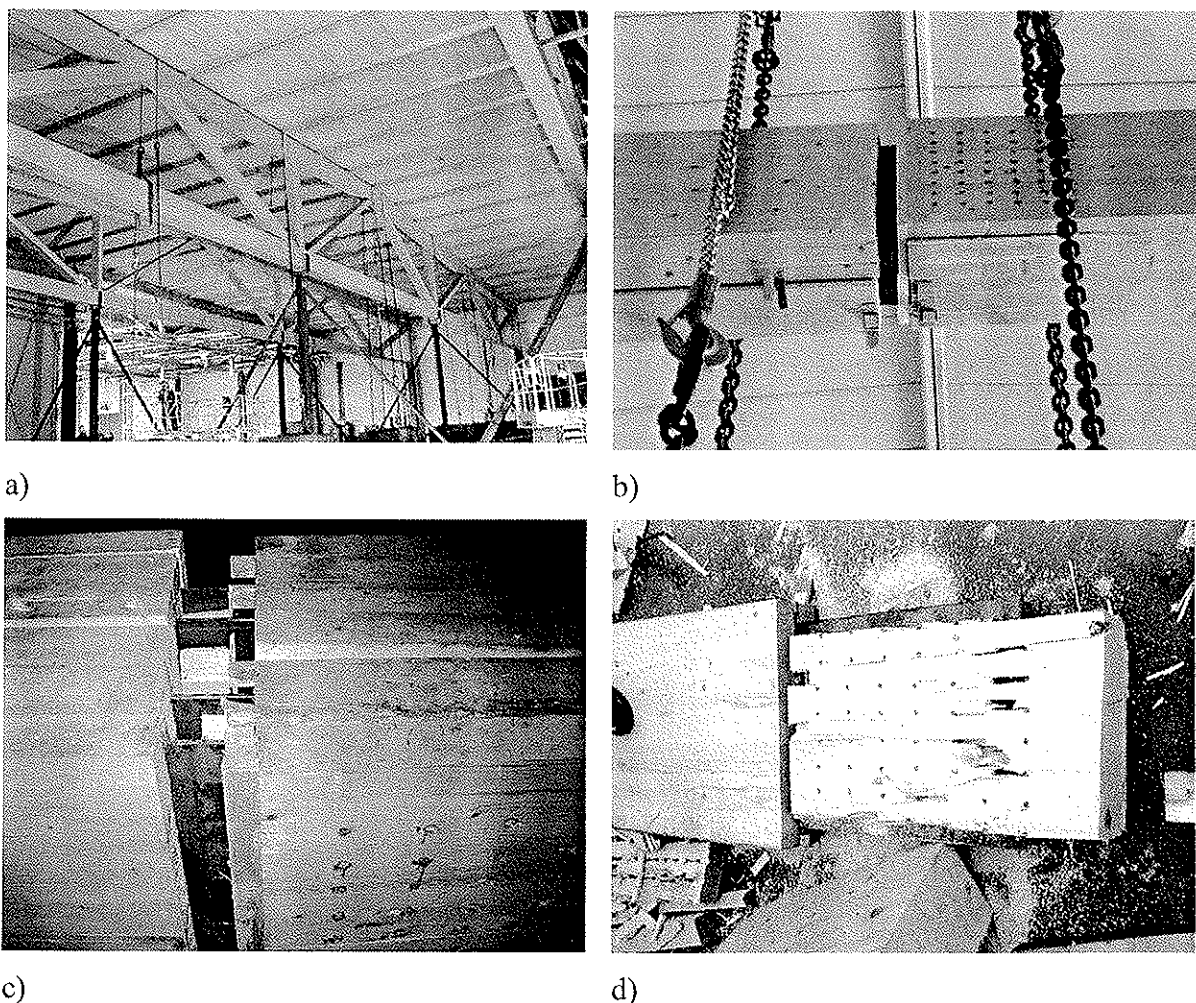
Figure 3. *a) Roof truss R38 before loading, b) and c) connection in the mid-span of the lower chord after loading, and d) mode of failure of the connection.*

3.2.2 Laboratory experiments

After the roof collapse, three tension experiments were performed with dowel joints of six shear planes and 4 x 4 dowels (S355 steel, d = 12 mm) at both ends the total wood cross-section being 240 x 225 mm (a_1 = 90 mm, a_2 = 40 mm, a_3 = 90 mm, a_4 = 52.5 mm, t_s = 56 mm, t_u = 49 mm, 8 mm wide steel plates slotted in 10 mm wide cuts in wood; see notations in appendix). The glulam was of Finnish strength class L40 with two top and bottom lamellae of grade MLT 30 and three middle lamellae of grade MLT 20. According to the Finnish NAD to Eurocode 5, this corresponds to GL 32. In all three tests the capacity was

nearly the same (COV = 4%) and the failure mode was block shear failure: first the wood cracked

Figure 4. *Dowel connections after testing.*

Table 2 *Calculated characteristic values of capacities R_k based on various code assumptions, and ratio of test values F (mean of three tests) to code values R (VTT research report RTE 1583/03).*

F_{mean} = 705 kN	ENV 1995	ENV + 1)	ENV + 2)	ENV + 1) + 2)	prEN	Annex A
R_k (kN)	1026 *)	**1008**	859	765	759	595
F_{mean}/R_k	0.69	**0.70**	0.82	0.92	0.93	1.18
k_2R_k (kN)	1159	**1139**	971	864	858	672
F_{mean}/k_2R_k	0.61	**0.62**	0.73	0.82	0.82	1.05

*) If tension strength of wood critical: R_k = 1132 kN.

ENV 1995: Calculation made in accordance with Eurocode 5 prestandard

ENV+1): Capacity of multiple shear plane connection calculated by multiplying the lowest shear plane capacity by the number of shear planes and number of fasteners.

ENV+2): Effective number of fasteners calculated based on prEN 1995-1-1 eqn (8.33)

ENV+1)+2): Both weakest shear plane and affected number of fasteners considered as above

prEN: Calculation in accordance with the latest Eurocode 5 (prEN 1995-1-1) without informative annex A. Glulam strength according to GL32/EN 1194:1999.

Annex A: Block shear capacity according to annex A of prEN 1995-1-1. No size effect correction for tension strength.

along the outer dowel lines on both sides, and the final failure was the tension failure of the remaining wood cross-section. A summary of the test results compared to various code versions is shown in Table 2. The mean of the test values is compared with calculated characteristic values, and also with acceptance criterion

$$F_{mean} \geq k_2 R_k \qquad (1)$$

where F_{mean} is the mean of the test values, k_2 is a factor depending on the sample size and coefficient of variation. According to Appendix A of ENV 1995-1-1 $k_2 = 1.13$, for six joints when COV $\leq$ 10%. R_k is the characteristic value of capacity in calculation.

3.3 Conclusions of failure

The Eurocode 5 ENV version which was used in the design is obviously not adequate. The full size experiment showed 50% capacity of the calculated characteristic value and laboratory experiments with smaller joints showed 60% capacity of the Eurocode ENV value. As a short term measure, a national supplement to the Eurocode 5 ENV version has been produced by Kevarinmäki concerning mainly the calculation of block shear failure and effective number of dowels in a joint (Appendix). It is based on the analysis of all old and new dowel joint tests that were made available to us.

There are, however, other reasons that have probably contributed to the failure in Jyväskylä:

- Failure may have started in a joint (see Fig. 1) in which most of the dowels were lacking (only seven dowels were in place instead of 33). However, the neighbouring truss should have carried the load, if there were no other problems.

- The quality of manufacturing of the joints was poor: tolerances of dowel hole locations and diameters were beyond the acceptable limits for dowel joints.

- The stability of the structure can be questioned: tall trusses were not adequately supported, and the compression chord was not properly fastened to the roof structure.

- The dowels were shorter than the width of the beam (151 mm vs. 215 mm) in order to have adequate fire resistance without extra protection. The holes were not open to both sides, and finally two trusses were placed side by side so that the visible surfaces had no holes. The design looked good and was good for fire protection, because the fasteners were hidden by wood. However, all dowels were not exactly centrally placed, and the absence of dowels could not be seen after installation of the trusses.

- It has been contended that the steel plates in the compression joints might have buckled, partly because of large manufacturing tolerances in the wood cutting. This was studied experimentally, and seems not to be a reason for collapse.

As a result of design and manufacturing problems the roof failed under a load which was only 25% of the intended load bearing capacity. The accident investigation commission is still working to establish the causes of the collapse. Once the investigation is completed a detailed final report will be published by the Accident Investigation Board. The views expressed in this paper are the conclusions of the authors, not necessarily those of the accident investigation commission.

4 Summary

This paper reports on the theoretical investigation of strength of sawn timber, which suggests that higher grades are relatively much better than low grades, with the consequence that structures made of C40 have clearly higher structural safety than structures made of C18, when present European strength grading and structural design standards are used.

Learning from the failures confirms that ENV 1995-1-1 is not adequate in the design of dowel-type tension joints and leads to overestimation of the load carrying capacity, which increases with the number of dowels. A new guideline is given in the Appendix to supplement ENV 1995-1-1. The upcoming version of Eurocode 5, EN 1995-1-1 will be safe in this respect, provided that also informative Annex A on block shear failure is followed. Our guideline in the Appendix is less conservative than in the upcoming Eurocode 5, and corresponds more closely to the test results.

Acknowledgement

References

ENV 1995-1-1, 1993, Eurocode 5 – Design of timber structures Part 1-1: General rules and rules for buildings. European Committee for Standardization CEN.

prEN 1995-1-1, 2002, Eurocode 5 - Design of timber structures, Part 1-1: General rules and rules for buildings. Final Draft 2002-10-09. Document CEN/TC 250/SC 5: N 195.

Hassinen, P., Koponen, S. & Tukiainen, P. 2003, Research report, Jyväskylän messupaviljongin B2 hallin kattorakenne, Kattoristikon R38 koekuormitus (Roof structure of B2 Hall of Jyväskylä Paviljonki, Testing of load-bearing capacity of R38 roof truss) made for Skanska Sisä-Suomi Oy (in Finnish, confidential)

Ranta-Maunus A., Fonselius M., Kurkela J. and Toratti T., 2001, Reliability analysis of timber structures. VTT Research Notes 2109. Espoo, Finland. 102 p. + app 3 p. ISBN 951-38-5908-8 (soft back edition), 951-38-5909-6 (URL: http://www.inf.vtt.fi/pdf/)

Ranta-Maunus, A., 2002, The effect of machine strength grading on the strength distribution of sawn timber based on numerical simulation. COST Action E24 & JCSS Workshop in Zürich, October 10-11, 2002.

Turk G., Ranta-Maunus A., 2003, Analysis of strength grading of sawn timber based on numerical simulation. VTT Research Notes. Draft, to be published 2003.

VTT research report RTE 1583/03 made for Wood Focus Finland (in Finnish, confidential)

Concise translation of VTT statement No. RTE2202/03 dated 9th June 2003

Made for the Ministry of Environment of Finland

Supplement to ENV 1995-1-1 and Finnish NAD:

Guideline for design of dowel and bolt joints under tension loads

This guideline is based on the dissertation by Andre Jorissen and Martin Schmidt, on existing design standards, and on the analysis of 216 experiments. Part of this information is confidential.

This guideline concerns joints loaded in the grain direction in structures made of sawn timber, glulam and LVL.

Eurocode 5, ENV 1995-1-1 with Finnish NAD can be used in the design of dowel-type joints if also the following additions or changes are followed:

1. Effective number of fasteners (replaces 6.5.1.2(3) in ENV 1995-1-1)

For a row of fasteners parallel to the grain direction, for loads parallel to the grain, the load carrying capacity is calculated using the effective number of bolts or dowels:

$$n_{i,ef} = \min \begin{cases} n_i \\ n_i^{0,9} \sqrt[4]{\dfrac{a \cdot t}{50 \cdot d^2}} \end{cases} \tag{A1}$$

where n_i is the number of fasteners in row i,

d is the fastener diameter,

$$a = \begin{cases} \min(a_1, a_3) & \text{for } n_i \ge 2 \\ a_3 & \text{for } n_i = 1 \end{cases} \tag{A2}$$

a_1 is the spacing distance in the grain direction,

a_3 is the end distance.

$$t = \begin{cases} t_u & \text{for double shear plane timber - to - steel - to - timber joints} \\ \min(t_s, t_u) & \text{for single shear plane timber - to - timber joints} \\ \min(t_s, 2t_u) & \text{for other joints} \end{cases} \tag{A3}$$

t_s is the thickness of the inner timber part in double or multiple shear plane joints or the thickness of timber on the head side of the bolt in a single shear joint,

t_u is the length of the dowel or unthreaded part of the bolt in the outer timber part.

2. Multiple shear plane joints (replaces 6.2.3 in ENV 1995-1-1)

In multiple shear plane joints the capacity of each shear plane will be calculated separately by dividing the joint into double shear plane connections. The capacity of the multiple shear plane joint is calculated by multiplying the minimum value of shear plane capacities by the number of shear planes.

3. Block shear failure

Block shear capacity of an end joint of a tensile member is calculated as

$$R_{l,d} = A_{l,net} \cdot k_l \cdot f_{t,0,d} \tag{A4}$$

where $f_{t,0,d}$ is the design value of the tension strength without size effect correction

$$k_l = \begin{cases} 1,45 & \text{for sawn timber and glulam} \\ 1,15 & \text{for (Kerto-S) LVL when } f_{t,0,k} = 38\,\text{N/mm}^2 \end{cases} \tag{A5}$$

$$A_{l,net} = (n_\perp - 1) \cdot (a_2 - d) \cdot t_{ef} \tag{A6}$$

$n_\perp$ is the number of parallel rows of fasteners in the direction perpendicular to the grain,

a_2 is the distance between the rows (see Fig. 6.3.1.2a in ENV 1995-1-1) in the direction perpendicular to the grain,

d is the diameter of hole made for the fastener

t_{ef} is the effective thickness of the timber member limited by the length of the smooth cylindrical part of the bolt or dowel.

Block shear failure calculation is not applied for connections where all fasteners are in the same row parallel to the grain ($n_\perp = 1$).

4. Glued laminated timber

If tensile members have dowel-type end joints, the members should be manufactured from homogenous glulam, all lamellae having the same strength class.

5. Manufacturing tolerances

Manufacturing tolerances are expected to meet the following tolerances:

- Length of smooth area of dowel or bolt inside wood members (t_s or t_u): - 2 mm, but not exceeding -5% of the wood member thickness

- Location of bolt or dowel in any part of the joint: $\pm$ 2 mm

If these tolerances are not met in manufacturing, the most unfavourable combinations have to be taken into account in the design calculation of joints.

INTERNATIONAL COUNCIL FOR RESEARCH AND INNOVATION
IN BUILDING AND CONSTRUCTION

WORKING COMMISSION W18 - TIMBER STRUCTURES

LOAD DURATION FACTORS FOR INSTANTANEOUS LOADS

A J M Leijten

Delft University of Technology

THE NETHERLANDS

B Jansson

Equilibrium Consulting Inc.

Vancouver

CANADA

Presented by: Ad Leijten

Ad Leijten began his presentation by giving an overview of the need to consider impact loading on guard rails and the choice of tropical hard wood. The research showed that the variation of dynamic strength as compared to static strength is dependent on species types. He concluded that impact-bending strength depends on wood species and loading rate. Discussions which followed related to the question of whether the effect is on a reduction of strength or an increase in loading due to the impact loading and the parameters which need to be considered in the research.

Load duration factors for instantaneous loads

A.J.M. Leijten

Delft University of Technology, The Netherlands

B. Jansson, MaSc.

Equilibrium Consulting Inc.

Vancouver BC, Canada

Introduction

There are a number of load cases such as earthquakes and single blasts where timber is exposed to substantially higher loading rates than in the standard short duration test. Examples of single blast loads are explosions but also impact by vehicles against a timber guardrail with loading times much less than one second sometimes up to of a few thousands of a second. Old test data shows that timber is well able to withstand impact loads. However, the validity of the old test data is questioned as more elaborate research indicates conflicting results.

Impact strength of connections

Very little is known about the impact performance of connections. Tests Girhammar, U. and Andersson, H. (1988) indicate a 20% increase in the embedment strength for a loading rate of 1250 mm/s compared to 2 mm/s.

Impact strength timber

A comprehensive test program was initiated at the Forest Products Laboratory, Madison, US to study the effect of rate of loading on the bending and compression parallel to the grain of two softwoods and two hardwoods; Sitka Spruce, Douglas-fir, Maple and Birch, respectively, Liska (1955). The planks were free of defects and as straight grained as possible. The dimensions were small: 1x1x4" for compression, 1x2x16" for bending of the softwoods and 1x1x16" for bending of the hardwoods. In both latter cases the span was 14.". The equilibrium moisture content ranged from 9 to 14%. Loading times ranged from 0.3 to 150 seconds. The bending tests were performed in a hydraulic testing machine with a constant head movement. The average of the controls (reference) mentioned in Figure 1 refer to the standard bending test results. The modification factors for accidental loading in many timber engineering design codes are based on these results. The bending strength increases with shorter time to failure rates for all wood species tested. At the highest loading rate the strength is about 20 to 30% higher than the bending strength at standardised loading rate. The load was determined by the deflection of a steel ring under one of the supports.
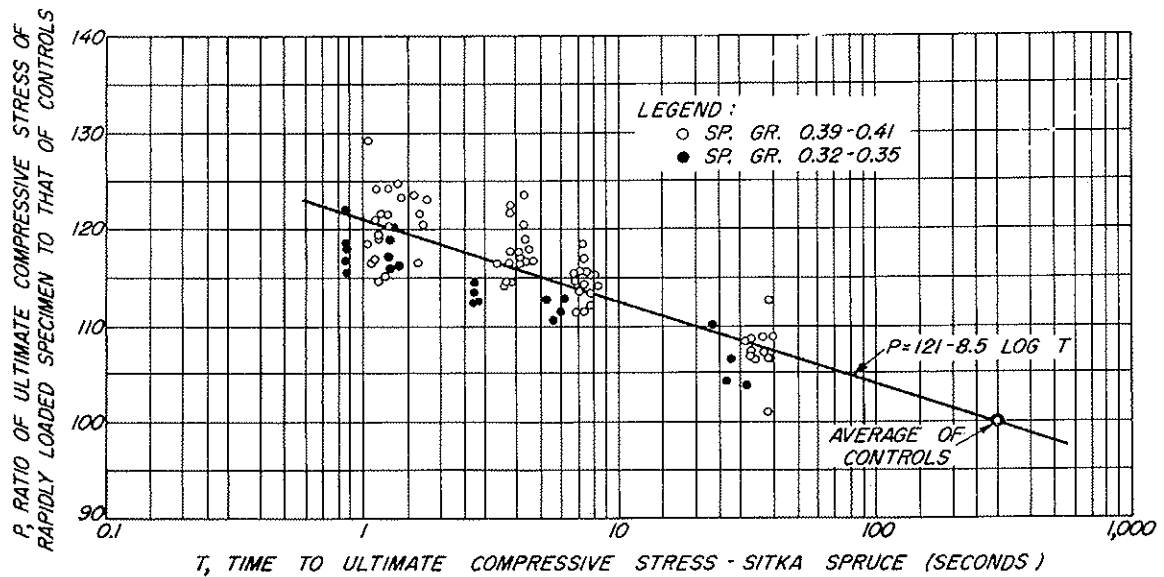
Figure 1: Ratio of static and impact bending strength versus loading rate for Maple, Liska (1955).

Mindess et. al. (1986) studied the impact bending strength on simply supported timber beams by dropping a weight (mass) at mid span from various heights. The three-point loading was accomplished by a fit-to-purpose built machine. Spruce beams of two commercial sizes were tested; 38x134x914 mm with a span 610 mm and 102x203x1530 mm with a span of 1220 mm. The smallest size beams were sampled in three categories. A) Defect free beams. B) Beams with a 35 mm square notch on the tension side of the beam. C) A knot at the tension side near the loading point. A drop height of 610 mm resulted in an impact velocity of 3,3 m/s. For the larger beams the weight was dropped from 1.5, 1.75 and 2.0m height resulting in an impact velocity of 5.1, 5.5 and 5.9 m/s respectively. On bases of the test results of the smaller beams it was concluded that the fibre length of the fractured part were much shorter than compared to the static bending test. For the more instrumented larger beams it was concluded that the bending strength and the fracture energies were lower than compared to the static bending test. The mean bending strength under impact appears to be 75% of the static strength. For the lower tail of the strength distribution the effect of impact appeared to be less dramatic. However, the test set-up did have a number of shortcomings that affected the strength results; one of which was the indentation of the compression zone caused by the shape of the loading tup, Sukontsasukkui at al. (2000). It should be mentioned that all previous researchers used load cells to determine the maximum load and to use these reading to obtain the bending strength without considering inertia effects.

Determination of impact strength

According to Johansson (1999) the use of load cell readings to treat the impact tests as static equivalent is a very deceptive indication of the true failure stress as the effect of inertia effects are disregarded. The internal moments and shear in the dynamic loaded beam must equilibrate not only the external applied force but also the inertia forces resulting from acceleration of the beam. One is to estimate the inertia effect by using an analytical model, the other is the use of computer simulation. Bantur et al. (1986) tested and analysed the impact results of single span concrete beams. He employed an analytical method to estimate the inertial effect and derived a closed form solution. The inertial load of

reinforced concrete beams accounted even up to 2/3 of the peak impact load. After the peak impact the inertia forces were still considerable and didn't drop rapidly.

Test results by Jansson

Jansson (1992) performed a comprehensive study of the impact strength of spruce-pine-fir beams but not before the test set-up used by Bantur et al. (1986) was modified in a way that the indentation of the loading tub into the compression zone of the beam was strongly reduced. Jansson used a load cell to determine the maximum load applied. His beams were loaded edge wise. He reports 651 impact tests on Spruce beams with dimensions of 38 x 89 x 1145 mm with a clear span of 1095 mm. The specimens were divided into two grades based on defects that appeared on the tension side over the mid half of the span. Defect free material was assigned class 1 material while beams with knots were assigned to class 2. Sub-groups of 31 beams were loaded in three point edge wise static (standardised) bending. The sub-group was tested either load controlled or deformation controlled. Results are shown in Table 1. As expected the mean maximum load appeared to be highest for Grade 1 while the coefficient of variation was smaller compared to Grade 2 (the c.o.v. is not given in Table 1).

The average *static* bending strength of Grade 1 material (defect free) was 82.1 MPa and 67.3 MPa for the Grade 2 (with knots). The differences in failure strength between the deformation controlled tests and load controlled tests were less than 18% for all loading rates.

Table 1:Overview test results by Jansson (1992)

Type of tests	target time to failure [sec]	Grade 1 (defect free)			Grad 2 (with knots)		
		number tests n	E-mod [MPa]	Mean max.Load [kN]	number tests n	E-mod [MPa]	Mean max.Load [kN]
DC	60	31	8903	13.6	31	8683	11.1
DC	3.5	31	8871	15.2	31	8691	12.3
DC	0.2	31	8866	15.4	31	8671	12.3
LC	60	31	8824	14.6	31	8693	12.2
LC	3.5	31	8911	14.7	31	8753	12.3
LC	0.2	31	8865	15.2	31	8587	11.9
Impact	0.03	62	8589	13.5	31	8539	11.9
Impact	0.02	62	8912	16.5	31	8485	12.5
Impact	0.01	62	8892	16	31	8832	13.8
Total		372			279		

DC= deformation controlled, LC=Load controlled

For the impact tests a weight of 345 kg was dropped from 50, 150 and 300 mm height resulting in a maximum impact velocity of 2,3 m/s. The average times to failure were 25, 17 and 10 milliseconds for Class 1 and 24, 13 and 9 ms for Class 2 material. The maximum force was measured directly by means of a load cell between the drop weight and the test specimen.

Simulation by means of Modal analysis was applied to enable to determine the portion of inertia load. He presented his results in three different ways to proof how different the conclusions can be depending on the method of analyses. Figure 2 and 3 represent the first method for Class 1 and 2 materials as applied traditionally and called Classic approach. The failure stresses from each loading rate are determined using the maximum value of the
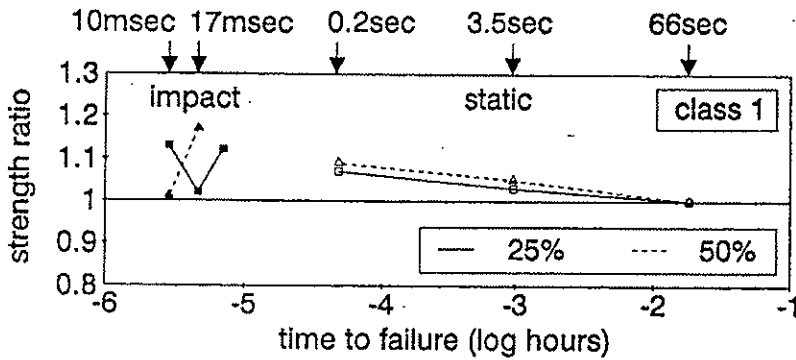
Figure 2: Classic approach, failure loads related to standard short duration, Class 1 material

load cell readings and divide it by the standard short duration strength resulting in the static duration of load. In this respect the effect of inertia is being neglected:

$$\text{Static DOL} = \frac{f_{static}}{f_{SSD}} \qquad (1)$$

were:

f_{stat} is the observed strength derived directly from the maximum load cell reading
f_{SSD} is the standard short duration strength

The Standard Short Duration strength is taken as the result of the load-controlled tests at 66s and 51s for Class 1 and 2 materials, respectively. In both figures 2 and 3 the classic approach shows a general tendency of increasing strength ratio with decreasing failure time. The 25% and 50% lines correspond to the non-parametric percentile values of the distribution. Class 2 material deviates from Class 1 material probably caused by the influence of knots. Class 1 material corresponds well with the findings of Liska (1955) given in Figure 1 for material free of knots. As mentioned earlier in the classic approach inertia effects are disregarded as the load cell readings include inertia effects.
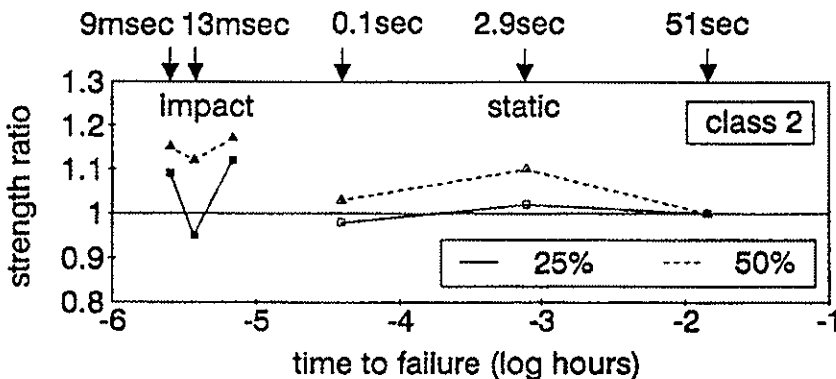
Figure 3: Classic approach, failure loads related to standard short duration, Class 2 material

Jansson makes an effort to evaluate the influence of inertia using modal analyses and finally presents his results as shown in Figure 4 and 5. The 25 and 50 ranking percentages values show a consistent tendency of decreasing strength with decreasing failure time. The dotted line in both figures represent the linear regression computed from both percentiles

4
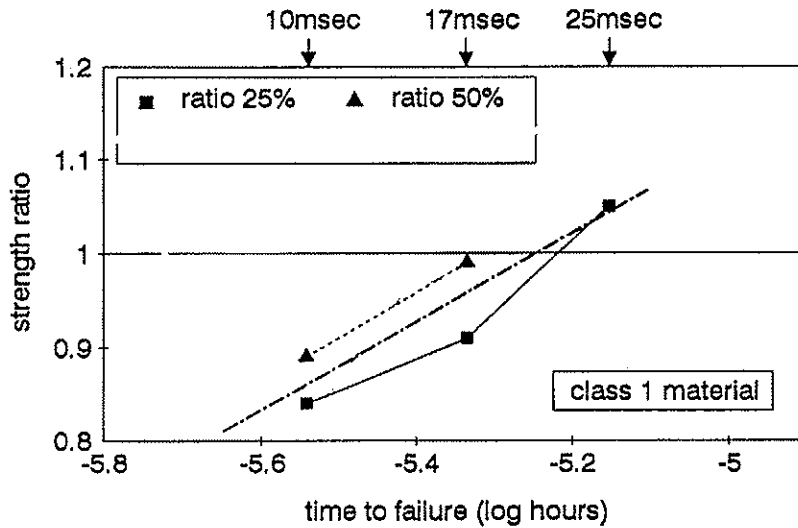
Figure 4: Strength decrease based on ranked modal strength, Class 1 material
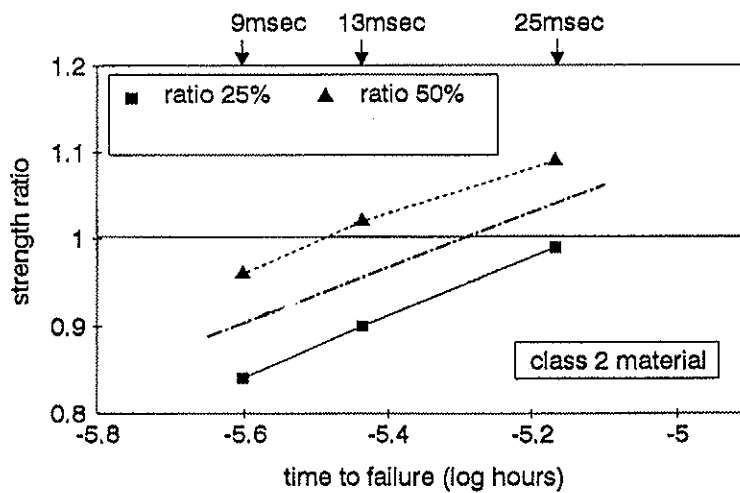
Figure 5: Strength decrease based on ranked modal strength, Class 2 material

values. Jansson also studied the failure modes in relation to the time to failure and found that compression initiated failure mode decreased with decreasing failure time. Material with strong tension zones developed more compression wrinkles in the compression zone, but as the failure time decreased the amount of failures in the tension zone increased and with that resulted in a decrease of failure strength.

Some of Jansson conclusions are:

- A strength decrease of 15% could be expected during impact loading for the weaker specimens compared to the static strength.

- The decrease in failure strength for higher loading rates was explained by the decreasing amount of compression initiated failure modes.

- The general practise of increasing the strength for impact loads should not be maintained.

Recent tests

All previous impact tests used wood species like Spruce and Pine. In relation to a project aimed at developing a timber guardrail the impact strength behaviour of other wood species was by assessed by Leijten (2000). The wood species were Angelim Vermelho (tropical hardwood), mean density 1091 kg/m³, Douglas Fir, 537 kg/m³, Ash, 711 kg/m³, Larch, 511 kg/m³ and three so-called heat threaded or heat modified wood species. Douglas Fir, density 472 kg/m³ was treated according to the PLATO process, (PLATO is a Dutch patented process). Spruce (Picea Abies), 461 kg/m³, and Pine (Pinus Silvestries), 458 kg/m³, were modified using the Finnish STELLAC process. Clear free were Angelim Vermelho, Douglas Fir and Ash while the others were of a commercial grade having knots and other deficiencies. The Plato wood was of the lowest grade involving the biggest knots. All specimens were conditioned at 80% RH and 20⁰ C until equilibrium was obtained. The density values specified above refer to this condition. Kloot (1954) showed that at about 10%-15% m.c. the impact resistance is the lowest. For higher and for lower m.c. the impact resistance increases. The target specimen dimensions were 40x130x1600mm. In Table 2 the batches for the static and impact tests, a total of 162 specimens, are given based on a balance of the modulus of elasticity.

The impact velocity was derived from the lateral impact speed of the guardrail test vehicle according to CEN/EN 1317, which was 7.0 m/s.

Table 2: Number of specimens of batches and MOE details

Wood	Batch Static test			Batch Impact test		
Species	Number of	mean	c.o.v	number of	mean	c.o.v
	Specimen	MOE		specimen	MOE	
	n	[N/mm2]	[%]	n	[N/mm2]	[%]
Angelim V.	11	18146	19	10	17496	15
Douglas	10	11161	23	10	11644	22
Ash	4	12587	29	7	12293	7
Larch	11	8122	20	10	7922	17
Plato (D)	12	9272	20	11	9821	15
Stellac (S)	13	12051	12	14	12161	13
Stellac (P)	17	9960	19	22	9689	19

The total mass of the drop piece was 199 kg and instrumented with an accelerometer.

To prevent too much indentation of the surface a solid cylindrical steel rod of 110 mm diameter was chosen as the striking loading head, Sukontasukkul (2000). To prevent any instability of the specimen it was decided to test the beams in flat-wise bending. The specimens were simply supported, span 1400 mm, and loaded by the drop-weight at mid span. It was decided to monitor the deflection at mid span by using a transducer (LVDT) attached to the bottom of the timber specimen directly underneath the impact location. With a high-speed video camera (9000 frames per second / one frame every 0.111 ms) the crack initiation was monitored. The readings from both accelerometer and LVDT were taken 50,000 times/s. To monitor the response of the instrumentation and the robustness of the test set-up the drop-weight height slowly increased from 10, 25, 50, 75, 100, 250, 500, 1000 mm and finally 2500 mm. For this purpose dummy specimens of clear free Larch were used. A phenomenon worth mentioning here and which appeared to be of importance in the interpretation of the test results was recorded by the high-speed video camera. Its

purpose was not only to monitor the attachment of the LVDT during impact and to determine the time to failure by the initiation of cracks but also to monitor the interaction between the beam and the drop-weight. The video pictures revealed that after the initial impulse transfer the beam speeded up more than the drop-weight resulting in a loss of contact. If the beam remained unbroken during this free flight the drop-weight made contact again and transferred a second impulse. This bouncing effect was also observed and recorded by the LVDT's as the time-deflection curve showed one or maximum two bumps. Finally, the drop-weight established a permanent contact and worked its way down until failure occurred. The output data from the impact test consisted of the time dependent position of the beam at mid span, time to failure, and the readings from the accelerometer. Time of failure was defined as the appearance of the first crack, which was taken from the video recordings. Also the accelerometer signalled the time to failure by an excess of shock waves. Only in some rare cases splits appeared that didn't initiate crack propagation straight away.

A dynamic simulation model based on so-called Thimoshenko elements was used to analyse the bending moment assuming linear elastic behaviour and was developed by A. Kok (1997). The simulation model was particular suited to load the beam by impulses and to attach lumped masses at any given time. Obviously, the model accounted for inertia effects. The model simulated the mid span time deflection relation well including the bouncing effect mentioned above. The dimensions, static modulus of elasticity and density where used as input. Although the dynamic modulus of elasticity is usually a 5% higher a sensitivity analyses showed that this didn't had a significant effect on the dynamic bending stresses.

Mean static versus mean impact strength

Bending strength [MPa]

	1	2	3	4	5	6	7
Standard [MPa]	125.2	72.2	92.8	55.1	27.7	41.4	50.1
Impact [MPa]	96.7	63.8	101.6	24.3	18.3	23.3	28.8
Impact/Standard	0.77	0.88	1.09	0.44	0.66	0.56	0.57
Failure time [ms]	7.4	7.2	11.1	6.4	3.2	4.6	4.8
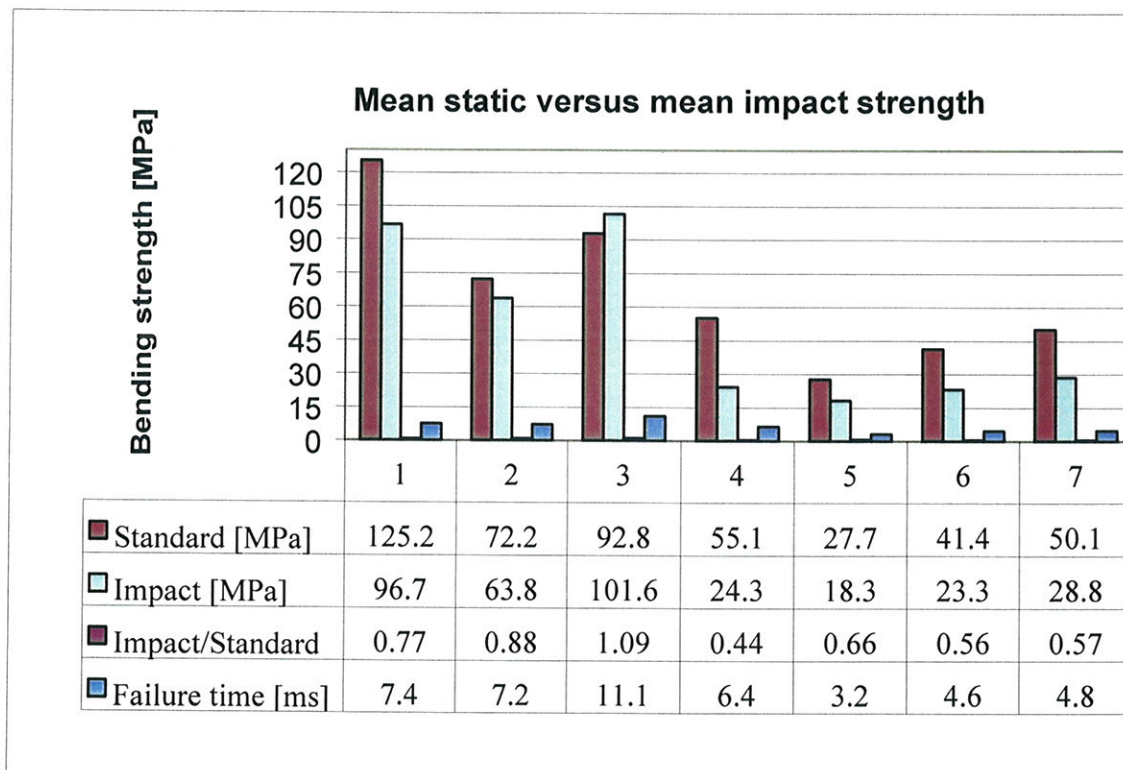
(1) Angelim Vermelho   (2) Douglas Fir   (3) Ash   (4) Larch

(5) Plato (Douglas Fir)   (6) Stellac (Spruce)   (7) Stellac (Pine)

Figure 6: Test results by Leijten (2000) comparing static and impact bending strength.

Figure 6 represents the overall results of the research. The mean impact strength (f_{dyn}) and static bending strength (f_{SSD}) are given. Also the strength ratio is determined and the mean

time to failure given. Although the number of test specimens per wood species is small the tendencies are clear. The mean impact bending strength is considerably smaller, 40 to 60%, than the mean standard static bending strength of all commercial wood species (with knots) such as Larch and the three heat-treated wood species. Only for Douglas and Ash both free of knots, the strength reduction is statistically not significant. In this respect the knot free hardwood Angelim Vermelho is an exception.

Bocchios et al. (2000) evaluated the same impact test results of Angelim Vermehlo and some Douglas Fir, however, not the complete data set. The evaluation was based on the deflection at failure disregarding any possible inertia effect. An equivalent static bending stress was determined and defined as the impact strength. This assumes a triangle moment distribution along the span of the beam from the moment of impact up to failure, which the dynamic simulations show not always to be correct, especially when inertia influence is high. Jansson (1992) already warned for this approach as misleading. Comparing both methods Leijten (2000) reports differences in mean impact bending strength of –5% to +30% depending on the time to failure (wood species).

A visual assessment of the type of failure with a focus on the length of the broken fibres revealed that long fibre failures for Ash and Angelim Vermelho were observed after impact failure followed by shorter fibre failure for Douglas fire and Larch. Especially, the heat-treated wood species, showed small to hardly any fibre length fracture.

Conclusions and proposal for change of modification factor for instantaneous loads

On the bases of the research evaluated the following conclusions can be drawn:
- In design of timber structures that are exposed to instantaneous loads the inertia effects cannot always be ignored. Design based on static equivalent methods can be very deceptive in reflecting the actual stress situation. For this reason a proper stress evaluation method like computer simulation methods is preferred.

- The strength modification factor for instantaneous loads currently in Eurocode 5, ($k_{mod}>1$) is based on impact tests of small clear specimens where the effect of inertia is disregarded.

- The impact bending strength is grade, wood species and loading rate dependent.

- Jansson (1999) and Leijten (2000) both demonstrated a general tendency that with increasing loading rate the bending strength decreases.

- Commercial grades with knots tend to show a higher degradation of the bending strength than clear free material. The strength degradation is substantial for heat-treated timber.

- Based on the test results evaluated it is difficult to propose instantaneous DOL factors as the shorter the time to failure the more the bending strength drops. However, for structural softwoods in Table 3 a proposal is given to change the duration of load factor for instantaneous load with high impact rates to be closer to reality than current code values.

Table 3: Proposed DOL factor, k_{mod}, for instantaneous loads for Eurocode 5 (EN1995-1-1) Service class I and II (m.c. 12-20%)

Material	Present factor k_{mod}	Proposed factor k_{mod}
Solid timber	1,1	0.85
Heat treated solid timber	-	0.6

References:

Bantur, A, Mindess, S, and Banthia, N., (1986), The behaviour of concrete under impact loading: Experimental procedures and method of analysis. Materials and Structures, Vol. 19, No. 113, pp. 371-378.

Bocchio, N., Ronca P. and Kuilen van de, J-W.(2001), Impact loading tests on timber beams, IABSE conference Lahto 2001, Innovative Wooden Structures and Bridges, IABSE Report Vol.85.

Girhammar, U. and Andersson, H. (1988), Effect of loading rate on nailed timber joint capacity. Journal of Structural Engineering, ASCI, Vol. 114.

Jansson, B. (1999), Impact loading of timber beams, RILEM Symposium on Timber Engineering, Stockholm, September 13-15.

Kloot, N.H. (1954), The effect of moisture content on the impact strength of wood, Australian Journal of applied Science, Vol.5 no.2, pp. 183-186.

Leijten A.J.M. (2000), Timber impact strength for guardrail application, Stevin Report 2000-1 /HE-40, Dep. of Civil Engineering, Delft University of Technology, The Netherlands.

Liska, J.A., (1955), Effect of rapid loading on the compressive and flexural strength of wood, Report 1767, Forest Products Laboratory, Forest Service, Madison, Wisconsin.

Kok, A. (1997), Lumped impulses, discrete displacements and moving load analysis, HERON 1997, vol.42, No. 1, p.3 -23, ISSN 0046-7316

Mindess, S and Madsen, B (1986), The fracture of wood under impact loading, Material and Structures, Vol. 19, No. 109.

Wood Handbook (1999), Wood as a engineering material, Report FPL-GTR-113, Forest Service, Forest Product Laboratory, Madison, Wisconsin.

Sukontsasukkui, P., Mindess, S., Banthia, N. (2000), Impact behaviour of parallel strand lumber (PSL), Proceedings of the World Conference on Timber Engineering, Whistler Resort, BC, Canada,

INTERNATIONAL COUNCIL FOR RESEARCH AND INNOVATION
IN BUILDING AND CONSTRUCTION

WORKING COMMISSION W18 - TIMBER STRUCTURES

STRUCTURAL DURABILITY OF TIMBER IN GROUND CONTACT

R H Leicester

C-H Wang

M N Nguyen

G C Foliente

CSIRO

C MacKenzie

TRADAC

AUSTRALIA

Presented by: Bob Leicester

Bob Leicester's presentation began with engineering definitions of the terms such as decay and decay front. He went on to describe the on-site tests carried out from which decay attack patterns on treated and untreated heartwood, corewood and sapwood were observed as a function of the maintenance procedure used. He went on to describe the model developed to predict the service life and its applicability to other forms of decay such as termite attack. He went on to answer questions relating to the current trend of not using preservatives such as CCA and design life.

STRUCTURAL DURABILITY OF TIMBER IN GROUND CONTACT

By R.H. Leicester[1], C-H Wang[1], M. N. Nguyen[1] G.C. Foliente[1], C. MacKenzie[2]
(1) CSIRO, Australia
(2) TRADAC, Australia

ABSTRACT

This paper describes the development of a model to predict the strength of timber poles and rectangular sawn sections subjected to in-ground attack by decay fungi. The models are based on data obtained from extensive in-ground stake tests that were monitored over a period of 30 years and a limited number of full size pole and rectangular sawn sections. The model takes into account timber species, preservative treatment, maintenance practice and local climate. The model predictions are in quantified form, and hence can be used to make cost-optimised decisions for asset management purposes.

1. INTRODUCTION

During the past few years several models to assess the durability of timber construction have been developed (Leicester 1999, 2001, Foliente *et al.* 2002). The following describes a model developed for evaluating the structural degradation of timber in ground contact. This model is based on the concept that decay in timber progresses on a front as indicated schematically in Figure 1. The decay front is taken to be the boundary between full strength undecayed wood and zero strength decayed wood. In this context, decayed wood is defined as wood that can be picked out with a pen knife. The structural load capacity of the residual timber section can be evaluated from the conventional principles of structural mechanics.

Details of the derivation of the durability model have been given in a recent IRG paper (Leicester *et al.* 2003). In the following only the final model equations will be presented.
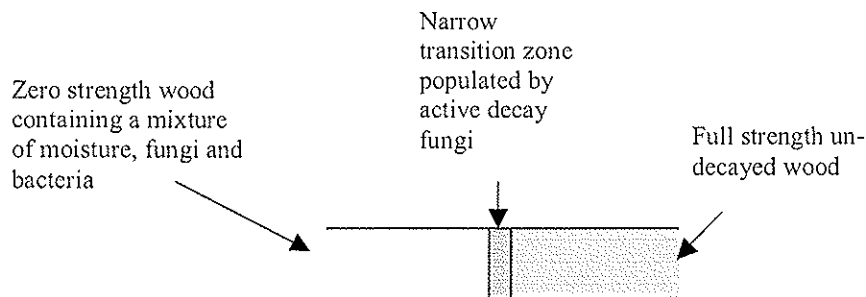
Figure 1. Schematic illustration of a decay front.

2. MODEL FOR THE DECAY OF STAKES

2.1 Tests of Small Stakes

The preliminary model was based on data obtained from small stakes of the dimensions shown in Figure 2. The stakes were placed at the 5 major sites around Australia as illustrated in Figure 3. The stakes comprised untreated outer heartwood of 77 species, with 10 replications at each site. There were also stakes of two species (*E. regans* and *P. radiata*) treated with various preservatives at three of the sites. All of this data comes from field studies monitored by J.D. Thornton and G.C. Johnson. Some of it is reported in a previous paper (Thornton *et al.* 1991). The species were left in situ for about 30 years, and the decay measured every few years by picking the stakes with a penknife. The

traditional score rating used for these stake assessments was converted into effective mm of depth of decay. On the basis of their performance, the species were subdivided into four durability classes (Thornton *et al.* 1997). An example of the data obtained is shown in Figure 4.
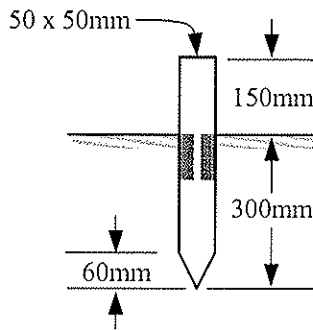
Figure 2. In-ground stake.
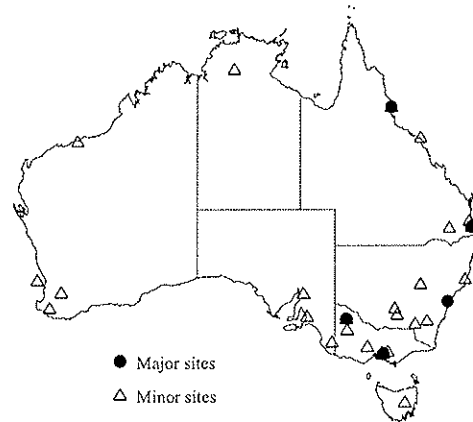
Figure 3. Test locations of in-ground stakes.
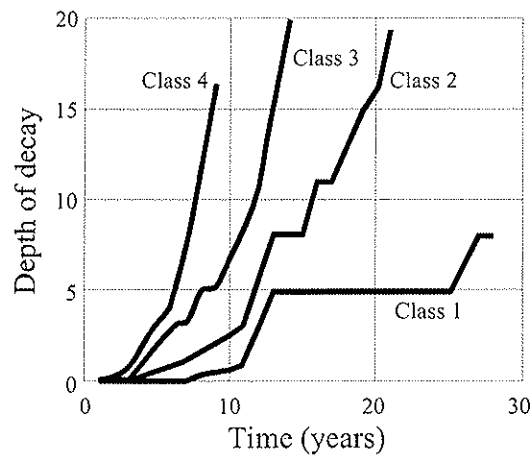
Figure 4. Measured 50-percentile values of decay of untreated in-ground stakes at Sydney; Classes 1–4 refer to durability classes after Thornton *et al.* 1997.

2.2 The Idealised Decay-Time Relationship

The assumption of the idealised progress of a decay front is illustrated in Figure 5. The features of this assumption are an initial lag, followed by a constant rate of decay. If a maintenance treatment is applied, the assumption is that there is an additional lag in the progress of the decay.

2.3 A Climate Index

The in-ground stakes were also used to investigate the effect of climate on decay. The most important climate factors affecting in-ground decay of timber are moisture content and temperature of the timber. Therefore, the climatic parameters chosen to create a climate index for in-ground decay were the mean annual rainfall, the number of dry months per year, and the mean annual temperature. A dry month is defined as the month during which the total rainfall does not exceed 5 mm. The value of 5 mm was chosen, because an analysis of the effect of rainfall for 12 typical soil types indicated that if the rainfall is less than 5mm per month, then the surface of the wood of in-ground stakes will dry below the fibre saturation point and halt surface decay.

2
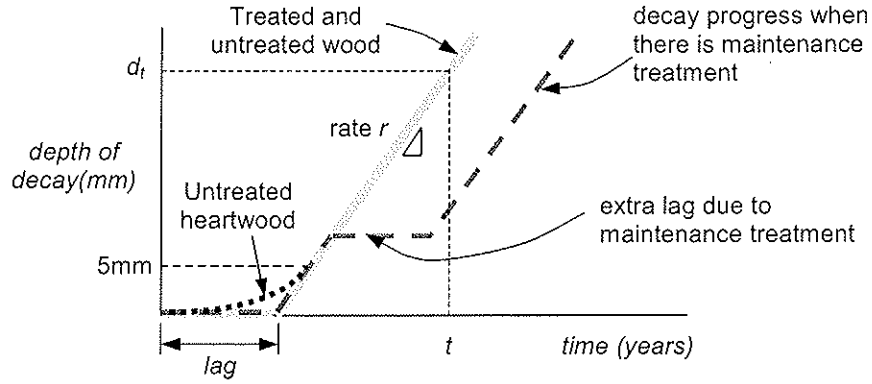
Figure 5. The idealised decay functions.

A model for a climate index was obtained by using information obtained from the stakes mentioned above, placed around Australia in the major and minor sites shown in Figure 4 for a brief 2 year period. By correlating the climate parameters with measured in-ground decay of the wood stakes, a climate index was derived that was proportional to the observed rates of decay of the untreated wood.

The climate index is expressed in terms of two functions, one related to the annual rainfall and the second to the mean annual temperature. The function $f(R_{mean})$, is based on the mean annual rainfall R_{mean} and is defined by

$$f(R_{mean}) = \begin{cases} 0 & \text{if } R_{mean} \le 250 \text{ mm or } N_{dm} > 6, \\ f_0(R_{mean})\left(1 - \dfrac{N_{dm}}{6}\right) & \text{if } R_{mean} > 250 \text{ mm and } 0 \le N_{dm} \le 6 \end{cases} \tag{1}$$

where

$$f_0(R_{mean}) = 10\left[1 - e^{-0.001(R_{mean} - 250)}\right] \tag{2}$$

in which N_{dm} denotes the number of dry months per year.

The other function $g(T_{mean})$, is based on the mean annual temperature T_{mean} and is given by

$$g(T_{mean}) = \begin{cases} 0 & \text{if } T_{mean} \le 5°C, \\ -1 + 0.2T_{mean} & \text{if } 5 < T_{mean} \le 20°C, \\ -25 + 1.4T_{mean} & \text{if } T_{mean} > 20°C. \end{cases} \tag{3}$$

The two functions $f_0(R_{mean})$ and $g(T_{mean})$ are shown in Figure 6. The climate index, I_{ig}, is defined as

$$I_{ig} = f(R_{mean})^{0.3} g(T_{mean})^{0.2} \tag{4}$$

Using this definition of a climate index together with data from the Met Bureau, a hazard map of Australia was drawn as shown in Figure 7, where the climate zones are defined as given in Table 1.

3

Table 1. Representative climate index values for the 4 hazard zones

In-ground Decay Hazard Zone	Representative I_{ig}	Boundary I_{ig}
A	0.5	1.0
B	1.5	2.0
C	2.5	2.5
D	3.0	

(a) Plot of $f_0(R_{mean})$ (b) Plot of $g(T_{mean})$
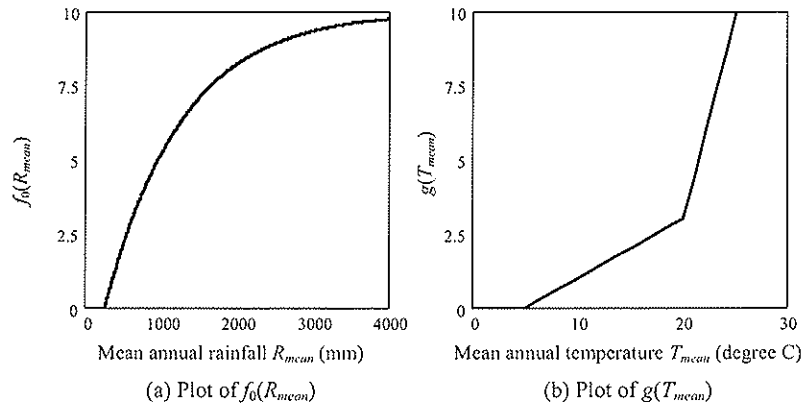
Figure 6. Functions of $f_0\left(R_{mean}\right)$ and $g\left(T_{mean}\right)$.
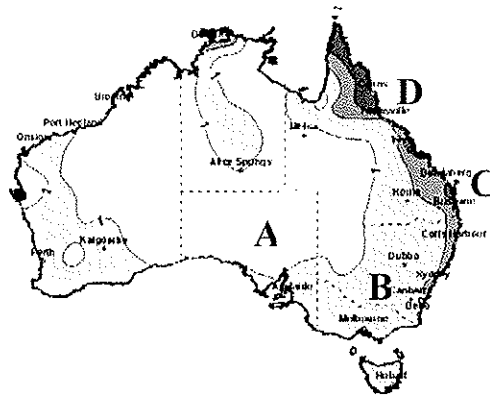
Figure 7. Hazard map based on equation (4).

2.4 Effect of Wood Location

This section presents the equations for a basic in-ground decay model for small clear stakes of timber. Definitions used for different types of wood are illustrated schematically in Figure 8. For convenience, the heartwood will be deemed to comprise two portions, an inner heartwood and an outer heartwood. In this paper, the inner heartwood will be denoted as 'core wood'. In the light of lack of definitive information, it will be assumed that the radius of core wood is half that of the total heartwood.

4
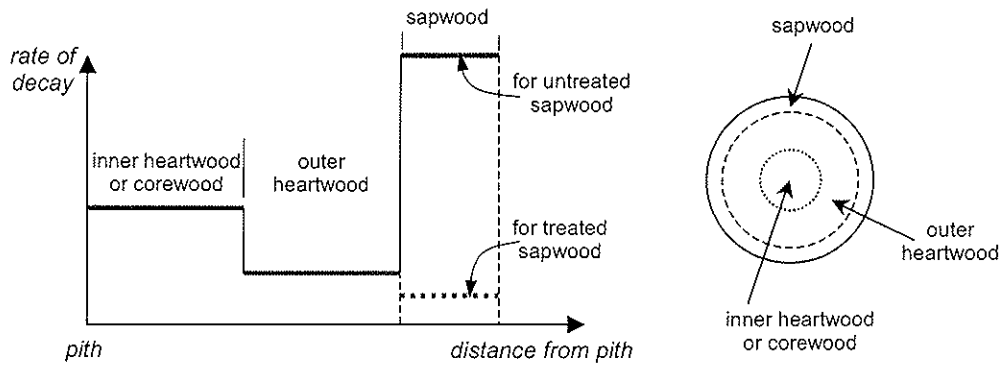
Figure 8. Schematic illustration of relative decay rates of different types of wood.

The outer heartwood, used for the stake tests, represents the most durable part of a tree. There will be an increased decay for the inner heartwood (corewood) and for the sapwood as indicated in Figure 8. The corewood is assumed to extend to half the distance between the pith and sapwood.

Data available on clear stakes relate only to the untreated outer heartwood. Limited information on the decay rates for untreated sapwood or for corewood. In this paper all decay rates of wood are stated in terms of the decay rate of outer heartwood.

2.5 Rate of Decay

2.5.1 Untreated outer heartwood

The decay rate of untreated outer heartwood, denoted by r_{heart}, is given by

$$r_{heart} = A \, I_{ig} \tag{5}$$

where the parameter A is given in Table 2 and I_{ig} denotes the climate index computed according to equation (4) and tabulated in Table 1.

Table 2. Decay parameters for untreated outer heartwood

Durability Class	A
Class 1	0.20
Class 2	0.55
Class 3	0.80
Class 4	1.85

2.5.2 Untreated corewood

The decay rate of untreated corewood denoted by r_{core} is taken to be given by

$$r_{core} = 3 \, r_{heart} \tag{6}$$

2.5.3 Untreated sapwood

The decay rate for untreated sapwood, denoted by r_{sap}, is taken to be given by

$$r_{sap} = 2 \, r_{heart, dc4} \tag{7}$$

where $r_{heart, dc4}$ denotes the decay rate of untreated outer heartwood of durability class 4.

5

2.5.4 Treated sapwood

In the model, it is assumed that for Australasian species of timber, only sapwood can be penetrated by preservative. For stakes preserved with CCA and creosote, this decay rate, denoted by r_{treat}, is taken to be given by

$$r_{treat} = r_{sap} / [\ 1 + B.C\ ] \qquad (8)$$

where   B = 80 for softwoods
         = 15 for hardwoods
         C = CCA retention (%kg/kg) for timber treated with CCA
         = 0.018 creosote retention (%kg/kg) for timber treated with creosote.

2.6 The Decay Lag

The decay lag, Figure 5, is taken to be given by

$$lag = 4 * r^{-0.3} \qquad (9)$$

where r is the corresponding decay rate evaluated according to equations (5)–(8).

In the following, the notation lag_{heart}, lag_{core}, lag_{sap} and lag_{treat} will be taken to denote the lag times for stakes of untreated outer heartwood, untreated corewood, untreated sapwood and treated sapwood respectively.

3. MODEL FOR FULL SIZE TIMBER MEMBERS

3.1 Calibration Procedure

For a full size members, the initial model is based on the model for small stakes and then modified as indicated from in-service observations. The following will illustrate the use of field data to modify and develop models for full size members by special reference to pole timbers. The pole models were developed on the basis of data obtained from 60 poles at the Wedding Bells test site north of Sydney (Gardner et al. 1994). For example, it has been noted that for CCA treated sapwood, the timber appeared to perform better in poles than in stakes, possibly because CCA leached from below ground timber in poles was being replaced by CCA leached from the above ground portions. Similarly it has been found that treatment of outer sapwood has an influence in delaying the decay of the inner corewood.

An important feature required for modelling full-size members is the need to decide on an attack scenario. Examples of assumptions used for decay patterns are shown in Figure 9. It is known from field observations that decay in a timber pole can initiate both from the perimeter progressing inwards and from the pith zone progressing outwards. Using a mix of both field observations and microbiology information, the models for inward and outward decay have been chosen. Figures 10 and 11 show two examples of models for the decay of hardwood timber poles. Other examples are given in the IRG paper cited earlier (Leicester et al. 2003).

If some sort of maintenance action is undertaken then the effect of such action is to add a further time lag to the progress of the decay, as illustrated in Figure 5. Table 3 lists values of the extra lag for each single application of a maintenance treatment.

6

Table 3. Effect of maintenance procedures

Maintenance procedure	Extra lag for each application of the maintenance procedure (yrs)	
	Perimeter decay	Centre decay
External diffusing chemical barriers: *(eg. Pastes containing copper, fluorine and boron salts)*	5	0
External non-diffusing chemical barriers: *(eg. Creosote or copper napthanate)*	2	0
External physical barriers: *(eg. Concrete collar or tar-enamel wrap)*	0	0
Insertion of internal diffusing chemicals	0	5

Case 1.
Decay from
pith zone

Case 2.
Decay from half
width cracks

Case 3.
Decay from
outer surface.

decay   d = depth of decay
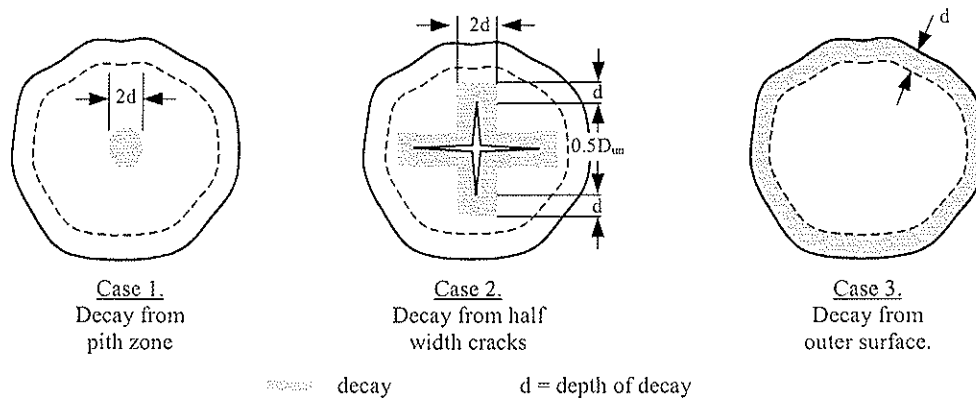
Figure 9. Examples of assumed attack patterns for in-ground poles.
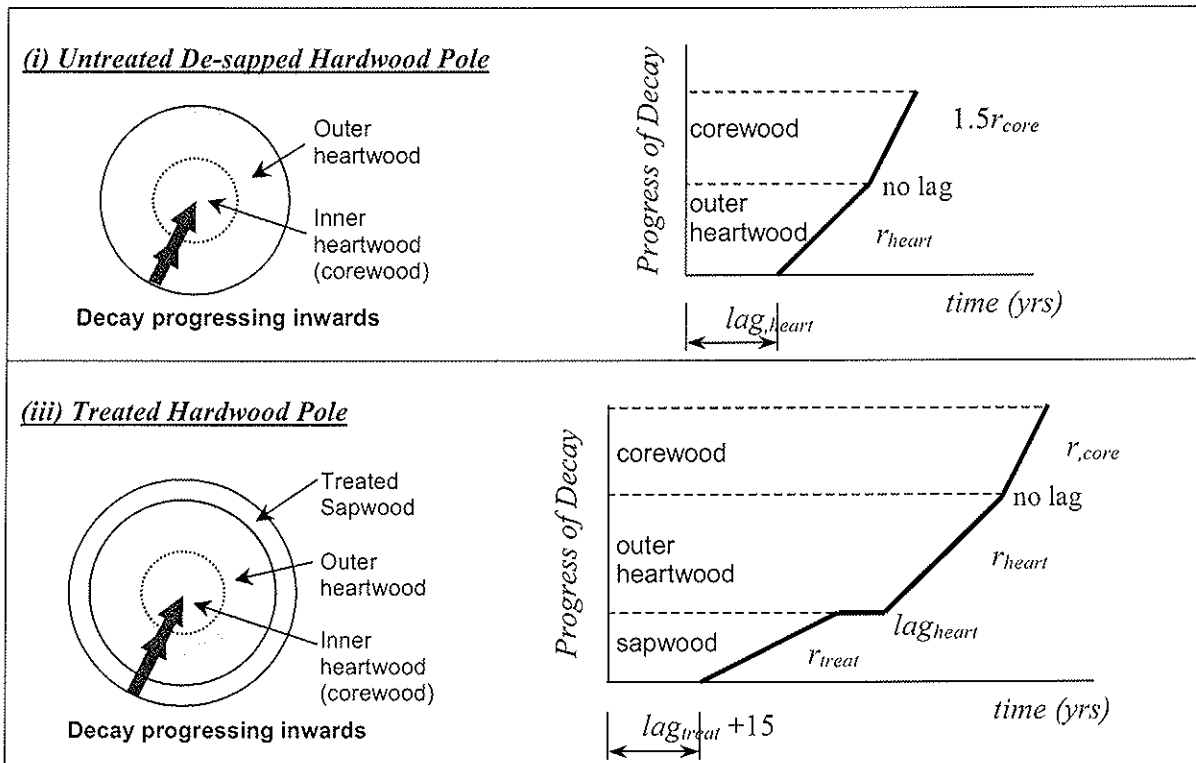
Figure 10. Decay of poles progressing inwards.
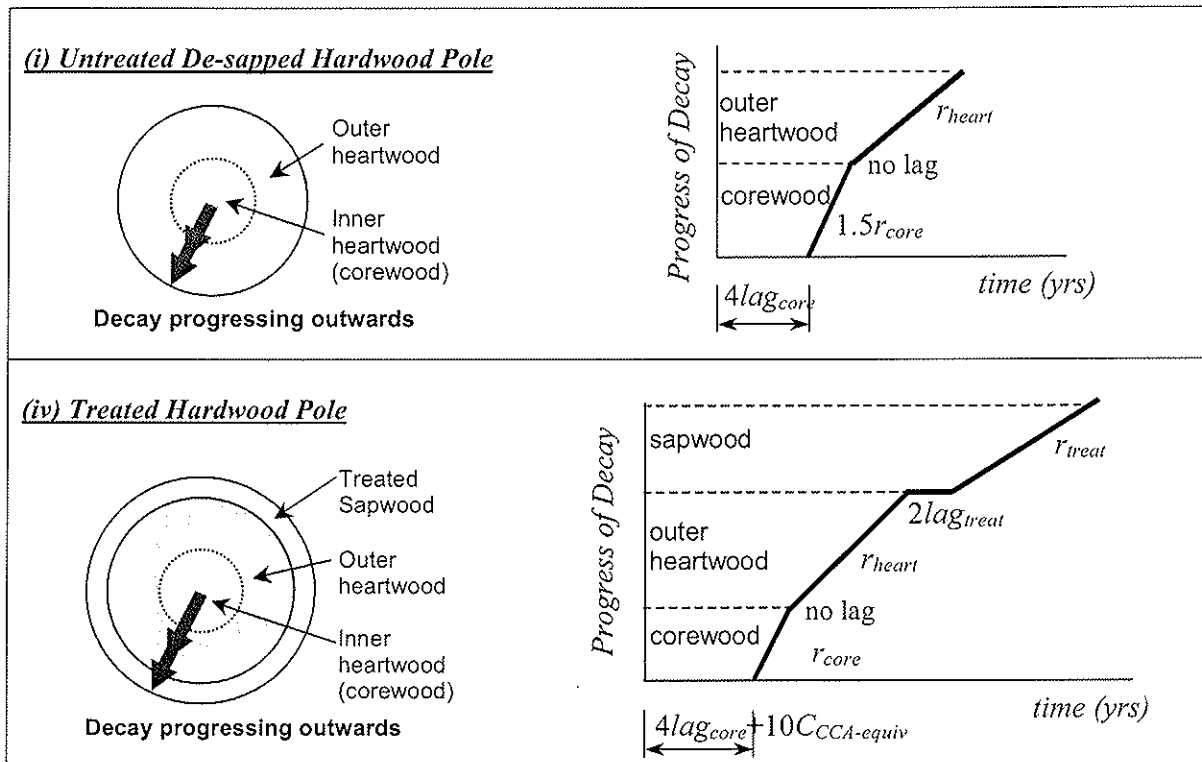
Figure 11. Decay of poles progressing outwards.

4.   APPLICATIONS

4.1   Asset Management

To illustrate the application of the models for service-life estimation of structural timber, the model for pole timbers will be used to examine the strength history of a round pole with a diameter of 400 mm, made from hardwood of durability class 2. It will be assumed to have a thickness of 15 mm sapwood treated with CCA preservative for hazard class 4 as specified in AS1604.1–2000; i.e., the preservative retention is 0.7 %kg/kg. It will be assumed that maintenance procedures will comprise the use of an external diffusing paste, applied at 25 and 30 years after installation. The site is assumed to be in hazard zone D shown in Figure 7.

The progress of the fungal decay of poles will be assumed to initiate from both the treated perimeter wood and the pith as illustrated in Figure 12a. The computed strength history of the typical pole is shown in Figure 12(b). This type of computation may be used for an asset management strategy where for example replacement of all poles may be required when the typical pole is assessed to have only 70% of its original strength capacity.

(a) Decay patterns
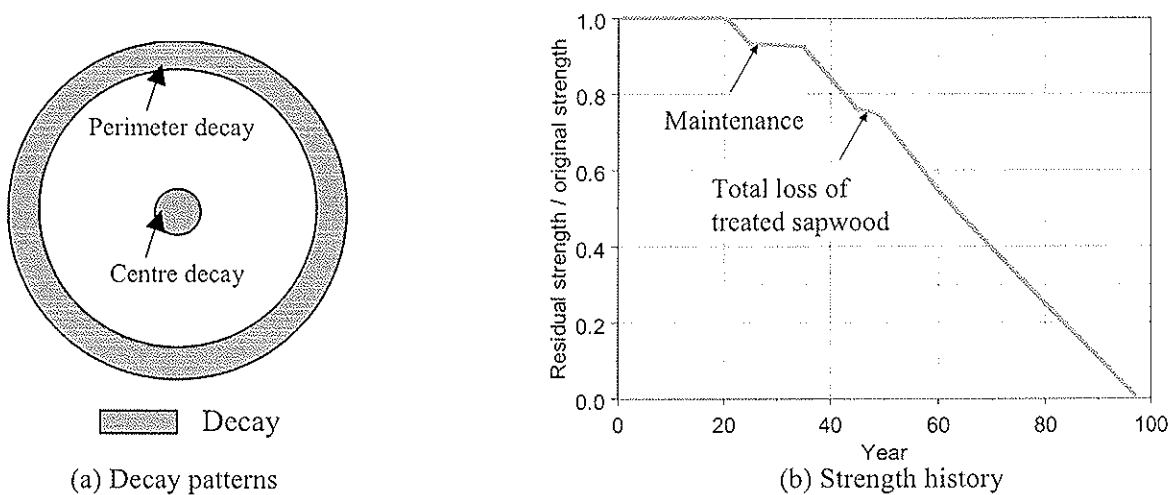
(b) Strength history

Figure 12. Strength history of the example pole.

4.2   Engineering Design Codes

For engineering design codes, the computed strength reduction may be expressed in the form

$$M = k_D M_o \qquad (10)$$

M = design bending strength capacity
M_o = value of M excluding durability considerations
k_D = durability factor

For the purpose of drafting engineering design standards it will be necessary to take into consideration the uncertainty associated with strength estimates. An example of this has been given in a previous paper (Leicester et al. 2001).

5.   CONCLUDING COMMENTS

Using the completed model, it is now possible to compute the deterioration over the years of the load capacity of structural elements constructed with timber in ground contact. The model is directly applicable to about 80 species of timber, CCA and creosote treatments and a variety of maintenance procedures. Through use of a climate index (based on rainfall and temperature parameters) the

procedure is applicable to all locations in Australia, from temperate to hot tropical regions and from rainforest to desert areas. With slight modifications, it should be possible to apply this model to any structure, fabricated from any species and located anywhere in the world.

Current progress is related to calibrating and modifying the model according to the experience of experts. In addition, it is necessary to find a procedure for taking into account the deterioration due to mechanical degradation that occurs in the arid regions of Australia.

Possibly the most important aspect of the engineering model described is that it provides a unified framework within which can be placed all types of knowledge, such as knowledge obtained from laboratory data, field data, expert opinion and accepted good practice. It can also be used to assess the monetary value of new knowledge.

6.   ACKNOWLEDGEMENTS

7.   REFERENCES

Foliente, G.C., Leicester, R.H., Wang, C-H., Mackenzie, C. and Cole, I.S. (2002). Durability Design for Wood Construction. *Forest Products Journal*, Jan, **52**(1), 10–19.

Leicester, R.H. (2001). Engineered Durability for Timber Construction. *Progress in Structural Engineering & Materials*, **2**(3).

Leicester, R.H., Wang, C-H. and Foliente, G.C. (2001). A Probabilistic Decay Attack Model of Timber In-ground. *Proc. ICOSSAR 2001 8th International Conference of Structural Safety & Reliability*, Newport Beach, CA.

Leicester, R.H. (1999). Durability Analysis of Timber Construction. *Proc. Pacific Timber Engineering Conference*, Rotorua.

Thornton, J.D., Johnson, G.C. and Nguyen, N.K. (1997). A Proposed Revision of Australia's Timber Durability Ratings. CSIRO Forestry and Forest Products, Victoria, Australia.

Thornton, J.D., Johnson, G.C. and Nguyen, N.K. (1991). An In-ground Natural Durability Field Test of Australian Timbers and Exotic Reference Species – VI: Results After Approximately 21 Years Exposure. *Material und Organismen*, **10**, 145–155.

Leicester, R.H., C-H Wang, C-H., Nguyen, M.N., Thornton, J.D., Johnson, G., Gardner, D., Foliente, G,.C. and MacKenzie, C. (2003)An Engineering Model For The Decay Of Timber In Ground Contact. *Proc. of The 34th Annual Meeting of IRG. The International Research Group on Wood Preservation*. Brisbane, Australia. May.

Gardner, W.D., Simpson, J.A. and Eldridge, R.H. (1994) Wedding Bells State Forest Pole Test Site report of the 1991 Inspection. Research Paper No. 26, Research Division, State Forests of NSW, Sydney, 66 pages.

10

INTERNATIONAL COUNCIL FOR RESEARCH AND INNOVATION
IN BUILDING AND CONSTRUCTION

WORKING COMMISSION W18 - TIMBER STRUCTURES

PROBLEMS WITH SHEAR AND BEARING STRENGTH OF LVL

IN HIGHLY LOADED STRUCTURES

H Bier

Carter Holt Harvey fibre-gen

NEW ZEALAND

Presented by: Hank Bier

Hank started his presentation by describing the background of the production of LVL in Australasia and the need for research due to the relatively large volume of production per capita. He went on to say that the aim of the research is to assess the reliability of the published shear and bearing capacity of the engineered products. From the test he concluded that only high grade specimens fail in shear, that shear characteristic based on bending is too conservative and that bearing failure needed to be examined. As a result follow on bearing tests were conducted from which he concluded that bearing deformation is important and that further work is necessary.

Problems with shear and bearing strength of LVL in highly loaded structures

Hank Bier

Carter Holt Harvey fibre-gen, New Zealand

1 Abstract

In most timber engineering design, neither shear nor bearing strength governs the design of bending elements such as beams and joists. However, when the structure carries very high loads over short spans, code values for shear begin to limit the design. Field experience suggests that for these structures, characteristic stresses based on codified test methods and evaluation of bearing and shear are simply, not realistic. The low variability of LVL means these effects can be studied in detail.

A test programme was undertaken to evaluate shear strength of LVL in single span and two span tests, on beams with and without bolt holes. As expected, shear failures were only observed in the very strongest LVL. The very high deformations observed showed that for concrete formwork elements, bearing deformation in the LVL support structure could become critical before shear, and standard engineering shear formulae may give misleading results.

An alternative bearing test was developed and used to assess bearing for beams where deformation control is critical. This test is based on identifying the onset of visible permanent set after repetitive loading, and limiting the design bearing stress accordingly. The information can be used to assist in the preparation of span tables for radiata pine LVL used to support concrete in formwork structures, and the concept could be used for other species.

2 Formulating the problem

Formwork for concrete is a critical use for high strength timber members. Loads are short term, usually very high, and failure can be dramatic if forms are not reliably designed. Engineered wood products like LVL or fabricated I beams compete with steel and aluminium where the components can be re-used many times on a concrete construction site. Engineered wood or LVL beams provide a solution for the formworker, and provided these beams can be re-used, they are economical, and light weight for their performance. In introducing a range of formwork support components to the Asian market in particular, the key feature in design has been to design for carrying very heavy loads over short spans. To do this effectively requires an understanding of real or unfactored loads for this application.

2.1 Load stresses

In permanent wood structures, the load for the life of the structure is usually much less than the total design load. Table 1 shows a summary of some unfactored loads and stresses.

Typically a 100 x 50 mm joist in light timber framing will span up to 1.8 m at 400 mm centres, and carry a load of approximately 0.8 kN. By contrast, in a formwork beam, the load achieves its maximum when the concrete is wettest, and is vulnerable to overload by impact or extra thickness of concrete before it is spread to the required slab thickness. Typically a 95 x 65 mm joist at 300 centres may carry a load of nearly 10kN over a span of 1.2 m. This means the shear stress in the light timber joist is about an order of magnitude less than in a formwork joist (0.15 MPa compared with 1.8 MPa for the formwork joist or 2.3 MPa for the bearer). Further as loads are transferred to larger section bearers, the bearing stress subjected by 3.6 Tonnes of concrete rises to about 5.2 MPa.

Table 1: Load extremes on small sized timber and LVL members

Action	LTF joist	LVL formwork joist	LVL form bearer
Size (mm x mm)	90 x 45	95 x 65	150 x 77
Span (m)	1.8	1.2	1.2
Spacing (mm)	400	300	1.2
Dead load (kPa)	0.5	0.2	0.3
Live load (kPa)	1.5 intermittent	24.7**	24.7**
Total load (kPa)	1.1 *	25	25
Load on beam (kN)	0.80	9.0	36
Shear stress (MPa)	0.15	1.1	2.3
Bearing stress (MPa)	0.10	1.8	5.2

* D+0.4L where 0.4 is the factor applied in seismic design for the load most likely to be there.

** Includes concrete in slab (0.9 m) and a 4kPa surcharge.

Clearly in formwork applications, a better understanding of shear and bearing strength is required. Designers of formwork cannot ignore these stress modes. Moreover, a review of the historical derivation of material properties show that the traditional test methods employed do not match the real strength and service demands of formwork structures.

2.2 Material strengths

2.2.1 Shear

Over many years of testing of thousands of pieces of radiata pine in-grade, the laboratory staff at the New Zealand Forest Research Institute observed very few failures in shear. Many test laboratories resort to publishing values from short span shear tests that are in fact, bending failures on a short span. Typically a technician will do the test, calculate shear stress at failure and this is then reported as the shear strength because it must be at least that high. The reality is that we do not have a reliable fix on the real shear strength of timber. The Canadians recognised this problem as noted by Madsen (p102) who reports

"most often, the beam will fail in bending or crushing even with small span to depth ratios". Accordingly, the team at British Columbia developed a "pure" shear test. However, formwork beams are not loaded in pure shear and most designs are carried out in field offices with limited time or access to sophisticated tools like Finite Element Methods. It was decided to carry out a short span test programme with spans close to those used in highly loaded formwork structures.

2.2.2 Bearing

A typical average bearing stress perpendicular to the grain for softwood (pines) published in ASTM D2555 is 250 psi with 28% c.v. These were 2" block tests on green clear wood tested to D143, and a factor of about 2 is given to obtain a dry value of about 500 psi or 3.5 MPa. This number represents the stress at the proportional limit, so is deformation bound, not safety or strength bound. Other values given in the ASTM test standards are for 0.1 inch (2.5 mm) or 0.04 inch (1 mm).

The average stress at 0.04 inches deformation (1mm) is about 1.8 times the proportional limit for a range of pines, so at 1 mm deformation the bearing stress is possibly 6.3 MPa. Modification factors in ASTM D245 suggest a reduction of 1.67 to adjust for in grade ring position(?), and the increase for dry use (19%) is 1.5. There is of course, no mention of LVL where multiple veneers on edge provide a more uniform bearing surface.

Madsen (p 292) has proposed an in-grade bearing test for solid timber using a stiff steel plate on a 150 mm long piece of lumber, and refers to other work (Hall) that models the analysis of compression perpendicular to the grain as a beam on elastic foundation. Figure 13.9 of Madsen shows a stress of around 4.5MPa for spruce pine fir at a limit determined from a 0.2% offset, resulting in a strain of about 0.022 or 2 mm deformation on the 89 mm deep timber.

Significantly, in the fabrication of formwork, construction specifications require very tight deformation control. The permitted deviation from the design shape is determined by the class of finish for the concrete surface. For high class finishes, deformations are limited to no more than 2 mm or span over 360, and for medium class finishes, 3 mm.

These tolerances can be exceeded easily by movement at the bearing surfaces if bearing limits are calculated using the stresses derived from traditional tests. Further, formwork components are used many times over in their useful life, and permanent indents due to bearing stress would be difficult to control when tolerances are so tight. The usual rules for engineering judgement of deformation in permanent structures simply do not apply and the search for a solution specific to highly loaded LVL members began.

What was required was a value that was not based on testing to large deformations. Rather a test was needed that could identify the onset of permanent deformation, so that the formwork beams could be used again and again without deterioration at bearing points that could differ from one job site to the next.

3 The test programmes

3.1 Shear

Veneer for LVL at our manufacturing plant is graded with both sonic velocity and resonance techniques to prescribed stiffness limits. For this test programme, three grades

were produced, and after lamination into 15 ply 45 mm thick billets, the co-efficient of variation of the MoE or bending stiffness within each grade was approximately 4% and for MOR about 9% for the 95 x 45 test pieces taken from the run. The average properties on standard bending tests at spans of 18 x depth were respectively:

	MoR (MPa)	MoE (GPa)
Grade 1	72.4	13.8
Grade 2	59.9	11.9
Grade 3	50.5	9.9

The material for the shear test samples was thus well characterised by the grading system.

For the shear tests each specimen was cut to 8 x depth, and tested in single point short span shear test on a span of 6 x depth or 570 mm as illustrated.
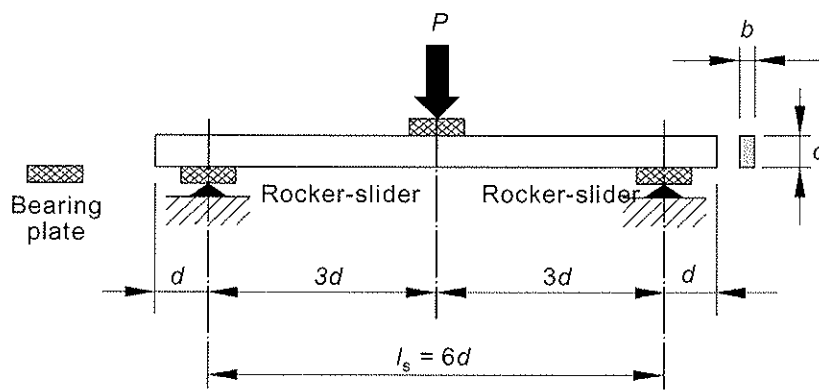
Figure 1: Single span bending/shear test to AS/NZS 4063

The type of failure was noted and equations to calculate bending and shear stress were:

Shear stress $= 3P / 4bd$

Bending stress $= 3PL / 2bd^2$

For those pieces that failed in bending, MOR and shear stress at failure (f_s) were calculated. For those pieces that failed in shear, bending stress (f_b) and ultimate shear stress (f_{su}) were calculated. The summarised properties are in Table 2 and illustrated in figure 2.

Table 2: Single span strength results (MPa) for three grades of 95 mm x 45 mm LVL

Grade	1	2	3	All
MOR in bending	69.2	65.5	59.0	
f_b at shear failure	72.7	63.5	65.9	
f_s at MOR	5.8	5.5	5.0	
f_{su} at shear failure	6.1	5.3	5.5	5.8
Bending failures	15	20	26	61
Shear failures	21	9	2	32
5% ile f_s at MOR	5.0	4.6	3.8	
5% ile f_{su}	5.6	(4.9)	(5.4)	5.1
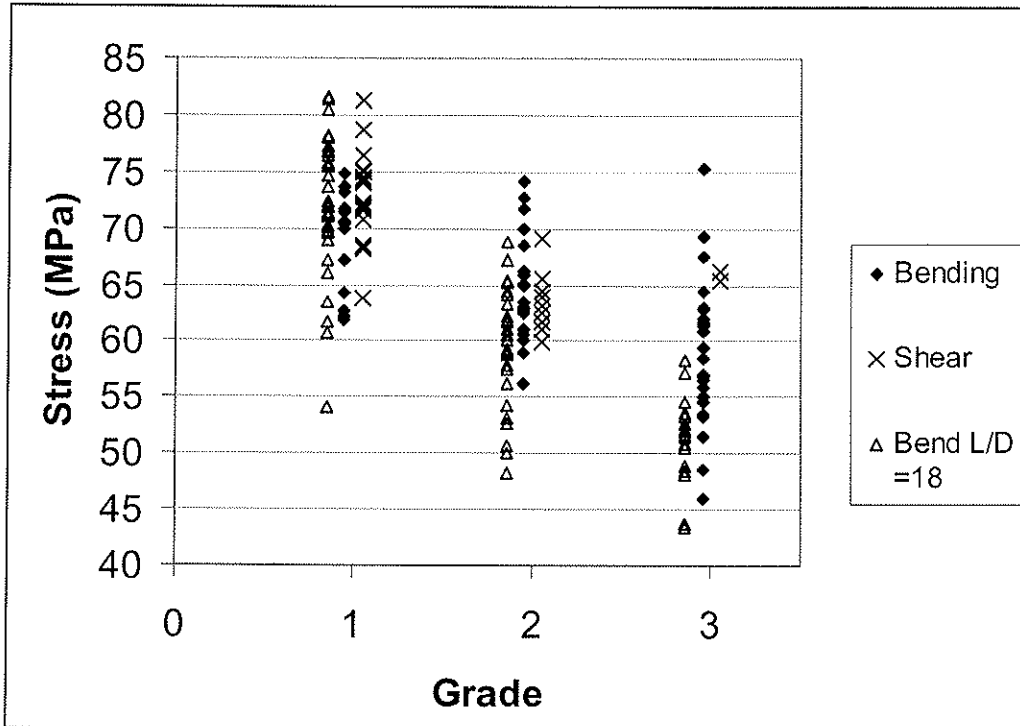
Figure 2: Bending stress at failure in bending and shear for short span tests, together with MOR from standard bending test (Bend L/D =18)

- there is a volume or test arrangement effect giving higher MOR's for the lower grades for shorter bending spans than the standard L/D of 18.

- only the strongest grade of LVL had sufficient bending strength to develop a shear failure in enough pieces to calculate a "real" 5%ile.

- The shear stress in bending failures is significantly below the "approximate" 5%iles for the lower grades. Shear strength based on these bending failures would be too low. A bending check should be the critical failure mode.

- Single span bending shear tests on lower grades of LVL used in formwork will not yield shear failures. The shear strength of the higher grade could be used because the effect of knots is to break the lines of principle stress and increase strength.

- Enough pieces that failed in shear to determine an all in shear strength for LVL. Using the Australian system, a basic working stress of 2.1 and a characteristic value of 6.2 (with $\phi = 0.8$) were calculated. These were published as 2 and 6 MPa.

3.2   Shear Tests on 150 mm and 75 x 35 mm LVL with holes

To assess the possible use of LVL with holes for easy assembly of forms, shear tests were done using two spans to match multiple span forms. The test arrangement is in figure 3. Because of the shorter spans expected in service, spans were reduced to 4d instead of 6d. Test spans were 600 mm and 300 mm for the two sizes. The shear stresses at ultimate load were calculated from.

Shear stress $= 0.516 \, P \, / \, bd$

Holes of 20 mm diameter through the neutral axis were drilled at the load points and at the supports. A matching sample without holes was also tested.

5
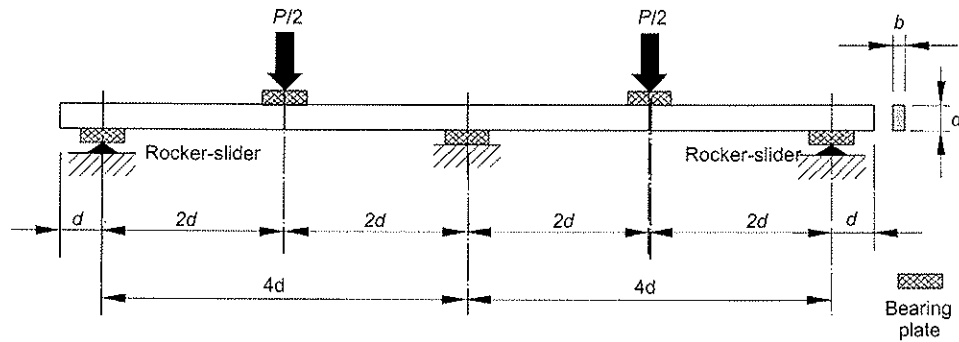
Figure 3: Two span bending/shear test (draft AS/NZS 4063 modified to shorter span).

The results of these tests are illustrated in figure 4;
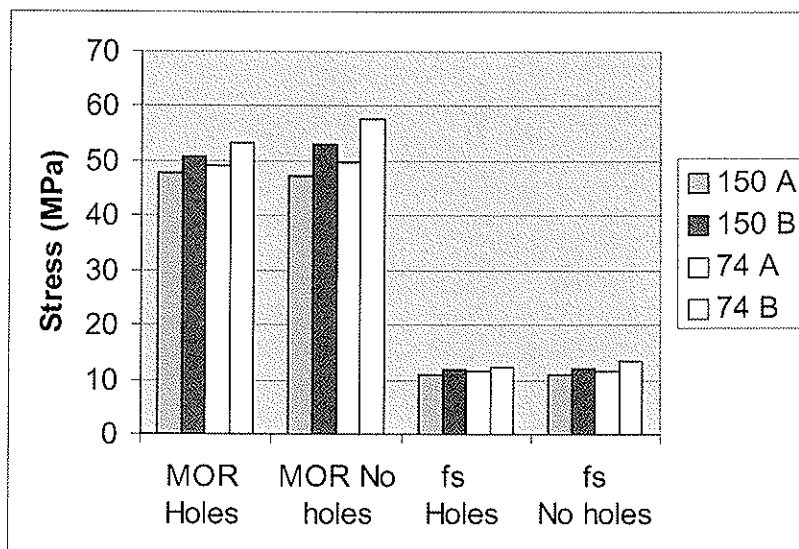
Figure 4: Summary of average bending and shear stresses from two span tests of two sizes and two sources (A and B)

There is no clear difference between the pieces with or without holes. This suggests a bolt able formwork product could be designed.

A peculiar result was that using the code formula given in AS/NZS 4063 the shear values are about twice what is determined from the single span test. It is suspected that the code formula proposed is actually meaningless for these short spans for deformations shown in the failed specimens in figure 5. The plane sections remain plane hypothesis is not valid. However, it is evident that for engineers using normal static equations, the lower strengths in the single span test become the governing shear criteria.

Large permanent compressive deformation occurred in the wood at the supports without inducing shear failures. This means bearing performance is a more serious design limit for loaded heavily loaded structures such as form work.

6
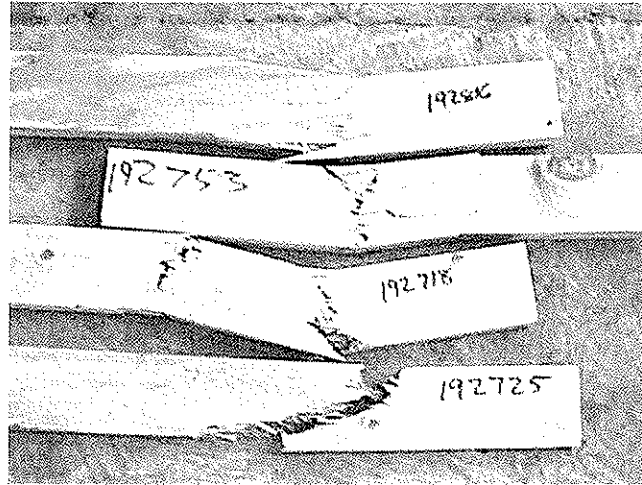
Figure 5a: Bending failures in 75 mm x 35 mm short span tests.
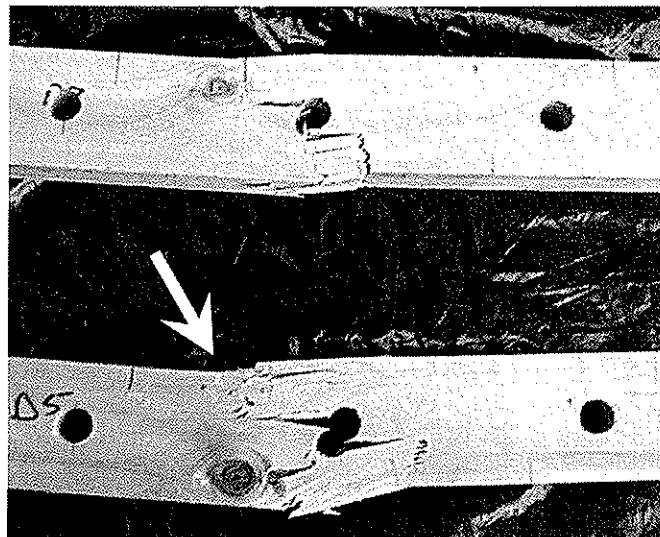
Figure 5b: May be shear failure? Arrow points to large bearing deformation.

3.3   Bearing

This bearing study was intended to explore the deformation perpendicular grain with the hope that a more rigorous analysis would follow. There was no serious attempt to provide for replicates, rather, could any sort of test be developed that might answer the question, "What determines the onset of permanent set in an LVL beam subject to repeated loading?"

Six pieces of LVL 35 mm x 75 mm x 250 mm long of a range of densities were selected for evaluation.

Each piece was subject to a compressive bearing load on the top edge with a:

(a)   25 mm long steel bearing flush with the end

(b)   50 mm long steel bearing centred approx 100 mm from the end

The full length of the bottom edge was supported on the test platten. The deformation into the top surface was measured with an LVDT alongside the load head. A second LVDT measured overall compression of the 75 mm depth. See figure 6.

The load was applied in 0.25 mm increments of surface deformation. After each increment, the load was completely removed, and the surface viewed for evidence of permanent (inelastic) damage or depression of the fibres. The deformation at which the first permanent set occurred was recorded, and marked on the load deformation curves.
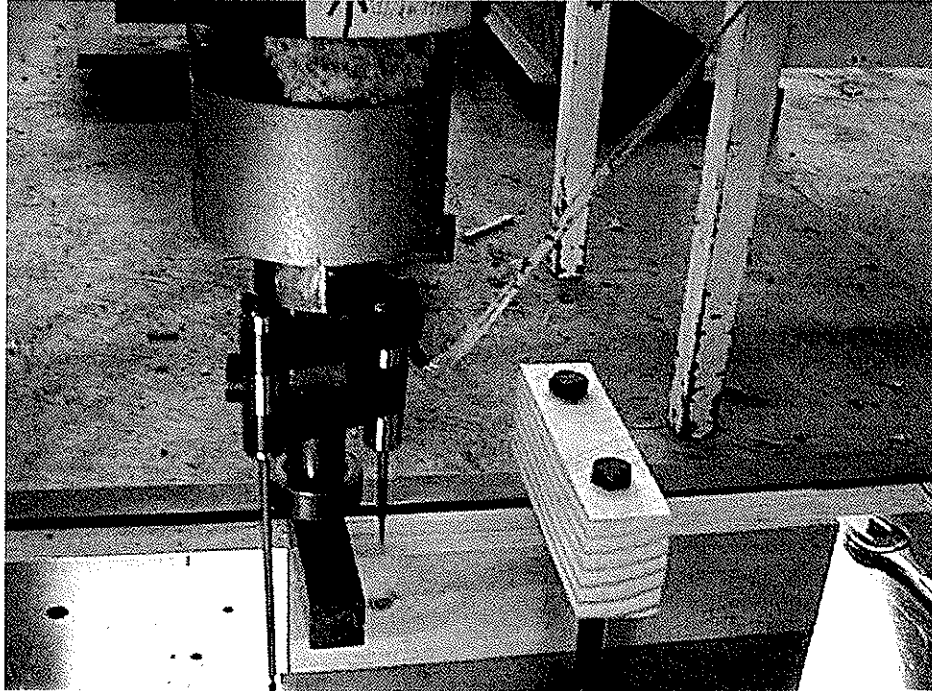
Figure 6: Test apparatus. LVDTs to measure indentation and overall compression.

Loads at the onset of visible residual set are highlighted in Table 3. The lower density specimens appeared to absorb more deformation without set, but permanent set is at similar loads. This suggests that fibre damage may occur at a definable stress level on the surface, rather than at a given depth of deformation.

The in-grade test reported by Madsen did not differentiate surface indentation from overall thickness reduction. The load deformation curves in figure 7 suggest that bearing deformation at the ends of the specimens is almost all at the surface whereas for the wider 50 mm bearing and higher loads about half of the compression deformation, was distributed into the mass of wood beneath the surface.

A lower bound for the 25 mm long end bearing stress is 8.1 MPa. For the inner bearing, the stress is 10.5 MPa. On average the onset of permanent set on the inner bearing was at about 0.6 mm for a stress about 12 MPa which is the same as the published bearing characteristic for formwork LVL. Also, total deformations of 1 to 1.5 mm are close to the limits of 2 mm and 3 mm used in practice.

So current designs are on the threshold of permanent deformation and close to design limits for forming concrete, and further testing is recommended.

A cyclic test regime is one option, and it is suggested that at least 10 cycles to various levels of surface deformation form part of the test to replicate service use. This would assess repeatability and could define a useful limit.

8

Table 3: Loads at increasing deformation on an LVL edge surface

25 mm bearing	Load (kN) at deformations (mm) of :						Permanent Indent at:
Density (kg/m³)	0.25	0.50	0.75	1.00	1.25	1.50	(mm)
500	1.6	4.2	6.8	**8.7**	9.3		1.00
504	1.2	2.7	4.4	5.8	**7.0**	8.1	1.25
511	2.0	5.1	**7.1**	8.8			0.75
537	2.8	6.0	8.3	**10.0**			1.00
545	1.8	5.4	8.0	**10.0**			1.00
570	2.3	6.0	**8.8**	10.6			0.75
50 mm bearing	Load at:						Permanent Indent at:
Density (kg/m³)	0.25	0.50	0.75				(mm)
500	1.6	12.0	**21.2**				0.75
504	8.0	**18.4**					0.50
511	7.6	18.0	**24.2**				0.75
537	6.4	16.8	**22.5**				0.75
545	6.0	19.6	**23.6**				0.75
570	10.0	**19.6**	23.2				0.50
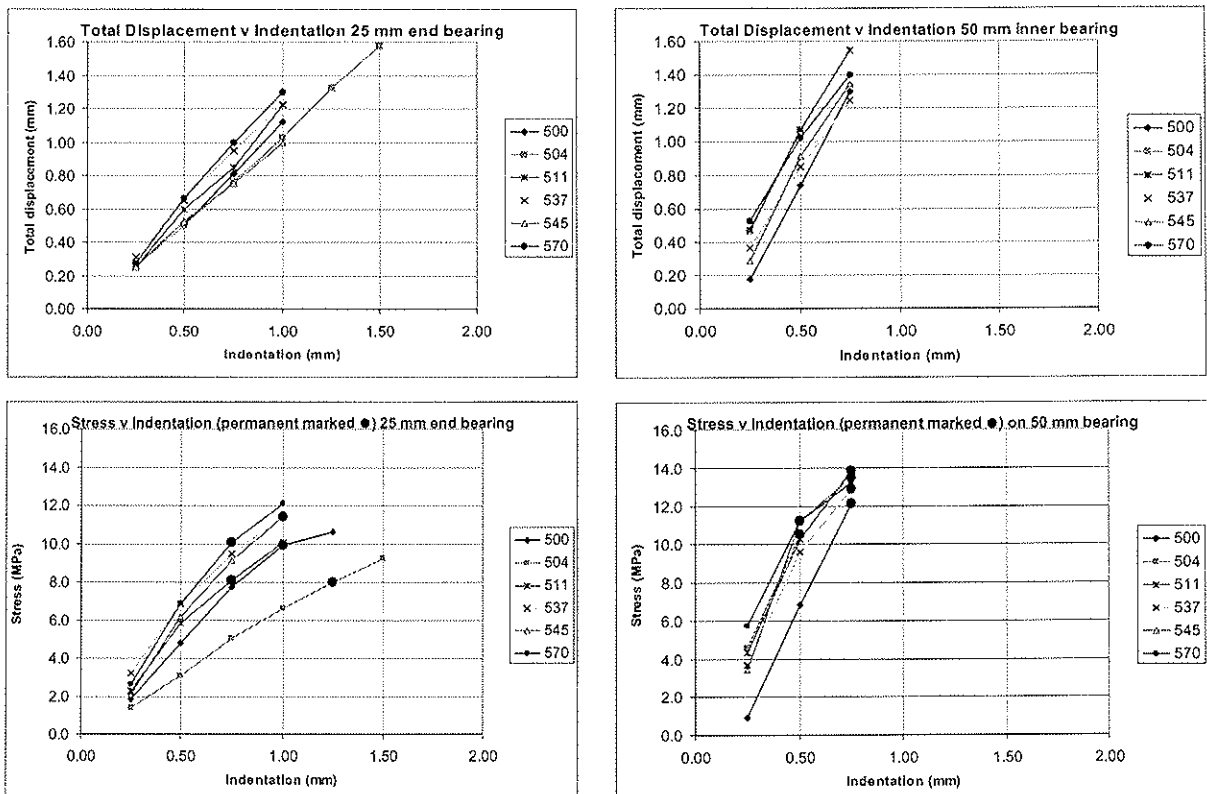
Figure 7: Load deformation curves

4 Conclusions

4.1 Shear

The shear strength of LVL can be determined for the very highest grades from a single short span bending shear test. Many specimens will not fail in shear, but a sufficient number can be obtained for derivation of a characteristic value.

For lower grades of LVL, bending failures are more likely to occur, because the material has insufficient bending capacity to mobilise a shear failure. Use the high grade strength.

A two span bending test programme showed that large deformations rendered standard formulae invalid and bearing performance could govern formwork design.

4.2 Bearing

Very limited data suggest that it may be possible to derive a more rigorous value for the onset of permanent bearing deformation to cover a range of typical bearing widths used in concrete formwork practice.

Currently used stress of 12 MPa for bearing in formwork is very close to the values obtained for a 50 mm wide bearing.

The total deformation of bearing members is significant relative to the 2 mm and 3 mm limits imposed in the design of formwork structures. Total deformation includes surface indentation and compression through the depth of the beam.

Further study and cyclic testing of formwork models is recommended to ensure serviceable formwork components in engineered wood.

5 Acknowledgements

6 References

1. ASTM D143, "Standard methods of testing small clear specimens of timber" American Society for Testing and Materials, Annual book of standards 1994

2. ASTM D245, "Establishing structural grades and related allowable properties for visually graded lumber" American Society for Testing and Materials, Annual book of standards 1994

3. ASTM D2555, "Establishing clear wood strength values" American Society for Testing and Materials, Annual book of standards 1994

4. AS/NZS 4063:1992 : Timber - Stress-graded - In-grade strength and stiffness evaluation

5. Madsen, B. Structural behaviour of Timber" 1992 Timber Engineering Ltd, Canada

INTERNATIONAL COUNCIL FOR RESEARCH AND INNOVATION
IN BUILDING AND CONSTRUCTION

WORKING COMMISSION W18 - TIMBER STRUCTURES

WEIBULL BASED DESIGN APPROACH

OF ROUND HOLES IN GLULAM

L Höfflin

S Aicher

Otto-Graf-Institute, Stuttgart

GERMANY

Presented by: Lilian Höfflin

Lilian began her presentation with an overview of the mechanical problem and also commented on the requirements of DIN 1052 and EC5. She went on to conclude that the Weibull approach agreed well with experimental results which showed strong size effects and moment influence.

She then went on to answer questions relating to the practical design use of the methodology presented and its impact on EC5 requirements. The methodology was well received by the participants.

Weibull based design approach

of round holes in glulam

Höfflin, L. and Aicher, S.

Otto-Graf-Institute, Stuttgart, Germany

1   Introduction

The bending capacity of glulam beams with holes is dominated by stresses perpendicular to grain at the periphery of the holes. The relevant material fracture resistance is tension strength and/or fracture energy perpendicular to grain. In case of rectangular holes with fairly sharp-edged corners of very small radii of curvature a linear fracture mechanics approach for modeling of the load capacity is plausible. Eurocode 5 employs for design an analogy to the fracture mechanics based design of rectangular end-notched beams. In case of round holes no quasi-singularity at the hole periphery exists, rendering at least linear fracture mechanics solutions of the design situation problematic. Nevertheless, in Eurocode 5 an attempt was made to extend the design model for rectangular holes to round holes by constructing some analogy between a tapered end-notch and a round hole.

For both types of holes, i.e. round and rectangular shaped ones, no moment contribution to the load capacity limit is considered. Especially the latter feature makes it difficult to modify the present Eurocode 5 solutions to account for arbitrary moment/shear force ratios.

This paper presents a different design model for round holes in glulam beams based on Weibull theory which shows a good agreement with experimental data.

2   Design model based on Weibull theory

2.1   Basics

The weakest link assumption in connection with the Weibull probability distribution represents a probabilistic theory well suited to describe bulk failure in very brittle materials with stochastically distributed defects. The theory is a very versatile tool to model size effects in combination with inhomogeneous stress stages. The application of the weakest link approach to timber is especially predestinated for all design/loading situations where, in presence of no stress singularities, tension strength perpendicular to grain, being besides shear strength parallel to fiber the most brittle wooden material property, is damage relevant. Since its first application to timber fracture in tension perpendicular to grain by Barrett (1974), the Weibull approach today is the well established method in many design codes to account for tension perpendicular to grain design of curved, tapered and pitched-

cambered glulam beams. Hereby, in general, rather large volumes are regarded whereas in case of the hole problem a rather localized area of increased tension stresses perpendicular to grain is relevant.

According to multiplication law of statistics, resulting in weak link assumption, the failure probability F of a given volume Ω, subject to an inhomogeneous stress distribution, can be written as

$$F = 1 - e^{\int_\Omega \ln S_E \, d\Omega} ,$$

(1)

where S_E is the survival probability of a unit volume element subjected to stress σ. Substituting, according to Weibull, for the unit survival probability the 2parametric exponential function

$$S_E = e^{-\left(\frac{\sigma}{\sigma_0}\right)^m}$$

(2)

the failure probability F of volume Ω becomes

$$F = 1 - e^{-\int_\Omega \left(\frac{\sigma(x,y,z)}{\sigma_0}\right)^m d\Omega} .$$

(3)

The damage relevancy of an inhomogeneous stress distribution within an certain volume as compared to constant stress conditions can be expressed by a fictive constant stress distribution, termed Weibull stress σ_{wei}, which has the same failure probability as the actual inhomogeneous stress state

$$\sigma_{wei} = \left(\frac{1}{\Omega} \int_\Omega \sigma^m(x,y,z) \, d\Omega\right)^{1/m} .$$

(4)

The ratio k_{dis} between the maximum value of the inhomogeneous stress distribution, σ_{max}, and the Weibull stress, σ_{wei},

$$k_{dis} = \frac{\sigma_{max}}{\sigma_{wei}}$$

(5)

thus defines the influence of the inhomogeneous stress distribution on strength in comparison to a constant stress distribution, hereby accounting for the stochastic defect distribution. Comparing at an arbitrary failure probability level the strengths f_1 and f_2 of two volumes Ω_1 and Ω_2 of the same material subject to different distributions of the same stress component one obtains

$$\frac{f_2}{f_1} = \frac{k_{dis,2}}{k_{dis,1}} \left(\frac{\Omega_1}{\Omega_2}\right)^{1/m} .$$

(6)

Assuming that volume Ω_1, following termed reference volume Ω_{ref}, is subject to a constant stress distribution, than $k_{dis,1} = 1$ and $f_1 = f_{ref}$, and omitting the index 2 one obtains the fictive strength f accounting for volume and inhomogeneous stress distribution

$$f = f_{ref} \, k_{dis} \left(\frac{\Omega_{ref}}{\Omega}\right)^{1/m} .$$

(7)

2

2.2   Load capacity estimation by the Weibull approach

Following it is assumed that the load capacity of the beam with a round hole is determined at any arbitrary, here at the characteristic probability level, simply by

$$\sigma_{t,90} = f_{t,90,k} \qquad (8)$$

where

$$f_{t,90,k} = f_{t,90,k,ref} \; k_{dis} \left(\frac{\Omega_{ref}}{\Omega} \right)^{1/m} . \qquad (9)$$

For design purpose, stress $\sigma_{t,90}$ is transferred to design stress $\sigma_{t,90,d} = \sigma_{t,90} \, \gamma_L$, where γ_L is averaged partial safety factor for load, and fictive strength is changed to fictive design strength by multiplying with (k_{mod}/γ_M) where γ_M is partial safety factor for the material and k_{mod} accounts for moisture and accumulated time of load duration.

Equations (8) and (9) are fully equal to the known design procedures for tension perpendicular to grain, e.g. for curved beams. In detail, acc. to Eurocode 5 reference volume and Weibull size exponent should be taken as $\Omega_{ref} = 0{,}01 \text{ m}^3$ and m = 5, and for characteristic tension strength perpendicular to grain of glulam, e.g. for strength class GL 32 (h) acc. to EN 1194, the value $f_{t,90,k,ref} = 0{,}5 \text{ N/mm}^2$ applies.

In order to use the Weibull theory/stress concept in design applicable manner to the regarded problem of a beam with a round hole, two essential steps are necessary:

i)   the maximum value $\sigma_{t,90}$ of the inhomogeneous tension perpendicular to grain stress field at the hole periphery must be determined and expressed by some fairly easy manageable, however fairly accurate approximated analytical equation. Hereby, all relevant influences of loading configurations and relative hole size have to be considered.

ii)   In order to account for the stochastic defect distribution in the highly tension stressed volume Ω, the stress distribution value k_{dis} has to be determined for different loading situations and hole to depths ratios; that necessitates the evaluation of the Weibull stress. In this context it is noteworthy, that no obvious boundaries, except for the hole periphery and beam width, exist for the determination of Ω.

ad i)   It was shown in Aicher and Höfflin (2001) that the maximum tension stress perpendicular to grain $\sigma_{t,90} = \sigma_{t,90,max}$ at the hole periphery conforms in a good approximation for an arbitrary moment/shear force ratio to

$$\sigma_{t,90} = \frac{3}{2} \frac{V}{b\,h} \left(1.23 + 0.82 \frac{d}{h} \right) + \frac{0.6\,M}{b\,h^2} \frac{d}{h} . \qquad (10)$$

ad ii)   The determination of k_{dis} and of the relevant volume Ω, so far not published, is outlined in the following chapter.

2.3   Determination of k_{dis} and relevant volume Ω

The locations at the hole periphery and the extensions of the tension perpendicular to grain stress fields depend on the loading situation, i.e. on the ratio of moment M to shear force

3
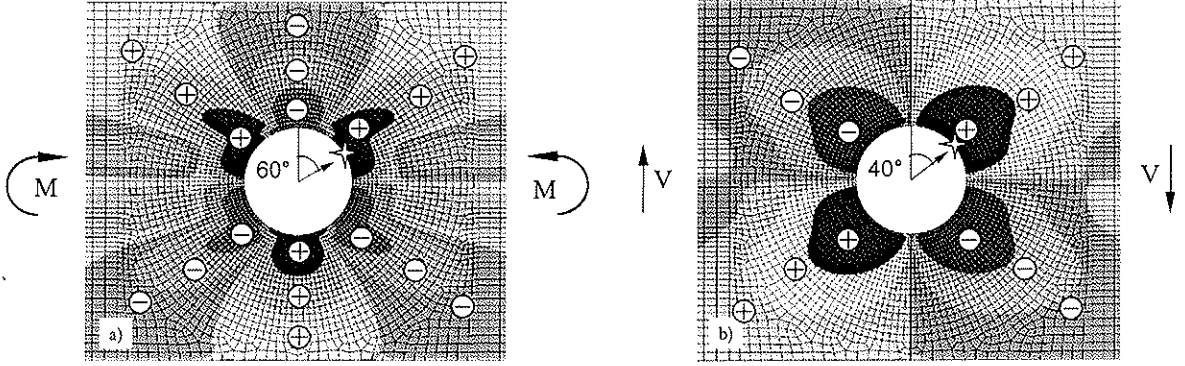
Fig. 1a, b: Stress distribution perpendicular to grain; the location (angle) of the highest tension stresses is marked with an asterisk
a) pure moment action
b) "pure" shear force action

V, the ratio of hole diameter to beam depth, d/h, and on the absolute beam depth h. Figures 1a and b show the distributions of stresses perpendicular to grain in the vicinity of a hole for two extreme M/V ratios. Figure 1a shows the case M/V $\to$ ∞, i.e. pure moment loading (V = 0), and Fig. 1b reveals the situation M/V $\to$ 0 being the fictive load case with a "pure" shear force (M = 0). This is discussed in detail in Aicher and Höfflin (2001) and has been verified experimentally via strain measurements (Aicher et al. 2003).

The stress distribution is very inhomogeneous along beam depth and length for both extreme and similarly for all arbitrary load cases. The problem posed was to define the damage relevant integration boundaries (see Fig 2a) for determination of the Weibull stress and hence of k_{dis}, as, except for the hole edge (and beam width), no obvious boundaries exist.

Further, for handling of combined load cases with arbitrary M/V ratios a joint integration range had to be determined.

In order to investigate different hole sizes and beam depths the area A (in the plane of the beam) of the integration volume Ω = b A is expressed by hole parameters (see Fig 2a). In y-direction, A is enclosed by two horizontal lines starting from the intercept points of the two angles φ_1 and φ_2 with the hole edge. In x-direction A is enclosed by the hole edge and the parallel curved line with a distance of ℓ = ξ d, i.e. a multiple of the hole diameter d.

By changing the integration ranges, quantities σ_{wei}, k_{dis} and Ω are influenced. A parametric study showed that it is possible to define a joint integration range for both extreme load cases, M/V $\to$ ∞ and M/V = 0, for which the k_{dis} value differs less than 1% from the results for the individual best fit integration ranges of the two load cases. Furthermore, it turned out that the d/h ratio has only a very small influence ($\leq$ 1%) on the k_{dis} value and therefore has not to be taken into account. The area of the derived joint integration range for all M/V load cases is defined as:

$$A = \Omega\, b = 0.5\, d\, (\cos(20°)\, d/2 - \cos(80°)\, d/2) = 0.1915\, d^2 \tag{11}$$

For the integration range acc. to eq. (11) the obtained k_{dis} values, as depending on the loading situation, are stated in Tab. 1.

Table 1: k_{dis} values for different moment/shear force ratios M/V

M/V	0 - 2 h	5 h	10 h	∞
k_{dis}	1.79	1.83	1.88	2.04
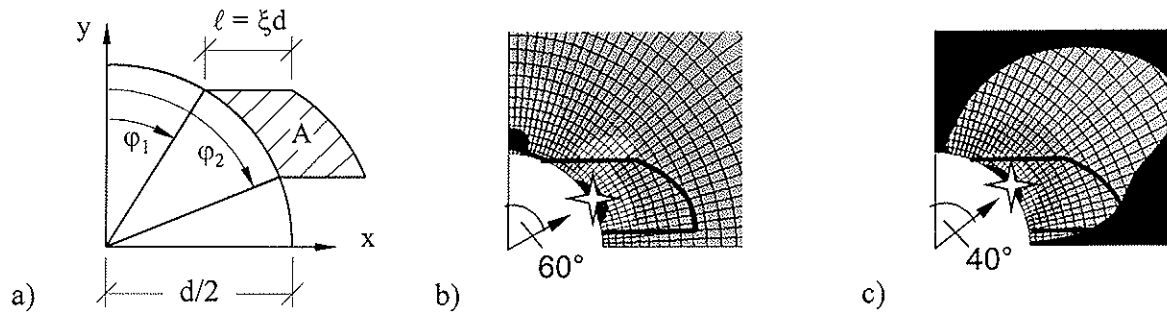
Fig. 2a-c: Integration area A

    a) definitions

    b) integration area A together with the tension stresses perpendicular to grain acc. to pure moment action

    c) integration area A together with the tension stresses perpendicular to grain acc. to "pure" shear force action

An evaluation of the (characteristic) shear force capacity acc. to the presented approach for different beam sizes and hole to depth ratios is given in chap. 4 altogether with a comparison to test results.

3 Tests

3.1 Literature review

Partly extensive experimental investigations on glulam beams with round holes with European spruce were performed in the past by Bengtsson and Dahl (1971), Kolb and Frech (1977), Johanesson (1977, 1983) and Pentalla (1980). Re-evaluation the European literature results forwarded despite indisputable individual merits of all cited investigations the following restrictions in the regarded context:

i)   apart from two exceptions, in each case only one specimen was tested per configuration of beam size, hole to depth ratio and moment/shear force ratio

ii)   the glulam quality/strength class differs between test series

iii)   the investigations covered in general a very small band of hole to depth ratios (predominantly d/h = 0.5)

iv)   the moment/shear force ratio did not exceed a ratio of 3h

v)   According to timber material science at the time of the investigations, size effects were not regarded; almost all tests were performed with beam depths of about 500 mm. Sometimes the holes were carefully placed in such a way that only clear wood occurred in the highest tension perpendicular to grain stressed corner of the hole.

vi)   the definitions of the given fracture loads differ; sometimes fracture load is equal to ultimate load, sometimes fracture load refers to some stage of crack development

In view of reasons i – vi, a project was conducted to set up a consistent data base, addressing the mentioned items, hereby using i.a. throughout the same glulam strength class (see below).

3.2 New tests at Otto-Graf-Institute

In extension to the experimental results presented in Aicher and Höfflin (2002) a considerable number (37) of additional full scale tests with beams with round holes were performed at Otto-Graf-Institute. The entity of performed calibration tests comprised two significantly different beam depths (h = 450 mm and h = 900 mm), three hole to depth ratios (d/h = 0.2, 0.3 and 0.4) and two moment to shear force ratios (M/V = 1.5 h and M/V = 5 h).

A schematic view of the test configuration with the used notations is given in Fig. 3. Each test series consisted of nominally five beams. Table 2 specifies the investigated beam configurations.

The two test series groups 450_1.5h_d/h and 900_1.5_d/h, differing by a scale factor of 2 for beam depth were performed in order to verify the assumed and model predicted large size effect. In each test series group three corresponding hole to depth ratios were regarded. For both test series groups the smallest sensible M/V ratio of 1.5 h was chosen; a minimum distance c ≥ 1.5 h between center of the hole and load application point is necessary for excluding stress disturbances induced by the support or loading point.
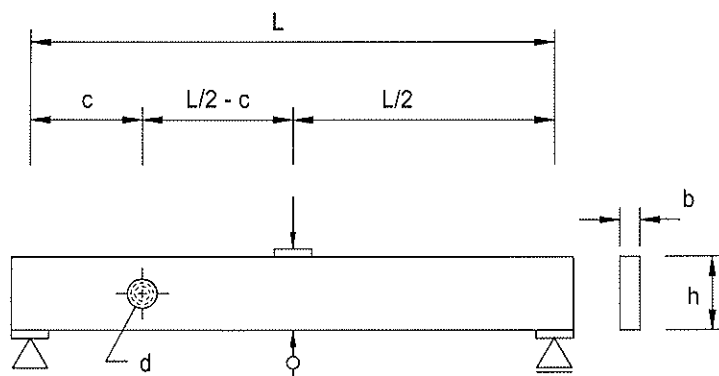
Fig. 3: Schematic view of the test configuration and geometry notations of the test beams

In order to verify the model predicted rather significant moment influence on the load capacity (not considered in Eurocode 5 at all), so far one test series 900_5.0h_03 was performed with a fairly high M/V ratio of 5h. Annotation: the experimental realization of large M/V ratios necessitates considerable beam lengths, here about 10 m. A comparison of test series 900_1.5h_0.3 and 900_5h_0.3, differing exclusively by the different M/V ratios, allows an unbiased assessment of the moment influence, of course within the limits of the small specimen numbers.

All tests were performed with homogeneously built-up glulam beams of strength class GL 32h acc. to EN 1194 (acc. to German national application document to EC 5 with glulam produced from machine stress graded laminations). The part of the beam in which the hole was placed was **not** particularly selected with respect to defects.

Table 2: Compilation of new tests at Otto-Graf-Institute

test series group	test series	beam depth	beam width	distance to support	moment/ shear force ratio	hole to depth ratio	hole diameter	No. of specimens
		h	b	c	M/V	d/h	d	
[-]	[-]	[mm]	[mm]	[mm]	[m]	[-]	[mm]	[-]
450_1.5h_d/h	450_1.5h_0.2	450	120	675	1.5 h	0.2	90	5
	450_1.5h_0.3					0.3	135	6
	450_1.5h_0.4					0.4	180	4
900_1.5h_d/h	900_1.5h_0.2	900	120	1350	1.5 h	0.2	180	5
	900_1.5h_0.3					0.3	270	6
	900_1.5h_0.4					0.4	360	6
900_5.0h_d/h	900_5.0h_0.3	900	120	4500 [1]	5 h	0.3	270	5

[1] the test set-up conformed in principle to Fig. 3, but consisted of more loading points

During the test performance in case of all beams three successive failure stages were observed, being

- the crack initiation in the center of the cross-sectional width at the highest stressed hole periphery. The location of the initial crack is in full agreement with a 3dimensional analysis of the problem regarding the actual cylindrical anisotropy of the laminations; for details see Aicher et al. (2003).

- the crack through full width at the hole periphery. The load when the crack in one hole corner was visible on both sides of the beam is termed as failure load in the following.

- the ultimate load with the collapse of the beam, following, in general, some stable/unstable propagation of the crack in direction of the beam length.

The quantitative test results are discussed subsequently altogether with the load capacity predictions of the Weibull (design) model.

4 Test results and model predictions

Figures 4a-c show the test results, the mean values of the individual test series and the estimated 5% fractiles acc. to lognormal distribution. The individual 5% fractiles were calculated from the mean value of each series and the mean coefficient of variation of all series. The graphs further show the characteristic shear force capacities predicted by the presented Weibull (design) approach.

Comparing the two test series 450_1.5h_d/h and 900_1.5h_d/h which differ only with respect to beam depth (Figs. 4a, b), a remarkable size effect was proven by the experiments. Comparing equal d/h ratios, the experimental mean and characteristic load capacities of the 2times higher beams increased in average by a factor of 1.44 ± 0.05. This agrees well with the model which predicts a characteristic load capacity increase by a factor of 1.52. Also the quantitative agreement of the experimental and theoretical 5% fractiles can be termed satisfying whereby the model, not yet calibrated to experimental results at all, predicts somewhat conservative loads. In case of test series group 450_1.5h_d/h, the average difference between experiment and model is 18%; in case of the larger beams (test series group 900_1.5h_d/h) the average difference is 14%.

The experimentally observed reduction of the shear force capacities by increasing the M/V ratio from 1.5 h to 5 h was very pronounced. The mean and characteristic values of test series 900_5.0h_0.3 (M/V = 5h) dropped by a factor of 1.67 compared to related test series 900_1.5h_0.3 (M/V = 1.5h). Quantitatively, the model predictions agree well with the experimental results of test series 900_5.0h_0.3; the difference between the predicted and the empiric 5% fractiles of the load capacities is 5%. Nevertheless, a difference between the empiric and the predicted moment influence has to be stated. The experimentally observed influence of an increased moment/shear force ratio results in a load capacity reduction factor of 0.6 which is 25% more severe than predicted by the model. At the time it is not fully evident whether this is bound to the small/minimum experimental basis (two test series of equal d/h ratio at one size level) or systematic. In the latter case an experimental model calibration could be easily performed.

a)

b)

c)
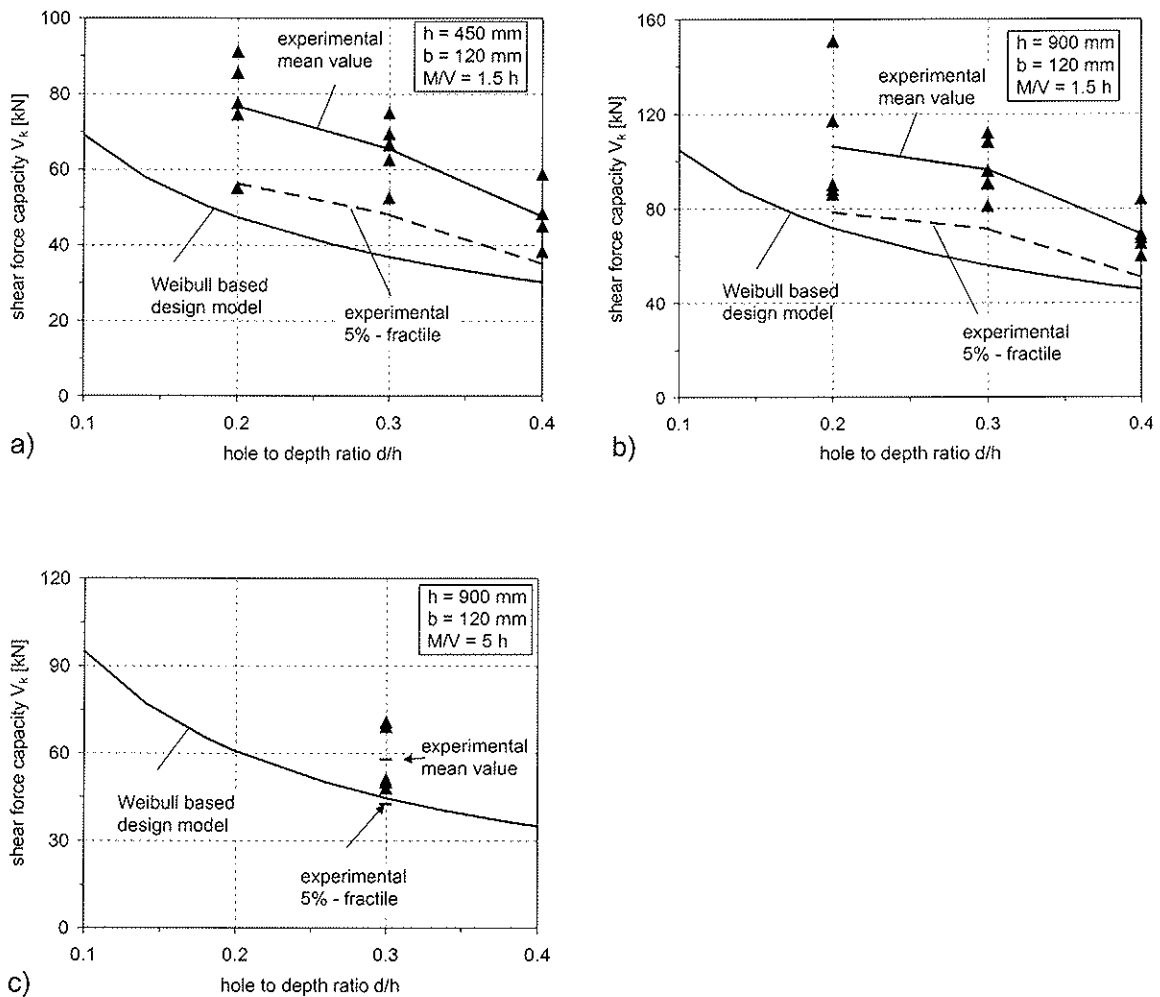
Fig. 4a-c: Test results, derived empiric 5% fractiles and predictions of the 5% fractiles of the load capacities acc. to the Weibull approach
a) series 450_1.5h_d/h   b) series 900_1.5h_d/h   c) series 900_5.0h_0.3

5 Comparison of Eurocode 5 and DIN 1052 solutions vs. the Weibull based model and test results

Figures 5a-c repeat the graphs already given in Figs. 4a-c, now including additionally the characteristic shear force capacities acc. to revised version of Eurocode 5 and latest draft of DIN 1052.

As lined out previously (Aicher and Höfflin, 2002), the Eurocode 5 solutions, as compared to DIN 1052, result in considerably (maximally 2.5times) higher characteristic load capacities. The discrepancy reduces for a constant moment/shear force ratio with increasing beam depth as the pure strength of materials approach of DIN 1052 does not account for any size effect. Contrary, the discrepancy strongly increases with growing M/V ratios, as Eurocode 5 does not account for any moment contribution to load capacity. Compared to both cited code approaches, the Weibull based model forwards the lowest load capacities.

The influence of the hole to depth ratio is mirrored by all models qualitatively in similar manner.
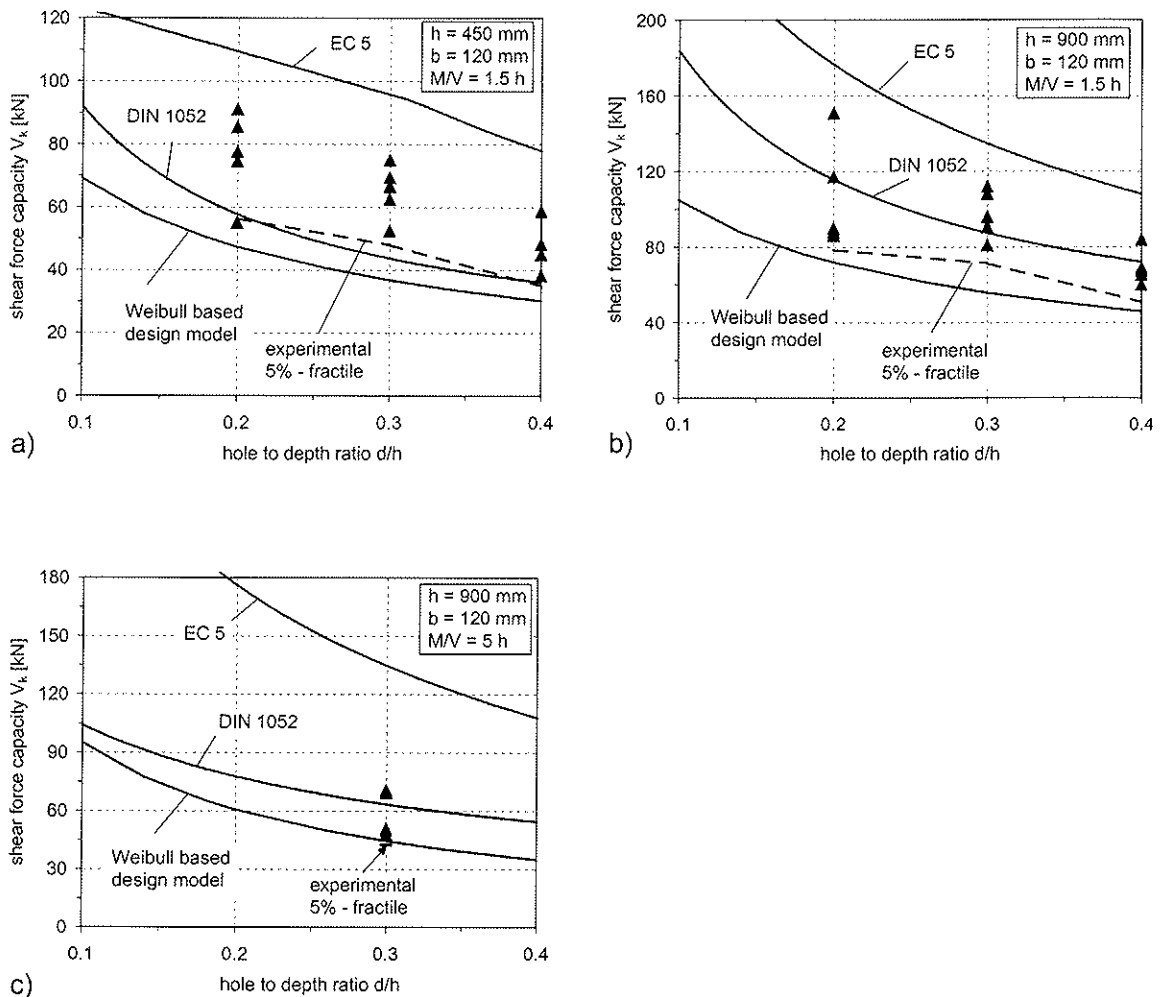
Fig. 5a-c: Test results, derived empiric 5% fractiles and computational solutions acc. to EC 5, DIN 1052 and the Weibull based model
a) series 450_1.5h_d/h   b) series 900_1.5h_d/h   c) series 900_5.0h_0.3

Comparing the three models with the experimental data base it is evident that the Weibull based design model predicts the characteristic load capacities of larger beams (here: h = 900 mm) and of loading conditions with higher moment/shear force ratios (here: M/V = 5h) best. For large beams with small M/V ratio (Fig. 5b) the design approaches acc. to Eurocode 5 and DIN 1052 forward in average of the three different hole to depth ratios overestimations of the characteristic load capacities of 110% and 35%, respectively. Compared hereto the Weibull based approach delivers a conservative approximation, which in average underestimates the characteristic load capacity by about 15%. For large beams with higher moment/shear force ratio, Eurocode 5 and DIN 1052 give overestimation of the characteristic load capacity by 220% and 50%, respectively, whereas the Weibull model differs just by 5% from the test results.

6 Conclusions

The presented, easily to apply design model for glulam beams with round holes overcomes inherent, partly considerable deficiencies of present code design approaches. The model accounts for both, size effect and moment influence on load capacity in transparent manner. Hereby, it allows selective calibrations to experimental results for all relevant influential parameters.

References

Aicher, S., Höfflin, L. (2001): Round holes in glulam members. Part 1: Analysis (in German). Bautechnik 78 (10), pp. 706-715

Aicher, S., Höfflin, L. (2002): Glulam beams with round holes – a comparison of different design approaches vs. test data. CIB-W18, Kyoto

Aicher, S., Höfflin, L., Reinhardt, H.-W. (2003): Verification of damage relevant strain distributions at round holes in glulam members (in German). Bautechnik (in press)

Barrett, J. D. (1974): Effect of size on tension perpendicular-to-grain strength of Douglas-Fir. Wood and Fiber Science, 6(2):126-143

Bengtsson, S., Dahl, G. (1971): Influence of holes near the support on the strength of glulam beams. (in Swedish). Lunds Tekniska Högskola, Adv. Byggnadsteknik II, master thesis

DIN 1052: Design of timber structures – General rules and rules for buildings. Final draft E DIN 1052 : BEKS-2002

Eurocode 5: Design of timber structures – Part 1-1; General rules and rules for buildings. Final draft prEN 1995-1-1, CEN/TC 250/SC 5 N195

Kolb, H., Frech, P. (1977): Untersuchungen an durchbrochenen Bindern aus Brettschichtholz. Holz Roh- und Werkstoff 35, pp. 125 – 134

Pentalla, V (1980): Reiällinen liimapuupalkki. Julkaisu 33, Div. Structural Eng. Helsinki University of Technology, Otaniemi

Johannesson, B. (1977): Holes in plywood beams and glued laminated timber beams. Publication S77:4, Chalmers University of Technology, Göteborg

Johannesson, B. (1983): Design problems for glulam beams with holes. Thesis, Div. Steel and Timber structures, Chalmers University of Technology, Göteborg

INTERNATIONAL COUNCIL FOR RESEARCH AND INNOVATION
IN BUILDING AND CONSTRUCTION

WORKING COMMISSION W18 - TIMBER STRUCTURES

EFFECT OF CHORD SPLICE JOINTS ON FORCE DISTRIBUTION IN TRUSSES WITH PUNCHED METAL PLATE FASTENERS

P Ellegaard

Department of Building Technology and Structural Engineering
Aalborg University

DENMARK

Presented by: Peter Ellegaard

Peter Ellegaard began his presentation by outlining the reasons and methodology used for the research. He also discussed the new guidelines given in EC5 and in the Danish code for the design of chord splice joints. The numerical aspects of the work is carried out using TrussLab. The work also included tests on trusses without chord splice joints for comparison purposes. He concluded that the influence on shear and axial forces is insignificant. More importantly he concluded that the new guidelines are not necessary.

Effect of Chord Splice Joints on Force Distribution in Trusses with Punched Metal Plate Fasteners

Peter Ellegaard, Assistant Professor

Department of Building Technology and Structural Engineering,
Aalborg University, Sohngaardsholmsvej 57
DK-9000 Aalborg, Denmark

1 Abstract

Splice joints in timber trusses with punched metal plate fasteners (nail plates) may be assumed rotationally stiff if their deformation has no significant effect upon the distribution of member forces according to Eurocode 5: Design of Timber Structures.

Two simple guidelines for the design and location of splice joints are given in Eurocode 5 for treating the splice joints rotationally stiff. The reasonability of these guidelines is discussed in this paper.

A finite element program TrussLab where the splice joints are given semi-rigid properties is used to analyse two triangulated trusses with three and four splice joints, respectively. The influence of the splice joints on section forces, rotations in the splice joints and global displacements of the trusses is analysed.

Based on the results of the calculations it seems that the guidelines for treating splice joints rotationally stiff do not necessarily lead to more realistic truss models.

2 Introduction

Normally splice joints are treated rotationally stiff and the nail plates are designed for the actual section forces (in Denmark this is common). There are no limitations to the location of the splice joints. However, in the new Danish timber code *DS 413 (1998)* and in *Eurocode 5 (2002)* rules are given to the location and to the design of rotationally stiff splice joints leading to larger nail plates or restrictions in the location of splice joints.

In Eurocode 5 section 5.4.2 (9) the following guidelines are given:

Splice joints used in lattice structures may be modelled as rotationally stiff if the actual rotation under load would have no significant effect upon member forces. This requirement is fulfilled if one of the following conditions is satisfied:

• splice joints with a load-carrying capacity, which corresponds at least to 1.5 times the combination of applied force and moment

1

- *splice joints with a load-carrying capacity, which corresponds at least to the combination of applied force and moment, provided that the wooden members are not subject to bending stresses which are greater than 0.3 times the member bending strength, and the assembly would be stable if all such connections acted as pins.*

Rules almost similar to those listed above are given in *Riberholt H. (1982)*. In *Riberholt (1989)* splice joints in bottom chord of triangulated trusses are mentioned as connections in which the slip should be considered when designing the truss because it is essential for the distribution of the section forces.

In *Blaß, H. J., Ehlbeck, J. & Kurzweil, L. (1997)* a number of tests with nail plate joints loaded to bending have been carried out. The ultimate load levels and the rotations in the joints were measured and it was found that the ultimate load level and the stiffness increase if there is contact between the timber members.

In *Bell, K. (1998)* two different models of a truss are analysed – one where the splice joints are rigid and one where they are assumed to be pinned. It is found that the bending moment distribution is dependent on the stiffness/rotation of the splice joints and that the real behaviour must be something in between.

In *Kevarinmäki, A. (2000)* design equations for chord splices are set up and they are compared with test results. It was found that timber contact is an important parameter that should be included in the design equations.

In this paper the effect of chord splices in trusses is analysed by a numerical program. The 2D finite element beam model (TrussLab) takes the effect of contact between timber members and non-linear behaviour of nail groups and joint lines into account. Besides the effect on force distributions the rotations in the splice joints, the global displacements and the gap size between the timber members of the splice joints are also discussed. Based on the results the guidelines in Eurocode 5 will be evaluated.

3 Modelling of Trusses

The geometry, the load case and the finite element model used to analyse the influence of splice joints for the two trusses are described in the following. A commercial finite element programme TrussCon is used to determine the dimensions of the timber and the sizes of the nail plates. In the commercial programme several load combinations are considered, however, in the calculations with TrussLab (semi-rigid behaviour of the splice joints and contact between timber members) only one load case is considered. The design of the trusses with TrussCon is based on Danish load and safety conditions according to *DS 410 (1982)* and *DS 409 (1982)* and the Danish timber code *DS 413 (1982)* - these codes are still valid in Denmark even though we have a new set of codes from 1998.

3.1 Geometry

The geometry of the two trusses W10 and W15 is shown in figures 1 and 2. The trusses are symmetrical (except for the splice joint in the bottom chord of truss W10) and the different locations of the splice joints are shown. For a description of the splice joint locations, see below the figures.
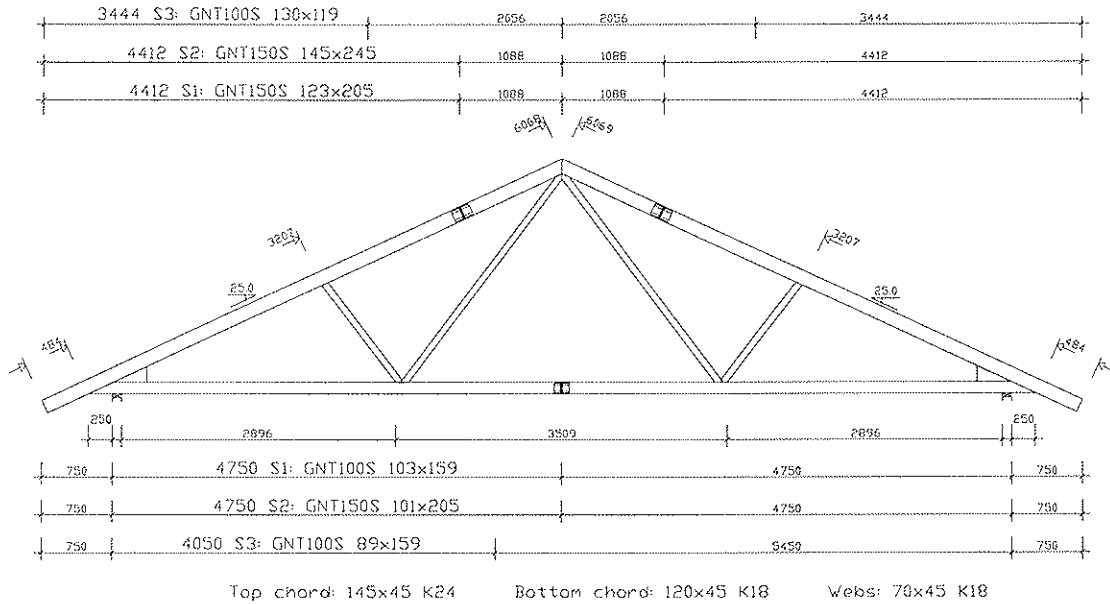
Figure 1. Geometry of triangulated W10 truss. Dimensions in mm.
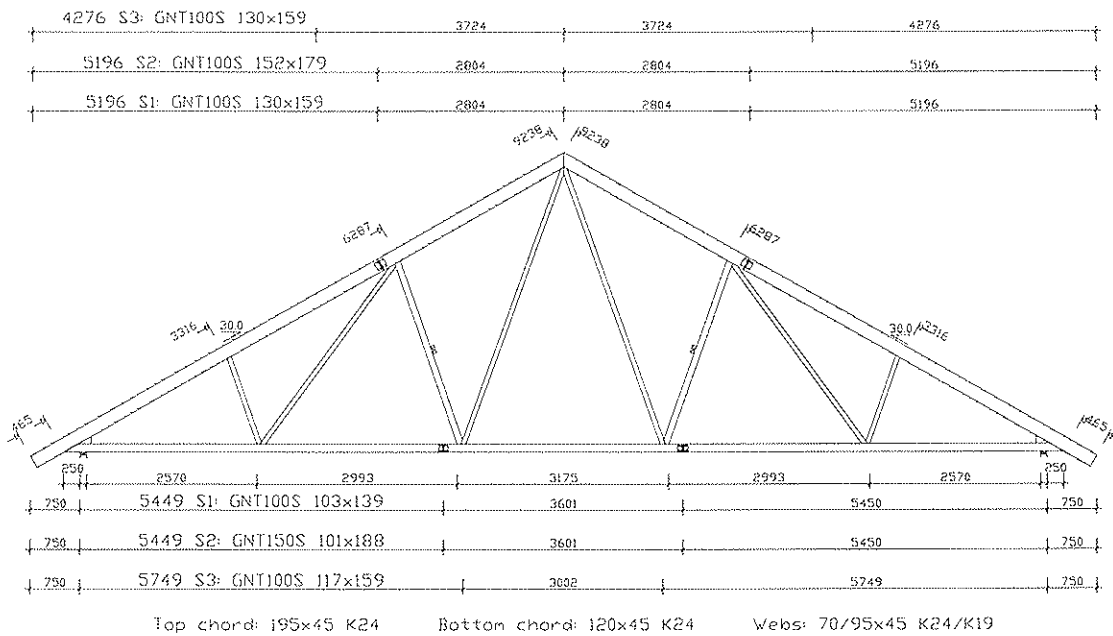
Figure 2. Geometry of triangulated W15 truss. Dimensions in mm.

In the analysis four different models S1-S4 with different splice joints have been set up for each of the two trusses:

- **S1**. The splice joints are located near maximum bending moment. The nail plates are utilised up to 100% (based on design values of the load and the strength). This model reflects the way the truss could be designed today – there are no restrictions in the location of the nail plates and they can be utilised 100%.

- **S2**. The splice joints are located near maximum bending moment. The nail plates are utilised up to 66%. This model reflects the way the truss could be designed according to the new guidelines in the codes – there are no restrictions in the location of the nail plates, but the nail plates can only be utilised up to 66%.

3

- **S3**. The splice joints are located where the timber members are subjected to bending stresses equal to 0.3 times the member bending strength. The nail plates are utilised up to 100%. This model reflects the way the truss could be designed according to the new guidelines in the codes – there are restrictions in the location of the nail plates, but the nail plates can be utilised up to 100%. The trusses are stable if all splice joints are pinned.

- **S4**. In this model the splice joints are fully stiff. This model is made for comparison with the models S1-S3 with semi-rigid splice joints.

When considering the utilisation of the nail plates both the anchorage capacity and the capacity of the joint line have been contemplated. The distributions of the bending moments correspond to the load case given in the next section.

It should be noted that for the W15 truss it was difficult to locate the splice joints in the bottom chord at maximum moment for models S1 and S2.

3.2 Load Case

The loads in the analysis correspond to $1.0 \cdot$ dead load $+ 1.3 \cdot$ snowload $+ 1.0 \cdot$ live load. This load case controls most of the timber dimensions and nail plate sizes in the splice joints. The load case for truss type W10 is shown in figure 3.
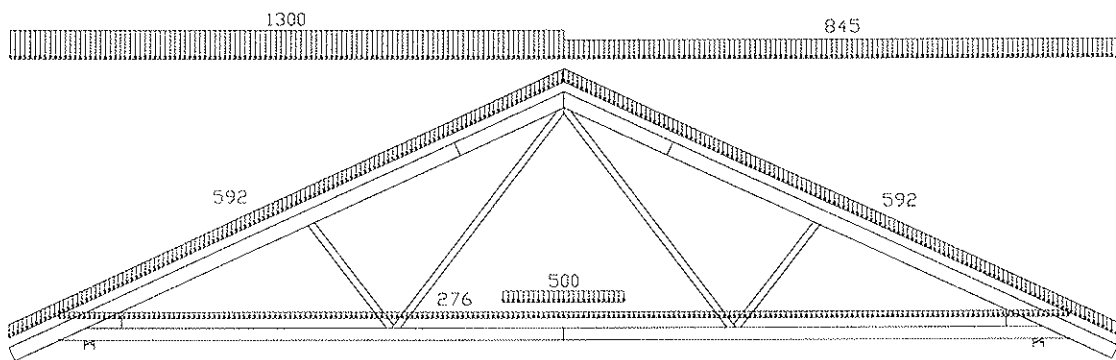
Figure 3. Loads [N/m] for truss type W10.

For truss type W15 the load case is similar.

3.3 Finite Element Model

Except for the splice joints the statical system for the trusses is taken directly from TrussCon where the beams can be either fully stiff connected or pinned. The splice joints are given semi-rigid behaviour as described below - the finite element program is named TrussLab, which is a toolbox developed under Matlab. For a detailed description of TrussLab, see *Ellegaard, P. (2002)*.

The different elements used in the joint modelling are described considering a heel joint of a timber truss, see figure 4.

4
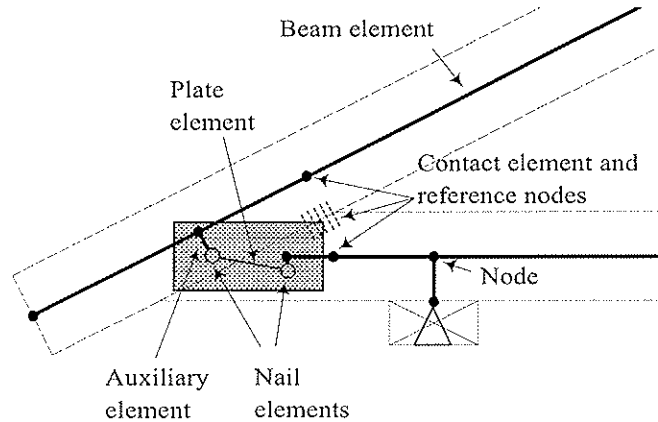
Figure 4. Heel joint used to explain the use of elements in TRUSSLAB.

Beam elements are used to model the timber members. The elements are located in the system line. Beam elements are also used as auxiliary elements. These auxiliary elements are used to transfer forces from nail groups to the system lines.

The stiffness of nail groups is taken into account by special nail elements. The nail elements connect beam elements with plate elements.

The behaviour of the nail plate over the joint line is modelled by a plate element. A plate element connects two nail elements. The nodes of a plate element and the corresponding nail elements are located at the centre of the respective nail groups.

Contact between timber members is modelled by a contact element. If there is an initial gap between the timber members the contact element is not activated until this gap is closed. The contact element refers to two nodes.

The material properties of the nail and plate elements are non-linear and the properties are determined from a number of tests, see *Ellegaard, P. (2002)*. The properties of the contact element are bilinear elastic.

The statical system for the W10 truss is shown in figure 5. The principle for the statical system for truss type W15 is similar.
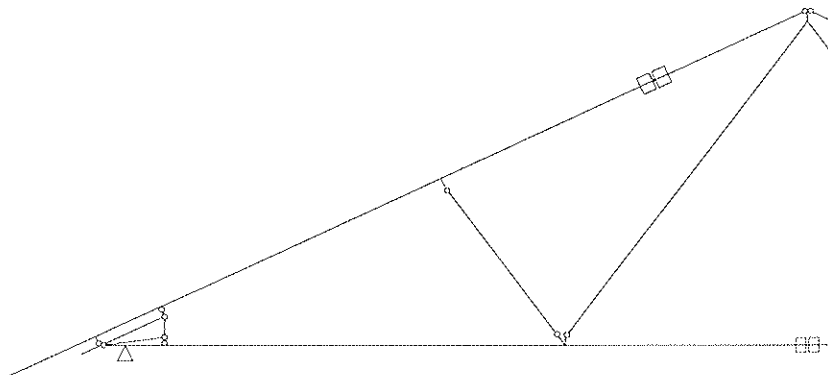
Figure 5. Statical system for the W10 – only half of the truss is shown due to symmetry.

For each type of truss and for each of the models S1, S2 and S3 three different sizes of initial gap between the timber members of the chord splices are analysed – 0.0 mm, 0.5

5

mm and 1.0 mm (all splice joints are given the same initial gap size). For gap sizes larger than 1.0 mm no contact between the timber members for the given load case is established.

4   Results from Calculations

From the results of the calculations in TrussLab it is found that there are only relative small changes in the distribution of the axial and shear forces. Therefore, only changes in the distribution of the bending moment are shown. To form a general overview the bending moment distribution for truss type W10 is shown in figure 6.
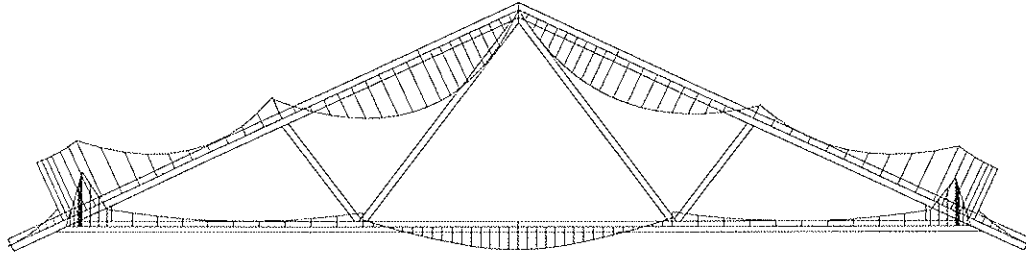
Figure 6. Bending moment distribution for the W10 truss type.

4.1   Truss Type W10

For the different models S1-S4 the values of the bending moment at four locations 1-4 (see figure 7) are listed in table 1.
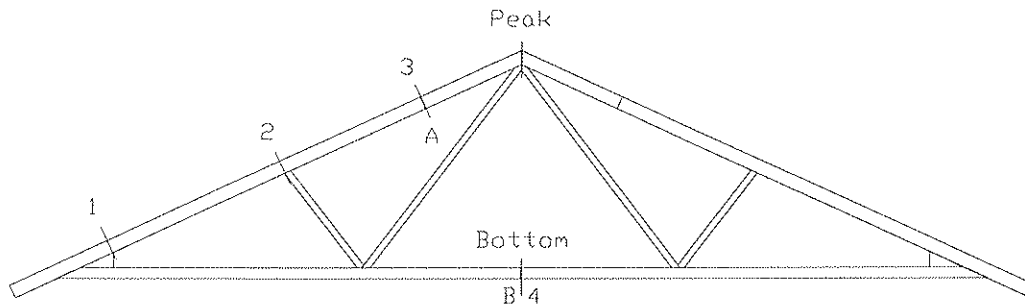
Figure 7. W10 truss with location of points where bending moments, rotations and displacements are calculated.

Truss model	Gap size	Bending moment [kNm]			
		1	2	3	4
W10 (S1)	0.0 mm	-1.71	-0.71	1.25	-0.56
	0.5 mm	-1.72	-0.76	1.22	-0.56
	1.0 mm	-1.72	-0.77	1.22	-0.56
W10 (S2)	0.0 mm	-1.71	-0.67	1.26	-0.56
	0.5 mm	-1.71	-0.70	1.25	-0.56
	1.0 mm	-1.71	-0.70	1.25	-0.56
W10 (S3)	0.0 mm	-1.73	-0.70	1.26	-0.57
	0.5 mm	-1.71	-0.70	1.25	-0.56
	1.0 mm	-1.74	-0.81	1.21	-0.56
W10 (S4)	--	-1.69	-0.65	1.28	-0.61

Table 1. Bending moments at locations 1-4 for truss type W10. The initial gap size is set to 0.0, 0.5 and 1.0 mm for each truss model.

The maximum moments at locations 1 and 3 for the three models S1-S3 compared with model S4 are only changed very little (< 3%). At location 2 the maximum deviation from model S4 is found for model S3 (gap = 1.0 mm) where the bending moment is 25% larger.

The deviations from the model with stiff splice joints (S4) become larger when the initial gap is larger. In general the distribution of the bending moments for the three models S1-S3 is relatively close.

The rotations in the splice joints and the vertical displacement at two locations (see figure 7) are listed in table 2.

Truss model	Gap size	Rotation [rad]		Displacement [mm]	
		A	B	Peak	Bottom
W10 (S1)	0.0 mm	0.0039	0.0048	-21.9	-8.0
	0.5 mm	0.0064	0.0056	-22.9	-8.3
	1.0 mm	0.0069	0.0056	-23.0	-8.4
W10 (S2)	0.0 mm	0.0027	0.0044	-21.4	-8.0
	0.5 mm	0.0039	0.0047	-22.0	-8.2
	1.0 mm	0.0039	0.0047	-22.0	-8.2
W10 (S3)	0.0 mm	0.0017	0.0043	-20.6	-8.1
	0.5 mm	0.0042	0.0052	-21.4	-8.5
	1.0 mm	0.0042	0.0052	-21.4	-8.5
W10 (S4)	--	0.0	0.0	-19.4	-7.8

Table 2. Rotations in splice joints A and B and displacements at two locations for truss type W10. The initial gap size is set to 0.0, 0.5 and 1.0 mm for each truss model.

The rotations and the displacements increase with larger initial gap. The models S2 and S3 lead to smaller rotations than S1, but the displacements at the bottom chord are slightly larger for model S3 than for S2 and S1. In general the displacements are 5-18% larger for the models S1-S3 compared with S4.

4.2 Truss Type W15

For the different models S1-S4 the values of the bending moment at three locations (see figure 8) are listed in table 3.
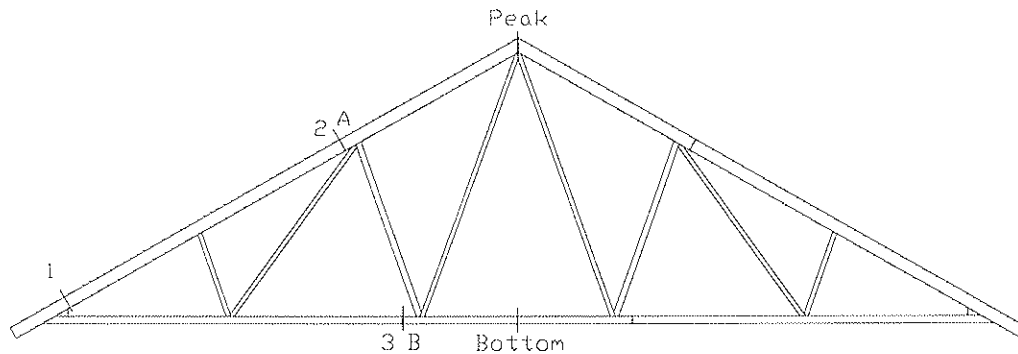
Figure 8. W15 truss with location of points where bending moments, rotations and displacements are calculated.

8

Truss model	Gap size	Bending moment [kNm]		
		1	2	3
W15 (S1)	0.0 mm	-3.88	-1.35	0.38
	0.5 mm	-3.88	-1.10	0.38
	1.0 mm	-3.88	-1.07	0.38
W15 (S2)	0.0 mm	-3.88	-1.39	0.37
	0.5 mm	-3.88	-1.22	0.38
	1.0 mm	-3.88	-1.22	0.38
W15 (S3)	0.0 mm	-3.88	-1.56	0.38
	0.5 mm	-3.88	-1.71	0.39
	1.0 mm	-3.89	-1.80	0.39
W15 (S4)	--	-3.88	-1.48	0.43

Table 3. Bending moments at four locations 1-3 for truss type W15. The initial gap size is set to 0.0, 0.5 and 1.0 mm for each truss model.

There is no noticeable change in the bending moments at locations 1 and 3 the four models amongst. At location 2 the changes compared with model S4 are between –21% (S3) and 28% (S1).

The rotations in the splice joints and the vertical displacement at two locations (see figure 8) are listed in table 4.

Truss model	Gap size	Rotation [rad]		Displacement [mm]	
		A	B	Peak	Bottom
W15 (S1)	0.0 mm	0.0013	0.0025	-11.7	-16.3
	0.5 mm	0.0035	0.0025	-11.9	-16.4
	1.0 mm	0.0038	0.0025	-11.9	-16.4
W15 (S2)	0.0 mm	0.0011	0.0027	-11.8	-16.4
	0.5 mm	0.0025	0.0027	-11.9	-16.5
	1.0 mm	0.0025	0.0027	-11.9	-16.5
W15 (S3)	0.0 mm	0.0016	0.0021	-11.8	-16.2
	0.5 mm	0.0043	0.0022	-12.0	-16.4
	1.0 mm	0.0056	0.0022	-12.1	-16.5
W15 (S4)	--	0.0	0.0	-11.2	-15.0

Table 4. Rotations in splice joints A and B and displacements at two locations for truss type W15. The initial gap size is set to 0.0, 0.5 and 1.0 mm for each truss model.

At location B the rotations are of the same magnitude. At location A the rotations are smaller for model S2 than for S1 and S3. The displacements for the models S1-S3 are of

the same magnitude and are 6-9% larger compared with model S4 where the splice joints are fully stiff.

4.3 Rotation due to Anchorage or Deformation in the Joint Line?

To analyse whether the rotations in splice joints are caused by rotations in the nail groups or by deformations of the nail plate in the joint line, a simple splice joint under four-point bending has been set up in TrussLab (span 2000 mm loaded at third points).

The splice joint is located at the middle of the beam and the nail plate is utilised 81% in anchorage capacity and 84% in the capacity of the joint line according to TrussCon. The ultimate load level is 2 x 3600 N (based on design values). The nail plate type is GNT150S.

Three models are set up in TrussLab (no contact between timber members is established):

1. One model where the nail plates are given "normal" stiffness (to find the total rotations).
2. One model where the joint line is stiff (to find the rotation of the nail groups).
3. One model where the nail groups are stiff (to find the rotations of the joint line).

The rotation of the nail groups/joint line at given load levels in relation to the total rotation is listed in table 5.

Load level	Nail group (model 2)	Joint line (model 3)
2 x 1000 N	83%	17%
2 x 2000 N	79%	21%
2 x 3000 N	77%	23%
2 x 4000 N	67%	33%
2 x 5000 N	43%	57%
2 x 6000 N	29%	61%

Table 5. Percentage influence to the rotations of the total rotation.

This simple analysis indicates that up to the ultimate load level the rotations are mainly due to rotations of the nail groups – for this type of nail plate.

5 Conclusion

As could be expected model S2 (splice joint near maximum moment and nail plates utilised up to 66%) leads to smaller rotations in the splice joints and smaller global displacements compared with model S1 (splice joint near maximum moment and nail plates utilised up to 100%). Due to the larger stiffness of the splice joints in model S2 the bending moments in the splice joints are also larger than for model S1.

However, when the splice joints are located closer to sections with zero moment (S3) the rotations and displacements are often larger compared with model S1. Moreover, it is not clear whether the influence on the bending moment distribution is larger for model S1 than for S3.

10

Therefore, it seems that the guidelines (especially the second one in Eurocode 5) for treating splice joints rotationally stiff do not necessarily lead to more realistic truss models compared with a situation with no limitations to the splice joints.

There are relatively large deviations between the results (moment distribution, rotations and displacements) achieved with the models S1-S3 compared with S4. To get a better agreement between real behaviour of a truss and the finite element models semi-rigidity of joints should be implemented. These joint models must include timber contact, since it is important to the stiffness and distribution of the section forces.

From a simple splice joint it is found that the rotations are mainly caused by the anchorage of the nails and not by deformations in the joint line (for GNT150S plate type).

6 References

Bell, K. (1998), 'Noen synspunkter på beregnings- og dimensjonerings-regler for takstoler og andre spikerplate-konstruksjoner' (in Norwegian) (Note on Analysis and Design of Timber Roof Trusses with Punched Nail Plates), Norwegian University of Science and Technology, 1998

Blaß, H. J., Ehlbeck, J. & Kurzweil, L. (1997), 'Berücksichtigung der Momentenübertragung von Nagelplattenverbindungen bei der Bemessung', Versuchsanstalt für Stahl, Holz und Steine, Abteilung Ingenieurholzbau, Universität Fridericiana Karlsruhe, 1997.

DS 409 (1982), 'Norm for sikkerhedsbestemmelser for konstruktioner' (in Danish) (Code of Practice for the Safety of Structures), Dansk Standard, 1. udgave/8.oplag, 1982.

DS 410 (1982), 'Norm for last på konstruktioner' (in Danish) (Code of Practice for Loads for the Design of Structures), Dansk Standard, 3. udgave/7.oplag, 1982.

DS 413 (1982), 'Norm for trækonstruktioner' (in Danish) (Code of Practice for the Structural Use of Timber), Dansk Standard, 4. udgave/6.oplag, 1982.

DS 413 (1998), 'Norm for trækonstruktioner' (in Danish) (Code of Practice for the Structural Use of Timber), Dansk Standard, 5. udgave/1.oplag, 1998.

Ellegaard, P. (2002), 'Analysis of Timber Joints With Punched Metal Plate Fasteners – With Focus on Knee Joints' Ph.D. Thesis, Department of Building Technology and Structural Engineering, University of Aalborg, Denmark, 2002.

Eurocode 5 (2002) - prEN 1995-1-1. Final draft of 1995-1-1, Version 2002-10-09, 'Eurocode 5 – Design of Timber Structures – Part 1-1: General Rules, General Rules and Rules for Buildings'. CEN Brussels, 2002.

Kevarinmäki, Ari (2000), 'Semi-rigid Behaviour of Nail Plate Joints', Ph.D. Thesis, Helsinki University of Technology, TKK-TRT-109, 2000.

Riberholt, H. (1982), 'Guidelines for Static Models of Trussed Rafters'. CIB-W18. 15-14-1. Karlsruhe, 1982.

Riberholt, H. (1989), 'Guidelines for Design of Timber Tussed Rafters'. CIB-W18. 22-14-1. Berlin, 1989.

INTERNATIONAL COUNCIL FOR RESEARCH AND INNOVATION
IN BUILDING AND CONSTRUCTION

WORKING COMMISSION W18 - TIMBER STRUCTURES

MONTE CARLO SIMULATION AND RELIABILITY ANALYSIS OF

ROOF TRUSSES WITH PUNCHED METAL PLATE FASTENERS

M Hansson

Lund University

SWEDEN

P Ellegaard

Aalborg University

DENMARK

Presented by: Martin Hansson

Martin Hansson began his presentation by describing the principles behind the use of load sharing system. He went on to describe the test data used in his research. He concluded that the strength of a roof truss taking experimental data as input parameters could be simulated. In the discussions which followed Martin clarified that by system he meant only a single roof truss rather than the whole roof.

Monte Carlo Simulation and Reliability Analysis of Roof Trusses with Punched Metal Plate Fasteners

Martin Hansson, Lund University, Sweden
Peter Ellegaard, Aalborg University, Denmark

1   Abstract

System effects are often found in timber structural systems e.g. due to transverse load distribution between different structural members. System effects are also related to the variation of strength within and between members. Most studies found in the literature have considered the variability between timber members, but the variability within members has been neglected mainly because of lack of data.

In this paper, Monte Carlo simulations of a W-truss are performed using a model describing the strength parameters between and within timber members. The timber members are connected by punched metal plate fasteners (nail plates). The variations in the properties of these joints have been estimated from experiments. The FE calculations are performed with TrussLab - a toolbox to MATLAB developed at Aalborg University. TrussLab takes contact between members and non-linear behaviour in the joints into account.

The system effect is estimated through a comparison of the simulations with a deterministic calculation of the roof truss using characteristic values as input to the model. The change of coefficient of variation also affects the reliability and is analysed. The total system effect is found to be between 10-20 % when timber failure is predominant, but less than 10% if the total failure is caused by failure in the plates or anchorage failure in the connection between nail plate and timber member.

2   Introduction

The reliability of roof trusses has been studied by for example Gupta et al. (1990). The timber strength variability between members was modelled as log-normally distributed and three types of models were analysed; pinned, rigid and semi-rigid joints. Changing only the behaviour of the joint, the probability of failure decreased with increased stiffness of the joint.

Dalsgaard Sørensen and Damkilde (2003) and Hansson and Thelandersson (2002) made simulations taking the variation within members into account. Both studies found system effects in the order of 10-20%. In Dalsgaard Sørensen and Damkilde (2003) the parameters in the sensitivity analysis showed minor influence on the simulated load-carrying capacity of the roof truss except for the coefficient of variation (COV) for the bending strength. The analysed parameters are shown in Table 1.

Table 1: Parameters in the sensitivity analysis by Dalsgaard Sørensen and Damkilde (2003).

Analysed parameter	COV (bending strength)	COV (MOE)	Statistical distribution (bending strength)	Correlation Strength parameters		
				Tension-bending	Compression-bending	MOE-bending
Alternative values	0.20/0.25	0.13/0.18	Log Normal, Normal, 2 parameter Weibull	0.8/0.7	0.9/0.8	0.8/0.7

In the engineering practice in Scandinavian countries, an increase of the bending strength is allowed in the top chord of a truss at moment peaks. This increase is based on proposal for Eurocode 5 by Riberholt (1990). For timber with a characteristic bending strength of 24 MPa and 18 MPa, the increase will be about 30% and 40%, respectively.

In Eurocode 5 (2002) a system effect factor (k_{sys}=1.1) may be multiplied by the member strength properties to take into account load distribution between similar parallel members connected by a continuous load distributing system. In this paper, one roof truss is analysed to take into account probabilistic system effect based on the reduced chance that a weak section will be placed at the most stressed point and structural load sharing where load can be distributed within the roof truss according to the stiffness in the different parts. The roof truss with nail plates is analysed using an advanced FE model taking non-linearity of the joints into account. The variability within and between timber members is simulated as well as the variability of the properties of the joints.

3 FE modelling of the system

The FE modelling of the truss is performed by TrussLab where the joints are modelled as semi-rigid with non-linear properties. The TrussLab model, the geometry of the truss and the load case are described in this section. For a detailed description of TrussLab, see Ellegaard (2002).

3.1 TrussLab model

The different elements used in the joint modelling for a heel joint are shown in Figure 1.
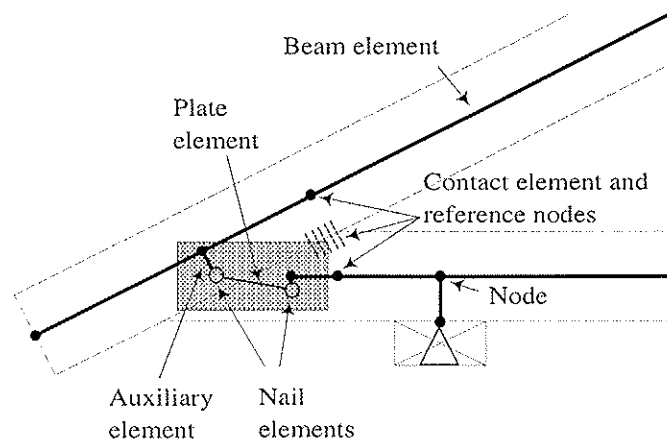
Figure 1: Heel joint used to explain the use of elements in TrussLab.

3.1.1 Beam element

Beam elements are used to model the timber members. The elements are located in the system line. Beam elements are also used as auxiliary elements to transfer forces from nail groups to the system lines. The length of each timber element is approximately 300 mm. Failure in the timber occurs when the stress exceeds the strength according to the expressions given in Eurocode 5 (2002).

3.1.2 Nail element

The stiffness of nail groups is taken into account by special nail elements. The nail elements connect beam elements with plate elements. The stiffness properties for one nail are shown in Figure 2. The relationship between force, p and displacement, Δ is described by eq. (1), see also Figure 2.

$$p(\Delta) = (p_0 + k \cdot \Delta)\left(1 - \exp\left(\frac{-kk \cdot \Delta}{p_0}\right)\right)$$

(1)
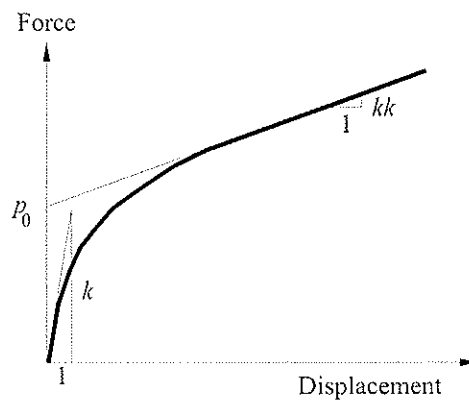
Figure 2: The nail force as a function of the displacement of the nail.

Besides the nail plate type, the stiffness parameters are dependent on the angle between the force direction and the main direction of the plate (α) and the angle between the force direction and the grain direction (β). The stiffness parameters are determined from four basic configurations where α and β are changed in steps of 90°. Hankinson's formula is used to determine the stiffness parameters for other than the four basic cases.

Failure in the nail groups is determined according to the expressions in Eurocode 5 (2002) – however, in these calculations the anchorage area is not reduced to an effective area (reduced by those parts of the surface which are beyond some specified dimension from the edges and ends).

3.1.3 Plate element

The behaviour of the nail plate over the joint line is modelled by a plate element. A plate element connects two nail elements. The nodes of a plate element and the corresponding nail elements are located at the centre of the respective nail groups. The plate element is made up of two types of small steel beams. One type has the same direction as the main direction of the nail plate and the direction of the other type is perpendicular to the main direction of the nail plate - see Figure 3. Depending on the geometry of the joint one or both types of plate beams are activated.

3
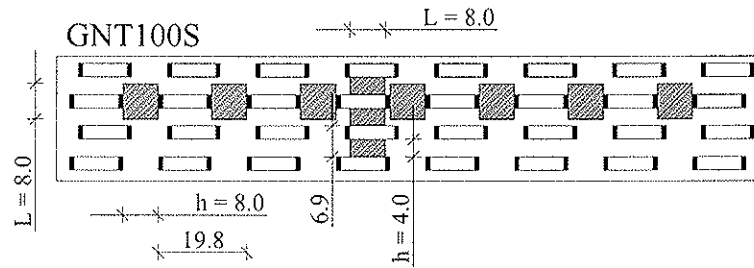
Figure 3: Geometry of the beams in the plate element for the GNT100S nail plate. Dimensions in mm. The thickness _t_ is 1.0 mm.

Each type of plate beams is given material properties with a stress-strain relation as shown in Figure 4.
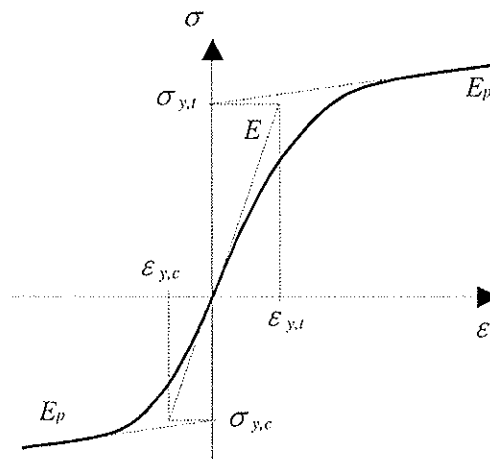
Figure 4: Definition of parameters for the beams in the plate element.

The failure criteria for the plate element are based on the axial, bending and shear stresses in each of the small plate beams - see Ellegaard (2002).

3.1.4 Contact element

Contact between timber members is modelled by contact elements. If there is an initial gap between the timber members, the contact element is not activated until this gap is closed. In the present calculations the initial gap sizes are set to 0.0 mm. Failure in contact zones is not considered.

4

3.2 Truss geometry and load

A roof truss manufacturer was asked to design the sizes and locations of the nail plates - the sizes of the timber members were prescribed. In the printout from the commercial software used, it can be found that for the given load cases (design loads) the utilisation for the timber is 74 % (with timber quality K18). According to the calculations, the utilisation for the nail plates is 51 % for the chosen sizes of the nail plates. The software takes the increase of bending strength at moment peaks according to Riberholt (1990) into account. The highest utilisation of the timber members is found in the top span of the top chord. According to the commercial programme, the highest utilised nail plate is located in the heel joint of the truss.

The geometry and the loads on the truss are shown in Figure 5. The load case corresponds to $1.0 \cdot$ dead load $+ 1.0 \cdot$ snowload $+ 1.0 \cdot$ live load.
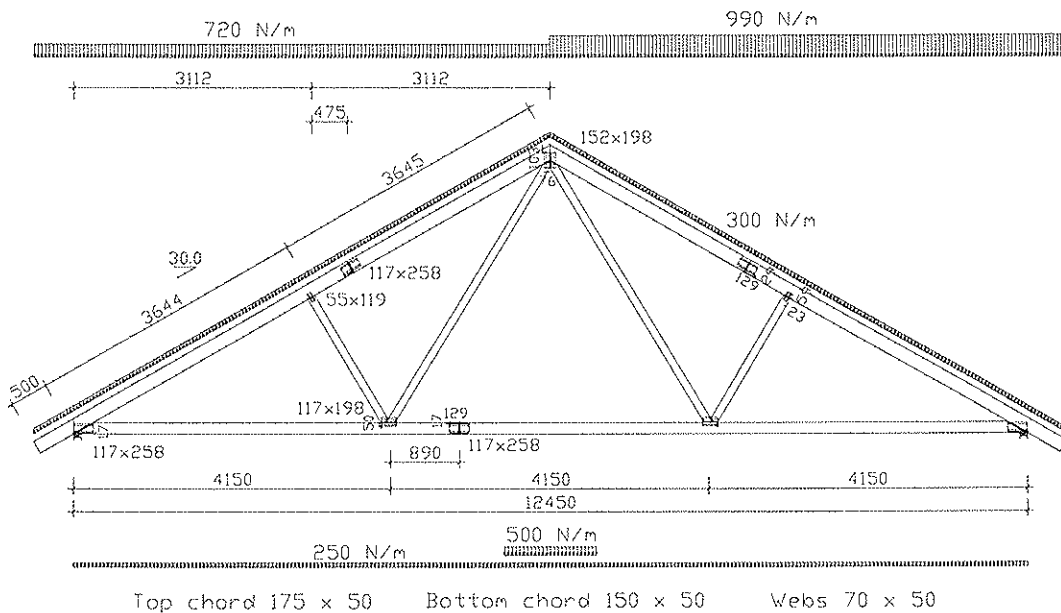
Figure 5: Geometry of the analysed truss. Dimensions in mm. All nail plates are type GNT100S. The truss is symmetrical except for the splice joint in the bottom chord.

4 Material properties

The input properties to the Monte Carlo simulations are described by lognormally distributed variables. The properties considered as stochastic variables are the strength and stiffness values of the timber and nail plates (both plate failure and anchorage failure).

4.1 Bending strength and modulus of elasticity of the beams

The bending strength profile of the timber members is modelled using a statistical model of the variability within and between members, Isaksson (1999). The bending strength $f_{m(i,j)}$ of section i in beam j is given by eq. (2), see also Figure 6.

$$f_{m(i,j)} = \exp\left(\mu + \tau_i + \varepsilon_{ij}\right)$$ (2)

where

μ is the logarithm mean of all weak sections in all beams.

τ_i is the difference between the logarithm mean of weak sections within beams i and μ. The mean equals zero and the standard deviation is σ_i.

ε_{ij} is the difference between weak section j in beam i and the value $\mu + \tau_i$. The mean equals zero and the standard deviation is σ_j.
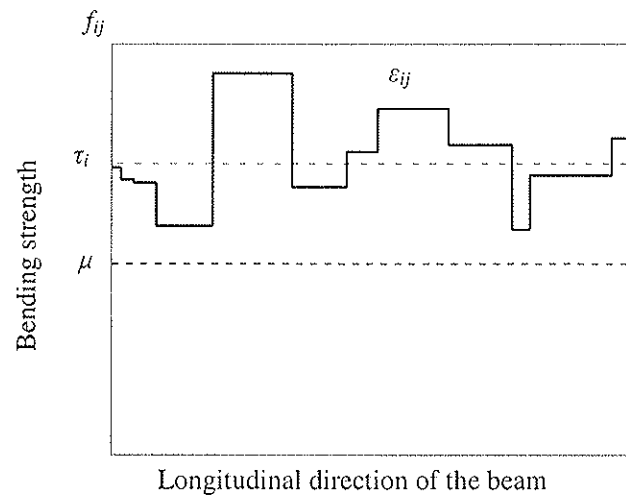
Figure 6: Model of bending strength variation in one timber beam, Isaksson (1999).

Isaksson (1999) found a coefficient of variation (COV) of 25 % for the bending strength. Of this variation 40 % is due to the variability within members and the rest is due to the variability between members. The COV given here is not the same as the one found by testing timber elements in four-point bending according to EN408 and EN384. These standards prescribe testing of one critical section within each member, but the input to the model is the result of testing all weak sections within the members. The standard test will result in a lower COV (about 20%).

6

The bending strength is modelled using the following parameters:

μ log N(3.9125,0) (expected value 50 MPa)

τ_i log N(0,0.0375)

ε_{ij} log N(0,0.025)

The modulus of elasticity (*MOE*) is correlated to the bending strength according to eq. (3), Dalsgaard Sørensen and Damkilde (2003). The *MOE* is further assumed to be constant within each timber beam. Based on experimental data, see Isaksson (1999), the correlation between bending strength and *MOE* is set to 0.8.

$$MOE_i = \mu_f \left[\ln(300) + 0.13\left(u_{f,i}\rho + u_E\sqrt{1-\rho^2} \right) \right]$$
       (3)

where

μ_f expected bending strength (50 MPa)

ρ correlation between bending strength and *MOE* (0.8)

$u_{f,i}$ outcome from a normal distribution N(0,1) used to generate bending strength in member *i*.

u_E outcome from a normal distribution N(0,1) which is independent of u_f

The length of a weak section is given by a gamma distribution Γ(2.5445, 194.12), i.e. the mean length of a weak section is around 500 mm, Isaksson (1999).

4.2 Tension, shear and compressive strength

Dalsgaard Sørensen and Damkilde (2003) showed that the correlation between the strength parameters have minor influence on the ultimate capacity of a roof truss. In this study, a deterministic relationship, found in prEN 338 (2002), is chosen. For tension strength $f_{t(i,j)}$ and shear strength $f_{v(i,j)}$ every section is computed from the corresponding bending strength, see eqs. (5) and (6). However, the compression strength $f_{c(i,j)}$ is based on the mean value of the bending strength in that particular beam, see eq. (7).

$$f_{t(i,j)} = 0.6 f_{m(i,j)}$$
       (4)

$$f_{v(i,j)} = 0.2 f_{m(i,j)}^{0.8}$$
       (5)

$$f_{c(i,j)} = 5 mean\left(f_{m(i,j)} \right)^{0.45}$$
       (6)

4.3 Anchorage properties

The input data for the nail plates (anchorage) are taken from experiments described in Ellegaard (2002), Nielsen (1996), Nielsen and Rathkjen (1994) and Jensen and Rasmussen (1993). The data are fitted to the force–displacement function (eq. (1)) using non-linear least-squares data fitting by the Gauss-Newton method (nlinfit in MATLAB). A restraint is set to *kk* (*kk* ≥ 1 N/mm) because TrussLab cannot have negative input of *kk* due to numerical issues. The properties are assumed to be uncorrelated except from p_0 and *kk* were a high negative correlation is expected and is set equal to –0.8 in the simulations.

Table 2: Input data for anchorage failure. p_0, k and kk are according to Figure 2. fa is the failure load for the nail plate. The data are per nail.

Direction		Number of experiments	fa		p_0		k		kk	
α	β		Mean [N]	COV [%]	Mean [N]	COV [%]	Mean [N/mm]	COV [%]	Mean [N/mm]	COV [%]
0	0	34	199.6	16.5	150.3	30.3	1974.8	44.5	127.2	121
90	0	10	189.0	17.8	137.9	28.4	2116.7	22.2	75.2	59.6
0	90	6	168.6	17.7	184.6	16.2	939.7	17.9	1	0
90	90	7	143.0	16.6	103.3	30.3	998.4	24.1	109.4	83.9

4.4 Plate properties

The number of tests available for this particular nail plate is not sufficient for statistical evaluation. However, since it is steel failure a low variation is expected and the mean values are taken from Ellegaard (2002), see Table 3. The COV of the nail plate properties, found in Table 3, is chosen as 5%.

Table 3: Mean values for the properties of the plate element, Ellegaard (2002).

	$\sigma_{y,t}$ [N/mm^2]	$\varepsilon_{y,t}$	$\sigma_{y,c}$ [N/mm^2]	$\varepsilon_{y,c}$
Beams in plate main direction	450	0.010	240	0.0053
Beams perpendicular to plate main direction	430	0.0075	240	0.0042

5 Monte Carlo simulations

The geometry of the roof truss is assumed deterministic in the Monte Carlo simulations. The load is increased by a load factor until ultimate load level is reached. The load factor is applied to all loads, even the permanent load. Further, only one load case is considered.

Although the utilisation in the calculation with the commercial software shows no large difference between anchorage/plate failure and timber failure, only anchorage and plate failure occurred in the simulations. However, for another truss design with other nail plate sizes there is a possibility that only timber failure occurs. Therefore, two different simulations are made: one with and one without anchorage and plate failure.

In Figure 7 the results from 1000 simulations can be found. Both anchorage failure and plate failure are included. However, all the "early" (below 5 percentile) failures are due to anchorage failure.
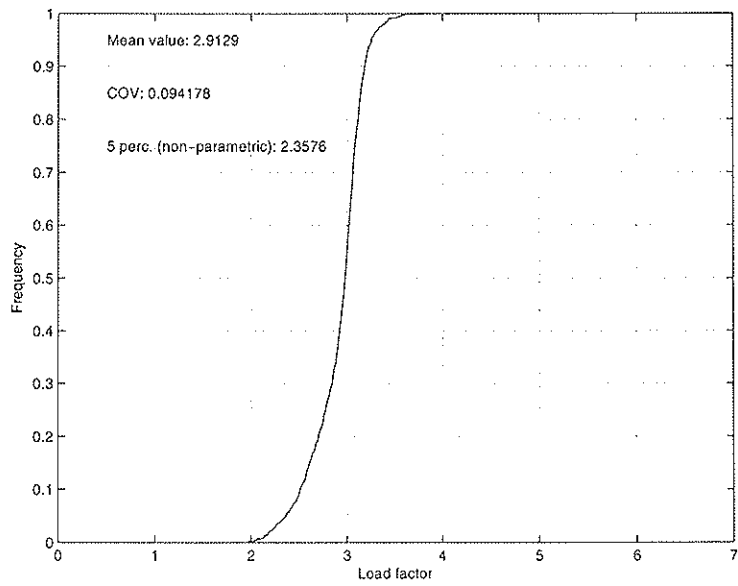
Figure 7: Frequency of the load factor at failure (nail plate failure included).

The results from the simulations when nail plate failure is not considered are shown in Figure 8. In about 60% of the cases, the dominating failure element is located just above the right-hand heel joint. The other failure elements are located in the bottom chord.
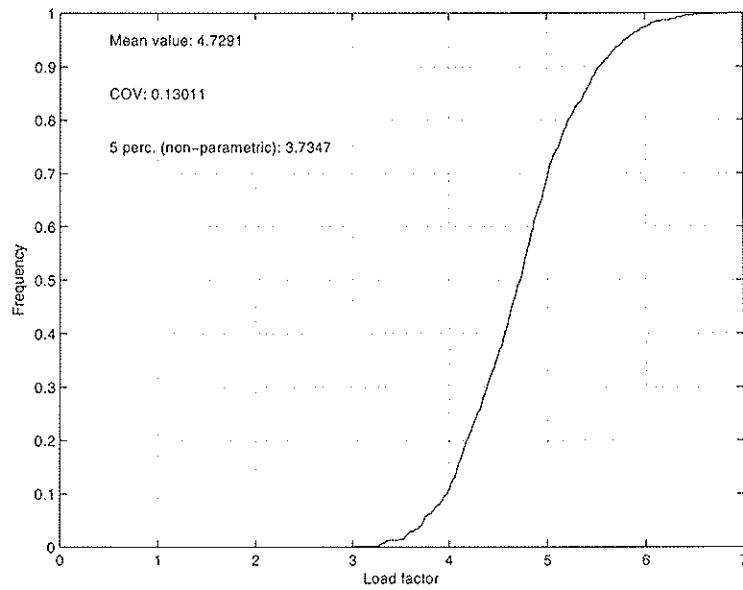
Figure 8: Frequency of the load factor at failure (nail plate failure excluded).

9

6   Results

To find an effect a deterministic calculation using the same model is performed and is to be compared with the simulations. The input to this deterministic calculation is the characteristic values (5 percentile values) for all stochastic variables. The load factor from both the simulation and the deterministic calculation can be found in Table 4.

Table 4: Summary of the results from the Monte Carlo simulations and the deterministic calculation with characteristic values.

Model type	Monte Carlo simulations Load factor			Deterministic calculation with characteristic values.
	Mean	COV	5-percentile non-parametric	Load factor
With plate failure	2.91	0.094	2.36	2.56
Timber failure	4.73	0.13	3.73	3.57

To make a fair comparison, both the change of characteristic value and the change of COV must be included. To analyse the change of COV the Danish code of practice, DS 409 has been used to get an indication of the influence of the reduced coefficient of variation. The partial safety factor for material properties γ_m is written, DS 409 (1998):

$$\gamma_m = \gamma_0 \gamma_1 \gamma_2 \gamma_3 \gamma_4 \gamma_5 \qquad\qquad (7)$$

where γ_0, γ_1, γ_2, γ_3, γ_4 and γ_5 take into account the consequences of failure, the failure mode (brittle or ductile failure), the dependence of COV in the material properties, accuracy of calculation model, the accuracy of the determination of the material properties and the control of the material production and workmanship respectively. The relation between COV and γ_2, the partial coefficient regarding the dependence of COV on the material properties, can be found in Table 5.

Table 5: The relation between COV and γ_2, DS 409 (1998).

COV	<0.05	0.1	0.15	0.2	0.25	0.3
γ_2	1.30	1.38	1.50	1.64	1.83	2.06

The change in COV is from 17 % (the input data of anchorage failure) to 9.4 % for the simulations including plate failure. When only timber failure is regarded, the change of COV is from 20% (as found in standard test of timber beams) to 13 %. However, it should be noted that the COV for the timber beams in the performed Monte Carlo simulations is 25%. In Table 6 the effect of change of characteristic value and coefficient of variation can be found.

Table 6: System effect due to change of characteristic values and COV.

Model type	Ratio between MC simulation and deterministic calc.	Change in COV	Ratio of γ_2 due to reduced COV (lin. interp. in Table 5)
With plate failure	2.36/2.56= 0.92	17%[*] → 9.4%	1.56/1.37= 1.14
Timber failure	3.73/3.57= 1.04	20% → 13%	1.64/1.45= 1.13

[*] COV from anchorage failure (see Table 2)

It can be seen that there is no system effect for plate failure if only the ratio between characteristic values is considered, but if the change of COV is included, a small effect is found. For trusses where timber failure is likely to occur, a system effect of about 10-20 % for

10

both the change in characteristic value and the decrease of COV are expected according to this study.

7   Summary

In the simulations, the only failure that was observed was failure in the nail plates for this specific roof truss. Therefore, additional simulations were performed ignoring failure in the nail plates. The system effect was estimated through a comparison of the simulations with a deterministic calculation of the roof truss using characteristic values as input to the model. The change of coefficient of variation also affects the reliability and was analysed. The total system effect was found to be between 10-20 % when timber failure is predominant, but less than 10% if the total failure was caused by anchorage failure in the connection between nail plate and timber member.

A more detailed study of the commercial software is desirable to determine if the joint models are accurate and if the engineering practice to increase bending strength at moment peaks is relevant.

8 References

Dalsgaard Sørensen J. and Damkilde L., (2003). *Load bearing capacity of roof trusses.* To be published. Aalborg University, Denmark.

DS 409, (1998). *Code of Practice for the Safety of Structures.* Danish Standard.

Ellegaard P., (2002). *Analysis of Timber Joints with Punched Metal Plate Fasteners*, Paper No 11, PhD Thesis, Aalborg University, Denmark.

Eurocode 5, (2002) *Design of Timber Structures – Part 1.1.* prEN 1995-1-1.CEN, Bruxelles, Belgium, Final draft 2002-10-09.

Gupta R. and Gebremedhin K.G., (1990). *Reliability analysis of semirigidly connected metal plate wood trusses.* International Timber Engineering Conference, Tokyo, Japan.

Hansson M. and Thelandersson S., (2002). *Assessment of probabilistic system effects on the reliability of timber trusses.* Material and Structures, Vol 35, pp 573-578.

Isaksson, T., (1999). *Modelling the variability of bending strength in structural timber.* Report TVBK-1015, Dept. of Structural Engineering, Lund University Sweden.

Jensen H. and Rasmussen H., (1993). *Undersøgelse af tandplader i stødsamlinger.* Master Thesis. In Danish, Aalborg University, Denmark.

Nielsen J., (1996). *Stiffness analysis of nail-plate joints subjected to short-term loads*, PhD Thesis, Paper No 2, Aalborg University, Denmark.

Nielsen J. and Rathkjen A., (1994). *Laterally loaded nail-plates*, Paper No 1, Aalborg University.

Olsson A., (2002). *Probabilistic Analysis and Optimization of Roof Trusses.* Submitted to Electronic Journal of Structural Engineering.

prEN 338, (2002). *Structural Timber – Strength Classes.* Final draft October 2002.

Riberholt H., 1990. *Proposal for Eurocode 5. Text on timber trussed rafters.* CIB-W18 23-14-2 Lisbon, Portugal.

INTERNATIONAL COUNCIL FOR RESEARCH AND INNOVATION
IN BUILDING AND CONSTRUCTION

WORKING COMMISSION W18 - TIMBER STRUCTURES

TRUSS TROUBLE

R H Leicester
P Paevere
G C Foliente

CSIRO

J Goldfinch

Koukourou Engineers

AUSTRALIA

Presented by: Bob Leicester

Bob Leicester began his presentation by considering a recent structural truss rafter roof collapse and nail plate pull out. He also described lateral stability issues related to truss roofs and also discussed heel joint failure modes, buckling and local effects.   His survey showed that nail plate pull out is not uncommon. In a particular case 12 out of 18 trusses had to be replaced due to nail plate pull out failures. From the study it is recommended that the strength of complex truss systems be verified via laboratory tests, that formal stability checks should be made for certain trusses and that special checks may need to be made for local grain slopes. Discussions centred on design code implications and the testing procedure for the heel joints.

TRUSS TROUBLE

By R.H. Leicester[1], J. Goldfinch[2], P. Paevere[1], G.C. Foliente[1]
(1) CSIRO, Australia
(2) Koukourou Engineers, Australia

ABSTRACT

Following many decades of extensive and highly successful applications of nail plated trusses in Australia, several unexpected incidents involving plated trusses occurred recently which have caused some concern and triggered investigations into the performance of these trusses. Among matters investigated have been the mechano-sorptive behaviour and structural mechanics of heel joints, creep buckling, brittle wood and quality control in fabrication and erection.

1.   INTRODUCTION

Since the 1960s, nail plated timber roof trusses have been used extensively and successfully in Australia for housing, community halls and commercial buildings. However in 2002 the double girder truss of a golf clubhouse in Adelaide collapsed killing two persons and were it not for the fortunate placement of a side wall, would have killed another 30 people. The collapse occurred after 7 years in service, without warning and on a quiet windless day. The only loading at the time was the dead load of the roof. Following an investigation on this collapse, the South Australian government issued a general hazard alert related to work place buildings using nail plate truss roofs. As a result a program to inspect the service condition of roof trusses was initiated. It was discovered that many existing trusses are either close to collapse, or appear to carry a risk of a collapse in the foreseeable future through teeth withdrawal due to mechano-sorptive and other effects.

Since the "problem" trusses follow conventional and apparently successful design forms, it is important to assess if there are potential future problems. The findings of some of the investigations undertaken for this purpose are discussed in the following.

2.   LOAD CAPACITY OF TRUSSES

2.1   Strength of the Heel Joint

It was suspected that the fatal collapse of the Adelaide clubhouse was initiated at the heel joint of a double girder truss. Accordingly the strength of this joint was studied through laboratory tests. A detailed report on the investigation of this truss is given elsewhere (Paevere *et al.* 2002).

The tested heel joint, shown in Figure 1, is of a type commonly used in Australia. The timber used was seasoned F17 Tasmanian Oak (an eucalypt hardwood). The nail plates used in the test were 2 mm thick, and comprised a designed structural plate and a smaller "comfort plate"; the purpose of the comfort plate was to hold the top and bottom chord members together near the support location. In both the clubhouse truss and the laboratory trusses, the wood at the heel joint was of good quality and the nail plate connections remained intact after failure of the heel joint.

The failure loads, expressed in terms of the heel reaction R, are given in Table 1 for four laboratory test trusses and for the clubhouse truss. The table also shows the bending strength of small clear wood specimens (10 x 10 mm section, 200 mm long) taken from the top chord of the heel joints.

The failure was by a split along the plane B–B followed by a transverse bending break across the plane C–C. It was not clear as to whether the transverse bending failure across the plane A–A preceded or followed the split along the plane B–B.

Table 1. Strength properties of the trusses investigated

Truss	Heel reaction R for a single truss (kN)		Bending strength of small clear specimens (Mpa)
	Short term test	After 7 years in service	
Club house truss	-	15.1	107
Lab No. 1*	23.4	-	162
Lab No. 2	22.6	-	152
Lab No. 3	30.1	-	108
Lab No. 4	37.2	-	-

* initial saw cut made at A-A (Figure 1)

If it is assumed that the clear wood of the laboratory tests has a bending strength of 140 Mpa, then the bending strength capacity of the section C–C corresponds to a heel joint reaction of 21.8 kN if C–C is half the timber section (i.e. 60 mm) and 38.7 kN if C–C is two thirds of the timber section (i.e. 80 mm). These values appear to be in line with the test data, and they also offer an explanation for the wide range noted for the ultimate strength capacity of the heel joint. It should be emphasised that the split along the plane B–B was the cause of a strength reduction by a factor of at least 2.0 in the load capacity of the truss heel; it is therefore important to speculate as to whether any structural analysis procedure would have predicted the occurrence of such a split.

To estimate the expected long duration strength of the clubhouse heel joint, a typical value of $R = 28$ kN may be taken from the short duration laboratory tests, a value of 1.3 for the difference in clear wood strengths between the timber of the clubhouse and laboratory heel joints, a factor of 1.25 for the duration of load effect, and a factor 1.15 for the double girder truss effect (Enjily and Whale 1994). Hence the expected long duration value is $R = 28/(1.3 \times 1.25 \times 1.15) = 15.0$ kN, which agrees with the computed in-service dead load on the failed clubhouse truss.

Extensive finite element modelling of the heel was undertaken. However, it was found that peak stress effects were very localised and very sensitive to assumptions used in modelling the heel joint. Hence the value of these studies was primarily in examining the assumptions of the structural action described above.
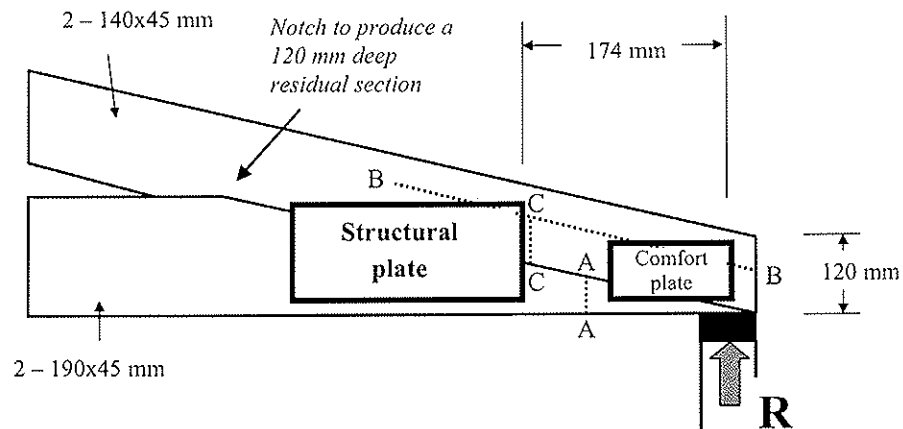
Figure.1 Scale drawing of heel of failed clubhouse truss.

2.2   Lateral Stability

Although it did not appear that the proximate cause of failure of the clubhouse truss had been due to buckling effects, it is possible that lateral buckling of the top chord exacerbated the situation. The opportunity was therefore taken to investigate the lateral restraint system of a typical truss construction. It has long been known that friction from roofing battens provides significant lateral restraint to the top chord of a truss, if the load to the truss is essentially applied via the battens (Leicester 1976). However, for the case of a girder truss the major part of the load is usually applied to the bottom chord.

For the case of the failed clubhouse double-girder truss, shown schematically in Figure 2, the buckling restraint is applied via 2.8 mm diameter nails that connect the tiling battens to the top chord and possibly also by the lateral cantilever action of the web members. The effectiveness of these restraints was investigated using a design procedure developed previously (Leicester 1975) and now incorporated into the Australian Timber Engineering Design Code (Standards Australia 1997). The results, shown in Figures 3 and 4, are not encouraging. In these Figures the term efficiency refers to the proportion of nail connections that are effective. Because many of the battens are spliced and many of the nails are associated with end splits of the battens, the efficiency in typical roof construction is probably in the range 0.2 – 0.5. Even if the number of nails were to be doubled, their restraint action would be inadequate.
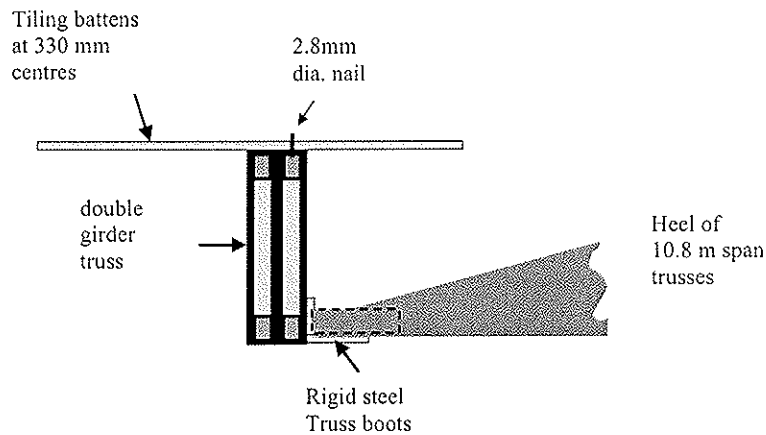
Figure 2. Schematic illustration of lateral support to failed double girder truss.
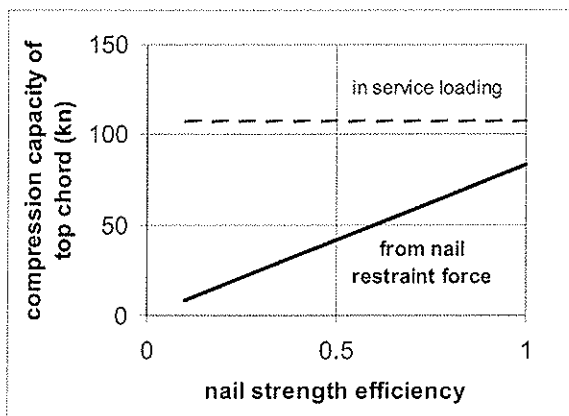
Figure 3. Effect of nail strength efficiency on the load capacity of the double girder truss.
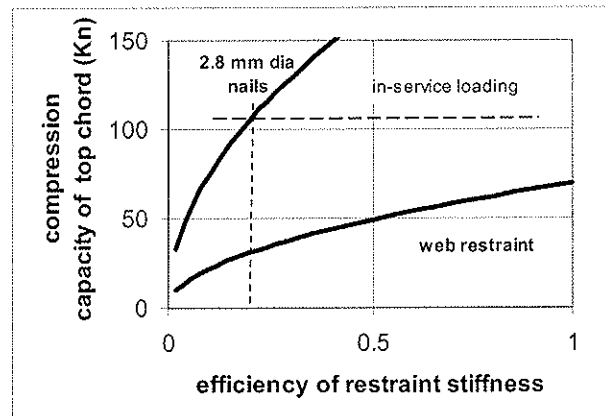
Figure 4. Effect of efficiency of restraint stiffness on the load capacity of the double girder truss.

2.3   Effect of Wood Quality

2.3.1   General

Grading rules often do not concern local effects that that affect the performance of toothed plates. These localised effects are difficult to cull out in general grading operations. For high risk structures it may be desirable to introduce special quality control procedures that target local effects.

2.3.2   Slope-of-grain

The Australian Standard AS 2082: Timber–Visually Stress-graded for Structural Purposes allows a slope of grain of 1:8 (corresponding to an angle of 7°) in F17 and A17 grade timber. However, in the failed truss there were some small local areas near the fracture point of the top chord that had a grain angle of 12°.

Figure 5 shows the effect of slope of grain on the strength of clear wood (Forest Products Laboratory 1999). Figure 6 shows the effect of slope of grain, as measured at the failure point of a set of parallel chord trusses (Leicester 1976).

From the above it is apparent that the slope-of-grain has a very marked effect on the strength of timber. Hence it is recommended that for critical structures, special checks should be made to ensure that excessive slope-of-grain does not occur at critical zones, particularly the heel joint. These checks can be made for example, by use of a hand lens or a mechanical slope-of-grain scriber.

2.3.3   Brittle wood

Although heartwood is not permitted by AS 2082 in members thinner than 175 mm, nevertheless small zones of brittle wood are often to be found in pieces of stress graded hardwood. Small clear wood specimens taken from a localised zone of brittle wood in the top chord of the failed clubhouse truss were found to have only 70% of the strength of similar specimens taken from the heel. It is recommended that some detection procedure be developed so as to ensure that brittle wood does not occur at critical locations such as at the heel joints of critical trusses.

2.3.4   Kino veins

Kino veins, also known as gum veins are frequently caused by forest fires and often occur along a growth ring of a eucalypt tree. The Australian Standard AS 2082 permits 'unlimited' tight gum veins and a limited quantity of loose gum veins. However, the occurrence of such gum veins along growth rings, particularly with back-sawn timber, can be detrimental to the performance of joints fabricated with nailed plates. An example of this was found at one joint of the failed double girder. The recommendation here is that for critical trusses, special inspection procedures should be adopted so as to ensure that gum veins do not occur at critical locations such as at heel joints.
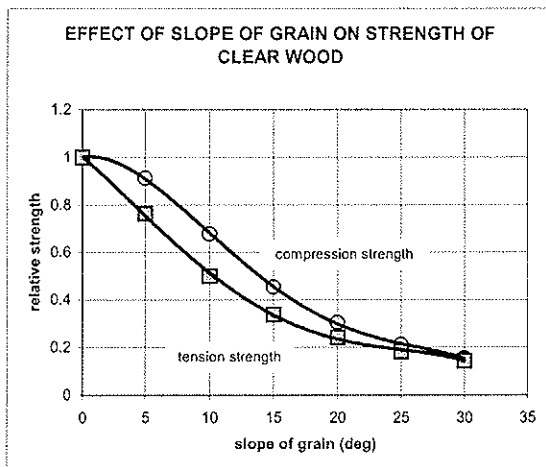
Figure 5. Effect of slope-of-grain on the strength of clear wood specimens (Forest Products Laboratory 1999).
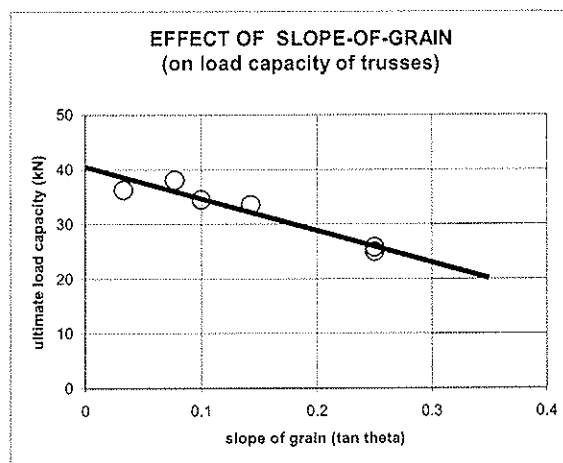
Figure 6. Effect of slope-of-grain of the top chord on the load capacity of a truss (Leicester 1976).

3. PLATE LIFT-OUT

3.1 The Problem

Following the collapse of the clubhouse truss and the consequent issuance of a Workplace Hazard Alert, one of the authors of this paper (J. Goldfinch) was commissioned to inspect the condition of several existing roof truss systems. To do this, sections of the roof were removed so as to gain viewing access to the heels of trusses. One disturbing feature noted was the lift-out of nail plate teeth.

In particular, severe plate lift out was noted in a series of 10 year old retirement home complexes, located along south-eastern Australia. Common features of these buildings were the use of seasoned pine, a common brand of 1.2 mm thick nail plate, low pitch trusses of about 10 m span and unsarked tile roof systems. In one complex it was noted that about 30% of the residential buildings had a lift-out at the heel joint exceeding 3.0 mm. If the lift-out exceeded 1.6 mm, remedial action was proposed, usually by repressing the plates, and then if necessary screwing plywood coverplates over the joint. However, often this could not be done because of excessive relative in-plane slip between the top and bottom chords; in such cases, the whole truss was replaced. For one particular meeting hall it was found necessary to replace 12 out of the 18 trusses for this reason. The bill for the upgrade of the trusses of these retirement complexes is expected to be $5–10 million, or more. Although this case study concerns an exceptionally poor performance and also the buildings concerned are associated with a nail plate that is no longer in use, nevertheless, the results are a wake up call to examine the phenomena of nail plate lift-out.

3.2 The Reasons for Plate Lift-out

Three types of lift-out observed are shown in Figure 7. The straight lift-out of a plate, shown in Figure 7(a) may be due to inadequate pressing, construction handling or just possibly to some as yet unknown moisture cycling effects. The convex plate "bounce back" as shown in Figure 7(b) is often the result of using timbers such as slash pine which have marked differences between early wood and latewood densities. The loss in joint strength due to this effect has been studied extensively (Mackenzie and McNamara 1994) and due allowance for this effect has been made in truss design procedures since about 1994.

The peeling effect as shown in Figure 7(c) is similar to that observed in a short term tension test to failure. It has also been observed in long duration tension tests where it is due to mechano-sorptive effects. Since these effects can lead to long duration failure, they have important practical implications, and will be considered further.

(a) plate pulls straight out

(b) plate "bounce back" to convex shape

(c) plate peeling at the edges
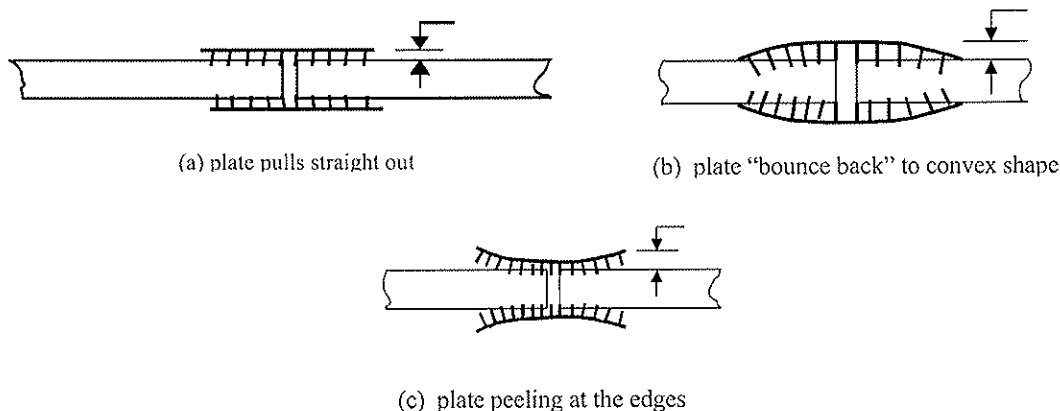
Figure 7. Observed types of plate lift-out.

3.3   Mechano-sorptive Effects

Long duration deformations of nail plate joints, subjected to tension loads under "natural" climate conditions of a shed in Melbourne, Australia have been described in a previous paper (Leicester and Lhuede 1992). Some of this data is reproduced in Table 2 and Figure 8 for the case of joints fabricated with seasoned radiata pine. It shows the nature of mechano-sorptive creep. In this data, the term "relative load" is used to denote the ratio between the applied load and the ultimate strength of a joint.

From Table 2 it is seen that for these plates, the relative creep deformation at 10 years is probably constant up to a relative load value of about 0.25. From another paper (Leicester *et al.* 1979), it can be estimated that the relative load value for failure at 10 years is about 0.4–0.7 for joints fabricated with seasoned softwood timber. Hence it may be postulated that the relative creep after 10 years is given as shown in Figure 9.

It can be shown that for a joint using nail plates evaluated according to AS 1649 and designed to be used as part of a truss system to support a tile roof, the ratio of the applied dead load to ultimate connector strength is about 0.3. This means that any unintended overstress on such a connector system will cause it to be operating in the high creep deformation regime, a situation that can lead to premature failure.

Some of the matters that can lead to an overstress are as follows:

(a)   The nailed plates are misplaced, so that one side of a joint is overstressed. An overstress by about 30% from this cause would not be unusual.

(b)   The nailed plate is evaluated incorrectly. Figure 10 shows data for the same nailed plate evaluated independently by three truss companies in Australia. It is noted that there is a spread of 30% in the assessed lower tail of the data. Some of these differences are probably due to differences in the sources of seasoned radiata pine used for these tests.

(c)   As shown in Figure 8, the effect of a wind on the joint can considerably increase the deformations obtained, due to the increased drying for each humidity cycle. This is likely to occur near the heel of a truss in an unsarked roof, particularly if the heel is located above an open wall cavity.

Information from North American sources is that the phenomenon of plate lift-out is rare and is known to occur only where moisture venting into a roof space is known to occur. The general absence of the phenomenon in North America may be due to the fact that most roofs there are sarked.

Table 2. Relative creep of plated joints after nine years under dead loads
(after Leicester and Lhuede 1992)

Spec. No.*	Load**	Deflection after nine years***	Residual Strength**
1	0.2	12.3	0.74
2	0.2	9.3	0.85
3	0.2	13.8	0.91
4	0.2	12.1	0.76
5	0.3	23.0	failed at 9 years
6	0.3	16.7	0.58
7	0.3	12.1	0.75
8	0.3	13.5	0.66

*   Sanford plate, dry radiata pine timber.
**   Relative to initial short duration strength
***   Relative to initial deflection
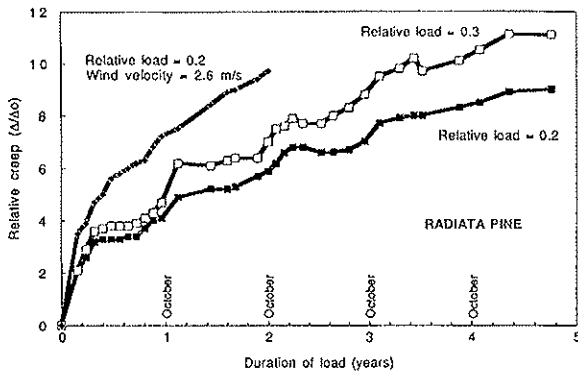
Figure 8. Measured deformations of Sanford plate.
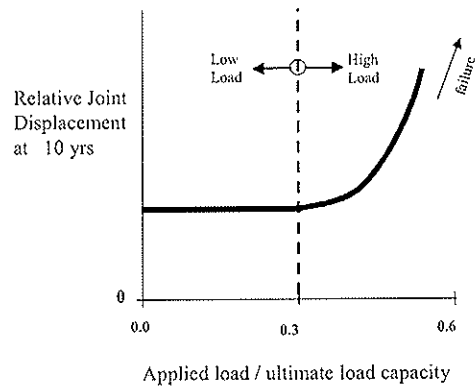
Figure 9. Schematic illustration of the effect of level of the applied loads on the deformation of toothed nail plate connector joints after 10 years.
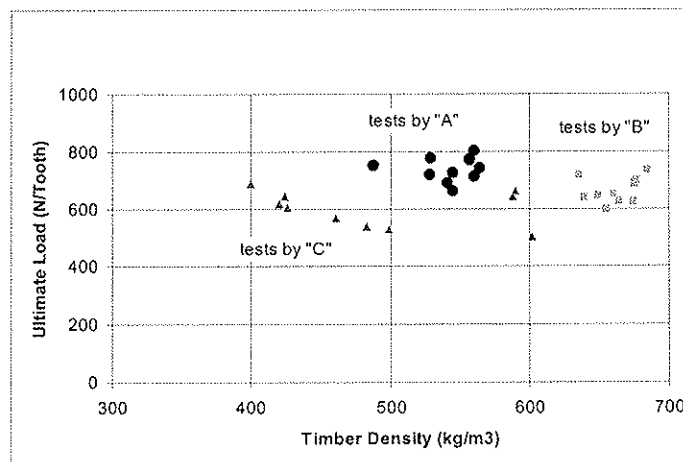
Figure 10. Test data obtained by three truss companies in the evaluation of the same nailed plate.

4. RECOMMENDATIONS

On the basis of the investigations described herein the following recommendations can be made for the design and fabrication of nail plated timber trusses that are intended for use as critical structures:

- The strength of heel joints should be assessed by direct laboratory tests to ensure that the correct failure mode is considered.

- For girder trusses loaded on the tension chord, a formal engineering analysis for the design of the system to laterally restrain the top chord should be undertaken.

- Special quality control checks should be undertaken to ensure that local slope-of-grain, brittle heart and gum veins are not present at connector plate locations.

- Heel joints should be designed so that the dead load in service does not exceed 0.15 of the short duration ultimate strength of the joint.

5. REFERENCES

Enjily,V. and Whale, L. (1994). The Performance of Trussed Girders Under Eccentric Loading. *Proc. Pacific Timber Engineering Conference*, Gold Coast, Australia, July, 496–509.

Forest Products Laboratory (1999). Wood Handbook–Wood as an Engineering Material. Technical Report FPL-GTR-113. Forest Products Laboratory. Forest Service, USDA, pp4–28 to 4–30.

Leicester, R.H. (1975.) Design of Bracing Systems for Timber Structures. *Proc. 17th Forest Products Research Conference*. Melbourne, Australia, Paper 1/31, May, 6 pages.

Leicester. R.H. (1976). Load Tests on Trusses with Lateral Restraints. Laboratory Report. Division of Building Research, CSIRO. Melbourne, Australia, 12 pages.

Leicester. R.H., Reardon, G.F. and Shuster, K.B. (1979). Toothed-Plate Connector Joints Subjected to Long Duration Loads. *Proc. 19th Forest Products Research Conference*, Melbourne, Australia, Paper 2/11, 7 pages.

Leicester. R.H. and Lhuede, E.P. (1992). Mechano-sorptive Effects on Toothed Plate Connectors. *Proc. IUFRO S.502 Meeting*, Bordeaux, France, August, 7 pages.

Mackenzie, C. and McNamara, R. (1994). Basic Working Loads for Truss Plate Connectors in Pinus Elliotti (Slash Pine). *Proc. Pacific Timber Engineering Conference*, Gold Coast, Australia, July, 2, 370–378.

Paevere, P.J., Leicester, R.H., Syme, M., Seath, C.A. and Banks, R. (2002). Investigation Into the Collapse of the Roof Structure at the Riverside Golf Club, Westlakes, Adelaide. CSIRO Internal Report BCE Doc. 02/161, June 80 pages.

Standards Australia (2000). AS1720.1–1997 Timber Structures. Part 1: Design Methods. Standards Australia, Sydney, Australia, incorporating Amendment Nos 1 & 2, 180 pages.

Standards Australia (2000). AS2082 Timber – Hardwood – Visually Stress-graded for Structural Purposes. Sydney, Australia, 49 pages.

Standards Australia (2001). AS1649 Timber – Methods of Test for Mechanical Fasteners and Connectors–Basic Working Loads and Characteristic Strengths. Sydney, Australia, 35 pages.

INTERNATIONAL COUNCIL FOR RESEARCH AND INNOVATION IN BUILDING AND CONSTRUCTION

WORKING COMMISSION W18 - TIMBER STRUCTURES

MONITORING LIGHT-FRAME TIMBER BUILDINGS:

ENVIRONMENTAL LOADS AND LOAD PATHS

I Smith
Y H Chui
University of New Brunswick

G McClure
G Doudak
McGill University

T Stathopoulos
Concordia University

M Bartlett
University of Western Ontario

M Mohammad
Forintek Canada Corp

CANADA

B Kasal
North Carolina State University

USA

G Foliente
P Paevere
CSIRO

AUSTRALIA

Presented by: Ian Smith

Ian Smith made the presentation on behalf of 10 authors in 7 institutions in 3 countries. He began by stating that the design of timber structures is basically subjective although the intention is to move towards a more performance/probabilistic approach. To be able to do so it is necessary to have synchronous data from full-scale timber structures which are complex. He went on to describe the various wooden buildings being monitored. The overall aim of the exercise is to achieve better design codes and rules leading to better building performance. He went on to inform participants of the expected project outcomes and technical challenges. The presentation was followed by an interesting discussion on the purpose, possible outcomes and implications for design of timber structures.

Monitoring light-frame timber buildings: Environmental loads and load paths

Ian Smith and Ying Hei Chui, University of New Brunswick, Canada
Ghyslaine McClure and Ghasan Doudak, McGill University, Canada
Ted Stathopoulos, Concordia University, Canada
Mike Bartlett, University of Western Ontario, Canada
Mohammad Mohammad, Forintek Canada Corp, Canada
Bo Kasal, North Carolina State University, USA
Greg Foliente and Phillip Paevere, CSIRO, Australia

Abstract

To date there has been little recognition of the need for systemic approaches toward structural analysis, design and fabrication of light-frame timber buildings. This paper discusses the strategy, method and progress of an integrated series of studies aimed at rectifying this deficiency. Three typical Canadian light-frame buildings are being monitored to determine environmental forces applied to them and how those forces flow from surfaces over which they are applied to the foundation. Experimentation is synergistic with, and linked to, laboratory studies and whole-building finite element modelling. Long-term goals are improved wind load design code provisions, development and validation of design level methods for sizing components of superstructures. When this was written, a pilot project had already proven the feasibility of real-time monitoring of light-frame buildings.

1   Introduction

Surprisingly few timber buildings have been tested at real-scale, even under laboratory conditions, with none (prior to now) having been studied systematically *in-situ* under the action of real environmental loads. This is despite much evidence that low-rise timber buildings are vulnerable to extreme storm and seismic events. Such buildings accounted for 65% of insured property damage from the 1994 Northridge earthquake, and 70% of insured damage from Hurricane Andrew in 1992 [1,2]. It has been estimated that between 1983 and 1995 world-wide economic losses due to wind and earthquake events were US$ 230 billion [3], with the majority attributed to hurricanes and tornadoes. Despite the huge sums involved and associated human suffering, negligible research has been oriented toward mitigation of damage to low-rise construction of any type.

1.1   General considerations

Ability to predict, at the design stage, whether any buildings will be safe and serviceable depends on:

- adequacy of knowledge about loads that may be experienced,
- ability to predict how loads will flow through the building and into components, and
- reliability of measurements of acceptable performance.

If knowledge is deficient on any of these counts, structural design calculations cease to be extrapolation tools and merely become means of proving comparative acceptability of alternative solutions.

Many gravity loads on buildings are known to quite high precision because geometry, construction materials and contents/occupancies are all well defined. Environmental loads like those due to storm flooding, rain and snow can be predicted in statistical terms with moderate precision, by extrapolating well documented evidence of historical events. For example, the likely maximum depth of snow on ground adjacent can be estimated reliably for a given return period indicating probability of occurrence. This presumes climatic conditions can be extrapolated from the past to the future over human time scales. Prediction of design snow loads on roofs is however less precise because buildings themselves influence snow accumulations. Environmental loads due to wind, and events like earthquakes can also be predicted within a statistical framework, but even less reliably than snow loads on roofs. Design level predictions of wind pressures on buildings are based on statistical estimates of likely peak wind speeds, physical relationships between wind speeds and pressures, and field or, primarily, wind tunnel determinations of pressure coefficients on building surfaces. The same general caveats as for the depth of snow on the ground apply. Pressure coefficients reflect generic or specific building shapes and surrounding terrain conditions. Overall, it is fair to say that design estimates for natural loads on buildings are less precise than might commonly be supposed.

By intent light-frame timber buildings provide dispersed redundant structural support to loads. Once complete, light-frame superstructures behave as an assembly of ribbed plates that are folded, interlocked and have openings. They do not behave as frameworks of ribs without plate elements attached, even though this is a dominant design presumption. It is very difficult to define what are the structural components, and what are the non-structural components, as confirmed by testing [4]. Complexity of modern building shapes combined with structural redundancy makes intuitive understanding of load carrying mechanism very difficult, or impossible. It is very difficult, for example, to say exactly what parts of systems attach roofs to walls or walls to the floors or foundations, or to assess attenuation of dynamic wind loads transferred to foundations. Design decisions about mass or load proportioning are also very difficult. It follows that predictions of forces in components are unreliable.

Building regulatory regimes in western countries do, or will soon, mandate structural design procedures requiring all buildings to be constructed in such a way that they have objectively measurable satisfactory performance [5]. Implementation is via what have become known as *performance-based building codes*, applicable to small buildings (those traditionally designed on the basis of prescriptive rules) and large buildings (those traditionally designed applying engineering principles). Performance-based codes lay down what a building system is to achieve in terms of either building physics or structural behaviour, rather than the old 'just do it like this' approach. For example, in Canada the new generation of building codes will require satisfaction of certain performance objectives. When fully developed and implemented new codes are intended to lead to great efficiencies in consumption of materials, and construction and operating costs based on life-cycle/environmental footprint considerations. In order to achieve this there must be changes to government regulations and development of new construction technologies (including design methods). Many national and international bodies are working toward establishment of suitable performance criteria and objectives. Little is being done to develop new structural design tools.

2

It follows from the above that neither loads on light-frame buildings, nor how they distribute those loads creating forces in members is well understood. Therefore, it is unclear how safe and serviceable light-frame buildings are, and impossible to say in what ways their structural performance can be improved. This is not said in order to alarm, but because recognition of the status quo is the starting point for improvement.

The remainder of this paper outlines a multi-institutional effort aimed at:
- improving knowledge of environmental (wind and snow) loads on typical low-rise buildings (under Canadian conditions),
- correlating field observations of wind loads with those expected on the basis of wind tunnel tests,
- measuring forces and deformations in test buildings and correlating them with applied loads, and
- developing numerical, and other, whole-building structural models (methods for extrapolating results beyond findings for the specific test buildings).

2   Related work on full-scale testing

Historically structural tests have focussed on determining the behaviour of isolated members, connections or subsystems. Therefore, behaviour is understood best for artificial situations, i.e. those that isolate elements from the context in which they are used. Although this simplifies testing, it severely hinders application of results. Countering this there is an emerging acceptance that performance of whole buildings can only be reliably assessed via full-scale tests [6-8].

2.1   Wind pressures on buildings
Texas Tech University has performed tests on buildings with flat and pitched roofs to determine wind pressures on surfaces [9]. A recent innovation is a house on flat terrain that sits on a turntable and can be rotated relative to the prevailing wind direction to observe how that influences pressure coefficients. Comparison of 1:100 scale and 1:50 scale measurements with real scale suggests that scaling effects on pressure measurements can be accounted for in a reliable manner. Current focus is local concentrations of pressures.

It is understood that the Florida Department of Community Affairs has launched the Florida Coastal Monitoring Project in collaboration with Clemson University, to monitor wind speed, and pressures on roofs, walls, in attic spaces and interior rooms, of ten houses. The main project objective is collection of data during hurricanes or other high-wind events.

2.2   Full-scale tests
The Cyclone Structural Testing Station at James Cook University in Australia has carried out tests on eight houses [4,10]. Although houses were constructed outdoors, loads were artificial with suction pressures simulated using Wiffle-tree arrangements. The objective was to determine whether similar houses are likely to have adequate performance under certain design wind speeds. Findings confirmed acceptability of performance of the structures and that stiffening effects of secondary (nominally non-structural) elements such as wall linings, ceilings and roof tiles can be considerable. No attempt was made to explain realistic load paths. More recently, CSIRO in Australia has carried out a test on a single-storey house in partnership with North Carolina State University. An L-shape plan was adopted to promote

torsion through the height of the system whatever the load arrangement. The building was subjected to series of non-destructive tests prior to final destructive testing. Reaction forces beneath all walls were measured. The CSIRO/NCSU experiment is the most accurately documented work so far [11]. The main purpose and value of the study is that it furnished the most comprehensive existing data for verification of whole-building models.

Clemson University has performed destructive tests on sixteen houses in coastal South Carolina [12]. The light-frame houses represented a range of ages (from about 5 to 50 years old: constructed between 1950 and 1996), sizes, styles and construction materials. Individual components, roof and wall sections were loaded artificially (e.g. by crane, suction box) to assess residual capacities in 'as built' and retrofit conditions. Whole buildings were not loaded. Although in a broad sense testing was similar to what can be done in a laboratory, boundary conditions tended to be more realistic. The data is aiding decisions about likely performance of similar construction under cyclone winds.

Texas Tech University has carried out experiments to assess capability of mobile homes to resist simulated hurricane force winds [9]. The 'wind' was generated by the propellers of a military transport aeroplane. Even though tests were unrealistic with regard to airflow characteristics they gave confidence in that strong winds can be resisted if mobile homes are adequately anchored to the ground.

Comprehensive overviews of whole timber building test can be found elsewhere [13,14].

3   Research strategy

Any holistic analytical capability relies on harmonious marriage of testing and modelling capabilities. Even accepting this it may not be obvious why it is sometimes necessary to test buildings in full-size. With timber it is impossible to use scale models in a manner that produces sensibly consistent effects on a number of physical and mechanical characteristics. Apart from wood materials themselves, mechanical joints cannot easily be scaled with regard to both strength and stiffness. Most importantly in many circumstances, effects of moisture gradients cannot be scaled.

Full-size building tests within laboratories are by definition of realistic size but often represent stripped-down construction. They employ artificial loading that may or may not be far from realistic. Whether loading is pushing and pulling (cyclic loads), or just pushing or pulling (static loads), structural modification is nearly always necessary to avoid force/stress concentration and localised damage of specimens. Modifications can quite considerable affect responses of specimen creating unrealistic failure mechanisms. Even though the importance of this can be debated, the basic premise that artificial loading produces some degree of artificial response cannot. *In-situ* full-size tests can have various characteristics, but for the purposes of this paper, *in-situ* (or field) tests are taken to be those done at realistic size with realistic construction, and involving real or very realistic loads. Full-size tests done *in-situ* are the only ones that can fully account for effects of construction details, physical environment, moisture movement, loading and ageing processes.

Following from the above, the strategy in research discussed in this paper is to carry out experiments on fully finished and full-realistic light-frame timber buildings, and to observe the responses of those building to natural environmental loads. The implication of this is that

loads applied to buildings and their structural response must be monitored simultaneously. In Canada the reliably available natural loading scenarios are winter snowfalls, and wind storms in autumn and spring seasons. These are therefore of primary interest to most of the authors, and the only natural loads anywhere that can be counted on to occur within a finite project. There is no intent or expectation that buildings will fail during the project, and they are expected to remain serviceable following completion of experiments. *In-situ* monitoring activities intertwine synergistically with development of numerical whole-building models, wind tunnel studies and component, and sub-system laboratory tests, Figure 1.
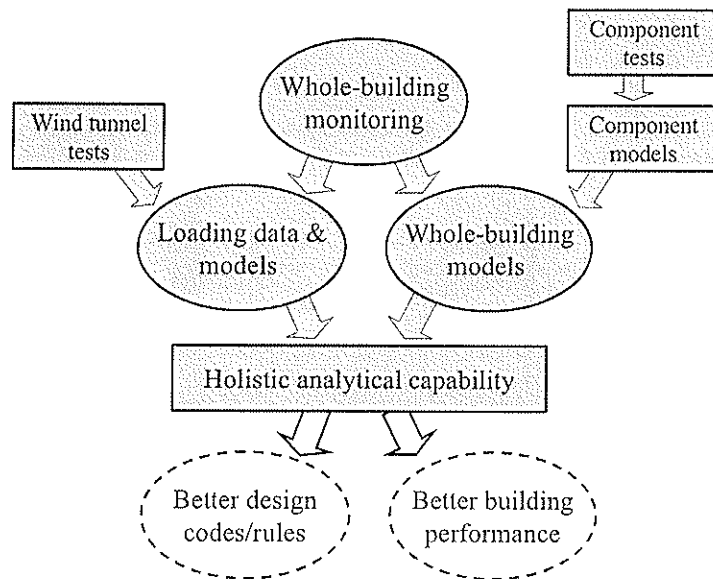
Figure 1 – Research strategy

As test buildings should never be damaged to any measurable extent, *in-situ* tests will only procure data about (and verify whole-building models for) response at low load-levels. Although this may raise concern about usefulness of results, in the context of failure predictions, the authors contend such concern is unnecessary. The key concept supporting this contention is that failure processes in structural systems always initiate on the local or subsystem level. Coalescence of local failures and their unstable propagation, to cause catastrophic whole-system failure, occurs well beyond the original strength impairing event(s) that engineers aim to prevent. The most important thing to know is the force and/or deformation along boundaries of subsystems or components. With this information in hand it is possible to predict quite easily failure behaviour of subsystems or components. Subsystem failure mechanisms are best studied via relatively simple and inexpensive testing and analysis of their behaviour in isolation (under well defined boundary force and restraint conditions). As an analogy, local failure determines the capacity of a very large notched glued-laminated timber girder. It is well accepted that simple fracture mechanics tests and theory are all that is needed to predict capacity, because most of the girder functions as a simple lever arm.

4   Preliminary project

A single storey industrial shed building in Sainte-Foy, Quebec, Canada was monitored to determine its displacement response to environmental (wind and snow) loads (Figure 2). Displacements were correlated with real-time estimates of environmental loads. Observations encompassed deformation of a continuous strip of the wall and roof. Artificial (static)

distributed and point loads were also applied to the structure to enhance understanding of how structural components interact. Limited finite element analysis was conducted for the rib stiffened roof subsystem and the overall assembly, with good agreement between predicted deformations and those observed under environmental or artificial loads. The global outcome of the monitoring study was that it confirmed theoretical expectations that composite action and load sharing are important mechanisms for light-frame shed buildings. It also proved feasibility of real-time monitoring, and thus opened the way for the main project described below. Some specific findings from the preliminary project are:

- estimates of wind pressures, based on instantaneous observations of wind speed and direction (measured with an anemometer mounted on a tower attached to the building), correlate with observed instantaneous deformations,
- snow loads on a parapet roof are approximately uniformly distributed and produce the same load deflection response as for a uniform water load created by flooding the roof,
- although wall to roof connections are semi-rigid with regard to moment transfer, to a reasonable approximation they can be regarded as pinned,
- tops of walls supporting roof joists spread to a measurable extent under service level gravity roof loads (normal snow accumulations), and
- the roof (plywood sheathing and insulation over wood I-joists at 0.61m centres) acts as a rigid diaphragm for the purpose of distributing wind loads.
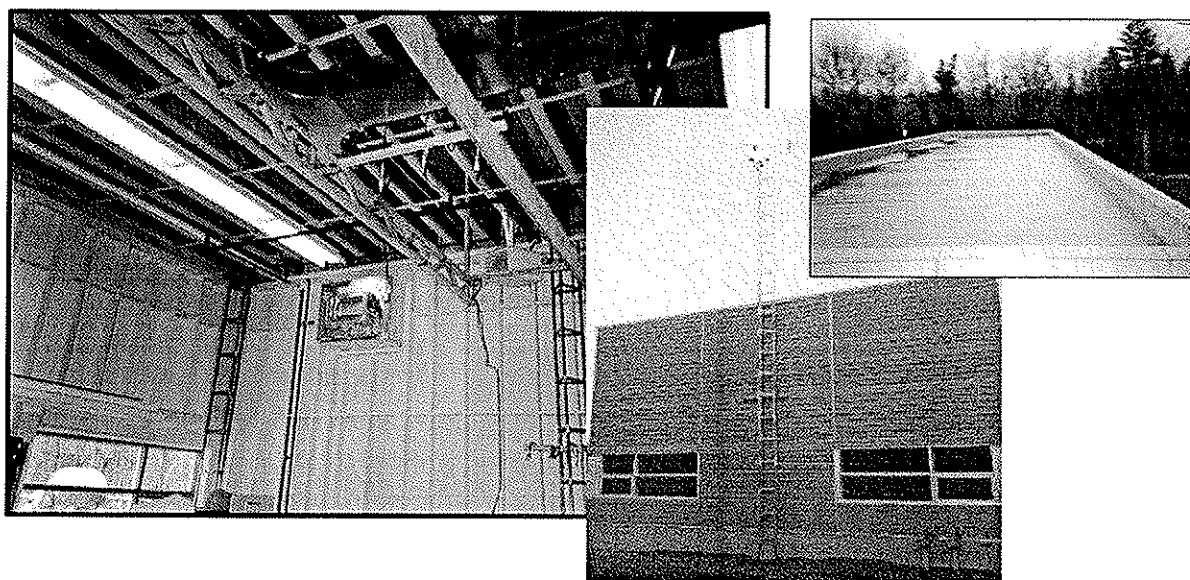
Figure 2 – *Structure 1*: Industrial light-frame building, Sainte-Foy

5   Main project

Three structures are being monitored as a collaborative exercise involving researchers from the universities of New Brunswick, McGill, Concordia and Western Ontario, and Forintek Canada Corp, from Canada; North Carolina State University from the USA; and CSIRO from Australia. The first building is the industrial shed (Structure 1) discussed in the last section. This building is reused because its structural arrangement is well defined making it relatively simple to understand and model. Also, it is immediately available as a test bed for proving test methods and protocols. Structures 2 and 3 are being specially built for the project. Both are variants of typical North American residential construction (single storey bungalow-type

buildings with about 16m x 8m footprints). Regular plan geometry and duo-pitch roofs are preferred because this is the geometry that equates to the standard case in the National Building Code of Canada and similar international documents. Residential buildings incorporate influences from many non-structural components, and their behaviour when complete is complex and difficult to understand and model, making them ideal for proving modelling capabilities. Structure 2 is to be located in Fredericton, New Brunswick, Canada. Figure 3 shows a draft architectural rendition of it. As can be seen, the internal wall openings and the arrangement of internal walls is irregular, which again facilitates verification of modelling capabilities. Structure 3 will be a modified version of Structure 2 and built in a location yet to be determined. Design of the two new buildings based on the so-called platform construction method.
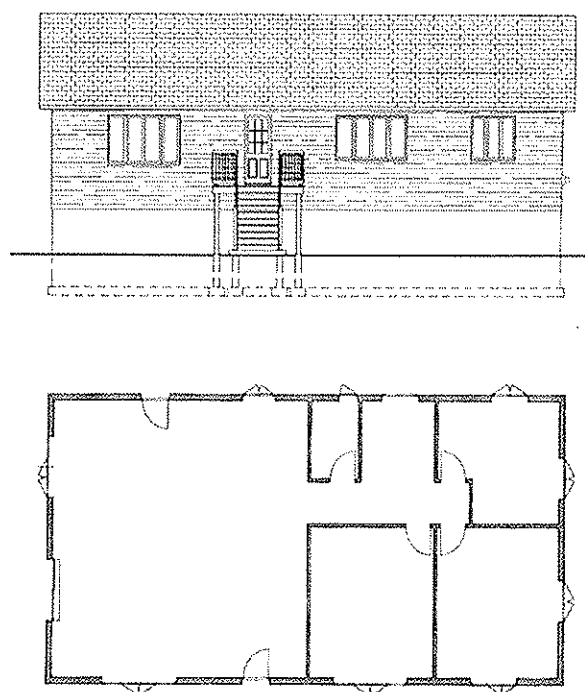
Figure 3 — *Structure 2*: Bungalow, Fredericton

The prime difference between Structures 2 and 3 will be in interfaces between subsystems. Structure 2 will have 'standard' nailed connection details, whereas new, and hopefully improved, details will be designed for the roof-to-wall and wall-to-foundation interfaces of Structure 3. The two buildings will sit side by side on an open field site and therefore be exposed to the same upstream terrain roughness. Care will be taken to avoid any critical interaction between them as far as wind flow is concerned. Matched scale models of structures will be tested in the wind tunnel at Concordia University.

Measurements to be taken for Structures 2 and 3 will include: wind speed and direction, snow load on the roof, internal and external wind pressures on wall and roof surfaces, internal forces at foundation-to-superstructure and wall-to-roof interfaces, and displacements (deflections and distortions) of stud walls and roof trusses. Measurements for Structure 1 are similar, except that there will be no observations of internal forces, because this would involve too much reconstruction. Structures 2 and 3 will be equipped with two series of 3-axis load cells (force measurements: vertically and horizontally parallel to external wall directions). The first series of load cells is to be located at the wall-to-superstructure

interface, i.e. under the floor platform that supports walls, at approximately 2m spacing. These will register the total loads transferred to the foundation. The second series of load cells will be located between roof trusses and supporting walls (trusses will be about 8m span and simply supported on the long external walls). The roof-to-wall load cells will be spaced at about 3m centres. The intents regarding what data will be recorded differ for the two sets of load cells. Apart from giving precise distributions of reaction forces, the lower series will enable the total applied forces to be measured (X, Y, Z or resultant senses). This means, for example, that errors in interpolation techniques for determining wind pressure distributions can be assessed (the buildings will be like giant wind tunnel specimens). The upper series of load cells are intended to provide point observations of forces that can be compared with model predictions. Figure 4 is a schematic rendition of the internal force measuring system for Structure 2.
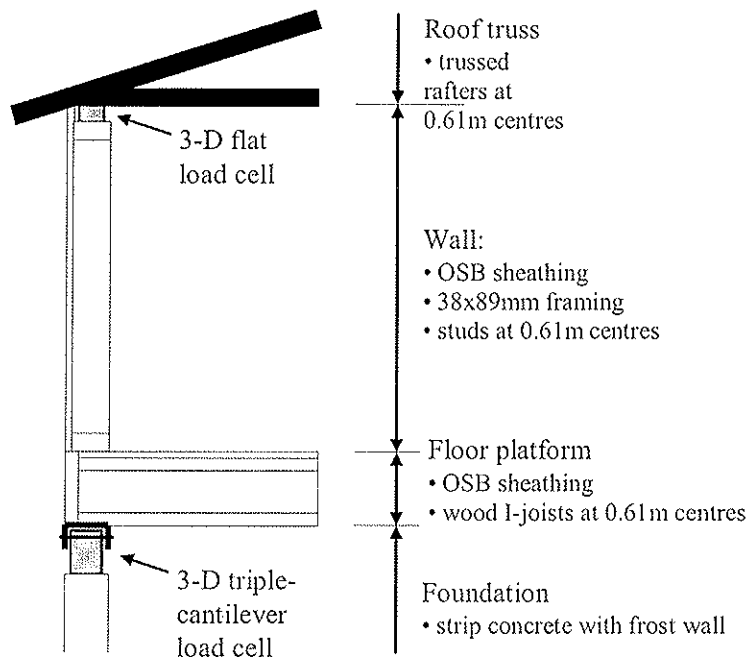
Figure 4 – Schematic of internal force measurements (*Structure 2*)

Apart from 'standard' deformation measuring instrumentation such as LVDTs, it is planned to use fibre optic devices that make possible an essentially infinite number of local strain observations from a single fibre that may be literally miles long.

6 Subsidiary studies

Apart from the *in-situ* monitoring, there are linked activities in progress, including:
- characterisation of properties of materials used to construct Structures 2 and 3,
- subsystem studies involving tests and finite element modelling, with the aim of verifying that flows of forces (load-paths) within walls and other subsystems can be predicted accurately if boundary forces and displacements are known,
- wind tunnel tests, and
- whole-building finite element modelling.

Simulated wind load tests carried out in the boundary layer wind tunnel at Concordia University are of particular importance. These use 1:200-scaled models of the actual buildings that are equipped with pressure taps on the outside and inside. Models must be tested for airflow in each of the principal wind directions, with upstream exposure representative of the upstream terrain roughness in the field. Pressure measurements at each tapping are carried out first to obtain mean and peak values of dimensionless pressure coefficients. These measurements are followed by area-load evaluations by combining the results from a number of taps located inside an area of interest. The approach for linking wind tunnel test data to actual measurements on structures is critical to success of the project. It consists of weighting the measured instantaneous loads on-line with appropriate influence coefficients in order to generate a set of values similar to those obtained in the field, where the actual generalised loads, including those in the foundation will have been measured directly. Several assumptions have to be made regarding the load transfer process, and similarity of the wind tunnel and field results will reveal which are more realistic. Success of this part of the study will have considerable impact on future wind tunnel testing procedures. The same approach will apply for building of other geometry (shape and size) and structural frameworks for which the pressure coefficient data may already be available.

Toward the end of the project emphasis will be placed on developing simplified (design level) analytical models. It is anticipated that design models will include rigid and flexible beams on elastic and inelastic foundations, rigid and flexible plates on elastic and inelastic foundations, spatial frame and possibly other models developed during the course of the research. In order to establish the performance criteria for light-frame wood buildings one must decide on limit states considering all possible failure modes (catastrophic and non-catastrophic). This cannot be done solely through experiments and one must use validated analytical models to simulate probable loading scenarios and building parameters. It is anticipated that relatively simple 3-D models will allow many simulations to be performed.

7   Progress to date

At the time of writing this paper the collaborative activities are 8 months old, with a planned duration of 4 years. Instrumentation has been reinstalled and enhanced for Structure 1, with the primary enhancement being installation of external pressure sensors. Considerable effort has been put into design of Structure 2 itself and its instrumentation system (e.g. design of special load cells, fibre optic strain-measurement trials). Structure 2 is to be built and instrumented by the end of 2003, with data collection commencing in early 2004. Structure 3 is to be built and instrumented in 2004/05. All subsidiary work mentioned in Section 6 has been commenced.

8   Concluding comments

The research discussed here will provide design approaches for wood light-frame construction that can realistically be expected to control structural reliability, especially under wind loads. This is particularly important with the advent of 'performance based design' methods that place emphasis on structures satisfying various end-use related performance objectives. Performance based design is intentionally product neutral. It potentially will wipe away timber's traditional advantage in markets where it has been deemed appropriate based on historical precedent rather than on objective proof of its suitability. Although there is little

doubt that timber will be reaffirmed as an appropriate light-frame building material, the forest products industry and the timber design community needs tools to make the objective proof of this a reality.

Acknowledgements

References

[1] Foliente, G. 1998. "Design of Timber Structures Subjected to Extreme Loads", Progress in Structural Engineering and Materials, 1(3): 236-244.

[2] Grant, R. 2000. "State Farm Insurance Company", Presentation to Technical Advisory Committee, Forintek Canada Corp, Vancouver, BC, Canada.

[3] Smolka, A. 1996. "Lessons from recent natural disasters", *In:* Proceedings of Asia-Pacific Symposium on Structural Reliability and its Applications, Tokyo, 12-14 November 1995. Tokyo: Nanae Corporation. [cited in Foliente 1998].

[4] Reardon, G. and Henderson, D. 1996. "Simulated wind loading of a two storey test house", Proceedings of International Wood Engineering Conference, Louisiana State University, Baton Rouge, LA, USA: 4.313-319.

[5] Foliente, G. C. 2000. "Developments in performance-based building codes and standards", Forest Products Journal, 50(7/8): 12-21.

[6] FPS. 1998. "Recent advances in understanding full-scale behavior of wood buildings", Special Publication 7275, Forest Products Society, Madison, WI, USA.

[7] Mettem, C.J., Bainbridge, R.J., Pitts, G.C. and Enjily, V. 1998. "Timber frame construction for medium-rise buildings", Progress in Structural Engineering and Materials, 1(3): 253-262.

[8] UWO. 2002. "Mitigating housing losses in extreme natural events", Proceedings of Workshop, 2 & 3 December 2002, Toronto, University of Western Ontario, ON, Canada (*on CD*).

[9] Mehta, K. 2002. "Full-scale testing at Texas Tech University", *In:* Proceedings of Workshop, 2 & 3 December 2002, Toronto, University of Western Ontario, ON, Canada (*on CD*).

[10] Henderson, D. 2002. "Experience derived from Australia's Cyclone Testing Station", *In:* Proceedings of Workshop, 2 & 3 December 2002, Toronto, University of Western Ontario, ON, Canada (*on CD*).

[11] Paevere, P., Foliente G.C. and Kasal, B. 2003. "Load-sharing and redistribution in a one-story woodframe building", ASCE Journal of Structural Engineering (Sept, *in press*).

[12] Reinhold, T. 2002. "Development of full-scale in-situ test facilities and experience gained from testing 16 houses in South Carolina", *In:* Proceedings of Workshop, 2 & 3 December 2002, Toronto, University of Western Ontario, ON, Canada (*on CD*).

[13] Doudak, G. 2000. "Monitoring of load paths in a wood structure", Research Report, Department of Civil Engineering and Applied Mechanics, McGill University, Montreal, QE, Canada.

[14] Paevere, P. 2002. "Full-scale testing, modelling and analysis of light-frame structures under lateral loading", PhD thesis, University of Melbourne, Melbourne, Australia.

[15] Kasal, B., Collins, M., Paevere, P. and Foliente, G.C. "Design models of light-frame wood buildings under lateral loads", ASCE Journal of Structural Engineering (*in press*).

INTERNATIONAL COUNCIL FOR RESEARCH AND INNOVATION
IN BUILDING AND CONSTRUCTION

WORKING COMMISSION W18 - TIMBER STRUCTURES

APPLICABILITY OF DESIGN METHODS TO PREVENT

PREMATURE FAILURE OF JOINTS AT SHEAR WALL CORNERS

IN CASE OF POST AND BEAM CONSTRUCTION

N Kawai

National Institute for Land and Infrastructure Management

H Isoda

Building Research Institute

JAPAN

Presented by: Naohito Kawai

Naohito Kawai began his presentation by stating that the objective of the research is to confirm the adequacy of design calculation (empirical and rigid beam) methodologies relating to the prevention of premature failure of joints at shear wall corners. He went on to describe the test specimens used and compared the test data against the predictions from both design methods. In conclusion he stated that both design methods give larger tensile force values than that observed experimentally and although the methods are applicable there are differences which will need to be verified using finite element methods.

Applicability of Design Methods to Prevent Premature Failure of Joints at Shear Wall Corners in Case of Post and Beam Construction

Naohito KAWAI

National Institute for Land and Infrastructure Management, Japan

Hiroshi ISODA

Building Research Institute, Japan

1   Introduction

In a simple method to confirm the structural performance of timber buildings with shear walls against earthquake and wind forces, shear strength of each story in one direction is assumed to be equal to the summation of those of shear walls in the same direction. However, this assumption is available at least when the premature failure of the joints at the corners of each shear wall is prevented.

Some design methods to prevent premature failure have been proposed, and one method was provided in a Notification under the Building Standard Law of Japan in 2000. In CIB-W18 meeting thirty-five 2002, the author introduced these design methods, and reported the comparison between calculation results and test results in case of wood framed construction.

In this paper, the results of series of lateral loading tests are summarized, which were conducted on two one-storied structures and six two-storied structures by post-and-beam construction with plywood sheathed shear walls or braced frames. Next, the calculation results using the design methods are compared with the test results. Finally, the applicability of these design methods to post-and-beam construction is discussed.

2   Design methods

There are some theories and design methods proposed in design manuals for post and beam construction with shear walls or braces, and for wood frame construction in Japan.

2.1   Empirical design method

Equation (1) shows the calculation method to obtain the required tensile strength considering transmitted tensile force from the shear walls on the upper floors. This calculation method was described in a structural design manual for allowable stress design of post and beam construction (HOWTEC 1988).

$$F_{a,i,j} = \sum_{i=k}^{n} \frac{L_{r,i}}{L_{e,i}} \frac{Q_{a,i,j}}{l_{i,j}} \beta_{i,j} h_i - G_{i,j} \tag{1}$$

where, $F_{a,i,j}$ is the tensile force at the bottom joint of shear wall number j on floor number i against the external force for allowable stress design, $L_{r,i}$ is required total effective wall length on floor number i, $L_{e,i}$ is existing effective wall length on floor number i, h_i is the height of the shear wall, $l_{i,j}$ is the length of the shear wall, $\beta_{i,j}$ is a factor considering the effect of restraint by surrounding members, $Q_{a,i,j}$ is the allowable shear strength of the shear wall and $G_{i,j}$ is the vertical load due to fixed load and superimposed load transmitted to the joint.

Effective wall length means the value obtained by multiplying actual wall length and multiplier, which is determined according to the allowable shear strength of the shear wall. The value of $\beta_{i,j}$ is 0.8 for shear wall that reaches the end of building, and 0.5 for others, which was determined empirically by some experimental results.

2.2 Modification considering ultimate state

In the ultimate state, shear force of each shear wall reaches the ultimate shear strength even if the total length of existing shear walls are far larger than required length. Equation (2) gives the required tensile strength in ultimate state not only for posts at shear wall end but also for posts between shear walls.

$$F_{u,i,j} = \sum_{i=k}^{n} \left| \frac{Q_{u,i,j}}{l_{i,j}} - \frac{Q_{u,i,j-1}}{l_{i,j-1}} \right| \beta_{i,j} h_i - G_{i,j} \tag{2}$$

where, $F_{u,i,j}$ is the tensile force at the bottom joint of shear wall number j on floor number i against the external force in the ultimate state, $Q_{u,i,j}$ is the ultimate shear strength of the shear wall and others are same as equation (1).

If the ratio between the ultimate strength and the allowable strength of shear wall is almost equal to that of joint, then equation (2) can be modified to the expression of allowable strength as Equation (3) by dividing both members by the ratio R. This equation is used in revised structural design manual for post and beam construction (HOWTEC 2001), and was also used as the bases of a provision of Notification No. 1460 in 2000 under the Building Standard Law of Japan.

$$F_{y,i,j} = \sum_{i=k}^{n} \left| \frac{Q_{y,i,j}}{l_{i,j}} - \frac{Q_{y,i,j-1}}{l_{i,j-1}} \right| \beta_{i,j} h_i - \frac{G_{i,j}}{R} \tag{3}$$

2.3 Rigid frame model

In a structural calculation manual for wood frame construction (Japan 2×4 builders association 2002), rigid frame model has been used to calculate the tensile force of joints at the bottom of shear wall end. In this paper, this method is not discussed as it is not usually applied to post and beam construction.

2.4 Precise model with rigid beam assumption

In the revised structural manual for houses with post and beam construction (HOWTEC 2001), equations (3) and (4) are proposed, based on the study by Inayama et al. (2001).

$$F_{a,1,i} = \frac{Q_{a,i-1}h}{2l_{i-1}} - \frac{Q_{a,i}h}{2l_i} - \frac{G\{l_{GL}L_L - L_{LR} - l_{Ri}(L_R - nl_{GR})\} + \left(\frac{h}{2} + h_u\right)(L_R - nl_{Ri})\sum Q_a}{L_L L_R - nL_{LR}} \tag{3}$$

$$F_{a,2,i} = F_{a,1,i} - \frac{Q_{a,i-1}h}{l_{i-1}} + \frac{Q_{a,i}h}{l_i} \tag{4}$$

where, $F_{a,1,i}$ is the tensile force at the bottom joint and $F_{a,2,i}$ is the tensile force at the top joint of the post number i, n is the number of posts, $Q_{a,i}$ is the allowable shear strength of the shear wall, h is the height of the shear wall, $\sum Q_a$ is summation of $Q_{a,i}$, l_i is the length of the shear wall, G is the vertical load due to fixed load and superimposed load transmitted to the upper beam, l_{GL} and l_{GR} are the distance between the vertical load G and left end post and right end post, l_{Li} is the distance between post number i and left end post, l_{Ri} is the distance between post number i and right end post, L_L, L_R and L_{LR} are;

$$L_L = \sum_{i=1}^{n} l_{Li} , \quad L_R = \sum_{i=1}^{n} l_{Ri} , \quad L_{LR} = \sum_{i=1}^{n} (l_{Li} l_{Ri})$$

and h_u is the height of centre of external forces applied to the upper floors, as;

$$h_u = \frac{\sum_{i=k+1}^{m} Q_i h_i}{Q_k} \tag{5}$$

where, Q_k is the shear force generated in the said storey number k, Q_i is the shear force generated in the storey number i, h_i is the height of the storey number i.

Equations (3) and (4) are derived for the model as shown in figure 1, using assumptions that upper beam behaves as a rigid body, and that all the joints at the top and bottom of posts are in elastic behaviour and have the same stiffness.
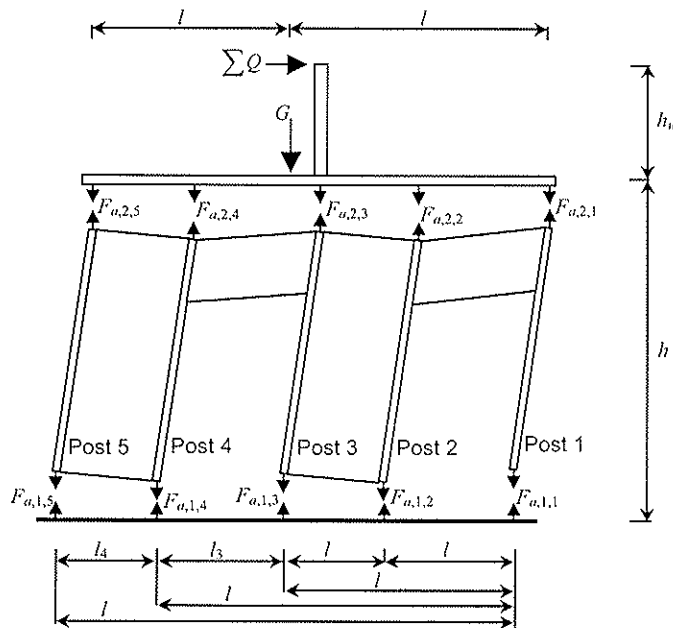
Figure 1   Precise model with rigid beam assumption (in case n = 4).

3

3 Experimental Results

3.1 Test method

3.1.1 Specimen

To study the applicability of the calculation and design methods mentioned above, cyclic loading test was conducted on two one-storied structures and six two-storied structures by post-and-beam construction with plywood sheathed shear walls or braced frames. Figure 2 shows the types of specimens, and Figure 3 shows configuration of representative two types of specimens. Table 1 shows the specification of members and fasteners.

Table 1. Specification of Members and Fasteners

Member or Fastener	Size (mm)	Species or Standard, etc.
Post	105*105	Pine (*Pinus sylvestris*)
Sill	105*105	Pine (*Pinus sylvestris*)
Beam	105*180	Pine (*Pinus sylvestris*)
Brace	105*30	Hem-fir
Plywood	t=9	JAS Class 1 (Hardwood)
Nail on plywood	l=50, d=2.75	JIS N50 @150
Plate at Brace End	t=2.3	Hexa-plate (Tanaka Co. Ltd)
Hold-down Fastener	t=6	25kN Type with 5 lugscrews (d=12)
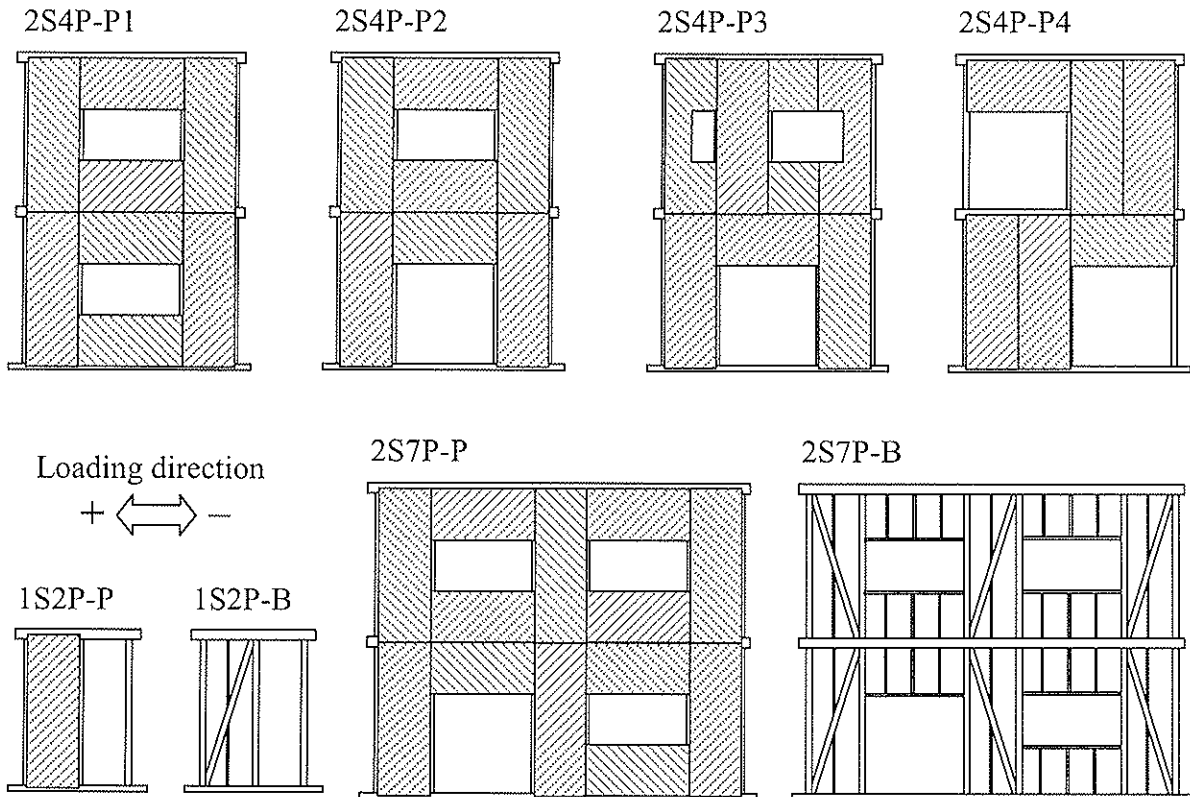
Figure 2. Types of structures tested.

4
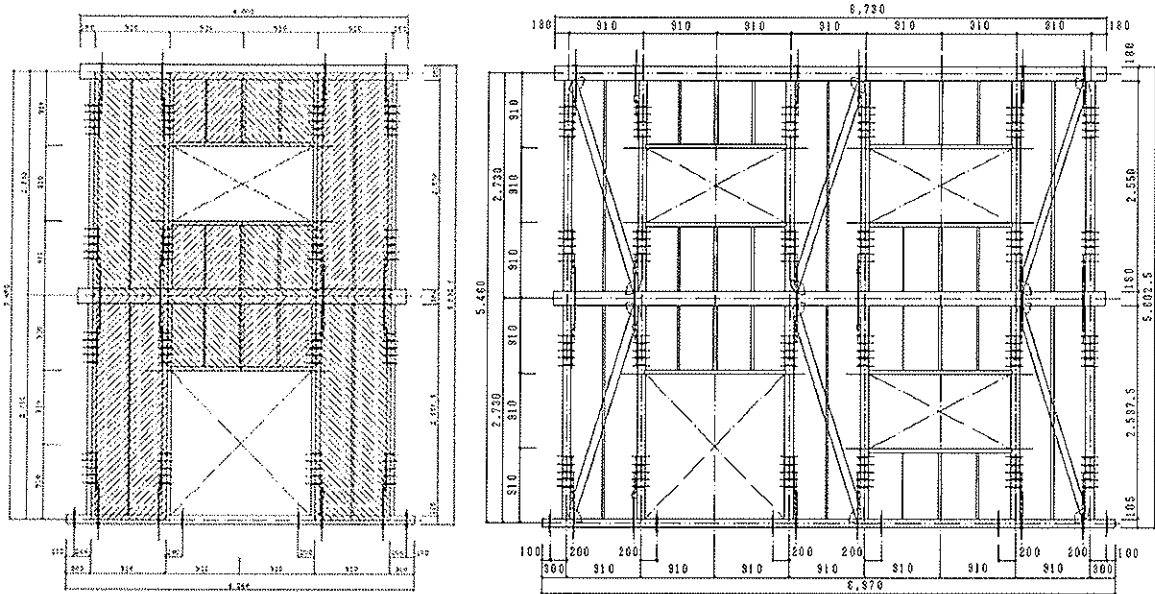
Figure 3.   Examples of configuration of the test specimens (2S4P-1, 2S7P-B).

3.1.2   Testing methods

Lateral loads were applied to the loading beams of both storey using oil jacks, with keeping the ratio of the second storey displacement to the first storey displacement as 1.4, which was determined considering distribution of seismic force for ordinary two-storey houses. Figure 4 shows the loading protocol. Displacement of each point was measured by LVDT, and the tensile force of each hold-down bolt was measured using centre-hall type load cell.
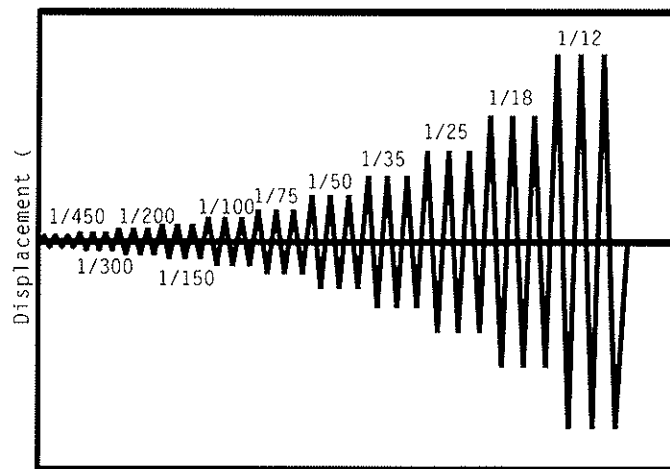
Figure 4.   Loading protocol.

3.2   Test results

Table 2 shows the observed properties of first storey and Figure 5 shows the examples of observed load-displacement curves of both stories.

Table 1.   Summary of test results – properties of first storey

Specimen	Loading direction	P_y (kN)	K (kN/mm)	P_{max} (kN)	D_{max} (mm)	μ
1S2P-P	+	6.35	0.39	11.3	108.6	6.07
	−	6.60	0.32	10.8	106.8	4.67
1S2P-B	+	6.74	0.31	12.5	68.7	3.97
	−	6.14	0.19	11.4	140.0	2.74
2S4P-P1	+	16.55	1.13	31.9	103.8	6.38
	−	19.86	1.01	31.5	74.5	5.21
2S4P-P2	+	17.11	1.04	30.3	107.9	7.21
	−	14.11	0.83	24.2	73.4	5.73
2S4P-P3	+	13.64	0.70	24.8	74.9	4.36
	−	15.87	0.93	27.6	72.7	4.06
2S4P-P4	+	15.74	0.47	22.8	52.8	2.51
	−	9.45	0.56	14.9	75.1	6.20
2S7P-P	+	29.59	1.88	50.4	76.9	4.84
	−	22.93	2.31	41.8	53.0	6.61
2S7P-B	+	15.19	0.87	28.3	76.9	6.03
	−	14.50	1.00	26.7	66.3	6.07

a) 2S7P-P

b) 2S7P-B
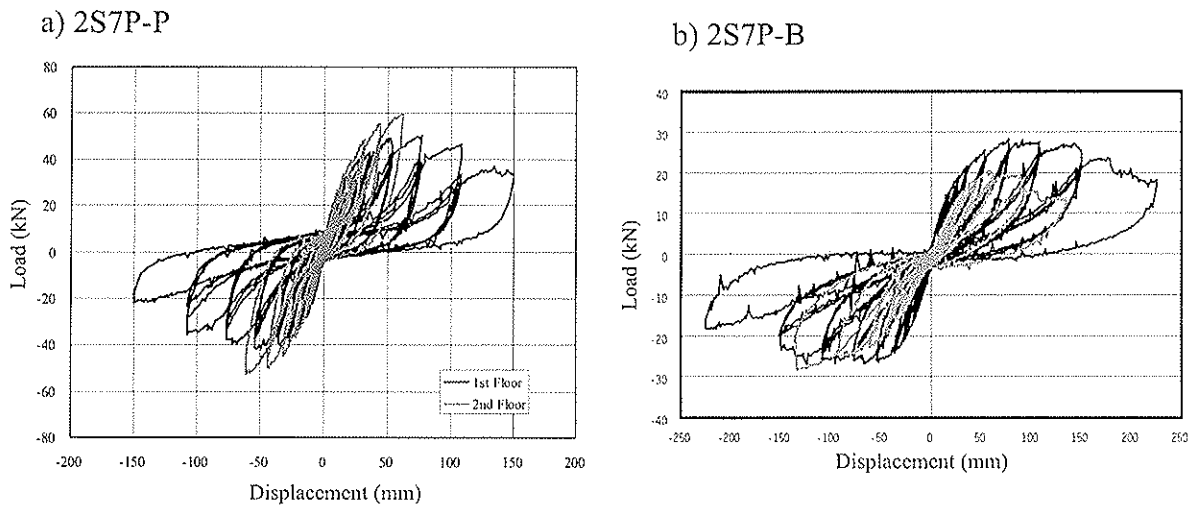
Figure 5   Examples of load-displacement curves.

4   Comparison of test result and design methods

4.1   Calculation of tensile force of joints

To discuss the adequacy of the design method mentioned above, tensile forces of joints at bottom corners of shear wall test specimens were calculated according those method, i.e.;

- Method 1: using empirical factor of 0.8 and 0.5 (see 2.1 and 2.2),
- Method 2: precise model with rigid beam assumption (see 2.4),

at the shear deformation angle of first storey of 1/120 radian, which is near to or a little beyond the yield strength .

To apply these methods to the test specimens, first, we picked up the value of shear force of each storey of each specimen, when the shear deformation angle of the first storey reached 1/120, and assuming the distribution of shear force. For the specimens with plywood, the distribution of shear force was calculated based on the equation of shear strength for perforated shear walls, which is described in a structural calculation manual for Japanese wood frame construction. For the braced frames, the distribution was calculated using the ratio of the shear strength of compression side to the tensile side observed in the one-storied specimen (1S2P-B) at the shear deformation of 1/120 radian.

Figure 6 shows the assumed distribution of shear force for all specimens at the shear deformation of the first storey of 1/120. These shear force were used for the calculation of tensile force of joints using Method 1 and 2 mentioned above, instead of actual yield strength. In this study, the effect of suspended wall and waist-high wall is considered using this assumption of distributed shear force, for both Methods 1 and 2.
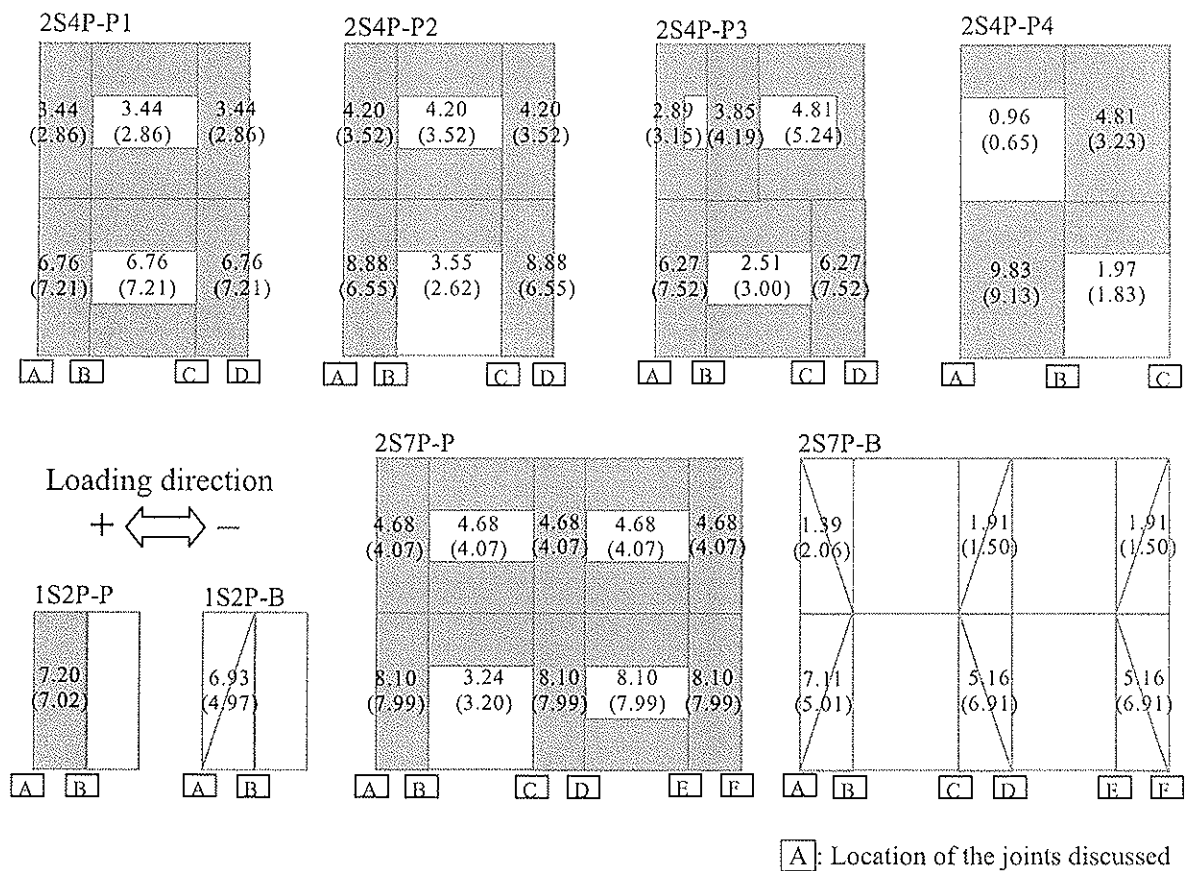
Figure 6. Assumed shear force (kN) of each part of the specimen at the shear deformation angle of the first storey of 1/120 radian.

5.2 Calculation results and discussions

Tables 2 shows the comparison of the tensile force of joints between the calculation results by Methods 1 and 2, and the test results. In this table, value of tensile force of each joint is

7

picked up as the value when the loading direction (plus or minus) is regarded to be critical for the joint.

Table 2. Comparison of tensile force of joints (kN) at shear deformation of first storey of 1/120 radian – test results and calculation results according to the design methods 1 and 2.

Specimen: 1S2P-P						
Test or	Joints					
Method	A (−)	B (+)				
Test	12.3	5.8				
Method 1	16.8	11.1				
Method 2	15.8	10.8				

Specimen: 1S2P-B						
Test or	Joints					
Method	A (−)	B (+)				
Test	8.4	9.4				
Method 1	11.9	10.4				
Method 2	11.2	10.4				

Specimen: 2S4P-P1						
Test or	Joints					
Method	A (−)	B (+)	C (−)	D (+)		
Test	17.0	0.2	Compression	14.5		
Method 1	24.2	7.7	7.55	24.5		
Method 2	22.5	−1.1	−0.4	22.4		

Specimen: 2S4P-P2						
Test or	Joints					
Method	A (−)	B (+)	C (−)	D (+)		
Test	15.4	0.7	Compression	12.8		
Method 1	24.2	13.8	10.5	31.4		
Method 2	20.9	3.7	2.3	27.3		

Specimen: 2S4P-P3						
Test or	Joints					
Method	A (−)	B (+)	C (−)	D (+)		
Test	17.3	1.5	Compression	13.2		
Method 1	25.6	9.0	9.0	20.8		
Method 2	24.2	1.8	2.5	20.8		

Specimen: 2S4P-P4						
Test or	Joints					
Method	A (−)	B (+)	C (−)			
Test	9.9	Compression	Compression			
Method 1	11.7	3.5	8.1			
Method 2	8.4	5.9	10.2			

Specimen: 2S7P-P						
Test or	Joints					
Method	A (−)	B (+)	C (−)	D (+)	E (−)	F (+)
Test	11.7	Compression	0.1	Compression	Compression	13.7
Method 1	29.0	13.2	12.6	9.6	9.0	30.7
Method 2	22.8	−1.5	11.1	7.7	−1.6	23.7

Specimen: 2S7P-B						
Test or	Joints					
Method	A (−)	B (+)	C (−)	D (+)	E (−)	F (+)
Test	6.5	11.3	Compression	Compression	9.2	5.3
Method 1	17.0	12.7	12.6	10.6	12.6	17.0
Method 2	11.6	7.9	10.9	8.3	7.5	11.6

( ): Loading direction (see Figure 6)

As Table 2 shows, there are tendencies that the Method 1 gives larger values of tensile force than the Method 2, and that both design methods give still larger values than the test results in average. The difference between calculation results and test results is larger at the inner posts than the end posts of the frames. For the posts at the end of the frames, both methods give near values of tensile force each other, and it seems that both methods are applicable for the practical design of joints at the end of the frames, though they are sometimes too conservative. For the posts at the end of frames, Method 1 always gives larger values than the test results, and it is remarkable that Method 2 sometimes gives smaller values compared with the test results.

One possible reason for the difference between the test results and calculation results of the specimens with plywood, is that the resistance of nails from plywood to framing members is not considered in the calculations.

As the reason of the difference between design methods and test results in tensile forces of hold down bolts, it can be pointed out that the distance of the stress centre of hold down bolts from the centre of post is not considered in the calculation. This eccentric setting of hold down bolts possibly decrease the tensile force generated in hold down bolts.

6 Conclusions

There are some design methods to calculate tensile forces of joints at the shear wall corner. To discuss the adequacy of two of these design methods for post and beam construction, a series of lateral loading tests were conducted on two one-storied structures and six two-storied structures by post-and-beam construction with plywood sheathed shear walls or braced frames, and the tensile forces at the joints obtained by these design methods and test results were compared.

As the results, there is a tendency that the two design methods give larger values than the test results in average, and the method using rigid beam assumption gives smaller values than the method using empirical factors. The difference between the calculation results and the test results is larger for the inner posts of the frames, but it seems that both design methods are applicable for the design of joints at end posts of the frames.

There are some possible reasons for the difference, such as lack of consideration for the effect of nails from plywood to framing members and distance between hold down bolt and centre of post.

7 References

HOWTEC. 1988. Guideline for the structural design and fire- proof design for three storey wooden houses (in Japanese).

HOWTEC. 2001. Allowable stress design for wooden houses by post and beam construction (in Japanese).

Inayama, M. and Murakami, M. 2001. Development of structural design method on conventional post and beam structures, Part 53 (in Japanese). Summaries of technical papers of annual meeting, Architectural Institute of Japan. Vol. C-1, pp369-370.

Japan 2×4 builders association. 2002. Structural design manual for buildings by wood frame construction (in Japanese)

8 Acknowledgment

INTERNATIONAL COUNCIL FOR RESEARCH AND INNOVATION
IN BUILDING AND CONSTRUCTION

WORKING COMMISSION W18 - TIMBER STRUCTURES

EFFECTS OF SCREW SPACING AND EDGE BOARDS ON THE

CYCLIC PERFORMANCE OF TIMBER FRAME AND

STRUCTURAL INSULATED PANEL ROOF SYSTEMS

D M Carradine
J D Dolan

Wood Materials and Engineering Laboratory
Washington State University

F E Woeste

Construction and Engineering Consultant
Blacksburg

USA

Presented by: David Carradine

David Carradine began his presentation by describing contemporary timber frame design methodologies using SIP panels. He went on to describe the testing protocols and the SIP roof panel configurations used in his experimental work. David went on to discuss the design implications based on the findings of the research.

Effects of Screw Spacing and Edge Boards on the Cyclic Performance of Timber Frame and Structural Insulated Panel Roof Systems

D. M. Carradine[1], J. D. Dolan, P. E.[1] and F. E. Woeste, P. E[2]

Abstract

Current understanding of the effects of screw spacing and installation of perimeter edge boards on behavior of timber frame and structural insulated panel (SIP) roof systems subject to earthquake loading is limited by a lack of test data on these systems. To assess the effects of screw spacing and edge boards on diaphragm stiffness, quasi-static cyclic stiffness tests were conducted on three 2.44 m (8 ft) deep and 7.32 m (24 ft) wide roof diaphragm assemblies, and two 6.10 m (20 ft) deep and 7.32 m (24 ft) wide roof diaphragm assemblies. Data from tests were collected and analyzed in order to determine the effects of screw spacing and the installation of an edge board versus no edge board on cyclic stiffness, strain energy, hysteretic energy, and equivalent viscous damping. A rationale for the cause of these effects was developed based on results of monotonic failure tests, that provided data on fastener breakage at failure. Data from monotonic and cyclic tests were incorporated in order to make design recommendations for timber frame and SIP structures subject to earthquake forces.

Introduction

Buildings all over the world have been constructed for centuries utilizing large timbers connected using wooden joints and secured with wooden pegs and wedges to create structural skeletons that are enclosed to provide shelter and interior spaces. Different cultures derived distinct construction methodologies, but all of these buildings using primarily wooden joints are considered timber frames. Timber frame construction has proved to be a dependable and enduring building system, although with the advent of industrialization and resulting ease of producing dimensional lumber during the early years of the 20th century, light-frame construction became much more common and replaced timber framing as the mainstay of low-rise wooden buildings. Nevertheless, a revival of interest in timber frame building in the United States occurred during the 1970s and since that time, the timber framing industry has grown to keep up with demand for timber frame houses, barns, churches, and other structures (O'Connell and Smith, 1999). European and Asian countries have also kept timber frame construction alive, even as other building methods have become more popular over the past 100 years.

Contemporary timber frame structures, especially in the United States, typically utilize structural-insulated panels (SIPs) attached to the timber frame skeleton to enclose the frame and create a functional structure. These panels consist of a layer of rigid insulation that is typically covered on one side by oriented strand board and on the other

---

[1] Research Engineer and Professor, respectively, Wood Materials and Engineering Laboratory, Washington State University, Pullman, WA 99164,
[2] Wood Construction and Engineering Consultant, 1502 Nelson Street, Blacksburg, VA 24060.

side by oriented strand board, gypsum drywall, or some other interior finish, such as tongue and groove paneling.

Lateral forces resulting from wind and earthquakes can induce considerable shear and bending stresses into building components. While timber frame structures are typically well within safety limits with regard to gravity loads, lateral loads can potentially exceed the stress limits of timbers and joints. One area prone to overstress in timber frame structures is the tenon portion of a beam because it is much smaller than the rest of the member, as illustrated in Figure 1, and is further limited in strength by holes for the wooden dowels and short edge distance from the dowel holes to the end of the tenon. When timber frame structures are loaded laterally under typical wind speeds or seismic ground accelerations, it is very likely that tenons on members where tension forces are induced will be overstressed if the contribution of building diaphragms and shear walls are not included in the structural analysis. Timber frame structures have an excellent performance record, and it is therefore believed that even though the frame alone does not have the strength to resist lateral loads, the contribution of SIPs or other cladding contributes to the ability of these structures to effectively resist lateral loading.

An initial investigation (Carradine et al., 2000) indicated that timber frame building design could benefit from incorporating SIPs as part of the lateral force resisting system of the building. Testing conducted on several timber frame and SIP roof diaphragm assemblies and subsequent data analyses provided critical information on the strength and stiffness of timber frame and SIP roof assemblies and served to quantify the contributions made by SIPs and the timber frames in resisting lateral loads applied to them. This knowledge was incorporated with existing procedures for diaphragm design of post-frame structures in order to develop a similar methodology for the design of timber frame buildings that included the SIPs as diaphragm elements for lateral load resistance.

While research included cyclic and monotonic diaphragm testing protocols for both seismic and wind design, the scope of this paper is limited to a discussion and interpretation of results from cyclic tests. Testing and analysis results from monotonic testing and design methodologies for resisting wind loads were presented in a paper currently in press.

Objective

The objective of this paper was to present results from cyclic testing of timber frame and SIP roof systems, to determine the effects of screw spacing and the installation of edge boards versus no edge boards on cyclic stiffness, strain energy, hysteretic energy, and equivalent viscous damping, and to incorporate these effects in order to make recommendations for designing timber frame buildings to resist earthquake loads.

Timber Frame and SIP Roof Assembly Testing

Typical timber frame roof construction composed of principle rafters and purlins lent itself most easily to the use of a simple beam test utilizing a single load applied to the center rafter of an assembly having three rafters and two bays. Roof assembly cyclic stiffness behavior was determined by displacing the center rafter, in a direction parallel to the rafters. In order to load the diaphragms as simply supported, deep beams, it was necessary to fabricate a system of steel brackets that held the outer rafters secure while

2

allowing for movement of the center rafter in a direction parallel to the longitudinal axes of the rafters. Displacements were induced in the center rafter utilizing a servo-hydraulic computer controlled 245 kN (55 kip) actuator with ±152 mm (6 in.) of travel that allowed for continuous monitoring of the loads applied to the specimens and displacement of the center rafter.

Low-level cyclic stiffness testing for all assemblies was accomplished utilizing the Basic Loading History quasi-static cyclic regime as described by Krawinkler et al. (2001). This regime was controlled by deformations and intended to represent a potentially damaging loading schedule from ground motions in the Los Angeles area of California. A reference deformation, Δ, representing the assembly's deformation capacity, is typically obtained from a monotonic test to failure. Cyclic loading was not utilized to induce failure into the diaphragms and therefore a maximum displacement of 6.4 mm (0.25 in.) was used for the cyclic testing in order to avoid any degradation of diaphragm stiffness prior to the monotonic strength and stiffness tests, and the remaining test cycles were scaled to reflect this maximum.

Tests were conducted on three basic test panel [2.44 m (8 ft) by 7.32 m (24 ft)] assemblies and two full-scale sized [6.10 m (20 ft) by 7.32 m (24 ft)] roof panel assemblies in order to determine cyclic parameter values, as well as how extrapolations could be made from test panel assemblies to full roof diaphragms. Figure 2 shows a plan view of the basic test panel assembly. Full-scale roof panel assemblies utilized ten SIPs and eight intermediate purlins, but were otherwise the same as the basic test panel assemblies. Construction of all tested assemblies was based on the most typically utilized timber frame joinery and SIP installation methods utilizing hardened steel screws, 229 mm (9 in.) long with shank diameter 4.8 mm (0.19 in.) and root diameter 4.3 mm (0.17 in.) to attach SIPs to timbers. Specific details on the fabrication of test specimens were provided by Carradine (2002). Each assembly was tested for configurations including the bare timber frame, timber frame with SIPs installed using screws at 610 mm (24 in.) on center (o.c.), timber frame with SIPs installed with screws at 305 mm (12 in.) o.c., and timber frame with SIPs installed with screws at 305 mm (12 in.) o.c. and 38 mm x 140 mm (1.5 in. x 5.5 in.) No. 2 Spruce-Pine-Fir edge boards installed. Installation of SIPs included 76.2 mm (3 in.) wide, oriented strand board (OSB) splines and polyurethane expanding foam at all SIP-to-SIP joints for all construction configurations.

Results and Interpretations of Roof Assembly Tests

According to the International Building Code 2003 (ICC, 2003), buildings must provide adequate strength, stiffness and energy dissipation through lateral and vertical force restraining systems to withstand ground accelerations based on geographic location. Determining cyclic stiffness and energy damping characteristics of timber frame and SIP roof systems was accomplished through cyclic load-deflection hysteresis analysis. These hysteresis analyses were derived from load-displacement curves resulting from the quasi-static cyclic tests. Results from cyclic regimes previously described provided load and deflection data for timber frame and SIP roof assemblies that were used to generate values for cyclic stiffness, strain energy, damped hysteretic energy and equivalent viscous damping for each assembly configuration. Load versus deflection plots for cyclic testing resulted in a series of hysteresis loops, rather than single lines obtained from monotonic tests.

3

A typical hysteresis loop plot is shown in Figure 3. Cyclic stiffness, like monotonic stiffness, represented a measure of load required to produce a specified displacement of the system being tested. Cyclic stiffness was obtained by calculating the slope of the line between points B and D in Figure 3 for hysteresis loops for the 7 primary peak cycles for each test configuration. Strain energy (S_c) was a measure of system potential energy, or energy associated with deformation of the assembly (Beer and Johnston, 1992) at a given displacement and was determined by totaling the area beneath triangles ABC and ADE in Figure 3 for each hysteresis loop. The area within a hysteresis loop represented the energy dissipated by the assembly for each cycle (Chopra, 1995) and was determined as hysteretic energy (H_e). Comparing energy dissipated per cycle per radian ($H_e/2\pi$) with strain energy (S_e) provided equivalent viscous damping ratios (η) for each hysteresis loop utilizing the following:

$$\eta = H_e/(2\pi\ S_c) \tag{1}$$

where,

η = equivalent viscous damping ratio, (decimal),
H_e = hysteretic energy, N-mm (lbs-in.), and
S_e = strain energy, N-mm (lbs-in.).

Equivalent viscous damping refers to energy dissipated from a vibrating system and is often utilized to quantify dissipated energy of cyclically loaded wood structural systems (Heine and Dolan, 1998).

Data from cyclic testing provided load and displacement values from which cyclic stiffness, strain energy, hysteretic energy and equivalent viscous damping were calculated for all assemblies. Table 1 provides numerical values for testing configurations for Assembly 2 for cyclic stiffness, strain energy, hysteretic energy and equivalent viscous damping at maximum displacements, provided as a typical example.

Trends in cyclic stiffness, strain energy, hysteretic energy and equivalent viscous damping for tested assemblies were observed to be consistent across the varied construction configurations and assemblies. The following discussion provides general trend information obtained from cyclic tests at maximum displacements for all assemblies. Assemblies 1, 2 and 3, which were 2.44 m x 7.32 m (8 ft x 24 ft) will be referred to as Assembly A specimens, while 6.10 m x 7.32 m (20 ft x 24 ft) Assemblies 4 and 5 will be referred to as Assembly B specimens.

Cyclic stiffness increased dramatically from the bare timber frame with the installation of SIPs using 610 mm (24 in.) o. c. screw spacing for all assemblies. Assembly A specimens averaged 11.5 times higher cyclic stiffness with installation of SIPs using 610 mm (24 in.) o. c. screw spacing, and cyclic stiffness for Assembly B specimens increased 18 times from the bare frame with the installation of SIPs using 610 mm (24 in.) o. c. screw spacing. Cyclic stiffness increased, on average, by 15% for Assembly A specimens and 12% for Assembly B specimens when SIP screw spacing was halved from 610 mm (24 in.) o. c. to 305 mm (12 in.) o. c. Edge board installation increased cyclic stiffness by an average 8% for Assembly A specimens and 5% for Assembly B specimens. Cyclic stiffness of completed Assembly B specimens was approximately twice that of Assembly A. As peak cyclic displacement increased, cyclic stiffness also increased for assemblies with SIPs installed, indicating stiffening within the

4

assemblies for increasing displacements. No degradation or decrease in stiffness was observed for completed assemblies subject to cyclic testing.

Calculation of strain energy for varied construction configurations and assemblies provided similar trends to those observed for cyclic stiffness. Strain energy for assemblies with SIPs installed using screw spacing of 610 mm (24 in.) o. c. were 8 times greater and 16 times greater than bare timber frames for Assembly A and Assembly B specimens, respectively. Decreasing screw spacing from 610 mm (24 in.) o. c. to 305 mm (12 in.) o. c. increased strain energy values by 18% for Assembly A specimens and 14% for Assembly B specimens. Strain energy increased 8% and 3% for Assembly A and Assembly B specimens, respectively, as a result of installing edge boards. Completed Assembly B specimens dissipated average strain energy approximately 3 times that of completed Assembly A specimens as displacements approached 6.4 mm (0.25 in.).

Similar to trends observed with cyclic stiffness and strain energy, hysteretic energy increased dramatically from the bare timber frame with installation of SIPs utilizing 610 mm (24 in.) o. c. screw spacing. Assembly A specimens dissipated 2.6 times as much hysteretic energy after initial SIP installation and Assembly B specimens dissipated 3.7 times as much hysteretic energy. Hysteretic energy calculations for increasing screw density and installing edge boards were not consistent enough to observe trends across configurations as some assemblies dissipated more energy and some less energy as screw density was increased and edge boards installed. Completed Assembly A specimens dissipated roughly half the hysteretic energy observed in completed Assembly B specimens at maximum cyclic displacements.

Equivalent viscous damping was a function of hysteretic energy and strain energy calculated utilizing an equation with strain energy in the denominator. Results from determining equivalent viscous damping for assembly configurations indicated that strain energy dominated the behavior of timber frame and SIP diaphragm assemblies as the trends for equivalent viscous damping were essentially the inverse of those for strain energy. Specifically, large decreases in equivalent viscous damping occurred after installation of SIPs using 610 mm (24 in.) o. c. screw spacing for all assemblies, followed by smaller decreases in equivalent viscous damping with decreased screw spacing and edge board installation. Installation of SIPs using 610 mm (24 in.) o. c. screw spacing reduced equivalent viscous damping from that of the bare timber frame by 72% for Assembly A specimens and 77% for Assembly B specimens. Increased screw spacing density to 305 mm (12 in.) o. c. reduced equivalent viscous damping 14% for Assembly A specimens and 18% for Assembly B specimens. Edge board installation reduced equivalent viscous damping by 5% for Assembly A specimens and 9% for Assembly B specimens. Equivalent viscous damping for completed Assembly B specimens was approximately 72% that of Assembly A specimens at maximum cyclic displacements.

Cyclic parameters described above for five timber frame and SIP roof assemblies follow trends that would be expected based on behavior of fasteners during tests to failure, in particular which screws were broken, bent and undamaged. The SIP screws dictated the behavior of the assemblies, which were fabricated with a very stiff SIP "plate" fastened with SIP screws to a frame of extremely stiff timbers, essentially pinned at the joints and free to rotate about those joints. As was observed during the tests,

5

dramatic changes in all cyclic characteristics were expected upon initial SIP installation due to the flexible nature of the timber frame and stiffness of the SIPs.

Cyclic stiffness exhibited a large increase with installation of SIPs onto the timber frame and continued to increase slightly with increased screw density and installation of edge boards. Increased screw density distributed the load going from timbers into the SIPs to a larger number of screws, resulting in more load being required to deflect the assembly the same displacement, and consequently higher cyclic stiffness. Edge board installation stiffened the plate created by the SIPs slightly, which induced more load sharing into the screws and again increased cyclic stiffness. Higher stiffness in Assembly B specimens over Assembly A specimens was attributed to the larger number of screws bent and broken. Strain energy increased similarly with increases in cyclic stiffness for the same reasons discussed above. Because no damage was caused during cyclic testing and the assemblies remained within their elastic range, strain energy increased as additional load was required to attain the same displacements.

Large increases in hysteretic energy were observed with installation of SIPs utilizing 610 mm (24 in.) SIP screw spacing, but trends in hysteretic energy from decreased screw spacing and edge board installation were somewhat inconsistent. This result was expected in the elastic range, as all conducted cyclic tests were, because hysteresis loop formation remains somewhat erratic until degradation of the system occurs and the loops become more distinct with increased displacements. Differences between hysteretic energy in Assembly A and Assembly B specimens were consistent with SIP screw data in that hysteretic energy dissipated by Assembly B specimens was approximately twice that of Assembly A specimens, and roughly twice the number of screws were damaged in Assembly B specimens as Assembly A specimens.

Equivalent viscous damping (Equation 1) was dominated by strain energy behavior, which resulted in equivalent viscous damping dropping significantly with installation of SIPs, and continuing to drop with decreased screw spacing and edge board installation, although at much smaller increments. Energy dissipation, or damping occurred as a result of friction among fasteners and components within the system as opposed to causing damage to materials comprising the assemblies. If cyclic displacements had been increased beyond the elastic range, damage would have occurred to the assemblies, reducing cyclic stiffness and strain energy, and an increase in hysteretic energy would have resulted in increased values for equivalent viscous damping. Additionally, utilization of hardened steel screws to attach SIPs to timbers had the effect of increasing cyclic stiffness and strain energy, but did not increase hysteretic energy because they did not have the ability to yield effectively. Use of fasteners with more ductility would have increased hysteretic energy and resulted in a more ductile assembly. Fasteners more ductile than the SIP screws utilized would likely have changed the effective dominance of strain energy and resulted in higher equivalent viscous damping ratios.

Timber Frame and SIP Design Recommendations

Current seismic design procedures in the IBC 2003 (ICC, 2003) do not contain provisions for the use of heavy timber frame construction. Because system response factors for timber frame buildings are not provided, design of heavy timber frame construction would need to be performed utilizing "Alternative Means and Methods",

6

which require building designers to assume a value for Response Modification Coefficient, R (R-value). Designers must also justify use of the assumed R-value and obtain approval from governing building officials prior to building approval. Justification of an R-value is based on several embedded assumptions, primarily for vertical lateral load resisting systems within a structure, including displacement capacity, ductility, stiffness and strength degradation, and hysteretic energy dissipation. While ample data is available for most seismic force resisting systems, there remains a lack of information regarding heavy timber frame and SIP construction vertical lateral load resisting elements. Testing conducted on timber frame and SIP roof systems, as discussed above, has provided some insight as to the behavior of these building types subject to seismic loads. Research conducted by Jamison (1997) on the cyclic and monotonic behavior of SIP shear walls indicated that SIP shear walls were extremely brittle when subjected to lateral loads, and were stiffer, less ductile and dissipated less energy than typical nailed wooden shear walls. Timber frame and SIP shear wall investigations at the University of Wyoming and available data indicated similar responses to lateral loads as the roof assemblies tested. National Earthquake Hazards Reduction Program (NEHRP) provisions for designing shear walls utilizing adhesive attachment of wall sheathing require that an R-value of 1.5 be used for calculating seismic forces as opposed to an R-value of 7 that is typically used for nailed shear walls (Building Seismic Safety Council, 2001). Adhesive attachment of sheathing to shear walls is only permitted in low seismic regions (i. e., Seismic Design Categories A and B). Based on stiffness and lack of ductility inherent within SIP shear wall elements, and the assumption that they behave more like shear walls utilizing adhesives for sheathing attachment than nailed shear walls, it is recommended that designers utilize an R-value of 1.5, the same as that for plain masonry shear walls and glued shear walls, which exhibit similar behavior when subject to lateral loads as SIP shear walls. Recommendations made with respect to IBC 2003 (ICC, 2003) seismic design procedures utilizing an R-value of 1.5 provide higher seismic forces applied to the building, resulting in conservative estimates of forces acting on timber frame members and are consistent with sound engineering practice.

Summary and Conclusions

Cyclic testing of timber frame and SIP roof systems provided data regarding ductility, strength and stiffness degradation, and energy dissipation of these assemblies. In general, timber frame and SIP roof assemblies proved to be extremely stiff structural systems that maintained their structural integrity up to cyclic displacements which coincided approximately with design loads. Cyclic characteristics of SIP and timber frame roof systems supported the assumption that SIPs create a very stiff plate that is connected to the flexible timber frame utilizing only the SIP screws. Timber frame and SIP roof assemblies tested cyclically within the elastic limit of the screws exhibited increases in cyclic stiffness and strain energy with decreases in screw spacing and installation of perimeter edge boards.

In addition to observed behavior of timber frame and SIP roof assemblies subject to cyclic loading, justification for estimating Response Modification Coefficient, R, for use with IBC 2003 (ICC, 2003) seismic design procedures, was based on research conducted on SIP shear walls, research regarding timber frame and SIP shear walls, and

comparisons with several other building systems including nailed shear walls, shear walls with adhesive attached sheathing and plain masonry shear walls. An R-value of 1.5 was recommended for calculating seismic forces on timber frame and SIP buildings as part of IBC 2003 (ICC, 2003) seismic design procedures. This R-value is based on the assumption of a brittle, stiff vertical lateral load resisting system with relatively low energy dissipation and provides conservative values for determining seismic forces on timber frame and SIP buildings.

References

Beer, F. P. and E. R. Johnston. 1992. *Mechanics of Materials 2ⁿᵈ Edition*. New York, NY: McGraw Hill, Inc.

Building Seismic Safety Council. 2001. *NEHRP Recommended Provisions for Seismic Regulations for New Buildings and Other Structures Part 1: Provisions (FEMA 368)*. Washington, DC: Building Seismic Safety Council.

Carradine, D. M., F. E. Woeste, J. D. Dolan and J. R. Loferski. 2000. Demonstration of wind load design of timber frame structures utilizing diaphragm action. *Transactions of the ASAE* 43(3): 729-734.

Carradine, D. M. 2002. *Methodology for the design of timber frame structures utilizing diaphragm action*, dissertation submitted to the faculty and staff of Virginia Polytechnic and State University in partial fulfillment of the requirements for the degree of Doctor of Philosophy in Biological Systems Engineering, Blacksburg, VA.

Chopra, A. K. 1995. *Dynamics of structures: theory and applications to earthquake engineering*. Upper Saddle River, NJ: Prentice Hall.

Heine, R. C. and J. D. Dolan. 1998. Monotonic and sequential phased displacement tests to determine short-term duration-of-load performance of stapled connections. Report No. TE-1998-001 submitted to International Staple, Nail and Tool Association.

International Code Council, Inc. (ICC). 2003. *International Building Code 2003*. Falls Church, VA: International Code Council, Inc.

Jamison, J. B. 1997. *Monotonic and cyclic performance of structurally insulated panel shear walls*, thesis submitted to the faculty and staff of Virginia Polytechnic and State University in partial fulfillment of the requirements for the degree of Master of Science in Civil Engineering, Blacksburg, VA.

Krawinkler, H., F. Parisi, L. Ibarra, A. Ayoub and R. Medina. 2001. Development of a testing protocol for wood frame structures. Report, Stanford University, Stanford, CA.

O'Connell, T and P. Smith. 1999. The North American timber frame housing industry. *Forest Products Journal* 49(1): 36-42.
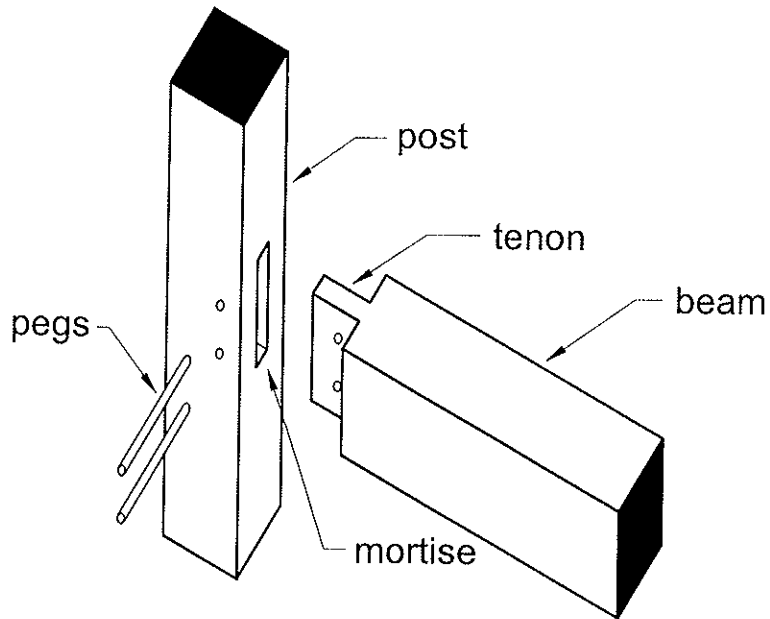
Figure 1. Typical elements of a mortise and tenon joint. Pegs are typically 25 mm (1 in.) in diameter and tenons are typically 38 mm (1-1/2 in.) to 51 mm (2 in.) thick.

38 mm x 140 mm (2x6) No. 2 SPF along roof perimeter, except at ridge, attached with 8d ring shank nails @ 203 mm (8") o.c.

1.22 m x 3.66 m (4'x12') SIP (typ.)

1.22 m (4'-0")

Ridge purlin

Rafter

11 mm x 76 mm (7/16"x3") OSB splines attached with 8d ring shank nails @ 203 mm (8") o.c.

Intermediate purlin

1.22 m (4'-0")

Post stub   Plate

3.66 m (12'-0")

3.66 m (12'-0")

SIPs attached to timbers with 229 mm x 4.8 mm (9"x0.19") diameter screws @ 305 mm (12") o.c.

Figure 2. Plan view of 2.44 m x 7.32 m (8 ft x 24 ft) basic test panel assembly.

9
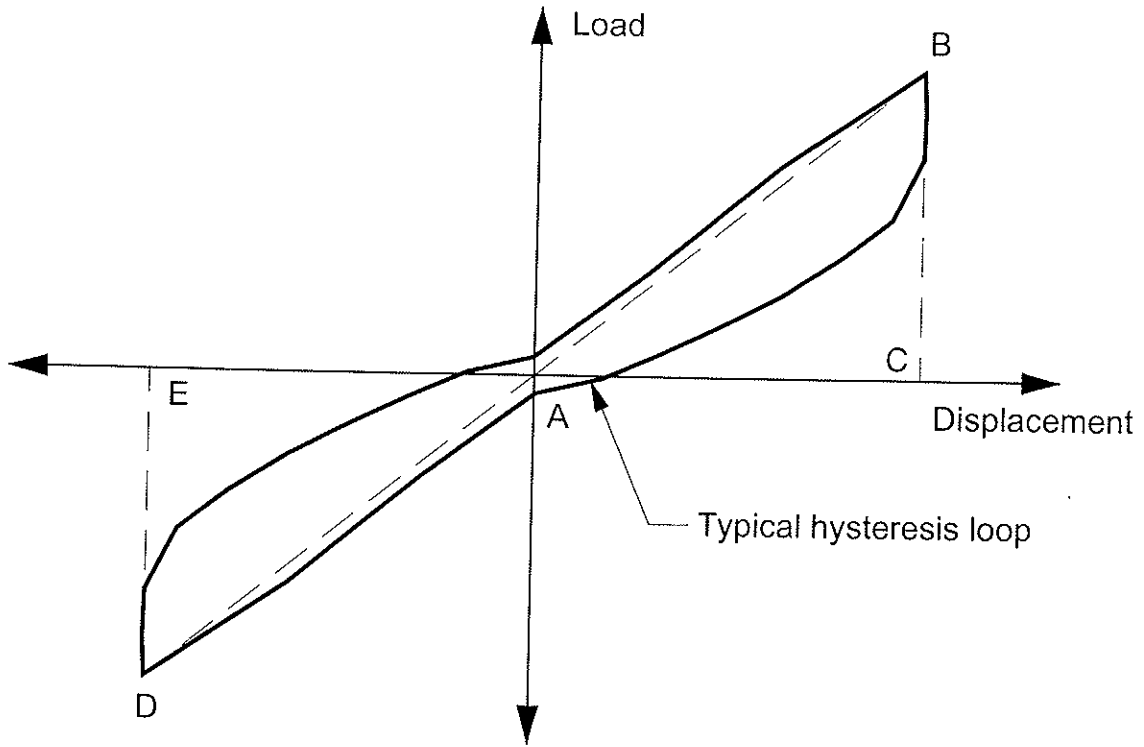
Figure 3. Example of typical hysteresis loop plot.

Table 1. Cyclic test parameters for various testing configurations of Assembly 2 at maximum displacements.

Test configuration	Cyclic stiffness	Strain energy	Hysteretic energy	Equivalent viscous damping
Bare timber frame	2,430 lbs/in. (426 N/mm)	7.39 lbs-in. (835 N-mm)	11.5 lbs-in. (1.30 kN-mm)	0.25
SIPs installed; screws 24" o.c.	26,600 lbs/in. (4.66 kN/mm)	73.1 lbs-in. (8.26 kN-mm)	33.5 lbs-in. (3.79 kN-mm)	0.073
SIPs installed; screws 12" o.c.	29,400 lbs/in. (5.15 kN/mm)	82.2 lbs-in. (9.39 kN-mm)	29.4 lbs-in. (3.32 kN-mm)	0.057
SIPs installed; screws 12" o.c., edge boards installed	32,700 lbs/in. (5.73 kN/mm)	85.6 lbs-in. (9.67 kN-mm)	29.4 lbs-in. (3.32 kN-mm)	0.055

INTERNATIONAL COUNCIL FOR RESEARCH AND INNOVATION
IN BUILDING AND CONSTRUCTION

WORKING COMMISSION W18 - TIMBER STRUCTURES

PSEUDO-DYNAMIC TESTS ON CONVENTIONAL TIMBER STRUCTURES

WITH SHEAR WALLS

M Yasumura

Department of Forest Resources Science
Shizuoka University

JAPAN

Presented by: Motoi Yasumura

Motoi Yasumura described typical 3 storey timber framed buildings using shear walls and their ability to withstand seismic effects before going on to describe the test method, specimens used in the pseudo dynamic testing conducted and the data obtained. He concluded that pseudo-dynamic testing is a useful approach for assessing the ground level storey behaviour and that the hysteretic model accurately predicted the first storey behaviour but under-estimate the second storey behaviour.

Pseudo-dynamic tests on conventional timber structures with shear walls

Motoi YASUMURA

Department of Forest Resources Science, Shizuoka University, Japan

1. Introduction

As the seismic performance of timber structures composed of shear walls is mainly governed by the mechanical properties of shear walls[1], the evaluation of seismic performance of shear walls is essential for the seismic design of timber structures. The lateral resistance of shear walls can be determined by the following four criteria obtained from the reversed cyclic lateral loading tests[2]; the initial stiffness, the yield strength, the ultimate strength and the ductility[3]. Although these criteria are indispensable for the evaluation of shear walls, they do not always predict the dynamic response of structures during the earthquakes. Pseudo-dynamic test is one of the most efficient methods to estimate the seismic performance of timber structures. To conduct a pseudo-dynamic tests of shear walls, we need to assume a mass which is the most sensitive to the earthquake response. In general, we consider the shear wall of the first story and apply the mass supported by that particular wall. However, the effects of shear walls of the upper story may not be negligible on the response of that of the first story.

To examine these problems, we conducted pseudo-dynamic tests on two-story timber structures with plywood-sheathed shear walls having an opening of different configurations, and the effects of the balance of the racking strength between the first and the second stories were studied. We also compared the responses of the first story with those of the test results of the individual shear walls.

The test results showed that the maximum displacement response of the first story became smaller when the resistance of the shear walls of the second story was smaller and that the maximum displacement responses of the first story were very close to those of pseudo-dynamic test results of the individual shear walls when the resistance of the shear walls of the second story were sufficiently large. These results indicate that the pseudo-dynamic tests of a single shear wall element with the mass supported by that particular wall show generally equal to or at least safe-side estimation of the response of the first story, and this method is appropriate to evaluate the seismic performance of the shear walls of the first story which are the most critical during the earthquake.

Time-history earthquake response analysis is another effective method to evaluate the seismic performance of timber structures. A good model of the cyclic behavior of shear walls is required to predict precisely the response. In this study the parameters of the hysteretical model of shear walls were determined from the reversed cyclic tests of the individual shear walls. The simulation predicted quite well the response of the first story, but tended to under-estimate the response of the second story. Further studies may be necessary to predict more precisely the seismic response of whole structures.

1

2. Specimens

Two groups of specimens were prepared. One consisted of plywood-sheathed shear walls with conventional post and beam frames of 3000mm width on center and 3000mm height (Group I) as shown in Fig.1, and the others were two story structures composed of shear walls in the first and the second stories attached only in one face of the structure (Group II) as shown in Fig,2.

Group I specimens consisted of 105-by 105mm posts and sill and 105-by 210mm beam of white . wood glued laminated timber. Posts placed at every 1000mm were connected to the sill and the beam with a steel pipe of 26.5mm diameter and hold down bolts (HD-B15). Two hold down bolts were used at the foot of posts and one at the top. Seven and a half millimeters thick lauan plywood JAS Type I was nailed on one side of the frame with N50 common nails at the interval of 150mm. In Group II specimens, steel braces of 16mm diameter were attached in vertical and horizontal frames perpendicular to the loading direction. No lateral resistant elements were attached in the vertical frame opposite to the shear walls.

Group I specimens had an opening of three different configurations at the center of the wall. Specimen W had an opening of 1000mm width and 1000mm height, specimen D had that of 1000mm width and 2000mm height, and specimen S had an opening of 1000mm width continuing from the sill to the top beam.

Group II specimens had the vertical diaphragm of the combination of Group I specimens as shown in Fig.3. Specimens WW, DW and SW had the shear walls with a window type opening (W) at the second story, and those with an opening of window (W), door (D) and slit (S) configuration at the first story, respectively. Specimen SS had shear wall with an opening of

Specimen W

Specimen D
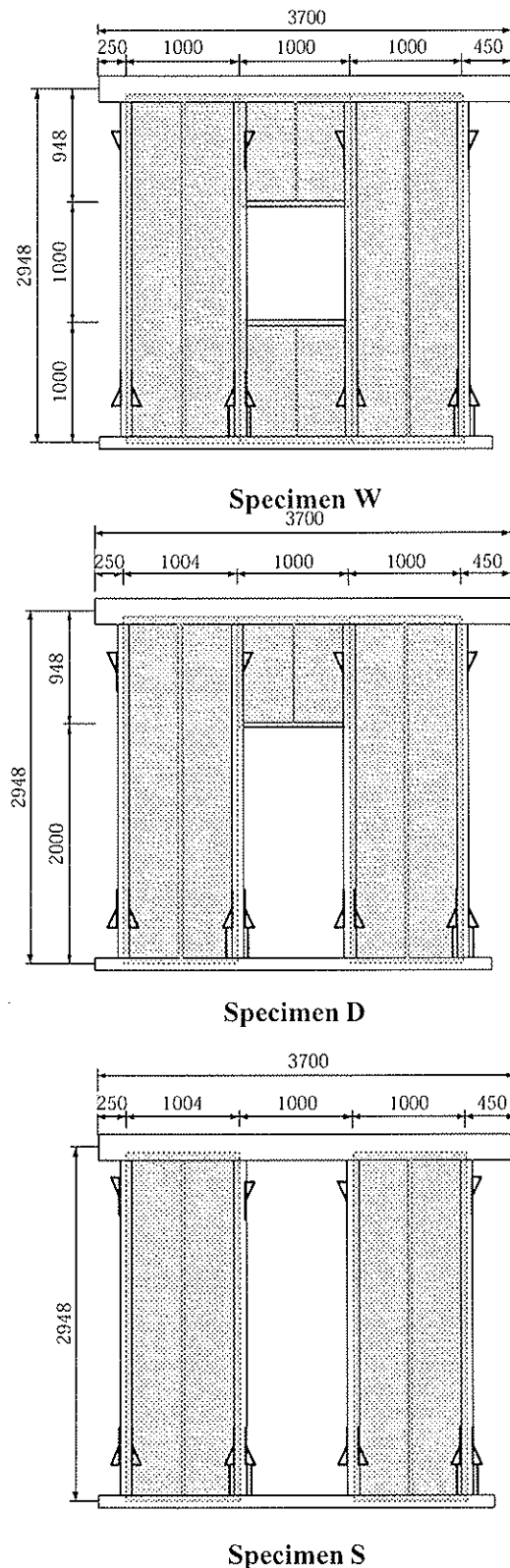
Specimen S

Fig.1 Shear wall specimens with an opening (Group I)

slit configuration (S) both at the first and the second stories. Specimen SHS had shear wall with an opening of slit configuration (S) at the first story and the shear wall of 1000mm width at the second story.

3. Test methods

Monotonic and reversed cyclic loading tests were conducted on Group I specimens to obtain fundamental data on load-deformation relationships. Then pseudo-dynamic tests by computer on line system (*Shimadzu 48000 system*) were conducted on each specimen. The accelerogram used for the pseudo-dynamic tests were based on the NS components of 1940 El Centro Earthquake linearly scaled to have the maximum ground acceleration of 0.4G. The mass and damping factor were supposed to be 5t and 2% for all the specimens.

For Group II specimens, the lateral loads were applied at the top of both the first and second stories as shown in Fig.2. Computer on line system (*Saginomiya ATC-20*) were used for the Pseudo-dynamic tests. The same accelerogram as used for Group I specimens, 1940 El Centro NS was applied. The mass of 2.5t were assumed for both the first and second stories.
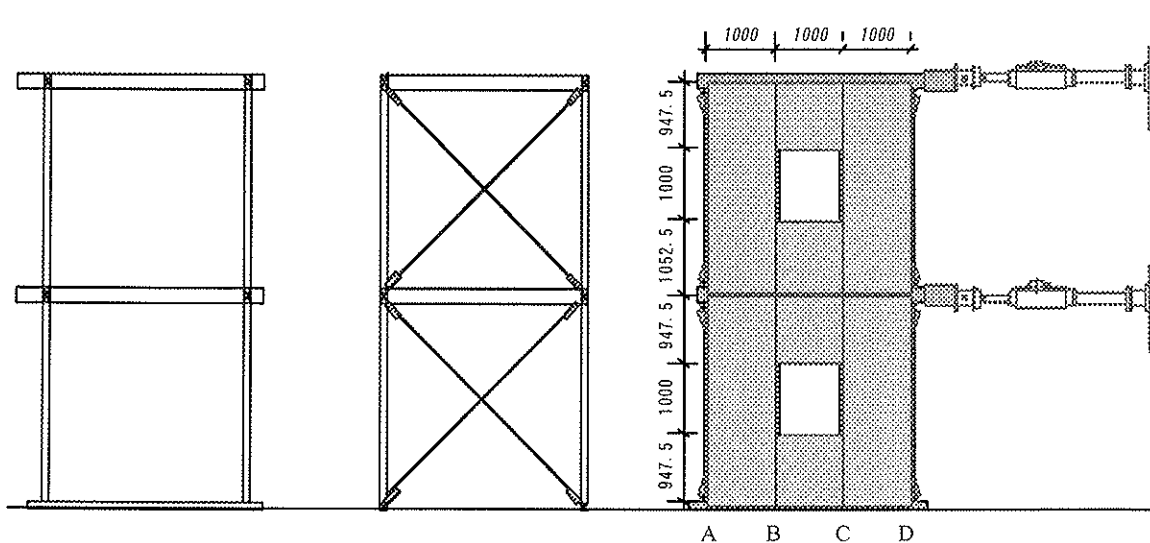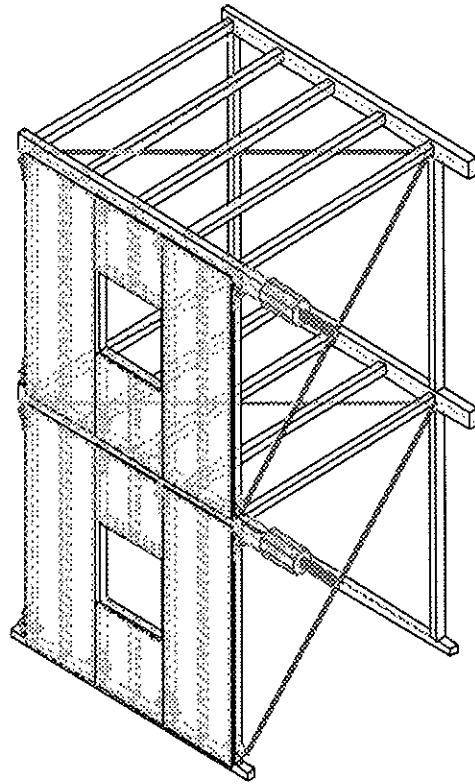
Fig,2 Overall description and test methods of Group II specimens

3
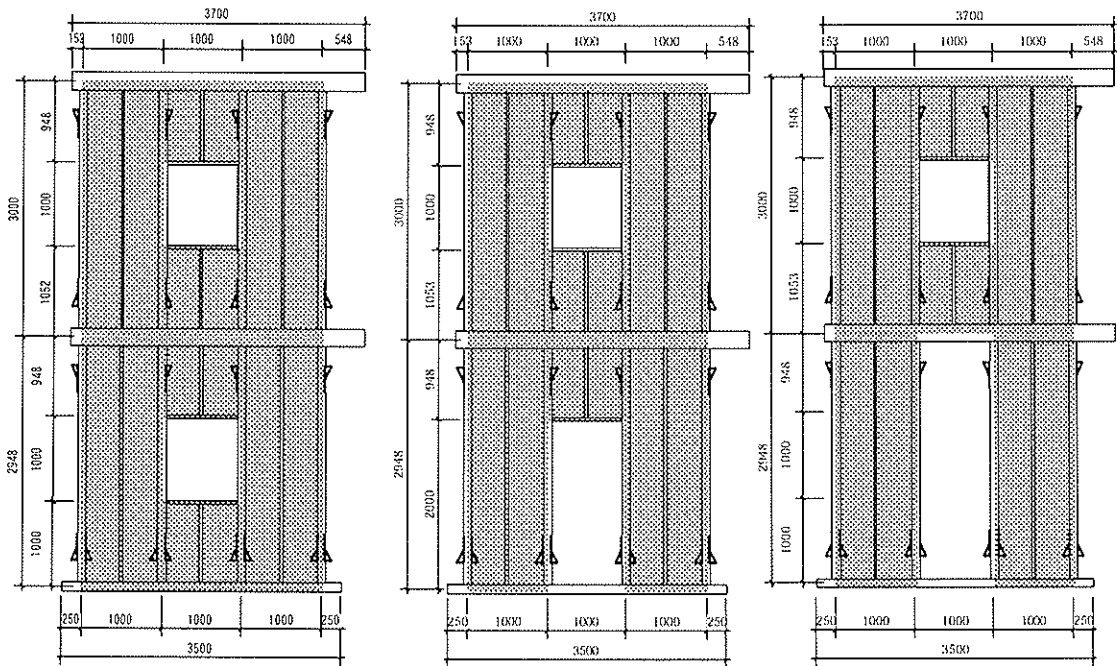
Specimen WW   **Specimen DW**   **Specimen SW**
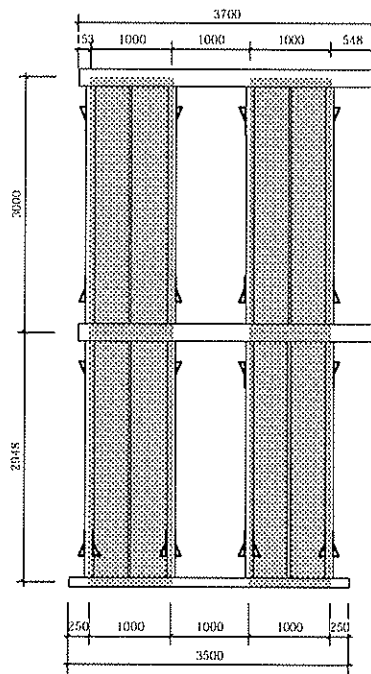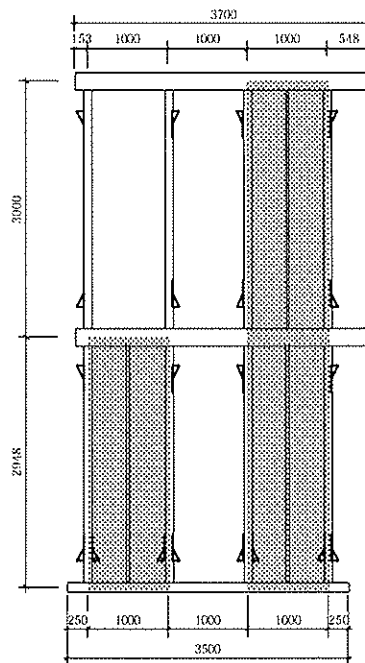
Specimen SS   **Specimen SHS**

Fig.3 Details in Groupe II specimens

4
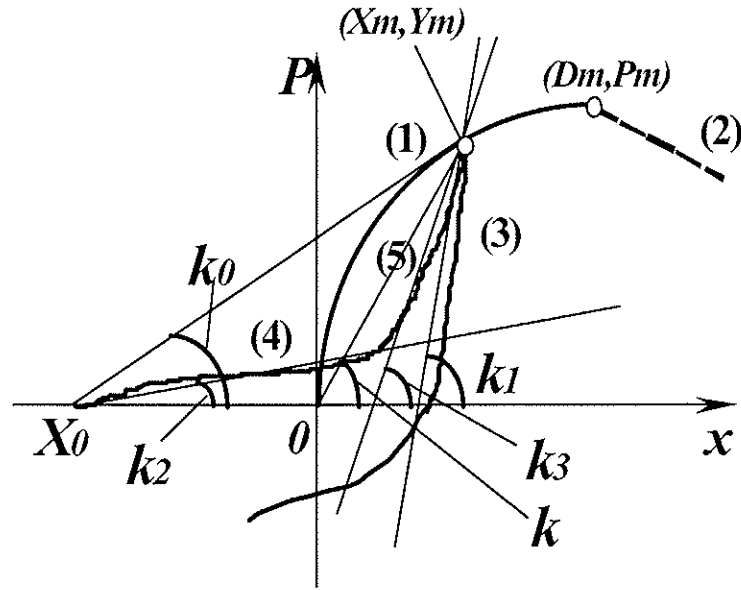
Fig.4 Modeling of load-displacement relationships of shear walls

4. Dynamic analysis

Time-history earthquake response analysis was conducted on Group I and II specimens. Single-degree-of-freedom lumped mass model was applied to the analysis. Load-displacement relationships of shear walls were obtained from the reversed cyclic loading tests of Group I specimens. A hysteretical model as shown in Fig.4 was assumed for the analysis[4]. The model includes;

1) Loading on the primary curves up to the maximum load
2) Loading on the primary curves over the maximum load
3) Unloading from the peak on the primary curve
4) Reloading with soft spring
5) Reloading toward the previous peak with hard spring
6) Unloading from the inner peak
7) Reloading toward the peak without slips

The primary curves up to the maximum load (1) and those over the maximum load (2) , are expressed as follows;

$$P = (P_0 + C_2 x)(1 - e^{-\frac{C_1 x}{P_0}}) \qquad (1)$$
$$P = Pm - C_3 |x - Dm| \qquad (2)$$

The parameters P_0, C_1 and C_2 were obtained from the enveloped curves of the load-displacement relationships in the reversed cyclic loading tests. The primary curves over the maximum load were obtained as the straight line determined by the drawn through the points corresponding to Pmax

5

and 0.8Pmax.

Unloading stiffens (3) and the reloading stiffness toward the previous peak (5) were based on the inclination of the straight line determined by the drawn through the origin and the peak on the primary curve (k). Reloading stiffness with soft spring (4) was based on the inclination of the straight line determined by the drawn through the peak on the primary curve and the crossing point of the X-axis (k_0).

$$k_1 / k = C_4 X_m^{C_5} + 1 \qquad (3)$$

$$k_2 / k_0 = 1 - C_6 |X_m - X_0|^{C_7} \qquad (4)$$

$$k_3 / k = C_8 X_m^{C_9} + 1 \qquad (5)$$

The parameters C_4 to C_9 were determined by approximating the relationships between k_1/k (k_2/k_0 or k_3/k) and the peak displacements of each cycle in the reversed cyclic tests. The same parameters were used for the shear walls of the same configuration at the first and the second stories. The input earthquake ground motions, the mass and the damping were the same as those of the pseudo-dynamic tests.

5. Results and discussions

Figure 5 shows the comparison of the simulated time history displacement response at the top of the first and the second stories of Group II specimens with the experimental results, and Fig. 6 compares the simulated lateral force-displacement relationships at the first and the second stories of Group II specimens with the experimental results. It shows that although the simulation of the first story response agreed comparatively well with the experimental results, the simulated response of the second story was approximately 50% smaller than the experimental results in most specimens.

Table 1 Maximum displacement response of Group I and II specimens

Specimen	Maximum displacement response of the first story (mm)			Maximum displacement response of the second story (mm)		
	Experiment	Simulation	ratio	Experiment	Simulation	ratio
W	39.09	53.17	0.74	---	---	---
D	52.09	58.04	0.90	---	---	---
S	60.01	64.72	0.93	---	---	---
WW	53.95	53.39	1.01	27.23	11.53	2.36
DW	58.88	56.58	1.04	28.57	11.16	2.56
SW	68.03	61.17	1.11	19.47	10.59	1.84
SS	62.70	58.73	1.07	26.71	16.09	1.66
SHS	35.52	28.44	1.25	76.58	60.06	1.28
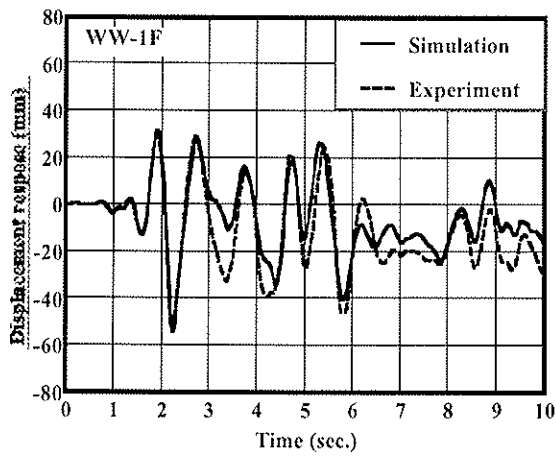
Specimen WW: 1st story
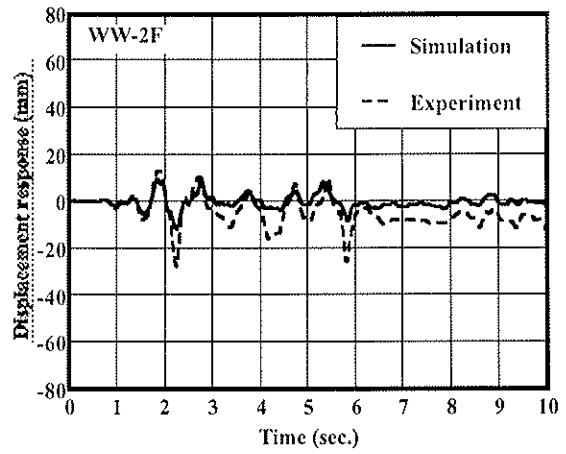
Specimen WW: 2nd story
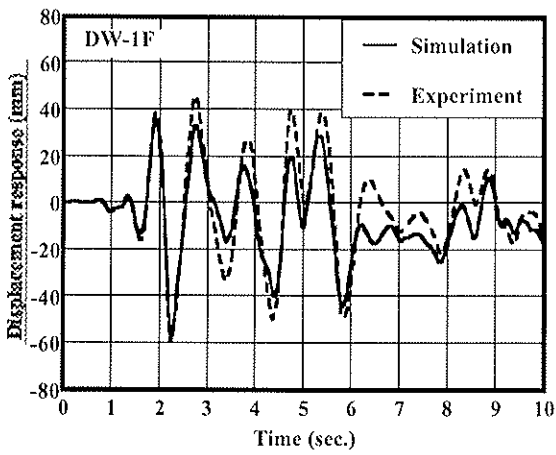
Specimen DW: 1st story
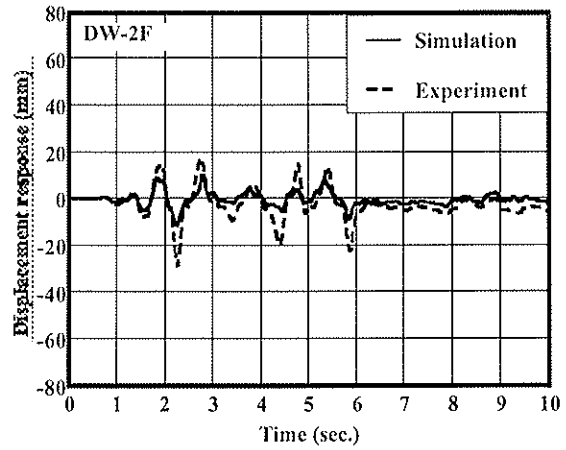
Specimen DW: 2nd story
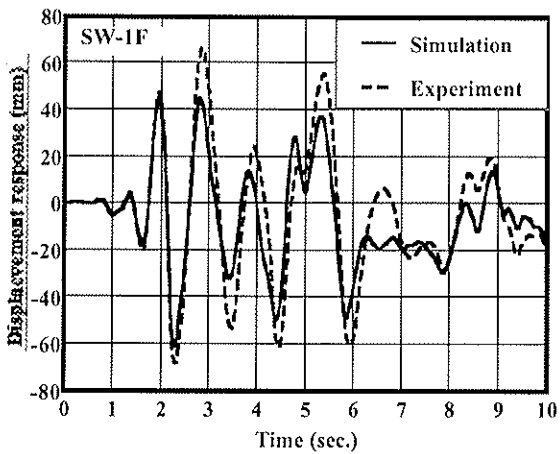
Specimen SW: 1st story
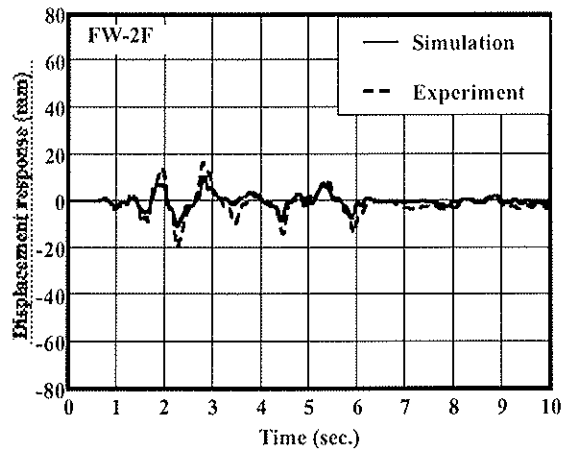
Specimen SW: 2nd story

Fig.5(a) Comparison of time hystory response by the pseudo-dynamic tests and simulation in Group II specimens(WW,DW,SW)

7

Specimen SS: 1st story

Specimen SS: 2nd story

Specimen SHS: 1st story

Specimen SHS: 2nd story
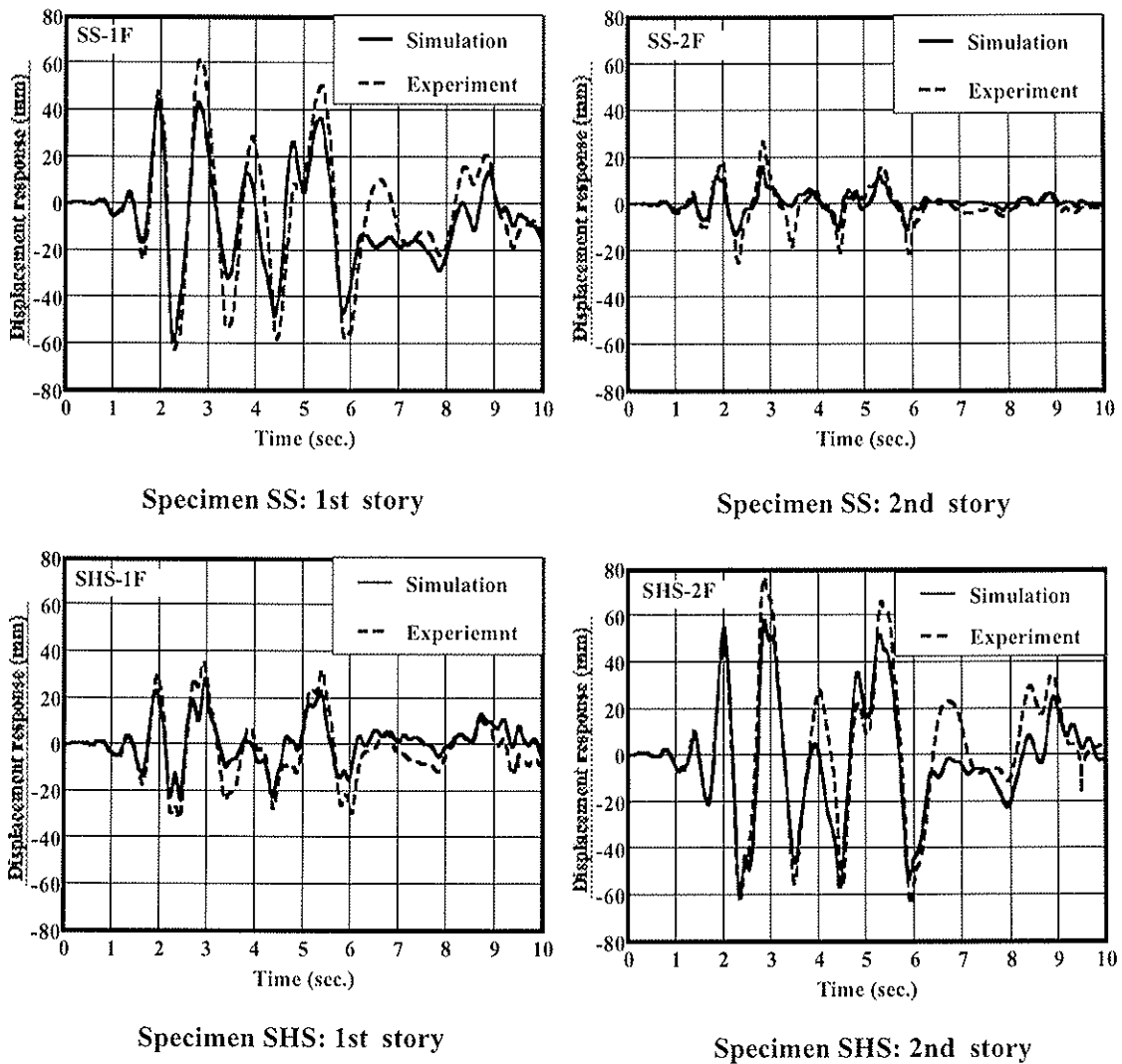
Fig.5(b) Comparison of time hystory response by the pseudo-dynamic tests and simulation in Group II specimens (SS, SHS)

This is probably because the displacement response of the second story was much smaller than that of the first story except for SHS, and the influence of the slips at the hold down bolts connecting the posts of the second and the first story is not negligible.

Table 1 shows the comparison of the maximum displacement response of the first story. It is notable that the maximum displacement response of the first story of Group II specimens whose shear walls of the second story were that with window type opening (W) was close to those of Group I specimens. This means that the pseudo-dynamic tests on single shear wall can be applicable to evaluate that of the first story of the two story building if the stiffness and strength of the second story are sufficiently large.

Table 2 shows the tensile force of the hold down bolts at the foot of posts in the first and the second stories when the horizontal displacement responses at the top of the specimen were the largest. It shows that the tensile forces were concentrated on the corner post near the loading points (A or D)
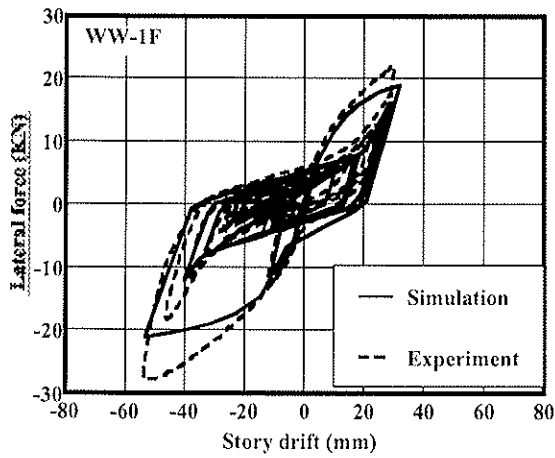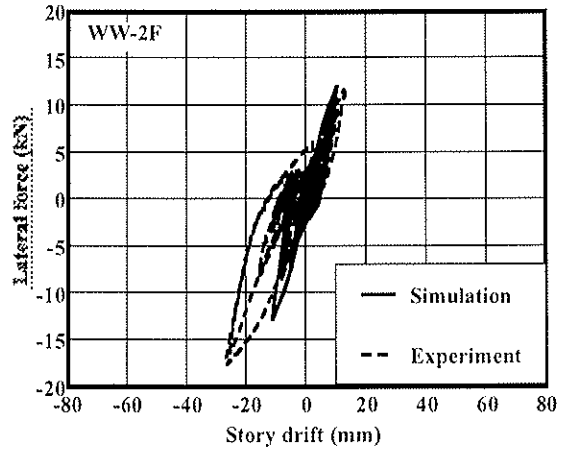
8

Specimen WW: 1st story   Specimen WW: 2nd story
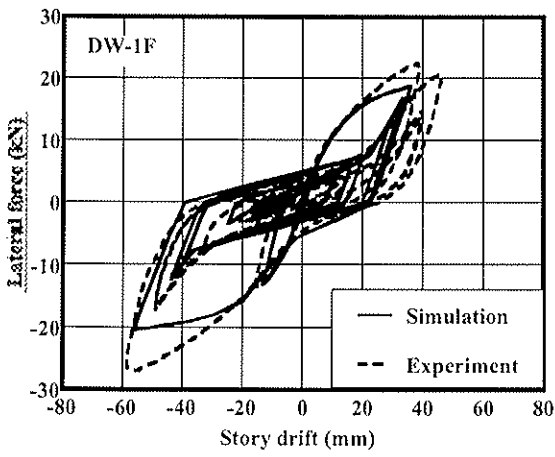
Specimen DW: 1st story   Specimen DW: 2nd story
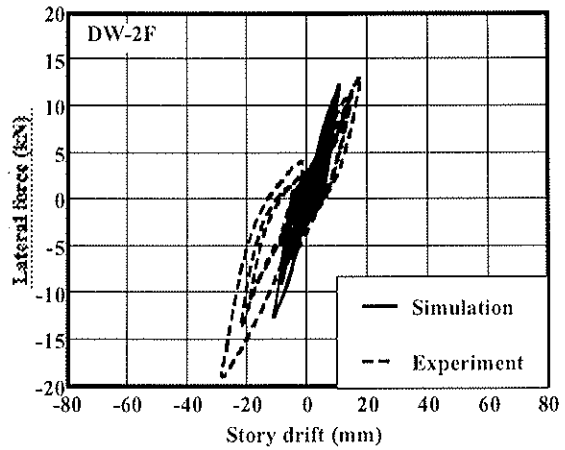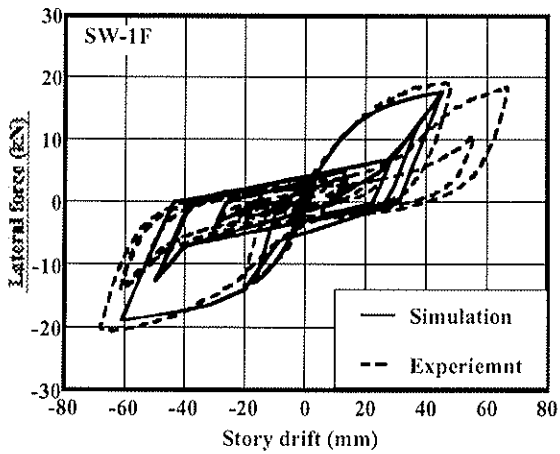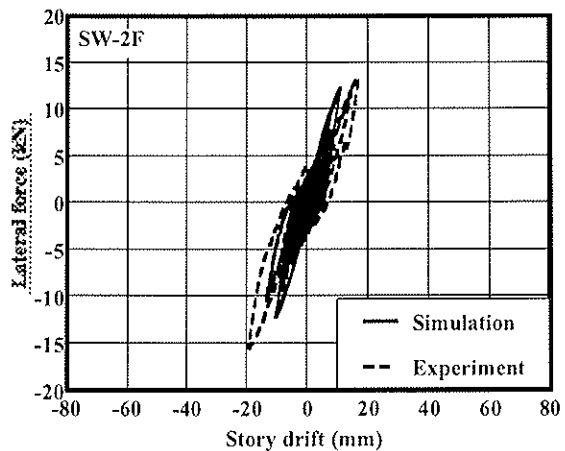
Specimen SW: 1st story   Specimen SW: 2nd story

Fig.6(a) Comparison of load-displacement relashionships by the pseudo-dynamic tests and simulation in Group II specimens (WW, DW, SW)

9

Specimen SS: 1st story

Specimen SS: 2nd story

Specimen SHS: 1st story

Specimen SHS: 2nd story
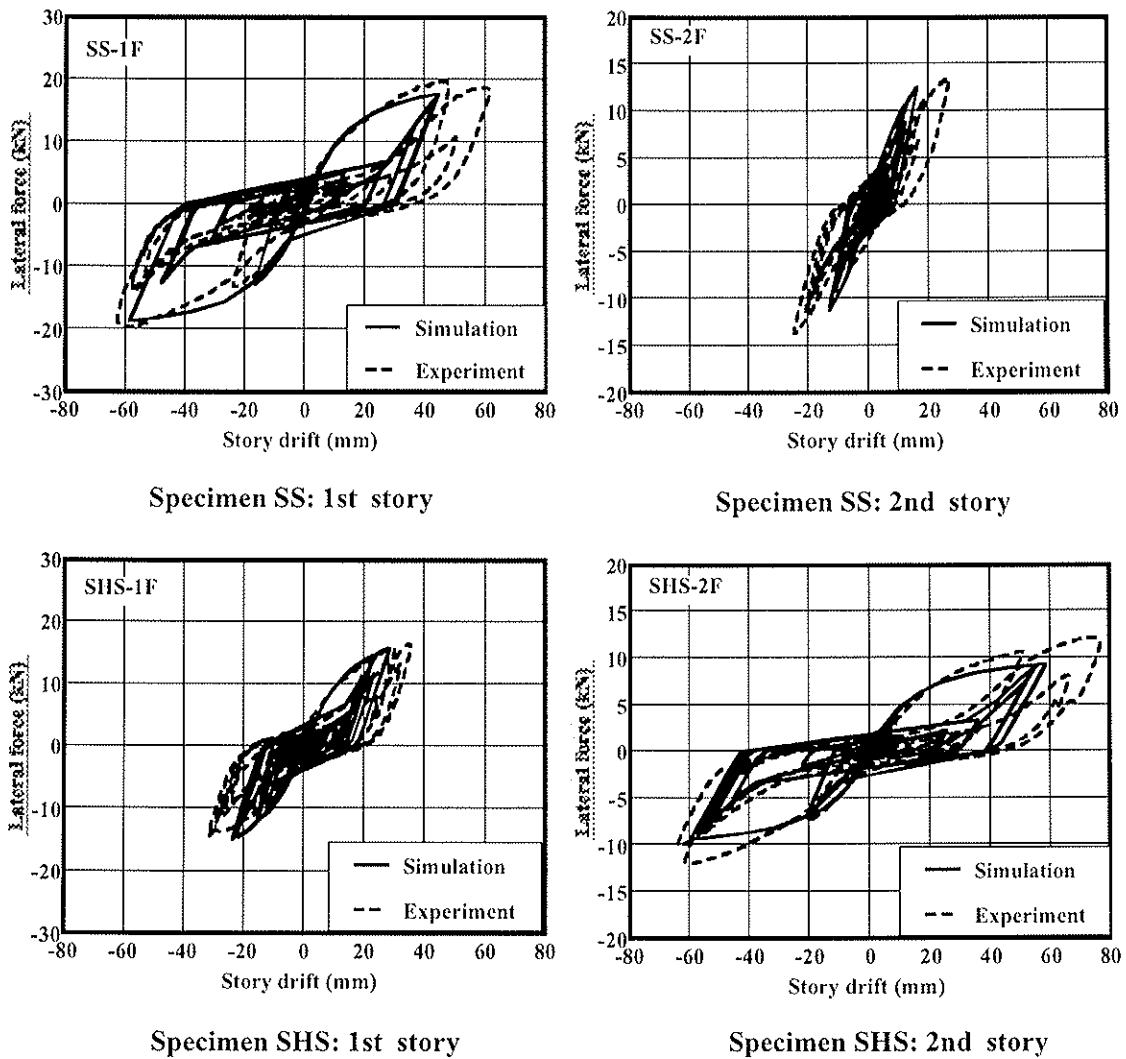
Fig.6(b) Comparison of load-displacement relashionships by the pseudo-dynamic tests and simulation in Group II specimens (SS, SHS)

and showed almost close values of 22 to 28kN regardless of the opening configuration except for the specimen SHS. In the specimen SHS, the tensile force of the corner posts were around 17kN and 30% smaller than other specimens. The tensile force of the third posts (C or B) varied from 4 to 19kN according to the different opening configuration. In general, the tensile force of the third posts (C or B) was larger when the opening was larger. In the specimen SHS, the tensile force of post B was somehow very small in the positive loading direction (D to A) and that of post C was very large (107% of post A) in the negative loading direction (A to D). This is because the tension force of the post of the second story was transmitted to the post of the first story by the hold down bolts connecting the foot of the posts of the second story and the top of that of the 1st story[4].

6. Conclusions

The following conclusions were led from the experimental and analytical studies.

1) The pseudo-dynamic tests of a shear wall with the mass supported by that particular walls show generally equal to or safe-side estimation of the response of the first story, and this method is appropriate to evaluate the seismic performance of the shear walls of the first story which are the most critical during the earthquake.

2) The simulation by the lumped mass time-history earthquake response analysis predicted quite well the response of the first story, but tended to under-estimate the response of the second story. Further studies may be necessary to predict more precisely the seismic response of whole the structures[5].

3) The tensile forces were concentrated on the corner post near the loading points and showed almost close values of 22 to 28kN regardless of the opening configuration except for the specimen SHS. The tensile force of the third posts (C or B) varied from 4 to 19kN according to the different opening configuration. As the effects of reducing the tensile force of the joints at the foot of inner posts are negligible, they should be considered in the design of joints connecting the posts to the sill[6].

7. Acknowledgements

Table 2 Tensil force of the hold down bolts at the foot of posts in the first and the second stories for the maximum horizontal displacement at the top of the specimens

Specimen	Loading direction	Lateral force (kN)		Tensile force of hold down (kN) at the 1st floor				ratio B/D or C/A
		1st story	2nd story	A	B	C	D	
WW	D to A	-7.31	-17.52	---	4.28	---	26.56	0.16
	A to D	10.28	11.00	22.04	---	6.73	---	0.31
DW	D to A	-4.08	-18.84	---	13.02	---	27.66	0.47
	A to D	6.98	13.08	21.78	---	14.94	---	0.69
SW	D to A	-5.79	-14.47	---	12.19	---	24.78	0.49
	A to D	7.98	10.59	21.63	---	18.77	---	0.87
SS	D to A	-3.24	-13.62	---	9.69	---	22.33	0.43
	A to D	4.21	13.42	25.02	---	19.48	---	0.78
SHS	D to A	3.12	-11.42	---	0.44	---	17.90	0.02
	A to D	7.48	8.47	16.89	---	18.01	---	1.07

8. References

1) Yasumura,M., Murota,T.,Nishiyama,I, Yamaguchi,N.(1988) Experiments on a three-storied wooden frame building subjected to horizontal load, Proc. of 1988 ICTE, Vol.2, pp262-275

2) ISO/DIS 16670: Timber structures – Joints made with mechanical fasteners – Quasi-static reversed-cyclic test method, 1998

3) Japan Two-by-four Home Builders Association: Structural calculation manual for wood-framed buildings,2002

4) Yasumura,M. (2001) Evaluation of damping capacity of timber structures for seismic design, Proc.of CIB-W18, paper 34-15-3

5) Richard,N.,Yasumura,M.,Davenne,L. (2003) Prediction of seismic behavior of wood-framed shear walls with openings by pseudodynamic test and FE model, J Wood Sci, 49: 145-151

6) Andreason,S., Yasumura,M., Daudeville, L.(2002) Sensitivity study of the finite element model for wood-framed shear walls, J Wood Sci, 48: 171-178

INTERNATIONAL COUNCIL FOR RESEARCH AND INNOVATION
IN BUILDING AND CONSTRUCTION

WORKING COMMISSION W18 - TIMBER STRUCTURES

EXPERIMENTAL INVESTIGATION OF LAMINATED TIMBER FRAMES WITH FIBER-REINFORCED CONNECTIONS UNDER EARTHQUAKE LOADS

B Kasal

North Carolina State University, Raleigh

USA

P Haller

A Heiduschke

Dresden University of Technology, Department of Civil Engineering

GERMANY

S Pospisil

I Jirovsky

M Drdacky

ITAM, Czech Academy of Sciences, Prague

CZECH REPUBLIC

Presented by: Bo Kasal

Bo Kasal indicated that his presentation is a follow on from the presentation by Peer Haller made in Kyoto last year. The problems with multi-storey heavy timber framed building in earthquakes relate to the relatively low mass and high strength/mass ratios of the structures. He went on to describe the full–scale and small (1:4) scale model tests conducted. He concluded by raising the various issues which should be resolved before composite reinforcements are used practically. Discussions on the paper included the need to relate W18 papers to at least work reported in previous W18 proceedings.

EXPERIMENTAL INVESTIGATION OF LAMINATED TIMBER FRAMES WITH FIBER-REINFORCED CONNECTIONS UNDER EARTHQUAKE LOADS

B. Kasal*[1], P. Haller[3], S. Pospisil[2], I. Jirovsky[2], A.Heiduschke[3], M. Drdacky[2],
[1] North Carolina State University, Raleigh, NC 27695-8005, USA,
bo_kasal@ncsu.edu, phone 919 515 5725, fax 919 513 3496
[2] ITAM, Czech Academy of Sciences, Prague, Czech Republic
[3] Dresden University of Technology, Department of Civil Engineering, Dresden, Germany

1   Abstract

1:4 scaled models and full-size two-story laminated timber frames were subjected to a series of shake-table experiments. Two different designs were tested: (i) typical design and (ii) frames with densified and fiber reinforced connections. The full-size frames had the footprint of 2400 x 3300 mm and a height of 5200 mm. The tests included sinusoidal sweeps of low amplitudes, arbitrary loading simulating earthquakes of different magnitudes (0.25-1.0g), and a sinusoidal dwell at the first natural frequency. Individual beam-to-column connections were tested to establish a nonlinear moment-rotation relationship that was used to model the connection behavior. 1:4 scaled models of frames and joints were tested prior to full-scale experiments. The fiber-reinforced connections enhanced the performance of the frames due to the higher load-carrying capacity and ductility.

2   Introduction

Wood structures traditionally perform well under dynamic loads such as earthquakes due to their low mass and high ductility of mechanical connectors. Experience from North America with light frame construction shows that the light frame buildings (LFB) are relatively safe and even under strong ground motions a total building collapse is rare. While LFB's contain large number of redundant ductile connections (nailed connections), heavy timber frames must rely on a finite number of beam-to-column connections that will be potentially overloaded during a strong motion earthquake. This increases the demands on connections in terms of ductility, moment capacity and reliability. While beam and columns behave linearly and exhibit brittle failure modes, beam-to-column connections are nonlinear, have certain ductility but can also exhibit brittle failure modes as shown further on in this paper.

Heavy timber frames are a viable alternative for steel and reinforced concrete frames used for essential structures in earthquake zones due to their low mass and excellent fire resistance of large wood cross sections. It appears that the limiting factors in the design are beam-to-column connections. Steel in various forms is almost exclusively used to facilitate connections between beams and columns. The connections can be either pinned or designed as moment connections (this is a predominant scenario). In either case, the designer has a limited space for placing the dowel-type fasteners that are used to connect beams to columns, limiting the capacity of the frames to transfer normal forces and/or moments.

Dowel bearing strength is correlated with the density of connected materials and increasing the density of the wood in the vicinity of joints will increase the overall connection capacity. Original research performed at TU Dresden [2,3] clearly shows increased capacity and ductility of simple monotonically loaded splices containing densified wood. Wood densification has been used for some time and the technology is readily available. While densifying wood material, the cell walls are damaged and this increases the susceptibility of the material to fail in tension perpendicular to fibers. Such failures if occur in connections will result in a brittle, catastrophic failure mode and that is unacceptable in structures loaded by earthquakes. Haller at al [3] used glass fiber non-woven fabric attached to the surface of the reinforced wood to prevent perpendicular-to-fibers tensile failure of connections.

In this paper, the performance of two story timber frames under dynamic loads and the relationship between laboratory connection tests and performance of connections within the frames will be examined.

3 Research program

The research program consisted of the following:
3.1 Testing of scaled models (1:4) of beam-to-column connections
3.2 Testing of full-scale beam-to-column connections
3.3 Shake-table tests of two-story scaled models (1:4) frames
3.4 Full-scale shake table tests of two-story frames

3.1 Testing of scaled models (1:4) of beam-to-column connections

The testing of scaled models of beam-to-column connection has been discussed by Kasal et al [5]. The goal of these experiments was to test various design scenarios and select the connection architecture that will be the most suitable for dynamic applications. Load-deformation characteristics are also needed for future analytical modeling. Moment capacity, energy dissipation (ductility) and failure modes were the variables that were used to select the candidates for full-scale experiments. Three different joint configurations were designed to test various options. The first connection type was a circle 54 mm in diameter consisting of 12 dowels with a diameter of 3 mm. The second joint had total of 8 dowels (4 dowels (d = 5 mm) and 4 dowels (d = 3 mm)), and the third connection had only 4 dowels (d = 5 mm). The joints were designed to meet the requirements of DIN 1052 T2 [1] for edge distance, end distance and spacing. We have tested joints with non-densified material (non-reinforced – control, and reinforced) and densified and reinforced material. The densification parameters, test protocol and results are described in Kasal et al [5]. The geometry of the connection is shown in Figure 1 (1:1 scale) except that the densified samples were used densified material throughout the entire cross section (20 x 40 mm).

3.2 Testing of full-scale beam-to-column connections

The full-size beam-to-column connections had the dimension shown in Figure 1 and were tested under the same protocol (DIN 1996) as small-scale connections. The goal of these experiments was to establish the moment and energy dissipation capacities needed to design the full-scale experiments and moment-rotation curves needed for analytical modeling.
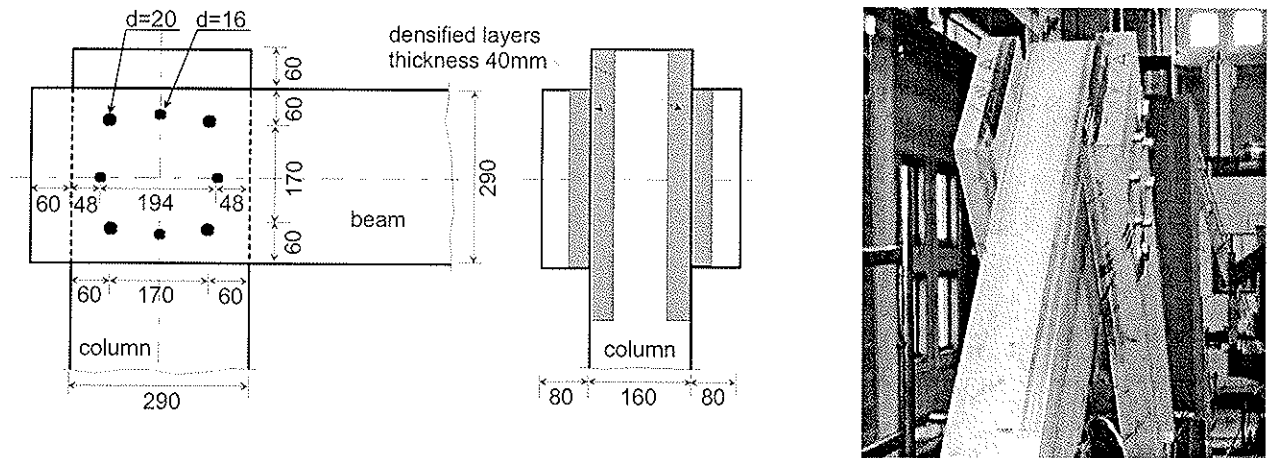
Figure 1. Connection detail and three-dimensional view of a partially densified and reinforced full-size specimen. Only first two laminations (2x20mm) at the interface between the beams and column were densified (Kasal et al 2002).

Three types of connections were tested: (i) control, made of non-densified, non-reinforced wood; (ii) beam-to-column connection with non-densified and reinforced wood; and (iii) beam-to-column connection containing layers of densified material reinforced with glass-fiber non-woven fabric. Typical rotation-moment relationships are shown in Figure 2.
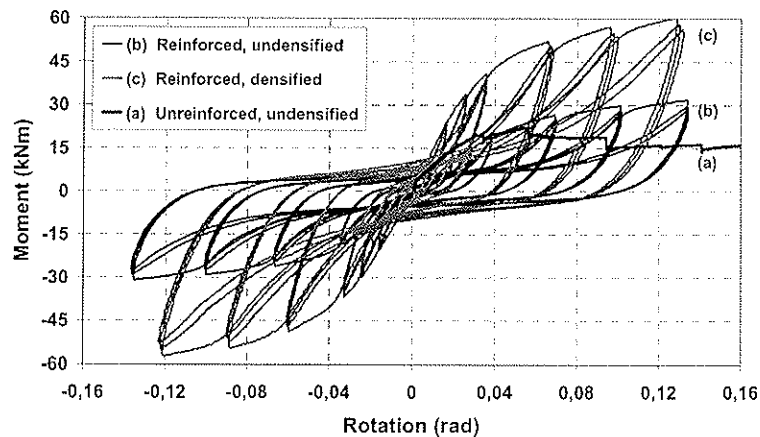
Figure 2. Typical moment-rotation curve for cyclically loaded full-scale beam-to-column connection.

Comparing the small-scale and full-scale tests revealed:

1. Densified material significantly increased strength and energy dissipation capacity of beam-to-column connections.
2. The use of densified wood increases the dowel bearing strength of the material and dowels or pins of larger diameters can be used while still exhibiting plastic hinges.
3. Application of non-woven reinforcing fabric minimizes the risk of brittle failure and significantly increases ductility of the connections.
4. Similar failure modes, behavior and relative properties of scaled and full-size connections allow one to use the scaled experiments to investigate dynamic behavior of subsystems and systems containing these connections.

3

3.3 Shake-table tests of two-story scaled models (1:4) frames

The goal of these tests was to study the qualitative behavior (joint rotations, failure modes) of the two story frames containing fiber reinforced densified/non-densified joints and establish a baseline for the full-scale tests. In addition, the data from the shake-table tests can be used to verify developed analytical models. Shake-table tests of the two story scaled models of frames were performed on a unidirectional shake-table at the Czech Academy of Sciences in Prague, Czech Republic. The test protocol included dynamic impact tests, sinusoidal sweep tests, arbitrary excitation in magnitudes up to 1.0 g simulating earthquake load. Each arbitrary signal was followed by a sinusoidal sweep function to determine the natural frequencies of the frames. The arbitrary signal was generated using SHR IEEE5 synthetic earthquake [6]. Two frame designs were tested: (i) typical design with non-densified reinforced material, and (ii) frame with densified and reinforced wood. The dimensions of the frame are in the Figure 3.
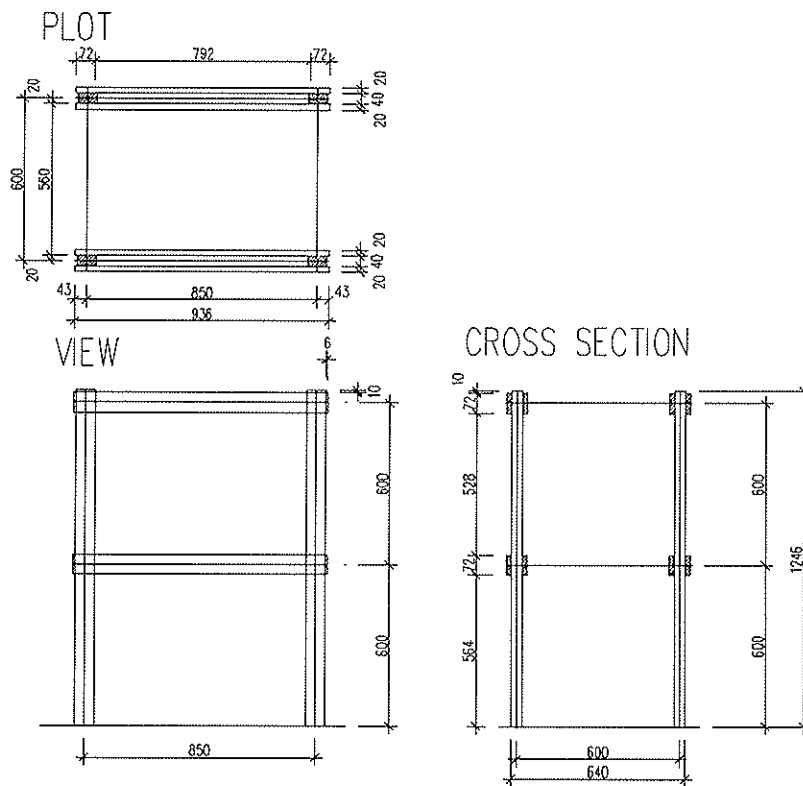
Figure 3. Dimensions of the 1:4 scaled frame (dimensions in mm).

The frames were constructed from Spruce wood. The decks were made of 5 mm thick plywood and 6x20 mm joists spaced 40 mm on center. The plywood was nailed to both surfaces of the joists. Lateral stiffness was established by shear walls made of 5 mm plywood and 5x20 mm vertical studs. One set of tests was performed on frame with steel cable x-braces restraining the frame in weak

4

direction – see Figure 5a. Densified wood had the average density of 900 kg/m^3, which represents about 50% densification. The frame was loaded by masses of 90 kg at the 1st floor level and 70 kg at the 2nd floor level. The masses simulated full dead and live load and steel disks of 10 kg mass each were used to simulate the distributed load. The frames were tested under the angles of 0 and 45 degrees with respect to the bents. The 45 degree angle generated torsions in the frame.

3.4 Full-scale shake table tests of two-story frames

The full-scale frame design is shown in Figure 4. The goal of the tests was to investigate the system performance under dynamic loads. The frames were made of the same material (Spruce) as the 1:4 scaled frames. The zones with densified wood were extending 600-1200 mm beyond the joints and finger jointing was used to facilitate the transitions between non-densified and densified material.
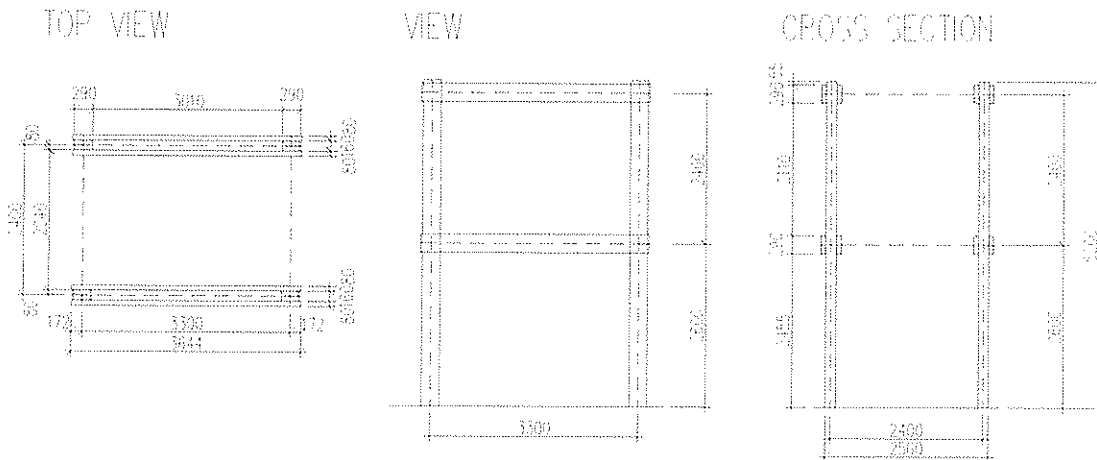
Figure 4. Full-frame dimensions (in mm).

Two frames were manufactured: (i) a control made of non-densified material (density of 0.44 g/cm^3) without reinforcement, and (ii) a frame with partially densified and reinforced material (further "densified frame") (see Figure 1). The densified wood had the density of 0.85 g/cm^3. The control specimen was horizontally laminated while the densified frame had members vertically laminated.

(a) (b)
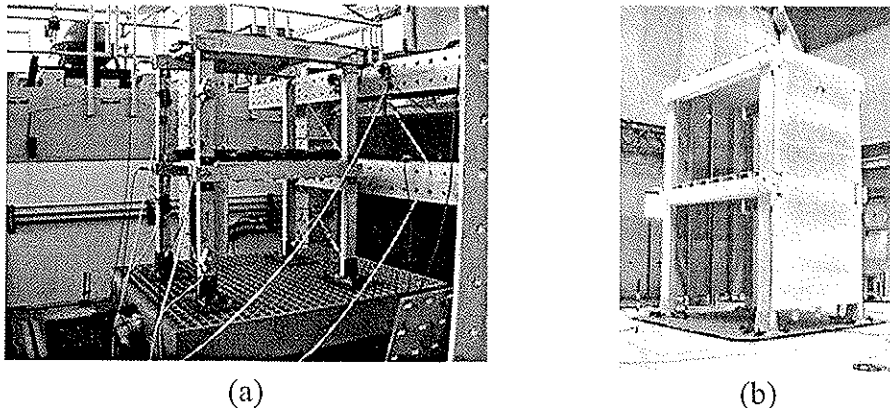
Figure 5. Shake table test setup. Scaled model test (a), and full-scale test (b).

Vertical lamination was necessary to introduce reinforcement at interfaces between laminations such that it was effective when connections were loaded by moments. Details of the densification process and parameters of the reinforcing fabric are reported in [5]. The test setup is shown in

Figure 5. Concrete blocks with masses of 360 kg/block were used to simulate the dead and live load. Two blocks were used on the roof (720 kg total) and four on the floor (1440 kg total). The masses simulated full dead and live loads. We have decided to use full loads (instead of 50%) based on small-scale experiments where we were unable to induce frame failure even under sinusoidal excitation at the 1st natural frequency.

4   Results and discussion

The transfer function (TF) comparing the table acceleration input and output from the top corner accelerometer is shown in Figure 6. The TF shows the magnitude of the amplification. At resonance frequency (phase = 90 degrees), the amplifications are significant.

(a)   (b)
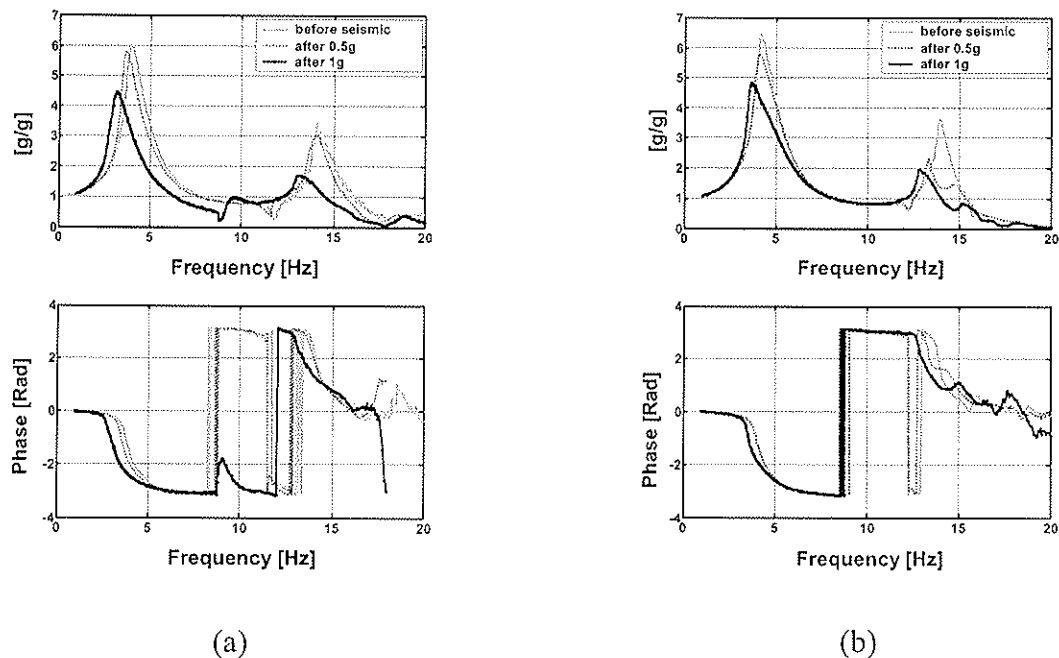
Figure 6. Transfer function for the upper top corners of the frame with non-densified reinforced connections (a) and densified and reinforced connections (b).

The arbitrary excitation did not cause failure and cracks in the material for either of the tested frame. The typical frame design (non-densified and non-reinforced, horizontally laminated) exhibited longitudinal cracks due to the tension perpendicular to grain after a sinusoidal dwell test at the frame fundamental frequency - Figure 7. The sinusoidal dwell test produced maximum drifts of 100 and 70 mm for typical and densified frames, respectively. The densified frame did not have any visible damage after the sinusoidal dwell test. The lack of cracks can be attributed to the radial reinforcement that prevented the brittle cracks from occurring. This is consistent with the cyclic tests of connections where significant rotations had to be imposed before cracks started to develop.
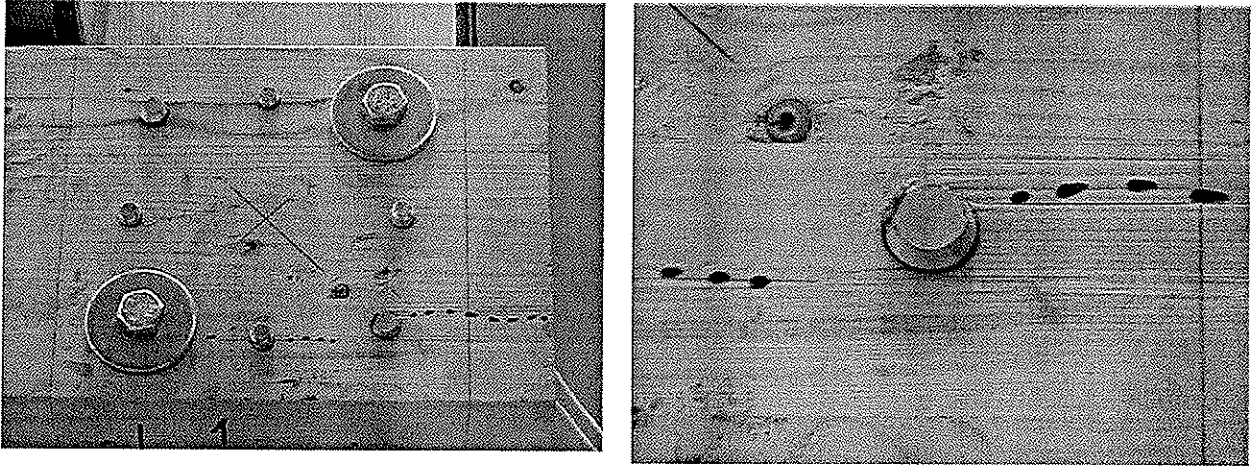
Figure 7. Cracks developing in the vicinity of steel dowels after sinusoidal dwell test.

The rotation between beam and column (joint rotation) for the upper corner of the densified frame loaded by a strong motion earthquake is shown in Figure 8. Comparing the experimentally measured rotations with the standard joint test (Figure 9) reveals that the actual joint rotations are extremely small as compared with amplitudes prescribed by the standard test [8].
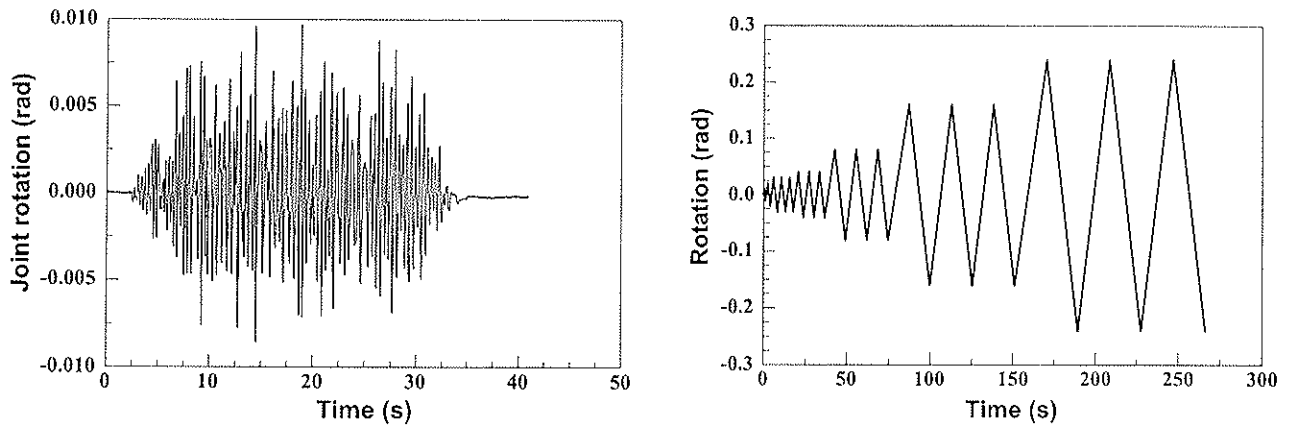
Figure 8. Rotation between the beam and column at the top corner of the densified frame loaded by an artificial earthquake excitation of 1.0g (a), and test protocol used for connection tests (b).

Figure 8 and Figure 9 indicate that the standard test protocol does not provide enough information in the range of displacement that can be expected in a real structure (Figure 8). If strength and stiffness degradation are important parameters, then the standard test protocol used in this experiment will not yield required data to identify the degradation of the system in the range of displacements that are likely to occur in the real system. Comparing Figure 9b with Figure 8a shows that the standard test will reach the maximum rotation that the joint experienced in two cycles.
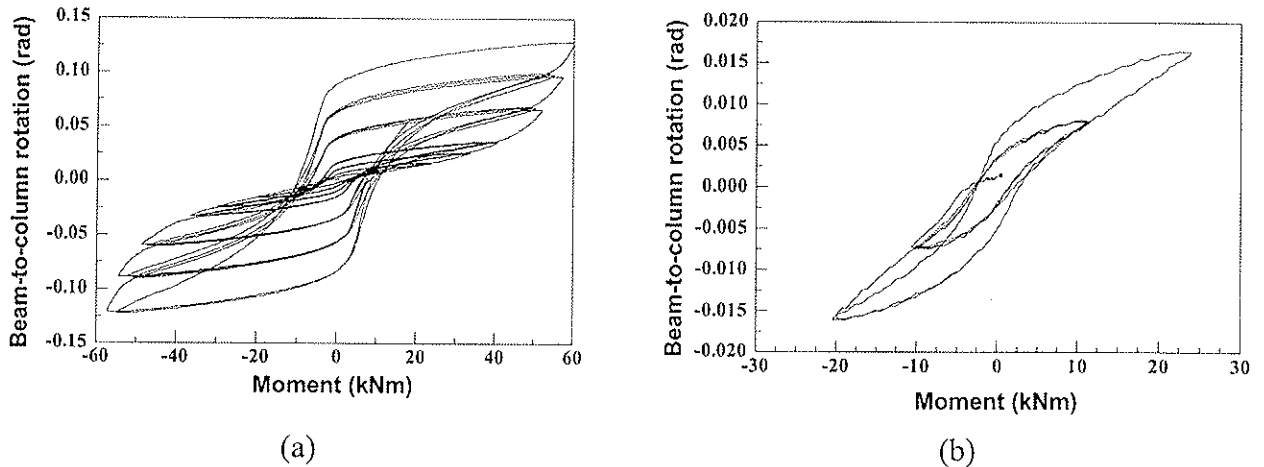
Figure 9. Reinforced densified beam-to-column connection cyclic test - full scale, reinforced and corner with densified material – see Figure 1). Full test result (a), and first two cycles (b).

5 Conclusions

Reinforcing beam-to-column connections of laminated heavy timber frames increases the moment and energy dissipation capacity of the joints and structural systems with these joints. Using densified material further enhances the connection performance provided that such connections are reinforced to prevent brittle failures in tension perpendicular to fibers.

Standard cyclic connection tests used in this work reach the practical deformation range too rapidly and do not give enough information about joint behavior under small rotations. Shake table tests of small and full-size frames revealed qualitatively same behavior of both structures but similitude theory cannot be used to make inferences from small-scale tests due to the nonlinear behavior of the system.

5 References

1. DIN 1052 T2 Timber Structures – Mechanical joints; Beuth Verlag, Berlin, Germany. 1988.
2. Haller P. Technische Textilien im Holzbau und ihre Möglichkeiten in der Verbindungstechnik, Bauen mit Textilien, Berlin: Ernst & Sohn, 1997 Heft 1, S. 11
3. Haller P, Wehsener J, Birk T. Embedding characteristics of fibre reinforced and densified timber joints; proceedings, CIB-W18-meeting, Venice, Italy, August 2001.
4. Haller, P. and, J. Wehsener. 2003. Entwicklung innovativer Holzverbindungen aus Pressholz und Glasfaserbewehrung, Forschungsbericht, irb-Verlag, Stuttgart.
5. Kasal B, Heiduschke A, Haller P. Fiber-reinforced beam-to-column connections for seismic applications. Paper submitted to CIB W16 committee meeting. Kyoto. Japan. 2002
6. Institute of Electrical and Electronic Engineers (IEEE), Standard 344, Recommended Practice for Seismic Qualification of Class 1E Equipment for Nuclear Power Generating Stations, 987.

INTERNATIONAL COUNCIL FOR RESEARCH AND INNOVATION
IN BUILDING AND CONSTRUCTION

WORKING COMMISSION W18 - TIMBER STRUCTURES

EFFECT OF TEST CONFIGURATIONS AND PROTOCOLS ON THE

PERFORMANCE OF SHEAR WALLS

F Lam

D Jossen

J Gu

N Yamaguchi

H G L Prion

Department of Wood Science, University of British Columbia, Vancouver

CANADA

Presented by: Frank Lam

In his introduction Frank Lam discussed the possibility of an earthquake in Vancouver before going on to describe the test protocol, specimens and results obtained. The aim of the research is to investigate the influence of test configuration and protocols on the performance of shear walls. He observed that hold-down devices allow full racking capacity to be developed. He concluded that hold down devices have a strong influence on the behaviour of the structure. More importantly a large number of load cycles in testing may not truly reflect structural behaviour in an earthquake. Hence he recommended that cyclic testing protocols should consider the total energy dissipation characteristics of the structure under expected earthquake excitation.

Effect of test configurations and protocols on the performance of shear walls

F. Lam[1], D. Jossen[2], J. Gu[3], N. Yamaguchi[4], H.G.L. Prion[1]

Department of Wood Science, University of British Columbia, Vancouver Canada

1. Introduction

A series of full scale static and reversed-cyclic tests on 1.82 m x 2.67 m Japanese post and beam shear walls sheathed with OSB panels were conducted at the University of British Columbia to evaluate their performance under different configurations and protocols. Lateral performance of shear walls tested with hold-down devices or tie rods (hydraulically controlled) are compared. Different cyclic test protocols are also considered including protocol recognized by Japanese Ministry of Land, Infrastructure and Transport (MLIT), Consortium of University for Research in Earthquake Engineering (CUREE) developed near-fault protocol, and a University of BC (UBC) protocol. Different failure modes were observed under the various test configurations and protocols. There was significantly increase in the ultimate strength when hold-down devices and dead weight were used in comparison with the hydraulically controlled tie rod system. The envelope of the cyclic load deflection curves from the CUREE near-fault protocol and the UBC protocol matched the monotonic test results well.

2. Experimental studies

Figure 1 shows a typical Japanese post and beam shear wall with OSB sheathing panel under lateral load tests. The sill and top beam of test specimen were mounted to two steel channels using a total of eight 12.7 mm bolts. The bottom channel was fixed to the reaction floor by steel angles. The top channel was guided laterally by rollers and attached to a MTS hydraulic actuator. In Phase I, MTS Micro-Controller (458.10) and Material Testing Function Generator were used to drive the actuator. In Phase II, MTS FlexTest GT digital controller and Hydraulic Manifold (293.11A) were used. A PC-based data acquisition system recorded the data with a frequency of 10 Hz. As shown in Figure 1, hydraulic controlled tie rods were used to apply the dead loads to the structure in Phase I while, in Phase II, steel weights were installed onto the top steel channel to represent the dead loads.

---

[1] Associate Professor, University of British Columbia Vancouver BC Canada
[2] Research Assistant Swiss Engineering School for the Timber Industry (SISH) Biel-Bienne Switzerland
[3] Ph.D. Student University of British Columbia Vancouver BC Canada
[4] Senior Research Engineer, Building Research Institute, Tsukuba City, Japan

All the post and beam/sill members were 105 mm x 105 mm Hem-fir timber except in phase I Hem-fir 105 mm x 135 mm timber was used as the top beams. The vertical studs were Hem-fir 30 mm x 105 mm members. Schematic details of the frame used in Phase II can be found in Figure 2. The walls were built following Japanese method of construction, with mortise and tenon joints and "T" connectors (Figure 3). All connection plates and nails were obtained from Japan. JAS grade 910 mm x 2580 mm x 9 mm thick OSB was used as sheathing panels with the longitudinal axis parallel to the height of the wall. Common 6D nails were used to fasten the panels to the frame members. The nail spacing (perimeter and field) was 150 mm. In Phase II, standard Japanese hold-down devices (HDB-20 bracket and LS 12, 4 x lag screws) were applied to the four corners of each specimen, as recently required in Japan.

Static push-over tests were conducted first in both phases of the test program. Based on the static test results, in Phase I reversed-cyclic tests were conducted following an older version of the Japanese test protocol in used until 2000 and a load protocol proposed by the University of BC (UBC protocol) (He et al. 1999). In Phase II, the current Japanese load protocol (Tsukuba Building Test Laboratory, 2001) and CUREE near-fault cyclic test protocol (Krawinkler et al. 2001) were followed. The current Japanese test method is authorized by Japan Ministry of Land, Infrastructure and Transport (MLIT), former Minister of Construction (MOC). Both the UBC and CUREE near-fault protocols have significantly fewer small cycles. Loading rates were 0.13 mm/sec for the monotonic tests, 2.4~4 mm/sec for the UBC protocol, 4 mm/sec for the old Japanese protocol, 0.14~1 mm/sec for the CUREE near-fault protocol and 0.08~0.7 mm/sec for MLIT protocol. Vertical load representing a total load of 2.275 kN/m from two stories over an area of 1.82 m x 1.82 m was applied onto the specimen. A description of the test configurations is shown in Table 1.
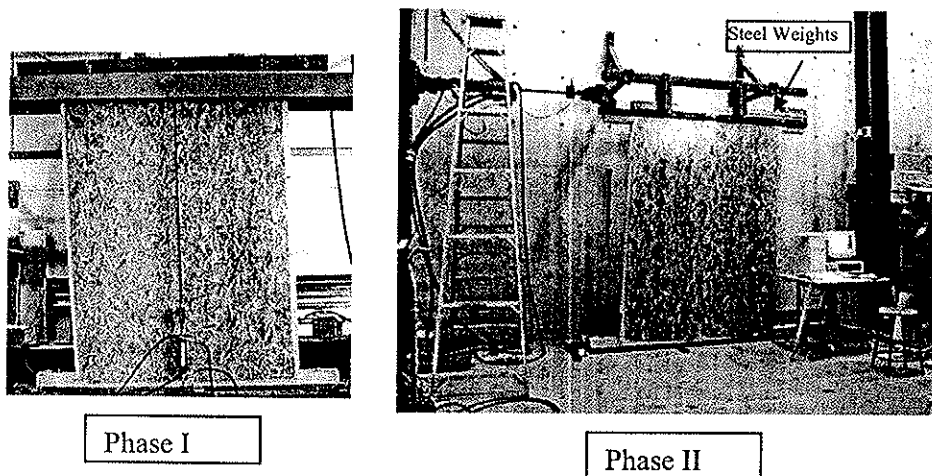
Figure 1. Test setup.
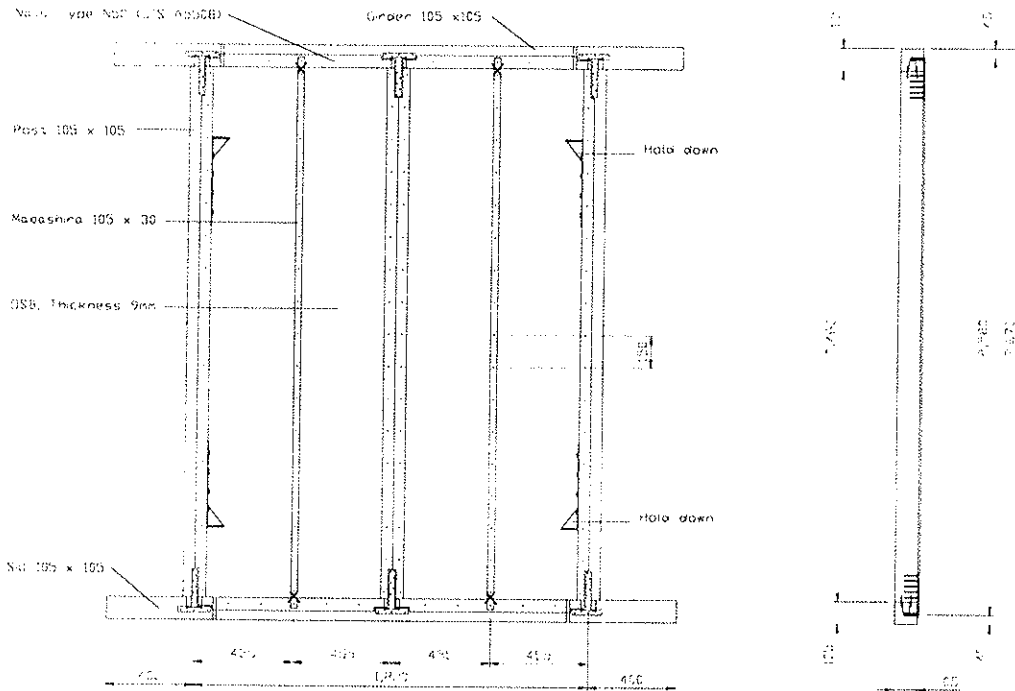
Figure 2. Details of a test specimen.
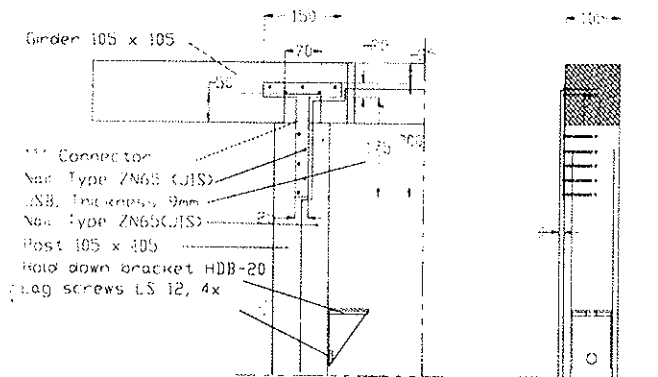
Figure 3. Mortise and Tenon joint and "T" connector.

Table 1. Test configurations.

Wall number	Test phase	Hold-down	Load type	Protocol
1	Phase I	No	Tie rod	Monotonic
2	Phase I	No	Tie rod	Monotonic
3	Phase I	No	Tie rod	Japanese (old)

3

4	Phase I	No	Tie rod	UBC
5	Phase II	Yes	Steel weight	Monotonic
6	Phase II	Yes	Steel weight	Japanese (current)
7	Phase II	Yes	Steel weight	CUREE near-fault
8	Phase II	Yes	Steel weight	CUREE near-fault

3. Test results and discussions

The test results are summarized in Table 2. P_{max} is defined as the maximum load carrying capacity; Δ_{max} is the displacement at maximum load; $\Delta_{0.8}$ is the post peak load displacement at 0.8 P_{max}.

Table 2. Japanese shear wall summary test results.

Wall	P_{max} (kN)	Δ_{max} (mm)	$\Delta_{0.8}$ (mm)	$\Delta_{0.8}/\Delta_{max}$
1	10.50	50.8	115.5	2.27
2	10.59	78.8	112.9	1.43
3	10.36/-11.92	66.5	101.3	1.52
4	12.49/-9.65	50.4	57.9	1.15
5	20.62	114.6	134.0	1.17
6	20.62/-16.08	72.0	87.4	1.21
7	20.76/-17.05	114.6	127.4	1.11
8	19.89/-15.86	117.6	141.2	1.20

The monotonic test results of Walls 1 and 2 (Table 2 and Figure 4) showed that the maximum load of the Japanese wall without hold-down is about 10.5 kN. Their load displacement curves show a plateau around the maximum load; therefore, precise estimation of Δ_{max} is difficult. Under the cyclic tests, Wall 3 has a peak load of 10.36 kN under one load direction and a peak load of -11.92 kN under reversed loading (Table 2). The asymmetric shape of the load deformation curve results from damage in the wall specimen during the leading half of the load cycle. Figure 5 shows the load displacement curves of Wall 3 together with the corresponding monotonic envelop curve for Wall 2. The monotonic test results can be considered as the backbone curve of Wall 3 with reasonable agreement. For Wall 4 subject to UBC protocol, its peak load is 12.49 kN, which is slightly higher than that of Wall 1 (Figure 6). After the peak load was reached, the load capacity decreased significantly. The response during the final push over load sequence also shows significant reduction from the monotonic curve. This behaviour can be explained by the different failure modes observed in the tests. In the monotonic test, the nail pull out in the vertical line of the T-connector was observed. In the cyclic test, the presence of tension perpendicular to grain failures as well as nail pull out failures (horizontal line) at the both sill to post connections (Figure 7) were found. With proper adjustment of nail location (closer to the base), the tension perpendicular to grain failures might be avoided. Furthermore, evidence of compression perpendicular to grain damage in the sill was also observed during cyclic loading from the action of the stud under compressive load.

4

In Phase II, Walls 5 to 8 were tested with hold-down. Wall 5 has a maximum load of 20.62 kN. Its load displacement curve also exhibited a good ductility (see Figure 4). For Wall 6 tested under MLIT protocol, the peak load is 20.62 kN, which happens to coincide with the monotonic result. After the peak load was reached, significant drop in load can be observed resulting from nail fatigue type failures (Figure 8). For Walls 7 and 8 subjected to the CUREE near-fault protocol, their load displacement curves are close to each other (Figure 9). Their backbone curves, as well as the peak load, fit the monotonic result very well.
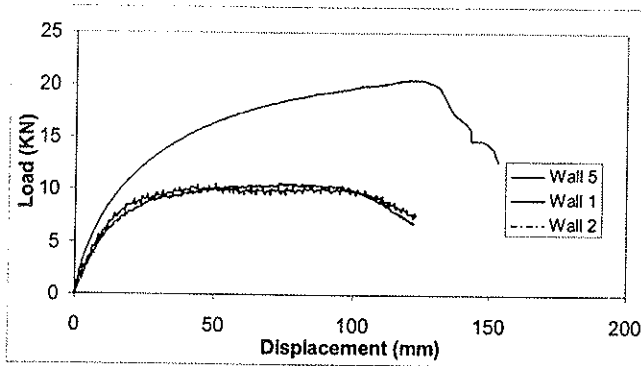
Figure 4. Comparison of monotonic tests.
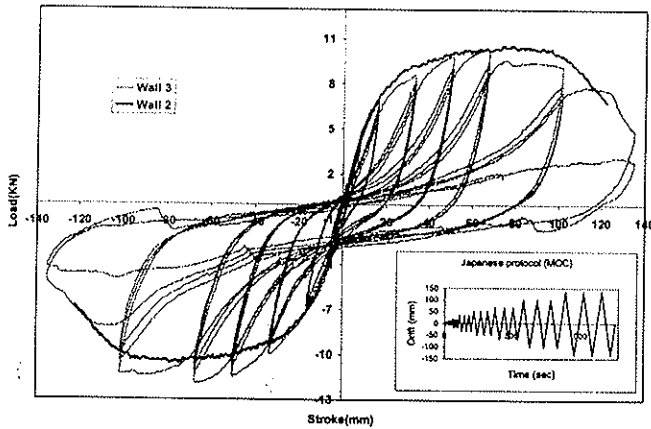
Figure 5. Load displacement curve under Japanese (old) test protocol (Wall 3).

5
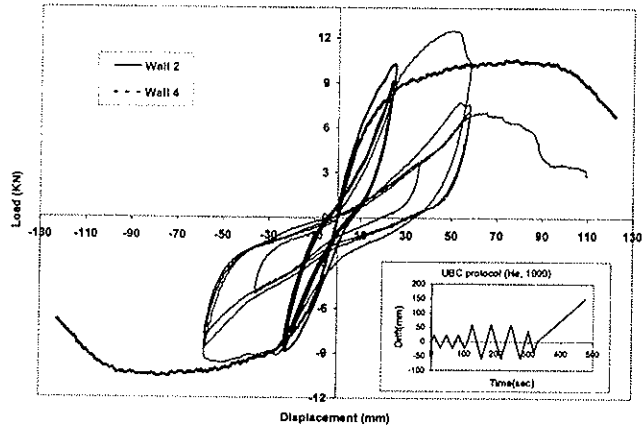
Figure 6. Wall under UBC protocol (Wall 4).
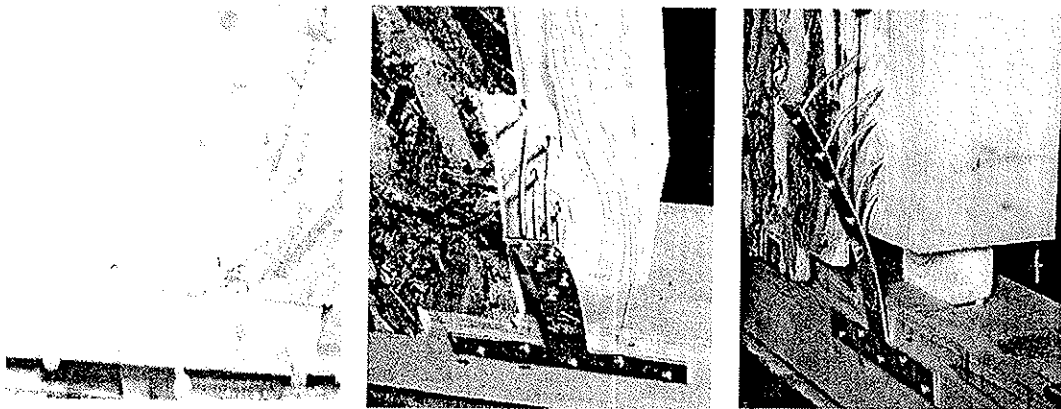
Figure 7. Uplift at the push end in Phase I tests.
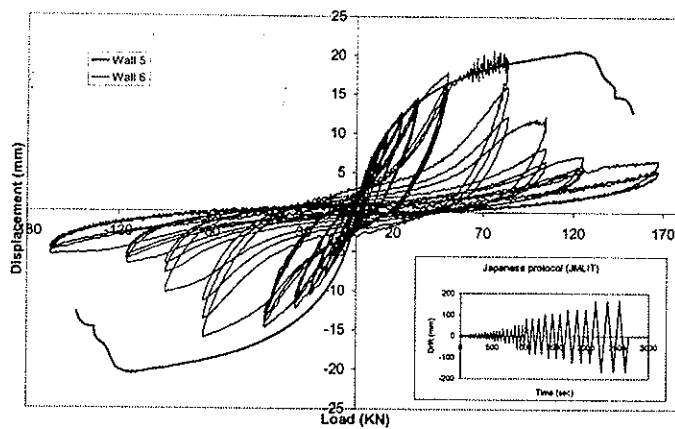
Figure 8. Load displacement curve under Japanese (current) test protocol (Wall 6).

6
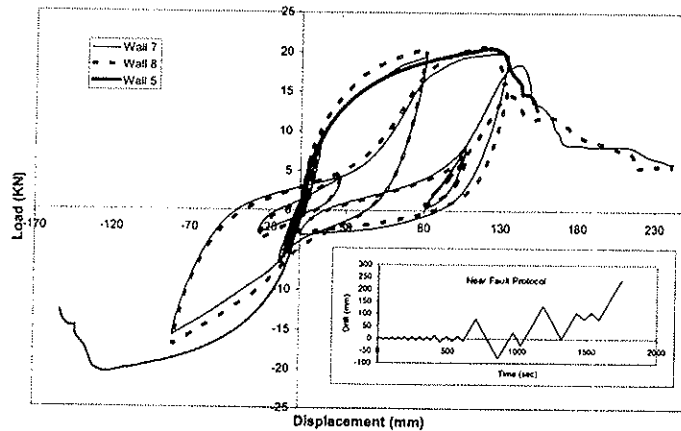
Figure 9. Load displacement curve under near-fault protocol (Wall 7 & Wall 8).
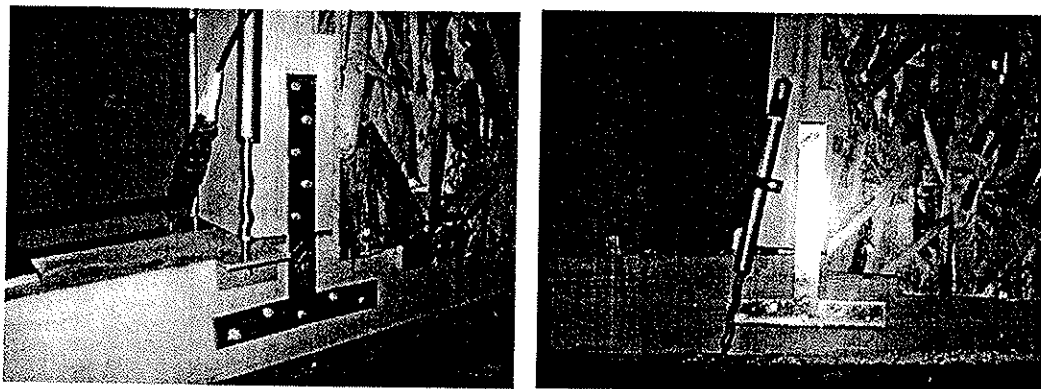
Figure 10. Negligible uplift at the push end in Phase II tests (only rotation angle).

3.1 Variation of shear wall

In Phase I, Walls 1 and 2 have identical configuration and test procedures. The monotonic load deformation curves are very close to each other (Figure 4). In Phase II, another set of identical walls (Walls 7 and 8) were tested under same test conditions. Again reasonably close results were observed (Figure 9). In these cases nail withdrawal type failures in the sheathing to framing were dominant. Although the results seem to be fairly repeatable, one must exercise caution because if wood failure modes are present one can expect much higher variation.

3.2 Effect of hold-down devices

Compared with the monotonic results in Phase I (Walls 1 and 2) and Phase II (Wall 5), Wall 5 shows significantly higher capacity than the walls in Phase I. For the monotonic tests, Phase I has the average peak load of 10.55 kN while Phase II has the peak load of 20.62 kN. The improvement of load carrying capacity can be attributed to the

7

reinforcement effect of the hold-down devices which prevented failure of the sill to post connection (including nail pull out and tension perpendicular to grain).

In Phase I without the hold-down devices, the sheathing to framing nail connections have to contribute to resisting the uplift forces; especially after the failure of the T-connector. In Phase II with the hold-down devices installed, the uplift potential was transferred directly to ground by the hold-down (Figure 10); so the nail connectors contributed primarily to the racking resistance. This effect of hold-down is consistent with observation from the tests of steel plate corner reinforcement (Durham et al 1996).

3.3   Effect of load protocols

Among the test protocols used, the MLIT protocols have long load sequences, while the UBC protocol and the CUREE developed near-fault protocol used fewer groups of large cycles. From Figure 8, the wall under Japanese protocol experienced an early peak load at a smaller displacement followed by a substantial drop in the load carrying capacity. It can be explained by low cycle fatigue failures of the nails around the wall perimeter, many of which fell to the ground or could be easily removed from the wall during the test. Although the field nails were still in position, they did not contribute much to the wall strength. In Figure 9, the load displacement curve under the CUREE near-fault protocol matched well with monotonic rests. It was also observed that few perimeter nails failed under low cycle fatigue. Since nail fatigue failures were not observed from damaged buildings in actual or simulated earthquakes (Durham 1998), the test protocols with fewer cycles seem to reflect the actual performance more realistically. This observation agreed with the results from North American light frame shear walls (He et al. 1999, Durham 1998). The maximum load of Wall 4 is higher than that of monotonic test (Figure 6). However, its substantial drop in capacity after the peak load can be attributed to the failure of T connectors, rather than the premature failure of nails between sheathing panels and posts (Stefanescu 2000).

4.   Conclusions

To investigate the influence of different configurations and protocols on the performance of Japanese shear wall, Japanese protocols, UBC protocol and CUREE developed near-fault protocol were followed. The test results showed that the backbone curves of the UBC and CUREE near-fault protocols, agreed with the monotonic test results. The protocols with long load sequence gave a similar backbone curve prior to achieving peak loads with monotonic test results. After peak loads, significant drop in capacity can be observed compared to the monotonic test results resulting from premature failure of the nail connectors.

Comparing the results from two test phases indicates that hold-down devices significantly increased the strength of walls. The test results also show that the variation of wall strength was not significant when nail withdrawal type failures of the sheathing to frame connectors were expected.

8

5. References

Durham, J. P., Ventura, C. E., Latendresse, V. and Prion, H. G. L. (1996). "Seismic resistance of shearwalls with steel plate corner reinforcements." Proceedings of the International Wood Engineering Conference, Vol. 2, New Orleans, USA, 550-557

Durham, J. P. (1998). "Seismic response of wood shearwalls with oversized oriented strand board panels." M.A.Sc thesis, University of British Columbia, Vancouver, BC, Canada

He, M., Magnusson, H., Lam, F., and Prion, H.G.L. (1999). "Cyclic performance of perforated wood shear walls with oversize oriented strand board panels." Journal of Structural Engineering, ASCE, 125(1), 10-18

Krawinkler, H., Parisi F., Ibarra L., Ayoub A., Medina R.(2001). "Development of a Testing Protocol for Wood Frame Structures". CUREE-Caltech woodframe project report, Stanford University, CA USA.

Lam, F., Prion, H.G.L and He, M. (1997). "Lateral Resistance of Wood Shear Walls with Large Sheathing Panels." Journal of Structural Engineering. ASCE, 123 (12), 1666-1673

Stefanescu, M. (2000). "Lateral Resistance of Traditional Japanese Post-and-beam Frames under Monotonic and Cyclic Loading Conditions." Master thesis, University of British Columbia, Vancouver, BC, Canada.

Tsukuba Building Test Laboratory Center of Better Living. (2001). "Testing method for wooden shear walls and its shear strength coefficient (bairitu)." Technical Report. Tsukuba, Japan. (Test Method is authorized by Japan MLIT).

INTERNATIONAL COUNCIL FOR RESEARCH AND INNOVATION
IN BUILDING AND CONSTRUCTION

WORKING COMMISSION W18 - TIMBER STRUCTURES

COMPARISON OF MONOTONIC AND CYCLIC PERFORMANCE

OF LIGHT-FRAME SHEAR WALLS

J D Dolan

Washington State University

A J Toothman

U.S. Army Corp. or Engineers

USA

Presented by: Dan Dolan

Dan Dolan reported that the research, comparing the performance of shear walls constructed with 4 different sheeting materials was carried out at the Brooks Forest Products Research Centre at Virginia Tech. He then described the results obtained and also discussed the design code implications as the test results showed that the design code requirements gave values less than that obtained experimentally. In the discussion Dan confirmed that he used 9mm sheathing with 24 inches stud spacing – this was sufficient to prevent buckling problems.

COMPARISON OF MONOTONIC AND CYCLIC PERFORMANCE OF LIGHT-FRAME SHEAR WALLS

By:
James D. Dolan Washington State Univeristy, USA
and
Adam J. Toothman U.S. Army Corp. or Engineers, USA

ABSTRACT:
A total of 31 shear walls were tested under monotonic and cyclic loading to (1) determine the resistance to lateral loading of shear walls with various sheathing materials; (2) examine the effect of fully reversed cyclic loading on the specimens; and (3) compare the monotonic and cyclic performance of the walls. Tests were conducted on 1.2 x 2.4m (4 x 8ft) walls, constructed of oriented strand board (OSB), hardboard, fiberboard, or gypsum wallboard. Four-foot long walls were chosen because it represents the maximum ratio that can be used for gypsum wallboard. The 2:1 aspect ratio is also the maximum aspect ratio permitted by the United States buildings codes for wood structural panels used to resist seismic forces without further reduction in design values. Two walls of each sheathing material were tested under both monotonic and cyclic loading. All walls in this study incorporated the use of overturning anchors in the form of mechanical hold-downs. The monotonic tests were conducted according to ASTM E564, while the cyclic tests were conducted to the recently adopted ASTM standard E2126. A comparison of the monotonic and cyclic tests leads to several key dissimilarities. In general, the performance of the shear walls when tested cyclically decreased, although the degree of reduction depends on the sheathing material. Hardboard panels tested under cyclic loading performed similar to the monotonic tests. The peak load during cyclic tests was actually larger than its corresponding monotonic test. Fiberboard panels also performed in a similar manner when tested under cyclic and monotonic loading. OSB panels did not perform as well when subjected to cyclic loading. The peak load was reduced by 12%, and the energy dissipation was 27% lower when tested under cyclic loading. Gypsum panels performed poorly under cyclic loading. Peak load reduction was 16%, failure displacement decreased by 38mm (1.5 in.), and the amount of energy dissipation was nearly reduced by one-half when subjected to cyclic loading.

INTRODUCTION:

The lateral load resisting mechanism in a residential house is typically referred to as a shear wall. Shear walls are used to resist three major load-carrying components: vertical loads, transverse wind loads, and in-plane lateral forces imposed by wind and seismic forces. Shear walls support the horizontal diaphragm and transfer the lateral forces down to the next level or foundation of the structure. Hurricanes and earthquakes are two major loads that can lead to collapse or expensive repairs to houses. This study focuses on understanding how light-frame shear walls sheathed with various types of sheathing materials perform when subjected to cyclic loading.

Wood structures have historically performed well when subjected to lateral loads. This performance is due partly to wood's low weight/high stiffness ratio, and the ductility and redundancy of light-frame wood systems. As a result of the ductility, or ability to

Λ

deform without breaking, shear walls have a capacity to dissipate large amounts of energy produced by earthquakes and hurricanes (Leiva-Aravena 1996).

Plywood and OSB are primarily used as the sheathing material for shear walls. However, other materials such as fiberboard and hardboard can also be effectively used as sheathing material to resist shear loads in houses. This study investigates these two products as well as gypsum wallboard to the lateral resistance of shear walls.

ASTM E72 and ASTM E564 are the two traditional monotonic test procedures used in the United States to evaluate the performance of shear walls. The older of the tests, ASTM E72, covers standard tests of walls, floors, and roof elements. This test is broader based than strictly a racking test (Skaggs and Rose, 1996). ASTM E72 was developed to reference sheathing materials against an accepted norm of 200mm deep by 25mm thick horizontal siding (Griffiths, 1984). The test method was designed to isolate the effects due to the sheathing panel, and not the behavior of the structural assembly or system. Researchers felt that ASTM E72 yielded unrealistic values because the use of a steel rod "hold-down" did not represent true wall behavior.

Due to the assumed unrealistic failure values from the use of the steel rod, ASTM E72 was replaced with ASTM E564. The E564 method simulates realistic of construction practices for wall assemblies (Griffiths, 1984).

Many studies have evaluated and predicted the performance of shear walls subjected to monotonic loading (Price and Gromala 1980; Wolfe 1983; Griffiths 1984; and Dolan 1989). The focus of most recent shear wall studies is the performance of the walls under earthquake loading. Cyclic tests were slow to develop due to the complication of the testing method and the lack of consensus on a test protocol for conducting such tests (Rose 1998). Although no standard cyclic loading procedure has been adopted until recently, there have been many research projects on the cyclic performance of light-frame shear walls (Gray and Zacher 1988; Dolan 1989; Rose 1998).

Heine (1997) compared the effects of monotonic and cyclic loading on 12.2m (40ft) long walls. He determined that the effects of the loading procedure was dependant on the amount of overturning restraint. Loads resisted by walls restrained from overturning were reduced by as much as 23% when tested cyclically, but walls without hold-down devices actually increased in strength when tested under cyclic loading. Johnson (1997) also compared the effects of loading on 12.2m (40ft) long walls with various amounts of openings. He determined that walls loaded cyclically reached peak load at a smaller displacements and reduced in strength when compared to monotonic test results. He attributed the reduction to fatigue of the nails from subjecting the walls to repeated fully reversed cycles.

Dinehart and Shenton (1998) performed shear wall tests to study the effects of static and cyclic loading. Their research showed that the ultimate loads achieved from static tests were slightly larger than from dynamic tests. However, the ductility of the wall from cyclic loading was between 34% and 42% less than the corresponding static ductility. Results suggest that actual load factors will be significantly smaller than the intended design value. The failure mode for monotonic loading was nail withdrawal, while the failure mode from cyclic loading was nail fatigue.

Salenikovich (2000) tested walls 0.6m (2ft), 1.2m (4ft), 2.4m (8ft), and 3.6m (12ft) subjected to monotonic and cyclic loading. Walls with overturning restraints experienced a reduction in ultimate strength and failure displacement when subjected to cyclic loading. However, there was no significant difference in unrestrained wall performance under the cyclic and monotonic loading conditions.

2

TEST PROGRAM:

Specimens were built in accordance with standard construction practice. The framing for the 1.2 x 2.4m (4 x 8ft) walls were constructed from stud or better Spruce-Pine-Fir (SPF). The walls consisted of a double top plate connected to the studs, which were then connected to a single bottom plate. The double end studs and intermediate studs were connected to the top and bottom plates using two 16d common nails in each end. The double end studs were nailed together using two 16d common nails at 305mm (12in.) on center. The studs were cut to a length of 2324mm (91 ½ in.) so that the total height of the wall was eight feet. The four sheathing materials used different types of nails and nail spacing. Table 1 lists the type and thickness of sheathing panel, along with its corresponding nail and nail spacing.

Table 1: Sheathing materials and nailing schedule

Sheathing		Nails		
			Nail Spacing (o.c.)	
Material	Thickness	Type	Edge	Field
OSB	11mm (7/16 in.) per US VPA DOC PS-2	8d common (Ø 3.33mm x 63.5mm long) (Ø 0.131" x 2 ½" long)	152mm (6in.)	305mm (12in.)
Hardboard	9mm (3/8 in.) per ANSI/AHA 135.4 and 135.6	6d box (Ø2.5 x 51mm long x 6.8mm Øhead) (Ø 0.099" x 2" long x 0.266" Ø head)	102mm (4in.)	203mm (8in.)
Fiberboard	12mm (½ in.) per ASTM C209	11ga. Galv. roofing nail (Ø 3 x 38mm long x Ø 9.5mm head) (Ø 0.12" x 1 ½"long x Ø 3/8" head)	102mm (4in.)	152mm (6in.)
Gypsum (GWB)	12mm (½ in.) per ASTM C36	11ga. Galv. roofing nail (Ø 3 x 38mm long x Ø 9.5mm head) (Ø 0.12" x 1 ½"long x 3/8" Ø head)	178mm (7in.)	406mm (16in.)

Test Setup

The walls were tested in a horizontal position as shown in Figure 1. No dead load was applied in this setup, which is a conservative representation of a typical shear wall. The bottom and top plates of the wall was attached to 76 x127mm (3 x 5 in.) steel beams with 16mm (5/8 in.) anchor bolts spaced at 610mm (24 in.) on center. For the walls with hold-downs, 16mm (5/8 in.) bolts were used to attach the hold-down to the steel beam. To avoid interference of the sheathing with the support, the narrow face of the beam was in contact with the bottom plate. This arrangement allowed the sheathing to move over the top of the steel beam without meeting any resistance, which would add false loads on the wall. The top steel beam was attached to the programmable hydraulic actuator, which provided the racking force to the wall.
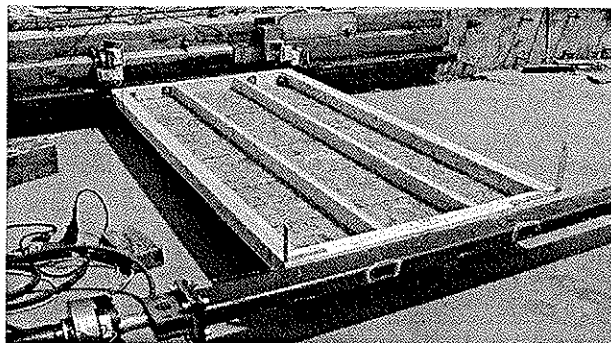
Figure 1: Test setup with wall in-place

In this investigation, eight channels of the data acquisition system were used to take readings on the walls. The reader is referred to Toothman (2002) for a detailed description of the instrumentation used for the tests.

Test Procedure

The monotonic tests were conducted according to ASTM E564 at a constant rate of 17 mm/min (0.67 in./min) until failure or until the actuator reached its maximum displacement of 152mm (6 in.). Unlike the specifications in ASTM E564, the unloading phases were omitted as the load was applied continuously until failure. This procedure was done because of the limited information that unloading phases provide.

All cyclic tests were in accordance with ASTM E2126 Method A. ASTM E2126 follows closely the SPD procedure developed by TCCMAR (Porter 1987) with a few changes. The SPD procedure is based solely on the FME, while ASTM E2126 takes into account the FME and ductility ratio when determining the initial amplitude of each phase in the protocol.

The loading schedule and waveform pattern for a typical wall are shown in Table 2 and Figure 2. FME and the ductility ratio values (μ), as determined from the monotonic tests, for each sheathing material are listed in Table 3. From the loading schedule defined by ASTM E2126, and shown in Table 2, it is possible that one phase will have a lower initial displacement than the previous phase. During phase five, if the ductility factor is not greater than 20, then the amplitude of the initial cycle will not be greater than 100% FME. Anytime this situation occurred, the phase was not included when forming the envelope curves and only increasing displacement amplitudes were included.

Table 2: Amplitude of initial cycle

Pattern	Phase	Amp. of Initial Cycle % FME
1	1	25
	2	50
	3	75
2	4	100
	5	5μ
	6	10μ
	7	20μ
	8	40μ
	9	60μ
	10	80μ
	11	Increase by 20μ Until failure

Figure 2: ASTM E2126 waveform pattern

Table 3: FME and ductility ratio values (μ) for wall specimens

Sheathing Material	FME (in.)	Ductility Ratio, μ
OSB	0.5	10
Hardboard	0.45	9
Fiberboard	0.55	7.5
Gypsum Wallboard	0.55	7.5

RESULTS:

This section discusses results of the monotonic and cyclic tests. It should be noted that all walls tested incorporated hold-down anchors. Shear wall parameters compared are peak load, displacement at failure, energy dissipation, and ductility. Figures 3 through 6 show load displacement relationships for OSB, hardboard, fiberboard, and gypsum, sheathed walls respectively.
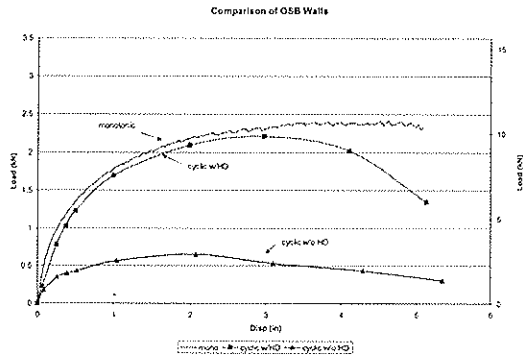
Figure 3: Load-displ. for OSB walls.
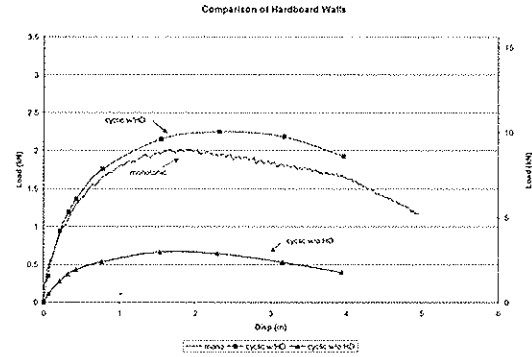
Figure 4: Load-displ. for hardboard walls.
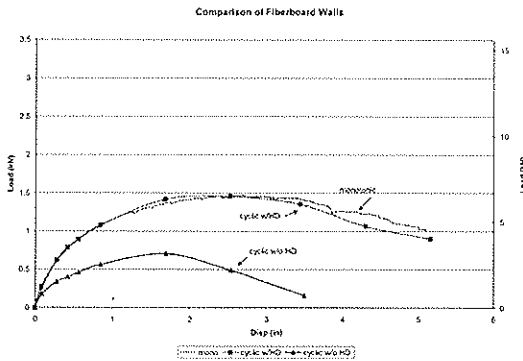
Figure 5: Load-displ. for fiberboard walls.
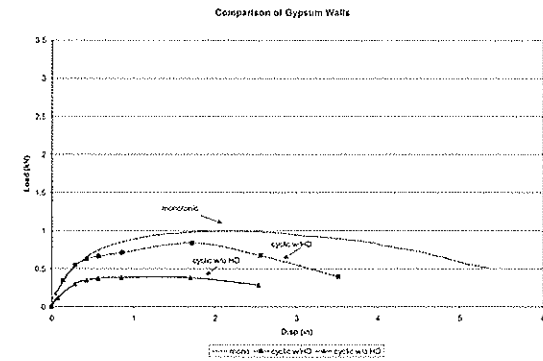
Figure 6: Load-displ. for gypsum walls.

Peak Load

Peak load values for the monotonic and cyclic tests with hold-downs are displayed in Table 4, along with the reduction that occurred from testing under cyclic loading. The sheathing material that experienced the largest reduction was gypsum wallboard. The gypsum's strength dropped from 4.4 kN (1.0 kips) to 3.7 kN (0.84 kips) or 16%. OSB-sheathed walls experienced a 12% decrease, while the fiberboard panels experienced a 3.9% decrease in strength. All of the sheathing materials reduced in strength when tested cyclically except for hardboard-sheathed walls, which actually increased in strength. The hardboard wall's strength increased by 0.76 kN (0.17 kips) or 8.2%.

One surprising observation was that hardboard reached a higher maximum load than OSB during cyclic loading, but OSB reached a higher maximum load during monotonic testing. One reason may result from the amount of overturning restraint, which allowed the force to be resisted by all the nails along the entire perimeter of the wall. Hardboard panels had a dense nailing schedule of 102mm (4 in.) around the perimeter, and the nails never tore through the sheathing, but instead, always withdrew from the framing. OSB had a perimeter nailing schedule of 152mm (6 in.), and the nails were observed to tear through the sheathing in some areas. Once a nail tore through the sheathing, that nail was incapable of transferring load between the sheathing and framing. When a nail withdrew

from the framing, it could still transfer shear, but the nail bent and moved through a larger displacement before transferring significant forces. Although the nails in OSB were larger than the nails in hardboard, the amount of nails and failure mode may have contributed to the increased resistance to cyclic loading.

As shown in the load-displacement curves, walls typically reached maximum load at a larger displacement when tested under monotonic loading. Continuous, fully reversed cycles caused the nails to fatigue and fail at a much lower displacement than when subjected to monotonic loading. The displacement at peak load of the OSB walls decreased by 21.8mm (0.86 in.), or 22%. Fiberboard walls reached peak load at a displacement 22.4mm (0.88in.) less than its corresponding monotonic test (26% decrease). Gypsum walls reached peak load at a displacement 13.3mm (0.52in.) less than its corresponding monotonic tests (23% decrease). The displacement at peak load for hardboard walls stayed nearly the same during the cyclic tests. The reason can be explained by the fact that the peak load was higher when tested under cyclic loading. The nail behavior and overturning restraints also contributed to the ability to undergo larger deflections under cyclic loading.

Table 4: Peak load comparison of monotonic and cyclic tests

Material	Monotonic		Cyclic		Reduction		
	(kN)	(kips)	(kN)	(kips)	(kN)	(kips)	%
OSB	11.2	2.51	9.8	2.21	1.33	0.3	12.0
Hardboard	9.3	2.08	10.0	2.25	-0.76	-0.17	-8.2
Fiberboard	6.8	1.52	6.5	1.46	0.27	0.06	3.9
Gypsum	4.4	1.00	3.7	0.84	0.71	0.16	16.0

Displacement at Failure

The failure load in this study was taken to be $0.8F_{peak}$. Since this is obviously based on the maximum load, the walls with the highest strength will also have the largest load capacity at failure. However, the displacement capacity of a structure is an important parameter to investigate and is not a function of the maximum load. The ability of a structure to dissipate more energy results from it being able to deform without failing.

Displacements at failure are compared in Table 5. Every cyclic test experienced a reduction in the failure displacement when compared to its corresponding monotonic test. The average reduction in the displacement at failure for all of the tests was 14%. The largest reduction occurred during gypsum sheathed wall tests. Failure displacement decreased by 39mm (1.55 in.), or 37%. During monotonic tests, nails in the gypsum would easily tear through the sheathing, but since the loading was in one direction, the wall could still resist load while undergoing large deformations. During fully reversed cycles, the nails would tear through the sheathing in both directions, which enabled the wall to fail at a lower displacement due to nail head pull through.

Table 5: Displacement at failure comparison of monotonic and cyclic tests

Material	Monotonic		Cyclic		REDUCTION		
	(mm)	(in.)	(mm)	(in.)	(mm)	(in.)	(%)
OSB	142	5.6	116	4.6	25	1.0	18%
Hardboard	117	4.6	106	4.2	10	0.4	9%
Fiberboard	117	4.6	109	4.3	8	0.3	7%
Gypsum	104	4.1	65	2.6	38	1.5	37%

OSB-sheathed walls experienced a reduction in failure displacement of nearly 25mm (1 in.) during the cyclic tests. The displacement at failure of hardboard and fiberboard appeared to be the least affected by the cyclic loading. The average reduction was only 9.7 mm (0.38 in.), or 8%. The decrease in failure displacement can be attributed to the nail behavior. During monotonic testing, the nails are pulled in only one direction at a constant rate. During cyclic loading, the nails are subjected to many fully reversed cycles, which produces fatigue.

Elastic Stiffness

Elastic stiffness for this study is defined as the slope of the secant line that passes through the origin and the point on the load-displacement curve equal to $0.4F_{peak}$. From monotonic tests, elastic stiffness is taken directly from the load-displacement curve. Elastic stiffness is calculated using the initial cycle envelope curve when considering cyclic tests. There was a wide variation in the elastic stiffness within the individual pair of tests.

Due to the variation of the elastic stiffness, a definite relation between the elastic stiffness and the loading procedure cannot be established. As shown in Table 6, the elastic stiffness increases in some cases and decreases in others when subjected to cyclic loading.

Table 6: Elastic stiffness comparison of monotonic and cyclic tests

Material	Monotonic		Cyclic with HD		CHANGE		
	(kN/mm)	(kip/in)	(kN/mm)	(kip/in)	(kN/mm)	(kip/in)	(%)
OSB	0.76	4.31	0.57	3.27	0.18	1.05	24
Hardboard	0.73	4.18	0.93	5.27	-0.19	-1.09	-26
Fiberboard	0.38	2.18	0.51	2.91	-0.13	-0.73	-33
Gypsum	0.39	2.22	0.45	2.56	-0.06	-0.34	-15

Elastic stiffness of the tests should be similar since the value is calculated at a point equal to forty percent of peak load. At this point, the wall has not yielded and should not matter how many cycles the wall has been subjected to. The values displayed in Table 5.4 are relatively close, and given the inherent variation in testing of full-scale wood specimens, the practical effect of loading protocol on elastic stiffness can be assumed to be negligible.

Ductility

Ductility values alone do not provide much insight into the performance of the walls. Ductility is a function of the elastic stiffness, yield displacement, and failure displacement. Therefore, ductility should be considered along with other shear wall parameters. The ductility ratio used for this study is the failure displacement divided by the yield displacement (Table 7).

Table 7: Ductility comparison of monotonic and cyclic tests

Material	Monotonic	Cyclic	CHANGE	
OSB	7.2	7.7	0.5	6%
Hardboard	8.7	10.4	1.7	16%
Fiberboard	7.3	9.4	1.9	20%
Gypsum	10.0	8.9	-1.1	-12%

Ductility values calculated from the cyclic tests varied by a large amount when compared to monotonic tests. Ductility tended to slightly increase or stay the same when

tested cyclically. Although the failure displacement decreased during cyclic loading, the yield displacement also decreased, which increased the ductility.

Energy Dissipation

Energy dissipation is important when discussing the performance of a shear wall. Lateral force that is exerted on a structure and transferred to the shear wall produces large amounts of energy that must be absorbed in order to avoid failure. The energy dissipated during monotonic tests is calculated by determining the area under the load-displacement graph. The total amount of energy dissipated during cyclic tests is the summation of all the cycles. However, for comparison purposes, the energy dissipation calculated in Table 8 was determined from the area under the average initial envelope curve. The limits of the energy dissipation are from the point of zero displacement to the failure displacement, which was taken at a displacement equal to $0.8F_{peak}$.

Table 8: Energy dissipation comparison of monotonic and cyclic tests

Material	Monotonic		Cyclic		Change		
	(kN-m)	(kip-ft)	(kN-m)	(kip-ft)	(kN-m)	(kip-ft)	(%)
OSB	1.31	0.97	0.96	0.71	0.35	0.26	26
Hardboard	0.95	0.70	0.91	0.67	0.04	0.03	4
Fiberboard	0.66	0.49	0.63	0.46	0.04	0.03	5
Gypsum	0.41	0.30	0.23	0.17	0.17	0.13	42

As shown in Table 8, the amount of energy dissipated by the walls under cyclic loading decreased when compared to monotonic tests. This occurred because the peak load and failure displacement was normally higher during monotonic tests, which increased the area under the load-displacement curve. As stated before, the cyclic tests dissipated much more total energy than the monotonic tests due to the numerous cycles that overlapped, but for comparison purposes only the initial envelope curve is considered. Because of the numerous cycles applied during the cyclic tests, nail fatigue contributed to the decreased energy dissipating capacity of the walls.

Response curves of the four sheathing materials behaved differently when considering energy dissipation. OSB panels experienced a large reduction in strength when tested cyclically. The energy reduction was 27% and can be explained by the failure displacement of the walls. During monotonic tests, OSB panels did not experience a sudden drop in strength after reaching peak load. Nails in the OSB would bend, but they were still attached to the wall and could resist load through a large displacement. When tested cyclically, OSB experienced a definite drop in strength after reaching peak load, which was a result of nail fatigue and tear out. The response during the two loading conditions were nearly identical until reaching peak load, but quite different after peak load (Figure 3).

The reduction in energy dissipation of hardboard and fiberboard-sheathed walls was small. The reduction during hardboard tests was 4%, while the reduction during fiberboard tests was only 6% when subjected to cyclic loading. As shown in Figures 4 and 5, the average response was nearly identical during monotonic and cyclic tests. For both loading conditions, the nail behavior was similar. During the hardboard tests, the sheathing nails pulled out of the framing until the sheathing panels were no longer affectively attached to the framing. The sheathing nails in the fiberboard typically pulled out of the framing, or tore through the weak panels during monotonic and cyclic loading. Similar nail behavior allowed the walls to fail in the same manner and at the same displacement.

Gypsum wallboard experienced the largest reduction of energy when tested cyclically (43%). This was not surprising given the ease of which the nails in the gypsum could tear through the sheathing. The actuator displacement moved at a much more rapid speed during the cyclic tests. The increased rate damaged the gypsum sheathing more drastically than the slower, more constant rate experienced during monotonic tests.

CONCLUSIONS:

A total of 31 walls were tested during this study to determine and compare the effects of monotonic and cyclic loading on shear walls with various sheathing materials. The sheathing materials investigated are oriented strandboard (OSB), hardboard, fiberboard, and gypsum wallboard. All of the walls were 1.2 x 2.4m (4 x 8ft), and to be conservative there were no gravity loads applied to the walls. All of the tests were performed with hold-downs. Monotonic tests were performed according to ASTM E564, while the cyclic tests were performed according to ASTM E2126. The conclusions drawn from the cyclic tests are:

(1) In general, the performance parameters decreased when the cyclic tests were compared to the monotonic tests. The most drastic reduction was observed during the gypsum-sheathed tests, followed by the OSB-sheathed tests.

(2) Hardboard panels tested under cyclic loading performed similar to the monotonic tests. The peak load during cyclic tests was actually larger than its corresponding monotonic test (8%). The displacement at failure decreased by 9%, and the energy dissipation reduced by only 4% when subjected to cyclic loading.

(3) Fiberboard panels also performed in a similar manner when tested under cyclic and monotonic loading. The peak load only decreased by 0.27 kN (0.06 kips), which was a reduction of 4%. The displacement at failure decreased by 7%, and the energy dissipation reduced by 5% when subjected to cyclic loading.

(4) OSB panels tested cyclically did not perform as well as when tested monotonically. The peak load reduction was 1.33 kN (0.3 kips), or 12%, and the energy dissipation was 27% lower when tested under cyclic loading.

(5) Gypsum panels performed poorly under cyclic loading. The peak load reduction was 16%, the failure displacement decreased by 38mm (1.5 in.), and the amount of energy dissipation was nearly reduced by one-half when subjected to cyclic loading.

LITERATURE CITED

American Society for Testing Materials. (1998). Standard Test Methods of Conducting Strength Tests of Panels for Building Construction, ASTM E72-98, West Conshohocken, Pennsylvania.

American Society for Testing Materials. (1995). Standard Practice for Static Load Test for Shear Resistance of Framed Walls for Buildings, ASTM E564-95, West Conshohocken, Pennsylvania.

American Society for Testing Materials. (2001). Standard Test Methods for Cyclic (Reversed) Load Test for Shear Resistance of Framed Walls for Buildings, ASTM E2126-01, West Conshohocken, Pennsylvania.

Dinehart, D.W., Shenton, H.W., and Elliott, T.E. (1998). "Comparison of Static and Dynamic Response of Timber Shear Walls," *Journal of Structural Engineering*, Vol. 124, No. 6, pp 686-695.

Dolan, J.D. (1989). *The Dynamic Response of Timber Shear Walls*, thesis submitted in partial fulfillment of the Doctor of Philosophy Degree at the University of British Columbia, Vancouver, British Columbia.

Gray, R.G. and Zacher, E.G. (1988). "Dynamic Testing of Wood Shear Panels," *Architecture*, Vol. 77, No. 3, pp. 121-124.

Griffiths, D.R. (1984). "Determining the Racking Resistance of Timber Framed Walls," *Proceedings of the Pacific Timber Engineering Conference, Auckland, New Zealand, Vol. 1, Timber Construction.* Institute of Professional Engineers, Wellington, New Zealand, pp 504-512.

Heine, C. (1997). *The Effect of Tie-Down Anchorage on Long Shear Walls with Openings,* thesis submitted in partial fulfillment of the Masters of Science Degree at Virginia Polytechnic Institute and State University, Blacksburg, Virginia.

Johnson, A.C. (1997). *Monotonic and Cyclic Performance of Long Shear Walls with Openings,* thesis submitted in partial fulfillment of the Masters of Science Degree at Virginia Polytechnic Institute and State University, Blacksburg, Virginia.

Leiva-Aravena, L. (1996). "Behavior of Timber-Framed Shear Walls Subjected to Reversed Cyclic Lateral Loading," Proceedings of the 1996 International Wood Engineering Conference – Volume 2, New Orleans, pp 201-206.

Porter, M.L. (1987). "Sequential Phase Displacement (SPD) Procedure for TCCMAR Testing." In: *Proceedings, 3rd Meeting of the Joint Technical Coordination Committee on Masonry Research.* U.S.- Japan Coordinated Earthquake Research Program, Tomamu, Japan.

Price, E.W. and Gromala, D.S. (1980). "Racking Strength of Walls Sheathed with Structural Flakeboards made from Southern Species," *Forest Products Journal,* Vol. 30, No. 12, pp 19-23.

Rose, J.D. (1998). "Preliminary Testing of Wood Structural Panel Shear Walls Under Cyclic (Reversed) Loading." *APA Research Report 158. APA – The Engineered Wood Association,* Tacoma, Washington.

Salenikovich, A.J. (1999). *Racking Performance of Light-Frame Shear Walls.* thesis submitted in partial fulfillment of the Doctor of Philosophy Degree at Virginia Polytechnic Institute and State University, Blacksburg, Virginia.

Skaggs, T.D. and J.D. Rose. (1996). "Cyclic Load Testing of Wood Structural Panel Shear Walls." *Proceedings of the 1996 International Wood Engineering Conference, New Orleans,* 2:195-200.

Toothman, A. (2002). Performance of Shear Walls with Different Sheathing Materials. thesis submitted in partial fulfillment of the Master of Science Degree at Virginia Polytechnic Institute and State University, Blacksburg, Virginia.

Wolfe, R.W. (1983). Research Paper FPL 439- Contribution of Gypsum Wallboard to the Racking Resistance of Light-Frame Walls. United States Department of Agriculture, Forest Products Laboratory, Madison, WI.

INTERNATIONAL COUNCIL FOR RESEARCH AND INNOVATION
IN BUILDING AND CONSTRUCTION

WORKING COMMISSION W18 - TIMBER STRUCTURES

PREDICTED RELIABILITY OF ELEMENTS AND CLASSIFICATION

OF TIMBER STRUCTURES

L Ozola

Latvia University of Agriculture, Jelgava

LATVIA

T Keskküla

Estonia Agricultural University, Tartu

ESTONIA

Presented by: Lilita Ozola

After acknowledging her co-author, Lilita Ozola discussed the approaches used to address the issue of uncertainties in design parameters. She went on to describe her database of timber framing systems, the sampling scheme used and the procedure used for determining the 5th percentile strength values. She proposed 3 classes of timber structures for design purposes, based on the required degree of reliability. Discussion centred on the relevance of the research to EC5.

Predicted reliability of elements and classification of timber structures

Lilita Ozola
Latvia University of Agriculture, Jelgava, Latvia
Tõnu Keskküla
Estonia Agricultural University, Tartu, Estonia

Abstract

The study is devoted to the assessment of uncertainties involved in the design procedure of structural timber elements. The discussed quantities refer to the measured variability of: wood strength values, buckling factor values and geometric characteristics of structural element sections. The probability calculations are carried out and the distributions of predicted load bearing capacity in different stress states are presented.

The inference about the necessity of correction of partial safety factors for structural timber elements with regard to their stress state is carried out based on the analysed probabilities distributions related with the amount of the influencing factors everyone of which, for example, strength and stiffness properties, section modulus, as well design model presumptions have a certain uncertainty level.

The proposal for the classification system of timber structures related to their safety and reliability is presented.

1   Introduction

While designing timber structures involves the decision making at the widest area of uncertainties. All quantities (material and product properties, environmental effects, geometrical data, actions) involved in the timber engineering calculations are associated with a considerable uncertainty. The uncertainty is due to significant inherent variability of affecting quantities, due to the limited information on these quantities and due to the idealizations of design model as well as many other influencing factors (Reliability..., 1991).

In this study the statistical description of some affecting quantities – strength of wood, buckling factor and geometric characteristics of structural elements- section area and modulus is presented. The predicted value of load bearing capacity of structural timber element is considered as a basic variable which is dependent on the material strength and stiffness properties, and the geometric characteristics of the element as well. The results in the treatment of variability of load bearing capacity of timber elements in bending and longitudinal buckling leads to the suggestion that the partial safety factors should be determined in the relation with the amount of affecting factors.

The comprehensive judgement on the problems in design practice and the construction of timber elements as well as research results on uncertainties involved demands the necessity of the elaboration of classification system of timber structures as related to the probability of their survival under the action in the most unfavourable combination.

2 Statistical description of affecting variables

2.1 Geometric characteristics

During the last years we have obtained large data sets of geometric characteristics of softwood structural timber elements which were inspected after a longterm service (12 up to 17 years) in livestock buildings. General softwood timber framing systems were selected (Figure 1). A large quantity of cross section measurements were carried out on beams and studs- in three sections for every beam and column using trammel. More than 3,300 of real cross-section dimensions for bending members and of about 530 sections for elements in longitudional buckling were fixed.
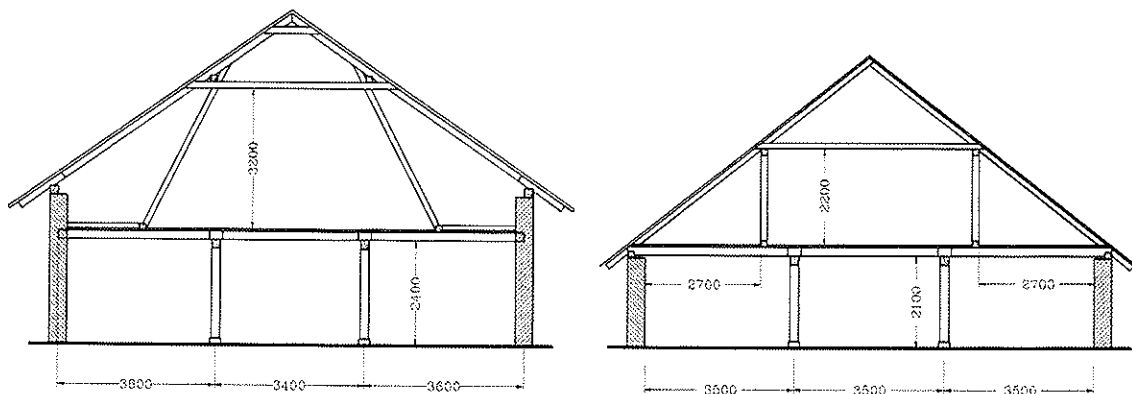
Figure 1. *General schemes of inspected timber framings in livestock buildings*

The statistical description of geometric data sets are presented in the relative terms- as the distributions about sample mean value. The histograms for particular data samples of column section area values and the reduced distribution for all population are displayed graphically in Figure 2. The variability of column section area characteristics is described by the mean coefficient of variation $v\{A/A_{mean}\}= 0.033$ for data samples (A_1, ..) of section area values and $v\{i/i_{mean}\}= 0.025$ for section radius of inertia values.

The data samples of geometric characteristics for bending members (beams and girders)- data sets (W-0, W-1,...) of section modulus relative values against the main stiffness axis of section are seen graphically displayed in Figure 3. The variability of section modulus and modulus of inertia values are characterised by the coefficients of variation: $v\{W/W_{mean}\}= 0.052$ and $v\{J/J_{mean}\}= 0.059$.
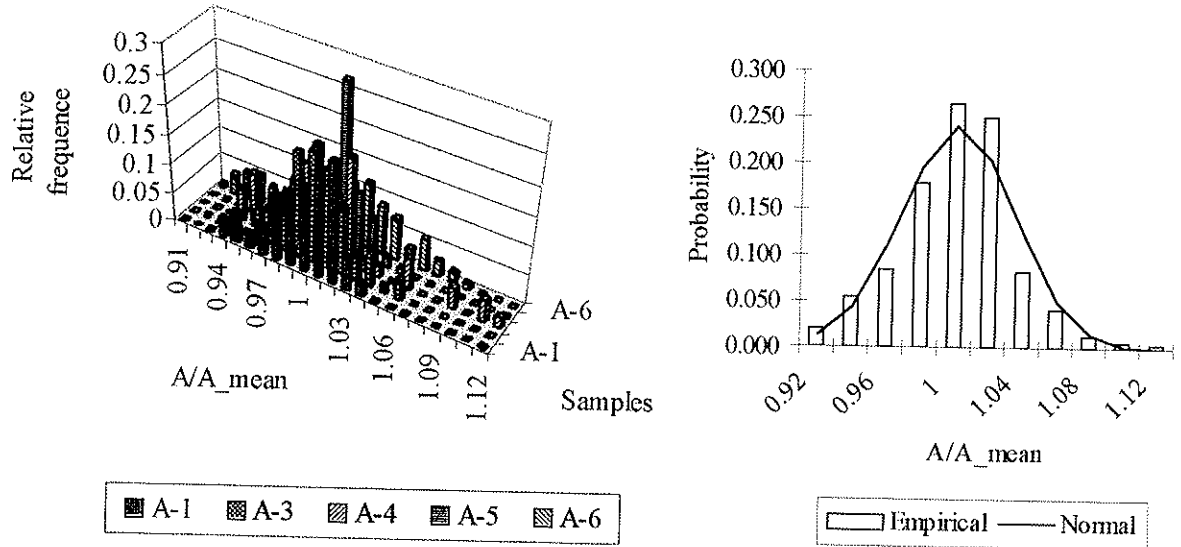
Figure 2. *Timber column section area variables: A- histograms of relative section area values, B- distribution of the ones reduced to quazi permanent population (5 samples in total) with normal curve superimposed*
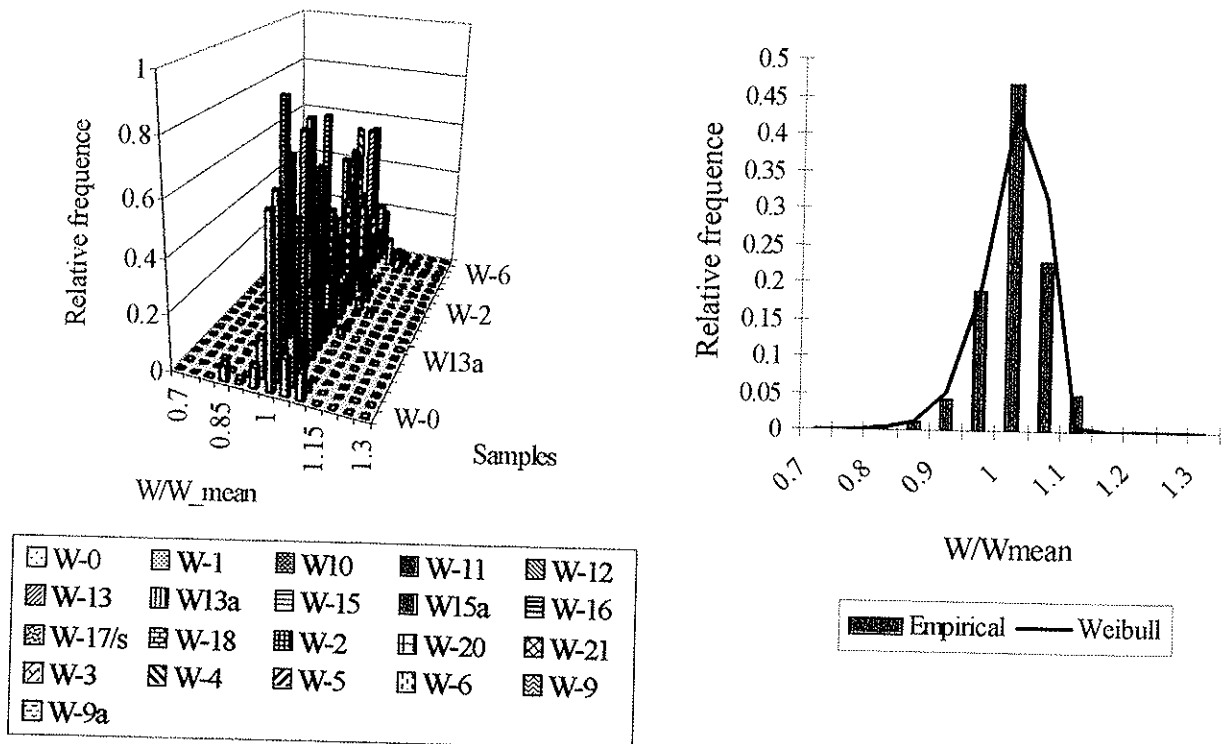
Figure 3. *Distributions of section moments of beams: A- histograms representing beam groups in inspected buildings, B- quazi-permanent population- all samples*

3

2.2 Wood strength properties

We have obtained some large data samples of the compression strength values of clear wood (*Pinus Silvestris*) standard specimens subjected to a short-term static load tests. Standard specimens (20x20x30 mm) were cut out from test pieces after loading in longitudinal buckling (20x20x300 mm). During the test the moisture content of wood was from 6 up to 8 percent. The obtained strength values are reduced to 12% moisture content using the reduction factor 0.04 per 1% of moisture content. The whole data set consists of 717 specimens. As this data set covers a wide range of wood density values, two different strength data samples were selected corresponding to wood density (ρ) ranges: sample DL includes the strength data for specimens with density less than 500 kg/m³ and sample DH includes the ones for specimens with density more than 500 kg/m³ (see distributions in Figure 4). This selection was done with purpose to clear up the relation exists or not of variation range of properties and density. For absolute values of characteristics for whole data set and both samples see in Table 1.

Table 1. *Statistical characteristics of compression strength and wood density data sets*

Sample	Size	Compression strength (at 12% moisture content)			Density of dry wood		
		mean value, N/mm²	standard deviation N/mm²	coefficient of variation	mean value, kg/m³	standard deviation kg/m³	coefficient of variation
Whole data set	717	54.8	7.84	0.143	502	56.73	0.113
DL	358	49.938	5.99	0.12	460.06	30.24	0.0657
DH	359	59.85	6.05	0.101	542.58	45.32	0.0835
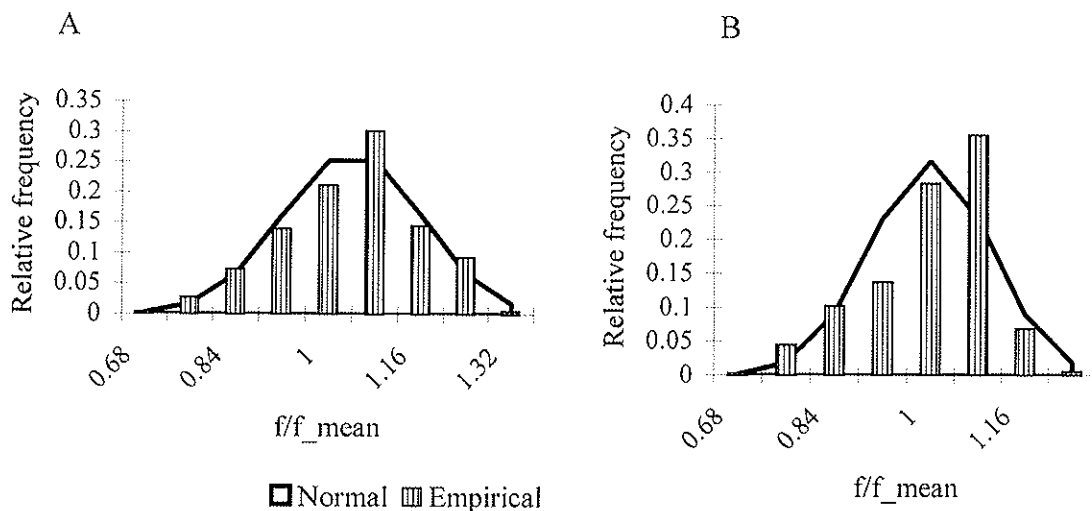
Figure 4. *Graphical displays of strength data distributions about their mean values with normal curves superimposed: A- sample DL (ρ≤500 kg/m³), B- sample DH (ρ>500 kg/m³)*

4

2.3 Treatment of buckling factor variable

The data groups of buckling factor values were obtained by testing series of free supported softwood timber specimens (20 x 20 x 300 mm) in axial compression (longitudinal buckling). The stress value after which the loss of linear proportionality between the longitudional force and transversal displacement values was observed, was assumed as a critical stress (f_{cr}). After that the standard samples were cut out and tested in compression to obtain the ultimate limit stress f_u value. The buckling factor values were estimated as ratio $k_c = f_{cr}/f_u$. The distribution (Figure 5) is described by the following characteristics: mean value $\mu\{k_c\}= 0.68$, standard deviation $\sigma\{k_c\}= 0.08$, coefficient of variation $v\{k_c\}= 0.12$. Note that there was no significant differences observed in statistical descriptions of buckling factor values as regard to above inspected density ranges.
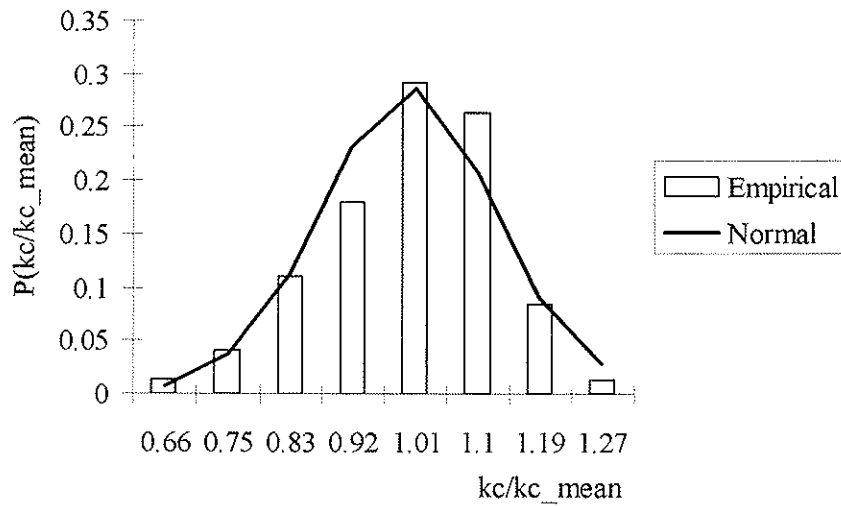
Figure 5. *Distribution of the relative buckling factor values with normal curve superimposed*

3. Variation of load bearing capacity of structural elements

All variables tested in the probabilistic meaning are assumed as mutually independent events. The predicted probability of load bearing capacity for structural elements is calculated according to the multiplication rule of probability. The probability of each load bearing capacity value is calculated by multiplying the probabilities of influencing factors as it is expressed by the formulaes (1) and (2).

The probability of predicted value of load bearing capacity for bending elements:

$$P(M_{k,DL(DH)}/M_{k,mean,DL(DH)})= P(f_{i,dl(dh)}/f_{mean,DL(DH)}) \times P(W_i/W_{mean}); \qquad (1)$$

and the one for elements in longitudinal buckling:

$$P(N_{k,DL(DH)}/N_{k,mean,DL(DH)})=P(f_{i,DL(DH)}/f_{mean,ds})\times P(A_i/A_{mean})\times P(kc_{i,dl(dh)}/kc_{mean,DL(DH)}), \qquad (2)$$

where $P(M_{k,DL(DH)}/M_{k,mean,DL(DH)})$, $P(N_{k,DL(DH)}/N_{k,mean,DL(DH)})$- the probabilities of the relative characteristic values of load bearing capacity corresponding to density range DL or DH, $P(f_{i,ds}/f_{mean,DL(DH)})$- the probability of relative material resistance value in corresponding wood density group, $P(W_i/W_{mean})$, $P(A_i/A_{mean})$- the probabilities of geometric characteristics

of sections, $P(kc_{i,dl(dh)}/kc_{mean,DL(DH)})$- the probability of the relative buckling factor value corresponding to density range DL or DH.

The statistical characteristics of treated load bearing capacity variables are summarized in Table 2 and distributions of predicted load bearing capacity values are shown in Figure 6.

Table 2. *Statistical characteristics of predicted load bearing capacity*

Element stress state	Density range	Predicted mean	Coeficient of variation
Bending	DL: $\rho < 500$ kg/m³	1.03	0.146
	DH: $\rho > 500$ kg/m³	0.99	0.136
Longitudinal buckling	DL: $\rho < 500$ kg/m³	1.1	0.17
	DH: $\rho > 500$ kg/m³	1.05	0.167
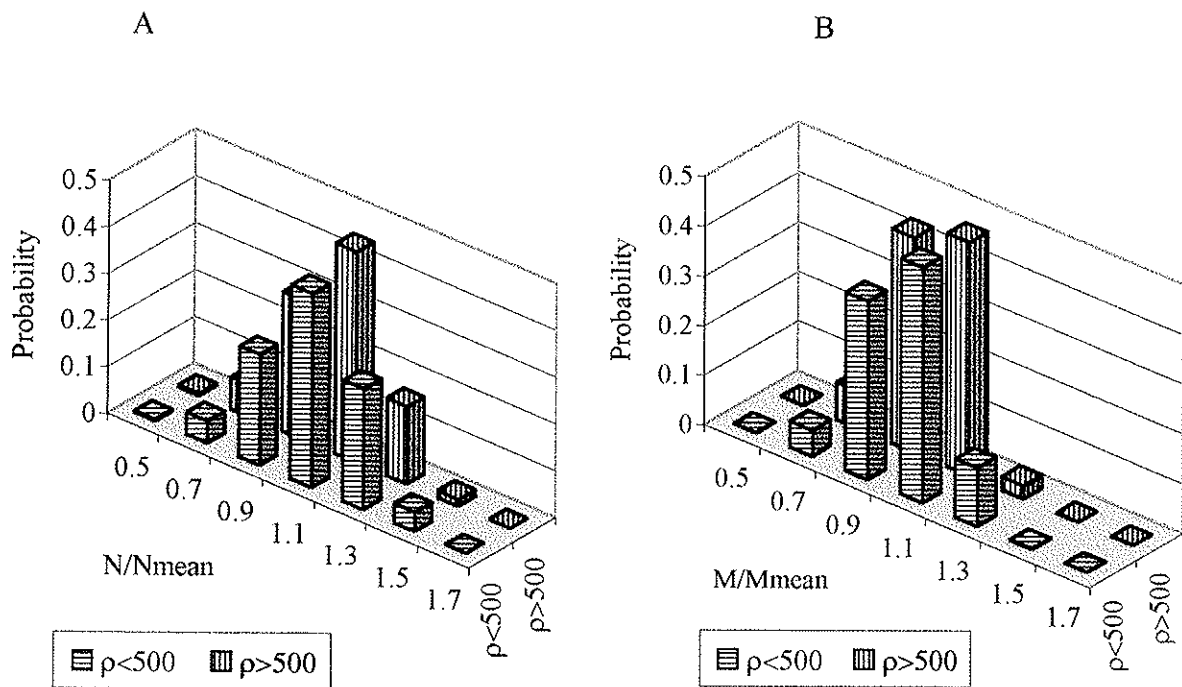
Figure 6. *Distributions of load bearing capacity relative values: A- bending elements; B- elements in longitudinal buckling*

Let us assume that the load factors are characterised by the independent constant value (=1) as the loads are not measured in this study. Therefore the task may be reduced to one component case and the limit state is described by a simple equation:

$$g = X - 1/\gamma \qquad (3)$$

where X- load bearing capacity variable; γ- the safety factor between loading and resistance part. Function g constantly increases with increasing of X values.

Assuming the normal distribution law for load bearing capacity variables, the probability of failure is

$$P(g < 0) = \Phi\left(\frac{1/\gamma - \mu_X}{\sigma_X}\right) = \Phi(-\beta) \qquad (4)$$

where Φ is the distribution function of the standardized normal distribution (Christensen R. (1996)); μ_X - mean value and σ_X - standard deviation of resistance variables; β - reliability index. Using Partial Safety Factor Method's solutions (Ditlevsen & Madsen (1996)) the reliability index (β) and probability P(g<0) values are calculated for different safety factor (γ) values. The results of calculations are given in Table 3.

It is clear from Table 3 that the safety factor is very sensitive to the number of affecting factors. For the beam elements it is satisfactory to adopt the safety factor $\gamma = 1.7$ to ensure the reliability index approximately $\beta = 2.93$-3.0. For the elements in longitudinal buckling the value of $\gamma = 2.0$ relates with values of $\beta = 3.14$-3.19.

Table 3. *Results of failure probability calculations*

Stress state	Density range	Partial safety factor γ	Statistics of resistance variable		Reliability index	Probability of failure P(g<0) (Brownlee 1977)
			mean	standard deviation		
Bending	DL	1.2	1.03	0.151	1.30	0.0968
	DH	1.2	0.99	0.134	1.17	0.121
Buckling	DL	1.2	1.1	0.188	1.42	0.0778
	DH	1.2	1.05	0.175	1.24	0.10749
Bending	DL	1.5	1.03	0.151	2.41	0.00798
	DH	1.5	0.99	0.134	2.41	0.00798
Buckling	DL	1.5	1.1	0.188	2.3	0.01072
	DH	1.5	1.05	0.175	2.19	0.01426
Bending	DL	1.5	1.03	0.151	2.93	0.00169
	DH	1.5	0.99	0.134	3.00	0.00135
Buckling	DL	1.5	1.1	0.188	2.72	0.00326
	DH	1.5	1.05	0.175	2.64	0.00415
Bending	DL	2.0	1.03	0.151	3.51	0.00022
	DH	2.0	0.99	0.134	3.66	0.00013
Buckling	DL	2.0	1.1	0.188	3.19	0.00071
	DH	2.0	1.05	0.175	3.14	0.00084

When making consideration on the safety of timber structures it is essential to appreciate that the analysis of large data samples does not really reflect the essence of the matter of such complicated structural material as timber.

The knowledge of wood as a structural material continues to improve every dozen of years. Nevertheless time is too far when the full scale population of data and mathematical models for all features of the behaviour of structural timber elements will be obtained. And it is not necessary to apply statistical methods to describe every timber engineering problem, since many are purely deterministic or easily solved using the past experience or information available in the sources such as databooks, specifications, design guides, and in known physical relationships. Some mechanism for the evaluation of timber structures as related to the reliability is necessary as soon as possible.

4. Classification of timber structures as related to designed reliability level

The necessity of classification of timber structures originates from many controversial or complicated situations in practice when one should prove the advantages or limitations of the unreliable solutions of timber structures. It is necessary both - from the safety and economical considerations to elaborate the classification system for the load bearing structures.

It is recommended to classify the timber structures in three classes as related to the reliability:

Class 1   structures with lowest designed degree of reliability;

Class 2   timber structures with medium designed degree of reliability;

Class 3   timber structures with highest designed degree of reliability.

The degree of reliability of a timber structure should be assessed taking account of (ISO 2394):

- the cause and mode of failure of a structure or structural element
- the possible consequences of failure;
- the choice of the values of action variables and calculation parameters;
- consideration of durability;
- the accuracy of the design models used.

Let us have some considerations based mainly on design practice and professional judgement.

The prediction of possible failure mode in the limit state is a very significant factor. The structural element which would be likely to collapse suddenly without a previous warning may be defined as brittle and should be designed having larger safety margins than one for which the collapse is preceded by some kind of warning (deformations etc.) in such a way that measures can be taken to limit the consequences. Degree of reliability may be assessed by the following criteria (see Table 4):

1   elements with the trend towards a brittle failure (tensile elements, elements with sections stressed in shear up to design resistance value, glue joints with high concentration of shear stress and the like);

3   elements with the trend towards a plastic failure mode and possibility of brittle failure mode is low (bended elements, compressed elements and elements in longitudinal buckling with the slenderness ratio more than 70, nailed and bolted joints, nail plate joints and the like);

6   elements with trend towards a plastic failure mode (bended elements, compressed elements and elements in longitudinal buckling with the slenderness ratio less than 70, nailed and bolted joints prevented from a brittle failure through shear planes, joints with toothed rings and the like).

The possible consequences of failure may be measured in terms of risk to life, injury, potential economic losses and by social inconveniences taking place after failure. The

degree of reliability may be assessed according to the consequences of failure by the following criteria:

2 risk to life high, social inconveniences very great. This criteria is satisfactory for temporary structures and buildings having no human activities;

4 risk to life medium, social inconveniences considerable (for livestock buildings, warehouses and the like);

6 risk to life low, social inconveniences small or negligible (for public buildings).

The degree of reliability is closely pertained by checking appropriate values in really possible combinations of actions on the structure. In such case the criteria are selected as follows:

1 the structure is checked on permanent and variable actions in fundamental combinations using decreased values of partial safety factors;

2 the same using normal values of partial safety factors;

3 the structure is checked on permanent, variable and accident actions in all possible combinations using normal or increased values of partial safety factors. The complete action models are considered.

The effects of uncertainty of the material matter itself showing the fluctuations of the physical properties and geometric characteristics of elements from sample to sample is assessed by the following criteria:

1 materials are selected by visual grading method;

2 materials are selected by mechanical grading method and geometric sizes are controlled;

3 materials are selected by mechanical grading method or testing, geometric sizes are controlled, safety factors for material and elements are involved according to the observed distributions of values.

The durability of the timber structure and the structural elements in their environment should remain fit for use during their design lifetime under appropriate maintenance. The criteria of durability are choosed as follows:

1 the structure satisfy the required performance criteria and system integrity is ensured;

2 the structure is manufactured and erected with confirmity of design requirements, the service conditions correspond to the same as designed and the necessary protective measures are realised;

3 the structure is manufactured and erected with the confirmity of design requirements using testing machines and special instruments for the quality control; the environmental conditions correspond to the same as designed; the necessary protective measures are realised and a periodical inspection of structures is ensured during the service.

Design models shall describe the timber structure and its behaviour up to the limit state under the consideration, accounting for relevant actions and environmental influences. At the same time the calculation model always represents the real structure as a simplified system in which more decisive factors are obligatory and the less important ones are

neglected. Actually, the design conception on timber structure includes as a minimum three models: action model, structural model (definition of elements and connection types as regards to degree of freedom), and resistance models by which wood resistance values corresponding to the action effects (duration of load, moisture content, direction of grains, effects of plastic behaviour of the material, geometrically linear versus geometrically nonlinear response) are determined.

The criteria for the assessment of fitting the design model with the real structure are selected as follows:

2   simplified loading and design models are used for determining internal forces, load duration and effects of service conditions are encountered in resistance model;

4   the correct design model is used for determining internal forces, load duration and service effects are encountered, the time-dependent behaviour (creep) of elements is considered;

6   the correct design model is used and geometrically nonlinear response of structure is considered, load duration and service effects are encountered, the time-dependent behaviour (creep) of elements is considered, the experimental verification of original models are carried out.

The appropriate quality control policy must be adopted and implemented with the purpose to achieve an adequate confidence that the designed and erected structure fulfil the specified requirements. The criteria are selected as follows:

1   the code requirements are considered in design and construction; general visual inspection and quality control is carried out;

3   the review of design documents is carried out by the expert commission; the manufacturing and erection processes are followed by the control measures including sampling and testing procedures detailed in the structural design standards; the control of service conditions and appropriate maintenance regime of structures is provided;

6   both quality control and compliance control of materials and structures are realised, for example, proof tests of real structures are performed, every produced unit is inspected.

Table 4. *Proposed criteria for differentation of timber structures as related to reliability*

Condition	Minimum of criteria for classes		
	1	2	3
Predicted failure mode	1	3	6
Risk, possible consequences of failure	2	4	6
Checking of action variables	1	2	3
Checking of material properties and of elements geometric uncertainties	1	2	3
Durability and maintenance	1	2	3
Design models used	2	4	6
Quality control level	1	3	6

5   Conclusions

The probabilistic calculations of timber elements based on the tested variables proved that a considerable decrease of reliability is expected for the elements in longitudinal buckling the capacity of which to resist external forces is affected by much more factors than in bending. It means that the safety factor for the structural elements elements should be determined not only for materials.

This study did not prove the idea that variation of properties depends on density of wood. May be variation in low density ranges is more expanded, but not particularly.

The system for the classification of timber structures should be developed. It is very important in the current situation when different building codes exist in European countries.

6   References

Brownlee K.A. (1977). Statistical theory and methodology in science and engineering. Translation in Russian (Moscow).

Christensen R. (1996). Analysis of variance, design and regression. Applied statistical methods. London: Chapman & Hall.

Ditlevsen O., Madsen H.O. (1996). Structural Reliability Methods. Chichester: JOHN WILEY & SONS.

ISO 2394:1998(E). General principles on reliability for structures.

Reliability-Based Design of Engineered Wood Structures (1992). Edited by Jozsef Bodig// Series E. Applied Sciences. Vol 215/ Proceedings of the NATO Advanced Research Workshop on Reliability-Based Design of Engineered Wood Structures in Florence, Italy, 2-5 Juny, 1991.- Kluwer Academic Publishers.

**INTERNATIONAL COUNCIL FOR RESEARCH AND INNOVATION
IN BUILDING AND CONSTRUCTION**

WORKING COMMISSION W18 - TIMBER STRUCTURES

CALIBRATION OF RELIABILITY-BASED TIMBER DESIGN CODES:

CHOOSING A FATIGUE MODEL

I Smith

University of New Brunswick

CANADA

Presented by: Ian Smith

Ian Smith began his presentation by stating that although most engineers take "static" fatigue into account they frequently neglect the effects of "cyclic" fatigue. He showed that the choice of damage model is a major factor that controls reliability predictions and that common interpretation of static fatigue data does not match the expectations from theoretical mechanics. He then went on to discuss the features which need to be taken into account when choosing a damage model before suggesting a simple mathematical model. He concluded that damage models should be consistent with experimental data but this does not mean that they have to be complex. Discussion centred on the use of terms static and cyclic fatigue and the relationship of the work reported to other standard fatigue work on timber.

Calibration of reliability-based timber design codes: Choosing a fatigue model

Ian Smith, University of New Brunswick, Canada

Abstract

Because wood is a rheological material, even quite low level stresses have the potential to degrade the residual strength of timber structures. Therefore it is important to account for fatigue processes when calibrating timber design code. This paper addresses both philosophical and practical aspects of questions surrounding essential features of fatigue models incorporated into reliability based code calibration exercises. Focus is on issues such as whether there is a certain level of stress below which fatigue damage will never occur and whether calculations need to account for both effects of load cycling and accumulated time under load. It is shown that, in a broad sense, it is unimportant whether fatigue predictions incorporate allowance for a threshold stress level, and that cyclic load induced fatigue need only be considered under low cycle fatigue situations where the loading frequency is sensibly measured in Hertz.

1   Introduction

Fatigue is the process of progressive localised permanent structural change occurring in materials subjected to conditions that produce sustained or fluctuating stress and strains at some point or points, and that may culminate in cracks or complete fracture after time or sufficient number of fluctuations [1].

Fatigue failure results from sustained or cyclic application of stress less than is required to cause in-elastic behaviour or fracture under monotonic loading of short duration. Damage initiates as micro cracks that subsequently aggregate, leading eventually to macro cracking and failure. Not all materials exhibit pronounced rheological characteristics (can flow under certain conditions), but wood does, which is why the above definition of fatigue incorporates a time argument. Fatigue in wood must depend on the number of stress cycles, rates of stressing and time for which peak stress is applied.

This paper addresses the question of what is the most suitable type of fatigue process (damage accumulation) model for incorporation into structural reliability simulations of timber structures. Discussion is focussed on the following issues:
- whether there is evidence to support assertions that fatigue only occurs if a certain threshold level of stress is exceeded,
- whether adoption of the so-called equal rank assumption biases interpretation of fatigue data and calibration of damage accumulation models,
- whether available evidence justifies use of complex damage accumulation models, and
- whether there is need to account for both static and cyclic fatigue effects in reliability calculations.

Although illustrative case studies are employed, focus is on conceptual issues.

1

2 Threshold stress level for damage accumulation[1]

For repetitive cyclic stress a fatigue limit is thought to exist for wood [2,3] and structural timber connections [4].[2] There is some dissenting opinion [5], but on balance opinion is favourable to the notion. The fatigue lives of wood components are smaller under reversed (through-zero) cyclic stress than under non-reversed (one-side-of-zero) cyclic stress having the same peak stress [6], with the most damaging situation being fully reversed loading (stress ratio $R = -1$)[3]. Nielsen [7] has proposed the existence of a critical R *value* under reversed loading, R_{crit}, above which the effects of stress-reversal are negligible. His order of magnitude estimate is $R_{crit} = -0.5$, but that value is inconsistent with the findings of Tsai and Ansell [7] who imply R_{crit} is close to zero. Possibly the value depends upon the strength level of a material, where strength level FL is the ratio of the actual strength to the theoretical strength of undamaged wood substance, with lumber and glulam having lower FL values than clear wood. Interestingly, fracture mechanics theory predicts rheological materials such as wood will always eventually fail under stress, irrespective of a fatigue limit [7]. What is clear from the literature is that, if a fatigue limit exists it has no unique value.

Tests have revealed that static fatigue (effect of sustained loading) can have a major effect on residual strength of various types of structural wood product [1]. Despite a few studies of quite long duration [8,9], stress levels have been too high for practical proof regarding the existence, or absence, of a threshold stress level σ_o below which damage will never accumulate. Existence of such a threshold has been postulated and incorporated in some empirical models for predicting damage due to static fatigue [1], with values of σ_o estimated to lie in a range of 0.35 to 0.55 for softwood lumber [10]. The higher values of σ_o are associated with higher quality lumber, which is contrary to fracture mechanics based expectations [7]. Fitting of threshold stress levels involves adoption of damage functions that presuppose they exist beyond the temporal range of data. Proposed empirical damage models incorporate up to seven (5 is common) calibration constants. Quite different combinations of model constants can lead to equally good fits of models to their calibration data [11], with one of those constants being σ_o. It seems unwise to read much into estimates of σ_o in the literature.

What is actually known from static fatigue tests is that, if ascending levels of constant stress are applied to matched groups of specimens there is an inverse relationship between the magnitude of the stress and the average time to failure. Despite material matching processes, strengths of individual specimens within a set vary and therefore actual σ can only be approximated. There is usually quite large variability in times to failure, T, with values being positively skewed, Figure 1(a). An approximately linear relationship exists between the level of applied constant stress σ and $\log_{10}T$, Figure 1(b). Static fatigue experiments (like cyclic fatigue experiments) will never identify existence of a threshold stress level below which stress induced damage never occurs, because wood is a rheological material. Obviously, this is not the same as saying there are no levels of stress that may be discounted.

---

[1] Stress level $= \sigma =$ ratio of peak applied stress to static strength determined in a test of about 0.1 hour duration.

[2] Fatigue limit = level of stress at or below which repetitive stress cycles will never cause failure.
[3] Stress ratio $= R =$ ratio of minimum to maximum stress (or load) during repetitive stress cycles.
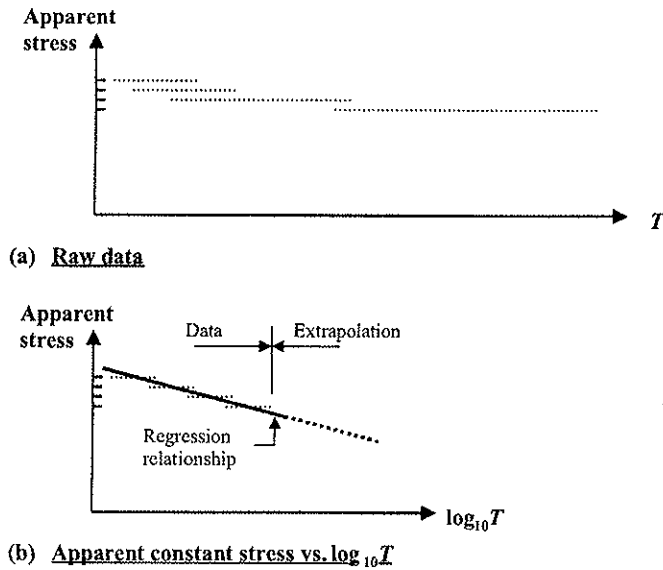
Figure 1 - Trend in static fatigue data (based on [1])

3 Equal rank assumption

Various researchers have employed the so-called equal rank assumption as a means of refining estimates of the σ for each specimen within a group subjected to the same absolute stress. The approach is an artificial means for smoothing data trends and extending the range of stress considered. Under the equal rank assumption it is presumed that the ordering of observed times to failure under a certain level of absolute stress is positively correlated with cumulative frequency in the static strength distribution [12]. With this mapping procedure it is possible to plot relatively smooth stress level versus time to failure (σ - $\log_{10}T$) trends from static fatigue data. Resultant plots tend to exhibit well defined negative curvature in σ - $\log_{10}T$ relationships at about the lowest deduced σ, Figure 2. Trends of the type depicted in Figure 2(b) have been taken a prima-facie evidence for existence of threshold stress levels applicable to static fatigue conditions [1]. However, as already mentioned, there is little physical evidence to support the deduction, and theoretical arguments against it (Section 2). Analysts should exercise caution before accepting 'equal rank interpretations' of data, not to mention being cognisant of links between this and subsequent use of resulting relationships in, for example, structural reliability based code calibration exercises.

4 Choice of a damage model

The vast majority of techniques for predicting fatigue damage in wood adopt the empirical damage index (state variable) approach. A few models have been proposed with a partially correct physical basis, but as yet these are not developed to the level where they can be calibrated and used with much confidence [1]. Remarks below concentrate on choosing an empirical model function likely to perform robustly as an extrapolation tool.

3
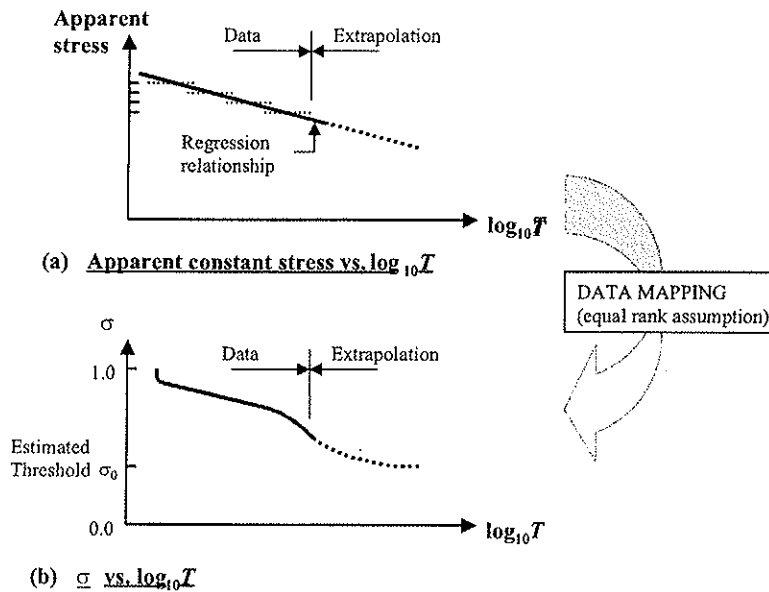
Figure 2 - Equal rank interpretation of static fatigue data (based on [1])

The major objection to empirical damage models is that most parameters have no strict physical meaning and it is very difficult to supplement models to account for factors such as moisture conditions and member size. Model 'constants' cannot always be calibrated in a straightforward manner and their values can be highly sensitive to presumptions that underpin the calibration exercise (Section 3). Stress levels considered by various researchers have been too high, and thus times to failure too short, for experimentally based elucidation of which is the best form of empirical damage accumulation function. Difficulty in obtaining consistent fit of models across ramp loading rates [13-15] implies they do not mimic how the rate of loading affects damage accumulation. It has been shown that although damage at the micro to macro scales is highly sensitive to the rate of loading, massive wood members and some types of joint are not, because they permit redistribution of stress as loading proceeds [1]. There is need for careful consideration when deciding implications of data and in use of extrapolation tools (models). The 'best' choice of an empirical damage model is undoubtedly application dependent, which is why there is no consensus on the matter.

Proposed empirical damage accumulation models overestimate residual strengths of specimens that survived sustained stress (or the proportion of survivors) because it is impossible for them to have an equally good fit over a different ranges of time [15]. As already implied (Section 2), the rate of damage will cascade once a failure surface/path that cannot be arrested is established, and a damage threshold stress will not exist independent of the load history. It has been observed for mechanical systems that variability in fatigue life depends primarily on uncertainty about individual specimens rather than on uncertainty about details of the stochastic load history [16]. By analogy uncertainty about lifetimes of wood members, connections or systems mainly depends on uncertainty about the extent of the initial damage, i.e. accuracy with which the stress level during the first pulse of in-service loading can be deduced.

4

When selecting a damage threshold stress level σ_o, logic suggests it should apply uniformly whatever the nature of the physical process that develops stress. The value should equal the fatigue limit as observed under repetitive cyclic loading, because that is the only parameter that can estimated within finite experimental budgets. Neglecting chemical and biological decomposition of the wood, it is plausible that damage will not occur provided a certain σ_o is never exceeded due to any causative agent. Any threshold stress should probably be lower than most estimates in the literature [1]. As alluded to already, because of its rheological nature, wood has 'memory' and damage is load path dependent. The current threshold stress level for any piece of material is dependent on the stress history and a function of the current level of damage [1,13,17]. Unpublished tests at the University of New Brunswick suggest that for structural lumber a reasonable initial value of σ_o is 0.2 (applicable to the nominally undamaged state). There exists interaction between static and cyclic fatigue effects [1], and in the general (but not necessarily the specific) case fatigue models need to reflect that.

Based on all the evidence available, an appropriate form of empirical damage model is thought to be [1]:

$$dD = \sum_{i=1}^{I} \left(\int_0^{t_i} 10^{(A-\sigma_i)/B} dt_i + \frac{1}{N_i} \right) \qquad \text{if } \sigma_i > \sigma_{o,i} = \sigma_{o,0}(1 - D_{i-1})^C$$

$$dD = 0 \qquad \text{if } \sigma_i \leq \sigma_{o,i} = \sigma_{o,0}(1 - D_{i-1})^C \qquad (1)$$

where: $0 \leq D \leq 1$ is a damage index with $D = 0$ corresponding to the undamaged state and $D = 1$ corresponding to the failure state, t_i is the period for the ith load cycle, N_i is the pure fatigue life for the peak stress level associated with the ith load cycle, σ_i is the stress ratio at time t ($0 \leq t \leq t_i$), $\sigma_{o,i}$ is the threshold stress level for the ith load cycle, $\sigma_{o,0}$ is the threshold stress level when $D = 0$, D_{i-1} is the damage level at the end of the $(i-1)^{th}$ load cycle, and A, B and C are calibration constants. Constants A and B are calibrated based on pure static fatigue tests. In the absence on other information, C can be taken as 1.0. Determination of N_i should account for dependency on loading frequency and the waveform [1]. When the loading frequency is low the associated term in equation (1) is null. The equation combines the well-known Palgrem-Miner rule with the relatively simple Gerhards damage models that the timber engineers are already familiar with [18-20]. The formulation of the model is preferred to others because while being relatively simple it still incorporates a 'memory effect'. Also, ability to perform explicit integration of the function makes its use practical. Equation (1) can be extended to encompass factors such as reversed loading and mechanosorptive effects, as outlined elsewhere [1].

5 Importance of cyclic versus static fatigue effects

As should be self evident, 'low cycle fatigue' (LCF) failures associated with high loading frequencies (e.g. seismic events, fluttering of roof panels during cyclones) are strongly influenced by the rate of stressing.[4] However, it is unclear in other circumstance whether both rate of stressing (cyclic fatigue effect) and time under loading (static fatigue effect) need to be considered. There is no simple answer to this question, and it is addressed here by considering a 'high cycle fatigue' (HCF) situation caused by repetitive loads applied at moderately high frequency.[5] Let us consider behaviour of a single-track short span railway

---

[4] LCF is commonly taken as referring to situations where failure occurs due to less than 10,000 stress cycles.

[5] HCF is commonly taken as referring to situations where failure occurs due to more than 10,000 stress cycles.

bridge of 3.6m span having five simply supported parallel stringers that share wheel loads in proportion to their flexural rigidities.[6] Live load is from wheels of type EDM GP-38 locomotives and 263k freight cars, each of which exerts maximum axle loads $F_{axle} = 292kN$. Dead load is relatively small and neglected here. Force pulses produced by axles crossing the bridge are as shown in Figure 3. As shown in the figure, the duration of the force pulse is linearly proportional to the speed of a train.
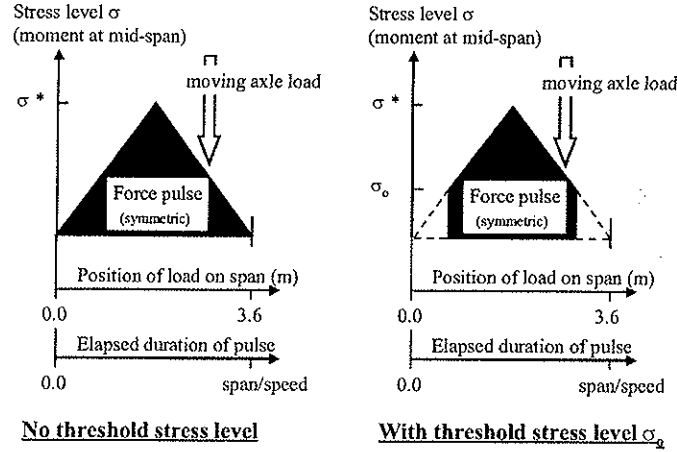
Figure 3 - Definition of force pulses on stringers: railway bridge (from [1])

Based on the above problem definition, the number of axle passes to failure is predicted for each stringer using the general form of the empirical damage accumulation model in equation (1). As discussed in Section 4, the first term in the expression for dD accounts for static fatigue effects and is proportional to the duration of a force pulse with more damage done per cycle the slower trains travel. The static fatigue damage per axle pass is:

$$dD_{static} = \frac{-BL(10^{(A-\sigma^*)/B} - 10^{(A-\sigma_o)/B})}{2.3026s\sigma^*} \qquad (2)$$

where s is the speed of the train, and other parameters are as previously defined. For the purposes of this problem it is presumed that $A = 0.880$ and $B = -0.120$, which corresponds to a relatively severe rate of damage accumulation. The second term in equation (1) accounts for effects of the rapid loading and unloading rates (cyclic fatigue effect), with the increment in dD per axle pass being:

$$dD_{cyclic} = 10^{-12.5(1-\sigma^*)} \qquad (3)$$

This corresponds to the stress level versus fatigue life relationship in Figure 4. Strictly, any expression for dD_{cyclic} should be a function of loading frequency (train speed) and the waveform [1]. Such refinement is excluded here as it does not influence predictions, as shown later.

Peak stress levels vary quite significantly between bridge stringers because of variability in both flexural rigidity that controls the proportion of the axle load carried, and variability in undamaged static strength. It is assumed for the purposes of calculation that failure of any stringer causes failure of the bridge. The bridge as a whole fails after $10^{7.6}$ axle passes if only the cyclic fatigue effect is considered. When static fatigue only, or static plus cyclic fatigue,

---

[6] This and other illustrative problems in this paper as discussed in more detail within the book by Smith et al [1].

6

is considered, the number of axle passes to fail the bridge depends on the train speed. Results are given in Table 1 for two train speeds and two assumptions about the parameters that control the influence of a threshold stress level on lives of stringers. For the various stringers, the predicted number of axle passes to cause failure is about two to three orders of magnitude less for static fatigue alone than for cyclic fatigue alone. Clearly the static fatigue effect dominates predictions. As shown in Table 1, existence of a threshold stress level has a secondary influence on results. Taking the least estimate of lifetime, the bridge is predicted to fail after $10^{5.3}$ axle passes. To a good approximation, predictions for full implementation of equation (1), i.e. $dD = dD_{static} + dD_{cyclic}$, are the same as those for $dD = dD_{static}$, because $dD_{static} \gg dD_{cyclic}$.
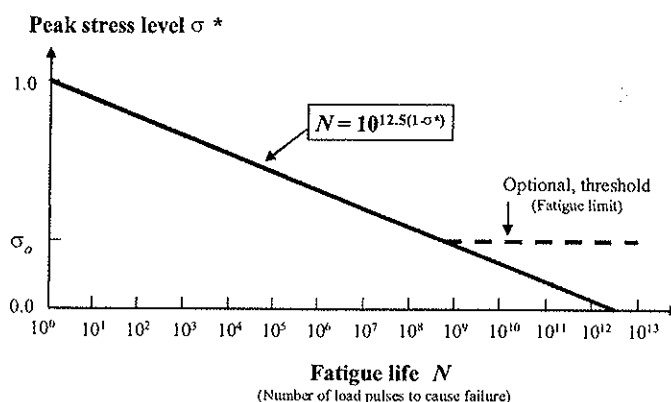
Peak stress level σ *

Figure 4 - Peak stress level vs. pure fatigue life relationship: railway bridge (from [1])

**Table 1** - Number of axle passes to cause failure: railway bridge: [7]

Train speed	Threshold stress level parameters	Static fatigue effect only	Static + cyclic fatigue effects
30 km/hr.	$\sigma_{o,0} = 0.0$	$10^{5.3}$	$10^{5.3}$
	$\sigma_{o,0} = 0.3$; $C = 0.0$	$10^{5.4}$	$10^{5.4}$
60 km/hr.	$\sigma_{o,0} = 0.0$	$10^{5.6}$	$10^{5.6}$
	$\sigma_{o,0} = 0.3$; $C = 0.0$	$10^{5.7}$	$10^{5.7}$

Results for models with a threshold stress level that degrades as damage accumulates ($C > 0.0$) are intermediate between those obtained assuming $\sigma_{o,0} = 0.0$; and $\sigma_{o,0} = 0.3$, $C = 0.0$. To illustrate, if $\sigma_{o,0} = 0.3$ and $C = 1.0$ the number of axle passes to fail the bridge would be $10^{5.34}$, instead of $10^{5.31}$ when $\sigma_{o,0} = 0.0$. Although it is not possible to generalise the outcome of one problem, it is clear that dD_{cyclic} can be expected to make no appreciable contribution to dD in many circumstances, e.g. snow loads on roofs, most floor occupancy loads. As a rule of thumb the cyclic fatigue effect can be expected to be negligible in circumstances where one would feel it nonsensical to quote the loading frequencies in Hertz.

---

[7] Assumptions about the threshold stress level are taken to be on the extremes implied by the literature, with $\sigma_{o,0} = 0.0$ representing no threshold and $\sigma_{o,0} = 0.3$; $C = 0.0$ representing a threshold expected to ameliorate damage accumulation rates quite significantly.

6 Importance of threshold stress level: static fatigue

As an illustrative problem, behaviour of flat roofs in Ottawa, Canada will be considered. Roofs have 38 x 235mm joists of Spruce-Pine-Fir, No. 2 grade, spaced at 400mm on centre and plywood sheathed attached by nominal nailing. For that type and size of lumber, the 5-percentile static moment capacity is 5.4kNm, and the maximum span that building regulations permit is 4.1m for domestic construction. In analysis joists are assumed to be simply supported at each end and subject to only dead and snow loads, Figure 5, i.e. potentially critical load conditions occur when heavy repetitive snow loads combine with dead load. Snow loading follows an Extreme Type I distribution with mean value of 1.09kPa (CoV = 0.935). The simulated dead load is 0.5kPa. Simulated stress levels σ range from just above 0.0 to over 0.8 depending on joist span (stress level σ is proportional to span^2).
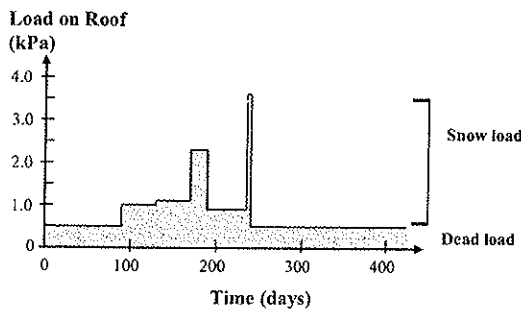
Figure 5 - Segment of simulated load history: flat roofs in Ottawa (from [1])
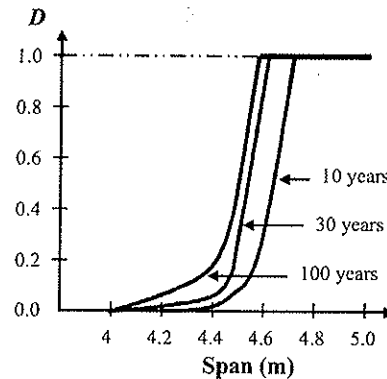
Figure 6 - Effects of joist span and time in service on damage index D for 5th percentile joist: flat roofs in Ottawa (from [1])

Again damage accumulation calculations are based on equation (1). Because snow accumulates slowly any rate of loading effects on damage are negligible and the cyclic fatigue effect need not be considered. The damage model reduces to:

$$dD = \sum_{i=1}^{I} \int_0^{t_i} 10^{(A-\sigma_i)/B} dt_i \qquad \text{if } \sigma_i > \sigma_{o,i} = \sigma_{o,0}(1 - D_{i-1})^C$$

$$dD = 0 \qquad \text{if } \sigma_i \le \sigma_{o,i} = \sigma_{o,0}(1 - D_{i-1})^C \qquad (4)$$

Here constants A and B are taken to be 0.9 and -0.05 respectively, based on the data by Hoffmeyer [9]. Parameters $\sigma_{o,0}$ and C that control evolution of the threshold stress level ($\sigma_{o,i}$) are taken to be 0.2 and 1.0 respectively. It can be shown that in a relative sense little damage occurs in periods when σ_i is less than about 0.4, and in practical terms results are unaffected if it is assumed $\sigma_{o,0} = 0.0$. Randomness between joists in parameters controlling damage accumulation rates (A, B, C and $\sigma_{o,0}$) is ignored here.

Because joist strengths vary both within and between roofs, stress levels, and therefore damage accumulation and likelihood of failure are stochastic processes. Accumulation of D is illustrated in Figure 6 for a joist that corresponded to the lower 5-percentile strength level (when new), as a function of span and time under load. As can be seen, such a joist should experience no appreciable damage if used within its permitted span range (span $\le$ 4.1m), but could acquire significant damage if the span were longer. It follows that some very weak joists can be expected to fail even if used at the permitted span. However, all joists in almost

every roof are substantially under utilised, from a strength point of view. Therefore roof failures are very unlikely and even if one joist in a particular roof fails, that roof is unlikely to collapse. Table 2 indicates how time to failure varies with joist span and gives estimates of annual probabilities of failure of roof joists (per joist per year basis).

Table 2 - Effect of span on time to failure and probability of failure: flat roofs in Ottawa

Span (m)	Approx. time to failure of 5%tile joist (years)	Approx. annual probability of failure (per joist)
4.0	∞	10^{-6}
4.2	2×10^3	10^{-5}
4.4	100	10^{-4}
4.6	< 10	10^{-2}
4.8	< 5	10^{-1}
5.0	< 1	1.0

It needs to be emphasised that above mentioned results, and results of similar studies, are highly dependent on model constants, especially A and B. Often there is a high degree of uncertainty about suitable values of those parameters. As is discussed by Smith et al [1], structural reliability predictions are highly sensitive to assumptions about variability in damage accumulation rates between nominally identical components and systems. Those assumptions can be much stronger influences on 'allowable spans' that almost any other variable (e.g. service life, choice of damage model, safety index). The issue of component versus system reliability is the only issue that is not automatically swamped by vagaries of knowledge about variability in damage rates. With the current levels of knowledge about selection of damage model parameters, it would be foolish to presume static fatigue predictions for wood components yield anything other than 'hand waving' estimates of failure rates. This is why results are an aid to rather than substitute for engineering judgement.

7 Conclusions

The broad conclusions from this paper are that:

- although predictive capabilities of damage should be consistent with experimental observations and theoretical concepts, this does not mean they have to be complex,
- it is relatively unimportant whether fatigue models incorporate allowance for a threshold stress level, and
- cyclic load induced fatigue need only be considered under low cycle fatigue situations where the loading frequency is sensibly measured in Hertz.

References

[1] Smith, I., Landis, E. and Gong, M. 2003. "Fracture and fatigue in wood", John Wiley & Sons, Chichester, UK.
[2] Kyanka, G.H. 1980. "Fatigue properties of wood and wood composites", *International Journal of Fracture*, 16(6): 609-616.
[3] Ansell, M.P. 1995. "Fatigue design for timber and wood-based materials", Lecture E22. *In:* "Timber Engineering STEP: Design – details and structural systems", *Eds.* Blass, H.J.,

Aune, P., Choo, B.S., Gorlacher, R., Griffith, D.R., Hilson, B.O., Racher, P. and Steck, G., Centrum Hout, Almere, The Netherlands: E22/1-E22/8.

[4] Hayashi, T., Sasaki, H. and Masuda, M. 1980. "Fatigue properties of wood butt joints with metal plate connectors", *Forest Products Journal*, 30(2): 49-54.

[5] Rosenthal, D. 1964. "Introduction to properties of materials", D. Van Nostrand Co., Inc., Princeton, NJ, USA.

[6] Tsai, K.T., and Ansell, M.P. 1990. "The fatigue properties of wood in flexure", *Journal of Material Science*, 25: 865-878.

[7] Nielsen, L.F. 1996. "Lifetime and residual strength of wood", Report: Series R, No. 6, Department of Structural Engineering and Materials, Technical University of Denmark, Lyngby, Denmark.

[8] Gerhards, C.C. 2000. "Bending creep and load duration of Douglas-fir 2 by 4s under constant load for up to 12-plus years", *Wood and Fiber Science*, 32(4): 489-501.

[9] Hoffmeyer, P. 2003. "Strength under long-term loading", *In:* "Timber Engineering", *Eds.* Thelandersson, S. and Larsen, H.J. John Wiley & Sons, Chichester, UK.

[10] Foschi, R.O., Folz, B.R. and Yao, F.Z. 1989. "Reliability-based design of wood structures", Structural Research Series Report No. 34, University of British Columbia, Vancouver, BC, Canada.

[11] Aicher, S. and Dill-Langer, G. 1997. "Damage modelling of glulam in tension perpendicular to the grain in variable climate", Paper number 30-9-2, Proceedings of CIB-Working Commission 18: Timber Structures, Meeting 30, International Council for Research and Innovation in Building and Construction, Rotterdam, The Netherlands.

[12] Madsen, B. 1992. "Structural behaviour of timber", Timber Engineering Ltd., North Vancouver, BC, Canada.

[13] Gerhards, C.C. and Link, C.L. 1987. "A cumulative damage model to predict load duration characteristics of lumber", *Wood and Fiber Science*, 19(2): 147-164.

[14] Daneff, G. 1997. "Response of bolted connections to pseudodynamic (cyclic) loading", MScFE thesis, University of New Brunswick, Fredericton, NB, Canada.

[15] Cai, Z., Rosowsky, D.V., Hunt, M.O. and Fridley, K.J. 2000. "Comparison of actual vs. simulated failure distributions of flexural wood specimens subjected to 5-day load sequences", *Forest Products Journal*, 50(1): 74-80.

[16] Crandall, S.H. and Mark, W.D. 1963. "Random vibration in mechanical systems", Academic Press, New York, NY, USA.

[17] Leicester, R.H. 1990. "Failure in two-cycle fatigue", *Theoretical and Applied Fracture Mechanics*, 13: 161-164.

[18] Palgren, A. (1924) "Die lebensdauer von kugallagern", *Ver. Deut Ingr.*, 68: 339-341.

[19] Miner, M.A. 1945. "Cumulative damage in fatigue", *Journal of Applied Mechanics*, 12(3): A159-164.

[20] Gerhards, C.C. (1979) 'Time –related effects of loading on wood strength: a linear cumulative damage theory', *Wood Science*, 11(3): 139-144.